



U.S. DEPARTMENT OF
ENERGY

Office of
Science

Program and Abstracts for the

Inaugural
Experimental Condensed Matter Physics
Principal Investigators Meeting

Rockville Hilton
Rockville, Maryland
August 9–12, 2011

Materials Sciences and Engineering Division
Office of Basic Energy Sciences
US Department of Energy

This document was produced under contact number DE-AC05-06OR23100 between the U.S. Department of Energy and Oak Ridge Associated Universities.

The research grants and contracts described in this document are supported by the U.S. DOE Office of Science, Office of Basic Energy Sciences, Materials Sciences and Engineering Division.

Foreword

This volume summarizes the scientific content of the 2011 Experimental Condensed Matter Physics Principal Investigators Meeting sponsored by the Materials Sciences and Engineering Division of the DOE Office of Basic Energy Sciences (BES). The purpose of the meeting was to bring together researchers funded by BES in this important research area so that they could get a view of the broad range of research that is being supported by the Experimental Condensed Matter Physics program. While recent research highlights were presented, the focus of the meeting was on topics that the PIs felt were the most exciting new research directions. This meeting was useful to DOE-BES in assessing the state of the program, charting future directions, and identifying programmatic needs. We hope that the meeting fostered a collegial environment that stimulated discussion of new ideas and provided unique opportunities to develop or strengthen collaborations among PIs. We plan to hold a similar meeting biannually.

This inaugural meeting was held August 9–12, 2011, at the Rockville Hilton in Rockville, Maryland. The meeting was attended by more than 100 scientists, with 46 oral and approximately 35 poster presentations in two poster sessions. We were very pleased to have two plenary speakers: Prof. Ramamoorthy Ramesh introducing the DOE SunShot Initiative and Prof. Séamus Davis providing an overview of the Center for Emergent Superconductivity EFRC.

The Experimental Condensed Matter Physics Program covers a broad range of research activities, supporting experimental research aimed at gaining fundamental understanding of the relationships between electronic structure, particularly in the case of strong correlation among electrons, and the properties of complex materials such as superconductors and magnetic materials. A particular emphasis is placed on investigating the physics of one- and two-dimensional systems, including nanostructures, as well as studies of electronic structure under extreme conditions such as low temperatures and high magnetic fields. The program has a longstanding investment in research to understand unconventional superconductors, including the high-temperature cuprate family and the recently discovered class of iron-based superconductors. In the last few years the program has increased support for studies of spin physics and nanomagnetism, and has begun to explore whether cold atom research can provide insight into open questions about correlated electron behavior in hard condensed matter systems. Also supported is the development of new techniques and instruments for characterizing the electronic states and properties of materials under extreme conditions, such as in ultra low temperatures (millikelvin) and ultra high magnetic fields (100 Tesla). Improving the understanding of the electronic behavior of materials on the atomic scale is relevant to the DOE mission, as these structures offer enhanced properties that could lead to dramatic improvements in technologies for energy generation, conversion, storage, delivery, and use.

We organized the meeting into ten different sessions that cover the broad range of activities supported by the program—correlated electrons, magnetism and spin physics, low-dimensional systems, superconductivity, and topological insulators—as well as two poster sessions.

We thank all the participants for their investment of time and for their willingness to share their ideas with the meeting participants. We also want to gratefully acknowledge the excellent support provided by Ms. Lee-Ann Talley and Ms. Joreé O’Neal of the Oak Ridge Institute for Science and Education and by Ms. Teresa Crocket of BES, without whom this meeting would not have happened.

Dr. Andrew Schwartz
Program Manager, Experimental Condensed Matter Physics
Materials Sciences and Engineering Division
Office of Basic Energy Sciences
Department of Energy

Table of Contents

Foreword	i
Table of Contents	iii
Agenda.....	xi

Session 1: Correlated Electrons

Complex States, Emergent Phenomena and Superconductivity in Intermetallic and Metal-Like Compounds

*P. Canfield, S. Bud'ko, J. Clem, D. Johnston, A. Kaminski, V. Kogan, R. Prozorov,
J. Schmalian, and M. Tanatar* 1

Superconductivity and Magnetism in d- and f-Electron Materials

M. Brian Maple.....5

Correlated and Complex Materials

Brian C. Sales, Lynn A. Boatner, David K. Christen, and David G. Mandrus9

Atomic Engineering Oxide Heterostructures: Materials by Design

H. Y. Hwang, J. Stohr, Y. Hikita, and C. Bell..... 13

Nanostructured Materials: From Superlattices to Quantum Dots

Ivan K. Schuller 17

Session 2: Magnetism and Spin Physics

Magnetic Films and Nanomagnetism

Sam Bader.....21

Optical Study of Spin Dynamics in Semiconductor Nanowires

Fengyuan Yang and Ezekiel Johnston-Halperin25

Spin Polarized Electron Transport through Aluminum Nanoparticles

Dragomir Davidović29

Spin-Polarized Scanning Tunneling Microscopy Studies of Nanoscale Magnetic and Spintronic Nitride Systems

Arthur R. Smith33

Fundamental Studies of High-Anisotropy Nanomagnets

David J. Sellmyer, Ralph Skomski, and George Hadjipanayis.....37

Session 3: Low-Dimensional Systems

Investigation of the Quantum Limit Transport Phenomena in Graphene <i>Philip Kim</i>	41
Microwave- and Terahertz- Photo-Excited Transport in Low Dimensional Electron Systems <i>Ramesh G. Mani</i>	45
Probing the Electronic Structure and Dynamics of Low-Dimensional Condensed-Matter Systems using Femtosecond Probes <i>Richard Osgood, Peter Johnson, and Andy Millis</i>	49
Optical Spectroscopy of Defects and Dopants in Nanocarbon Materials <i>Lukas Novotny</i>	53

Session 4: Superconductivity

Tailoring Near Isotropic High Temperature Superconductivity in Iron Pnictides <i>Wai-Kwong Kwok, Ulrich Welp, Alexei E. Koshelev, Vitalii Vlasko-Vlasov, and George W. Crabtree</i>	57
Origin of Superconductivity in Structurally Layered Materials <i>Athena Sefat</i>	61
Towards a Universal Description of Vortex Matter in Superconductors <i>Leonardo Civale</i>	65
High Magnetic Fields as a Probe to Unveil the Physical Properties of the Newly Discovered Fe Oxypnictide Superconductors and Related Compounds <i>Luis Balicas</i>	69

Session 5: Two-Dimensional Electron Systems

Novel Temperature Limited Tunneling Spectroscopy of Quantum Hall Systems <i>Raymond Ashoori</i>	73
Microwave Spectroscopy of Electron Solids: Fractional Quantum Hall Effect and Controlled Disorder <i>Lloyd Engel</i>	77
Emergent Phenomena in Quantum Hall Systems Far From Equilibrium <i>Michael Zudov</i>	81

Quantum Electronic Phenomena and Structures

Wei Pan, Michael P. Lilly, Ken S. K. Lyo, John L. Reno, Lisa A. Tracy, George T. Wang, and Rohit P. Prasankumar 85

Cold Exciton Gases in Semiconductor Heterostructures

Leonid Butov 89

Session 6: Low-Dimensional Systems

Measurement of Single Electronic Charging of Semiconductor Nano-Crystals

Marc A. Kastner 93

Colloidal Quantum Dot Films, Transport and Magnetotransport

Philippe Guyot-Sionnest 96

Novel sp²-Bonded Materials and Related Nanostructures

Alex Zettl 100

Spectroscopy of Degenerate One-Dimensional Electrons in Carbon Nanotubes

Junichiro Kono 101

Symmetries, Interactions, and Correlation Effects in Carbon Nanotubes

Gleb Finkelstein 105

Session 7: Superconductivity

Quasiparticle Recombination in BSCCO Probed by Time-Resolved ARPES and Optical Reflectivity

R. J. Birgeneau, E. Bourret-Courchesne, A. Lanzara, D. H. Lee, J. Orenstein, R. Ramesh, and A. Vishwanath 109

Infrared and Angle Resolved Photoemission Studies of High-Temperature Superconductors and Related Systems

Christopher C. Homes, Tonica Valla, and Peter D. Johnson 113

The Nature of Fermi Arcs, Pseudogaps, and Electron Scattering Rates in Cuprate High-T_c Superconductors

Dan Dessau 117

Experimental Study of Severely Underdoped Ultrathin Cuprate Films

Thomas R. Lemberger 120

Spectroscopic Imaging STM Studies of Complex Electronic Matter

J. C. (Séamus) Davis 123

Session 8: Topological Insulators

Quantum Transport in Topological Insulator Nanoelectronic Devices <i>Pablo Jarillo-Herrero</i>	127
Focused Research Center in Correlated Electron Materials <i>Ziqiang Wang, Hong Ding, Vidya Madhavan, and Willie Padilla</i>	130
Infrared Hall Effect in Correlated Electronic Materials <i>H. Dennis Drew</i>	134

Session 9: Superconductivity

Quantum Materials at the Nanoscale <i>P. Abbamonte, R. Budakian, J. N. Eckstein, L. H. Greene, A. J. Leggett, D. J. Van Harlingen, A. Bezryadin, S. L. Cooper, E. H. Fradkin, T. Hughes, N. Mason, and S. Vishveshwara</i>	139
Engineering of Mixed Pairing and Non-Abelian Quasiparticle States of Matter in Chiral p-Wave Superconductor Sr_2RuO_4 <i>Ying Liu</i>	143
Tunneling and Transport in Nanowires <i>Allen M. Goldman</i>	147
Single Atom and Molecule Manipulation and Its Application to Nanoscience and Technology <i>Saw-Wai Hla</i>	151
Time-Resolved Synchrotron Studies of Spin and Charge Dynamics in Solids <i>D. B. Tanner, D. H. Reitze, C. J. Stanton, and G. L. Carr</i>	155

Session 10: Magnetism

Properties of Spintronic Materials and Nanostructures via Novel Characterization Techniques <i>Charles S. Fadley, Peter J. Fischer, Frances Hellman, and Jeffrey B. Kortright</i>	159
Digital Synthesis: A Pathway to New Materials at Interfaces of Complex Oxides <i>Anand Bhattacharya</i>	164
Time-Resolved Spectroscopy of Insulator-Metal Transitions: Exploring Low-Energy Dynamics in Strongly Correlated Systems <i>Gunter Luepke</i>	168

Competing Interactions in Complex Transition Metal Oxides
L. E. De Long, Gang Cao, Todd Hastings, and S. S. Seo..... 172

Exploration of Artificial Frustrated Magnets
Peter Schiffer, Vincent Crespi, and Nitin Samarth 175

Poster Sessions

Poster Session I..... 179

Poster Session II 181

Poster Abstracts

Quantum Transport in Magnetic and Non-Magnetic 2D Correlated Insulators
Philip W. Adams..... 183

Experimental Study of Correlations and Induced Superconductivity in Graphene
Eva Y. Andrei 187

Probing Nanocrystal Electronic Structure and Dynamics in the Limit of Single Nanocrystals
Moungi G. Bawendi 191

Developing Functionality in Quantum Dots
Jonathan Bird 195

Integrated Growth and Ultra-Low Temperature Transport Study of the 2nd Landau Level of the Two-Dimensional Electron Gas
Gabor Csathy and Michael Manfra 199

Magnetic and Superconducting Properties of Materials Studied by the ⁹⁹Ru, ¹⁸⁹Os, ¹¹⁹Sn, ⁵⁷Fe and ¹⁹¹Ir Mössbauer Effects in External Magnetic Fields
Michael DeMarco and Dermot Coffey..... 203

Experiments on Quantum Hall Topological Phases in Ultra Low Temperatures
Rui-Rui Du..... 207

Fabrication of Graphene Devices for Electron Flow Imaging
Adam Graham, Wei Li Wang, Sagar Bhandari, David C. Bell, and Robert Westervelt..... 211

Linear and Nonlinear Optical Properties of Metal Nanocomposite Materials
Richard F. Haglund, Jr. 212

Science at 100 Tesla <i>Neil Harrison, Fedor F. Balakirev, Jonathan Betts, Scott Crooker, Marcelo Jaime, Ross McDonald, Albert Migliori, and John Singleton</i>	216
Emerging Materials <i>John F. Mitchell, Kenneth E. Gray, and B. J. Kim</i>	220
Ballistic Acceleration Phase of a Supercurrent <i>Milind N. Kunchur and Gabriel Saracila</i>	224
Interfaces in Epitaxial Complex Oxides <i>Hans M. Christen, Gyula Eres, Ho Nyung Lee, T. Zac Ward, Christopher M. Rouleau, Jon Z. Tischler, Ben C. Larson, and Anter El-Azab</i>	225
Transport Studies of Quantum Magnetism: Physics and Methods <i>Minhyea Lee</i>	229
Studies of Interband Modes and Fermi Surface Features in Very Clean MgB₂ Films <i>Qi Li</i>	231
Emergent Behavior of Magnet-Superconductor Hybrids <i>Igor F. Lyuksyutov, W. Wu, and D. G. Naugle</i>	235
Electronic and Optical Processes in Novel Semiconductors for Energy Applications <i>A. Mascarenhas, Brian Fluegel, Kirstin Alberi, and Aleksey Mialitsin</i>	239
Investigations of the Material Dependence of the Casimir Force <i>Umar Mohideen</i>	243
Nanostructure Studies of Strongly Correlated Materials <i>Douglas Natelson</i>	244
Magnetic Nanostructures and Spintronic Materials <i>Michael Pechan</i>	248
Thermopower near the 2D Metal-Insulator Transition <i>Myriam P. Sarachik, Alex Punnoose, and Sergey V. Kravchenko</i>	252
Photonic Systems <i>Joseph Shinar, Rana Biswas, Kai-Ming Ho, and Costas Soukoulis</i>	255
Infrared Optical Study of Graphene in High Magnetic Fields <i>Dmitry Smirnov and Zhigang Jiang</i>	259

Probing the Origins of Conductivity Transitions in Correlated Solids: Experimental Studies of Electronic Structure in Vanadium Oxides <i>Kevin E. Smith</i>	264
Indirect Excitons in Coupled Quantum Wells: New Studies with Dark Excitons <i>David Snoko</i>	267
Simulating Strongly Correlated Electrons with a Strongly Interacting Fermi Gas <i>John E. Thomas</i>	271
Investigations of Electron Correlation in Complex Systems <i>J. G. Tobin, S. W. Yu, B. W. Chung, G. W. Waddill</i>	275
Spatial Extent of Near-Band Edge Modification due to Lattice Disorder <i>A. Steigerwald, A. B. Hmelo, K. Varga, L. C. Feldman, and N. Tolk</i>	279
Novel Nanoscale Morphologies and Atomistic Processes Control on Surfaces <i>K. M. Ho, M. Hupalo, P. A. Thiel, M. C. Tringides, and C. Z. Wang</i>	283
A Synergistic Approach to the Development of New Hydrogen Storage Materials Part II: Nanostructured Materials <i>A. Paul Alivisatos, Jeffrey R. Long, Jeffrey J. Urban, and Alex Zettl</i>	287
Phase Diagram for Iron-Chalcogenide Superconducting Films <i>Barrett O. Wells and Joseph I. Budnick</i>	291
Author Index	295
Participant List	297

BES Experimental Condensed Matter Physics Principal Investigators Meeting

AGENDA

Tuesday, August 9, 2011

- 4:00 – 6:00 pm **Registration**
- 6:00 – 7:00 pm ******* Working Dinner *******
- 7:10 – 7:30 pm **Welcome**
Andy Schwartz
Program Manager, Experimental Condensed Matter Physics
- 7:30 – 8:00 pm **Division and Program Updates**
Linda Horton
Director, Division of Materials Science and Engineering
- 8:00 – 8:45 pm **DOE SunShot Initiative**
Ramamoorthy Ramesh
Program Manager, EERE
- 8:45 – 9:45 pm **Informal Discussions**

Wednesday, August 10, 2011

- 7:30 – 8:30 am **Breakfast**

Session 1

Correlated Electrons

- 8:30 – 8:50 am Paul Canfield (*Ames Lab*)
Complex States, Emergent Phenomena and Superconductivity in Intermetallic & Metal-Like Compounds
- 8:50 – 9:10 am Brian Maple (*UCSD*)
Superconductivity and Magnetism in d- and f-Electron Materials
- 9:10 – 9:30 am Brian Sales (*ORNL*)
Correlated and Complex Materials
- 9:30 – 9:50 am Harold Hwang (*SLAC*)
Atomic Engineering Oxide Heterostructures: Materials by Design

9:50 – 10:10 am Ivan Schuller *UCSD*
Nanostructured Materials: From Superlattices to Quantum Dots

10:10 – 10:40 am ***** **Break** *****

Session 2

Magnetism and Spin Physics

10:40 – 11:00 am Sam Bader (*ANL*)
Magnetic Films and Nanomagnetism

11:00 – 11:20 am Fengyuan Yang (*Ohio State*)
Optical Study of Spin Dynamics in Semiconductor Nanowires

11:20 – 11:40 am Dragomir Davidovic (*Georgia Tech*)
Spin Polarized Electron Transport through Aluminum Nanoparticles

11:40 – 12:00 pm Art Smith (*Ohio Univ.*)
Spin-Polarized Scanning Tunneling Microscopy Studies of Nanoscale Magnetic and Spintronic Nitride Systems

12:00 – 12:20 pm David Sellmyer (*Nebraska*) and
George Hadjipanayis (*Delaware*)
Fundamental Studies of High-Anisotropy Nanomagnets

12:20 – 2:00 pm ** **Working Lunch / Small Group Discussions** **

Session 3

Low-Dimensional Systems

2:00 – 2:20 pm Philip Kim (*Columbia*)
Investigation of the Quantum Limit Transport Phenomena in Graphene

2:20 – 2:40 pm Ramesh Mani (*Georgia State*)
Microwave- and Terahertz- Photo-Excited Transport in Low-Dimensional Electron Systems

2:40 – 3:00 pm Rick Osgood (*Columbia*)
Probing the Electronic Structure and Dynamics of Low-Dimensional Condensed-Matter Systems Using Femtosecond Probes

3:00 – 3:20 pm Lukas Novotny (*Rochester*)
Optical Spectroscopy of Defects and Dopants in Nanocarbon

3:20 – 3:50 pm ***** **Break** *****

Session 4	Superconductivity
3:50 – 4:10 pm	Wai Kwok (ANL) <i>Tailoring Near Isotropic High Temperature Superconductivity in Iron Pnictides</i>
4:10 – 4:30 pm	Athena Sefat (ORNL) <i>Origin of Superconductivity in Structurally Layered Materials</i>
4:30 – 4:50 pm	Leonardo Civale (LANL) <i>Towards a Universal Description of Vortex Matter in Superconductors</i>
4:50 – 5:10 pm	Luis Balicas (NHMFL) <i>High Magnetic Fields as a Probe to Unveil the Physical Properties of the Newly Discovered Fe Oxypnictide Superconductors and Related Compounds</i>
5:10 – 5:30 pm	Poster Introductions
5:30 – 6:00 pm	***** Break *****
6:00 – 7:30 pm	Working Dinner and Plenary Talk
6:30 – 7:15 pm	Séamus Davis (BNL) <i>EFRC: Center for Emergent Superconductivity</i>
7:30 – 9:30 pm	Poster Session I

Thursday, August 11, 2011

7:30 – 8:30 am **Breakfast**

Session 5	Two-Dimensional Electron Systems
8:30 – 8:50 am	Ray Ashoori (MIT) <i>Novel Temperature Limited Tunneling Spectroscopy of Quantum Hall Systems</i>
8:50 – 9:10 am	Lloyd Engel (NHMFL) <i>Microwave Spectroscopy of Electron Solids: Fractional Quantum Hall Effect and Controlled Disorder</i>
9:10 – 9:30 am	Michael Zudov (Minnesota) <i>Emergent Phenomena in Quantum Hall Systems Far from Equilibrium</i>
9:30 – 9:50 am	Wei Pan (SNL) <i>Quantum Electronic Phenomena and Structures</i>
9:50 – 10:10 am	Leonid Butov (UCSD) <i>Cold Exciton Gases in Semiconductor Heterostructures</i>

10:10 – 10:40 am ******* Break *******

Session 6

Low-Dimensional Systems

10:40 – 11:00 am Marc Kastner (*MIT*)
Measurement of Single Electronic Charging of Semiconductor Nano-Crystals

11:00 – 11:20 am Philippe Guyot-Sionnest (*Chicago*)
Colloidal Quantum Dot Films: Transport and Magnetotransport

11:20 – 11:40 am Alex Zettl (*LBNL*)
Novel sp²-Bonded Materials and Related Nanostructures

11:40 – 12:00 pm Jun Kono (*Rice*)
Spectroscopy of Degenerate One-Dimensional Electrons in Carbon Nanotubes

12:00 – 12:20 pm Gleb Finkelstein (*Duke*)
Symmetries, Interactions, and Correlation Effects in Carbon Nanotubes

12:20 – 2:00 pm **** Working Lunch / Small Group Discussions ****

Session 7

Superconductivity

2:00 – 2:20 pm Joe Orenstein (*LBNL*)
Quasiparticle Recombination in BSCCO Probed by Time-Resolved ARPES and Optical Reflectivity

2:20 – 2:40 pm Chris Homes (*BNL*)
Infrared and Angle Resolved Photoemission Studies of High-Temperature Superconductors and Related Systems

2:40 – 3:00 pm Dan Dessau (*Colorado*)
The Nature of Fermi Arcs, Pseudogaps, and Electron Scattering Rates in Cuprate High-T Superconductors

3:00 – 3:20 pm Tom Lemberger (*Ohio State*)
Experimental Study of Severely Underdoped Ultrathin Cuprate Films

3:20 – 3:40 pm Séamus Davis (*BNL*)
Spectroscopic Imaging STM Studies of Complex Electronic Matter

3:40 – 4:10 pm ******* Break *******

Session 8	Topological Insulators
4:10 – 4:30 pm	Pablo Jarillo-Herrero (<i>MIT</i>) <i>Quantum Transport in Topological Insulator Nano-electronic Devices</i>
4:30 – 4:50 pm	Vidya Madhavan (<i>Boston College</i>) <i>Focused Research Center in Correlated Electron Materials</i>
4:50 – 5:10 pm	Dennis Drew (<i>Maryland</i>) <i>Infrared Hall Effect in Correlated Electronic Materials</i>
5:10 – 5:30 pm	Poster Introductions
5:30 – 6:00 pm	***** Break *****
6:00 – 9:30 pm	Working Dinner and Poster Session II

Friday, August 12, 2011

7:30 – 8:30 am **Breakfast**

Session 9	Superconductivity
8:30 – 8:50 am	Dale Van Harlingen (<i>Illinois</i>) <i>Quantum Materials at the Nanoscale</i>
8:50 – 9:10 am	Ying Liu (<i>Penn State</i>) <i>Engineering of Mixed Pairing and Non-Abelian Quasiparticle States of Matter in Chiral P-Wave Superconductor Sr₂RuO₄</i>
9:10 – 9:30 am	Allen Goldman (<i>Minnesota</i>) <i>Tunneling and Transport in Nanowires</i>
9:30 – 9:50 am	Saw Hla (<i>Ohio Univ.</i>) <i>Single Atom and Molecule Manipulation and Its Application to Nanoscience and Technology</i>
9:50 – 10:10 am	David Tanner (<i>Univ. of Florida</i>) <i>Time-Resolved Synchrotron Studies of Spin and Charge Dynamics in Solids</i>
10:10 – 10:40 am	***** Break *****

Session 10	Magnetism
10:40 – 11:00 am	Chuck Fadley (<i>LBNL</i>) <i>Properties of Spintronic Materials and Nanostructures via Novel Characterization Techniques</i>
11:00 – 11:20 am	Anand Bhattacharya (<i>ANL</i>) <i>Digital Synthesis: A Pathway to New Materials at Interfaces of Complex Oxides</i>
11:20 – 11:40 am	Gunter Luepke (<i>William & Mary</i>) <i>Time-Resolved Spectroscopy of Insulator-Metal Transitions: Exploring Low-Energy Dynamics in Strongly Correlated Systems</i>
11:40 – 12:00 pm	Lance De Long (<i>Univ. of Kentucky</i>) <i>Competing Interactions in Complex Transition Metal Oxides</i>
12:00 – 12:20 pm	Peter Schiffer (<i>Penn State</i>) <i>Exploration of Artificial Frustrated Magnets</i>

Session 1

Correlated Electrons

The Ames Laboratory Complex States, Emergent Phenomena and Superconductivity in Intermetallic & Metal-like Compounds FWP

PIs: P. Canfield (FWP Leader) canfield@ameslab.gov, S. Bud'ko budko@ameslab.gov, J. Clem clem@ameslab.gov, D. Johnston johnston@ameslab.gov, A. Kaminski kaminski@ameslab.gov, V. Kogan kogan@ameslab.gov, R. Prozorov prozorov@ameslab.gov, J. Schmalian schmalian@ameslab.gov, M. Tanatar tanatar@ameslab.gov

FWP web page: <http://www.ameslab.gov/dmse/fwp/complex-states>

SCOPE

This FWP has been specifically assembled to create, study, and understand materials with novel electronic and magnetic ground states. It intimately links design, growth, characterization, modeling and theory within a National Laboratory setting, allowing for the rapid identification, understanding and control of systems of interest. The FWP has many powerful techniques at its disposal, ranging from a wide variety of synthetic methods, through an extensive range of thermodynamic, transport and spectroscopic measurements, to sophisticated modeling and theory. The strength of this FWP is its ability to cycle through the “think, make, measure, understand, control, think” cycle rapidly and efficiently. The goal of this FWP is the design, discovery, characterization, understanding and ultimately control over materials with complex and potentially useful properties. In this presentation I will review some of the primary capabilities of our FWP with the hope of enhancing inter-laboratory collaborations within this program. I will highlight some of our ongoing research in correlated electron systems (ranging from high T_c superconductivity to field induced quantum criticality in heavy fermion systems) and outline some of our plans for future work.

RECENT PROGRESS

The priority of this FWP is the development and understanding of model systems combined with agile and flexible response to, and leadership in, a rapidly-changing materials landscape. Within this context, some of the systems that have been recently focused on include: Fe-based, and related, superconductors, and correlated electron systems with small, or vanishing, moments, because of their combined promise to serve as model systems as well as starting points for developing better, energy-relevant properties. To accomplish this goal, three highly intermeshed classes of activities will operate both in series and in parallel:

- Design and growth (Canfield, Bud'ko, Johnston, Schmalian, Kogan)
- Advanced Characterization (Bud'ko, Kaminski, Prozorov, Tanatar)
- Theory and modeling: (Clem, Kogan, Schmalian)

During the 2008 – 11 period the FWP has been able to make significant progress in the fields of correlated electron systems, the physics associated with local moment ordering and the effects of internal and external fields on the ordered states, and, of course, superconductivity. The primary focus of the FWP efforts has been on the Fe-base superconductors. During the past three years we have made key contributions in the areas of:

--Growth and measurement of RFeAsO single crystals
--Growth and measurement of the first BaFe₂As₂ single crystals
--Discovery of CaFe₂As₂ and its extreme pressure sensitivity
--Studies of compounds related to BaFe₂As₂
--Determination of T-x phase diagrams for Ba(Fe_{1-x}TM_x)₂As₂ (TM = Co, Ni, Cu, Rh, Pd), establishment of unifying T-e phase diagrams, and established empirical rules for superconductivity

--London penetration depth and thermal transport measurements across pnictide series
--Theoretical description of FeAs-based superconductors.

We also made significant advances in understanding several aspects of the physics of cuprates. We had found evidence that the pseudogap state and superconductivity are associated with two different energy scales. These initial angle resolve photoelectron spectroscopy (ARPES) results prompted us to study the in-plane magnetic penetration depth in optimally doped Bi-2201 using muon-spin rotation. The results of these measurements indicated that for underdoped samples the segments of the Fermi surface only near the nodes contribute significantly to the superconducting condensate; whereas antinodal regions, where spectral gap is largest, do not point to the possibility of competition between pseudogap and superconductivity. In other work, we discovered decisive evidence for competition between pseudogap and superconductivity in cuprates. We conducted pioneering quantitative ARPES studies of the spectral weights of the features associated with the pseudogap and superconductivity and demonstrated that the pseudogap competes with the superconductivity by depleting the spectral weight available for pairing. This represents a major shift in thinking about the role of the pseudogap in problems with the cuprates and a possibility to improve their superconducting properties by suppressing the pseudogap.

In addition to our extensive work on superconductivity the FWP has developed and studied several classes of correlated electron materials. These include the RT_2Zn_{20} series, a highly tunable family of dilute rare earth bearing materials that manifest both 4f and 3d correlations. For example, for $T = Fe, Ru, Os, Co, Rh,$ and Ir , the YbT_2Zn_{20} materials are all heavy fermions, formally doubling the number of such compounds (i.e. $\gamma > 400$ mJ/mol-K²). In addition, we continued research into earlier T- and R-based HF systems including LiV_2O_4 and $YbAgGe$, a system we discovered could manifest a rare example of Yb-based field induced quantum criticality. Theoretically we developed a new approach to dimensional reduction and emergent symmetries at a quantum critical point in frustrated magnets and analyzed Kondo-lattice screening in a d-wave superconductor.

We also continued to study rare earth, local moment magnetism; we used the tunnel diode resonator (TDR) and magneto-optics (MO) to study local moment ordering in previously established model systems ($RAgSb_2$, $CeSb$, and $Nd_2Fe_{14}B$). In Kerr microscopy studies of high-purity, low pinning, single crystals of $Nd_2Fe_{14}B$, we discovered fractal-domain patterns and in $CeAgSb_2$, we found that even weakly ferromagnetic systems can be imaged via Kerr rotation from as-grown, mirror-like surfaces, giving better spatial resolution than a garnet-based indicator. In $Fe_{0.25}TaS_2$, real-time MO images reveal unusual slow dynamics of dendritic domain formation. We also extended the use of TDR measurements to local moment systems and found them to be very sensitive to long range magnetic ordering and metamagnetism. TDR was used to collect high-density, temperature and field dependent data to construct a detailed, anisotropic, low temperature H-T phase diagram of $TmNi_2B_2C$ and $ErNi_2B_2C$, probe multiple phase transitions in $CeSb$ and, on a phenomenological level, to detect the difference in the dynamic response between weak itinerant and local moment ferromagnets in a variety of materials.

FUTURE PLANS

We plan to pursue a variety of synthetic efforts aimed at better understanding the physics of the current Fe-based materials as well as finding other, new, examples of exotic, hopefully high temperature, superconductivity. To gain a clearer understanding of the $BaFe_2As_2$ system we plan detailed studies of transition metal doping series, including Ru , to compare with our hydrostatic pressure work as well as Cr and Mn to better understand the conspicuous difference between electron and hole doping via TM substitution. Initial results on lightly Cr -doped $BaFe_2As_2$

indicate the higher temperature structural / magnetic phase transition may not be split and also remains first order in nature. A combination of thermodynamic, transport and microscopic measurements should help elucidate the potentially different physics associated with doping with TM lighter than Fe. In addition to single doping series, the $\text{Ba}(\text{Fe}_{1-x}\text{Co}_x)_2\text{As}_2$ series will be used as a well understood starting point for double doping experiments. For example Cr and Mn will be doped into both underdoped and overdoped sides of the $\text{Ba}(\text{Fe}_{1-x}\text{Co}_x)_2\text{As}_2$ superconducting dome so as to try to separate effects associated with band filling and disorder.

More broadly, on the high risk / high payoff extreme of our synthesis agenda, we plan to identify and study a wide variety of transition metal-based compounds that manifest reduced moment, antiferromagnetic ordering. We will synthesize the parent materials, either in single crystalline or polycrystalline form and then use hydrostatic pressure (up to 8 GPa) and / or site substitution to try to suppress the antiferromagnetism with the hope of stabilizing new examples of exotic superconductivity.

Using the various doping series developed in the FWP, the evolution of the Fermi surface in electron, hole, and isoelectronically doped iron arsenic superconductors and its relation to superconductivity will be studied. These studies will help shed light on the relationship between superconductivity and magnetism, and also possibly provide additional information about the nature of superconducting pairing in these materials. We have some very interesting preliminary data that revealed unusual behavior of the reconstructed Fermi surface in electron doped materials. Further detailed studies and extension of these measurements to hole doped materials will be a crucial component in elucidating the interesting physics of these materials.

We will also determine, or set limits on, the in-plane anisotropy associated with the orthorhombic state in the parent, CaFe_2As_2 , SrFe_2As_2 , and BaFe_2As_2 compounds as well as the underdoped $\text{Ba}(\text{Fe}_{1-x}\text{TM}_x)_2\text{As}_2$ series members. The detwinning required to accomplish this has already been achieved (as confirmed via direct visualization as well as x-ray diffraction). We plan to combine optical microscopy and x-ray studies with transport measurements to determine the effects of detwinning on the normal as well as superconducting properties of these crystals

In addition, the FWP will be developing new measurements and synthesis capabilities that will allow for better access to, and understanding of, these novel states. We are commissioning new pressure cells that allow for measurements of resistivity and magnetization up to 14 GPa and 10 GPa respectively and we are developing a TDR under pressure system ($0.35 \text{ K} < T < 300 \text{ K}$, $H < 14 \text{ T}$, $P < 90 \text{ kbar}$) so as to measure a.c. susceptibility. We also plan to use TDR technique for precision measurements of the Knight shift in metallic superconductors. We plan to extend the TDR technique to provide angular as well as frequency resolution. We are in the final stages of deploying in house, thermal transport measurements, down to 50 mK, in fields up to 14 T.

We are also upgrading our ARPES system with two new, crucial: (i) Replace the aging SES2002 with a state of the art R8000 electron analyzer. This result in an increase of the energy resolution down to sub-meV range, an increase of the angular acquisition range from 10 to 40 deg., and an increase in transmission figure by four and extend the kinetic energy range from 5 eV to 0.5 meV range. (ii) Add a laser based, tunable low energy VUV photon source. These two combined will have enormous impact on the performance of the laboratory-based ARPES system at the Ames Laboratory allow performing (spatially resolved) ARPES microscopy measurements with μm resolution and increase the photoelectron escape depth to increase bulk sensitivity.

Finally, with recently awarded funding we will be building a suite of reactive material, Ar-based, glove boxes that will allow for more ready use of alkali and alkali-earth metals, specifically Li, as both a solvent and solute.

SELECTED PUBLICATIONS (out of over 250) FROM 2008 – 2011:

See <http://www.ameslab.gov/dmse/fwp/complex-states> for full list/links

“FeAs-Based Superconductivity: A Case Study of the Effects of Transition Metal Doping on BaFe₂As₂”, Canfield PC and Bud'ko SL, Annual Review of Condensed Matter Physics, **1**, 27, 2010.

“The puzzle of high temperature superconductivity in layered iron pnictides and chalcogenides”, Johnston DC, Adv. in Phys., **59**, 803, 2010.

“Pressure induced superconductivity in CaFe₂As₂”, Torikachvili MS, et al., Phys. Rev. Lett., **101**, 2008,

“Momentum dependence of the superconducting gap in NdFeAsO_{0.9}F_{0.1} single crystals measured by angle resolved photoemission spectroscopy”, Kondo T, et al., Phys. Rev. Lett. **101**, 147003, 2008.

“Lattice and magnetic instabilities in CaFe₂As₂: A single-crystal neutron diffraction study” Goldman AI, et al., Phys. Rev. B, **78**, 100506, 2008.

“Effects of Co substitution on thermodynamic and transport properties and anisotropic H-c₂ in Ba(Fe_{1-x}Co_x)₂As₂ single crystals”, Ni N, et al., Phys. Rev. B, **78**, 214515, 2008.

“K-Doping Dependence of the Fermi Surface of the Iron-Arsenic Ba_{1-x}K_xFe₂As₂ Superconductor Using Angle-Resolved Photoemission Spectroscopy”, Liu C, et al., Phys. Rev. Lett., **101**, 177005, 2008.

“First-order structural phase transition in CaFe₂As₂”, Ni N, et al., Phys. Rev. B, **78**, 014523, 2008.

“Structural transition and anisotropic properties of single-crystalline SrFe₂As₂”, Yan JQ, et al., Phys. Rev. B, **78**, 024516, 2008.

“Coexistence of Competing Antiferromagnetic and Superconducting Phases in the Underdoped Ba(Fe_{0.953}Co_{0.047})₂As₂ Compound Using X-ray and Neutron Scattering Techniques”, Pratt DK, et al., Phys. Rev. Lett, **103**, 087001, 2009.

“Decoupling of the superconducting and magnetic/structural phase transitions in electron-doped BaFe₂As₂”, Canfield PC, et al., Phys. Rev. B, **80**, 060501, 2009.

“Nematic Electronic Structure in the "Parent" State of the Iron-Based Superconductor Ca(Fe_{1-x}Co_x)₂As₂”, Chuang TM, et al., Science, **327**, 181, 2010

“Phase diagrams of Ba(Fe_{1-x}M_x)₂As₂ single crystals (M=Rh and Pd)”, Ni N, et al., Phys. Rev. B, **80**, 024511, 2009.

“Effects of Nematic Fluctuations on the Elastic Properties of Iron Arsenide Superconductors”, Fernandes RM, et al., Phys. Rev. Lett, **105**, 157003, 2010.

“Three- to Two-Dimensional Transition of the Electronic Structure in CaFe₂As₂: A Parent Compound for an Iron Arsenic High-Temperature Superconductor”, Liu C, et al., Phys. Rev. Lett, **102**, 167004, 2009.

“Magnetic order in BaMn₂As₂ from neutron diffraction measurements”, Singh Y, et al., Phys. Rev. B, **80**, 100403, 2009.

“Competition between the pseudogap and superconductivity in the high-T_c copper oxides” Kondo T, et al., Nature, **457**, 296, 2009.

“Probing Fractal Magnetic Domains on Multiple Length Scales in Nd₂Fe₁₄B”, Kreyssig, A., et al., Phys. Rev. Lett., **102**, 047204, 2009.

“Multiple regions of quantum criticality in YbAgGe”, Schmiedeshoff, G. M., et al., Phys. Rev. B, **83**, 180408, 2011.

Superconductivity and Magnetism in d- and f-electron materials

Principal Investigator: M. Brian Maple
Bernd T. Matthias Professor of Physics
Department of Physics, University of California, San Diego
La Jolla, California 92093-0319
mbmaple@ucsd.edu

Project Scope

The primary emphasis of this project is on the physics of superconducting, magnetic, heavy fermion, non-Fermi liquid, and other types of strongly correlated electron phenomena in novel transition-metal, rare-earth, and actinide based oxides and intermetallic compounds with a focus on the growth of high quality single crystal specimens. Materials investigated include Fe-pnictide high-temperature superconductors, unconventional U-based superconductors, magnetically ordered rare-earth compounds, and heavy fermion *f*-electron materials. The anisotropic normal and superconducting state properties of these materials are studied as a function of concentration of chemical constituents, oxygen vacancy concentration, temperature, pressure, and magnetic field in order to obtain information about the underlying electronic, lattice, and magnetic excitations involved in the superconductivity, the symmetry of the superconducting order parameter, and the electron pairing mechanism. Physical properties of high- T_c superconductors and thermoelectric materials that are important for their performance in technological applications have been characterized. Phenomena associated with the interplay between superconductivity and other types of spin and charge order are of particular interest.

Recent Progress

Much of our recent research falls into seven principal categories: correlated electron behavior in the noncentrosymmetric $Ln_2T_{12}P_7$ compounds, Fe-pnictide based superconductors, valence fluctuations in $Ce_{1-x}Yb_xCoIn_5$, superconductivity and magnetism in LnT_4X_{12} filled skutterudites, high temperature superconductivity in the cuprates, the interplay between weak ferromagnetism and superconductivity in UCoGe based materials, and hidden order, magnetism, and superconductivity in URu₂Si₂. Highlights of this research are summarized below.

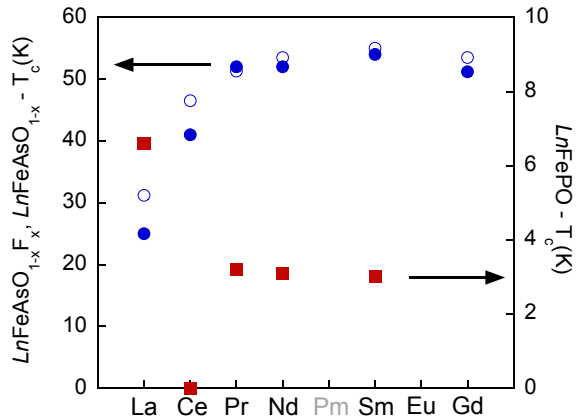
The temperature (T) - magnetic field (H) phase diagram for single crystals of the noncentrosymmetric compound Yb₂Fe₁₂P₇ was reported. This system exhibits a crossover from a magnetically ordered non-Fermi-liquid (NFL) phase at low H to another NFL phase at higher H . The crossover occurs near the value of H where the magnetic ordering temperature (T_M) is no longer observable, but not where T_M extrapolates smoothly to $T = 0$ K at a possible quantum critical point (QCP), indicating the occurrence of a quantum phase transition between the two NFL phases. The lack of a clear relationship between the extrapolated QCP and NFL behavior suggests an unconventional route to the NFL ground states. We have also explored the behavior of other members of this “2-12-7” family of compounds including U₂Fe₁₂P₇, which displays antiferromagnetic behavior below 14 K and possible metamagnetism, and Sm₂Fe₁₂P₇, which appears to be a new heavy fermion,

itinerant ferromagnet with a Curie temperature of ~ 6 K.

We grew single crystals of the Fe-based pnictide superconductor LaFePO. Specific heat data suggest either that only a small fraction of the sample is superconducting or that the superconductivity is characterized by an unusually small specific heat jump. We subsequently showed that the superconductivity becomes bulk-like if the crystals are annealed in oxygen. An infrared and optical study carried out in collaboration with D. Basov's research group found clear evidence of electronic correlations in metallic LaFePO with the kinetic energy of the electrons reduced to half of that predicted by band theory of nearly free electrons. This suggests that electronic many-body effects are important in the iron pnictides despite the absence of a Mott transition. We also reported superconductivity in two new members of the $LnFePO$ series ($Ln = Pr$ and Nd). A comparison of the evolution of the superconducting T_c with the substitution of the different lanthanide ions for the $LnFePO$ series and the $LnFeAsO_{1-x}F_x$ and $LnFeAsO_{1-\delta}$ series has supplied evidence supporting a different mechanism of superconductivity for the P- and As-based compounds.

X-ray diffraction, electrical resistivity, magnetic susceptibility, and specific heat measurements on the system $Ce_{1-x}Yb_xCoIn_5$ ($0 \leq x \leq 1$) reveal that many of the characteristic features of the $x = 0$ correlated electron state are stable for $0 \leq x \leq 0.775$, and that phase separation occurs for $x > 0.775$. The stability of the correlated electron state is apparently due to cooperative behavior of the Ce and Yb ions, involving their unstable valences. Low-temperature NFL behavior is observed which varies with x , even though there is no readily identifiable quantum critical point. The superconducting critical temperature T_c decreases linearly with x towards 0 K as $x \rightarrow 1$, in contrast to other heavy fermion superconductors where T_c scales with T_{coh} . We conclude that $Ce_{1-x}Yb_xCoIn_5$ belongs to a growing class of systems in which the NFL behavior occurs in the absence of an obvious QCP. These results also suggest that valence fluctuations may play a role in the unconventional SC and NFL behavior in pure $CeCoIn_5$.

An invited article, entitled "Non-Fermi liquid regimes and superconductivity in the low temperature phase diagrams of strongly correlated d - and f -electron materials," was published in a special issue of the Journal of Low Temperature Physics. The materials discussed in this article were primarily ones where the NFL behavior either occurs far away from a QCP, within an ordered phase, or may not be associated with any putative QCP. We focused on compounds that were prepared in the principal investigator's group at the University of California, San Diego over the past 20 years. In particular, we emphasized the point that it remains unknown whether NFL physics is universal, or if a multitude of unique subclasses exist.



A comparison of the evolution of the superconducting transition temperature T_c versus lanthanide Ln for the series $LnFePO$ (solid squares), the optimally fluorine doped compounds $LnFeAsO_{1-x}F_x$ (solid circles), and the oxygen deficient compounds $LnFeAsO_{1-\delta}$ (open circles).

Future Plans

In the future we will build upon research on materials that we have investigated recently, revisit some previously studied materials with new approaches and/or prepared with new methods, and continue to search for new materials exhibiting correlated electronic behavior.

The ThCr_2Si_2 -type FeAs-based superconductors have been extensively studied in single crystal form due to the relative simplicity of growing rather large crystals via a flux growth technique. Studies of the ZrCuSiAs -type FeAs-based superconductors such as $\text{LnFeAsO}_{1-\delta}$ and $\text{LnFeAsO}_{1-x}\text{F}_x$, with their significantly higher critical temperatures, have been largely restricted to polycrystalline samples. However, recently a few groups have reported the growth of “1111” type FeAs based superconductors in single crystal form with dimensions up to several mm. We have launched an effort to grow a number of LnFeAsO based compounds in single crystal form. The availability of single crystalline samples will help to elucidate the complex interplay of superconductivity and magnetism that develops in these materials.

It was recently reported that a new class of filled skutterudite compounds with the chemical formula $M\text{Pt}_4\text{Ge}_{12}$ (M = rare earth or alkaline earth metal) can be formed by standard synthesis techniques. For the compounds where M = Sr, Ba, La, Pr, and Th, superconductivity is observed. For Sr and Ba, the superconducting transition temperatures are $T_c = 5.35$ K and 5.10 K, respectively, and it is thought that the superconductivity is BCS like and emerges from electron-phonon interactions supported by the Pt-Ge cage structure. For La and Pr, the superconductivity occurs at a surprisingly high temperature, $T_c \sim 8.3$ K, and thermodynamic measurements indicate strong coupling for $\text{PrPt}_4\text{Ge}_{12}$. $\text{ThPt}_4\text{Ge}_{12}$ was also found to be a clean-limit strong-coupling superconductor with $T_c = 4.62$ K. Additionally, the compounds where M = Eu and Nd are reported to be antiferromagnets, while the Ce compound shows intermediate valence for the Ce ion. These observations open a new direction for research in the filled skutterudite compounds that merits further investigation. We will attempt to synthesize new members of this series in our ongoing effort to explore correlated electron phenomena in the context of filled skutterudite materials.

Extensive studies of the $\text{URu}_{2-x}\text{Re}_x\text{Si}_2$ system in our laboratory indicate that the hidden order (HO) phase is suppressed by $x \approx 0.1$. Motivated by the richness of the $\text{URu}_{2-x}\text{Re}_x\text{Si}_2$ phase diagram, we have begun studies of $\text{URu}_{2-x}\text{T}_x\text{Si}_2$ for other transition metals T . For example, a recent study for $T = \text{Fe}$ revealed that the HO/large moment antiferromagnetic (LMAFM) phase boundary $T_0(x)$ undergoes a two-fold increase from 17.5 K at $x = 0$ to ~ 42 K at $x \approx 0.8$. These studies will provide important insight concerning the mysterious HO phase whose order parameter has eluded identification for more than two and a half decades. The reduction of the unit cell volume through the substitution of the smaller isoelectronic Fe ions for Ru will enable the interrelation of the HO and LMAFM phases to be investigated without the necessity of applying an external pressure. We intend to follow up with investigations of single crystals in order to determine whether the complex phase diagram of $\text{URu}_{2-x}\text{Fe}_x\text{Si}_2$ can be explained in terms of valence electron concentration tuning or a more complex scenario.

Further investigations of the interesting and large class of noncentrosymmetric $M_2T_{12}Pn_7$ where $M = \text{Zr}, \text{Hf}, \text{Ln}, \text{Th}, \text{U}$, $T = \text{Fe}, \text{Ni}, \text{Co}, \text{Mn}$, and $Pn = \text{P}, \text{As}$ will be performed. Efforts will be made to synthesize these materials in single crystal form and to characterize them by measurements of x-ray diffraction, electrical resistivity, specific heat, and magnetization measurements. These noncentrosymmetric compounds may yield unconventional superconductivity with mixed singlet and triplet spin pairing, exotic types of magnetic order via the Dzyaloshinskii-Moriya interaction, and unconventional quantum critical behavior.

Selected Publications

- L. Shu, R. E. Baumbach, M. Janoschek, E. Gonzales, K. Huang, T. A. Sayles, J. Paglione, J. O'Brien, J. J. Hamlin, D. A. Zocco, P.-C. Ho, C. A. McElroy, and M. B. Maple, "Correlated Electron State in $\text{Ce}_{1-x}\text{Yb}_x\text{CoIn}_5$ Stabilized by Cooperative Valence Fluctuations," *Physical Review Letters* **106**, 156403 (2011).
- M. Janoschek, R. E. Baumbach, J. J. Hamlin, I. K. Lum, and M. B. Maple, "The non-centrosymmetric heavy fermion ferromagnet $\text{Sm}_2\text{Fe}_{12}\text{P}_7$," *Journal of Physics: Condensed Matter* **23**, 094221 (2011).
- R. E. Baumbach, J. J. Hamlin, M. Janoschek, I. K. Lum, and M. B. Maple, "Magnetic, thermal, and transport properties of the actinide based noncentrosymmetric compounds $\text{Th}_2\text{Fe}_{12}\text{P}_7$ and $\text{U}_2\text{Fe}_{12}\text{P}_7$," *Journal of Physics: Condensed Matter* **23**, 094222 (2011).
- M. B. Maple, R. E. Baumbach, N. P. Butch, J. J. Hamlin, and M. Janoschek, "Non-Fermi Liquid Regimes and Superconductivity in the Low Temperature Phase Diagrams of Strongly Correlated d - and f -Electron Materials," *Journal of Low Temperature Physics* **161**, 4 (2010) - Invited review Article.
- R. E. Baumbach, J. J. Hamlin, L. Shu, D. A. Zocco, J. R. O'Brien, P.-C. Ho, and M. B. Maple, "Unconventional $T - H$ Phase Diagram in the Noncentrosymmetric Compound $\text{Yb}_2\text{Fe}_{12}\text{P}_7$," *Physical Review Letters* **105**, 106403 (2010).
- N. P. Butch and M. B. Maple, "The suppression of hidden order and the onset of ferromagnetism in URu_2Si_2 via Re substitution," *Journal of Physics: Condensed Matter* **22**, 164204 (2010).
- M. M. Qazilbash, J. J. Hamlin, R. E. Baumbach, Lijun Zhang, D. J. Singh, M. B. Maple, and D. N. Basov, "Electronic correlations in the iron pnictides," *Nature Physics* **5**, 647 (2009).
- N. P. Butch and M. B. Maple, "Evolution of Critical Scaling Behavior near a Ferromagnetic Quantum Phase Transition," *Physical Review Letters* **103**, 076404 (2009).
- B. J. Taylor and M. B. Maple, "Formula for the Critical Temperature of Superconductors Based on the Electronic Density of States and the Effective Mass," *Physical Review Letters* **102**, 137003 (2009).
- R. E. Baumbach, J. J. Hamlin, L. Shu, D. A. Zocco, N. M. Crisosto, and M. B. Maple, "Superconductivity in LnFePO ($\text{Ln} = \text{La}, \text{Pr}$ and Nd) single crystals," *New Journal of Physics* **11**, 025018 (2009).
- R. W. Hill, S. Li, M. B. Maple, and L. Taillefer, "Multiband Order Parameters for the $\text{PrOs}_4\text{Sb}_{12}$ and $\text{PrRu}_4\text{Sb}_{12}$ Skutterudite Superconductors from Thermal Conductivity Measurements," *Physical Review Letters* **101**, 237005 (2008).
- S. K. Goh, J. Paglione, M. Sutherland, E. C. T. O'Farrell, C. Bergemann, T. A. Sayles, and M. B. Maple, "Fermi-Surface Reconstruction in $\text{CeRh}_{1-x}\text{Co}_x\text{In}_5$," *Physical Review Letters* **101**, 056402 (2008).

Correlated and Complex Materials

Principal Investigators

Brian C. Sales, ORNL (salesbc@ornl.gov)

Lynn A. Boatner (boatnerla@ornl.gov)

David K. Christen (christendk@ornl.gov)

David G. Mandrus (mandrusdg@ornl.gov)

Project Scope

The physics of correlated and complex materials is addressed using the combination of materials synthesis, compositional tuning, and crystal growth. The overarching theme is the discovery and investigation of novel cooperative phenomena and new forms of order in complex transition metal oxides, pnictides and Zintl phases. Phenomena such as charge and orbital ordering, coupling of magnetism and ferroelectricity, unconventional superconductivity, vortex pinning and dynamics, low carrier density ferromagnetism, and anharmonic phonons in thermoelectric materials are studied. A substantial fraction of the effort is devoted to the discovery of innovative materials and the growth of large single crystals of fundamental interest to condensed matter physics. The composition of these materials are carefully controlled, and the effects of compositional tuning on the basic physics of the materials are studied using X-ray and neutron diffraction, and measurements of magnetization, specific heat, and electrical and thermal transport properties. Once the materials have been prepared and characterized, in-depth experiments such as inelastic neutron scattering, photoemission, and scanning tunneling microscopy are performed in order to obtain a deeper understanding of the relevant physics. Some of the materials investigated are promising for energy-related applications such as superconductors for grid applications and thermoelectrics for energy conversion.

Recent Progress

Most of our recent research has focused on two broad areas (1) the relationship between magnetism and superconductivity in the iron-based superconductors and (2) insights into how good thermoelectric performance may be related to unusual physical properties such as anharmonic phonons, strong electron-phonon coupling, and a high dielectric constant. The ultimate goal of (1) is to prepare crystals and design experiments that will enhance our fundamental understanding of the origin of superconductivity and magnetism in the Fe pnictide and chalcogenide materials. The goal of (2) is to provide microscopic insights into possible routes to better thermoelectric materials, and a more quantitative understanding of heat transport in solids.

One of the interesting and puzzling features exhibited by all of the iron-based superconductors well above T_c is the qualitative difference between the DC magnetic susceptibility measured with a SQUID and the susceptibility at finite frequency measured using either NMR or neutron scattering. This is illustrated in Fig 1. Only the dynamic susceptibility appears to correlate with superconductivity with Co concentrations from 6% to 26%. The Knight shift and the DC susceptibility are qualitatively the same in the paramagnetic region for all Co concentrations

Another interesting question that often arises when discussing the Fe-based superconductors, is whether the Fe magnetism should be regarded as localized or itinerant. Most of the neutron data has been analyzed using localized Heisenberg models, whereas much of the physics is better understood from an itinerant point of view. We have shown that core level X-ray spectroscopy and photoelectron experiments, that can measure on very fast timescales, detect both local moment behavior and itinerant behavior with the same technique (Ref 3). The results can be understood using ideas that were developed for iron metal above its Curie temperature about 30 years ago; the key idea being the existence of two types of spin fluctuations: one very fast that depends on the band width, and one much slower that depends on the appropriate time average of the fast fluctuations. In most metallic magnets both local and itinerant behaviors are found to be necessary to describe the total magnetic response and we expect that to also be the case for the iron-based superconductors.

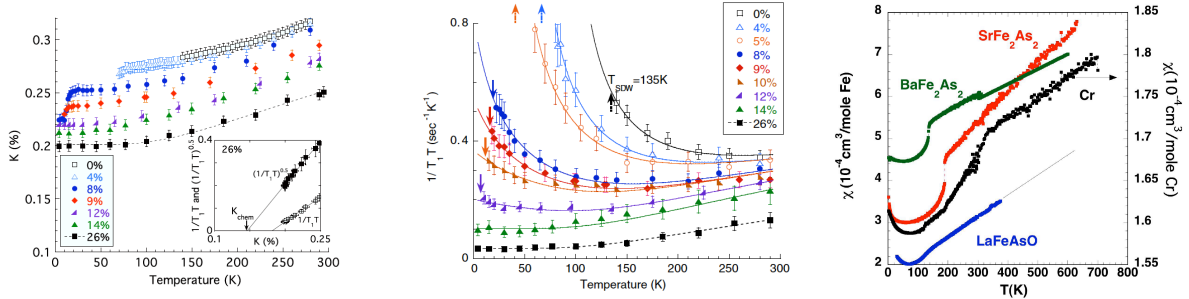


Fig 1 (Left) Knight shift (K) vs temperature for a family of Co-doped BaFe_2As_2 crystals (Middle) Spin-lattice relaxation rate $1/T_1T$ for same crystals with $f = 56.5$ MHz. The relaxation rate measures the integral of the imaginary part of the dynamical spin susceptibility for all wavevectors \mathbf{q} in the first Brillouin zone. The strength of the paramagnetic spin fluctuations can be fit to a Curie-Weiss law (Ref 1). (Right) DC susceptibility for three of the parent compounds and Cr metal. Like the Knight shift, in the high-temperature paramagnetic regime the susceptibility increases linearly with temperature. This origin of this increase is still under debate (Ref. 2).

Thermoelectric materials can be used to convert heat directly into electricity with no moving parts. Most good thermoelectric materials are narrow-gapped semiconductors that have a large electrical conductivity, a high Seebeck coefficient and a low thermal conductivity. In many thermoelectric materials the electrons and phonons are assumed to be weakly interacting and are treated as independent subsystems. We recently showed, however, that interactions between the electron and phonon systems must be considered to understand the temperature dependence of many of the properties of the unusual narrow-gap semiconductor FeSi, (Ref. 4). We also showed that the strong electron-phonon coupling in this compound invalidated the common approximation of dividing the total thermal conductivity into independent electronic and lattice components: $\kappa_{\text{total}} = \kappa_{\text{electronic}} + \kappa_{\text{lattice}}$. (Ref. 5).

Lead Telluride is a good thermoelectric material in the 400-700 K temperature range. Above room temperature the lattice thermal conductivity is surprisingly low for a binary compound with a simple rocksalt structure. Neutron scattering measurements on a large PbTe single crystal and first-principles computations of the phonons show a strong anharmonic coupling between the ferroelectric transverse optic mode and the longitudinal acoustic modes for temperatures above 200 K. This interaction extends over a large portion of reciprocal space, and directly affects the heat carrying phonons. These results provide a microscopic picture of why many good thermoelectric materials are found near a lattice instability of the ferroelectric type.

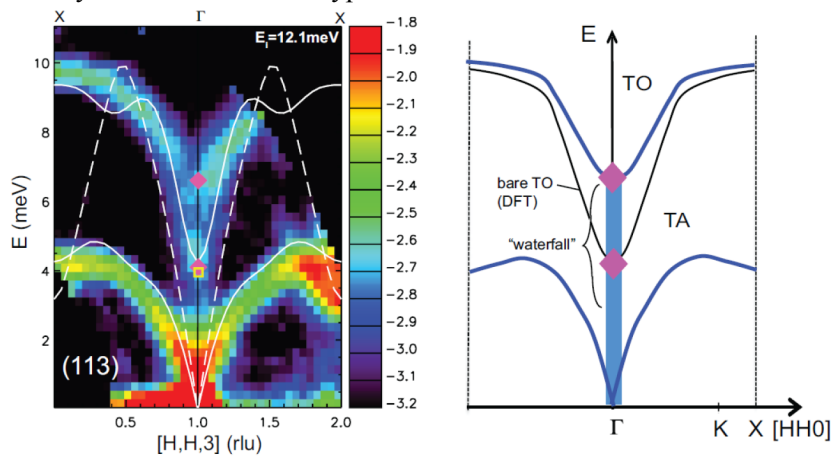


Fig. 2 Inelastic neutron scattering data (left) showing the presence of a waterfall effect arising from strong non-harmonic mixing of optical and acoustic lattice vibrations (right) in PbTe.

Future Plans

There are still many questions regarding the relationship between magnetism and superconductivity in the iron-based superconductors. Many of these questions can only be addressed using inelastic neutron scattering from relatively large well-characterized single crystals. We plan to grow and characterize more large crystals from the Co-doped BaFe_2As_2 system. These crystals will be used by our neutron collaborators to test detailed theoretical predictions concerning magnetism and superconductivity in these materials. We have recently grown large crystals of $\text{TlFe}_{1.6}\text{Se}_2$, and we have discovered two unusual phase transitions. With decreasing temperature there is a decrease in the ordered Fe moment and a localization of carriers associated with the transitions. There is indirect evidence that these phase transitions are associated with orbital order. We plan to study these transitions using inelastic and elastic x-ray and neutron scattering, resonant ultrasound spectroscopy, and optical spectroscopy. In addition, since this compound is chemically and structurally similar to superconducting compositions where part of the Tl is replaced by an alkali metal, this study should provide additional understanding of what is required for iron-based superconductivity.

One of the requirements for a good thermoelectric material is high carrier mobility. Several good thermoelectric materials (e.g. PbTe or GeTe) have a high dielectric constant due to the proximity to a ferroelectric phase transition. Does a high dielectric constant lead to a high carrier mobility? To address this question we will collaborate with Hans Christen's group to systematically study the effects of the dielectric constant on carrier mobility in a series of $\text{KTa}_{1-x}\text{Nb}_x\text{O}_3$ single crystals. In this model system the ferroelectric phase transition temperature can be tuned anywhere from 0 to 700 K by varying the Nb content. If a high dielectric constant does increase carrier mobility, this may suggest a new route to design better thermoelectric materials and as well as improve the performance of oxide electronics.

Most of the recent improvements in the performance of thermoelectric materials have resulted from a reduced lattice thermal conductivity. The amount of heat carried by phonons in a solid is poorly understood. For example, with the possible exception of Si, the amount of heat carried by phonons that have mean free paths, Λ , in a narrow range (e.g. $1\ \mu\text{m} < \Lambda < 10\ \mu\text{m}$) is not known. We plan to collaborate with Olivier Delaire and use inelastic neutron scattering, neutron linewidths, and model calculations to measure phonon lifetimes in single crystals of several good thermoelectric materials. The goal of this research is to obtain a better fundamental understanding of heat transport in solids. We also plan to collaborate with a group at MIT that has developed a new transient thermoreflectance spectroscopy technique to sort out the amount of heat carried by phonons with a particular mean free path. This information should complement the neutron work.

Publications

The nature of our research is highly collaborative and from Jan 2008 to the present we have published over 120 papers including 24 PRL's, 1 Nature, 1 Nature Physics, 1 Nature Materials, 1 PNAS, and 47 PRB's. Some of our more interesting and original papers are listed below.

1. F. L. Ning, K. Ahilan, T. Imai, A. S. Sefat, M. A. McGuire, B. C. Sales, D. Mandrus, P. Cheng, B. Shen and H. -H. Wen, "Contrasting Spin Dynamics between Underdoped and Overdoped $\text{Ba}(\text{Fe}_{1-x}\text{Co}_x)_2\text{As}_2$ ", *Phys. Rev. Lett.* **104**, 037001 (2010).
2. B. C. Sales, M. A. McGuire, A. S. Sefat and D. Mandrus, "A Semimetal Model of the Normal State Magnetic Susceptibility and Transport Properties of $\text{Ba}(\text{Fe}_{1-x}\text{Co}_x)_2\text{As}_2$ ", *Physica C* **470**, 304 (2010).
3. F. Bondino, E. Magnano, M. Malvestuto, F. Parmigiani, M. A. McGuire, A. S. Sefat, B. C. Sales, R. Jin, D. Mandrus, E. W. Plummer, D. J. Singh and N. Mannella, "Evidence for Strong Itinerant Spin Fluctuations in the Normal State of $\text{CeFeAsO}_{0.89}\text{F}_{0.11}$ Iron-Oxypnictide Superconductors", *Phys. Rev. Lett.* **101**, 267001 (2008).
4. O. Delaire, K. Marty, M. B. Stone, P. R. C. Kent, M. S. Lucas, D. L. Abernathy, D. Mandrus and B. C. Sales, "Phonon Softening and Metallization of a Narrow Gap Semiconductor by Thermal Disorder", *PNAS* **108**, 4725 (2011).

5. B. C. Sales, O. Delaire, M. A. McGuire, A. F. May, “Thermoelectric Properties of Co-, Ir, and Os-doped FeSi Alloys: Evidence for Strong Electron-Phonon Coupling” *Phys. Rev. B.* **83**, 125209 (2011).
6. O. Delaire, J. Ma, K. Marty, A. F. May, M. A. McGuire, M.-H. Du, D. J. Singh, A. Podlesnyak, G. Ehlers, M. D. Lumsden, and B. C. Sales, “Giant Anharmonic Phonon Scattering in PbTe” *Nature Materials –advanced online publication June 7, 2011*.
7. A. S. Sefat, R. Y. Jin, M. A. McGuire, B. C. Sales, D. J. Singh, and D. Mandrus, “Superconductivity at 22 K in Co-doped BaFe₂As₂ Crystals” *Phys. Rev. Lett.* **101**, 117004 (2008).
8. M. A. McGuire, A. D. Christianson, A. S. Sefat, B. C. Sales, M. D. Lumsden, R. Jin, E. A. Payzant, D. Mandrus, Y. Luan, V. Keppens, V. Varadarajan, J. W. Brill, R. P. Hermann, M. T. Sougrati, F. Grandjean, and G. J. Long “Phase Transitions in LaFeAsO: Structural, magnetic, elastic, and transport properties, heat capacity, and Mossbauer spectra” *Phys. Rev. B.* **78**, 094517 (2008).
9. M. A. McGuire, R. P. Hermann, A. S. Sefat, B. C. Sales, R. Jin, D. Mandrus, F. Grandjean, and G. J. Long, “Influence of the rare-earth element on the effects of the structural and magnetic phase transitions in CeFeAsO, PrFeAsO, and NdFeAsO”, *New J. Phys.* **11**, 025011 (2009).
10. B. C. Sales, A. S. Sefat, M. A. McGuire, R. Y. Jin, D. Mandrus, and Y. Mozharivskij, “Bulk superconductivity at 14 K in single crystals of Fe_{1+y}Te_xSe_{1-x}” *Phys. Rev. B.* **79**, 094521 (2009).
11. R. M. Fernandes, L. H. VanBebber, S. Bhattacharya, P. Chandra, V. Keppens, D. Mandrus, B. C. Sales, A. S. Sefat, and J. Schmalian, “Effects of Nematic Fluctuations on the Elastic Properties of Iron Arsenide Superconductors”, *Phys. Rev. Lett.* **105**, 157003 (2010).
12. A. D. Christianson, M. D. Lumsden, S. E. Nagler, G. J. MacDougall, M. A. McGuire, A. S. Sefat, B. C. Sales, and D. Mandrus, “Static and Dynamic Magnetism in Underdoped Superconductor BaFe_{1.92}Co_{0.08}As₂” *Phys. Rev. Lett.* **103**, 087002 (2009).
13. M. D. Lumsden, A. D. Christianson, E. A. Goremychkin, S. E. Nagler, H. A. Mook, M. B. Stone, D. L. Abernathy, T. Guidi, G. J. MacDougall, C. de la Cruz, A. S. Sefat, M. A. McGuire, B. C. Sales, and D. Mandrus, “Evolution of spin excitations into the superconducting state in FeTe_{1-x}Se_x” *Nature Physics* **6**, 162 (2010)
14. M. D. Lumsden, A. D. Christianson, D. Parshall, M. B. Stone, S. E. Nagler, G. J. MacDougall, H. A. Mook, K. Lokshin, T. Egami, D. L. Abernathy, E. A. Goremychkin, R. Osborn, M. A. McGuire, A. S. Sefat, R. Jin, B. C. Sales, D. Mandrus, “Two-dimensional resonant magnetic excitation in BaFe_{1.84}Co_{0.16}As₂” *Phys. Rev. Lett.* **102**, 107005 (2009).
15. X. B. He, G. R. Li, J. D. Zhang, A. B. Karki, R. Y. Jin, B. C. Sales, A. S. Sefat, M. A. McGuire, D. Mandrus, and E. W. Plummer, “Nanoscale chemical phase separation in FeTe_{0.55}Se_{0.45} as seen via scanning tunneling spectroscopy” *Phys. Rev. B.* **83**, 220502 (2011)
16. M. A. McGuire, D. J. Gout, V. O. Garlea, A. S. Sefat, B. C. Sales, D. Mandrus, “Magnetic phase transitions in NdCoAsO”, *Phys. Rev. B.* **81**, 104405 (2010).
17. C. P. Cheney, F. Bondino, T. A. Calcott, P. Vilmercati, D. Ederer, F. Magnano, M. Malvestuto, F. Parmigiani, A. S. Sefat, M. A. McGuire, R. Jin, B. C. Sales, D. Mandrus, D. J. Singh, J. W. Freeland, and N. Mannella, “Orbital symmetry of Ba(Fe_{1-x}Co_x)₂As₂ superconductors probed with x-ray absorption spectroscopy” *Phys. Rev. B.* **81**, 104518 (2010).
18. P. Vilmercati, A. Fedorov, I. Vobornik, U. Manju, G. Panaccione, A. Goldoni, A. S. Sefat, M. A. McGuire, B. C. Sales, R. Jin, D. Mandrus, D. J. Singh, and N. Mannella, “Evidence for three-dimensional Fermi-surface topology of the layered electron-doped iron superconductor Ba(Fe_{1-x}Co_x)₂As₂”, *Phys. Rev. B.* **79**, 220503 (2010).
19. M. A. McGuire, A. S. Sefat, B. C. Sales, and D. Mandrus, “Iron substitution in NdCoAsO: Crystal structure and magnetic phase diagram” *Phys. Rev. B* **82**, 092404 (2010).
20. E. A. Goremychkin, R. Osborn, C. H. Wang, M. D. Lumsden, M. A. McGuire, A. S. Sefat, B. C. Sales, D. Mandrus, H. M. Ronnow, Y. Su, and A. D. Christianson, “Spatial inhomogeneity in RFeAsO_{1-x}F_x (R= Pr, Nd) determined from rare earth crystal-field excitations” *Phys. Rev. B.* **83**, 212505 (2011).

**Project Title: Atomic Engineering Oxide Heterostructures: Materials by Design, FWP
#10067**

PIs: H. Y. Hwang (hyhwang@slac.stanford.edu), J. Stohr (stohr@slac.stanford.edu), Y. Hikita (yasuyuki.hikita@gmail.com), & C. Bell (cbell1@slac.stanford.edu)

SLAC National Accelerator Laboratory

Project Scope: This FWP focuses on developing the science and technology of interfaces between transition metal oxides. In the search for emergent phenomena and ever higher functionality in devices, transition metal oxides have significant potential since they host a vast array of properties, such as orbital ordering, unconventional superconductivity, ‘colossal’ magnetoresistance, all forms of magnetic ordering and ferroelectricity, as well as (quantum) phase transitions and couplings between these states. Using atomic scale growth techniques, we explore the synthesis of novel interface phases, with a current emphasis on polar surface doping of quantum wells and control of interface dipole formation. X-ray probes are used to determine the static and dynamic electronic and magnetic structure in ultrathin films and superlattices. Heterostructures with low-density superconductors are used to explore new experimental regimes of low-dimensional superconductivity, particularly in the presence of tunable spin-orbit coupling and disorder. Together, these activities address the newly-revealed experimental opportunities enabled by atomically controlled growth of complex oxide heterostructures, and develop the fundamental design principles which underlie the creation of new electronic, magnetic, and superconducting states for science and technology.

Recent Progress: We have made significant progress on several fronts: the design of artificial interface dipoles to tune band alignments >2 eV; electronic and magnetic reconstructions of ultrathin manganite films and their interfaces; and reconstructions at atomic scale perovskite/non-perovskite heterointerfaces. In this presentation we focus on our recent developments in understanding and controlling the electronic structure of the $\text{LaAlO}_3/\text{SrTiO}_3$ interface and δ -doped SrTiO_3 .

The observation of conductivity, and superconductivity, in $\text{LaAlO}_3/\text{SrTiO}_3$ in an interface-specific manner has generated much research activity to determine the origins of the electronic structure. Mechanisms including the polar discontinuity, interdiffusion, and crystalline defects have all been raised and hotly debated as competing origins, while in reality multiple contributions likely coexist to equilibrate the electrochemical potential across the interface [9]. A puzzling issue is the inconsistency of various experimental probes for aspects of this problem; for example, $\text{Au}/\text{LaAlO}_3/\text{SrTiO}_3$ junctions indicate the presence of a large internal field across the LaAlO_3 , as would be expected from polar catastrophe models [2], while photoemission spectroscopy finds a much smaller internal field [M. Takizawa, S. Tsuda, T. Susaki, H. Y. Hwang, and A. Fujimori, “Electronic Charges and Electric Potential at $\text{LaAlO}_3/\text{SrTiO}_3$ Interfaces Studied by Core-Level Photoemission Spectroscopy,” *Phys. Rev. Lett.*, in review

(arXiv:1106.3619)]. Recently, we have found an extreme sensitivity of the interface carrier density and conductivity to polar surface adsorbates, which can be varied by a factor of three by room temperature adsorbate exposure, providing opportunities for chemical sensing [Y. Xie, Y. Hikita, C. Bell, and H. Y. Hwang, “Control of Electronic Conduction at an Oxide Heterointerface Using Surface Polar Adsorbates,” *Nature Comm.*, in review (arXiv:1105.3891)]. Going further, the present/absence of a surface screening metal dramatically changes the strength of the internal electric field across the heterostructure. Taken together, these results address many of the long-standing discrepancies in studies of this interface – the surface boundary conditions are dramatically coupled to the interface, and vary between experimental configurations.

The low-temperature ground state of the $\text{LaAlO}_3/\text{SrTiO}_3$ interface has recently been mapped using scanning SQUID microscopy. In addition to a superfluid density with strong spatial variations ($\sim 80\%$), a large density of magnetic dipoles are observed, indicating a strong competition between superconductivity and ferromagnetism, resulting in their coexistence on a sub-micron scale [J. Bert, B. Kalisky, C. Bell, M. Kim, Y. Hikita, H. Y. Hwang, and K. A. Moler, “Direct Imaging of the Coexistence of Ferromagnetism and Superconductivity at the $\text{LaAlO}_3/\text{SrTiO}_3$ Interface,” *Nature Phys.*, in review]. By contrast, δ -doped SrTiO_3 , another 2D superconductor we have examined, exhibits a homogeneous uniform superconducting state with no signs of magnetism. These results are consistent with theoretical suggestions that the $\text{LaAlO}_3/\text{SrTiO}_3$ interface electrons have several competing instabilities, characteristic of strongly correlated electrons.

Future Plans: *Mesoscale superconductivity.* The use of surface adsorbates allows the tuning of the interface carrier density and mobility over a broad range, robust to ultra-low temperatures, spanning much of the superconducting phase diagram. Spectroscopic experiments will hopefully provide a deeper microscopic understanding of this phenomenon, in particular the possibility of chemio-adsorption in some cases, not just physio-adsorption. Together with AFM-based [5] and conventional lithographic techniques, a number of approaches to crossing the 2D-1D superconducting transition will be explored.

The recent finding of microscopic coexistence of ferromagnetism and superconductivity in $\text{LaAlO}_3/\text{SrTiO}_3$ is just the beginning of a systematic experimental effort to understand and manipulate these phases. For the magnetism, the LaAlO_3 thickness dependence and interface-termination dependence should shed further light on this unexpected behavior. If technically feasible (for the largest dipoles), spectroscopy via PEEM would give information on the microscopic origins of the magnetic instability, whether arising from Ti $3d$ states, or in O $2p$ ligand field states. Furthermore, the demonstrated ability to span the superconducting phase diagram via back-gate field effects is technically compatible with scanning-SQUID, enabling the study of the density dependence of interface magnetism and superconductivity, and their interplay. It is noteworthy that this system has strong broken inversion symmetry and spin-orbit coupling, in addition to magnetism and superconductivity, and thus could be a host for

unconventional edge states as has been recently theoretically proposed. Toward that end, we plan to study whether scanning probes can be used to manipulate and arrange the spatial distribution of the competing ground states.

An interesting point of contrast to study in parallel is δ -doped SrTiO₃. Unlike back-gated LaAlO₃/SrTiO₃, which rapidly loses mobility in the 2D limit upon depletion, δ -doped SrTiO₃ exhibits significant mobility enhancements in the 2D limit, as more of the electron wavefunction extends into the undoped region. This may provide the first experimental system to explore 2D superconductivity in the clean limit, for which many intriguing (reentrant) states have been theoretically proposed. Recent results [11] have already demonstrated significant mobility improvements over the past 2 years, for which the electronic structure of the normal state can be probed for all thicknesses via quantum oscillations. Another direction planned (preliminary experiments currently initiated) is the growth of two or more delta-doped regions; the variation of their separation can be used to engineer the coupling between 2D superconductors, and examine the resulting effect on transition temperature and anisotropic superconducting properties. This provides a flexible platform to study the role of inter-planar coupling in layers superconductors, which has played a central role in theoretical descriptions of quasi-2D organic superconductors and cuprates. In particular, the strong spin-orbit coupling relative to the superconducting gap [M. Kim, Y. Kozuka, C. Bell, Y. Hikita, and H. Y. Hwang, "Intrinsic Spin-Orbit Coupling in Superconducting δ -Doped SrTiO₃ Heterostructures," *Phys. Rev. Lett.*, in review (arXiv:1106.5193)] suggests that coupled bi-layers can generate novel symmetry superconducting states.

Publications:

1. Y. Kozuka, M. Kim, H. Ohta, Y. Hikita, C. Bell, and H. Y. Hwang, "Enhancing the Electron Mobility via Delta-Doping in SrTiO₃," *Appl. Phys. Lett.* **97**, 222115 (2010).
2. G. Singh-Bhalla, C. Bell, J. Ravichandran, W. Siemons, Y. Hikita, S. Salahuddin, A. F. Hebard, H. Y. Hwang, and R. Ramesh, "Built-In and Induced Polarization Across LaAlO₃/SrTiO₃ Heterojunctions," *Nature Phys.* **7**, 80 (2011).
3. T. Yajima, Y. Hikita, and H. Y. Hwang, "A Heteroepitaxial Perovskite Metal-Base Transistor," *Nature Mater.* **10**, 198 (2011).
4. T. Higuchi, Y. Hotta, Y. Hikita, S. Maruyama, Y. Hayamizu, H. Akiyama, H. Wadati, D. G. Hawthorn, T. Z. Regier, R. I. R. Blyth, G. A. Sawatzky and H. Y. Hwang, "LaVO₄:Eu Phosphor Films with Enhanced Eu Solubility," *Appl. Phys. Lett.* **98**, 071902 (2011).
5. Y. W. Xie, C. Bell, Y. Hikita, and H. Y. Hwang, "Tuning the Electron Gas at an Oxide Heterointerface via Free Surface Charges," *Adv. Mater.* **23**, 1744 (2011).
6. H. K. Sato, J. A. Mundy, T. Higuchi, Y. Hikita, C. Bell, D. A. Muller, and H. Y. Hwang, "Nanometer-Scale Epitaxial Strain Release in Perovskite Heterostructures Using 'SrAlO_x' Sliding Buffer Layers," *Appl. Phys. Lett.* **98**, 171901 (2011).

7. Y. Hikita, M. Kawamura, C. Bell, and H. Y. Hwang, "Electric Field Penetration in Au/Nb:SrTiO₃ Schottky Junctions Probed by Bias-Dependent Internal Photoemission," *Appl. Phys. Lett.* **98**, 192103 (2011).
8. H. Y. Hwang, J. Levy, P. Maksymovych, G. Medeiros-Ribeiro, and R. Waser, eds., *Oxide Nanoelectronics*, MRS Symposium Proceedings v1292, Cambridge University Press (2011).
9. T. Higuchi and H. Y. Hwang, "General Considerations of the Electrostatic Boundary Conditions in Oxide Heterostructures," in *Multifunctional Oxides*, edited by E. Tsymbal, C. B. Eom, R. Ramesh, and E. Dagotto, Oxford University Press, in press (arXiv: 1105.5779).
10. R. Yamamoto, C. Bell, Y. Hikita, H. Y. Hwang, H. Nakamura, T. Kimura, and Y. Wakabayashi, "Contrasting the Structure of n-type and p-type LaAlO₃/SrTiO₃ Interfaces," *Phys. Rev. Lett.* **107**, 036104 (2011).
11. M. Kim, C. Bell, Y. Kozuka, M. Kurita, Y. Hikita, and H. Y. Hwang, "Fermi Surface and Superconductivity in Low-Density High-Mobility δ -Doped SrTiO₃," *Phys. Rev. Lett.*, in press (arXiv:1104.3388).
12. Y. Ishida, H. Kanto, A. Kikkawa, Y. Taguchi, Y. Ito, Y. Ota, K. Okazaki, W. Malaeb, M. Mulazzi, M. Okawa, S. Watanabe, C.-T. Chen, M. Kim, C. Bell, Y. Kozuka, H. Y. Hwang, Y. Tokura, and S. Shin, "Common Origin of the Circular-Dichroism Pattern in ARPES of SrTiO₃ and Cu_xBi₂Se₃," *Phys. Rev. Lett.*, in press.
13. B. Kim, D. Kwon, T. Yajima, C. Bell, Y. Hikita, B. G. Kim, and H. Y. Hwang, "Reentrant Insulating State in Ultrathin Manganite Films," *Appl. Phys. Lett.*, in press.

Title: Nanostructured Materials: From Superlattices to Quantum Dots
Principal Investigator: Prof. Ivan K. Schuller
Institution: University of California – San Diego
Email: ischuller@ucsd.edu

Project Scope

This project is dedicated to the main issues which arise when magnetic materials are nanostructured in one, two and three dimensions. This comprehensive project includes preparation of nanostructures using thin film (Sputtering and MBE) and lithography (electron beam and self assembly), characterization using surface analytical, scanning probe, high-resolution scattering (X-ray and Neutron) and microscopy techniques and measurement of physical properties (magnetotransport, magnetic and magneto-optical). All preparation of unique materials and devices, most structural and physical characterization are performed in the PI's laboratory at UCSD. Sophisticated structural and magnetic studies at the nanoscale are performed in collaboration with others at major facilities of DOE funded national labs. Many collaborations, which crucially rely on materials and devices prepared under this grant, are underway at major DOE facilities (synchrotrons and neutron) and other research universities. General physical phenomena investigated include; exchange bias, effect of confinement on magnetic properties, proximity effects in magnetic hybrids, and induced phenomena by the application of external driving forces such as time varying electric and magnetic fields, light and other types of radiation. In all cases, a crucial ingredient in the studies is the reduction of complex, highly correlated materials to the nanoscale, where fundamental changes may occur in their physical properties.

Recent Progress

Recent, exhaustive studies have led to a variety of interesting, unexpected and/or novel results described in detail in many of the publications produced during the past two years. Highlights include:

- i) The use of neutron and synchrotron sources and conversion electron Mossbauer measurements to unravel the spatial dependence of uncompensated spins in exchange biased systems. Two particularly interesting and unexpected discoveries were; a) the presence of pinned and unpinned moments in the AF and b) the critical role of bulk pinned-uncompensated moments in the AF.
- ii) Connections between length scales and exchange bias, showing that depending on the relative domains sizes in the FM and AFM positive, negative or dual hysteresis loops may appear.
- iii) Discovery of highly unquenched orbital moments in Fe-metallophthalocyanine as never found before in any organic material. This synchrotron experiment was

- only possible because of the availability of highly ordered epitaxial Fe metallophthalocyanine films grown by us, using Molecular Beam Epitaxy.
- iv) Quantitative determination of the field profile of magnetic vortices a four-force neutron scattering experiment in magnetic nanodots grown over macroscopic areas,
 - v) Discovery of avalanches in the transport of VO₂ highlighting the fractal and self similar nature of the metal-insulator transition in transition metal oxides
 - vi) Control of spin injection and the effect of surface scattering in nonlocal spin propagation.

An additional important and crucial ingredient is the education of the next generation scientists and technologists in state of the art forefront instrumentation, experimental and theoretical techniques. In addition to publications and patents the young investigators were invited to give major talks at important meetings in the field. Many of the students and postdocs funded under DOE sponsorship are pursuing very successful careers in the magnetic, electronics, sensor and semiconductor industries. Some have pursued academic careers in major and/or teaching academic institutions such as universities and national labs. Thus this project has been actively contributing to the scientific and technological human resource basis of the nation.

Future Plans

General physical phenomena which will be investigated include; exchange bias, effect of confinement on magnetic properties, a variety of proximity effects in magnetic hybrids, and induced phenomena due to external time varying electric and magnetic fields, light and other types of radiation. In all cases, a crucial ingredient is the reduction of complex or highly correlated materials to the nanoscale, where fundamental changes may occur in their physical properties. We will extend our studies to fast time scales, where many unexpected effects have already been observed by others and us.

Specific physical phenomena, which will be studied, include the:

- i) Development of tunable antiferromagnets and study of collective superlattice effects in metal-oxide superlattices,
- ii) Investigation of the origin of pinned uncompensated-moments giving rise to exchange bias and their relevance to the development of new systems with enhanced exchange bias and temperature stability,
- iii) Engineering of novel nanomagnetic patterned structures which should give rise to unusual transport properties,
- iv) Growth of oxide-magnetic hybrids which modify their properties when subject to light and or temperature,
- v) Studies of the effect of conductivity changes on spin transmission in non-magnetic materials, and
- vi) Fast time behavior of hybrid nanostructures.

In all these cases, we have developed the ideas and the conceptual framework for new experiments. These indicate that much new physics will be uncovered some of which is impossible to predict a-priori.

In addition to producing new science and uncovering new scientific guiding principles, this research will probably lead to new applications in important technological areas for DOE such as sensors, electronics and data storage. In particular, this may have direct relevance to the future of modern electronics in areas such as reconfigurable circuits, fault tolerant computing, self-repairing electronic systems, and molecular spintronics.

SELECTED PUBLICATIONS DURING 2008-2010

1. Temperature and angular dependences of dynamic spin-polarized resonant tunneling in CoFeB/MgO/NiFe junctions, *C. W. Miller, I. K. Schuller, R. W. Dave, J. M. Slaughter, Yan Zhou, and J. Akerman, J. Appl. Phys. 103, 07A904 (2008).*
2. Antiferromagnetic domain size and exchange bias, *M.R. Fitzsimmons, D. Lederman, M. Cheon, H. Shi, J. Olamit, I. Roschin, and I.K. Schuller, Phys. Rev. B. 77, 224406 (2008).*
3. Angular dependence and origin of asymmetric magnetization reversal in exchange-biased Fe/FeF₂ (110), *A. Tillmanns, S. Oertker, B. Beschoten, G. Guntherodt, J. Eisenmenger, and I.K. Schuller, Phys. Rev. B. 78, 012401 (2008).*
4. Direct measurement of depth-dependent Fe spin structure during magnetization reversal in Fe/MnFe₂ exchange-coupled bilayers, *W. Macedo, B. Sahoo, J. Eisenmenger, M. Martins, W. Keune, V. Kuncser, R. Rohlsberger, O. Leupold, R. Ruffer, J. Nogues, K. Liu, K. Schlage, and I.K. Schuller, Phys. Rev. B 78, 224401 (2008).*
5. Multiple avalanches across the metal-insulator transition of vanadium oxide nanoscaled junctions, *A. Sharoni, J. Ramirez, and I.K. Schuller, Phys. Rev. Lett. 101, 092503 (2009).*
6. Role of the antiferromagnetic bulk spin structure on exchange bias, *R. Morales, Z.-P. Li, J. Olamit, K. Liu, J.M. Alameda, and I.K. Schuller, Phys. Rev. Lett. 102, 097201 (2009).*
7. Relevance of length scales in exchange biased submicron dots, *Z.-P. Li, R. Morales, and I. K. Schuller, Appl. Phys. Lett. 94, 142503 (2009).*
8. Control of spin injection by direct current in lateral spin valves, *F. Casanova, A. Sharoni, M. Erekhinsky, I. K. Schuller, Phys. Rev. B. 79, 184415 (2009).*
9. Anomalous magnetization reversal mechanism in unbiased Fe/FeF₂ investigated by means of the magneto-optic Kerr-effect, *A. Tillmanns, T. Blachowicz, M. Fraune, G. Guntherodt, and I. K. Schuller, J. Magn. Magn. Mater. 321, 2932(2009).*
10. Evolution of the local superconducting density of states in ErRh₄B₄ close to the ferromagnetic transition, *V. Crespo, J. G. Rodrigo, H. Suderow, S. Vieira, D. G. Hinks, and I. K. Schuller, Phys. Rev. Lett. 102, 237002 (2009).*
11. First-order reversal curve measurements of the metal-insulator transition in VO₂: signatures of persistent metallic domains, *J. G. Ramirez, A. Sharoni, Y. Dubi, M. E. Gomez, and I. K. Schuller, Phys. Rev. B. 79, 235110 (2009).*

12. Angular dependence of vortex-annihilation fields in asymmetric cobalt dots, *R. K. Dumas, T. Gredig, C.-P. Li, I. K. Schuller, and K. Liu, Phys. Rev. B. 80, 014416 (2009).*
13. Measurement of the vortex core in sub-100 nm Fe dots using polarized neutron scattering, *I. V. Roschin, C.-P. Li, H. Suhl, X. Batlle, S. Roy, S. Sinha, S. Park, R. Pynn, M. R. Fitzsimmons, J. Mejia-Lopez, D. Altbir, A. H. Romero, and I. K. Schuller, Euro. Phys. Lett. 86, 67008 (2009).*
14. Three-dimensional spin structure in exchange-biased in antiferromagnetic /ferromagnetic thin films, *R. Morales, M. Velez, O. Petravic, I. Roschin, Z.-P. Li, X. Batlle, J. M. Alameda, and I. K. Schuller, Appl. Phys. Lett. 95, 092503 (2009).*
15. Novel laser-induced dynamics in exchange-biased systems, *A. Porat, S. Bar-Ad, and I. K. Schuller, Euro. Phys. Lett. 87, 67001 (2009).*
16. Surface enhanced spin-flip scattering in lateral spin valves, *M. Erekhinsky, A. Sharoni, F. Casanova, and I. K. Schuller, Appl. Phys. Lett. 96, 022513 (2010).*
17. The fabrication of ordered arrays of exchange biased Ni/FeF₂ nanostructures, *M. Kovylyna, M. Erekhinsky, R. Morales, I. K. Schuller, A. Labarta, and X. Batlle, Nanotechnology 21, 175301 (2010).*
18. Highly unquenched orbital moment in textured Fe-phthalocyanine thin films, *J. Bartolome, F. Bartolome, L. M. Garcia, G. Filoti, T. Gredig, C. Colesniuc, and I. K. Schuller, Phys. Rev. B. 81, 195405 (2010).*
19. Development of vortex state in circular magnetic nanodots: theory and experiment, *J. Mejia-Lopez, D. Altbir, P. Landeros, J. Escrig, A.H. Romero, I. Roschin, C.-P. Li, M.R. Fitzsimmons, X. Batlle, and I. K. Schuller, Phys. Rev. B. 184417 (2010).*
20. Frequency Mixer Having Ferromagnetic Film, *A. Khitun, I. Roschin, K. Galatsis, M. Bao, and K. L. Wang, US 2008/0224740A1; September 18, 2008. PATENT*
21. Exchange-bias based multi-state magnetic memory and logic devices and magnetically stabilized magnetic storage, *I. Roschin, O. Petravic, R. Morales, Z.- P. Li, X. Batlle, and I. K. Schuller, US 2010/ 7764454; July 27, 2010. PATENT*

Session 2

Magnetism and Spin Physics

**BES Experimental Condensed Matter Physics Principal Investigators Meeting
Rockville, Maryland, August 9-12, 2011**

**Magnetic Films and Nanomagnetism*
Materials Science Division, Argonne National Laboratory**

Sam Bader, Group Leader

Materials Science Division, Argonne National Laboratory, Argonne, IL 60439

Phone: (630) 252-4960; Fax: (630) 252-5219; Email: bader@anl.gov

Our vision is to address the grand challenges in condensed matter and materials physics via the exploration of the realm of nanomagnetism. Nanomagnetism is connected to fundamental questions of how the energy demands of future generations will be met via the utilization of wind turbines as a viable alternate energy source, and electric vehicles as alternatives to continued fossil-fuel consumption. Nanomagnetism is connected to the question of how the information technology revolution will be extended via the advent of spintronics and the possibilities of communication by means of pure spin currents. Nanomagnetism provides deep issues to explore in the realms of nanoscale confinement, physical proximity, far-from-equilibrium phenomena, and ultrafast and emergent behavior, and can even provide a window on the bio-realm via new therapeutic techniques and insights. While magnetism is regarded as the oldest field in all of science, nanomagnetism is fresh and vibrant and helped usher in the era of nanoscience and nanotechnology. The next decade will provide new insights, concepts and rewards, given the recent infrastructural advances in fabrication and characterization facilities, and the ever-increasing computational power available to the research community that our group at Argonne now enjoys.

The three hot issues that our group is poised to address and illuminate encompass:

- (i) spin dynamics,
- (ii) spin transport, and
- (iii) the creation of new multilayer materials,

based on metallic heterostructures. Our program in *spin dynamics* will provide insights into *artificial magnonic materials*. The proposed work will advance our fundamental understanding of linear and nonlinear excitations in magnetic nanostructures. Our program in *spin transport* focuses on the physics of pure spin currents. It is only recently that spin currents have been recognized as a possible means to communicate without charge currents, potentially eliminating some of the wasted heat that impedes further transistor miniaturization. Due to this heat, information technology is becoming an energy technology issue, as well as a U.S. economic competitiveness issue. Finally, *the quest for new functional materials via nanoscale multilayering* enables us to create systems that possess unusual synergistic properties that may otherwise be mutually exclusive. Such systems include exchange spring nanomagnetic composites with low or no rare-earth content than can still exceed today's commercial capabilities as used in electric motors and generators. Or ferromagnetic-superconducting multilayers that support an exotic interfacial pairing mechanism even though the individual components can be as simple as elemental layers. Such multilayering also enables us to explore the energetics and transport mechanisms underlying organic spintronic heterostructures. The concepts and materials explored within this program also provide samples worthy of advanced characterization at BES major characterization facilities.

* Work supported by the U.S. Department of Energy, Office of Science, Basic Energy Sciences, under contract No. DE-AC02-06CH11357.

Recent Progress:

Quantifying Spin Hall Effects: Spin Hall effects interconvert spin and charge currents even in nonmagnetic materials and, ultimately might facilitate spin transport without the need for ferromagnets. We showed how spin Hall effects can be quantified by integrating permalloy/normal-metal bilayers into a coplanar waveguide. A *dc* spin current in the normal metal can be generated via spin pumping by exciting the ferromagnetic resonance of the Py. Using this approach we could determine the spin Hall angle, which is the ratio of the spin-Hall-to-charge conductivity. This technique is adaptable to various materials, providing trends with the periodic table for charge-to-spin current conversion efficiency. In particular, a giant spin Hall effect had recently been reported for Au. Our studies via spin pumping and also via mesoscopic Au Hall bar structures were used to determine a spin Hall effect value that is more than an order of magnitude lower than the previously reported giant value.

Functionalized Magnetic Microdisks: Most magnetic vortices studied to date involve arrays on a substrate. Here we investigated an aqueous suspension of lithographical Fe-Ni microdisks (50-nm thick, ~1- μ m diameter). The hysteresis loop is typical for magnetization reversal due to nucleation, displacement and annihilation of the vortices. A small external magnetic field causes the vortex center to (reversibly) displace, inducing a magnetic moment proportional to the field strength. As a result, the microdisks physically rotate in solution until the plane of the disk is aligned along the field direction. The transmitted light intensity from an external laser, increases when the field is *on*, and decreases when field is *off*. The finding could have applications in low-energy consumption magneto-optic devices. Furthermore, we showed (with CNM and Univ. of Chicago) that an *ac* field induces oscillations of the microdisks when attached, via a linker antibody, to human brain cancer cells in aqueous solution. The oscillations transmit a mechanical force to the nucleus, that compromises the integrity of the cell membrane, and initiates programmed cell death. Weak fields (<100 Oe) applied at low frequency (few tens of Hz) for only 10 min were sufficient to induce cell death in 90% of the cells. The external power in our experiments is 10^5 times smaller than in hyperthermia usage of magnetic nanoparticles.

Organic Spin Valves: The energy barrier at organic/electrode interfaces has been a source of confusion with respect to charge injection efficiency in organic electronic devices. It also contributes to the present controversy in *organic spintronics*, where there are claims that, for example, the lowest-unoccupied-molecular-orbital (LUMO) level of the organic semiconductor Alq₃ is low enough to support electron injection from ordinary ferromagnetic metals in a spin-valve geometry. We directly measured the electron injection barrier at the interface between Alq₃ and metal electrodes using hot electrons injected from a tunnel barrier. We reported the energy barrier for electron injection (2.3 eV at the Fe/Alq₃ interface, and 2.2 eV for Al/Alq₃.) Our results are consistent with the known Alq₃ transport gap derived from inverse photoemission spectroscopy, proving that claims of molecular spin transport in "organic spin valves" are not supported by intrinsic material properties. They also underscore the need to understand the charge transport mechanism in organic spintronic devices before spin transport can be understood.

- **Future Plans**

Magnonic Crystals: We will experimentally and theoretically investigate artificial magnonic materials based on 2D arrays of magnetic dots. Due to the intrinsic degeneracy of the ground state of an individual dot, arrays of such dots will have multiple configurations separated by energy barriers. We expect that, by applying a proper sequence of magnetic pulses it will be possible to select a stable, static configuration. The magnon frequencies depend both on resonance frequencies of the individual dots and on the strength of the dipolar inter-dot coupling. By varying the dot size, it is possible to tune these frequencies from sub-GHz (via the gyrotropic mode in a magnetic vortex ground state) to ~ 10 GHz (via the uniform precession mode in a uniform ground state.) The proposed work will advance our fundamental understanding of linear and nonlinear excitations in nanostructured magnetic systems and should transform the field of microwave magnetic materials, possibly leading to novel ultra-fast and energy efficient signal processing devices.

Lateral Spin Valves: We will tailor the spin current generation via electrical injection using our lateral spin valves. We will investigate the influence of current bias on the spin accumulation for different types of contacts. One variation for the ferromagnetic injector contact is to use superlattices with perpendicular magnetic anisotropy, such as Co/Pd or Co/Pt. Due to the perpendicular anisotropy it will be possible to inject spins and control their 3D orientation, since in-plane magnetic fields can be used to tilt the magnetization in arbitrary directions. We will also extend the range of materials for spin injection. One choice will be Pd, to see if ferromagnetism can be induced via spin accumulation. Another choice will be low-T ferromagnets, such as CuNi alloys, where spin-injection might increase the ordering temperature.

Spin Pumping: We will deepen our understanding of spin-pumping-initiated spin Hall effects by determining the temperature dependence of spin Hall conductivities. We will determine the underlying spin scattering mechanism via the T dependencies. A major question is to identify the role of impurities. Recent theoretical work speculates that an orbital-dependent Kondo effect for Fe in Au can give rise to a giant spin Hall effect in gold. The effect would be even stronger for rare earth impurities and represents a way to generate pure spin currents with long spin diffusion lengths for which the intrinsic spin Hall effect is small.

Spin Triplet Superconductivity: A ferromagnet with inhomogeneous magnetization in proximity to a thin superconductor is a key ingredient for the production of spin triplet interfacial pairing. However, so far there has been no control over the tunability of the interface. We will use hard-soft ferromagnetic exchange spring bilayers as the inhomogeneous source. The pitch of the twist of the soft ferromagnetic layer can be tuned via changing the magnitude of the field or via sample rotation. The proposed film structure will have the advantage that the magnetic inhomogeneity can be tuned at-will within a single sample, providing an unambiguous test of the presence of spin triplet superconductivity.

Ultrastrong Permanent Magnets: Nanocomposites of high-anisotropy Mn alloys and a soft phase, such as Fe(Co) or Fe₃B, might provide properties comparable to that of rare-earth-containing permanent magnets. In addition to the usual need of exchange-springs to optimize the microstructure to obtain effective coupling, there are two additional issues that arise: (i) it is not known whether the exchange coupling between the Mn-alloys and Fe or Co is ferromagnetic or AF; and (ii) the formation of a pure, single-phase of the ordered-alloys is difficult. The difficulty is that the DO₂₂ phase is a highly distorted tetragonal structure, and the Mn tends to segregate because of peritectic reaction and because Mn diffusion through MnBi is exceedingly slow.

List of Publications resulting from DOE sponsored research 2008-2011

1. J. S. Jiang, J. E. Pearson, S. D. Bader, "Direct Determination of Energy Level Alignment and Charge Transport at Metal/Alq₃ Interfaces via Ballistic-Electron-Emission Spectroscopy", *Phys. Rev. Lett.* **98**, 072505 (2011).
2. Yaohua Liu, S. G. E. te Velthuis, J. S. Jiang, Y. Choi, S. D. Bader, A. A. Parizzi, H. Ambaye, and V. Lauter, "Magnetic Structure in Fe/Sm-Co exchange spring bilayers with intermixed interfaces", *Phys. Rev. B* **83**, 174418 (2011).
3. S. D. Bader and S. S. P. Parkin, "Spintronics" *Ann. Rev. Cond. Matt. Phys.* **1**, 71 (2010).
4. D. H. Kim, E. A. Rozhkova, I. Ulasov, S. D. Bader, T. Rajh, M. Lesniak, V. Novosad, "Biofunctionalized magnetic vortex microdisks for targeted cancer cell destruction", *Nat. Matls.* **9**, 165 (2010).
5. O. Mosendz, J. E. Pearson, F. Y. Fradin, G. E. W. Bauer, S. D. Bader, A. Hoffmann, "Quantifying spin Hall angles from spin pumping: Experiments and Theory" *Phys. Rev. Lett.* **104**, 046601 (2010).
6. G. Mihajlović, J. E. Pearson, S. D. Bader, A. Hoffmann, "Surface spin flip probability of mesoscopic Ag wires", *Phys. Rev. Lett.* **104**, 237202 (2010).
7. O. Mosendz, J. E. Pearson, F. Y. Fradin, S. D. Bader, A. Hoffmann, "Suppression of spin-pumping by a MgO tunnel-barrier", *Appl. Phys. Lett.* **96**, 022502 (2010).
8. G. Mihajlovic, M. S. Patrick, J. E. Pearson, S. D. Bader, M. Field, G. J. Sullivan, A. Hoffmann, "Temperature dependent nucleation and annihilation of individual magnetic vortices", *Appl. Phys. Lett.* **96**, 112501 (2010).
9. G. Mihajlovic, D. K. Schreiber, Yuzi Liu, J. E. Pearson, S. D. Bader, Amanda Petford-Long, A. Hoffmann, "Enhanced spin signals due to native oxide formation in Ni₈₀Fe₂₀/Ag lateral spin valves", *Appl. Phys. Lett.* **97**, 112502 (2010).
10. O. Mosendz, V. Vlaminck, J. E. Pearson, F. Y. Fradin, G. E. W. Bauer, S. D. Bader, A. Hoffmann, "Detection and quantification of inverse spin Hall effect from spin pumping in permalloy/normal metal bilayers", *Phys. Rev. B* **82**, 214403 (2010).
11. O. Mosendz, G. Mihajlović, J. E. Pearson, P. Fischer, M.-Y. Im, S. D. Bader, A. Hoffmann, "Imaging of lateral spin valves with soft x-ray microscopy", *Phys. Rev. B* **80**, 104439 (2009).
12. S. T. Chui, V. Novosad, S. D. Bader, "Finite frequency response of small magnetic structures under an external static field", *Phys. Rev. B* **80**, 054419 (2009).
13. G. Mihajlović, J. E. Pearson, M. A. Garcia, S. D. Bader, A. Hoffmann, "Negative Nonlocal Resistance in Mesoscopic Gold Hall Bars: Absence of the Giant Spin Hall Effect", *Phys. Rev. Lett.* **103**, 166601 (2009).
14. J. Fassbender, J. Grenzer, O. Roshupkina, Y. Choi, J. S. Jiang, S. D. Bader, "Tuning exchange spring magnets by ion irradiation and annealing", *J. Appl. Phys.* **105**, 023902 (2009).
15. J. S. Jiang, J. E. Pearson, S. D. Bader, "Absence of Spin Transport in the Organic Semiconductor Alq₃" *Phys. Rev. B* **77**, 035303 (2008); *Virt. J. Nanoscale Sci. & Tech.*, Jan. 14, 2008.
16. Y. Choi, J. S. Jiang, J. E. Pearson, S. D. Bader, J. P. Liu, "Element-specific recoil loops in Sm – Co / Fe exchange-spring magnets" *J. Appl. Phys.* **103**, 07E132 (2008).
17. B. Roldan-Cuenya, W. Keune, R. Peters, E. Schuster, B. Sahoo, U. von Hörsten, W. Sturhahn, J. Zhao, T. S. Toellner, E. E. Alp, S. D. Bader, "High-Energy Phonon Confinement in Nanoscale Metallic Multilayers", *Phys. Rev. B* **77**, 165410 (2008).
18. P. Cadden-Zimansky, Ya. Bazaliy, L. M. Litvak, J. S. Jiang, Jiyeong Gu, C.-Y. You, M. R. Beasley, S. D. Bader, "Asymmetric Ferromagnet-Superconductor-Ferromagnet Switch", *Phys. Rev. B* **77**, 184501 (2008).
19. R. Cheng, S. D. Bader, F. Y. Fradin, "Strong Surface Magnetic Anisotropy of Ultrathin Fe on Curved Pt(111)", *Phys. Rev. B* **77**, 024404 (2008) pp. 1-6.
20. Y. Liu, Y. Q. Wu, M. J. Kramer, Y. Choi, J. S. Jiang, Z. L. Wang, J. P. Liu, "Microstructure Analyses of a Bilayer Sm-Co/Fe Exchange Spring Permanent Magnet", *Appl. Phys. Lett.* **93**, 192502, (2008).
21. K. S. Buchanan, M. Grimsditch, F. Y. Fradin, S. D. Bader, V. Novosad, Driven dynamic mode-splitting of the magnetic vortex translation resonance, *Phys. Rev. Lett.* **99**, 267201 (2007); *Virt. J. Nanoscale Sci. & Tech.*, Jan. 14, 2008.

Project Title: Optical Study of Spin Dynamics in Semiconductor Nanowires

Principle Investigator: Fengyuan Yang
 Department of Physics, The Ohio State University
 Email: fyyang@physics.osu.edu

Co-PI: Ezekiel Johnston-Halperin
 Department of Physics, The Ohio State University
 Email: ejh@physics.osu.edu

Project Scope:

The central goal of this DOE project is to investigate spin relaxation behavior in quasi-1D semiconductor systems through optical spin injection into semiconductor nanowires and detection of spin relaxation time using time-resolved pump-probe techniques. Optical investigations of spin relaxation have been performed in bulk semiconductors (3D), semiconductor quantum wells (2D), and quantum dots (0D). Exceptionally long spin lifetime (~100 ns) and spin diffusion length over 100 micrometers have been discovered in bulk GaAs. If semiconductor spintronics is to fulfill its promise to become a next generation technology, these extraordinary properties must persist in semiconductors with lateral dimensions down to tens of nanometers. More importantly, a number of theoretical reports have predicted that as the lateral dimensions of semiconductors are reduced to the order of the electron mean free path, the spin relaxation time exhibits a surprising increase near the one-dimensional (1D) limit. In order for the realization of this goal, the semiconductor nanowires must be able to absorb a circularly-polarized light for optical excitation of spin carriers. However, the quasi-1D geometry and the dielectric mismatch between the nanowires and their environment lead to a large anisotropy in optical absorption between the parallel and perpendicular direction to the nanowire axis. This optical anisotropy prohibits the optical excitation of spin-polarized carriers in semiconductor nanowires by circularly polarized light. In this DOE project, we have overcome the optical polarization anisotropy by coating the nanowires with a matching dielectric material of sufficient thickness, which allows us to characterize the spin relaxation in semiconductor nanowires.

Recent Progress

1. Role of defect states in charge transport in InP nanowires synthesized by PLD

Spin relaxation and optical properties in semiconductor nanowires are sensitive to defect

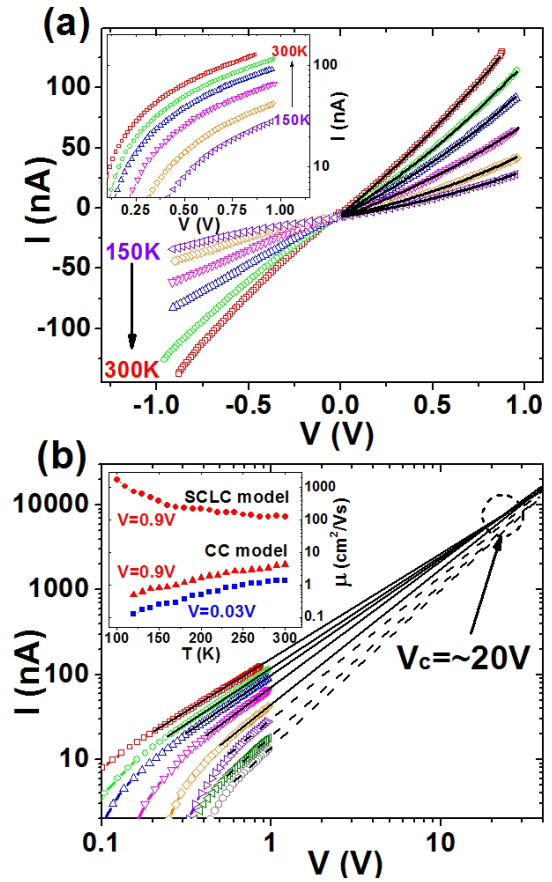


Fig. 1. (a) Temperature dependent I-V plots and fitting to the Schottky model. Inset is the semi-log plot of showing non-exponential function dependence on V. (b) A log-log plot of the same data shows linear behavior, $I \sim V^S$, with slope increasing as temperature decreases. The extrapolations of the linear fits converge to a crossover point (V_c). Inset: electron mobility calculation in different models: circles for SCLC model, squares for CC model.

states in nanowires. The surfaces of semiconductor nanowires are particularly susceptible to formation of defect states due to oxidation and dangling bonds, which are problematic for optical and electrical performance of the nanowires. In order to understand the role of defect states in nanowires, we investigated the charge transport mechanisms in Se-doped *n*-type InP nanowires grown by pulsed laser deposition (PLD) using single nanowire field-effect transistor (FET) device. The contact resistance is small from the 2-probe and 4-probe current-voltage (I-V) measurements. The current as a function of gate-bias shows *n*-type behavior that saturates at negative gate-bias. Qualitatively similar behavior has been reported in InAs nanowires with high mobility ($16000 \text{ cm}^2/\text{V}\cdot\text{s}$), where the saturation was attributed to the presence of surface traps. This result suggests that there exists a parallel transport channel that shorts the band transport at negative gate bias where the *n*-type nanowire is fully depleted.

The temperature dependence of the I-V curves reveals non-linear behavior that persists to room temperature (Fig. 1a). The inset in Fig. 1a is a semi-log plot and shows significant nonlinearity for all temperatures, indicating that the transport is non-Schottky. The linearity at high bias seen in log-log plots (Fig. 1b) suggests that a power law, rather than the exponential dependence predicted by the Schottky model, more appropriately describes electronic transport in these systems. Temperature and gate dependent I-V measurements reveal three distinct transport regimes, i) at high bias and high temperature the wires exhibit space-charge limited current (SCLC), ii) at low bias and high temperature the nanowire transport is dominated by nearest-neighbor hopping (NNH) and iii) at low bias and low temperature variable-range hopping (VRH) dominates. Further, we find that the crossover temperature between NNH and VRH can be tuned by a gate bias, indicating that electron-electron correlations can be controlled *in situ*. These results highlight the complexity of charge transport in these materials and demonstrate the critical role played by defects in these quasi-1D structures.

2. Synthesis of III-V semiconductor nanowires and core-shell nanowire heterostructures using MOCVD

Due to the limited capability in controlling the growth of III-V nanowires by PLD and the significant amount of defects in PLD-produced nanowires, we have switched to metal-organic chemical vapor deposition (MOCVD) for the epitaxial growth of III-V nanowires on GaAs(111)B and GaAs(100) substrates (insets of Fig. 2). GaAs nanowires with essentially no tapering have been obtained by controlling the

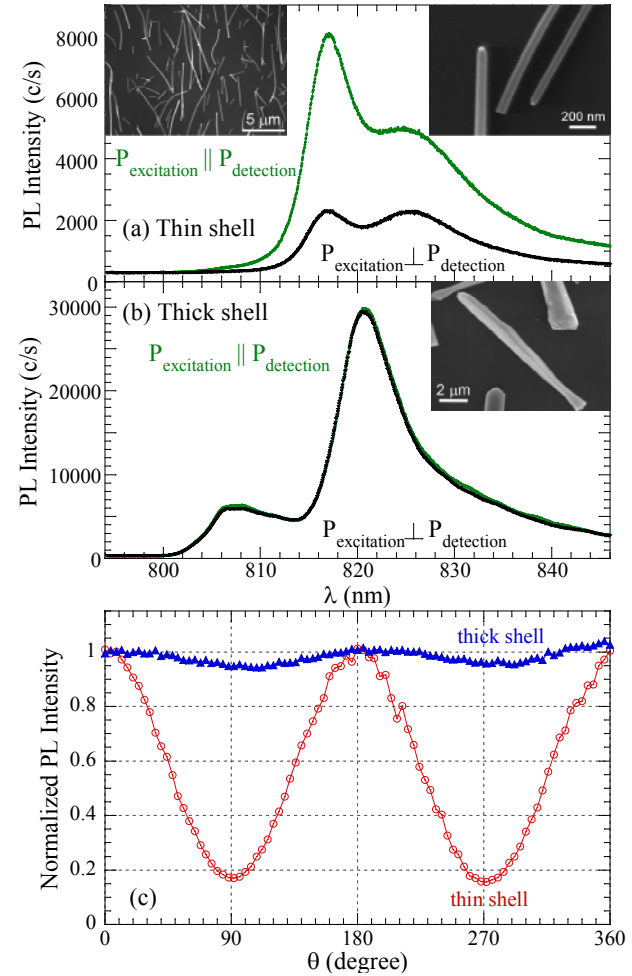


Fig. 2. PL spectra of 30-nm GaAs nanowires with (a) a 15-nm (thin) $\text{Al}_{0.35}\text{Ga}_{0.65}\text{As}$ shell and (b) a 500-nm (thick) $\text{Al}_{0.35}\text{Ga}_{0.65}\text{As}$ shell for the linear polarization of the excitation light parallel (green) and perpendicular (black) to the detection polarization. The core-shell nanowires were grown by MOCVD and then transferred to Si substrates for PL measurements (insets: SEM images of the transferred nanowires). (c) Angular dependence of normalized PL intensity ratio P_{\perp}/P_{\parallel} for GaAs nanowires with thin (red) and thick (blue) nanowires, where θ is the angle between the polarization orientations of the excitation light and the detection polarizer.

substrate temperature (450°C), V/III sources ratio, and Au nanoparticle density. More importantly, MOCVD offers the capability to fabricate core-shell nanowire heterostructures by first growing GaAs core nanowires at 450°C, followed by the growth of a shell (e.g. AlGaAs) at a higher temperature such as 650°C. The protection and passivation of the core nanowire surface by the shell greatly minimizes the surface defect density. The AlGaAs shell with a larger band gap also provides a confinement for the core GaAs nanowire. As a result, the core-shell structured nanowires exhibit a very bright photoluminescence (PL) as shown in Fig. 2, indicating high-efficiency optical absorption and radiative recombination, which are highly desirable for optical study of spin relaxation in nanowires.

3. Pronounced PL polarization anisotropy in GaAs nanowire arrays and minimization of such anisotropy through dielectric matching with thick AlGaAs shells

The MOCVD-grown nanowires were first transferred from GaAs substrates onto Si substrates for PL measurements to avoid interference from the substrates. Bare GaAs nanowires show no PL peak due to significant amount of surface trap states which completely prohibit radiative recombination. In order to enable photoluminescence of GaAs nanowires, we fabricated core-shell nanowires with a 30-nm GaAs core nanowire and a 15-nm $\text{Al}_{0.35}\text{Ga}_{0.65}\text{As}$ shell which passivates the surface of the core nanowire and essentially eliminates the surface trap states. As a result, a bright photoluminescence was observed as shown in Fig. 2a. The main peak at $\lambda = 817$ nm is from the GaAs band edge emission and the shoulder peak at $\lambda = 826$ nm can be attributed to donor states which is commonly seen in GaAs wafers. We systematically varied the angle between the linear polarization of the excitation laser, $P_{\text{excitation}}$, and the detection polarizer, $P_{\text{detection}}$, to characterize the polarization anisotropy. There is a significant difference in the PL intensity between $P_{\text{excitation}} \parallel P_{\text{detection}}$ and $P_{\text{excitation}} \perp P_{\text{detection}}$, especially for the band edge emission at $\lambda = 817$ nm. Fig. 2c shows normalized polarization anisotropy over the complete 360° range, which gives a minimum of only 0.15 at $\theta = 90^\circ$ and 270° ($P_{\text{excitation}} \perp P_{\text{detection}}$), indicating that the nanowire array (inset of Fig. 2a) is largely aligned.

In order to minimize the polarization anisotropy for optical spin excitation in nanowires, we synthesized core-shell nanowires with a thick $\text{Al}_{0.35}\text{Ga}_{0.65}\text{As}$ shell (inset of Fig. 2b) which has a thickness of 550 nm (diameter 1.10 μm) at the thick end and a thickness of 310 nm (diameter: 650 nm) at the thin end. The reason for the nonuniform diameter is due to that during the nanowire growth, the thick end of the nanowires is away from the GaAs substrate and absorbs more source gases while the thin end is close to the substrate and sees less source gases. This nonuniformity should not affect the optical properties of the core nanowires since optical excitation and luminescence only happen within the core nanowires as long as the shell is thick enough. As expected, the PL of the core-shell nanowires with thick shells exhibits essentially no polarization anisotropy, as shown in Figs. 2b and 2c. The small peak at $\lambda = 806$ nm in Fig. 2b is due to the defect states in the $\text{Al}_{0.35}\text{Ga}_{0.65}\text{As}$ shell. Since this peak is spectrally distinguishable from the PL of the core GaAs nanowires, it does not interfere with the optical characterization of the core nanowires.

Our original plan was to use oxides, e.g. TiO_2 and Ta_2O_5 , to coat the III-V nanowires to minimize the polarization anisotropy for spin dynamics studies using pump-probe techniques. The core-shell nanowires with thick AlGaAs shells provide a better material system for this purpose with the following advantages: (1) the core nanowires and shells are grown by MOCVD in the same run, providing clean epitaxial interfaces between the core nanowires and the shells with little defect states; (2) the AlGaAs shell has essentially identical dielectric constant as the GaAs nanowires, resulting in an ideal dielectric matching for optimal spin excitation; (3) the doping type and carrier density in the core nanowires and shells can be individually controlled and tuned for systematic studies of spin relaxation.

In order to avoid nanowires transfer from GaAs substrates to Si wafers, we have also grown $\text{In}_{0.1}\text{Ga}_{0.9}\text{As}$ nanowires with an $\text{Al}_{0.35}\text{Ga}_{0.65}\text{As}$ shell on GaAs(100) substrates since the luminescence of the $\text{In}_{0.1}\text{Ga}_{0.9}\text{As}$ nanowires is spectrally well separated from that of the GaAs substrate. The elimination of the

need for nanowire transfer provides III-V nanowire arrays of very high density which is desirable for pump-probe measurements of spin relaxation due to the high signal-to-noise level.

Future Plans

The GaAs-AlGaAs core-shell nanowires with bright PL and essentially no optical anisotropy (Fig. 2c) offer the desired materials for the study of spin relaxation in 1D systems using optical pump-probe techniques. Recently, we performed Time Resolved Kerr Rotation (TRKR) measurements of spin relaxation time in GaAs epi-layers grown by MOCVD (Fig. 3). The spin relaxation time is $\tau = 1.4$ ns at 50 K and exceeds 90 ns at 5 K at a doping level of $n = 4 \times 10^{16} \text{ cm}^{-3}$, indicating the high quality of MOCVD-grown GaAs. With the availability of the pump-probe optical techniques and the high quality nanowires, we are well positioned to investigate spin physics in 1D semiconductors in the near future.

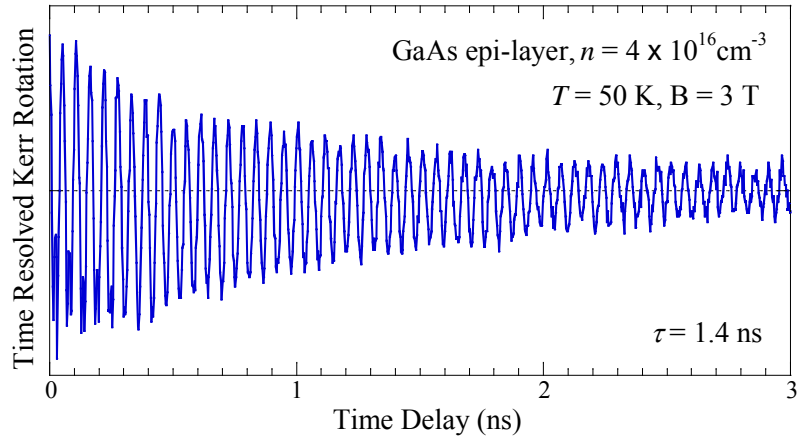


Fig. 3. Time Resolved Kerr Rotation (TRKR) measurement of spin relaxation time in a GaAs epi-layer with a doping level $n = 4 \times 10^{16} \text{ cm}^{-3}$ at $T = 50$ K and a magnetic field $B = 3$ T. The obtained spin relaxation time is $\tau = 1.4$ ns.

The current plan includes studies of spin relaxation time as a function of applied magnetic field strength and temperature, and the resulting behavior will be analyzed to determine the dominant spin scattering mechanism (such as Dresselhaus or Rashba dominated scattering). The theoretical predictions also suggest that studies of spin relaxation time as a function of nanowire diameter may reveal the dramatic suppression of D'yakonov and Perel' (DP) spin scattering. If this is in fact the case, these studies will reveal both a significant increase in spin relaxation time and a change in the temperature and magnetic field dependence consistent with the onset of the next-most dominant scattering mechanism.

List of publications

1. Dongkyun Ko, Xianwei Zhao, Kongara Reddy, Oscar Restrepo, Nandini Trivedi, Wolfgang Windl, Nitin Padture, Fengyuan Yang, and Ezekiel Johnston-Halperin, "Role of defect states in charge transport in semiconductor nanowires," *submitted to Phys. Rev. Lett.*
2. Lei Fang, Xianwei Zhao, Yi-Hsin Chiu, Dongkyun Ko, DongSheng Li, Nitin Padture, Fengyuan Yang, and Ezekiel Johnston-Halperin, "Controlling the polarization anisotropy through oxide coating in InP and ZnO nanowires," *submitted to Appl. Phys. Lett.*

Spin Polarized Electron Transport Through Aluminum Nanoparticles

Dragomir Davidović

dragomir.davidovic@physics.gatech.edu

School of Physics, Georgia Institute of Technology, 837 State Street, Atlanta, Georgia 30332

Ferromagnetic nanoparticles have drawn increasing interests because of their novel behavior and potential application in miniaturization of magnetic memory. Technological breakthroughs require further understanding of magnetization dynamics in ferromagnetic nanoparticles. In this project, we study the magnetic properties of Co nanoparticles by tunneling spectroscopy and microwave pumping. These two techniques enable us to study the coupling between electron tunneling and magnetization dynamics as well as magnetic damping.

In our recent experiment, we study the electrical and magnetic properties (Fig. 1) of single Co nanoparticles with 2-5nm in diameter. We observed magnetic excitations in nanoparticles generated by tunnel current. As shown in Fig. 2, the switching field of the nanoparticles, indicated by arrows, decreases with voltage, especially near the Coulomb blockade threshold. In the red loop of the inset in Fig. 2C, a current pulse applied when the magnetic field is below the switching field switches the nanoparticle from Coulomb blockade state into the current carrying state suggesting a magnetic reversal. In a magnetically excited nanoparticle, the magnetic energy needed for switching will be reduced. Thus, the reduction of the switching field with bias voltage, as well as the switching of the magnetization by applying a current pulse, demonstrate that the tunnel current excites the nanoparticle magnetically.

In another experiment, we successfully integrate the tunneling spectroscopy and microwave pumping using device with new geometry (Fig. 3). We study the effect of repeated nanosecond microwave pulses with various spacing between pulses T_s on Co nanoparticles at 4.2K. As shown in Fig. 4C and D,

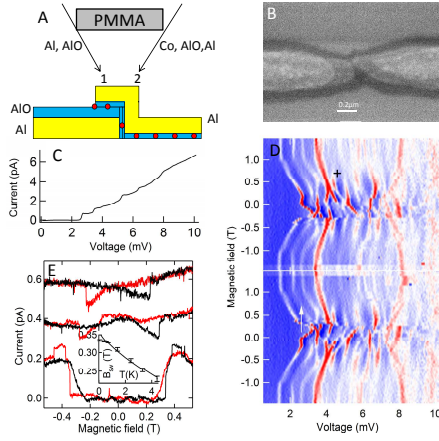


Figure 1: A: Sketch representing sample fabrication process. B: Scanning electron micrograph of a typical device. C: Current versus bias voltage curve at $T = 15\text{mK}$. D: Differential conductance versus magnetic field and voltage at base temperature ($\sim 15\text{mK}$). Top and bottom panel in D correspond to decreasing and increasing magnetic field, respectively. Blue (red) regions correspond to low (high) conductance. E: Current versus magnetic field at voltage 2.4mV , showing the hysteresis loop at $T = 60\text{mK}$, 2.4K , and 4.4K (bottom to top), with current offsets 0.2pA (for clarity). Black (red) line correspond to increasing (decreasing) field. Inset: Switching field versus temperature.

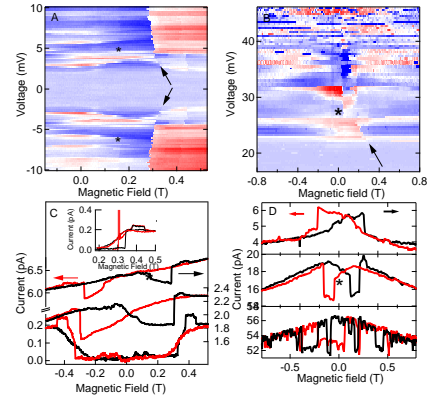


Figure 2: A, C: Sample 1 at $15\text{-}60\text{mK}$. B, D: Sample 2 at $15\text{-}60\text{mK}$. A, B: Current versus increasing magnetic field and voltage of sample 1 and 2 respectively. Red (blue) regions correspond to high (low) current. Black arrows point to the switching field versus voltage. Black stars indicate additional magnetic switches. C: Current hysteresis loops at voltage 2.4mV , 5.2mV , and 10mV (bottom to top). D: Current hysteresis loops at 26mV , 32mV , and 44mV (top to bottom). Black (red) lines correspond to increasing (decreasing) magnetic field. Inset: Hysteresis loops zoomed-in near the switching field. Red and black represent the loop with and without voltage pulse respectively.

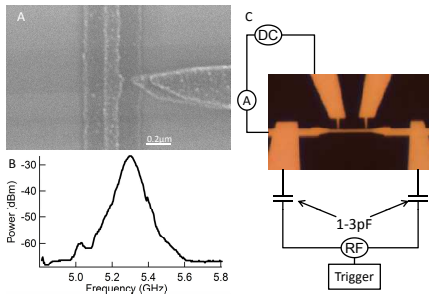


Figure 3: A: Scanning electron micrograph of a typical device. B: Fourier spectrum of repeated microwave pulses. C: Scheme of electrical circuit.

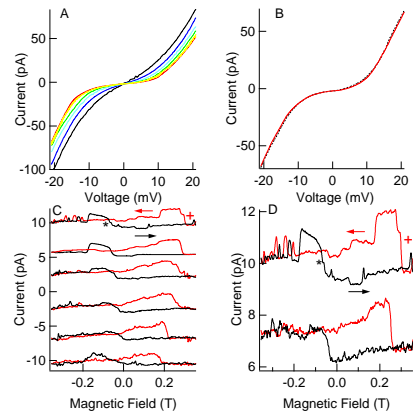


Figure 4: A: Average I-V curves at 27K, 16.6K, 13.1K, 9.3K, 5.8K, and 4.2K (from top to bottom at positive bias voltage). B: Average I-V curves at $T_s = 10\mu s$ (red) and $1.25\mu s$ (black). C: Average current loops at 4.2K when $T_s = \infty$ (no microwave), $1000\mu s$, $10\mu s$, $5\mu s$, $2.5\mu s$, and $1.25\mu s$ (top to bottom). The right and left arrow corresponds to increasing and decreasing magnetic field respectively. D: Average current loops at 4.2K and 7K (top to bottom). Current loops with finite T_s in C and 7K in D are offset down with 4pA spacing.

the reduction caused by microwave pulses with $T_s = 1.25\mu\text{s}$ is much stronger than that from the temperature increase from 4.2K to 7K while the electron temperature in the leads at $T_s = 1.25\mu\text{s}$ is estimated to be less than 4.4K (Fig. 4A and B). These results demonstrate that magnetic excitations in Co nanoparticles are pumped directly by microwave pulses, not by ordinary sample heating. The reduction of switching field is still observable at $10\mu\text{s}$ pulse spacing, which implies that the spin relaxation time in our Co nanoparticles is in the order of microsecond.

In the future work, we plan to extend the application of electron tunneling and microwave pumping techniques in our study of nanoparticles.

We will use the gate to tune the nanoparticles so that electron can tunnel into a majority level. We want to see if tunneling into majority level can stabilize magnetization dynamics against thermal fluctuations, thereby suppress superparamagnetism.

We can use the microwave to induce CESR in Al nanoparticles and FMR in Co nanoparticles. We want to explore these effect to improve our understanding of the spin and magnetization dynamics in these nanoparticles.

We will study the effects of nonequilibrium white noise on magnetization dynamics in Co nanoparticles to directly test the Brown model of magnetic reversal by properly tuning the microwave pulses.

Publications

Microwave coupled electron tunneling measurement of Co nanoparticles. W. Jiang, F. Tijiwa Birk, and D. Davidović, *Applied Physics Letters* (Accepted) (2011).

Electronic Properties of Au-Graphene Contacts. C. E. Malec, and D. Davidović, *Phys. Rev. B* (Accepted) (2011).

Transport in graphene tunnel junctions. C. E. Malec, and D. Davidović, *Journal of Applied Physics* **109**, 064507 (2011).

Magnetoresistance in an aluminum nanoparticle with a single ferromagnetic contact. F. Tijiwa Birk, and D. Davidović, *Physical Review B* **81**, 241402 (2010).

Modeling electron-spin accumulation in a metallic nanoparticle. Y. G. Wei, C. E. Malec, and D. Davidović, *Physical Review B* **78**, 035435 (2008).

Spin-polarized electron tunneling through an aluminum particle in a non-collinear magnetic field. F. Tijiwa Birk, C. E. Malec, and D. Davidović, *Physical Review B* **79**, 245425 (2008).

Project Title: Spin-Polarized Scanning Tunneling Microscopy Studies of Nanoscale Magnetic and Spintronic Nitride Systems

Principal Investigator: Arthur R. Smith

Institution: Nanoscale & Quantum Phenomena Institute
Ohio University
Office of Research & Sponsored Programs

E-mail: ohiousmith@gmail.com

Project Scope: The scope of this project is to investigate the properties of nanoscale magnetic and spintronic nitride systems. Of particular interest is to investigate nitride surfaces such as wurtzite gallium nitride covered with magnetic atoms. As the central experimental technique, we utilize ultra-high vacuum scanning tunneling microscopy and spin-polarized scanning tunneling microscopy (SP-STM). Both room temperature and low-temperature STM systems are employed in this project in order to address key questions regarding especially the magnetic and spintronic properties at the nanometer or atomic length scales. Samples investigated are prepared using molecular beam epitaxy and transferred *in-situ* to the adjoining STM chamber for investigation.

Recent Progress: In recent investigations, we have found that gallium nitride surfaces, when exposed to magnetic transition metal atoms, result in a range of novel, well-ordered structures. Whereas the origins of magnetic properties of transition metal-doped bulk gallium nitride layers were controversial and difficult to unravel due to the problems of cluster formation and inhomogeneities, these well-ordered magnetic-containing surface structures open new possibilities for development of magnetic nitride systems for future spintronic applications. For example, in several cases we find $\sqrt{3} \times \sqrt{3} - R30^\circ$ surface structures in which Mn atoms are bonded to either Ga or N or both. In the first situation – found at the Ga-polar wurtzite-GaN surface – this results in a magnetic surface with either antiferromagnetic or ferromagnetic ground state, dependent on Mn content. Additional growth of Mn and Ga on this template leads to stoichiometrically controllable Mn_xGa_y ultra-thin alloy films with direct spintronic applications. In the case of Mn on the N-polar w-GaN surface, our current work points toward both N- and Ga-bonding of the Mn atoms, with a structural model which has not previously been seen, and which may be considered as a 2-D MnGaN surface alloy.

Until very recently, we have been exploring these systems at room temperature mainly with regular STM and mostly in zero applied magnetic fields. However, in order for these promising systems to lead to novel, futuristic device applications, it will be essential to fully explore their electronic, magnetic, and spintronic properties with a tool capable of unprecedented spin *and* spatial resolution. SP-STM is such a tool which is capable of mapping spin structure of surfaces down to the nanometer and even atomic scale using magnetic tips. Further critical requirements for characterizing these systems fully are the capability of applying external magnetic fields and the ability to vary the temperature.

Therefore, the exciting directions of the current research project are to begin exploring these magnetic-on-nitride 2-D surface systems using SP-STM and spin-polarized scanning tunneling spectroscopy, both under applied magnetic fields and in different temperatures. For this purpose, we have developed two state-of-the-art SP-STM systems, one working in room temperature and the second working in low and variable temperatures. Confirming the viability of these directions, in our most recent STM experiments we find that application of small fields in the range from ~ 20 G to ~ 300 mT at room temperature leads to direct and appreciable changes in the spectroscopic signature of a surface 2-D magnetic nitride system. Shown in Fig. 1(a) is an STM image without spin polarization of the Mn/N-polar wurtzite GaN $\sqrt{3}\times\sqrt{3}$ -R30° surface structure obtained with a normal tungsten tip. The surface contains a few defects; however, overall it is a perfectly arranged near-hexagonal-type structure. Each unit cell is thought to contain one

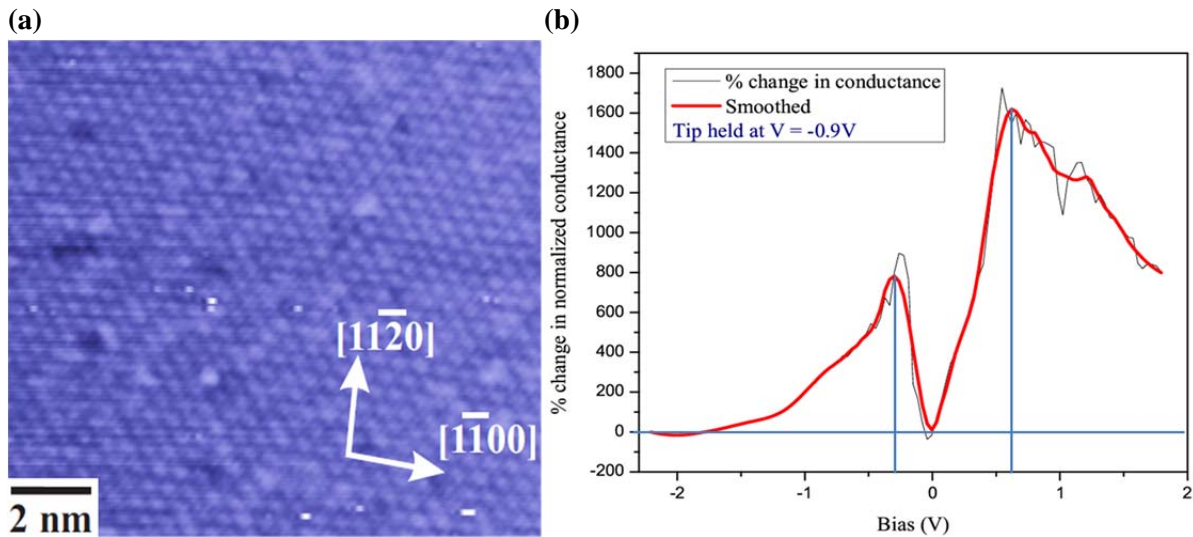


Fig. 1. (a) STM image of $\sqrt{3}\times\sqrt{3}$ -R30° Mn/GaN surface; (b) percent change in normalized conductance (with applied field of ~ 300 mT versus without the applied field) as a function of sample bias.

Mn atom, and this is confirmed through recent first-principles calculations by our theory collaborators. The spectroscopy of this surface, however, presents an unprecedented behavior, namely that at zero perpendicular applied magnetic field, we see a weakly metallic behavior, but at finite small perpendicular applied fields, the surface conductance is strongly increased within the vicinity of two distinct energy windows, one on either side of the Fermi level. This result is presented in Fig. 1(b) which shows a plot of the percent change in the normalized conductance *with* versus *without* applied perpendicular field. As can be seen, normalized conductance increases by as much as 1600% on the positive bias side. Such a dramatic increase is truly unexpected, strongly motivating further work to explain it. Control experiments have also been done, confirming that the effect is only seen for the Mn-reconstructed surface and not for the bare GaN surface.

Future Plans: While the significance of this finding has yet to be fully understood, such novel behavior as a function of applied magnetic field, within a single fractional monolayer of magnetic atoms at the surface of a wide-bandgap semiconductor, and at room temperature, is certainly rare and unexpected. Furthermore, these new findings suggest that spintronic nitride surface structures comprise a rich class of surfaces which have only begun to be investigated and which have excellent potential for futuristic nanoscale device applications.

With two fully operational SP-STM systems, one working in room temperature and one in low temperature, and both having applied magnetic field functionality, the sky is the limit to what we can do next, since these systems are each coupled to molecular beam epitaxy (and for the low-temperature system, pulsed laser epitaxy) growth facilities for nitride spintronic material systems. In the immediate future, we plan of course to explore in greater detail the intriguing phenomena shown above, in order to gain a comprehensive understanding of the observed behavior.

With respect to the findings presented in Fig. 1, we are currently working to further probe this effect using SP-STM. One possibility is that application of a small magnetic field induces an ordered magnetic (correlated) state within the layer which in turn influences the electronic properties. Application of magnetic STM tips offers the possibility of extracting the magnetic spin component from the STM signal and as such may help to shed light on the origins of this interesting new phenomenon.

As this project represents only one outcome of our recent experimental work with manganese, future work will as well involve the use of other transition metal (and rare earth) atoms to explore if there is something special about Mn which results in what we have seen here, or whether a similar phenomenon can also be observed for other TM's (or RE's) on GaN.

Ordered magnetic states for ultra-thin magnetic systems on GaN surfaces will indeed comprise one of the principal foci of our lab's future investigations. We have also had significant success recently exploring the growth and properties of monolayer systems of MnGa on the Ga-polar GaN(0001) surface. In this case, the special structure of the Ga-rich, Ga-polar "1×1" (pseudo-1×1) surface structure plays an important role in determining the ordered Mn-induced structures which occur. In the case of sub-monolayer Mn deposition, we expect an antiferromagnetically-ordered arrangement of Mn spins to occur for the lowest-coverage stripe phase, based on theoretical calculations performed by our collaborator. As the Mn concentration is increased on the surface, the structure evolves, ultimately becoming an ideal template for ferromagnetic MnGa layers. These layers have been also grown over the thickness range from one to several tens of monolayers, which results in well-ordered epitaxial layers.

While it is important for practical applications to explore these materials' room-temperature properties, low-temperature SP-STM measurements in applied magnetic fields allow the investigation of additional fundamental properties. Therefore, this is certainly one of our future key research directions.

Publication List (2008-2011):

68. [Influence of Growth Temperature and Cr:N Flux Ratio on the Properties of Chromium Nitride Thin Films](#), Yinghao H. Liu, Kangkang Wang, Wenzhi Lin, Abhijit Chinchore, Meng Shi, Jeongihm Pak and Arthur R. Smith, Thin Solid Films (2011), in press.

67. [Efficient Kinematical Simulation of Reflection High-Energy Electron Diffraction Streak Patterns for Crystal Surfaces](#), Kangkang Wang and Arthur R. Smith, Comp. Phys. Commun. **182**, 2208 (2011).

66. [A Modular Designed Ultra-High-Vacuum Spin-Polarized Scanning Tunneling Microscope with Controllable Magnetic Fields for Investigating Epitaxial Thin Films](#), Kangkang Wang, Wenzhi Lin, Abhijit V. Chinchore, Yinghao Liu, and Arthur R. Smith, Rev Scientific Instruments **82**, 053703 (2011).

65. [Structural Controlled Magnetic Anisotropy in Heusler \$L1_0\$ -MnGa Epitaxial Thin Films](#), Kangkang Wang, E. Lu, J. W. Knepper, F.-Y. Yang, and A. R. Smith, *Applied Physics Letters* **98**, 162507 (2011).
64. [Novel Two-Dimensional Mn Structure on the GaN Growth Surface and Evidence for Room-Temperature Spin Ordering](#), Kangkang Wang, Noboru Takeuchi, Abhijit Chinchore, Wenzhi Lin, Yinghao Liu, and Arthur R. Smith, *Phys. Rev. B* **83**, 165407 (2011).
63. [Reflection High Energy Electron Diffraction and Atomic Force Microscopy Studies of \$Mn_xSc_{1-x}\$ Alloys Grown on MgO\(001\) Substrates by Molecular Beam Epitaxy](#), Costel Constantin, Abhijit Chinchore, and Arthur R. Smith, *Mater. Res. Soc. Symp. Proc.* (2011), **1295**: mrsf10-1295-n05-37; doi:10.1557/opl.2011.458.
62. [Structural, Magnetic, and Electronic Properties of Dilute MnScN\(001\) Grown by RF Nitrogen Plasma Molecular Beam Epitaxy](#), Costel Constantin, Kangkang Wang, Abhijit Chinchore, Han-Jong Chia, John Markert and Arthur R. Smith, *Mater. Res. Soc. Symp. Proc.* (2011), **1290**: mrsf10-1290-i08-02; doi:10.1557/opl.2011.178.
61. [Growth of Epitaxial Iron Nitride Ultrathin Film on Zinc-Blende Gallium Nitride](#), Jeongihm Pak, Wenzhi Lin, Kangkang Wang, Abhijit Chinchore, Meng Shi, David C. Ingram, Arthur R. Smith, Kai Sun, J. M. Lucy, A. J. Hauser, and F. Y. Yang, *J. Vac. Sci. Technol. A* **28(4)**, 536 (2010).
59. [Magnetic and Electronic Properties of Fe_{0.1}Sc_{0.9}N/ScN\(001\)/MgO\(001\) Films Grown by Radio-Frequency Molecular Beam Epitaxy](#), Costel Constantin, Kangkang Wang, Abhijit Chinchore, Han-Jong Chia, John Markert, Arthur R. Smith, *Mater. Res. Soc. Symp. Proc. Vol.* **1198**, 1198-E07-22 (2010).
58. [Epitaxial Growth of Ferromagnetic Delta-phase Manganese Gallium on Semiconducting Scandium Nitride \(001\)](#), Kangkang Wang, Abhijit Chinchore, Wenzhi Lin, David C. Ingram, Arthur R. Smith, Adam J. Hauser, and Fengyuan Yang, *Journal of Crystal Growth* **311**, 2265 (2009).
57. [Delta-Phase Manganese Gallium on Gallium Nitride: a Magnetically Tunable Spintronic System](#), Kangkang Wang, Abhijit Chinchore, Wenzhi Lin, Arthur R. Smith, and Kai Sun, *Mat. Res. Soc. Symp. Proc.* **1118**, K06.06 (2009).
56. [Atomic Layer Structure of Manganese Atoms on Wurtzite Gallium Nitride \(000-1\)](#), Abhijit Chinchore, K. Wang, W. Lin, J. Pak, and A. R. Smith, *Applied Physics Letters* **93(18)**, 181908 (2008).
55. [Molecular Beam Epitaxial Growth of Zinc-Blende FeN\(111\) on Wurtzite GaN\(0001\)](#), Wenzhi Lin, Jeongihm Pak, David C. Ingram, and Arthur R. Smith, *J. Alloys & Compounds* **463**, 257 (2008).

- **Project Title and Principal Investigators**

Fundamental Studies of High-Anisotropy Nanomagnets

David J. Sellmyer, University of Nebraska, dsellmyer@unl.edu

Ralph Skomski, University of Nebraska, rskomski2@unl.edu; rskomski@neb.rr.com

George Hadjipanayis, University of Delaware, hadji@physics.udel.edu

- **Project Scope**

This project is focused on a key class of materials important in magnetism and nanoscience. The specific target is nanometer-length-scale and real-structure control of structures as a means of creating nanomaterials with high magnetic anisotropy and high coercivity. Innovative aspects of the research include synthesis of new magnetic nanostructures with special fabrication techniques. The proposed research consists of three main parts. The first is aimed at preparation and properties of nanoscale clusters and particles where anisotropic structures and surface effects are expected to lead to new high-anisotropy nanomagnets. Both rare-earth-free and rare-earth-containing Co-Fe-rich systems are explored. The second part is focused on new thin-film nanomagnets and unconventional alloy structures. Here, the goals are to control the coercivity and anisotropy in hexagonal and related structures, where exchange and anisotropy effects of substitutional and interstitial doping are investigated. The third part is aimed at understanding the effects of spatial confinement on magnetic hardening in nanoscale structures undergoing structural transformations. This topic is highly important in magnetic nanomaterials since many of them have to be thermally processed to create nanophases with desired hard magnetic properties.

- **Recent Progress**

The concept of achieving a useful high-energy-product magnet through appropriate nanostructuring of known hard and soft phases has been tantalizing researchers since the idea was first proposed. The field has received added impetus recently because of the potential scarcity of rare-earth metals used in today's best permanent magnets. We have investigated two-phase nanostructures of hard $L1_0$ -ordered FePt and soft iron-rich fcc FePt experimentally and by model calculations. The Fe-Pt thin films were produced by epitaxial co-sputtering onto MgO and have a thickness of about 10 nm. They form two-phase dots that cover a large fraction of the surface but are separated from each other. X-ray diffraction and TEM show that the c -axis of the phase FePt is aligned in the direction normal to the film plane. The experimental and theoretical hysteresis loops indicate nearly ideal exchange coupling, and excellent magnetic properties are obtained, including high values of coercivity (51 kOe), saturation magnetization (1287 emu/cc), and nominal energy product (54 MGOe).

Rare-earth transition-metal (R-TM) alloys show superior permanent magnetic properties in the bulk, but the synthesis and application of R-TM nanoparticles remains a challenge due to the requirement of high-temperature annealing above about 800 °C for alloy

formation and subsequent crystalline ordering. We have developed a single-step method to produce highly ordered R-TM nanoparticles such as YCo_5 and Y_2Co_{17} , without high-temperature thermal annealing by employing a cluster-deposition system and investigate their structural and magnetic properties. The direct ordering is highly desirable to create and assemble R-TM nanoparticle building blocks for future permanent-magnet and other significant applications.

We also have observed unusual spin correlations and a Kondo effect in the strong, high-temperature ferromagnet MnBi. Transport spin polarization measurements show polarization values from 51% to 63% and a large magnetoresistance. Relativistic band-structure calculations indicate that in spite of almost identical densities of states at E_F , the large Fermi velocities lead to the high transport spin polarization. Doping of MnBi with Pt leads to a resistance minimum (Kondo effect) below 10 K. First-principle calculations show that Mn atoms are displaced by Pt to interstitial sites where they couple antiferromagnetically with the Mn sublattice, and these spin correlations give rise to the Kondo effect.

- **Future Plans**

The fabrication of exchange-coupled nanocomposite magnets faces several challenges. This includes (i) achieving a uniform mixture of hard and soft phases with a characteristic length scale of order 10 nm, (ii) arranging the nanostructure so that the coercivity remains high as the fraction of high-magnetization soft phase is increased, (iii) aligning the easy anisotropy axes of the hard-phase grains, and (iv) fabricating dense-packed bulk magnets for practical use.

Randomly oriented anisotropy axes reduce the maximum energy product $(BH)_{\text{max}}$ to somewhat more than one-fourth of the "aligned" value. Thus the $(BH)_{\text{max}}$ values obtained for isotropic nanocomposite magnets thus far are limited to about 25 MGOe [200 kJ/m^3], which is about 40% of the best aligned $\text{Nd}_2\text{Fe}_{14}\text{B}$ -type magnets. It has been possible to produce $L1_0$ -based single phase thin-film platelets with excellent alignment and coercivity, but this has been possible so far for *two-phase* nanostructures only in our recent work.

We are investigating experimentally and by model calculations two-phase nanostructures of hard $L1_0$ -ordered FePt and soft iron-rich fcc Fe-Pt. The thin films are produced by epitaxial co-sputtering onto MgO (001) and have variable thicknesses. They form two-phase dots that cover a large fraction of the surface and studies of exchange coupling between the dots are underway. X-ray diffraction and TEM show that the c -axis of the phase FePt is aligned in the direction normal to the film plane.

We intend to further study ultrahard magnets based on the $L1_0$ structure by pursuing $\text{Fe}_{65}\text{Co}_{35}$ as the major component of the soft phase. This alloy has the largest known polarization value, $J_s = 24.5 \text{ kG} = 2.45 \text{ T}$. The structure sought will consist of $L1_0$ (Fe, Co)Pt as the hard phase, and fcc Fe-Co-Pt as the soft phase. Properties that may be

achievable include $J_s \approx 1.8$ T, $B_c \approx 1.0$ T and an energy product greater than 60 MGOe (480 kJ/m^3). We will use micromagnetic modeling to guide the nanostructuring.

Additional systems to be studied include (MnBi:Fe):Fe-Co nanocomposites and SmCo_5 nanoparticles. The latter will be prepared in a newly designed cluster-deposition system enabling alignment of ordered clusters before deposition on the substrate.

- **Selected Recent DOE Publications (one page)**

1. Y. Liu, T.A. George, **Ralph Skomski** and **D.J. Sellmyer**, "Aligned and Exchange-Coupled FePt-Based Films," *Appl. Phys. Lett.* (submitted).
2. P. Kharel, **R. Skomski**, P. Lukashev, R. Sabirianov, and **D.J. Sellmyer**, "Spin Correlations and Kondo Effect in a Strong Ferromagnet," *Phys. Rev. B* (in press).
3. P. Kharel, P. Thapa, P. Lukashev, R.F. Sabirianov, E. Y. Tsybal, **D.J. Sellmyer**, and B. Nadgorny, "Transport Spin Polarization of High Curie Temperature MnBi Films," *Phys. Rev. B* **83**, 024415 (1-6) (2011).
4. B. Balamurugan, **R. Skomski**, X. Li, S. Valloppilly, J. Shield, **G.C. Hadjipanayis**, **D.J. Sellmyer**, "Cluster Synthesis and Direct Ordering of Rare-Earth Transition-Metal Nanomagnets," *Nano Lett.* **11**, 1747-1752 (2011).
5. T. Mukherjee, S. Michalski, **R. Skomski**, **D.J. Sellmyer**, C. Binek, *et al.*, "Overcoming the Spin-Multiplicity Limit of Entropy by Means of Lattice Degrees of Freedom: A Minimal Model," *Phys. Rev. B* **83**, 214413 (2011).
6. P. K. Sahota, **R. Skomski**, A. Enders, **D.J. Sellmyer**, and A. Kashyap, "Anisotropy of Zigzag Chains of Palladium," *J. Appl. Phys.* **109**, 07E322 (1-3) (2011).
7. B. Balasubramanian, **R. Skomski**, X.Z. Li, V.R. Shah, **G.C. Hadjipanayis**, J.E. Shield, and **D.J. Sellmyer**, "Magnetism of Cluster-Deposited Y-Co Nanoparticles," *J. Appl. Phys.* **109**, 07A707 (1-3) (2011).
8. A. Kashyap, **R. Skomski**, P. Manchanda, J.E. Shield, and **D.J. Sellmyer**, "Layered Transition-Metal Permanent-Magnet Structures," *J. Appl. Phys.* **109**, 07A714 (1-3) (2011).
9. V. Sharma, P. Manchanda, **R. Skomski**, **D.J. Sellmyer**, and A. Kashyap, "Anisotropy of Heavy Transition Metal Dopants in Co," *J. Appl. Phys.* **109**, 07A727 (1-3) (2011).
10. M.A. Peck, Y. Huh, **R. Skomski**, R. Zhang, P. Kharel, M.D. Allison, **D.J. Sellmyer**, and M.A. Langell, "Magnetic Properties of NiO and (Ni,Zn)O Nanoclusters," *J. Appl. Phys.* **109**, 07B518 (1-3) (2011).
11. P. Kharel, **R. Skomski**, and **D.J. Sellmyer**, "Spin Correlations and Electron Transport in MnBi: Au Films," *J. Appl. Phys.* **109**, 07B709 (1-3) (2011).
12. N.G. Akdogan, **G.C. Hadjipanayis**, **D.J. Sellmyer**, "Novel $\text{Nd}_2\text{Fe}_{14}\text{B}$ Nanoflakes and Nanoparticles for the Development of High Energy Nanocomposite Magnets," *Nanotechnology* **21**, 295705 (2010); N.G. Akdogan, **G.C. Hadjipanayis**, **D.J. Sellmyer**, "Novel $\text{Nd}_2\text{Fe}_{14}\text{B}$ Nanoflakes and Nanoparticles for the Development of High Energy Nanocomposite Magnets," *Nanotechnology* **21**, 339802 (2010) (figure correction).
13. **R. Skomski**, A. Kashyap, A. Solanki, A. Enders, and **D.J. Sellmyer**, "Magnetic Anisotropy in Itinerant Magnets," *J. Appl. Phys.* **107**, 09A735 (1-3) (2010).
14. **R. Skomski**, Y. Liu, J. E. Shield, **G.C. Hadjipanayis**, and **D.J. Sellmyer**, "Permanent Magnetism of Dense-Packed Nanostructures," *J. Appl. Phys.* **107**, 09A739 (1-3) (2010).

15. P. Kharel, **R. Skomski**, R.D. Kirby, and **D.J. Sellmyer**, “Structural, Magnetic and Magneto-Transport Properties of Pt-Alloyed MnBi Thin Films,” *J. Appl. Phys.* **107(9)**, 09E303-1-09E303-3 (2010).
16. B. Balamurugan, **R. Skomski**, **D.J. Sellmyer**, “Magnetic Clusters and Nanoparticles,” in *Nanoparticles: Synthesis, Characterization and Applications*, Eds. R.S. Chughule, R.V. Ramanujan (American Scientific Publishers, California, 2010), pp. 127-162.
17. E. Kockrick, **R. Skomski**, **D.J. Sellmyer**, *et al.*, “Mesoporous Ferromagnetic MPt@Silica/Carbon (M=Fe, Co, Ni) Composites as Advanced Bifunctional Catalysts,” *Chemistry of Materials* **22**, 1624-1632 (2010).

Session 3

Low-Dimensional Systems

Project Title:

DE-FG02-05ER46215: Investigation of the Quantum Limit Transport Phenomena in Graphene

Principal Investigator: **Philip Kim**

Institution: Department of Physics, Columbia University

Email: pk2015@columbia.edu

Project Scope

In the last three years, under the DOE BES support on the project “Investigation of the Quantum Limit Transport Phenomena in Graphene,” we have performed electrical and thermoelectrical transport measurements in order to study the electronic structure of this exotic low-dimensional system in the quantum limit. During this time, we have developed experimental processes to create extremely high quality graphene samples by suspending the active channel area, to fabricate Corbino devices to investigate bulk transport, and to create thermoelectric devices for entropy transport in graphene. In particular, our major DOE- supported research achievements are: (i) the production of ultrahigh mobility graphene samples; (ii) investigation of thermoelectric and magnetothermoelectric effects in graphene; (iii) the discovery of magnetic field effect induced symmetry-breaking in bilayer graphene; (iv) the discovery of the fractional quantum Hall effect (FQHE) in graphene; (v) investigation of bulk transport in magnetically induced insulating state using a Corbino geometry; and (vi) the observation of a multicomponent FQHE in graphene. The DOE funding has been the major source of support for carrying out these projects in the PI’s group.

Recent Progress

Ultrahigh mobility graphene production: We have demonstrated the fabrication of electrically contacted suspended graphene and have achieved the best reported mobility of carriers in graphene. Besides opening new avenues for studying the intrinsic physics of Dirac fermions, this improvement demonstrates the dominant role played by extrinsic scattering in limiting the transport properties of unsuspended graphene samples. From this result, we infer that much of the scattering in traditional graphene-on-silica devices is not intrinsic but rather results from the interaction with the substrate underlying the graphene. Near room temperature we observe a $\sim 120,000 \text{ cm}^2/\text{Vs}$ mobility, higher than in any known semiconductor.

Thermoelectric and magnetothermoelectric transport in graphene: We investigated thermoelectric transport in graphene. The conductance and thermoelectric power (TEP) of graphene is simultaneously measured using a microfabricated heater and thermometer electrodes. The sign of the TEP changes across the charge neutrality point as the majority carrier density switches from electron to hole. The gate dependent conductance and TEP exhibit quantitative agreement with the semiclassical Mott relation. In the QH regime at high magnetic field, the tensor components of the TEP show quantized behavior. Because of its sensitivity to electron-hole asymmetry, TEP measurements provide a complementary experimental tool to further study quantum transport phenomena in high mobility graphene samples.

Symmetry breaking of the zero energy Landau level in bilayer graphene: We reported on the eightfold symmetry-breaking of the zero-energy Landau level in bilayer graphene systems in a strong magnetic field. We found that this unusual zero-energy quantum Hall octet, while intact at lower magnetic fields, splits up completely into eight separate Landau levels when exposed to 35

T. In this high-field regime, the eightfold degeneracy in the zero-energy Landau level is completely lifted, exhibiting new quantum Hall states. In a single particle picture, among the zero-energy BLG octet degeneracy, the Zeeman effect can lift the real spin degeneracy, however the remaining quartet symmetry cannot be lifted by a magnetic field. Therefore, the observed spontaneous octet symmetry-breaking at high magnetic fields strongly suggests the role of many-body effects near the charge neutral point in BLG.

Observation of the fractional quantum Hall effect in graphene: We have demonstrated the fabrication of ultra-high mobility graphene devices by suspending the samples above the substrate. In these ultraclean suspended graphene devices, we observed a signature of the FQHE, indicated by plateaus in the two-terminal conductance. We also have fabricated multi-terminal suspended graphene devices with better designed voltage probe contacts which minimize mechanical deformation of the samples and suppress the hot spot formation. In these devices we observe fully-developed integer quantum Hall states appearing at magnetic fields as low as 2 T. By measuring the temperature dependence of these resistance minima, the energy gap for the 1/3 fractional state in graphene is determined to be ~ 20 K at 14 T.

Corbino Device Measurement of Graphene Quantum Hall Effect: We investigated the spin character of the $\nu = 0$ QH state in monolayer graphene by measuring the conductance of this state as a function of in-plane magnetic field. Our experiments involved both two-terminal measurements of high-mobility suspended graphene, where the insulating character of both the bulk and the edges are measured in parallel, and measurements of on-substrate graphene using a Corbino probe geometry, where the bulk conductance can be measured independently of any edge state effects.

Multicomponent Fractional Quantum Hall Effect in Graphene: Exploiting our recent success of fabricating high quality graphene devices using a hexagonal boron nitride substrate, we have just started to investigate magneto-transport of these devices. The Hall mobility at high density is $\sim 30,000$ cm²/Vs; the charged-impurity mobility, which dominates at low density, is in excess of 100,000 cm²/Vs as determined by fitting straight lines to the linear portion of the conductivity; the charge inhomogeneity, estimated from the resistivity peak width at the charge neutrality point (CNP), is of order 10^{10} cm⁻². All three metrics indicate this sample to be of exceptionally high quality and consistent with previous measurements of similar graphene/h-BN devices at low magnetic fields. We observe an unexpected hierarchy in the emergent FQHE states that may be explained by strongly interacting composite Fermions with full SU(4)-symmetric underlying degrees of freedom. The FQHE gaps are measured from temperature dependent transport to be up to 10 times larger than in any other semiconductor system. The remarkable strength and unusual hierarchy of the FQHE described here provides a unique opportunity to probe correlated behavior in the presence of expanded quantum degrees of freedom.

Future Plan

Building on the successful progress described in the previous section, we plan to focus our interest on *investigation of the role of electron interactions in graphene* as described below:

High mobility homogeneous graphene sample production: In order to reach the quantum transport limit in graphene, obtaining high mobility, homogeneous samples is crucial. In particular, the study of many-body correlations near the charge neutrality point, where the electron-electron (e-e) interactions become stronger, is only possible in highly homogeneous

samples. Using high quality single crystals of h-BN, we have recently demonstrated the preparation of well-controlled atomic layers of h-BN using mechanical exfoliation techniques similar to graphene preparation. The method is based on extremely thin crystalline layered insulators that can be prepared with very high quality, and atomically controlled, thickness. For further improvement of sample preparation and developing complex graphene hybrid structures, we can utilize multiple co-laminating processes. We will further improve the quality of the interface by controlling the environment, performing the co-lamination process in a glove box with inert gas.

Searching for highly correlated fractional quantum Hall effect: The possibility of discovering correlated electronic states in graphene and its bilayer, including novel many-body ground states and their unique elementary excitations, provides the major motivation for this part of the proposal. Monolayer and bilayer graphene differ from conventional 2D electronic systems such as GaAs/AlGaAs quantum wells in two major ways. First, as we discussed in introduction section, graphene support an expanded spin-like internal degeneracy (termed pseudospin) in comparison with most other 2D electronic systems. Second, the orbital structure of the wavefunctions in graphene and its bilayer are different, leading to different effective interactions within a partially filled Landau level. In this section, we discuss ongoing and future experiments aimed at novel behavior arising from these two differences: SU(4) quantum Hall ferromagnetism with spin/pseudospin textured excitations and potential non-abelian fractional quantum Hall states in bilayer graphene.

Electron correlation in double layer graphene nanostructures:

Our recently demonstrated ability to transfer graphene without degradation of sample quality, together with high-quality BN, a complimentary wide band gap dielectric, opens the possibility of realizing novel graphene-based device architectures by alternately stacking the two materials.

Interaction induced thermoelectric transport in graphene: Inheriting our successful demonstration of thermopower (TEP) and magneto-thermopower (MTEP) measurement in graphene, we plan to use TEP and MTEP measurement to probe the e-e interactions in high quality graphene samples with reduced disorder. This includes the the electron-hole plasma at high temperatures, which is described by hydrodynamics, and MTEP in the FQH regime.

Electron transport in graphene at extreme charge density: Another potential direction for the study of e-e interactions in graphene is the investigation of single and multilayer graphene samples in the extreme carrier density limit, where Fermi energies reach values beyond $E_F > 1$ eV, corresponding to carrier densities of $n > 10^{14}$ cm⁻². In this “metallic” regime graphene’s properties are expected to be strongly modified because of trigonal warping and the increased size of the Fermi surface, as well due to additional high energy subbands in multilayer graphene.

Magnetic moment measurement in graphene: Thermodynamic bulk probes of the QHE, such as magnetization, provide complementary information to that obtained from transport measurements. Exploiting the mechanical stability of graphene, we will develop a novel tool for measuring magnetization in graphene using a suspended sample as its own torque magnetometer.

Publications acknowledged the current DOE grant

- K. I. Bolotin, K. J. Sikes, Z. Jiang, G. Fundenberg, J. Hone, P. Kim, and H. L. Stormer, Ultrahigh electron mobility in suspended graphene, Solid State Communications **146**, 351-355 (2008).

- K. I. Bolotin, K. J. Sikes, J. Hone, H. L. Stormer and P. Kim, Temperature dependent transport in suspended graphene, *Phys. Rev. Lett.* **101**, 096802 (2008).
- Y. M. Zuev, W. Chang, and P. Kim, Thermoelectric and magnetothermoelectric transport measurements of graphene, *Phys. Rev. Lett.* **102**, 096807 (2009).
- Y. Zhao, P. Cadden-Zimansky, Z. Jiang and P. Kim, Symmetry breaking of the zero energy Landau level in bilayer graphene, *Physical Review Lett.* **104**, 066801 (2010)
- K. I. Bolotin, F. Ghahari, M. D. Shulman, H. L. Stormer and P. Kim, Observation of the Fractional Quantum Hall Effect in Graphene, *Nature* **462**, 196-199 (2009).
- F. Ghahari, Y. Zhao, P. Cadden-Zimansky, K. Bolotin, P. Kim, Measurement of the $\nu = 1/3$ fractional quantum Hall energy gap in suspended graphene, *Phys. Rev. Lett.* **106**, 046801 (2011)
- C. R. Dean, A. F. Young, P. Cadden-Zimansky, L. Wang, H. Ren, K. Watanabe, T. Taniguchi, P. Kim, J. Hone, K.L. Shepard, Multicomponent fractional quantum Hall effect in graphene, arXiv:1010.1179; *Nature Physics*, *in press*.

Project Title: Microwave- and terahertz- photo-excited transport in low dimensional electron systems

Principal Investigator: Ramesh G. Mani

Institution: Georgia State University, Atlanta, GA

Email: rmani@gsu.edu; mani.rg@gmail.com

Project Scope: This experimental project aims to compare low temperature transport- and photo-excited transport in low dimensional electronic systems based on high mobility GaAs/AlGaAs heterostructures and sheets of carbon known as graphene. The motivation for the project stems from the understanding that subjecting materials to conditions far from equilibrium can lead to otherwise-unattainable properties, and that a comparative study of the dark and photo-excited transport can serve as a path to identifying the non-equilibrium steady-state properties of such systems. Some interesting examples of emergent behavior in a driven, steady-state, non-equilibrium system are the radiation-induced zero-resistance states and associated magneto-resistance oscillations in the quasi two dimensional GaAs/AlGaAs system, where microwave and terahertz photoexcitation helps to produce giant magneto-resistance oscillations, with vanishing resistance states at the oscillatory resistance minima at liquid helium temperatures. Such zero-resistance states in the quasi two dimensional electron system (2DES) exhibit activated transport without, remarkably, a concomitant quantum Hall effect. This project includes an in-depth study of the radiation-induced transport in the GaAs/AlGaAs system and a search for related phenomena in graphene. Such a study of the microwave- and terahertz- photo-excited transport is also expected to identify new types of radiation sensors for the microwave and terahertz bands, spectral bands including many potential future applications.

Recent Progress:

Linear-polarization-sensitivity of the radiation-induced magneto-resistance oscillations in GaAs/AlGaAs devices: The microwave and terahertz radiation-induced magneto-resistance oscillations in the 2DES are characterized by B^{-1} periodic oscillations in the diagonal magnetoresistance, R_{xx} , of the 2DES at cryogenic temperatures, T . These R_{xx} oscillations show a strong sensitivity to T and the microwave power, P , at modest P . Proposed mechanisms for such oscillations include radiation-assisted indirect inter-Landau-level scattering by phonons and impurities (the displacement model), non-parabolicity effects in an ac-driven system (the non-parabolicity model), a radiation-induced steady state non-equilibrium distribution function (the inelastic model), and the periodic motion of the electron orbit centers under irradiation (the radiation driven electron orbit model).

Under typical experimental conditions, some or all of these mechanisms can contribute towards sufficiently large amplitude radiation-induced magneto-resistivity oscillations such that, theoretically, at the oscillatory minima, the magneto-resistivity is able to take on negative values. According to theory, negative resistivity triggers, however, an instability in the uniform current distribution, leading to current domain formation, and the experimentally observed zero-resistance states.

Although these theories suggest radiation-induced magneto-resistance oscillations, they differ with respect to their predictions on, for example, the microwave polarization sensitivity in the radiation-induced oscillations. Here, the displacement model predicts that the oscillation-amplitude depends on whether the microwave electric field, E_{ω} , is parallel or perpendicular to the dc -electric field, E_{DC} . On the other hand, the inelastic model unequivocally asserts polarization insensitivity to the radiation-induced magneto-resistance oscillations. Polarization immunity, in the radiation-driven electron orbit model, depends parametrically upon the damping factor, γ , exceeding the frequency of the microwave field. Finally, the non-parabolicity model suggests a perceptible polarization sensitivity for linearly polarized microwaves, while indicating the absence of such oscillations for circularly polarized radiation. Here, we investigate the effect of rotating, *in-situ*, the polarization of linearly polarized microwaves relative to long-axis of Hall bars. Strikingly, we find that the amplitude of the radiation-induced magneto-

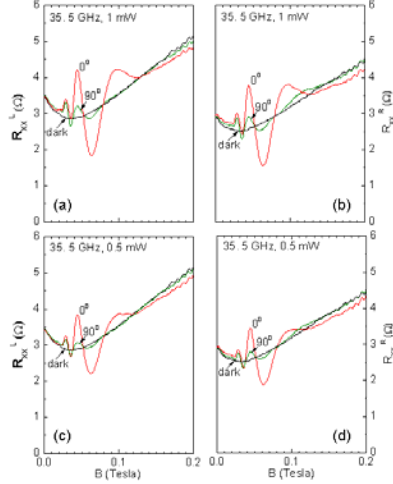


Figure 1. Microwave-induced magneto-resistance oscillations in R_{xx} at 1.5 K are shown at $f = 35$ GHz for $P = 1$ mW in panels (a) and (b) and for $P = 0.5$ mW in panels (c) and (d). The R_{xx} measured on the left (right) side of the Hall bar, see Fig. 1, is shown as R_{xx}^L (R_{xx}^R). Each panel shows a set of three traces: a dark curve (black), a curve (red) obtained at $\theta = 0^\circ$, a trace (green) obtained at $\theta = 90^\circ$. All panels exhibit reduced amplitude radiation-induced magneto-resistance oscillations at $\theta = 90^\circ$.

amplitude of the resistance oscillations are remarkably responsive to the relative orientation between the microwave antenna and the current-axis in the specimen, indicating a striking linear polarization sensitivity in the radiation-induced magnetoresistance oscillations.

Microwave induced electron heating in the regime of the radiation-induced magnetoresistance oscillations: Here, we examine quantitatively the nature of electron heating due to microwave photo-excitation in the high mobility two dimensional electron systems by exploring the influence of microwave photoexcitation on the amplitude of Shubnikov-de Haas (SdH) oscillations in a regime where the cyclotron frequency, ω_c , and the microwave angular frequency, ω , satisfied $2\omega \leq \omega_c \leq 3.5\omega$. Specifically, the electron heating due to microwave excitation was extracted by comparing the damping of the amplitude of Shubnikov-de Haas oscillations due to microwave excitation with the damping of the same oscillations due to bath temperature changes in the dark, see Fig. 2. In good agreement with theoretical predictions, the results indicated modest

resistance oscillations are remarkably responsive to the relative orientation between the linearly polarized microwave electric field and the current-axis in the specimen.

Figure 1 exhibits the diagonal resistance R_{xx} vs. B at $f = 35.5$ GHz. Fig. 1(a) and (b) show the results obtained at a source-power $P = 1$ mW, while Fig. 1(c) and(d) show the same obtained at $P = 0.5$ mW. Here, R_{xx}^L and R_{xx}^R represent the measurement on the left (L) and right (R) sides of the Hall bar device. Each panel of Fig. 1 includes three traces: A dark trace (in black) obtained in the absence of microwave photoexcitation. A $\theta = 0^\circ$ trace in red, where the MW antenna is parallel to the long-axis of the Hall bar. Finally, the panels of Fig. 1 also exhibit, in green, the $\theta = 90^\circ$ traces, where the MW antenna is perpendicular to the long-axis of the Hall bar. A remarkable feature is observed when one compares the red (0°) and green (90°) traces within any single panel of Fig. 1. Such a comparison indicates that the amplitude of the radiation-induced magneto-resistance oscillations is reduced at the $\theta = 90^\circ$ MW antenna orientation. Finally, the period and the phase of the radiation-induced magnetoresistance oscillations are unchanged by MW-antenna rotation; this feature is readily apparent in Fig. 1. Thus, we find that, although, the frequency and the phase of the photo-excited magneto-resistance oscillations are insensitive to the polarization, the

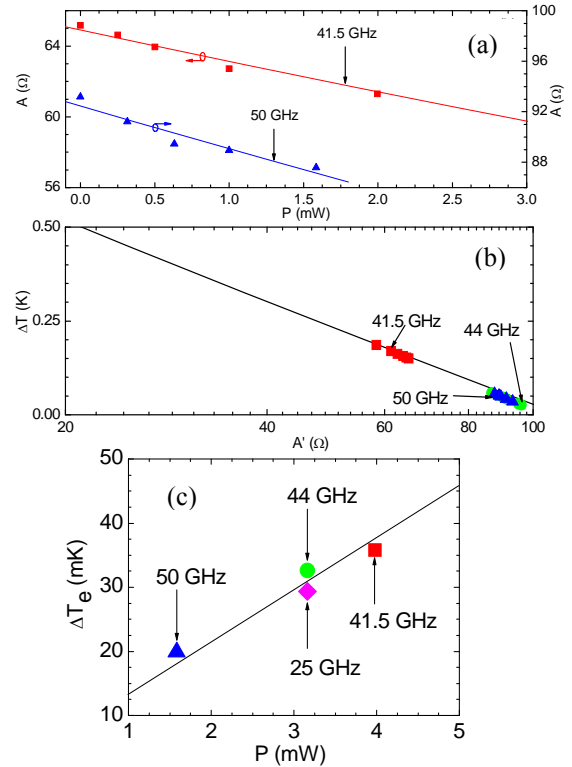


Figure 2. (a) SdH oscillation amplitude A vs. P is shown for 41.5GHz at 1.6K and 50GHz at 1.5K. (b) This panel illustrates the effect of T (Solid line) and P (Solid symbols) on A , the amplitude of SdH oscillations. Panel (c) shows a plot of maximum ΔT_e vs peak- P (solid symbols), with a line to guide the eye.

heating, i.e., $\Delta T/\Delta P \sim 9\text{mK/mW}$, over the examined regime.

Future Plans:

*Photoexcited transport in epitaxial graphene:** Graphene refers to the one atom thick honeycomb lattice of carbon atoms that is rolled up into carbon nanotubes and stacked into layers in graphite. Graphene constitutes a truly two-dimensional electronic system because the electronic wave function is confined to a single atomic layer, unlike in other planar (quasi) two-dimensional electronic systems. The linear dispersion relation in zero-gap semiconductors usually associated with relativistic particles provides for additional interesting electronic properties, such as the anomalous quantum Hall effect. It is also possible to open up a bandgap in graphene ribbons by size quantization. Finally, this material promises

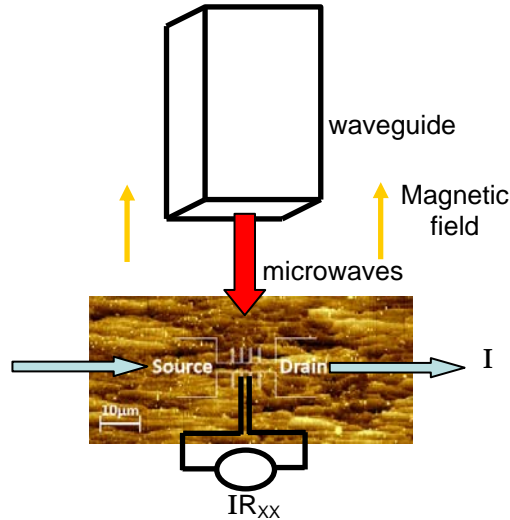


Figure 3. A schematic of the measurement on epitaxial graphene is superimposed on an AFM image of the material.

extraordinarily high mobility at room temperature, which can potentially be exploited for high speed device applications. Due to these and other interesting properties, graphene is now viewed as a complementary material to Silicon for future electronics. Yet, the realization of large area graphene films is a technological challenge. Epitaxial graphene, which evolves from the thermal decomposition of the surface layers of SiC, is thought to be a route to realizing large area graphene films. Here, we carry out a transport study of epitaxial graphene under microwave photo-excitation to 50 GHz, and have obtained some preliminary results. Furnace grown epitaxial graphene films are realized by the thermal decomposition of 4H insulating SiC. The graphene realized by this method is overlaid on steps of the underlying SiC substrate. It is characterized by a carrier density of 10^{13} cm^{-2} . Small Hall bar devices with Au/Pd contacts are fabricated on the c-face of this material by e-beam lithography. Transport measurements of the type shown in Fig. 3 are being carried out at liquid Helium temperatures under

microwave photo-excitation. Some preliminary results are available.

*Work is carried out in collaboration with J. Hankinson, C. Berger, and W. de Heer of the School of Physics, Georgia Institute of Technology.

Remote Sensing of radiation-induced transport: In these experiments, we hope to correlate transport measurements in GaAs/AlGaAs with concurrent “remote sensing” measurements of the 2DES, where the remote sensing is carried out using microwave sensors located at a distance from the 2DES. Such measurements will serve to correlate the reflection and absorption properties of the 2DES with the transport observations.

Microwave photo-voltaic effect in the regime of the radiation-induced magneto-resistance oscillations in the GaAs/AlGaAs 2DES: The photo-voltaic effect induced by microwave radiation in the 2DES in a perpendicular magnetic field has been considered both theoretically and experimentally. As mentioned above, microwave photo-excitation produces inverse-B periodic oscillations in the diagonal resistance that lead into novel zero-resistance states in the low temperature limit. The photo-excitation also produces a concomitant photo-voltage effect, which includes strong fluctuations and is fully reproducible. The photo-voltage fluctuations have well defined magnetic field symmetry although they are expected to be enhanced in the vicinity of cyclotron resonance. This work will examine this microwave and terahertz photovoltaic effect and correlate the results with magneto-transport.

List of Publications:

- “Evolution of Shubnikov-de Haas oscillations under photoexcitation in the regime of the radiation-induced zero-resistance states,” R. G. Mani, *Physica E* 40, 1178 (2008).
- “Narrow-band radiation-sensing in the Terahertz and microwave bands using the radiation-induced magnetoresistance oscillations,” R. G. Mani, *Appl. Phys. Lett.* 92, 102107 (2008).
- “Band-limited radiation-sensing using the radiation-induced magneto-resistance oscillations,” R. G. Mani, *Intl. J. Mod. Phys. B* 23, 2703-2707 (2009).
- “Phase study of oscillatory resistances in microwave irradiated and dark GaAs/AlGaAs devices: Indications of an unfamiliar class of integral quantum Hall effect,” R. G. Mani, W. B. Johnson, V. Umansky, V. Narayanamurti, and K. Ploog, *Phys. Rev. B* 79, 205320 (2009).
- “Nonlinear growth with the microwave intensity in the radiation-induced magnetoresistance oscillations,” R. G. Mani, C. Gerl, S. Schmult, W. Wegscheider, and V. Umansky, *Phys. Rev. B* 81, 125320 (2010).
- “Transport study of Berry’s phase, the resistivity rule, and quantum Hall effect in graphite,” A. Ramanayaka and R. G. Mani, *Phys. Rev. B* 82, 165327 (2010).
- “Sublinear radiation power dependence of photoexcited resistance oscillations in two dimensional electron systems,” J. Inarrea, R. G. Mani, and W. Wegscheider, *Phys. Rev. B* 82, 205321 (2010).
- “Hall effects in doubly connected specimens,” A. Kriisa and R. G. Mani, *IEEE Trans. In Nanotechnology* 10, 179 (2011).
- “Comparative study of microwave radiation-induced magnetoresistance oscillations in GaAs/AlGaAs devices,” R. G. Mani, W. Wegscheider, and V. Umansky, *IEEE Trans. In Nanotechnology* 10, 170 (2011).
- “Microwave induced electron heating in the regime of the radiation-induced magnetoresistance oscillations,” A. Ramanayaka, R. G. Mani, and W. Wegscheider, *Phys. Rev. B* 83, 165303 (2011).
- “Observation of linear polarization sensitivity in the radiation-induced magneto-resistance oscillations,” R. G. Mani, A. Ramanayaka, and W. Wegscheider, *Phys. Rev. B* (accepted for publication).
- “Linear polarization rotation study of the radiation-induced magnetoresistance oscillations,” A. N. Ramanayaka, R. G. Mani, J. Inarrea, and W. Wegscheider, *Phys. Rev. B* (Submitted for publication).
2011 APS March Meeting Abstracts of Work-in-progress:
- “Transport study under microwave photoexcitation in epitaxial Graphene,” R. G. Mani, J. Hankinson, C. Berger, and W. de Heer, *Bull. Am. Phys. Soc.* 56, Abstract# x11.00004, March 24, 2011
- “Scanning Tunneling Microscope study of Atomic steps in Gold films on Muscovite Graphite,” Olesya Sitnikova and R. G. Mani, *Bull. Am. Phys. Soc.* 56, Abstract# W21.00004, March 24, 2011
- “Microwave induced electron heating in the regime of the radiation-induced magnetoresistance oscillations,” A. Ramanayaka, R. G. Mani, and W. Wegscheider, *Bull. Am. Phys. Soc.* 56, Abstract# x11.00003, March 24, 2011
- “Remote sensing of transport in microwave photo-excited magnetoresistance oscillations in the GaAs/AlGaAs system,” Tianyu Ye, G. Chand, A. Ramanayaka, R. G. Mani, and W. Wegscheider, *Bull. Am. Phys. Soc.* 56, Abstract# x11.00006, March 24, 2011
- “Microwave photo-voltaic oscillations in the GaAs/AlGaAs system,” G. Chand, T. Ye, A. Ramanayaka, R. G. Mani, and W. Wegscheider, *Bull. Am. Phys. Soc.* 56, Abstract# x11.00011, March 24, 2011.

Probing the Electronic Structure and Dynamics of Low-Dimensional Condensed-Matter Systems Using Femtosecond Probes

Richard Osgood,* Peter Johnson,** and Andy Millis***

*osgood@columbia.edu

Departments of Applied Physics and Applied Mathematics, Columbia University

** pdj@bnl.gov,

Departments of Condensed Matter and Materials Science, Brookhaven National Laboratories

*** millis@phys.columbia.edu,

Department of Physics, Columbia University

ABSTRACT

Scope

This program has the goal of understanding the physics of emergent properties in artificially nanostructured materials. In our case, emergent behavior in complex systems is due to the role of confinement both lateral and vertically in evolving new and unexpected materials response. Our focus is emergent properties in *surface* systems. Surfaces enable the use of the powerful tool of momentum-resolved photoemission (ARUPS) for probing electron motion and the tuning of a system by altering of the surface composition, reconstruction, or confinement. In addition, our program also will have a growing emphasis on measuring time-dependent dynamic phenomena. Recent instrumentation upgrades at Columbia and Brookhaven enhance our measurements, using these advanced techniques. We will seek to answer such questions as:

- Are there new electronic phases near surfaces in one-atom-wide wires or in nanoparticles, and can theoretical constructs be developed to examine such systems?
- What are the emergent dynamic properties arising from lateral confinement in 1 and 2D confined systems?
- Can we probe many-body effects in exfoliated freestanding graphene?
- What are the limits to synthesizing large-scale uniform nanoarrays, for area probes such as photoemission?

Our program is designed to take maximum advantage of the collaborations in condensed matter physics, which we have developed within the last few years. These include, for example, experimental techniques developed at Columbia for preparing monolayer and thin-multilayer exfoliated single crystal samples, for probing with microRaman scattering probes, and for fabricating exfoliated and electronically tunable sample structures. In addition, our program leverages the numerous collaborations developed at BNL in STM, nanofabrication, and synchrotron measurements and at the third-generation synchrotron source, ELETTRA, in Trieste. Our focus in ultrafast laser photoemission also seeks to utilize the complementary instrumentation at BNL and at Columbia University for examining high-energy-resolution and high-temporal-resolution photoemission, respectively.

Recent Progress

The excited-state properties of condensed-matter systems have traditionally been an area of much interest but not fully explored. Excited states play a role in many areas of materials physics from ion or X-ray irradiation to carrier transport under high bias. Our program examines the electronic structure and dynamics of excited low-dimensional nanosystems. These surfaces can couple into a variety of elementary excitations and even change surface phases. While we can

and have examined 1D (see Refs. 1, 3, 6, and 10) and 2D (Refs. 2, 4, 5, and 7-9) systems such as atomic wires using strongly biased tunneling microscopy (see **Fig. 1**), we have recently explored using nonlinear femtosecond photoemission to excite and probe states many eV above the Fermi level in 1D nanostructured surfaces and in monolayer epitaxial graphene.

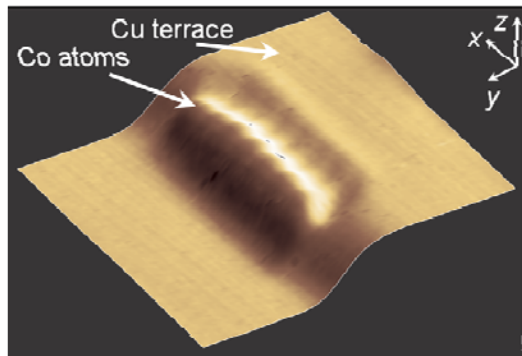


Fig. 1. Single-atom wire of Co on Cu(775).

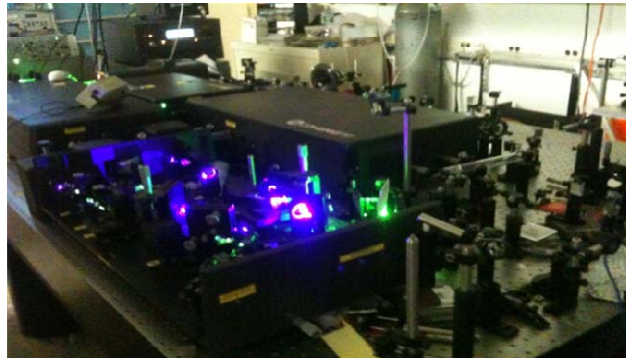


Fig. 2. Two-photon photoemission laser system at Columbia University.

- Specifically, for example, our work has used femtosecond laser sources (see **Fig. 2**) to probe the excited states at the interfaces of epitaxial graphene on Ir(111) in order to understand how transport occurs on the graphene surfaces and at the metal/graphene interface. Both the photoemission linewidth and the directly measured temporal lifetime using pump-probe photoemission measurements provide information on the surface scattering and nature of the excited state lifetime. Finally our studies have yielded information on the growth of graphene from submonolayer islands. Thus our results show that electrons can be trapped on nanometer-scale graphene surface islands, where trapping is shown by upward shifts in the excited electronic states. (Ref. 9).
- In addition, we have demonstrated also that photoemission with this intense ultrafast laser source could be used to perform photoemission from bulk states as far as $\sim 3\text{-}5\text{eV}$ above E_F on single-crystal metals both on planar flat surfaces and nanostructured surfaces. In this case, we show that using wavelength tuning, we can map out the excited state structure of states on either flat or vicinal-cut surfaces with regular step arrays formed by the monolayer steps. In our future work, we will use our normally unoccupied state photoemission to examine crystals of correlated electron materials and graphene interlayer states and excited state dynamics of these systems. (Refs. 5 and 8).
- Finally we have completed an initial study of the electronic structure of small samples of free-standing exfoliated monolayer graphene. This crystal is an ultrathin flexible membrane, which exhibits out-of-plane deformation or corrugation. Our measurements have developed a technique to measure the band structure of such free-standing graphene by angle-resolved photoemission. Our results show that a major issue is to unfold the fact that photoelectron coherence is limited by crystal corrugation. However, we have shown that by combining surface morphology measurements of the graphene roughness with angle-resolved photoemission, energy-dependent quasiparticle lifetime and band-structure measurements can be extracted; see **Fig. 3**. Our measurements use our development of an analytical formulation for relating the crystal corrugation to the photoemission linewidth. With this approach our angle-resolved photoemission spectroscopy measurements have shown that, despite significant

deviation from planarity of the crystal, the electronic structure of exfoliated suspended graphene is nearly that of ideal, undoped graphene; we also have measured the Dirac point to be within 25 meV of E_F . Further, we have shown that suspended graphene behaves as a marginal Fermi liquid, with a quasiparticle lifetime that scales as $(E - E_F)^{-1}$. See Ref. 2, 4 and 7 for more details.

Future plans

Our future plans for the next year are as follows:

- *Quasiparticle Dynamics on “Tuned” Step Arrays:* We will examine the emergence of new dynamics properties with confinement using nanoarrays. Ultrafast pump/probe measurements will be used to study lifetime in nanosystems with the goal being to understand the interrelation of dynamics and confinement in artificially fabricated nanosystems. Measurements will use both ultrafast and ultrahigh-energy-resolution ARPES techniques to examine dynamics processes such as scattering rates versus parallel momentum and the corresponding electronic structure of the arrays, respectively.
- *Kondo and Magnetic Physics on Stepped Surfaces - Tuning Lateral Confinement and Atom Placement:* We have formed atom chains of Co at step edges or precisely space neighboring atoms using adjacent step edges and are examining the resulting structures for either magnetic or Kondo interactions. Our experiments, using vicinal step arrays will examine the coupling of the surface and bulk substrate electronic states with those of the chains. We have carried out measurements of the STS spectra as a function of temperature at the BNL-CFN low-temperature STM (with the Sutter Group). We are currently analyzing this data and, in conjunction with many-body theory, are examining the interrelation of spin and structure in the chain. We are preparing two papers in this area; Ref. 10 is on the verge of being submitted.

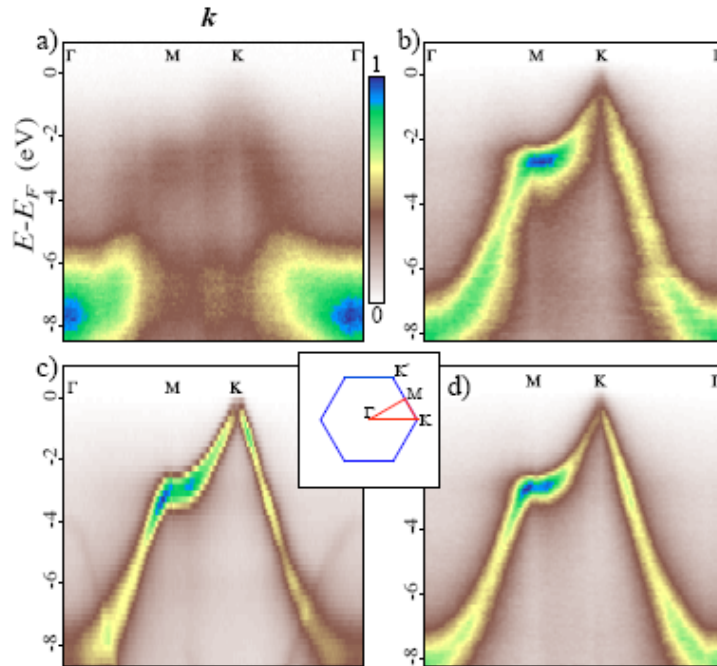


Fig 3. ARPES data along symmetry directions in Brillouin zone for graphene and graphite. (a) SiO₂ supported graphene ($\hbar\omega = 90$ eV). (b) Suspended graphene ($\hbar\omega = 84$ eV). (c) Kish graphite ($\hbar\omega = 90$ eV). (d) Suspended graphene ($\hbar\omega = 50$ eV). Inset shows 2D graphene Brillouin zone.

- *Nanoprobng of Electronic Structure of 2D systems:* Probing the photoemission of free-standing graphene and other free-standing 2D systems is a continuing objective of our research. Our results to date show clearly and for the first time that high quality photoemission data can be obtained as shown in **Fig. 3**; however, the challenges of small sample size and interactions with the underlying, supporting surface, has required careful attention. We have found that sample preparation and tradeoffs are important considerations in obtaining the best possible data and we have developed a theoretical treatment to “remove” the effects of surface corrugation from the photoemission data. We will now extend these measurements to known flat graphene systems, i.e., such as graphene on BN, which have recently been obtained in exfoliated form. Our first paper in this area is given in Ref. 7 below.

Recent references for our work

1. S. Wang, M.B. Yilmaz, K.R. Knox, N. Zaki, J.I. Dadap, R.M Osgood, Jr., T. Valla, and P.D. Johnson, “Electronic Structure of Co-Decordated Vicinal Cu(775) Surface: High-Resolution Photoemission Spectroscopy.” *Phys. Rev. B* **77**, 115448 (2008)
2. K.R. Knox, S. Wang, A. Morgante, D. Cvetko, A. Locatelli, T.O. Mentès, M.A. Niño, P. Kim, and R.M. Osgood, Jr., “Spectromicroscopy of Single and Multilayer Graphene Supported by a Weakly Interacting Substrate.” *Phys. Rev. B (Rapid Comms)*, **78**, 201408 (2008)
3. N. Zaki, D. Potapenko, P.D. Johnson, and R.M. Osgood, Jr., “Atom-Wide Co Wires on Cu(775) at Room Temperature.” *Phys. Rev. B* **80**, 15, 155419 (2009)
4. A. Locatelli, K.R. Knox, D. Cvetko, T.O. Mentès, M.A. Niño, S. Wang, M.B. Yilmaz, P. Kim, R.M. Osgood, Jr., A. Morgante, “Corrugation in Exfoliated Graphene: An Electron Microscopy and Diffraction Study.” *ACS Nano* **4**, 8, 4879 (2010)
5. Z. Hao, J.I. Dadap, K. Knox, M. Yilmaz, P.D. Johnson, R.M. Osgood, Jr., “Nonequilibrium Band Mapping of Unoccupied Bulk States Below the Vacuum Level by Two-Photon Photoemission.” *Phys. Rev. Lett.* **105**, 017612 (2010)
6. N. Zaki, K. Knox, R.M. Osgood, P. D. Johnson, J. Fujii, I. Vobornik, and G. Panaccione, "Surface states on vicinal Cu(775): STM and photoemission study", *Phys. Rev.* **83**, 205420 (2011).
7. K.R. Knox, A. Locatelli, M.B. Yilmaz, D. Cvetko, T.O. Mentès, M.A. Nino, P. Kim, A. Morgante, and R.M. Osgood, Jr. "Making ARPES Measurements on Corrugated Monolayer Crystals: Suspended Exfoliated Single-Crystal Graphene" *Phys. Rev. B* (2011 – accepted for publication).
8. M. B. Yilmaz, J. I. Dadap, K. R. Knox, N. Zaki, Zhaofeng Hao, P. D. Johnson, and R. M. Osgood, Jr., “Nonequilibrium resonant two-photon photoemission band mapping using a tunable femtosecond source,” submitted to *New Journal of Physics*, (under review) 2011
9. D. Niesner, J. Dadap, M. Kralj, M. Petrovic, K. Knox, N. Zaki, R. Bhandari, P. Yeh, R. M. Osgood, T. Fauster, “Trapping surface electrons on graphene islands,” To be submitted, PRL
10. Junichi Okamoto and A. J. Millis, “One-dimensional physics in transition-metal nanowires: Phases and elementary excitations,” To be submitted, *Phys. Rev. B*

Optical Spectroscopy of Defects and Dopants in Nanocarbon Materials

DOE Grant Number: DE-FG02-05ER46207

Lukas Novotny (novotny@optics.rochester.edu)

University of Rochester, The Institute of Optics, Rochester, NY, 14627.

1. Program Scope

The objective of this project is to control and understand the influence of defects and dopants on the physical properties of carbon nanotubes and graphene. The physical properties of these nanocarbon materials are strongly affected by impurities and structural defects. For example, a conducting graphene sheet turns into a semiconductor when it is cut into a narrow ribbon. Furthermore, its edges give rise to localized states that have a strong influence on transport properties. Thus, the intentional generation of defects and dopants in nanocarbons provides an opportunity to engineer electronic and optical properties, similar to semiconductor device technology.

2. Recent Progress

We use *near-field Raman spectroscopy* to zoom-in on single defects and dopants. This method uses a metal tip as an optical antenna to localize and enhance incident laser radiation and to interact locally with nanocarbon materials. The technique makes it possible to measure local electronic and structural properties with a spatial resolution of 10-20 nm and has been used to record high-resolution spatial maps of optically active phonons and localized photoemission.

To our surprise, the intensity of Raman lines turned out to be non-uniform along most nanotubes that we studied. The nanotubes were mostly arc-discharge, HiPCO, or CVD grown tubes. We tentatively assigned the non-uniform Raman intensity distribution to defects in the tube structure. It was also suggested that the observation could be related to interactions of the tube with the supporting substrate. However, a series of experiments finally confirmed that the substrate has a minor effect on the Raman lines and that the observed localization of modes was indeed due to nanotube inhomogeneities. The best evidence comes from measurements that were performed on nanotubes grown by different methods but using the same substrate. We found that some tubes are uniform over many tens of microns in length whereas other tubes show a high density of localized features. The so far nicest tubes were provided by our collaborator Ernesto Joselevich at Weizmann Institute in Israel. These tubes are grown by CVD on intentionally miscut quartz surfaces, where they wind up in the form of serpentines, as shown in Fig. 1. Once we had highly uniform nanotube samples at hand we set out to quantitatively understand the mechanism of near-field Raman enhancement [9].

Our studies revealed that the near-field Raman intensity is inversely proportional to the 11^{th} power of the separation between the tip and the nanotube. The results show that for defect-free nanotubes all phonon modes exhibit the same enhancement behavior, which indicates that the Raman enhancement process is not significantly influenced by the symmetry of the Raman mode, and is mainly defined by the properties of the tip acting as an optical antenna. In order to be able to quantify experimental data and to relate measurements to intrinsic material properties we developed an analytical theory of local field

enhancement in one-dimensional (1-D) systems, such as semiconductor nanorods or carbon nanotubes. An extension of the theory to 0-D (e.g. molecules or quantum dots), 2-D (e.g. graphene or quantum wells), and 3-D (e.g. bulk materials) materials follows essentially the same steps.

In our experiments, a sample with self-organized carbon nanotube serpentines was raster-scanned underneath a laser-irradiated gold tip and Raman scattering spectra were acquired pixel-by-pixel. Near-field Raman images were generated by integrating the spectra over the spectral ranges associated with discrete phonon peaks. Fig. 1(a) shows a large-scale confocal Raman image. The contrast (color scale) in the image renders the intensity of the G band. Fig. 1(b) shows a corresponding near-field Raman image acquired in the boxed area in (a). The resulting resolution of ≈ 20 nm is defined by the tip radius. A line-cut along the blue line in image (b) is depicted in Fig. 1(c). It is evident, that near-field imaging not only improves resolution but it also improves the signal-to-noise ratio. To evaluate the near-field enhancement we placed the tip over the nanotube at a fixed location and recorded Raman spectra as a function of the tip-sample separation Δ . Fig. 1(d) shows the corresponding Raman spectra for the smallest and largest separation. The two spectra are offset for clarity. The radial breathing mode (RBM) frequency $\nu_{RBM} = 262$ cm^{-1} identifies the nanotube as a semiconducting (10,2) tube, whose energy gap for the second optical transition E_{22} is in resonance with the incident laser energy. The near-field spectrum also clearly features the intermediate frequency mode (IFM) occurring at 865 cm^{-1} , and the G^- and G^+ peaks occurring at 1545 cm^{-1} and 1585 cm^{-1} , respectively. Notice that the disorder-induced D band (~ 1350 cm^{-1}) cannot be observed, indicating that the serpentine nanotube has a low defect density.

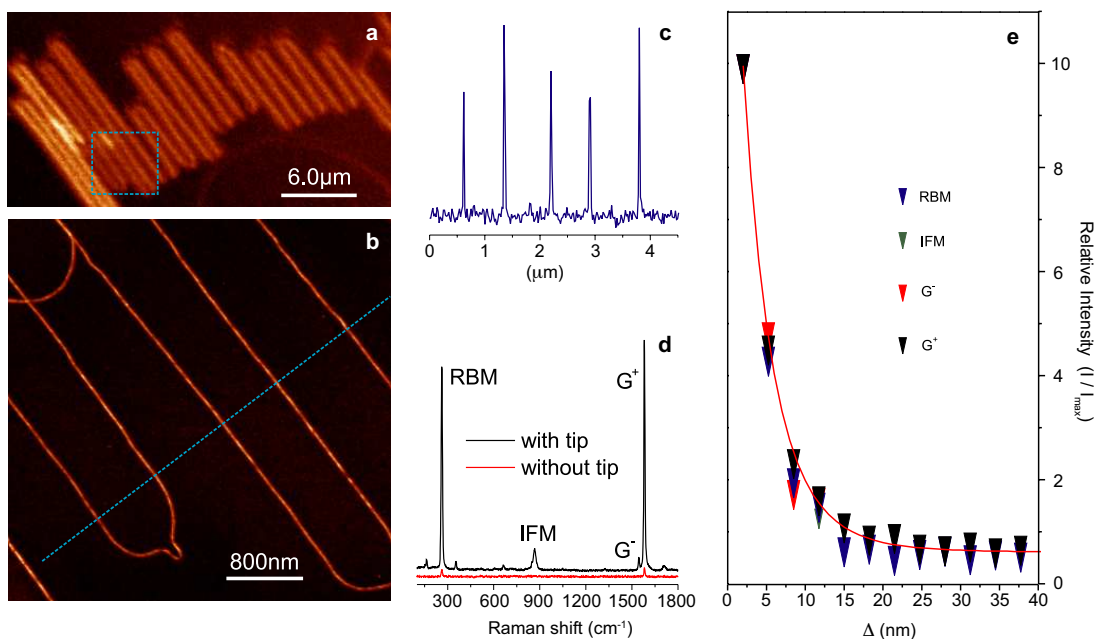


Figure 1: Near-field Raman spectroscopy of serpentine carbon nanotubes grown on a quartz substrate. (a) Confocal Raman image corresponding to the G band intensity of a semiconducting nanotube. (b) Near-field Raman image corresponding to the G band intensity recorded in the boxed area in panel (a). (c) Intensity profile obtained along the blue line in panel (b). (d) Far field Raman spectrum (red curve) and near-field Raman spectrum (black curve) recorded at a fixed location. (e) Approach curves for the RBM, IFM, G^- and G^+ bands. From Ref. [9].

Fig. 1(e) shows the intensities (integrated areas) of several Raman peaks as a function of the tip-sample separation Δ . All Raman intensities are normalized with the corresponding values at shortest separation ($\Delta \sim 2$ nm). Interestingly, they all exhibit the same distance dependence. The red curve in Fig. 1(e) is a fit to the experimental data according to our theoretical result. It can be seen from Fig. 1(e) that our theoretical predictions are in good agreement with the experimental data. Notice that all modes present the same distance dependence, that is, within the resolution of our measurements, all phonon modes get enhanced by the same factor. Thus, our results show that the near-field enhancement does not depend on the symmetry of the Raman mode, but mainly on the field enhancement factor provided by the near-field probe used in the experiment. We emphasize, however, that this behavior is restricted to isolated tubes and that significant variations between the different Raman modes occur for nanotubes with high defect densities. For example, for double-wall nanotubes we observed that the outer tube screens the fields that are experienced by the inner tube. Consequently, a weaker enhancement is observed for the radial breathing mode of the inner tube.

We have also investigated energy transfer between tubes and the coupling between tubes and the supporting dielectric substrate. Tube-tube interactions were studied by measuring the photoluminescence spectra of a pair of intersecting semiconducting SWNTs [5]. In the case of dissimilar nanotubes [structures (9,1) and (6,5)] we observed exciton energy transfer between the tubes. The exciton transfer rate has been determined to be 0.5 ps^{-1} and the energy transfer mechanism was found to follow a simple Förster type process, similar to energy transfer between fluorescent molecules. We have quantified the energy transfer efficiencies between two nanotubes for different inter-nanotube distances and determined that efficient transfer is limited to a few nanometers because of competing fast nonradiative relaxation responsible for low photoluminescence quantum yields [5, 8].

To study nanotube-substrate interactions we have combined Raman scattering with electric force microscopy. Surprisingly, we observed that the nanotube-on-quartz system exhibits a mixture of semiconductor and metal behavior, depending on the orientation between the tube and the substrate. Contact with a supporting substrate has been broadly studied as either a drawback or a solution for developing nanotube-based nanotechnologies. Researchers have for example studied the interaction of SWNTs with silicon substrates as a possible route for the integration between SWNTs and silicon-based microelectronics.

We used CVD grown serpentine nanotubes as described above. The supporting vicinal $\alpha\text{-SiO}_2$ substrate is insulating, and terminated with parallel atomic steps. At the temperature of nanotube growth, the surface contains exposed unpassivated Si atoms, thus promoting a strong tube-substrate interaction, especially when the nanotube lies *along* a step. Alternatively, when the nanotube lies *across* the surface steps, the interaction is discontinuous and weaker. The grown serpentine SWNTs consist of parallel straight segments connected by alternating U-turns. The straight segments lie along the quartz steps, while the U-turns lie across the steps, so that the tube-substrate interaction is modulated along the tube. We have analyzed Raman spectra along single serpentine nanotubes and observed systematic variations in the G band lineshape [10]. In particular, the periodic change on the tube-substrate interaction existing in our SWNT serpentine generates a set of alternate doped-undoped tube segments, which follows from the periodic appearance of the G' feature on the low-frequency side of the G band. This observation is also backed by electric force microscopy (EFM) measurements performed on the same serpentine nanotubes [10].

3. Future Plans

In our future work we will study localized states near the edges of graphene. In particular, we are interested to extract the electron coherence length from the measurement of the spatial profile of the Raman d band near the graphene edge. To this end, we will complete a cryogenic Raman instrument and measure d band localization as a function of temperature.

4. DOE sponsored publications 2008-2011

- [1] L. G. Cançado, A. Hartschuh, and L. Novotny, "Tip enhanced Raman scattering of carbon nanotubes," *J. Raman Spectrosc.* **40**, 1420–1426 (2009).
- [2] I. O. Maciel *et al.*, "Electron and phonon renormalization at defect/doping sites in carbon nanotubes," *Nature Mat.* **7**, 878 – 883 (2008).
- [3] H. Qian, C. Georgi, N. Anderson, A. A. Green, M. C. Hersam, L. Novotny, and A. Hartschuh, "Exciton energy transfer in pairs of single-walled carbon nanotubes," *Phys. Stat. Sol. B* **245**, 2243–2246 (2008).
- [4] H. Qian, P. T. Araujo, C. Georgi, T. Gokus, N. Hartmann, A. A. Green, A. Jorio, M. C. Hersam, L. Novotny, and A. Hartschuh, "Visualizing the local optical response of semiconducting carbon nanotubes to DNA-wrapping," *Nano Lett.* **8**, 2706–2711 (2008).
- [5] H. Qian, C. Georgi, N. Anderson, A. A. Green, M. C. Hersam, L. Novotny, and A. Hartschuh, "Exciton transfer and propagation in carbon nanotubes studied by near-field optical microscopy," *Nano Lett.* **8**, 1363–1367 (2008).
- [6] H. Qian, N. Anderson, C. Georgi, L. Novotny, and A. Hartschuh, in *Tip-enhanced optical microscopy, Nano-Optics and Near-Field Optical Microscopy*, A. Zayats and D. Richards, eds., (Artech House, 2009).
- [7] A. Hartschuh, H. Qian, C. Georgi, and L. Novotny, "Tip-enhanced near-field optical microscopy of carbon nanotubes," *Anal. and Bioanal. Chem.* **394**, 1787 (2009).
- [8] C. Georgi, M. Boehmler, H. Qian, L. Novotny, and A. Hartschuh, "Probing exciton propagation and quenching in carbon nanotubes with near-field optical microscopy," *Phys. Stat. Sol. B* **246**, 2683–2688 (2009).
- [9] L. G. Cançado, A. Jorio, A. Ismach, E. Joselevich, A. Hartschuh, and L. Novotny, "Mechanism of Near-Field Raman Enhancement in One-Dimensional Systems," *Phys. Rev. Lett.* **103**, 186101 (2009).
- [10] J. Soares *et al.*, "Modulating the electronic properties along carbon nanotubes via tube-substrate interaction," *Nano Lett.* in print (2010).
- [11] D. A. Bonnell *et al.*, "Imaging physical phenomena with local probes," *Rev. of Mod. Phys.*, submitted (2010).
- [12] R. Beams, L. G. Cancado, and L. Novotny, "Low temperature Raman study of the electron coherence length near graphene edges," *Nano Lett.* **11**, 1171-1181 (2011).

Session 4

Superconductivity

Tailoring Near Isotropic High Temperature Superconductivity in Iron Pnictides

WAI-KWONG KWOK wkwok@anl.gov
ULRICH WELP welp@anl.gov
ALEXEI E. KOSHELEV koshelev@anl.gov
VITALII VLASKO-VLASOV vlasko-vlasov@anl.gov
GEORGE W. CRABTREE crabtree@anl.gov

Materials Science Division, Argonne National Laboratory, Argonne IL 60439, USA

PROJECT SCOPE

Since the discovery of high temperature superconductivity (HTSC) in cuprates, novel superconductors have been discovered at a steady rate, including $Ba_{1-x}K_xBiO_3$, boro-carbides, MgB_2 and recently the new families of Fe-based pnictides. Each new group brings to light fascinating new properties, be it unconventional gap symmetries and pairing mechanisms, multiple gaps, effect of pairbreaking scattering, or interplay with magnetism. For these materials, standard notions on how superconducting properties (such as critical fields, specific heat, penetration depth, thermal conductivity, NMR relaxation rates etc.) behave as a function of temperature or magnetic field need to be re-evaluated if we are to achieve a consistent picture of the new superconducting behavior. This project integrates experiments and theory aimed at understanding the effects of multiple gaps, gap anisotropy and pair-breaking impurity scattering on thermodynamic and transport properties of unconventional superconductors, in particular the recently discovered Fe-based pnictides. On the experimental side we conduct measurements of the angular dependent specific heat, thermal conductivity, and normal state resistivity to probe the anisotropic phase diagram, the quasiparticle density of states and the electron scattering rates. We modify scattering processes through the controlled introduction of additional scattering centers in the form of correlated line scattering centers by heavy ion irradiation at Argonne's ATLAS accelerator and Michigan State's National Superconducting Cyclotron, and of uncorrelated point and cluster scattering centers by proton irradiation at Western Michigan University and by electron irradiation at Argonne's van de Graaff accelerator. The experimental work is conducted in close synergy with our theoretical investigations. Quantities such as the thermal conductivity, density of states and upper critical field are obtained from analytical and numerical solutions of the quasi-classical Usadel equation and of the Bogolyubov equations.

RECENT PROGRESS

We developed a membrane-based steady-state ac-micro-calorimeter capable of measuring sub-microgram superconducting crystals. We have obtained the anisotropic phase diagram and the anomaly at T_c for a range of single crystal Fe-pnictide superconductors. For example, Fig. 1 shows the superconducting transitions of optimally doped $\text{SmFeAsO}_{0.85}\text{F}_{0.15}$ and $(\text{Ba,K})\text{Fe}_2\text{As}_2$ in magnetic fields along the crystallographic c -axis. In zero-field, $\text{SmFeAsO}_{0.85}\text{F}_{0.15}$ displays a clear cusp-like anomaly in C/T with height of $\Delta C/T_c = 24 \text{ mJ/molK}^2$ at $T_c = 49.5 \text{ K}$, which is substantially smaller than the prediction based on the scaling $\Delta C/T_c \sim T_c^2$ that has been reported for various 122 based materials. In magnetic fields applied along the c -axis, pronounced superconducting fluctuations induce strong broadening and suppression of the specific heat anomaly which can be well described using three-dimensional lowest-Landau-level scaling with an upper critical field slope of -3.5 T/K and anisotropy of $\Gamma = 8$. The small value of $\Delta C/T_c$ implies a modest value of the Sommerfeld coefficient $\gamma \sim 8 \text{ mJ/molK}^2$ indicating that $\text{SmFeAsO}_{0.85}\text{F}_{0.15}$ is characterized by a modest density of states and strong coupling. In contrast, $(\text{Ba,K})\text{Fe}_2\text{As}_2$ has a specific heat anomaly of $\Delta C/T_c = 100 \text{ mJ/molK}^2$ – in line with the $\Delta C/T_c \sim T_c^2$ -scaling – and a mean-field like evolution of the transitions in field. The anisotropy is found to be low, $\Gamma \sim 2.5$, consistent with the near absence of superconducting fluctuations.

Our preliminary theoretical work has shown that in s^\pm -superconductors non-magnetic inter-band scattering induces quasi-particle states at the Fermi energy E_F even for vanishingly small impurity concentrations. These strongly affect all the low-temperature thermodynamic and transport properties of the superconductor such as specific heat, thermal conductivity, surface impedance,

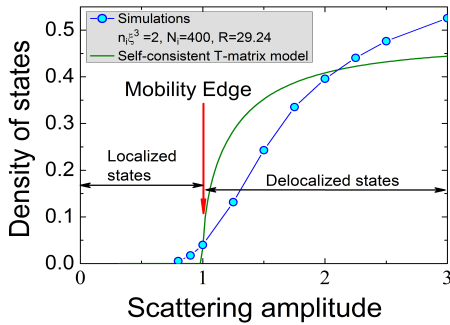


Figure 2. Representative dependence of the density of states at the Fermi energy on the scattering strength of impurities at fixed concentration for the two-band s^\pm superconductor with identical amplitudes of intraband and interband scattering. The mobility edge was evaluated by analysis of the localization length of states. Result obtained within the analytical self-consistent T-matrix approach is also shown by solid green line.

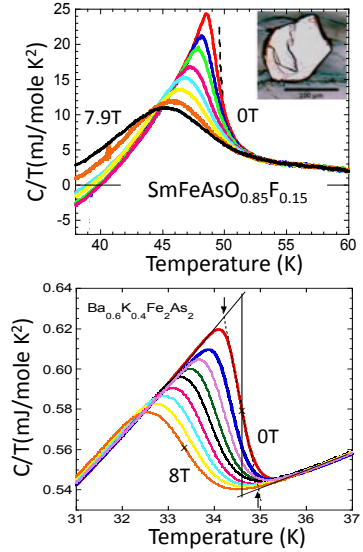


Figure 1. Comparison of the specific heat of optimal doped Sm-1111 and Ba-122 single crystals in magnetic fields up to 8 Tesla. Inset shows the size of the Sm-1111 crystal ($108 \times 97 \times 7 \mu\text{m}^3$).

magnetic penetration depth, relaxation rates and dielectric function. By numerically solving the two-band Bogolyubov equations for s^\pm superconductors, we explore the behavior of the density of states and localization properties of the quasiparticles. On general grounds, one can expect two qualitatively different regimes (see Fig. 2). At a small concentration of pair-breaking impurities, the scattering-induced quasi-particle states are localized at the scattering site, reminiscent of Shiba resonances in conventional superconductors, and their mobility edge is located at finite energy. In this case, these states only influence the low-temperature thermodynamic properties but do not contribute to the transport. At some critical concentration of impurities the scattering-induced states overlap and delocalize; the mobility edge approaches zero energy. Then these states will contribute to transport and should lead to distinctly different behavior than at low concentration addressed in our experimental work described above.

FUTURE PLANS

Our preliminary work found that heavy ion irradiation has a profound effect on the phase diagram and superconducting transition of $\text{Ba}_{0.6}\text{K}_{0.4}\text{Fe}_2\text{As}_2$ as shown in Fig. 3. Upon irradiation to a dose-matching field of $B_0=2$ T the upper critical field slopes increase significantly. Heavy-ion irradiation yields an almost isotropic superconductor with enormous upper critical fields. This result implies that by modifying scattering processes in a multi-band superconductor almost isotropic response can be created directly addressing one of the grand challenges of an isotropic high T_c superconductor.

Building on these results, we will perform a systematic study of quasi-particle scattering effects in FeAs-superconductors. Our initial experimental efforts will focus on single crystals of $\text{BaFe}_2(\text{As}_{1-x}\text{P}_x)_2$. This material is very clean, to the extent that de Haas van Alphen oscillations could be observed for various doping levels. Therefore, it is an ideal platform for our investigations of quasi-particle scattering effects. Starting with pristine samples, we will introduce increasing amounts of additional scattering centers in a controlled way through irradiation with electrons, protons or heavy ions, thereby producing a series of crystals with various doping levels and spanning the entire range from the clean to the dirty limit.

We will investigate the temperature and field (-angle) dependence of the electronic specific heat, thermal conductivity, electric conductivity and Hall effect, and the changes of T_c and the anisotropic phase diagram with impurity concentration. These quantities yield complimentary information on the normal quasi-particles within energy of order $k_B T$ around the Fermi level, and allow for the detailed characterization of the superconducting ground state by correlating our experimental results with theoretical predictions. The electronic specific heat is a direct measure of the total electron density of states, and therefore directly reflects the gap symmetry and the presence of sub-gap states. Thermal conductivity is the ideal quantity to probe quasi-particle transport properties in the superconducting state where the electrical conductivity is shorted out by the superconducting condensate. These measurements allow the detailed investigation of the evolution of sub-gap states with scattering amplitude.

In addition to pair-breaking scattering, finite density of states at the Fermi level can also arise due to the formation of nodes in the gap. Nodes can either be enforced by symmetry such as in d-wave gaps or be ‘accidental’ as has been discussed for s^\pm gaps. In order to separate these two mechanisms (pair-breaking scattering versus nodes) we will perform specific heat and thermal conductivity measurements as *function of field angle*. Quasi-particles located in planes that are perpendicular to the field direction experience a shift in energy. Therefore, by rotating the magnetic field, areas on the Fermi surface that have a gap smaller than this shift can be mapped out since a characteristic angular dependence of the specific heat and thermal conductivity will arise due to the nodal structure. In contrast, sub-gap states due to pair-breaking scattering do not introduce additional angular dependence. Furthermore, accidental nodes are smeared out by impurity scattering. Therefore, our studies on samples with varying purity will yield detailed information on the evolution of the gap-structure with scattering amplitude.

We will also perform detailed high-resolution measurements of the normal state magneto-resistivity and Hall effect in order to obtain independent information on impurity scattering. Initially we will use two or three-band formulations of a Drude-type transport model to fit our transport data with the aim to deduce band-resolved charge carrier concentrations and mobilities.

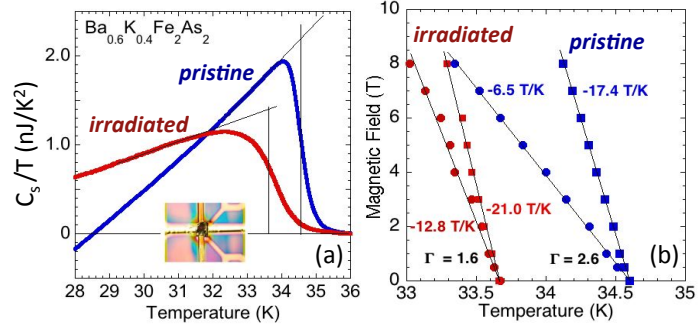


Figure 3. (a) Temperature dependence of the specific heat of an optimal-doped $(\text{Ba}, \text{K})\text{Fe}_2\text{As}_2$ crystal at $H=0\text{T}$, before and after 1.4 GeV Pb-ion irradiation. Micro-calorimeter (inset). (b) Upper critical field phase diagram before and after irradiation.

LIST OF PUBLICATIONS

- Anisotropic phase diagram and superconducting fluctuations of single-crystalline $\text{SmFeAsO}_{0.85}\text{F}_{0.15}$*
U. Welp, C. Chaparro, A. E. Koshelev, A. E. W. K. Kwok, A. Rydh, N. D. Zhigadlo, J. Karpinski, S. Weyeneth, Phys. Rev. B 83(10) 100513 (2011)
- Thermal conductivity in the mixed state of a superconductor at low magnetic fields*
A. A. Golubov, A. E. Koshelev, Phys. Rev. B 83(22) (2011)
- Anisotropic phase diagram and strong coupling effects in $\text{Ba}_{1-x}\text{KxFe}_2\text{As}_2$ from specific-heat measurements*
U. Welp, R. Xie, A. E. Koshelev, W. K. Kwok, H. Q. Luo, Z. S. Wang, G. Mu, H. H. Wen, Phys. Rev. B 79(9), 094505 (2009).
- Magneto-optical study of $\text{Ba}(\text{Fe}_{1-x}\text{M}_x)_2\text{As}_2$ ($M=\text{Co}$ and Ni) single crystals irradiated with heavy ions*
R. Prozorov, M. A. Tanatar, B. Roy, N. Ni, S. L. Bud'ko, P. C. Canfield, J. Hua, U. Welp, W. K. Kwok, Phys. Rev. B 81(9), 094509 (2010).
- Statistics of the subgap states of s_{\pm} superconductors*
A. Glatz and A. E. Koshelev, Phys. Rev. B 82(1) 012507 (2010)
- London penetration depth in $\text{Ba}(\text{Fe}_{1-x}\text{T}_x)_2\text{As}_2$ ($T=\text{Co}, \text{Ni}$) superconductors irradiated with heavy ions*
H. Kim, R. T. Gordon, M. A. Tanatar, J. Hua, U. Welp, W. K. Kwok, N. Ni, S. L. Bud'ko, P. C. Canfield, A. B. Vorontsov, R. Prozorov, Phys. Rev. B 82(6) 060518 (2010).
- Vortex pinning by compound defects in $\text{YBa}_2\text{Cu}_3\text{O}_{7-d}$*
J. Hua, U. Welp, J. Schlueter, A. Kayani, Z. L. Xiao, G. W. Crabtree, W. K. Kwok, Phys. Rev. B 82(2), 024505 (2010).
- Understanding the role of heavy ion-irradiation induced surface columnar nanostructures through FESEM imaging*
A. Chiodoni, F. Laviano, R. Gerbaldo, G. Ghigo, L. Gozzelino, E. Mezzetti, B. Minetti, W. K. Kwok, Physica C 470(19), 914 (2010).
- Specific heat and phase diagrams of single crystal iron pnictide superconductors*
U. Welp, G. Mu, R. Xie, A. E. Koshelev, W. K. Kwok, H. Q. Luo, Z. S. Wang, P. Cheng, L. Fang, C. Ren, H. H. Wen, Physica C 469(9-12), 575-581 (2009).
- Calorimetric determination of the upper critical fields and anisotropy of $\text{NdFeAsO}_{1-x}\text{Fx}$ single crystals*
U. Welp, R. Xie, A. E. Koshelev, W. K. Kwok, P. Cheng, L. Fang, H. H. Wen
Phys. Rev. B 78(14), 140510(R) (Oct 2008).
- Growth and superconductivity of FeSe_x crystals*
U. Patel, J. Hua, S. H. Yu, S. Avci, Z. L. Xiao, H. Claus, J. Schlueter, V. K. Vlasko-Vlasov, U. Welp, W. K. Kwok, Appl. Phys. Lett. 94(8), 082508 (2009).
- Stability of dynamic coherent states in intrinsic Josephson-junction stacks near internal cavity resonance*
A. E. Koshelev
Phys. Rev. B 82(17), 174512 (Nov 2010).
- Coupled domain structures in superconductor/ferromagnet Nb-Fe/garnet bilayers*
V. K. Vlasko-Vlasov, U. Welp, W. K. Kwok, D. Rosenmann, H. Claus, A. A. Buzdin, A. Melnikov
Phys. Rev. B 82(10), 100502 (Sep 2010).
- Matching effect and dynamic phases of vortex matter in $\text{Bi}_2\text{Sr}_2\text{CaCu}_2\text{O}_8$ nanoribbon with a periodic array of holes*
S. Avci, Z. L. Xiao, J. Hua, A. Imre, R. Divan, J. Pearson, U. Welp, W. K. Kwok, G. W. Crabtree, App. Phys. Lett. 97(4) 042511 (Jul 2010).
- Coexisting multiple dynamic states generated by magnetic field in $\text{Bi}_2\text{Sr}_2\text{CaCu}_2\text{O}_{8+d}$ stacked Josephson junctions*
Y. D. Jin, H. J. Yong-Duk, H. J. Lee, A. E. Koshelev, G. H. Lee, M. H. Bae
- Effect of sample geometry on the phase boundary of a mesoscopic superconducting loop*
G. R. Berdiyrov, S. H. Yu, Z. L. Xiao, F. M. Peeters, J. Hua, A. Imre, W. K. Kwok
Phys. Rev. B 80 (6), 064511 (Aug 2009).
- Magnetoresistance oscillations in superconducting granular niobium nitride nanowires*
U. Patel, Z. L. Xiao, A. Gurevich, S. Avci, J. Hua, R. Divan, U. Welp, W. K. Kwok
Phys. Rev. B 80(1), 012504 (2009).
- Soft magnetic lithography and giant magnetoresistance in superconducting/ferromagnetic hybrids*
V. K. Vlasko-Vlasov, U. Welp, A. Imre, D. Rosenmann, J. Pearson, W. K. Kwok
Phys. Rev. 78(21), 214511 (2008).

“Origin of Superconductivity in Structurally Layered Materials” (ERKCM70)

Oak Ridge National Laboratory

Athena S. Sefat, sefata@ornl.gov

Project Scope: Our overarching goal is to lay a foundation for predicting superconducting materials by documenting similarities and differences between the two high-temperature superconducting classes. This project involves a strong synthesis component for the design of new or improved iron- and copper-based materials, and also those without such 3*d*-elements, with input from electronic structure calculations. Beyond synthesis, our characterization efforts involve determination of lattice and magnetic structures, and thermodynamic and transport measurements. Elastic and inelastic neutron scattering tools at ORNL are used to find lattice and magnetic structures, and magnetic excitations. Through collaborations, the effects of applied pressure and studies of superconducting gap and Fermi surface structures are pursued. Because the mechanism of high-temperature superconductivity remains unknown, our project focuses on tackling several specific queries such as those listed here: Are there specific structural features that stabilize a superconducting state? What are the roles of chemical substitutions or applied pressure? What is the role of magnetic ions in relation to superconducting charge carriers?

Recent Progress: Research has been ongoing (see Publications section). Below is an outline of our some of our most recent findings.

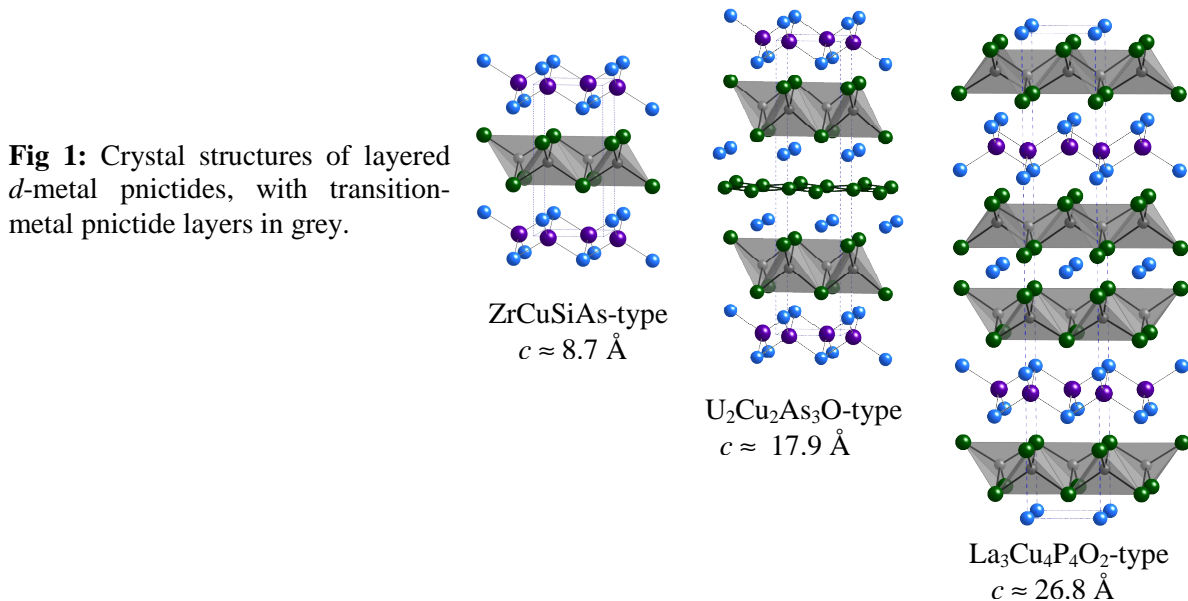
- The superconducting behavior in Sr₄V₂O₆Fe₂As₂ is dependent on synthesis conditions: the superconducting transition temperature is high for samples with most crystalline impurities; it decreases with increases in *c*-lattice parameter.
- For NdFeAsO_{0.86}F_{0.14}, we find a single gap feature below the superconducting transition temperature ($T_C = 48$ K) by the use of scanning tunneling microscopy/spectroscopy. Data result in BCS temperature dependence of the energy gap $\Delta(T)$, with $2\Delta(0)/k_B T_C \approx 4.3$.
- The crystal structure and electrical resistance data of EuFe₂As₂ give evidence of a tetragonal to a collapsed-tetragonal phase at 8 GPa, and superconductivity at 41 K under pressure.
- Temperature dependence of the electronic specific heat on the various concentrations of Co-doped BaFe₂As₂ superconductors show that the gap structure does not change significantly as a function of doping, and data can not be described by a single isotropic *s*-wave gap.
- EuCo₂As₂ undergoes a tetragonal to a collapsed-tetragonal phase at 4.7 GPa, a behavior that is common to the AT₂As₂ (*A* = Ca, Sr, Ba) parents of superconductors. No superconducting transition is found with pressure.
- In CeFeAsO, magnetism on the Fe and Ce is found to coexist up to 15 GPa. No superconducting feature is observed up to 50 GPa.
- For NdCoAsO, the antiferromagnetic phase is found to be stable under 53 GPa and down to 10 K without signs of superconductivity. This result shows that superconductivity may not be favored in cobalt-based materials.
- NdCoAsO gives three magnetic phase transitions that are suppressed as cobalt is replaced with Fe. No superconducting transition is observed for 20% chemical doping.
- The electronic and local crystal structure of CeFeAsO_{0.89}Fe_{0.11} superconductor and its undoped CeFeAsO parent show that the total DOS within 2 eV below E_F is dominated by Fe 3*d* states. There are indications of Fe *d*-electron itinerancy. The occupied Ce 4*f* states are located at ~1.7 eV below E_F and show a main 4*f*¹ configuration. The total and partial DOS extracted from x-ray spectroscopy data show good agreement with calculations.

- Changes in the elastic properties of BaFe_2As_2 parent and $\text{BaFe}_{1.8}\text{Co}_{0.2}\text{As}_2$ superconductor show that the structural order (orthorhombic to tetragonal phase) is induced by magnetic fluctuations and that both magnetic and nematic phases are important low energy excitations.
- Annealing significantly improves some superconducting characteristics of Co-doped BaFe_2As_2 crystals: transition temperature increases; electronic specific heat in superconducting state decreases; Schottky-like contribution suppresses. The optimally doped material is fully gapped.
- By the use of point-contact Andreev reflection spectroscopy, a gap size of $\sim 3 - 4$ meV with the energy gap $\Delta(T)$, with $2\Delta(0)/k_B T_C \approx 2.0-2.6$, is found for $(\text{Ba}_{0.6}\text{K}_{0.4})\text{Fe}_2\text{As}_2$ ‘122’ superconductor. This gap is smaller than those reported for ‘1111’ superconductors.
- Chromium-doped BaFe_2As_2 show strong magnetism in diffraction results, which can explain the absence of superconductivity. The average spin-density-wave (SDW) moment is independent of small Cr doping levels. However, the SDW moment decreases rapidly beyond 30% doping, at which point a new competing G-type antiferromagnetic phase dominates.
- For $\text{FeTe}_{0.5}\text{Se}_{0.5}$ superconductor, two types of magnetic excitations are found: a resonance at $(0.5,0.5,0)$ and incommensurate fluctuations on either side of this wave vector. With different x , the resonance is fixed in position while the incommensurate excitations move. Such unusual relation between the resonance and incommensurate magnetism with superconductivity show that a common behavior of the low energy magnetic excitations may not be necessary for electron pairing.
- The effects of magnetism and vortex lattice disorder in cobalt-doped BaFe_2As_2 superconductors are found to cause uncertainty in values of magnetic penetration depth (λ) determined by transverse-field muon spin rotation.

Future Plans: Three areas of focus are described below.

- a) *Do certain crystal structures give a superconducting state? Here we explore the possibility of synthesis of new superconductors and characterize materials by means of basic physical property measurements.*

Part of our effort will be focused on the discovery of new superconducting materials by exploratory synthesis. Certain layered structures such as $\text{U}_2\text{Cu}_2\text{As}_3\text{O}$ and $\text{La}_3\text{Cu}_4\text{P}_4\text{O}_2$ may instigate a superconducting state. These structures are similar to the Fe-based superconductors (e.g. ZrCuSiAs-type structure in $\text{SmFeAsO}_{0.9}\text{F}_{0.1}$, $T_C = 55$ K) since they are tetragonal, have layers of transition metal pnictides and have transition metals in tetrahedral coordination (see Figure 1).



b) **What is the role of chemical substitution on the quantum phase transition between the magnetic and a possible superconducting phase?** Here we synthesize doped-materials and characterize them by means of basic physical property measurements, neutron-scattering experiments, and electronic structure calculations.

Part of our program will yield information and insight into the structural and magnetic transitions, as well as find the role of spin fluctuations and phonons in producing a superconducting state. This can be done by studying the role of chemical substitutions (x) in already well-known parent materials. For example, it is puzzling that doping of BaFe_2As_2 by $\sim 10\%$ electrons on iron crystal site gives superconductivity [Sefat et al., *Phys. Rev. Lett.* **101** (2008), 117004.], but holes do not give the same effect [Sefat et al., *Phys. Rev. B* **79** (2009), 224524.]; see Figure 2. In addition, it is difficult to understand why electron doping with metals of the same column ($3d$ or $4d$), which are so different in size, induce superconductivity for the same T_C and at the same doping level [Ni et al. *Phys. Rev. B* **80** (2009), 024511.]. One of our immediate questions is if Mo-doping duplicates Cr-doping in BaFe_2As_2 system, and what underlying electronic structure may stabilize a magnetic phase in favor of a superconducting dome.

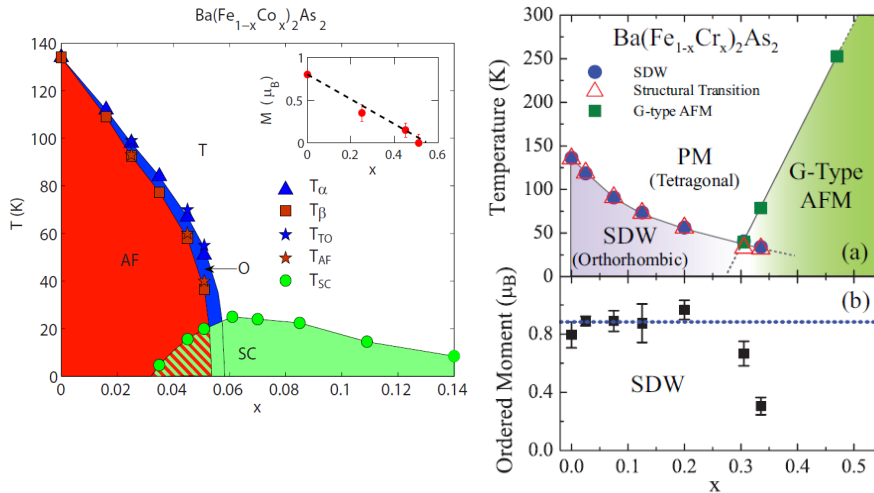


Fig 2: Phase diagrams of temperature (T) versus chemical doping (x) in BaFe_2As_2 . Left is the electron doping result by means of cobalt [Lester et al., *Phys. Rev. B* **79** (2009), 144523]; right is the hole-doping result by means of chromium [Marty et al., *Phys. Rev. B* **83** (2011), 060509.].

c) **What is the intrinsic behavior of a single crystal?** Here we will attempt to synthesize crystals by various crystal growth methods, find their chemical stoichiometries, and characterize the crystals by means of basic physical property measurements.

We have shown using a combination of powder X-ray and neutron diffraction, first principles calculations, temperature- and field-dependent magnetization, heat capacity and resistivity data that the superconducting behavior of ' $\text{Sr}_4\text{V}_2\text{O}_6\text{Fe}_2\text{As}_2$ ' is dependent on synthesis conditions, particularly, heating profiles result in unintentional chemical doping (Figure 3, left) [Sefat et al. *Physica C* **471** (2011), 143.]. Because such polycrystalline materials contain numerous impurities, it would be essential to find the behavior of the pure crystal.

In addition, the coexistence of superconductivity and antiferromagnetism is found in Bridgman grown $\text{AFe}_{2-y}\text{Se}_2$ crystals, with different T_N values perhaps dependent on uncertainty in the iron content (see Figure 3, right) [Liu et al. *Euro. Phys. Lett.* **94** (2011), 27008.]. It would be interesting to grow more homogenous crystals out of flux, with better control over stoichiometry and determine the y value.

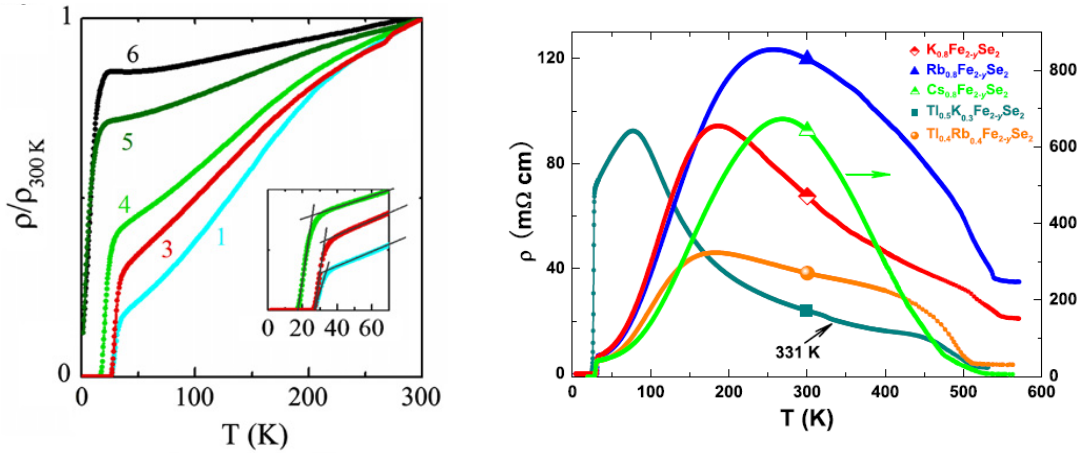


Figure 3: Left is the normalized temperature dependence of electrical resistivity for ‘Sr₄V₂O₆Fe₂As₂’ materials synthesized in different conditions; samples 5 and 6 are not superconductors down to 1.8 K [Sefat et al. *Physica C* **471** (2011), 143.]. Right is the temperature dependence of the resistivity for AFe_{2-y}Se₂ showing the coexistence of superconductivity and antiferromagnetic phases [Liu et al. *Euro. Phys. Lett.* **94** (2011), 27008.].

Publications: From *April 15, 2010 (start of the project) to the present time*, we have published **27** scientific manuscripts in journals such as *Phys. Rev. Lett.* (3), *Chem. Mater.* (2), and *Phys. Rev. B* (12). A few of these are listed below:

- Uhoya, W.; Stemshorn, A.; Tsoi, G.; Vohra, Y. K.; Sefat, A. S.; Sales, B. C.; Hope, K. M.; Weir, S. T., “Collapsed tetragonal phase and superconductivity of BaFe₂As₂ under high pressure,” *Phys. Rev. B* **82** (2011), 144118.
- Sales, B. C.; McGuire, M. A.; May, A. F.; Cao, H. B.; Chakoumakos, B. C.; Sefat, A. S., “Unusual phase transitions and magnetoelastic coupling in TiFe_{1.6}Se₂ single crystals,” *Phys. Rev. B* **83** (2011), 224510.
- Sonier, J. E.; Huang, W.; Kaiser, C. V.; Cochrane, C.; Pacradouni, V.; Sabok-Sayr, S. A.; Lumsden, M. D.; Sales, B. C.; McGuire, M. A.; Sefat, A. S.; Mandrus, D. “Magnetism and disorder effects on muon spin rotation measurements of the magnetic penetration depth in iron-arsenic superconductors,” *Phys. Rev. Lett.* **106** (2011), 127002.
- Marty, K.; Christianson, A. D.; Wang, C. H.; Matsuda, M.; Cao, H.; VanBebber, L. H.; Zarestky, J. L.; Singh, D. J.; Sefat, A. S.; Lumsden, M. D. “Competing magnetic ground states in non-superconducting Ba(Fe_{1-x}Cr_x)₂As₂,” *Phys. Rev. B: Rapid Comm.* **83** (2011), 064513.
- Gofryk, K.; Vorontsov, A. B.; Vekhter, I.; Sefat, A. S.; Imai, T.; Bauer, E. D.; Thompson, J. D.; Ronning, F. “Effect of annealing on the specific heat of Ba(Fe_{1-x}Co_x)₂As₂,” *Phys. Rev. B* **83** (2011), 064513.
- Fernandes, R. M.; VanBebber, L. H.; Bhattacharya, S.; Chandra, P.; Keppens, V.; Mandrus, D.; McGuire, M. A.; Sales, B. C.; Sefat, A. S.; Schmalian, J. “Effect of nematic fluctuations on the elastic properties of iron arsenide superconductors,” *Phys. Rev. Lett.* **105** (2010), 157003.
- Mook, H. A.; Lumsden, M. D.; Christianson, A. D.; Nagler, S. E.; Sales, B. C.; Jin, R.; McGuire, M. A.; Sefat, A. S.; Mandrus, D.; Egami, T.; dela Cruz, C., “Unusual relationship between magnetism and superconductivity in FeTe_{0.5}Se_{0.5},” *Phys. Rev. Lett.* **104** (2010), 187002.
- Gofryk, K.; Sefat, A. S.; McGuire, M. A.; Sales, B. C.; Mandrus, D.; Thompson, J. D.; Bauer, E. D.; Ronning, F., “Doping-dependent specific heat study of the superconducting gap in Ba(Fe_{1-x}Co_x)₂As₂,” *Phys. Rev. B*, **81** (2010), 184518.
- Lu, X.; Park, W K; Yuan, H. Q.; Chen, G. F.; Luo, G. L.; Wang, N. L.; Sefat, A. S.; McGuire, M. A.; Jin, R.; Sales, Mandrus, D.; Gillett, J.; Sebastian, S. E.; Greene, L. H., “Point-contact spectroscopic studies on normal and superconducting AFe₂As₂-type iron pnictide single crystals,” *Supercond. Sci. Technol.* **23** (2010), 054009.

Towards a universal description of vortex matter in superconductors

PI: Leonardo Civale,

Superconductivity Technology Center, Los Alamos National Laboratory

e-mail: lcivale@lanl.gov

Project Scope

Superconducting vortex physics has been a major field in condensed matter and statistical physics since the discovery of the oxide high temperature superconductors (HTS). Vortices in HTS have a complex phase diagram in the magnetic field - temperature (\mathbf{B} - T) space¹ with a proliferation of several topological vortex phases. The rich vortex physics in HTS arises from the much larger influence of thermal fluctuations as compared to conventional low temperature superconductors (LTS). It is important noticing, however, that there is not a hard boundary between LTS and HTS vortex phenomenology. In any superconductor (SC) the vortex behavior is determined by the *intrinsic properties* of the vortex matter and the *extrinsic effects* resulting from material *inhomogeneities* that create a potential energy landscape. The central idea of this project is obtain a comprehensive vortex physics description that is **universal**, in the sense that it should be applicable to all or at least a broad variety of SC. We are working in coordinated experimental and theoretical effort to attain this objective. Our focus is on interactions between vortices with material inhomogeneities with emphasis on the influence of thermal fluctuations. Our project is fundamental-science oriented in terms of the methodology and expected outcome, but we intend to obtain results applicable not only to model systems but also to materials of technological relevance, including predictions valid for new superconductors that can be discovered in the future.

Recent progress

The oxide HTS exhibit rich vortex physics due to the strong thermal fluctuations arising from the small coherence length (ξ) and large anisotropy (γ). Iron-based superconductors are a whole new family of materials spanning broad ranges of critical temperatures (T_c), ξ and γ , where the generality of the ideas developed for the oxides can be tested. The multi-band superconductivity in these compounds introduces a new level of complexity. Valuable information can also be obtained from MgB_2 , a chemically simpler two-band superconductor.

To obtain a general perspective, we have investigated vortex matter in superconductors spanning broad ranges of T_c and γ , from $\gamma=1$ to $\gamma > 6$ and from $T_c < 10\text{K}$ to $T_c \sim 90\text{K}$ (see Figure 1). This allows us to perform comparative analyses at fixed T_c and/or γ . Also, we studied samples with different degrees of disorder; from very clean single crystals to films with the strongest pinning obtained so far. We have manipulated the pinning landscape both chemically (by adding second phases and tuning the growing conditions) and through irradiations (protons to introduce random defects and heavy ions to create aligned columnar defects). We use transport and magnetization methods to study the upper critical fields (H_{c2}), melting lines (H_m), critical currents densities (J_c) and dynamics (flux creep). Of particular relevance was the use of the pulsed-fields facilities at the NHMFL-LANL to explore the high field phenomenology, and the analysis of the angular dependences.

Co-doped iron-arsenide 122 films: (from the group of Prof. H. Hosono, Tokyo Inst. of Technol., Japan). After an initial study of $\text{SrFe}_{1.8}\text{Co}_{0.2}\text{As}_2$ ($T_c \sim 19\text{K}$), we focused on biaxially

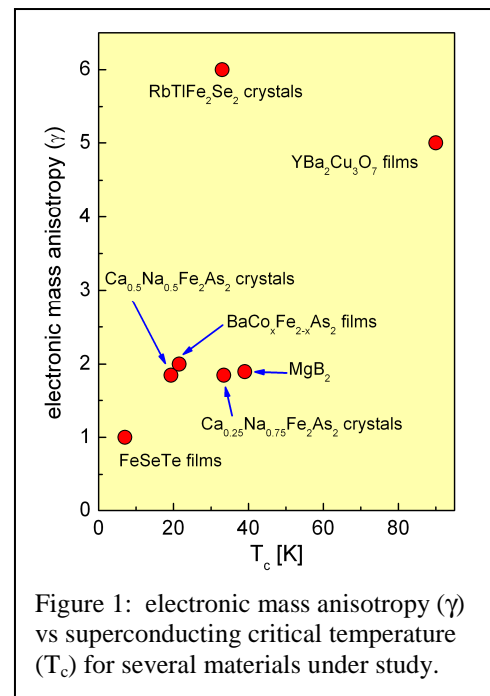


Figure 1: electronic mass anisotropy (γ) vs superconducting critical temperature (T_c) for several materials under study.

oriented $\text{BaFe}_{2-x}\text{Co}_x\text{As}_2$ films grown by Pulsed Laser Deposition on $(\text{La,Sr})(\text{Al,Ta})\text{O}_3$ substrates, which are more stable and have better crystalline quality, with $T_c = 21\text{K}$ and $\Delta T_c < 1\text{K}$. We determined H_{c2} , H_m and J_c as a function of field orientation (Θ). In the T-H region studied we found that $H_{c2}(\Theta)$ can be modeled using a single band with $\gamma = 2$. This simplified description is valid since the predictions of the two band model and a single-band with low anisotropy are almost identical near T_c . Unlike observations on single crystals of the same composition with similar T_c and γ , we found a broadening of the resistive transition $\rho(T)$ with increasing H , indicating the presence of a vortex liquid phase. This was the first clear observation of a vortex liquid in a superconductor with such low T_c and small anisotropy. $H_m(\Theta)$ does not follow the anisotropic scaling observed in $H_{c2}(\Theta)$; instead it shows a large peak centered at $H//c$ indicative of *strong* correlated pinning. Consistently, we found that $J_c > 1 \text{ MA/cm}^2$ at 4 K and 1 T, about 2 orders of magnitude higher than in the $\text{SrFe}_{2-x}\text{Co}_x\text{As}_2$ films. A large $J_c(\Theta)$ peak for $\mathbf{H}||c$ confirms the presence of strong correlated disorder.

Ca_{1-x}Na_xFe₂As₂ single crystals: (Renmin Univ. of China, Beijing). We investigated the effect of doping on the crystalline structure and superconducting properties for $x = 0.5, 0.6, 0.75$. The maximum $T_c \sim 33.4$ K occurs at $x \sim 0.75$, corresponding to a charge carrier density different than in doped BaFe_2As_2 and SrFe_2As_2 . We determined the vortex phase diagram and pinning regimes of the $x = 0.75$ and $x = 0.5$ ($T_c \sim 19\text{K}$) crystals. As in the Co-doped films, in the T-H region studied (up to 15T) $H_{c2}(\Theta)$ can be described by a single band anisotropic model, and remarkably $\gamma = 1.85 \pm 0.05$ is the same for both crystals, independently of the Na content. In the $T_c \sim 33$ K crystal we detected a narrow vortex-liquid phase. In contrast to the Co-doped films, neither $H_m(\Theta)$ nor $J_c(\Theta)$ show evidence of correlated pinning. We explored the time relaxation of J_c and extracted the flux creep rate $S(T,H)$. Both crystals show qualitatively similar behavior, with elastic collective creep at low T and H and a crossover to plastic creep above a boundary $T_{cr}(H)$ that coincides with the upper end of the regime $J_c \propto H^{-\alpha}$ originated in pinning by sparse random nanoparticles. The glassy exponent μ for the $x=0.75$ crystal is $\mu \sim 0.7$ to 1, a value range frequently observed in $\text{YBa}_2\text{Cu}_3\text{O}_7$ and consistent with collective creep, while for the $x=0.5$ crystal $\mu \sim 3$ to 3.3, above the highest μ predicted by collective creep models. Our results point to the need to explore more examples of vortex matter in systems with intermediate influence of thermal fluctuations.

Co-doped BaFe₂As₂ single crystals: (grown at ISTEC, Japan). We are exploring these crystals as a link between the $\text{Ca}_{1-x}\text{Na}_x\text{Fe}_2\text{As}_2$ single crystals and the Co-doped films, with intermediate $T_c \sim 23\text{K}$ and similar anisotropy $\gamma \sim 2$ near T_c . In contrast to the Co-doped films they show no correlated pinning, and as compared to the $\text{Ca}_{1-x}\text{Na}_x\text{Fe}_2\text{As}_2$ single crystals they exhibit different pinning regimes, in particular a maximum in $J_c(H)$ at intermediate fields (“fishtail effect”). The creep rates $S(T,H)$ are similar to the $\text{Ca}_{0.25}\text{Na}_{0.75}\text{Fe}_2\text{As}_2$ system, but the crossover from elastic to plastic creep occurs at a temperature intermediate between the two $\text{Ca}_{1-x}\text{Na}_x\text{Fe}_2\text{As}_2$ crystals with T_c of 19K and 33K. We have irradiated one of these Co-doped crystals with protons to introduce random point defects, and are currently repeating the vortex studies. Initial results show an increase in J_c , disappearance of the fishtail, and a decrease in S .

Tl_{0.58}Rb_{0.42}Fe_{1.72}Se₂ single crystals: We are studying this new superconductor in collaboration with the Zhejiang Univ. (China) and the NHMFL-LANL. $H_{c2}(T)$ for $\mathbf{H}||c$ increases linearly with decreasing T , reaching $H_{c2}(T=0) \sim 55$ T, while a larger $H_{c2}(T=0)$ with a strong convex curvature is observed for $\mathbf{H}\perp c$. The anisotropy of H_{c2} decreases with decreasing T . The analysis based on the Werthamer-Helfand-Hohenberg model shows that $H_{c2}(T=0)$ is orbitally limited for $\mathbf{H}||c$, but the effect of spin paramagnetism may play a role on the pair breaking for $\mathbf{H}\perp c$. $H_{c2}(\Theta)$ near T_c is consistent with a single-band model with $\gamma \sim 6$, and that $\rho(T)$ broadens upon increasing of H , indicating the presence of a vortex liquid.

ReBa₂Cu₃O₇ thin films: We studied $J_c(H,T)$ and $H_{irr}(\Theta)$ in $\text{Y}_{0.77}\text{Gd}_{0.23}\text{Ba}_2\text{Cu}_3\text{O}_y$ with random BaZrO_3 nanoparticles and in $\text{YBa}_2\text{Cu}_3\text{O}_y$ films grown by metal organic deposition. Both films have mixed pinning landscapes with large $\text{RE}_2\text{Cu}_2\text{O}_5$ particles (diameter $\sim 80\text{nm}$) and high density of twin boundaries. In addition $\text{YGdBCO}+\text{BZO}$ films have a high density of BZO nanoparticles (diameter $\sim 25\text{nm}$). J_c , H_{irr} , and S

above $T \sim 40\text{K}$, are greatly affected by the BZO nanoparticles, resulting in a higher H_{irr} and improved J_c along the c axis and at intermediate Θ , while at low T both types of films show similar behavior.

We also investigated a series of $(\text{Y,Gd})\text{Ba}_2\text{Cu}_3\text{O}_y$ films with BaMO_3 ($M=\text{Zr, Nb, Sn}$) additions. The engineered pinning landscapes consisted mainly of random nanoparticles, and we were able to control their size ($D = 22$ to 83 nm) and density ($n = 0.1$ to $13 \times 10^{21}/\text{m}^3$). J_c gradually increases with increasing n , both for $\mathbf{H} \parallel c$ and $\mathbf{H} \parallel 45^\circ$. The films with higher n show nearly isotropic J_c , indicating that spherical nanoparticles pin vortices over a broad angular range. The nature of the vortex melting transition systematically changes by changing n . In films with large n we observed a Bose-glass like transition at both $\mathbf{H} \parallel c$ and $\mathbf{H} \parallel 45^\circ$, with similar exponents than in YBCO single crystals with correlated disorder.

Bulk polycrystalline MgB_2 : (Dr. A. Serquis, Bariloche, Argentina) We had previously shown that MgB_2 doping of with carbon nanotubes (CNT) resulted in an enhancement of both H_{c2} (due to the reduction of the electronic mean free path induced by the C that dissolves in the matrix) and J_c (due to the pinning produced by the CNT that retain integrity). We have now explored the flux creep in undoped and CNT-doped polycrystalline MgB_2 . In both cases $S(T)$ is Anderson-Kim like with no evidence of glassy relaxation, in contrast to pnictides and oxides. Although the CNT doping increases J_c , it also increases S . This is consistent with the reduction in ξ due to doping. We used the pulsed-field facilities of the NHMFL to investigate $H_{c2}(T)$ in bulk polycrystalline MgB_2 doped simultaneously with C and Ca. These two elements dope different sites of the MgB_2 lattice, altering the intra- and inter-band scattering in dissimilar ways. The idea of this study is that these different effects on the electronic mean free path should reflect in the temperature dependence of H_{c2} . We are currently analyzing these results in the framework of Gurevich's model for H_{c2} in two-band superconductors.

Future plans

We will continue the study of Fe-based superconductors, the materials of most current interest due to their exciting novel physics, particularly their multi-band character, and the large H_{c2} . We established solid collaborations with some of the groups producing the best samples, and we will continue receiving both thin films and single crystals. One main focus will be the exploration of the angular dependences of the equilibrium and non-equilibrium states of the vortex matter. We will use the pulsed fields of the NHMFL-LANL to study $H_{c2}(T, \Theta)$, $H_m(T, \Theta)$, and the dissipative properties of the vortex liquid at very high fields. We will also continue using transport and magnetization tools to investigate the pinning properties, the nature of the solid phases, and the flux creep mechanisms. The overall goal will be to elucidate the complex relations between the multi-band character, the anisotropy, the presence or absence of vortex liquid phases, and the glassy (elastic) or non-glassy (plastic) dynamics. We have already irradiated several samples with protons and heavy-ions, and we plan to continue exploring the irradiation effects on the vortex matter in Fe-based, cuprates, and MgB_2 superconductors. We will focus on using irradiations to engineer well controlled mixed pinning landscapes (random+correlated) to investigate their combined and synergetic effects, and to manipulate the crossover between elastic and plastic dynamics.

As an example, we have received a new batch of $\text{BaFe}_{2-x}\text{Co}_x\text{As}_2$ films, with thicknesses from ~ 100 nm to ~ 500 nm. Our first goal is to investigate whether there is a thickness dependence of J_c , similar to the case of YBCO films, in order to determine the presence of interface pinning. The second goal is to explore the source of the correlated pinning along the c -axis. Our initial results suggest that there is no thickness dependence in J_c , and that the c -axis peak in $J_c(\Theta)$ remains visible for all thicknesses. We are also studying the effects of 3MeV proton irradiation on the vortex pinning in these films. We started with low doses to produce a small defect density and we plan to follow the evolution with dose. We found that the initial irradiation produces a small reduction in T_c and a small increase in J_c , only in limited H-T ranges. We are also pursuing proton irradiations in the $\text{Ca}_{1-x}\text{Na}_x\text{Fe}_2\text{As}_2$ single crystals. For the $T_c \sim 33\text{K}$ crystal we found that the initial irradiation increases J_c significantly, reducing the exponent α in the $J_c \propto H^{-\alpha}$ regime, and eliminates the field-independent J_c regime at high H .

With regards to MgB₂, we will explore flux creep in epitaxial films produced by reactive evaporation (Brian Moeckly, Superconductor Technologies, Inc.). These films are cleaner than the bulk MgB₂ samples (they have a much smaller H_{c2}) and also will allow us to investigate angular dependences, in contrast to polycrystalline samples.

We will expand the use of magnetic force microscopy (MFM) for direct visualization of vortices and vortex lattices in cuprates, Fe-based, MgB₂ and borocarbide superconductors. We will apply this tool to determine the temperature dependence of the penetration depth λ in multi-band superconductors, and to explore magnetic and non-magnetic pinning effects.

Publications

1. “Angular and field properties of the critical current and melting line of Sr(Fe_{1-x}Co_x)₂As₂ epitaxial films”, B. Maiorov, S.A. Baily, Y. Kohama, H. Hiramatsu, L. Civale, M. Hirano, and H. Hosono, *Supercond. Sci. Technol.* **22**, 125011 (2009).
2. “Direct measurements of the penetration depth in a superconducting film using magnetic force microscopy”, E. Nazaretski, J. P. Thibodaux, I. Vekhter, L. Civale, J. D. Thompson, and R. Movshovich, *Appl. Phys. Lett.* **95**, 262502 (2009).
3. “Vortex liquid-glass transition up to 60 T in nano-engineered coated conductors grown by metal organic deposition”, M. Miura, S. A. Baily, B. Maiorov, L. Civale, J. O. Willis, K. Marken, T. Izumi, K. Tanabe and Y. Shiohara, *Appl. Phys. Lett.* **96**, 072506 (2010).
4. “Vortex Viscosity in Magnetic Superconductors Due to Radiation of SpinWaves”, A. Shekhter, L.N. Bulaevskii and C.D. Batista, *Phys. Rev. Lett.* **106**, 037001 (2011).
5. “Liquid vortex phase and strong c-axis pinning in low anisotropy BaCo_xFe_{2-x}As₂ pnictide film”, B. Maiorov, T. Katase, S.A. Baily, H. Hiramatsu, T.G. Holesinger, H. Hosono and L. Civale, *Supercond. Sci. Technol.* **24**, 055007 (2011).
6. “Mixed pinning landscape at high temperature in nanoparticle-introduced YGdBa₂Cu₃O_y films grown by metal organic deposition”, M. Miura, B. Maiorov, S. A. Baily, N. Haberkorn, J. O. Willis, K. Marken, T. Izumi, Y. Shiohara and L. Civale, *Phys. Rev. B* **83**, 184519 (2011).
7. “Carbon nanotubes addition effects on MgB₂ superconducting properties”, A. Serquis, G. Pasquini and L. Civale, chapter in *Carbon Nanotubes / Book 5, in press* (2011).
8. “Highly aligned carbon nanotube forests coated by superconducting NbC”, G. Zou, H. Luo, S. Baily, Y. Zhang, N. Haberkorn, J. Xiong, E. Bauer, T. McCleskey, A. Burrell, L.Civale, Y.T. Zhu, J.L. MacManus-Driscoll, and Q.X. Jia, *Nature Communications, in press* (2011).
9. “Effect of doping on structural and superconducting properties in Ca_{1-x}Na_xFe₂As₂ single crystals”, N. Haberkorn, B. Maiorov, M. Jaime, I.O. Usov, M. Miura, G.F. Chen, W. Yu and L. Civale, *Phys. Rev. B, in press* (2011).

Submitted

1. “The effect of density and size of disorder on the vortex glassy phase in BaMO₃ (M=Zr, Nb, Sn) nanoparticles-introduced (Y,Gd)Ba₂Cu₃O_y films”, M. Miura, B. Maiorov, J.O. Willis, T. Izumi, Y. Shiohara, K. Marken, and L. Civale, *Phys. Rev. B, submitted* (2011).
2. “Role of carbon nanotube ribbon on the superconducting properties of epitaxial NbC films”, Y. Y. Zhang, F. Ronning, K. Gofryk, N. A. Mara, N. Haberkorn, G. Zou, H. Wang, J. H. Lee, E. Bauer, T. M. McCleskey, A. K. Burrell, L. Civale, Y. T. Zhu and Q.X. Jia, *Nanoletters, submitted* (2011).
3. “Measurements of the temperature dependent magnetic penetration depth in MgB₂ thin film using magnetic force microscopy”, J. Kim, L. Civale, J.D. Thompson, R. Movshovich, B.H. Moeckly, C.S. Yung and E. Nazaretski, *Appl. Phys. Lett., submitted* (2011).
4. “Strong pinning and elastic to plastic vortex crossover in Na-doped CaFe₂As₂ single crystals” N. Haberkorn, M. Miura, B. Maiorov, G.F. Chen, W. Yu, and L. Civale *Phys. Rev. B, submitted* (2011).
5. “Upper critical field and thermally activated flux flow in single crystalline Tl_{0.58}Rb_{0.42}Fe_{1.72}Se₂” L. Jiao, Y. Kohama, J.L. Zhang, H.D. Wang, B. Maiorov, F.F. Balakirev, Y. Chen, L.N. Wang, T. Shang, M.H. Fang, and H.Q. Yuan. *Phys. Rev. B, submitted* (2011).

Experimental Condensed Matter Physics Principal Investigators Meeting

1. **DOE award #:** DE-SC0002613
2. **Project Title:** “*High magnetic fields as a probe to unveil the physical properties of the newly discovered Fe oxypnictide superconductors and related compounds*”
3. **Name of the PI:** Luis Balicas
4. **Name of the recipient (Institution):** National High Magnetic Field Laboratory-Florida State University
5. **Project Scope:** The goal of this project is to undertake a complete and concerted effort in the physical characterization of Fe pnictides and related compounds at high magnetic fields, aiming at:

i) Determining their magnetic field-temperature phase-diagram by exploring their transport and magnetic properties as a function of field, temperature, and pressure. How much of their phase diagram is occupied by the vortex-liquid, vortex-lattice and/or vortex-glass phases? Are there additional superconducting and/or magnetic phases at higher fields?

ii) Clarifying if the boundary between the normal metal and the superconducting phase can be explained in terms of single band or multi-band superconductivity, or multiple superconducting phases,

iii) Understanding the origin of their extremely high upper critical fields,

iv) Exploring the possibility of observing the de Haas van Alphen effect, in order to study the evolution of the topography of the Fermi surface(s) as a function of doping/pressure,

v) Characterizing their under-doped regime due to the possible existence of a pseudogap phase as in the cuprates.

6. (Very...) Recent Progress

- i) Disorder-dependent superconducting phase-diagram at high magnetic fields in $\text{Fe}_{1+y}\text{Se}_x\text{Te}_{1-x}$ (in particular for $x \sim 0.4$)

We compared the high-field phase-diagram for the $\text{Fe}_{1+y}(\text{Te},\text{Se})$ series, particularly the diagram for the optimally doping compound $\text{Fe}_{1+y}\text{Te}_{1-(x\sim 0.6)}\text{Se}_{x\sim 0.4}$ synthesized by two methods: the first method is based on a traveling-solvent floating zone growth technique (TSFZ), which leads to crystals of acceptable crystallinity displaying “non-metallic” resistivity above the superconducting transition, optimal T_c s, with transition widths $\Delta T_c \approx 1$ to 3 K, see Figs. 1 (a) and (b). We compared their behavior with crystals resulting from a second growth method based on the Bridgman-Stockbarger (BS) technique which, in our case leads to crystals of poorer crystallinity (i.e. larger mosaicity), wider transitions and frequently to non-optimal T_c s in as grown crystals, as previously reported by other groups. [1] These last single-crystals were subjected to an annealing procedure which leads to metallic resistivity, considerably sharper resistive transitions $\Delta T_c \approx 1$ K, and to superconducting transitions comparable to those reported in the literature for high quality BS-grown single crystals as measured by SQUID magnetometry. [2] The annealed crystals having a clear metallic behavior preceding superconductivity, display considerably higher upper-critical fields when compared to those showing poor metallicity, particularly for magnetic-fields applied along the inter-layer direction. This increase leads to a distinct shape of the $H_{c2}^c(T)$, i.e. from an approximately linear in T behavior as reported in Ref. [3], to the marked concave down curvature followed by saturation at lower temperatures as seen in Ref. [4]. An analysis of our experimental data using a multiband theory for $H_{c2}(T)$ [5] shows that $H_{c2}(T)$ is indeed strongly Pauli limited with a Maki parameter $\alpha_M \approx 7$ -10, and predicts the Farrel-Fulde-Larkin-Ovchinnikov (FFLO) state [6], which is characterized by modulated superconducting gap, below 7K, see Fig. 1 (c). A detailed single crystal x-ray analysis reveals that the annealing process does not affect the crystallinity or the degree of mosaicity of our single-crystals nor the fraction of interstitial iron. isotropic phase diagram which combined with the enhancement in $H_{c2}^c(T)$, suggests that the fluctuations in the content of interstitial Fe contributes strongly to the suppression of superconductivity. Finally, we found, through a scaling analysis of the fluctuation conductivity in the neighborhood of the superconducting transition, that the superconducting fluctuations in this system are two-dimensional in character. And this is consistent with our estimation for the inter-

plane coherence length in this system, which in agreement with other groups, indicates that it is smaller or of the order of the inter-planar distance.

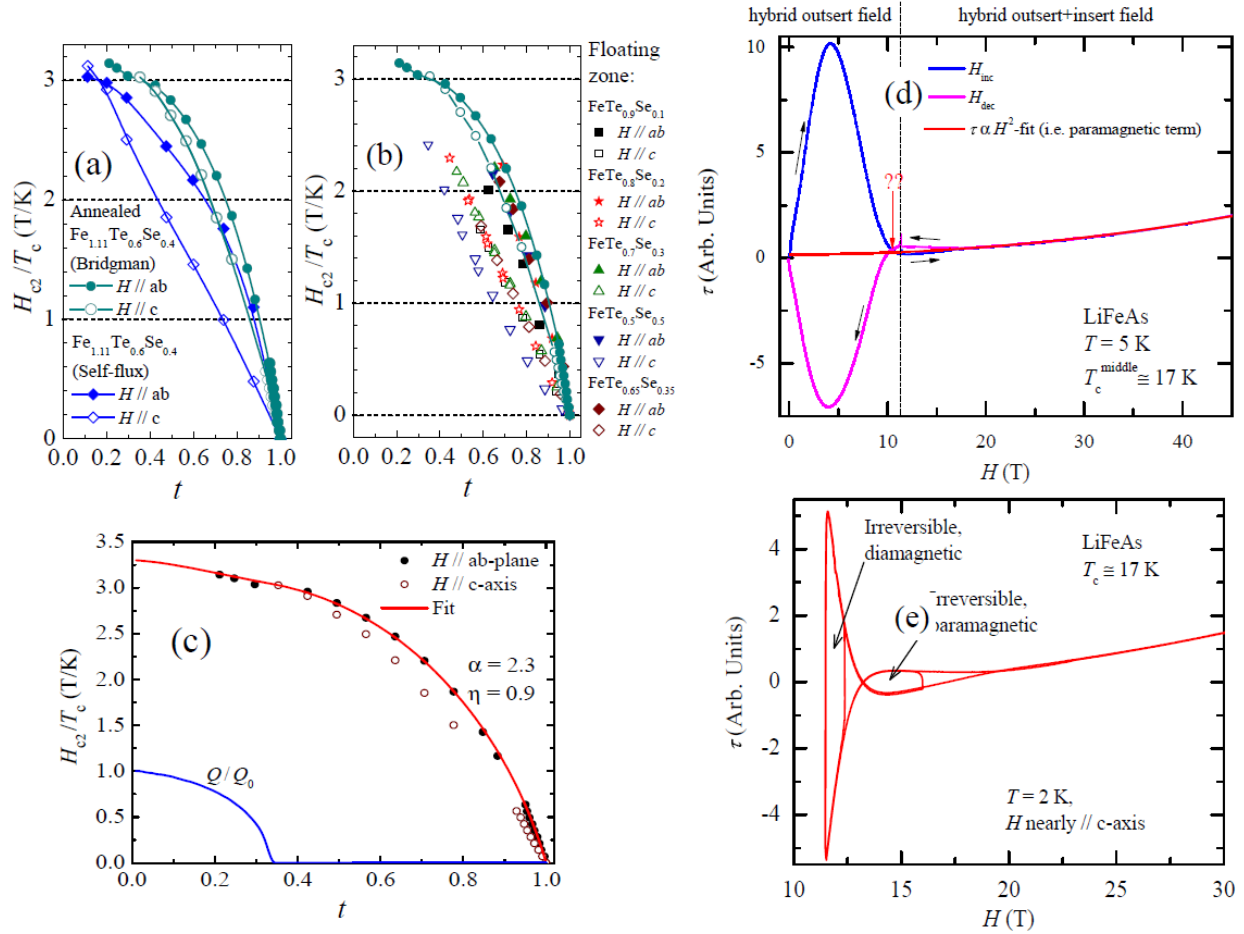


Fig.1. (a) Comparative superconducting phase-diagram under high magnetic fields where the upper critical field H_{c2} normalized by the superconducting transition temperature T_c , is plotted as a function of the reduced temperature $t = T/T_c$ for two single crystals: respectively for the Fe_{1+ δ} Se_{0.4}Te_{0.6} single crystal in Ref. [3] and for our annealed Fe_{1.11}Se_{0.4}Te_{0.6} (nominal stoichiometry) BS single-crystal. (b) Superconducting phase-diagram for several TSEZ grown single-crystals, where the phase-diagram for our annealed Fe_{1.11}Se_{0.4}Te_{0.6} BS single-crystal is also included. Open and solid markers depict the phase-boundary between metallic and superconducting states for fields along the c -axis and along a planar direction, respectively. All points for both graphs were extracted from the middle point of the resistive transition. (c) Upper critical fields H_{c2} as a function of $1-t$ where $t = T/T_c$ is the reduced temperature. Red lines are fits to a model discussed in Ref. [5] for a Pauli limited multi-band superconductor which assumes the emergence of a Farrel-Fulde-Larkin-Ovchnikov state (blue line). (d) Magnetic torque τ as a function of magnetic H for a nearly optimally doped LiFeAs single crystal ($T_c \cong 17$ K), at temperature of 5 K. Blue and magenta lines depict increasing and decreasing field sweeps, respectively. Notice, how a clearly large diamagnetic signal (broad peak) is followed by a small loop (whose beginning is indicated by the red arrow) which is characterized by a paramagnetic or nearly ferromagnetic response, before the reversible torque region is reached. Red line is a fit to $\tau \propto H^2$ which describes the paramagnetic component superimposed into the torque signal. Spikes observed at $H = 11.45$ T (paramagnetic irreversible torque region), correspond to the irreversible response associated with distinct field sweep rates, $\delta H/\delta t \cong 2$ T/min above 11.45 T (resistive insert of the hybrid magnet) and $\delta H/\delta t \cong 0.1$ T/min below 11.45 T (superconducting outsert of the hybrid magnet). (e) τ as a function of field in a limited scale, showing the different irreversible/hysteretic regimes in the vicinity of the upper critical field at a temperature $T = 2$ K.

ii) Paramagnetic Meissner response in the vicinity of H_{c2} in LiFeAs

The authors of Ref. [7] claim that the SC phase-diagram of LiFeAs can be well described within a theory for H_{c2} based on the multiband s^\pm pairing scenario within the clean limit, [8] assuming the existence of a FFLO like state for $H \perp c$ below 5 K. Stimulated by this preliminary report, we proceeded to perform high field torque measurements in LiFeAs single crystals in provenance of the group of C. W. Chu from the University of Houston. Since torque is proportional to magnetization which is a thermodynamic function of state, our goal was to obtain a thermodynamic confirmation, i.e. evidence for a phase transition within the superconducting state in the vicinity of the upper critical field which would indicate the presence of an additional phase-transition.

Figure 1 (d) and (e) show the magnetic torque as a function of the magnetic field (up to 45 T and 30 T, respectively) for a LiFeAs single-crystal close to optimal doping. For fields below 10 T one sees a typical hysteretic diamagnetic response, due to the pinning of vortices by either defects or geometrical barriers intrinsic to the crystal (collective pinning), which is characterized by a sharp peak whose amplitude and position in field depends on temperature. Remarkably, as the field further increased beyond 10 T, the sign of the irreversibility changes forcing the magnetic torque to display the same value for both increasing and decreasing field sweeps at a given field value (indicated by the red arrow). This crossing can only be consistent with an irreversible response which is paramagnetic or nearly ferromagnetic in nature, as if one was dealing with “antivortices”. In the literature one can indeed find reports of a “paramagnetic Meissner” response, for instance in the cuprates [9]. But in contrast to our results, it is usually observed only at extremely low magnetic fields, and is ascribed to the interplay between frustration among grains in granular samples and the d -wave symmetry of the superconducting gap [10]. In our case, this effect seems to disappear as the sample is rotated towards the ab -plane, which discards any role that one could associate with magnetic impurities, and indicates that this effect is intrinsically related to the superconducting phase diagram for fields along the inter-planar direction. Curiously, in the only compound for which the FFLO state is claimed to have been observed, i.e. CeCoIn₅, this state is claimed to coexist with a magnetic state presumably induced by the external field within the vortex cores associated with the complex vortex lattice structure associated with it [11]. Our results are suggestive of a similar scenario, although at this point we have to complete the phase diagram in Fig. 4, and check its reproducibility in several crystals and devices and techniques.

References

- [1] Y. Mizuguchi and Y. Takano, J. Phys. Soc. Jpn. **79**, 102001 (2010).
- [2] B. C. Sales *et al.*, Phys. Rev. B **79**, 094521 (2009).
- [3] M. Fang *et al.*, Phys. Rev. B **81**, 020509(R) (2010).
- [4] S. Khim, *et al.*, Phys. Rev. B **81**, 184511 (2010).
- [5] A. Gurevich, *et al.*, Phys. Rev. B **82**, 184504 (2010).
- [6] P. Fulde and R. A. Ferrell, Phys. Rev. **135**, A550 (1964); A. I. Larkin and Yu. N. Ovchinnikov, Sov. Phys. JETP **20**, 762 (1965).
- [7] K. Cho *et al.*, Phys. Rev. B **83**, 060502(R) (2011).
- [8] A. Gurevich, Phys. Rev. B **82**, 184504 (2010).
- [9] E. L. Papadopolou, *et al.*, Phys. Rev. Lett. **82**, 173 (1999).
- [10] M. Siegrist and T. M. Rice, Rev. Mod. Phys. **67**, 503 (1995).
- [11] M. Kenzelmann *et al.*, Science **321**, 1652 (2008)

7. Future plans:

Most of our attention in next year will be focused on three fronts:

- i. Understanding the origin of the paramagnetic like Meissner response in LiFeAs for fields close to the upper critical field. Does this correspond to a particular vortex state, or is this evidence for a phase transition within the superconducting state involving the superconducting order-parameter?
- j. Further refinement of the synthesis protocol of the FeSe_xTe_{1-x} series, with the goal of improving its crystallinity, reducing the amount of interstitial iron and the inhomogeneity of its distribution. The shape of the high field superconducting phase diagram seen by us and by other groups, shows a mild upturn at lower temperatures which can only be understood in

- terms of the presence of an additional superconducting phase akin to the so-called FFLO state characterized by a modulated superconducting gap. The synthesis of clean, high quality samples, currently one of our goals, is crucial to clarify this issue through thermodynamic measurements.
- k. Synthesis and physical properties of 122 Fe chalcogenide systems. These compounds seem to be radically different from the other Fe pnictide superconductors, where the magnetic moment of Fe is claimed to be very large. Also, for particular combinations of alkaline and iron concentrations, this system seems to undergo a phase transition towards an insulating state as in the cuprates. We want to study this interplay, and in particular clarify if or how the magnetism of Fe ions affects their superconducting phase diagram measured at high fields.
 - l. Search for further thermodynamic evidence for additional field-induced superconducting phases within the superconducting phase diagram of the Fe pnictide/chalcogenide compounds.
 - m. Continue our efforts to detect the de Haas van Alphen effect in these materials.
- 8. A list of publications resulting from DOE sponsored research that have been published in 2008-2011 (2009-2011 in our case):**
1. *Anisotropic phase diagram of the frustrated spin dimer compound $Ba_3Mn_2O_8$* , E. C. Samulon, K. A. Al-Hassanieh, Y.-J. Jo, M. C. Shapiro, L. Balicas, C. D. Batista, and I. R. Fisher, Phys. Rev. B **81**, 104421 (2010).
 2. *Possible Bose-Einstein condensate of magnons in single-crystalline $Pb_2V_3O_9$* , B. S. Conner, H. D. Zhou, Y. J. Jo, L. Balicas, C. R. Wiebe, J. P. Carlo, Y. J. Uemura, A. A. Aczel, T. J. Williams, and G. M. Luke, Phys. Rev. B **81**, 132401 (2010).
 3. *Atomic layers of hybridized boron nitride and graphene domains*, L. Ci, L. Song, C. H. Jin, D. Jariwala, D. X. Wu, Y. J. Li, A. Srivastava, Z. F. Wang, K. Storr, L. Balicas, F. Liu, P. M. Ajayan, Nat. Mater. **9**, 430 (2010).
 4. *Disorder-dependent superconducting phase-diagram at high magnetic Fermi surface evolution through a heavy-fermion superconductor-to-antiferromagnet transition: de Haas–van Alphen effect in Cd-substituted $CeCoIn_5$* , C. Capan, Y.-J. Jo, L. Balicas, R. G. Goodrich, J. F. DiTusa, I. Vekhter, T. P. Murphy, A. D. Bianchi, L. D. Pham, J. Y. Cho, J. Y. Chan, D. P. Young, and Z. Fisk, Phys. Rev. B **82**, 035112 (2010).
 5. *Short range ordering in the modified honeycomb lattice compound $SrHo_2O_4$* , S. Ghosh, H. D. Zhou, L. Balicas, J. S. Gardner, S. Hill, Y. Qiu, and C. R. Wiebe, J. Phys.-Condens. Mat. **23**, 164203 (2011).
 6. *Sequential Spin Polarization of the Fermi Surface Pockets in URu_2Si_2 and its Implications for the Hidden Order*, M. M. Altarawneh, N. Harrison, S. E. Sebastian, L. Balicas, P. H. Tobash, J. D. Thompson, F. Ronning, and E. D. Bauer, Phys. Rev. Lett. **106**, 146403 (2011).
 7. *Spin Liquid State in the $S=1/2$ Triangular Lattice $Ba_3CuSb_2O_9$* , H. D. Zhou, E. S. Choi, G. Li, L. Balicas, C. R. Wiebe, Y. Qiu, J. R. D. Copley, and J. S. Gardner, Phys. Rev. Lett. **106**, 147204 (2011).
 8. *Anisotropic Hysteretic Hall Effect and Magnetic Control of Chiral Domains in the Chiral Spin States of $Pr_2Ir_2O_7$* , L. Balicas, S. Nakatsuji, Y. Machida, and S. Onoda, Phys. Rev. Lett. **106**, 217204 (2011).
 9. *Multi-band superconductivity in $LaFeAsO_{0.9}F_{0.1}$ single crystals probed by high field vortex torque magnetometry*, G. Li, G. Grissonanche, A. Gurevich, N. D. Zhigadlo, S. Katrych, Z. Bukowski, J. Karpinski, and L. Balicas, Phys. Rev. B **83**, 214505 (2011).
 10. *Rearrangement of the antiferromagnetic ordering at high magnetic fields in $SmFeAsO$ and $SmFeAsO_{0.9}F_{0.1}$ single crystals*, S. Weyeneth, P. J. W. Moll, R. Puzniak, K. Ninios, F. F. Balakirev, R. D. McDonald, H. B. Chan, N. D. Zhigadlo, S. Katrych, Z. Bukowski, J. Karpinski, H. Keller, B. Batlogg, and L. Balicas, Phys. Rev. B **83**, 134503 (2011).
 11. *Floating zone crystal growth and structural distortion of $Pb_2V_3O_9$* , B.S. Conner, H.D. Zhou, L. Balicas, C.R. Wiebe, J. Whalen, T. Siegrist, J. Cryst. Growth **321**, 120 (2011).

Session 5

Two-Dimensional Electron Systems

Project Title: “Novel Temperature Limited Tunneling Spectroscopy of Quantum Hall Systems”

Principal Investigator: Raymond Ashoori (ashoori@mit.edu)

Institution: Massachusetts Institute of Technology

Project Scope:

Spectroscopic methods involving injection or ejection of electrons in materials have unique power in probing the electronic structure and interactions between electrons. The “single particle” spectrum obtained from techniques such as photoemission or tunneling spectroscopy is among the most fundamental and directly calculable quantities in theories of highly interacting systems. In ordinary superconductors, comparison of features in this spectrum with theory proved to be one of the primary experimental signatures validating the BCS theory of superconductivity. We are developing fundamentally new spectroscopic technique, time domain capacitance spectroscopy (TDCS), to measure the single-particle spectrum of the 2DES in semiconductors and of graphene without a perturbing scanning tip and with negligible electron heating, even when the in-plane conductivity of the system vanishes. The TDCS results have yielded unprecedented high-resolution measurements of the cold 2DES over a range of 20 meV (~200 Kelvin) above and below the Fermi surface. These measurements reveal the difficult-to-reach, beautiful, and surprising structure in this highly correlated system far from the Fermi surface. Our planned work extends the use of the TDCS technique to the 2DES at lower temperatures and with higher energy resolution, to edge states of the 2DES, and to the 2D hole system. The TDCS technique will be used to search for and characterize, with extraordinary resolution, features in the single-particle spectrum of semiconductors at energies both close to and well away from the Fermi energy. TDCS has already revealed a number of surprises in the quantum Hall system, and the work to be performed may reveal signatures of new quasiparticles, the nature of quantum Hall edge states, and the properties of the low carrier density 2D system as the carriers order to form an electronic crystal. With this progress, TDCS can grow to be applied to technologically important systems such as high-Tc superconductors, graphene, topological insulators, and spintronics systems to provide fundamental and previously unattainable data on the electronic properties of these materials.

Recent Progress:

We have made considerable progress since receiving our original grant in August of 2008, both in developing and improving our spectroscopic technique and in understanding the physics of low-dimensional electronic systems. In 2010, we published (with sole DOE support) a paper in *Nature* that describes striking and detailed features that appear in the spectrum of the quantum Hall system only at low temperatures (~100 mK) and at high magnetic fields. We have also observed a quasiparticle (a “plasmaron”) whose existence had first been predicted over 40 years ago. We have also developed a means to extract the dispersion

relation of quasiparticles within an electronic system and extract features such as changes to the mass of electrons that occur as a result of electron-electron interactions .

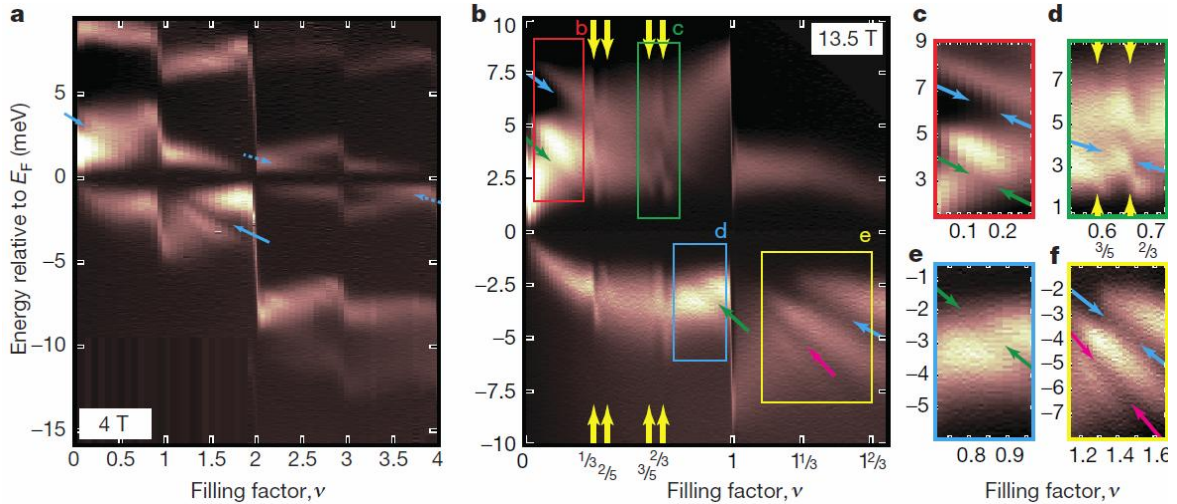


Figure 1 | High magnetic field TDCS spectra show ‘sash’ features: bright and dark diagonal lines across the spectrum. The horizontal axis in each spectrum is the electron density in the quantum well, expressed as a filling factor ν with $\nu=1$ corresponding to completely filling the lowest spin-polarized Landau level. The vertical axis is energy E measured from the Fermi energy E_F , with $E>0$ corresponding to injecting electrons into empty states in the quantum well and $E<0$ corresponding to ejecting electrons from filled states. Bright regions correspond to high single-particle density-of-states. a, Spectrum taken at a temperature of 100mK with a 4T perpendicular magnetic field. Features associated with the “ $\nu=1$ sash” are highlighted with a blue arrow, while another sash about $\nu=3$ is indicated with a dashed blue arrow. b, 13.5 T data, taken at 80 mK. The $\nu=1$ sash is similarly indicated with blue arrows, while the “ $\nu=1/2$ sash” that, when extrapolated, passes through the Fermi energy at $\nu=1/2$ is indicated with green. Sharp downward steps in the spectrum corresponding to chemical potential jumps at filling fractions corresponding to fractional quantum Hall plateaus are indicated with yellow arrows. The contrast for positive and negative energies has been adjusted separately in this spectrum. In c–f, selected regions of the spectrum in b are magnified and their contrast enhanced to ease identification of the features, indicated with arrows that match the colors in b.

Observation of Novel “Sash” Features: Application of a large magnetic perpendicular to a 2DES field produces massively degenerate Landau levels; within a Landau level the kinetic energy of the electrons is suppressed, and electron–electron interactions set the only energy scale. Coulomb interactions break the degeneracy of the Landau levels and can cause the electrons to order into complex ground states. We observed, in the high energy single particle spectrum of this system, salient and unexpected structure that extends across a wide range of Landau level filling fractions. The structure appears only when the two-dimensional electron system is cooled to very low temperatures, indicating that it arises from delicate ground state correlations.

As seen in Fig. 1, above, our TDCS results on a high mobility sample at low temperatures display a number of prominent “sash” features (see caption for an explanation of the meaning of these spectra; also see introductory section of this proposal for how these spectra are obtained). The bright (dark) regions in plots are regions of high (low) single-particle density of states (SPDOS). The plots display the SPDOS as a function of electron injection ($E > 0$) or ejection ($E < 0$) energy relative to the Fermi energy ($E = 0$ on the plots) as exchange-split Landau levels are filled with electrons (horizontal axis). The dark regions about the Fermi energy in each of the plots arise from a magnetic field-induced Coulomb gap that exists in two dimensions. In a simple picture, this gap develops because the magnetic field inhibits electrons already in the 2D system from moving away from the tunneling electron. The sash features appear as bright and dark lines cutting through the Landau level spectrum that appear to intersect with the Fermi energy at electron densities corresponding to filling fractions of $\nu = 1$, $\nu = 1/2$, and $\nu = 3$.

Amazingly, we find that the observed sashes disappear when the sample temperature is increased to a value far below the temperature equivalent of the energy at which the sash is seen. For instance, in Figure 1b, there are sash features occurring at 7 meV, or about 70 Kelvin, which disappear when the sample temperature is raised to 1 Kelvin. This behavior suggests that the high energy spectrum probes correlations in the ground state of the system. Hence, the high energy single-particle spectrum can be seen as a kind of microscope for electronic correlations.

Publications 2008-2011 resulting from DOE sponsorship:

O.E. Dial, R.C. Ashoori, L.N. Pfeiffer, K.W. West, “Anomalous structure in the single particle spectrum of the fractional quantum Hall effect”, Nature 464, pp. 566 – 570 (2010)

Lu Li, C. Richter, J. Mannhart, R. C. Ashoori, Coexistence of Magnetic Order and Two-dimensional Superconductivity at LaAlO₃/SrTiO₃ Interfaces (provisionally accepted for publication in Nature Physics)

O.E. Dial, R.C. Ashoori, L.N. Pfeiffer, K.W. West, “Observations of Plasmarons in a System of Massive Electrons” submitted for publication

Future Plans

Spectroscopy of the semiconductor 2DES at lower temperatures and with higher mobilities, Improvements to Experimental Apparatus and to Samples: The results shown above, as well as our prior work, were all performed at temperatures around 100 mK. As the resolution of our spectra is limited by the sample temperature, lower temperatures would allow us to obtain significantly more detailed structure. To improve signal to noise in the experiment, we are adding a second stage of amplification to the probe (amplifier at the 1K pot). To achieve low heating of the mixing chamber, we run our low temperature amplifier

(in the mixing chamber) at very low power (~ 5 mW) and a gain of less than unity (gain of about $2/3$). This means that the noise in the system is dominated by our room temperature 50W amplifier. By having a second stage amplifier (with a gain of about 10) at the 1K pot, we may be able to dramatically reduce the noise in the experiment. This will mean that we will be able to take significantly higher resolution data in the same amount of time as it now takes us for lower resolutions.

Composite Fermions: Composite fermion theory beautifully captures most of the features of the fractional quantum Hall effect by describing the 2D system as comprised of weakly interaction “composite fermions”. Essentially, electrons in this model bind even integer numbers of magnetic flux quanta (two flux quanta per electron for the simplest case) to themselves. One then treats the value of magnetic field for which there are two flux quanta per electron within the system (equivalent to filling factor $\nu=1/2$) as zero magnetic field for the composite fermions. Figure 2 shows possible identification of structures in our spectra that originate from composite fermions. In higher mobility samples and at lower temperatures, we may be able to see more features in the fan and to determine if we are indeed observing features originating from composite fermions.

Stripe and bubble phases: Spatial ordering of electrons into “stripe” and “bubble” features is thought to exist natively in the 2DEG around higher Landau level filling factors ($n>4$) and signatures of them may have appeared in transport properties of the 2D electron system at very low temperatures. They are thought to arise from a competition between long range Coulomb repulsion of electrons and short range exchange attraction (as well as the screening properties of the 2DEG for high Landau level filling). To date, the main experimental evidence for such structures comes from transport experiments revealing anisotropy in the sample conductance and evidence for pinning of a crystal in microwave conductivity studies. As we move to lower temperatures and higher mobilities, we will perform TDCS measurements in the hope of detecting signatures of this spatial ordering.

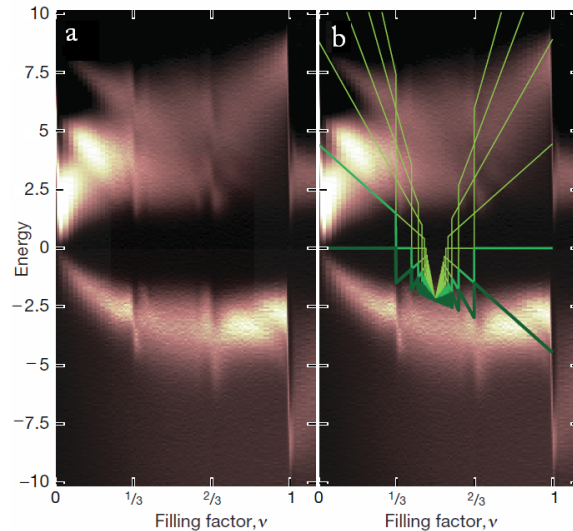


Figure 2: The 13.5T TDCS spectrum without (a) and with (b) the calculated composite fermion Landau fan superimposed allows identification of the two $\nu=1/2$ sash features (green line sloping down with left and right y-intercepts of +5 and -5 meV) a Landau level of the composite fermion fan closest to the Fermi surface. Lines suggested by the fan but not observed have been included to show alignment with chemical potential jumps (vertical glitches in data at $\nu=1/3$ and $\nu=2/3$ associated with known fractional quantum Hall states).

Microwave spectroscopy of electron solids: fractional quantum Hall effect and controlled disorder

Principal Investigator: Lloyd W. Engel, NHMFL/FSU, engel@magnet.fsu.edu

Project Scope

This project involves spectroscopic studies of solids of carriers in two-dimensional electron systems (2DES), in GaAs/Al_xGa_{1-x}As heterostructures. These solids, stabilized by mutual repulsion of carriers, are pinned by residual disorder, and exhibit a striking resonance in their rf or microwave spectra. This resonance is the motivation for studying these systems with microwave spectroscopy. Understood as a pinning mode, in which pieces of the solids oscillate within the potential of the disorder, the resonance is of interest both as the signature of a solid, and as a tool for the study of these solids. Fig. 1 explains the measurement technique, and shows an example of a resonance.

The electron solids are ubiquitous in low-disorder 2DES, in that they can be observed in many different ranges of Landau level filling, ν . The best known solid range is at the high magnetic field (B), low ν termination of the fractional quantum Hall series. In high quality n-type samples there is solid for ν both above and below the 1/5 fractional quantum Hall effect (FQHE), with a “reentrant” range of solid [1], located between the 2/9 and 1/5 FQHE. In higher Landau levels, there are other electron solid phases [2] which exhibit pinning modes: the “bubble” phases [3], lattices with multiple carrier guiding centers at each site, and the anisotropic “stripe” phases [4]. Within the ν ranges of quantum Hall plateaus, but not exactly at the quantizing “center” filling, ν_c , quasiparticles or holes have low partial Landau level filling $\tilde{\nu} = \nu - \nu_c$, and exhibit pinning modes [5] that behave as expected for a pinned Wigner solid of quasiparticles or quasiholes on top of one or more filled Landau levels.

Recent Progress

Evidence for Wigner crystals of 1/3 fractional quantum Hall quasiparticles

We have studied microwave conductivity spectra in the immediate vicinity of Landau level filling $\nu = 1/3$, with comparison to spectra taken near $\nu = 1$ in the same sample. The results are interpreted as due to Wigner crystallization of dilute fractionally charged quasiparticles. Fig. 2 shows the development of the resonance within the 1/3 FQHE.

Skyrmion solid near $\nu = 1$. In this work, skyrmion effects in the IQHWS around $\nu = 1$ effects are elucidated by systematic study of the dependence of the pinning mode on in-plane field, B_{\parallel} , which at fixed ν reduces the skyrmion spin. B_{\parallel} has essentially no effect on the pinning mode for ν just below 2, at which a Wigner crystal is composed of single Landau quasiholes. In contrast, B_{\parallel} increases the pinning frequency of the solid near $\nu = 1$ just under conditions for which the skyrmion sizes are predicted [6] to be significant. We find B_{\parallel} increases the pinning mode frequency only for small enough skyrmion density. This shows that spin size of skyrmions is affected by their mutual proximity [6], an illustration of the intertwined nature of charge and spin in this state.

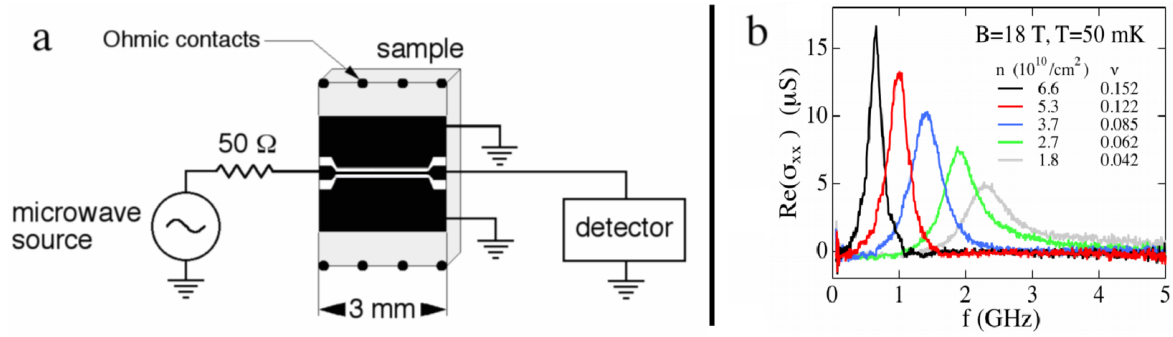


Figure 1: *a.* Schematic of measurement of a transmission line. The coplanar waveguide (CPW) transmission line is drawn to scale, as fabricated on the top of a sample. The highly conductive metal film that forms the CPW is shown as black. The metal side planes are grounded. *b.* Pinning mode of electron solid terminating the FQHE at high B . Density, n , is varied by means of a backgate.

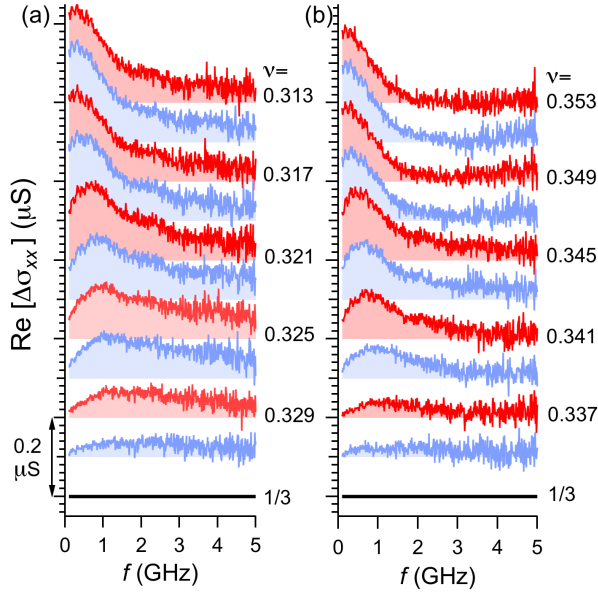


Figure 2: Spectra $\Delta\text{Re}(\sigma_{xx})(\nu)$ vs frequency, f , of pinning modes of quasiparticle/hole effect Wigner crystal near $\nu = 1/3$, taken for successive ν separated by steps of 0.002; successive spectra offset upwards for clarity. $\Delta\text{Re}(\sigma_{xx})(\nu)$ is $\text{Re}(\sigma_{xx})(\nu) - \text{Re}(\sigma_{xx})(\nu_c)$, where ν_c is the quantizing filling factor, $1/3$. Spectra are shaded to show zero. a) quasiholes, $\nu < 1/3$, b) quasiparticles, $\nu > 1/3$.

Quasi 3-D Wigner crystals: In-plane magnetic field effect on Wigner crystallization in wide quantum wells. Large in-plane magnetic field B_{\parallel} can be thought of as confining an electron to a magnetic length $l_{B_{\parallel}} = (\hbar/eB_{\parallel})^{1/2}$. When $l_{B_{\parallel}}$ is significantly less than the well width W , the carriers have some freedom the z -direction (growth direction) to alternate z from site to site, to minimize interelectron repulsion, forming a quasi-3D crystal [7]. Taking insulating behavior to indicate the presence of a pinned Wigner solid, references [7, 8] reported that applying B_{\parallel} shifted ν_s , the filling factor below which Wigner crystallization occurs, upward.

We have extensively studied the effect of B_{\parallel} on Wigner crystal formation as evidenced by the presence of the pinning mode. B_{\parallel} has more effect for larger carrier density, n . The quasi 3D states are expected to occur for this condition, since when the carriers are spaced far apart, it is less advantageous for them to avoid each other in the z direction.

Future Plans

Wigner solids of fractional quantum Hall quasiparticles

A natural extension of our recent results [9] on the resonance for ν just above and below $1/3$, would be to look for resonances within other FQH states. One of these is the spin transition [10] in the $2/3$ FQHE, another is the $1/5$ FQHE, for which the low ν and reentrant [1] electron solids are close by in filling. One possibility is to compare data on the different FQH states, to see the effects of different electron or composite fermion [11] (CF) Landau level. The Landau level affects the wave function of a carrier of the solid, and hence the coupling of the carrier to disorder and the resonance frequency. It may be possible (although challenging) to examine some of the delicate $N = 1$ Landau level states, which are of particular current interest.

Searching for resonances in other FQHE states than $1/3$ should be a matter of optimizing measuring techniques to more easily maintain the sensitivity needed to resolve the resonance signals, (which are comparatively small for FQH quasiparticle solids), while achieving better sample states. We have found that sample state can often be improved by using a transmission line with wider slots (see Fig. 1a): this may be due to reduced strain effects on the sample. Wider slots also can produce lower temperatures by reducing the effect of noise coming down the microwave coaxial cable to generate heat (mainly as resistive loss in the transmission line). Especially with wide slots, which reduce the sensitivity of the measurement, reduction of drift of the instrumentation is of great importance in looking at the small signals from the FQHWS pinning modes. Simply placing the room temperature instrumentation in a temperature-controlled (adequately cooled) box should greatly improve the spectra.

Samples with controlled disorder

These studies are intended to increase understanding of the pinning mode, while exploring the interplay of interaction and disorder in 2DES in high magnetic field. We will study the resonances of a series of samples in which the 2DES resides in $\text{Al}_x\text{Ga}_{1-x}\text{As}$, rather than pure GaAs. The random [12], point like disorder from the Al atoms is ideal for modeling in the context of weak pinning theory [13–15], and we propose to examine the x dependence of the resonance peak frequency, f_{pk} , with the aim of obtaining quantitative information on correlation lengths of solid order and shear moduli in the electron solids. At the same time we can investigate newly-reported reentrant phases [16] in these materials, and study the competition, strongly affected by disorder, between the FQH liquids and the electron solids.

The problem of understanding disorder is complicated by the several different kinds of disorder present in heterostructures in the low temperature limit: accidental impurities distributed throughout the material, interface roughness, and the potential of remote ionized dopants. As part of the study of samples of varying disorder we plan to measure pinning modes in heterostructure isolated field effect transistors (HIGFETs)[17], which have no deliberate dopants, and are populated by application of bias voltage to a nearby gate. Measurements of these devices at microwave frequency will require us to develop new techniques. Besides offering a different disorder environment, the devices have readily tunable density, and maintain good quality at lower densities than doped devices, potentially giving access to

conditions in which electron solids may be present for kinetic energy not completely frozen out by high magnetic field.

DOE-supported Publication List

G. Sambandamurthy, R. M. Lewis, Han Zhu, Y. P. Chen, L. W. Engel, D. C. Tsui, L. N. Pfeiffer, and K. W. West “Observation of Pinning Mode of Stripe Phases of 2D Systems in High Landau Levels,” *Phys. Rev. Lett.* **100**, 256801 (2008).

Han Zhu, G. Sambandamurthy, L. W. Engel, D. C. Tsui, L. N. Pfeiffer, and K. W. West, “Pinning mode resonances of two-dimensional electron stripe phases at high Landau levels”, *Physica B* **404**, 367-369 (2009).

G. Sambandamurthy, Han Zhu, Y. P. Chen, L. W. Engel, D. C. Tsui, L. N. Pfeiffer, and K. W. West, “Pinning modes of the stripe phases of 2D electron systems in higher Landau levels”, *Int J. Mod. Phys. B* **23**, 2628-2633 (2009).

Han Zhu, G. Sambandamurthy, L. W. Engel, D. C. Tsui, L. N. Pfeiffer and K. W. West, “Pinning mode resonances of 2D electron stripe phases: Effect of in-plane magnetic field”, *Phys. Rev. Lett.* **102**, 136804 (2009).

Han Zhu, G. Sambandamurthy, Yong P. Chen, Pei-Hsun Jiang, Lloyd Engel, D. C. Tsui, L. N. Pfeiffer, K. W. West, “Pinning mode resonance of a Skyrme crystal near Landau level filling factor $\nu = 1$ ”, *Phys. Rev. Lett.* **104**, 226801 (2010).

Han Zhu, Yong P. Chen, P. Jiang, L. W. Engel, D. C. Tsui, L. N. Pfeiffer, and K. W. West “Observation of a Pinning Mode in a Wigner Solid with $\nu = 1/3$ Fractional Quantum Hall Excitations”, *Phys. Rev. Lett.* **105**, 126803 (2010).

P. Jiang, A. F. Young, Philip Kim, L. W. Engel, and D. C. Tsui, “Quantum oscillations in graphene at microwave frequencies”, *Appl. Phys. Lett.* **97**, 062113 (2010).

References cited

- [1] H. W. Jiang *et al.* *Phys. Rev. Lett.*, 65(5):633–636, Jul 1990.
- [2] M. M. Fogler, A. A. Koulakov, and B. I. Shklovskii. *Phys. Rev. B*, 54(3):1853, 1996.
- [3] R M Lewis *et al.* *Phys Rev Lett*, 89(13):136804, 2002.
- [4] G. Sambandamurthy *et al.* *Phys. Rev. Lett.*, 100(25):256801, 2008.
- [5] Y. Chen *et al.* *Physical Review Letters*, 91(1):016801, 2003.
- [6] R. Côté *et al.* *Phys. Rev. Lett.*, 78(25):4825, 1997.
- [7] B. A. Piot *et al.* *Nat Phys*, 4(12):936, 2008.
- [8] W. Pan *et al.* *Phys. Rev. B*, 71(3):035302, 2005.
- [9] Han Zhu *et al.* *Phys. Rev. Lett.*, 105(12):126803, 2010.
- [10] J. P. Eisenstein *et al.* *Phys. Rev. B*, 41(11):7910, 1990.
- [11] J. K. Jain. *Phys. Rev. Lett.*, 63(2):199, 1989. doi: 10.1103/PhysRevLett.63.199.
- [12] Wanli Li *et al.* *Applied Physics Letters*, 83(14):2832, 2003.
- [13] H. A. Fertig. *Phys. Rev. B*, 59(3):2120–2141, Jan 1999.
- [14] R. Chitra, T. Giamarchi, and P. Le Doussal *Phys. Rev. B*, 65(3):035312, Dec 2001.
- [15] Michael M. Fogler and David A. Huse. *Phys. Rev. B*, 62(11):7553–7570, Sep 2000.
- [16] Wanli Li *et al.* *Phys. Rev. Lett.*, 105(7):076803, 2010.
- [17] B. E. Kane *et al.* *Applied Physics Letters*, 63(15):2132,1993.

Emergent Phenomena in Quantum Hall Systems Far From Equilibrium

Michael Zudov

School of Physics and Astronomy, University of Minnesota - Twin Cities, Minneapolis, MN 55455, USA

E-mail: zudov@physics.umn.edu Web: <http://groups.physics.umn.edu/zudovlab/>

Project Scope

The project expands upon a rapidly growing area of nonequilibrium transport phenomena recently discovered in very high Landau levels of two-dimensional electron systems (2DES) where Shubnikov-de Haas oscillations (SdHO) are not yet resolved. Among these phenomena are microwave-(MIRO) [1], phonon-[2], Hall field-[3] induced resistance oscillations, and several classes of combined oscillations [4]. Experimentally, all these effects often extend into the regime of separated Landau levels where other striking phenomena, such as microwave-induced zero-resistance states [5] and dc field-induced zero-differential resistance states [6] emerge. At the same time, the majority of theoretical proposals have been focusing on the regime of overlapping Landau levels and, as a result, their direct applicability to experiments remains limited. One of the objectives of the project is to understand how these and other emergent nonequilibrium transport phenomena evolve in the regime of *separated* Landau levels in a high-mobility 2DES and eventually explore their relevance in the quantum Hall effect regime.

Recent Progress

Giant microwave photoresistivity in high-mobility quantum Hall systems. We have recently observed a remarkably strong microwave photoresistivity effect in a high-mobility 2DES subject to a modest magnetic field and low temperature [7,8]. In contrast to MIRO which are observed at *all* cyclotron resonance harmonics and are known to *decay* away with increasing microwave frequency, this peak appears *only* near the *second* harmonic of the cyclotron resonance and *only* above a certain frequency f_0 (> 100 GHz, in our 2DES). Furthermore, this so-called X_2 peak [see Fig. 1 (a)] can be surprisingly strong, exceeding both MIRO and the dark resistivity by more than *one and two orders of magnitude*, respectively [8]. We have found that the peak appears in the regime *linear* in microwave intensity and quickly decays with increasing temperature. Appearing only in the separated Landau level regime, the peak cannot be explained by existing theories and its origin remains unclear.

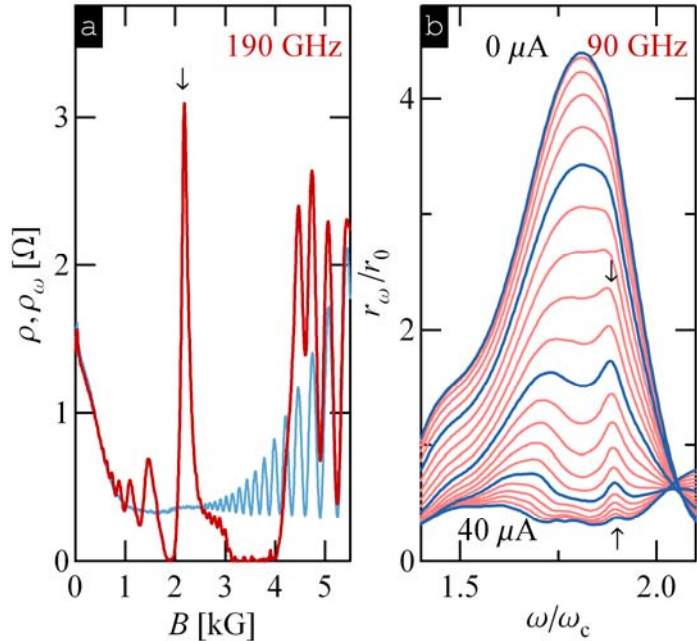


Fig. 1: (a) Magnetoresistivities measured without and with microwaves of $f = 190$ GHz. (b) Differential resistivity under microwaves of $f = 90$ GHz at currents from $I = 0$ to $40 \mu\text{A}$.

Nonlinear response of microwave photoresistance in a high mobility 2DES near the second harmonic of the cyclotron resonance. We have performed *nonlinear* transport studies of microwave photoresistance in a high-mobility 2DES over a wide range of microwave frequencies (up to 190 GHz) and dc currents (up to 100 μA) [9]. Remarkably, at a microwave frequency $f = 90$ GHz, which is lower than the critical frequency f_0 necessary for the observation of the X_2 peak at zero dc field, the peak shows up in nonlinear differential resistivity under modest dc fields, which apparently help to separate it from MIRO [Fig. 1 (b)]. Once developed, the X_2 peak persists over a wide range of dc currents and eventually evolves into a minimum (not shown). Most importantly, the position of the X_2 peak is largely *insensitive* to the applied dc field over the whole range of dc fields studied. This behavior is in contrast to the evolution of MIRO that shift to higher magnetic fields [4] in accordance with the “displacement” model [10]. Taken together, these findings give further evidence that the nature of the X_2 peak is different from that of MIRO and provide timely and important constraints for theoretical considerations.

Microwave Photoresistance in a 2D Electron Gas with Discrete Spectrum. In order to further investigate the regime of separated Landau levels, we have studied the evolution of linear response microwave photoresistance with the microwave frequency f , from 50 to 200 GHz [11]. In the overlapping Landau level regime, theory predicts that microwave photoresistivity oscillates as $\delta\rho_\omega \sim -\sin(2\pi\omega/\omega_c)$, where $\omega = 2\pi f$, ω_c is the cyclotron frequency. In this limit, the spacing between any cyclotron resonance harmonic and the closest maximum, called the phase $\varphi_n = n - \omega/\omega_c$, is close to 1/4 regardless of the microwave frequency. However, when the microwave frequency becomes sufficiently high, MIRO extend into the separated Landau level regime and the above expression is no longer valid. Here, the theory predicts that the phase φ_n will be *reduced* reflecting the ratio of the Landau level width Γ to the cyclotron energy, $\varphi_n \sim \Gamma/\omega_c$. This result implies that for a given (not-too low) ω , φ_n should increase with the oscillation order n (until it saturates at 1/4). At the same time one expects that, for a given n , φ_n will *decrease* with ω , while the number of peaks showing the reduced phase will *increase*. As a result, a comprehensive frequency dependence study is expected to yield information on how the Landau level width Γ evolves with the magnetic field.

Surprisingly, our recent experiments [11] revealed very unusual behavior. First, we confirmed that for a given ω , the phase φ_n is *decreasing* with *decreasing* $n \sim 1/B$, in agreement with previous studies [12]. At the same time, our analysis of the evolution of φ_n with

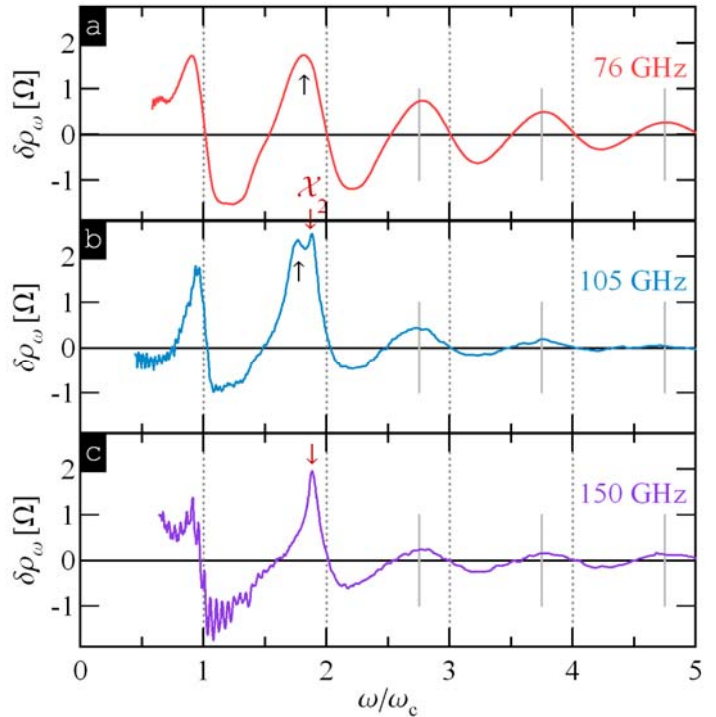


Fig. 2: Microwave photoresistivity $\delta\rho_\omega$ vs ω/ω_c at $f = 76$ GHz (a), 105 GHz (b), and 150 GHz (c).

$\omega \sim \omega_c \sim B$, does not show any noticeable decrease, as prescribed by $\varphi_n \sim \Gamma/\omega_c$. Instead, we find that for all n , φ_n remains roughly *the same* over the whole range of ω studied. We thus conclude that φ_n *depends strongly* on the oscillation order n , but not on the magnetic field. This finding clearly shows that the routinely observed reduced phase [11, 12] *cannot* be explained by the transition to the separated Landau level regime presenting a serious challenge for existing theories. Finally, this study revealed that the phase of the novel X_2 peak near the second harmonic of the cyclotron resonance [7-9] is also independent on B . Its value, however, is found to be significantly smaller (but not zero as proposed in [7]) than the MIRO phase (see Fig. 2 (b) where the X_2 peak appears on top of the second MIRO maximum).

Future Plans

It has been known for a long time that the amplitude of Shubnikov - de Haas Oscillations decreases when a high enough direct current is passed through the 2DES. The obvious candidate for such nonlinearity is the increase of the electron temperature which is caused by Joule heating. This scenario was investigated and confirmed in various 2DES [13], ranging from Si-inversion layers [14] to graphene [15]. On the other hand, many other studies [16] interpret dc field-induced suppression of the SdHO solely in terms of the so-called *inelastic* mechanism [17,18]. This mechanism originates from non-equilibrium distribution of electron states caused by electric field and was originally proposed to explain experiments on microwave photoresistance [1]. In addition to heating and inelastic mechanisms, there also exist the *displacement* mechanism [10,18] which stems from electric field-induced modification of impurity scattering rates and was successfully used to explain HIRO [3] as well as many other nonlinear phenomena [4]. Unfortunately Refs. 15 did not elaborate why (and if) heating and displacement mechanisms can be ignored in their experiments. In the near future we plan to systematically investigate the role of dc electric field on Shubnikov – de Haas oscillations (and in the regime preceding SdHO) in order to single out partial roles of heating, displacement, and inelastic contributions.

List of publications

- [A] M. A. Zudov, A. T. Hatke, L. N. Pfeiffer, K. W. West, “Microwave Photoresistance in a 2D Electron Gas with Discrete Spectrum” (2011) (submitted).
- [B] M. A. Zudov, A. T. Hatke, H.-S. Chiang, L. N. Pfeiffer, K. W. West, and J. L. Reno “Nonequilibrium transport in very high Landau levels”, *Journal of Physics: Conference Series* (2011) (in press).
- [C] A. T. Hatke, M. A. Zudov, L. N. Pfeiffer, and K. W. West, “Non-linear response of a high mobility two-dimensional electron system near the second harmonic of the cyclotron resonance”, *Physical Review B - Rapid Communications* **83**, 201301 (R) (2011) (published).
- [D] A. T. Hatke, M. A. Zudov, L. N. Pfeiffer, and K. W. West, “Giant microwave photoresistivity in a high-mobility quantum Hall system”, *Physical Review B – Rapid Communications* **83**, 121301(R) (2011) (published).
- [E] A. T. Hatke, M. A. Zudov, L. N. Pfeiffer, and K. W. West, “Resistance oscillations induced by the Hall field in tilted magnetic fields”, *Physical Review B – Rapid Communications* **83**, 081301(R) (2011) (published).

References

- [1] Zudov *et al.*, Phys. Rev. B **64**, 201311(R) (2001), Ye *et al.*, Appl. Phys. Lett. **79**, 2193 (2001), Hatke *et al.*, Phys. Rev. Lett. **102**, 066804 (2009).
- [2] Zudov *et al.*, Phys. Rev. Lett. **86**, 3614 (2001), Zhang *et al.* Phys. Rev. Lett. **100**, 036805 (2008), Hatke *et al.*, Phys. Rev. Lett. **102**, 086808 (2009).
- [3] Yang *et al.*, Phys. Rev. Lett. **89**, 076801 (2002), Hatke *et al.*, Phys. Rev. B **79**, 161308(R) (2009), Hatke *et al.*, Phys. Rev. B **83**, 081301(R) (2011).
- [4] Zhang *et al.*, Phys. Rev. Lett. **98**, 106804 (2007), Hatke *et al.*, Phys. Rev. Lett. **101**, 246811 (2008), Khodas *et al.*, Phys. Rev. Lett. **104**, 206801 (2010).
- [5] Mani *et al.*, Nature **420**, 646 (2002), Zudov *et al.*, Phys. Rev. Lett. **90**, 046807 (2003), Willett *et al.*, Phys. Rev. Lett. **93**, 026804 (2004), Smet *et al.*, Phys. Rev. Lett. **95**, 116804 (2005).
- [6] Bykov *et al.*, Phys. Rev. Lett. **99**, 116801 (2007), Romero *et al.*, Phys. Rev. B **78**, 153311 (2008), Hatke *et al.*, Phys. Rev. B **82**, 041304(R) (2010).
- [7] Dai *et al.*, Phys. Rev. Lett. **105**, 246802 (2010).
- [8] Hatke *et al.*, Phys. Rev. B **83**, 121301(R) (2011).
- [9] Hatke *et al.*, Phys. Rev. B **83**, 201301(R) (2011).
- [10] Durst *et al.*, Phys. Rev. Lett. **91**, 086803 (2003), Lei and Liu, Phys. Rev. Lett. **91**, 226805 (2003), Vavilov and Aleiner, Phys. Rev. B **69**, 035303 (2004), Khodas and Vavilov, Phys. Rev. B **78**, 245319 (2008).
- [11] Hatke *et al.*, submitted (2011).
- [12] Zudov, Phys. Rev. B **69**, 041304(R) (2004); Studenikin *et al.*, Phys. Rev. B **71**, 245313 (2005); Phys. Rev. B **76**, 165321 (2007).
- [13] Neugebauer and Landwehr, Phys. Rev. B **21**, 702 (1980), Sakaki *et al.*, Surf. Sci. **142**, 306 (1984), Hirakawa and Sakaki, Appl. Phys. Lett. **49**, 889 (1986), Leadley *et al.*, Semicond. Sci. Tech. **4**, 879 (1989), Ma *et al.*, Phys. Rev. B **43**, 9033 (1991), Balkan *et al.*, Phys. Rev. B **52**, 17210 (1995), Chow *et al.*, Phys. Rev. Lett. **77**, 1143 (1996), Tiras *et al.*, Phys. Rev. B **64**, 085301 (2001).
- [14] Neugebauer and Landwehr, Phys. Rev. B **21**, 702 (1980).
- [15] Tan *et al.*, arXiv:1104.3678 (2011).
- [16] Zhang *et al.*, Phys. Rev. B **75**, 081305(R) (2007), Phys. Rev. B **80**, 045310 (2009), Kalmanovitz *et al.*, Phys. Rev. B **78**, 085306 (2008), Romero *et al.*, Phys. Rev. B **78**, 153311 (2008), Vitkalov, Int. J. of Mod. Phys. B **23**, 4727 (2009).
- [17] Dmitriev, Mirlin, and Polyakov, Phys. Rev. Lett. **91**, 226802 (2003), Dmitriev *et al.*, Phys. Rev. B **71**, 115316 (2005).
- [18] Vavilov, Aleiner, and Glazman, Phys. Rev. B **76**, 115331 (2007).

Project Title: Quantum Electronic Phenomena and Structures

PIs: Wei Pan, Sandia National Laboratories (wpan@sandia.gov)
Michael P. Lilly, Sandia National Laboratories (mplilly@sandia.gov)
Ken S.K. Lyo, Sandia National Laboratories (sklyo@sandia.gov)
John L. Reno, Sandia National Laboratories (jlreno@sandia.gov)
Lisa A. Tracy, Sandia National Laboratories (latracy@sandia.gov)
George T. Wang, Sandia National Laboratories (gtwang@sandia.gov)
Rohit P. Prasankumar, Los Alamos National Laboratories (rpprasan@lanl.gov)

Collaborators: S.R.J. Brueck, University of New Mexico,
S. Das Sarma, University of Maryland
G. Gervais, McGill University, Canada
Z. Jiang, Georgia Tech
J. Kono, Rice University
D.C. Tsui, Princeton University

Project Scope:

We explore in this project quantum electronic and optical properties in MBE/CVD grown and/or lithographically patterned nanoelectronic structures. The proposed research address the issues of what novel types of quantum collective behaviors can emerge from nanostructures and how well this behavior can be controlled and manipulated. The Quantum Transport in Structured Semiconductors Thrust addresses quantum transport properties in low-dimensional semiconductor systems. We search and examine novel phenomena arising due to strong electron-electron interactions and the interplay between disorder and electron-electron interaction. The focus of the Growth and Properties of III-Nitride and III-V Nanowires Thrust is to synthesize high quality III-nitride and III-V heterostructure nanowires that may exhibit unexpected and exciting quantum electronic properties. Ultrafast time-resolved optical measurements are also utilized to examine carrier dynamics in these nanostructures.

Recent Progress:

Impact of disorder on the 5/2 non-Abelian quantum Hall state: The electron-electron (e-e) interaction plays an important role in two-dimensional electron systems (2DESs) and is known to induce novel quantum ground states, e.g., the many-body quantum Hall effect states. In addition to e-e interactions, disorder has a similarly important impact on the quantum states in 2DESs, and the interplay between disorder and e-e interactions remains a major line of research. Here, we present our recent results on how the nature of disorder affects the 5/2 energy gap and, thus, the stability of this state. The 5/2 fractional quantum Hall effect (FQHE) state has been at the center of current quantum Hall research due to the possibility of it being non-Abelian and, thus, having potential applications in fault-tolerant topological quantum computation. There is an urgent need to understand the impact of disorder on this FQHE state, since a larger energy gap at 5/2 would exponentially reduce error rates and make the envisioned quantum computation more robust. In this study, we compare the activation energy gap data obtained in two types of samples: symmetrically doped modulation quantum-well samples and undoped heterojunction insulated gate field-effect transistors (HIGFETs). In

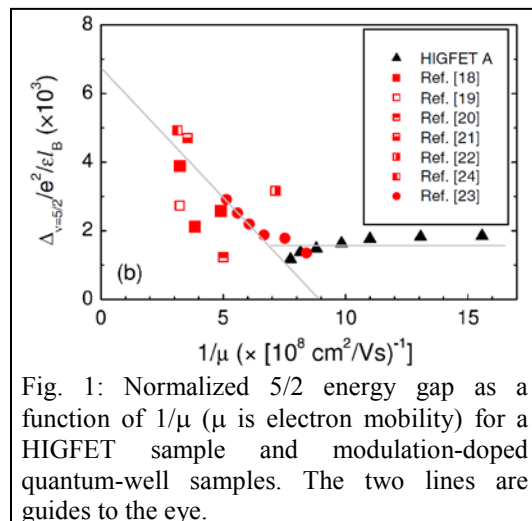


Fig. 1: Normalized 5/2 energy gap as a function of $1/\mu$ (μ is electron mobility) for a HIGFET sample and modulation-doped quantum-well samples. The two lines are guides to the eye.

modulation-doped quantum-well samples, where long-range Coulombic disorder dominates, the energy gap (shown as the squares and dots in Fig.1) drops quickly with decreasing mobility (or increasing disorder). On the other hand, in HIGFET samples, where the short-range neutral disorder dominates, the $5/2$ energy gap (the triangles in Fig. 1) shows only a weak mobility dependence. Our results clearly demonstrate that the two types of disorder play very different roles in affecting the stability of the $5/2$ state.

Re-entrant Negative Coulomb Drag in a 1D Quantum Circuit: Coulomb drag measurements were carried out between tunable vertically-coupled quantum wires. The wires are fabricated in a GaAs/AlGaAs double quantum well heterostructure with a 15 nm barrier separating the quantum wells. This design allows an independent control over the subband occupancy in each independently contacted

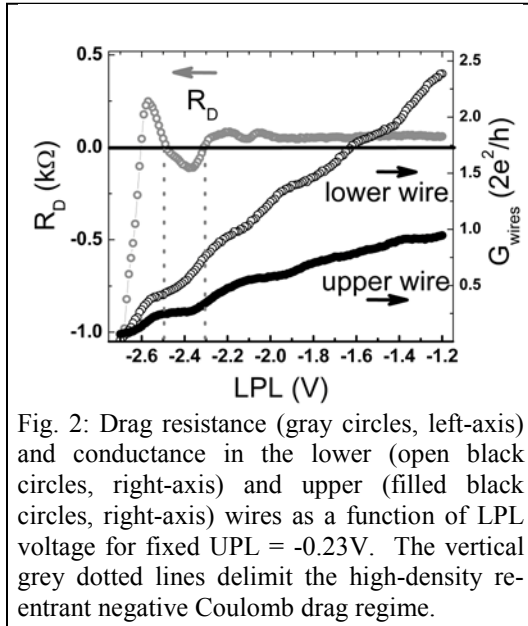


Fig. 2: Drag resistance (gray circles, left-axis) and conductance in the lower (open black circles, right-axis) and upper (filled black circles, right-axis) wires as a function of LPL voltage for fixed UPL = -0.23V. The vertical grey dotted lines delimit the high-density re-entrant negative Coulomb drag regime.

quantum wire, a first in a device with such a small interwire separation. The Coulomb drag signal is mapped out versus the number of subbands occupied in each wire, and regions of both positive and negative drag are observed. A single Coulomb drag trace taken from such a mapping is shown in figure 2 (gray circles, left-axis), along with the conductance in the lower wire (open black circles, right-axis) and in the upper wire (filled black circles, right-axis). Negative Coulomb drag signals are measured in two regimes: one at low electronic density when the drag wire is close to or beyond depletion and one at a higher electronic density when the drag wire has one or more single 1D subbands occupied. This re-entrant high density negative drag signal is delimited by the vertical dotted gray lines in figure 2. This is the first observation of a negative one-dimensional Coulomb drag signal in wires with a 1D subband occupancy greater than, or equal to one. We proposed the re-entrant negative drag signal in terms of localization, electron-hole asymmetry and band structure.

Spatial Distribution of Defect Luminescence on GaN Nanowires: The spatial distribution of defect and band-edge luminescence of GaN nanowires was studied using spatially-resolved cathodoluminescence (CL) imaging and spectroscopy (Ref. 30). Using this high resolution technique, defect-related yellow luminescence was revealed to be primarily surface-related (Fig. 3), possibly due to the diffusion of mobile point defects during growth. Mitigation of these surface defects will be key to controlling the nanowire electronic properties via interface engineering.

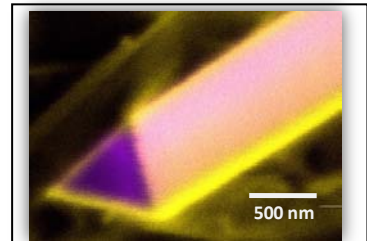


Fig. 3: CL image showing defect related yellow luminescence at the GaN nanowire surface, and band-edge emission at the core.

Carrier Dynamics in III-Nitride Nanowires: Optical pump-probe experiments were carried out on III-nitride nanowire ensembles, revealing that carrier relaxation through the defect states responsible for yellow luminescence increased with the nanowire growth temperature. Experiments also revealed that AlGaN and AlN shell layers of GaN nanowires passivate the surface defects. Recently, we have performed the first ultrafast optical experiments on single III-nitride nanowires, allowing us to uncover new physics that was obscured in experiments on nanowire ensembles.

Future Plans:

Spin polarization of the fractional quantum Hall states in the first excited Landau level: Surprisingly, very little data are available for the spin polarization of the fractional quantum Hall (FQH) states in this Landau level. On the other hand, answers to this question will help us to better understand the nature of these FQH states, in particular the $5/2$ and $12/5$ states, which are believed to be of non-Abelian and have potential applications in fault-tolerant topological quantum computation. We plan to systematically study the spin polarization utilizing the tilted magnetic field technique in ultra-high mobility two-dimensional electron systems. In particular, we will examine whether the transition from a FQH state to an anisotropic state at $5/2$ is a first order quantum phase transition, predicted by a theoretical model. Possible spin transition under tilt magnetic fields will also be examined for the $12/5$ state, a possible candidate of the more exotic parafermionic FQH state.

Double Quantum Wires: With the goal of studying 1D correlation physics we will use the new samples to measure 1D-2D tunneling, 1D-1D tunneling for a single subband and Coulomb drag between 1D wires. These transport measurements will probe the density of states and interwire electron-electron scattering due to Coulomb interactions. These effects should depend on the nature of the 1D ground state, and provide a useful tool to access Luttinger liquid effects. In addition to these dc transport techniques, we have developed a high frequency (\sim GHz) reflectometry technique for quantum computing measurements. While this is primarily for the detection of single electron events in quantum dots, we will try to make conductance measurements of single long quantum wires on the time scale of 100 nanosec to 1 microsec. The combination of double wire experiments and fast transport measurements has significant potential for new studies of quantum wires.

Spin Physics in 2D Holes: Building on recent successes in growth of high-mobility two-dimensional hole systems (2DHS) via C doping of (100) oriented GaAs/AlGaAs heterostructures, we propose to develop 2DHS at Sandia for experiments investigating the spin degree of freedom in nanostructures. After successful development of 2DHS, we propose to perform experiments investigating hole spins in bulk 2D systems. For example, measurements of the spin-orbit coupling can be made via magnetotransport. Another goal would be to experimentally determine the coupling between hole and nuclear spins in the host semiconductor using nuclear magnetic resonance (NMR) techniques, such as resistively-detected NMR, to verify the magnitude and form of the coupling predicted by theory.

Growth and Electronic Properties of Nanowires: We will focus on growth and characterization of core-shell nanowires, primarily Al(Ga)N/GaN and patterned InGaAs/GaAs nanowires, in order to continue our study of interface manipulation and engineering of nanowires, and the resulting effects on their electrical and optical properties. These core-shell nanowires will allow us to examine the novel structure and physics of 1D and 2D electron and hole gases that may be formed at the heterointerfaces in free-standing semiconductor nanowires, as predicted by our recent theoretical work (Ref 34). We will also fabricate and study the properties of Al(Ga)N/GaN nanowire heterostructures using a recently-developed top-down nanowire fabrication technique, which may yield nanowires with fewer point defects. Obtaining better understanding of and control over these phenomena could enable the development of ultrafast and ultraefficient nanowire-based electronic and photonic devices.

Ultrafast Dynamics in Nanowires: We will use terahertz (THz) time-domain spectroscopy (THz-TDS) to measure the conductivity of core-shell nanowires in a non-contact manner, which will enable us to study 1DEG/2DEG formation in these systems. Optical-pump terahertz-probe measurements will enable us to temporally resolve conductivity dynamics in these nanomaterials after ultrafast photoexcitation. Additionally, we will continue our pump-probe experiments on individual nitride nanowires. Our initial focus will be to optimize the spatial resolution of this technique, which should enable us to image carrier dynamics in individual nanowires with sub-100 fs temporal and sub-micron spatial resolution. Performing

such measurements will enable us to directly image, for example, the effects of radial heterostructuring on charge transport in a single GaN core/AlGaN shell nanowire, with direct impact on the use of these nanowires in nanoscale transistor and waveguide applications.

Selected Publications (2008-2011):

1. W. Pan, S. K. Lyo, J. L. Reno, J. A. Simmons, D. Li, and S. R. J. Brueck, *Applied Physics Letters* **92**, 052104 (2008).
2. W. Pan, J. S. Xia, H. L. Stormer, D. C. Tsui, C. Vicente, E. D. Adams, N. S. Sullivan, L. N. Pfeiffer, K. W. Baldwin, and K. W. West, *Physical Review B* **77**, 075307 (2008).
3. D. Huang, S. K. Lyo, K. J. Thomas, and M. Pepper, *Phys. Rev. B* **77**, 085320 (2008).
4. D.R. Luhman, W. Pan, D. C. Tsui, L. N. Pfeiffer, K. W. Baldwin, K. W. West, *Physical Review Letters* **101**, 266804 (2008).
5. S. K. Lyo, *Phys. Rev. B* **77**, 195306 (2008).
6. T.M. Lu, L. Sun, D. C. Tsui, S. Lyon, W. Pan, M. Mühlberger, F. Schäffler, J. Liu, Y. H. Xie, *Physical Review B* **78**, 233309 (2008).
7. E. Bielejec, J. L. Reno, S. K. Lyo and M. P. Lilly, *Solid State Communications* **147**, 79 (2008).
8. E. H. Hwang and S. Das Sarma, *Phys. Rev. B* **78**, 075430 (2008)
9. C. P. Morath, J. A. Seamons, J. L. Reno and M. P. Lilly, *Phys. Rev. B* **78**, 115318 (2008).
10. Q. Li, G. T. Wang, *J. Cryst. Growth*, **310**, 3706 (2008).
11. Q. Li, G. T. Wang, *Appl. Phys. Lett.*, **93**, 043119 (2008).
12. I. Arslan, A. A. Talin, G. T. Wang, *J. of Phys. Chem. C* **112**, 11093 (2008).
13. P. C. Upadhyaya, Q. Li, G. T. Wang, A. J. Fischer, A. J. Taylor, R. P. Prasankumar, *Semiconductor Science and Technology*, 2008.
14. A. A. Talin, G. T. Wang, E. Lai, R. J. Anderson, *Appl. Phys. Lett.*, **92**, 093105 (2008).
15. S. K. Lyo, *Phys. Rev. B* **79**, 125328 (2009).
16. D. Huang, S. K. Lyo, and G. Gumbs, *Phys. Rev. B* **79**, 155308 (2009).
17. W. Li, C. L. Vicente, J. S. Xia, W. Pan, D. C. Tsui, L. N. Pfeiffer, K. W. West, *Phys. Rev. Lett.* **102**, 216801 (2009).
18. J. A. Seamons, C. P. Morath, J. L. Reno and M. P. Lilly, *Phys. Rev. Lett.* **102**, 026804 (2009).
19. S. K. Lyo, *Phys. Rev. B* **79**, 125328 (2009).
20. C. P. Morath, J. A. Seamons, J. L. Reno and M. P. Lilly, *Phys. Rev. B* **79**, 041305 (2009).
21. G. T. Wang, Q. Li, A. A. Talin, A. Armstrong, Y. Lin, J. Huang, *ECS Trans.* **19**, 55 (2009).
22. R. P. Prasankumar, P. C. Upadhyaya, A. J. Taylor, *Phys. Stat. Solidi B* **246**, 1973 (2009).
23. Y. Lin, Q. Li, A. Armstrong, G. T. Wang, *Solid State Commun.*, **149**, 1608 (2009).
24. G. Stan, C. V. Ciobanu, T. P. Thayer, G. T. Wang, J. R. Creighton, K. P. Purushotham, L. A. Bendersky, R. F. Cook, *Nanotechnology* **20**, (2009). (Cover Article)
25. Q. Li, Y. Lin, J. R. Creighton, J. J. Figiel, G. T. Wang, *Adv. Mater.* **21**, 2416 (2009). (Cover Article)
26. W. Li., J.S. Xia, C. Vicente, N.S. Sullivan, W. Pan, D.C. Tsui, L.N. Pfeiffer, K.W. West, *Phys. Rev. B* **81**, 033305 (2010).
27. S.K. Lyo, *Phys. Rev. B* **81**, 115303 (2010).
28. D. Laroche, S. Das Sarma, G. Gervais, M.P. Lilly, and J.L. Reno, *Appl. Phys. Lett.* **96**, 162112 (2010).
29. P.C. Upadhyaya, Q.M. Li, G.T. Wang, A.J. Fisher, A.J. Taylor, R.P. Prasankumar, *Semi. Sci. Tech.* **25**, 024017 (2010).
30. Q.M. Li and G.T. Wang, *Nano Lett.* **10**, 1554 (2010).
31. W. Pan, J.L. Reno, D. Li, and S.R.J. Brueck, *Phys. Rev. Lett.* **106**, 156806 (2011).
32. W. Pan, N. Matuhara, N.S. Sullivan, K.W. Baldwin, K.W. West, L.N. Pfeiffer, and D.C. Tsui, *Phys. Rev. Lett.* **106**, 206806 (2011).
33. T.M. Lu, W. Pan, D.C. Tsui, P.C. Liu, Z. Zhang, and Y.H. Xie, accepted to *Phys. Rev. Lett.*
34. B.M. Wong, F. Leonard, Q. Li, G.T. Wang, *Nano Lett*, dx.doi.org/10.1021/nl200981 (2011)

Experimental Condensed Matter Physics Principal Investigators Meeting

Abstract

Project Title: Cold Exciton Gases in Semiconductor Heterostructures

Principal Investigator: Leonid Butov

Institution: University of California, San Diego

e-mail address: lvbutov@physics.ucsd.edu

webpage: <http://physics.ucsd.edu/~lvbutov>

Project Scope

An indirect exciton is a bosonic quasi-particle formed by an electron and a hole confined in separated quantum well layers. Due to their properties, indirect excitons form a model system both for the studies of basic properties of cold bosons and for the development of optoelectronic devices: (i) Indirect excitons have long lifetimes and can cool down to temperatures well below the temperature of quantum degeneracy. This gives an opportunity to realize cold excitons gases. (ii) Indirect excitons have built-in dipole moments and their energy can be controlled by voltage. This gives an opportunity to create a variety of potential landscapes for indirect excitons and use them as a tool for studying the physics of excitons. (iii) Indirect excitons have long spin relaxation times. This allows studying exciton spin transport and other spin-related phenomena. (iv) Indirect excitons can travel over large distances. This gives an opportunity to measure exciton transport by imaging spectroscopy. Within this project, we study excitons in lattices and moving lattices – conveyers, spin-related phenomena in cold exciton gases and coherent phenomena in cold exciton gases.

Recent Progress (since the start of the project in August 2010)

Electrostatic conveyer for excitons

We realized controlled transport of indirect excitons via moving lattices – conveyers created by a set of voltages applied to the electrodes on the sample surface. The wavelength of this moving lattice is set by the electrode periodicity, the amplitude is controlled by the applied voltage, and the velocity is controlled by the ac frequency. The excitonic conveyer realizes controlled transport of excitons as charged coupled devices (CCD) realize controlled transport of electrons. We found the dynamical localization-delocalization transition for excitons in the conveyers and determined its dependence on exciton density and conveyer amplitude and velocity [1, t5].

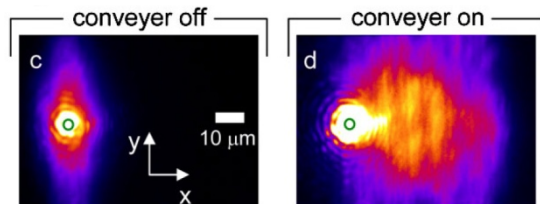


Fig. 1. Exciton conveyer. Exciton emission images for conveyer off and on. Exciton transport via conveyer is presented by the extension of the exciton cloud along the direction of the moving potential [1, t5].

Spin texture in a cold exciton gas

We observed spin textures in a cold exciton gas in a GaAs/AlGaAs coupled quantum well structure. Spin textures spontaneously form around the exciton rings, which serve as sources of cold excitons. The

observed phenomena include a vortex of linear polarization and extended coherence of excitons in the polarization vortex, a skew of the exciton fluxes in orthogonal circular polarizations and a corresponding four-leaf pattern of circular polarization, a ring of linear polarization, and a periodic spin texture. These phenomena emerge below a few Kelvin. The data indicate a ballistic exciton transport regime where the spin polarization is locked to the direction of particle propagation and scattering is suppressed [2, t1-t4].

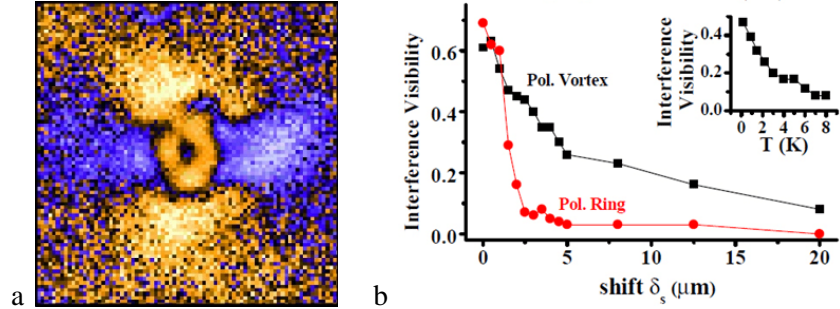


Fig. 2. An example of the observed exciton spin textures. (a) Polarization image showing exciton spin texture with x- and y-polarized excitons (yellow and blue). A ring of linear polarization and a vortex of linear polarization with polarization perpendicular to the radial direction are presented. (b) Visibility of interference between the emission of excitons, which are laterally separated by δ_s . Extended coherence of excitons is observed in the polarization vortex. Insert shows the temperature dependence [2, t1-t4].

Pattern of spontaneous coherence and phase singularities in a cold exciton gas

We observed pattern of spontaneous coherence and phase singularities in a cold exciton gas in a GaAs/AlGaAs coupled quantum well structure. Extended spontaneous coherence of excitons is observed in the region of the polarization vortices and in the region of the macroscopically ordered exciton state. The coherence length in these regions is much larger than in a classical gas, indicating a coherent exciton state with a much narrower than classical exciton distribution in momentum space, characteristic of a condensate. The observed phase singularities include phase domains and fork-like dislocations in the interference pattern. Extended spontaneous coherence, spin texture, and phase singularities are spatially correlated and emerge when the exciton gas is cooled below a few Kelvin [t1-t4].



Fig. 3. An example of the observed phase singularities. Fork-like dislocation in interference pattern characteristic of a phase singularity [t1-t4].

Excitons in 2D lattices

We developed a method to create 2D electrostatic lattices for excitons and realized square, triangular, and honeycomb lattices. Cold atoms in lattices have been intensively used for the exploration of condensed-matter physics. For excitons in electrostatic lattices, parameters of both the lattice, e.g., the lattice amplitude, and the particles, e.g., the exciton density, can be accurately controlled as for cold atoms in lattices. Parameters of excitons differ from the atomic ones by orders of magnitude. Therefore, studies of excitons in controllable lattices can give new insights into this field [t6].

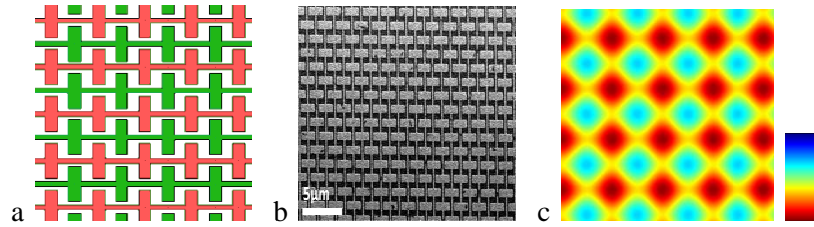


Fig. 4. An example of 2D lattices for excitons. (a) Schematic of electrode pattern, (b) SEM image of electrodes, and (c) exciton potential landscape for a square lattice. A color bar presents the exciton energy variation [t6].

Future Plans

The planned activities for the near future follow the proposal and the results of the first months of the research.

For the first part of the project – excitons in lattices – we plan to continue the study of excitons in 2D lattices. In particular, we plan to study exciton transport and localization-delocalization transition for excitons in 2D lattices.

For the second part of the project – exciton conveyers – we plan to develop exciton conveyers in circular geometry, i.e. stirring potentials, which can be used for generation and control of exciton vortices.

For the part of the project – spin related phenomena in cold exciton gases and coherent phenomena in cold exciton gases – we plan to study the observed spin textures, pattern of spontaneous coherence, and phase singularities in a cold exciton gas.

A list of publications and presentations at conferences and schools resulting from DOE sponsored research since the start of the project in August 2010

1. A.G. Winbow, J.R. Leonard, M. Remeika, Y.Y. Kuznetsova, A.A. High, A.T. Hammack, L.V. Butov, J. Wilkes, A.A. Guenther, A.L. Ivanov, M. Hanson, A.C. Gossard, Electrostatic Conveyer for Excitons, arXiv:1102.5329v1 (2011); Phys. Rev. Lett. 106, 196806 (2011).
2. A.A. High, A.T. Hammack, J.R. Leonard, Sen Yang, L.V. Butov, T. Ostatnicky, A.V. Kavokin, A.C. Gossard, Spin Texture in a Cold Exciton Gas, arXiv:1103.0321v1 (2011).
- t1. L.V. Butov, Cold Excitons, 2010 Michigan Summer School ‘Quantum Simulation and Metrology’, Ann Arbor, MI (Aug 2-13, 2010).
- t2. L.V. Butov, Cold Excitons, 3rd International School on Nanophotonics and Photovoltaics, Zakhadzor, Armenia (Sep 15-22, 2010).
- t3. L.V. Butov, Spin Texture in a Cold Exciton Gas, The 41st Winter Colloquium on the Physics of Quantum Electronics PQE-2011, Snowbird, Utah (Jan 2-6, 2011).
- t4. A.A. High, A.T. Hammack, J.R. Leonard, Sen Yang, L.V. Butov T. Ostatnicky, A.V. Kavokin, A.C. Gossard, Spin Texture in a Cold Exciton Gas, APS March Meeting 2011, Dallas, TX (Mar 21-25, 2011).
- t5. J.R. Leonard, A.G. Winbow, M. Remeika, Y.Y. Kuznetsova, A.A. High, A.T. Hammack, L.V. Butov, J. Wilkes, A.A. Guenther, A.L. Ivanov, M. Hanson, A.C. Gossard, Electrostatic conveyer for excitons, APS March Meeting 2011, Dallas, TX (Mar 21-25, 2011).
- t6. M. Remeika, L.V. Butov, M. Hanson, A.C. Gossard, Excitons in Electrostatic Lattices, APS March Meeting 2011, Dallas, TX (Mar 21-25, 2011).
- t7. Y.Y. Kuznetsova, J.R. Leonard, L.V. Butov, J. Wilkes, A.L. Ivanov, A.C. Gossard, Excitation energy dependence of the exciton inner ring, APS March Meeting 2011, Dallas, TX (Mar 21-25, 2011).

Session 6

Low-Dimensional Systems

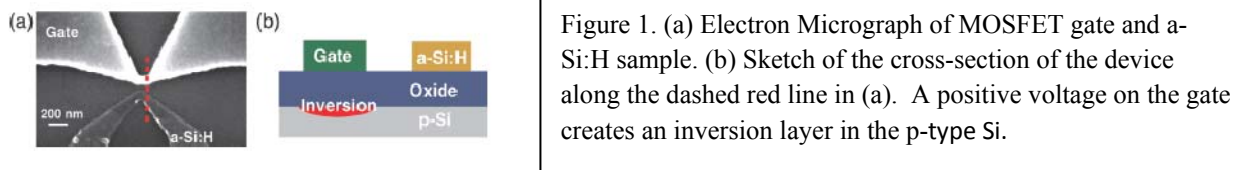
Project Title: Measurement of Single Electronic Charging of Semiconductor Nano-Crystals
PI: Marc A. Kastner, mkastner@mit.edu
Institution: Massachusetts Institute of Technology

Project Scope

The long-range goal is to use charge sensing to measure the motion of single electrons as they hop among the semiconductor nano-crystals in a two-dimensional array. Such nano-crystals have been identified as potentially useful for solar cells, because their optical absorption can be tuned, by varying their size, across the solar spectrum. In principle, a mixture of different sizes could be therefore used to improve solar cell efficiency beyond the Shockley-Queisser limit. While the optical properties of individual nano-crystals are well controlled and understood, the transport of electrons and holes through an array of such nano-crystals is not. Single-electron tunneling between quantum dots in GaAs heterostructures, in which the confinement is induced by nanometer-size electrodes, has been measured using narrow transistors as charge sensors. The technique allows the measurement of tunneling rates, and gives detailed information about what limits charge transport. We have fabricated nanometer-size charge sensors integrated with nanometer-size samples of nano-crystal arrays. Future work will be aimed at measuring the single-electron tunneling events as well as identifying possible collective motion of electrons.

Recent Progress

When we began this project there were two major technical obstacles that we had to overcome. The first was to integrate a nanometer-size transistor with a different material, in which the motion of electrons is to be measured. The second was to fabricate uniform nano-crystal films on the nanometer length scale. We have now overcome both of these hurdles.



We and others had great success in using narrow transistors (also called quantum point contacts) in GaAs/AlGaAs heterostructures as the charge sensors for observation of single-electron tunneling between quantum dots *in the same heterostructure*. However, no one had ever used a narrow transistor to measure charge motion in a nearby different material. Our first publications have announced that we have done this. We used electron-beam lithography to create narrow MOSFETs, ~ 100 nm wide, and to fabricate a similarly narrow strip of semiconductor, in the first case amorphous Si:H, nearby. An electron micrograph and sketch of the cross-section of the device are given in Figure 1. Applying a step voltage to the a-Si:H results in a transient change in conductance of the MOSFET because of the motion of charge in the a-Si:H, and this can be used to measure the resistance of the a-Si:H. The MOSFET is an electrometer integrated with the sample of interest, and because its input capacitance is very small, extremely large resistances can be measured. We can measure resistances four orders of magnitude larger using this technique than by measuring current in the same sample. Furthermore, the technique can be used even when the contacts are much more resistive than the sample, as we have recently demonstrated.

Figure 2(a) shows the transient observed in the conductance of the MOSFET when the step voltage is applied to the a-Si:H. This is converted to a conductance, and is measured as a function of temperature (Fig. 2b). The open circles are the data that can be measured with conventional methods. One can measure resistances as large as $\sim 10^{18} \Omega$ with the charge sensing method.

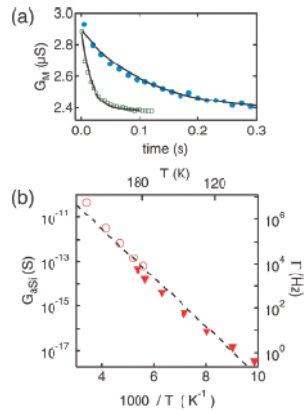


Figure 2. Conductance of the MOSFET G_M as a function of time at $T=125$ K (closed circles) and 140 K (open squares); the latter is offset for clarity. At $t = 0$ the voltage applied to one of the a-Si:H contacts is changed from -1.8 to -2.7 V. The solid lines are theoretical fits used to extract the conductance. (b) Conductance through the a-Si:H G_{aSi} , obtained from charge transients (closed triangles) and from measuring current (open circles) with a voltage bias across the a-Si:H of ≈ -2.3 V. For the charge transient measurement the rate of decay Γ is given on the right-hand axis. The dashed line is a fit to simply activated behavior.

Creating uniform films of nano-crystals has been a challenge that we have only recently met. In general, the large oleic acid cap molecules needed to produce nano-crystals that are very uniform in size, makes the tunneling of electrons between nano-crystals extremely slow, and thence the conductance extremely small. This has been overcome either by cap exchange with smaller molecules or annealing to degrade the cap molecules. However, these treatments generally lead to films that are cracked. We have found that exchanging the oleic acid capping ligand for n-butylamine while the nano-crystals are still in solution results in deposited films that are uniform and much more highly conducting. Furthermore, we are able to pattern these films using electron beam lithography and liftoff.

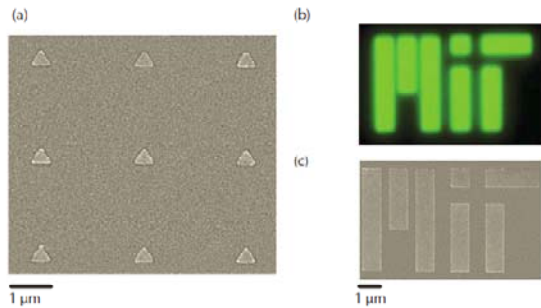


Figure 3. Examples of nano-crystal films patterned with electron-beam lithography. (a) Electron micrograph of triangles showing feature size as small as ~ 40 nm. (b) Photoluminescence from a patterned film, and (c) electron micrograph of the same pattern. The nano-crystals are CdSe.

Figure 3 shows examples of nano-crystal films patterned on the nanometer length scale. One can see that features as small as ~ 40 nm can be created using e-beam lithography and liftoff. The photoluminescence shows that the non-radiative recombination rate for nano-crystals in the patterned films is not radically increased.

Future Plans

Our plan is to now integrate the charge sensor with a narrow strip of nano-crystals nearby to search for single-electron tunneling and other charge fluctuations. The narrow MOSFETs generate their own single-electron signals, because of tunneling of electrons between the inversion layer and traps, probably in the oxide adjacent to it. For this reason, we are fabricating devices with two MOSFETs, one on each side of the nano-crystal film. We have shown that tunneling events inside one MOSFET are not detected by the second, but we expect that both MOSFETs will be sensitive to charge motion in the nano-crystal films. An electron micrograph of the dual-MOSFET structure is shown in Figure 4.

Single-electron tunneling will be detected if electrons tunnel over large enough distances. For lateral quantum dots in GaAs, such detection is effective if the tunneling distance is ~ 300 nm. Our measurements of the temperature dependence of the current-voltage characteristic on large area films have led us to conclude that the transport is limited by nearest-neighbor tunneling, in which case the tunneling distance

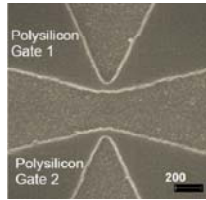


Figure 4. Electron micrograph of a double-MOSFET device. The nano-crystal film will be patterned between the two transistors and contacts will be made to it with gold electrodes outside the field of view.

would be too short to be observed by the MOSFETs. However, the large area and the cracking, mentioned above, may be influencing the results. We will first use our charge sensing to measure the current-voltage characteristic as a function of temperature on the crack-free, small area samples. We will then study the time dependence of the MOSFET conductance, looking for correlated transients in the two MOSFETs.

In addition to single-electron tunneling events, we may observe collective motion of electrons resulting from the long-range Coulomb interaction. It has been predicted that when the two-dimensional density of electrons or holes is commensurate with the density of nano-crystals, the Coulomb interaction will lead to a charge-density wave that is pinned. Because of disorder, it is much more difficult to observe such commensurability effects in large-area samples. However, in a small sample the correlation length of the hexagonal close-packed order of the nano-crystals can be comparable to the sample size, making the correlations more easily observable. It has been predicted that these correlations should result in large variations of the activation energy of the conductance as a function of gate voltage. We will search for this by using the Si substrate as a gate to add charge carriers to the nano-crystal film. In addition, the formation of a charge density wave may give rise to narrow-band noise if the pinning can be overcome with field. This would be observable with our charge sensors.

Publications

“Measuring charge transport in a thin solid film using charge sensing,” K. MacLean, T. S. Mentzel and M. A. Kastner, *Nano Letters* **10**, 1037 (2010)

“The effect of electrostatic screening on a nanometer scale electrometer,” K. MacLean, T. S. Mentzel and M. A. Kastner, *Nano Letters* **11**, 30 (2011)

"Colloidal Quantum Dot Films, Transport and Magnetotransport"

Philippe Guyot-Sionnest, The University of Chicago.

BES ECMP PI meeting, August 9-12 2011

Project Scope

Research in colloidal quantum dots (CQD) is increasingly applied towards applied electrooptical devices, including LEDs, PV and photodetection. Our DOE work is on the basic electrical properties of films of CQD. We study monodispersed dots. We investigate the effect of carrier density, temperature and matrix. CQD solids allow to test the models of conduction in disordered systems, in particular variable range hopping. The small density of state allows to observe effects of magnetic field on the conductance, such as spin-blockade and wave-function squeezing, and we are searching for magnetic polarons. The CQD solids also exhibit large 1/f conductance noise that is not quantitatively understood.

Recent progress

A. Magnetic polarons in magnetic impurity doped quantum dots. The RKKY model predicts that in a quantum dot, the coupling between magnetic impurities is strongly affected by unpaired electrons.¹ This allows for voltage-controlled magnetic materials. There are reports of such effect in epitaxial materials.^{2 3 4 5} Recently Gamelin et al showed that photoexcitation of one exciton in CdSe:Mn colloidal dots lead to a magnetic polaron.⁶ Over the past several years we investigated Mn²⁺ doping in various colloidal quantum dots, CdSe, CdS, ZnSe, and core/shells, and developed the ability to charge the dots with controlled average number of electrons. However we have not yet observed the expected changes in magnetic properties. At present there are no synthesis of monodispersed Mn²⁺ doped colloidal dots in which electrons or holes can be injected, and therefore this experiment may still be mostly a synthetic challenge. Systems that are currently being explored are HgTe:Mn, ZnTe:Mn/HgTe and ZnTe:Mn/CdTe core/shell systems. The development of these systems is in progress and the search for voltage tunable magnetic CQD solids is on-going.

B. Conduction in films of quantum dots. We finished a detailed study of the *dc* conductance of CdSe colloidal dot films. The model of variable range hopping conductivity predicts a crossover between Mott and Efros-Shklovskii as a function of temperature and density of states. This was observed using monodispersed CdSe colloidal quantum dot 3D solids where the density of states at the Fermi level is varied by electrochemistry⁷. The temperature dependence of the conductivity shows the 1/4 Mott exponent at low density, while the 1/2 Efros-Shklovskii exponent appears at high densities. That study gives us confidence that prior literature on disordered semiconductors is directly applicable to the conductivity in CQD solids

Recently, we developed HgTe colloidal dots. HgTe is a semi-metal with a zero energy gap. However small nanocrystals have a gap between the Γ_8 valence and conduction bands. Figure 1a show an absorption spectrum of the HgTe colloidal dots with an edge at 3 microns. Films of HgTe CQDs readily exhibit conductivity due to thermally excited carriers, and it is also strongly modulated by the electrochemical potential as shown in figure 1b. The 10⁵-fold increase in conductance occurs concurrently with the reversible current for reduction (negative side) and

oxidation (positive side). Overall, this new system responds extremely well to electrochemical doping, with stable, reversible and repeatable charging both for n and p-side.

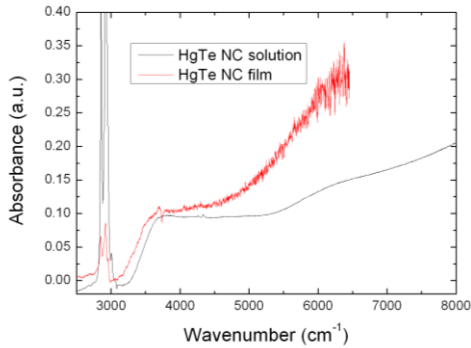


Fig 1a: room-temperature absorption spectra of HgTe NCs in TCE solution (black) and on Pt coated electrodes after crosslinking with hexanedithiol. The 3000cm^{-1} peak is due to hydrocarbons.

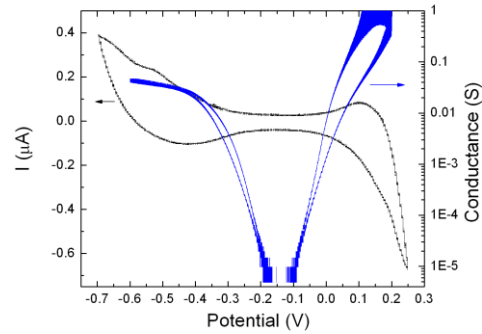


Fig 1b: Cyclic voltammetry (black) and conductance (blue) of the HgTe NC film at 210K

C. Magnetoresistance in colloidal quantum dot arrays as a function of charging and composition.

We study the magnetoresistance in pure CdSe or CdSe/CdS quantum dot films, where the MR is attributed to spin-blockade. Positive MR of 35% was obtained in films of CdSe/CdS dots, at high bias, low charging level and with mixed sizes.⁸ The explanation is that spin-blockade is most effective when the coupling between electrons of separate dots is weakest. Spin blockade should be more effective in one-dimensional channels and at lower bias. We investigate samples in Anodized Aluminum Oxide (AAO) with pores adjustable between 20 and 60 nm diameter as shown in Fig. 2a. The results are rather similar to prior results with interdigitated electrodes except for a more robust MR at higher temperature (fig.2c) and for lower biases of a few volts (fig.2b).

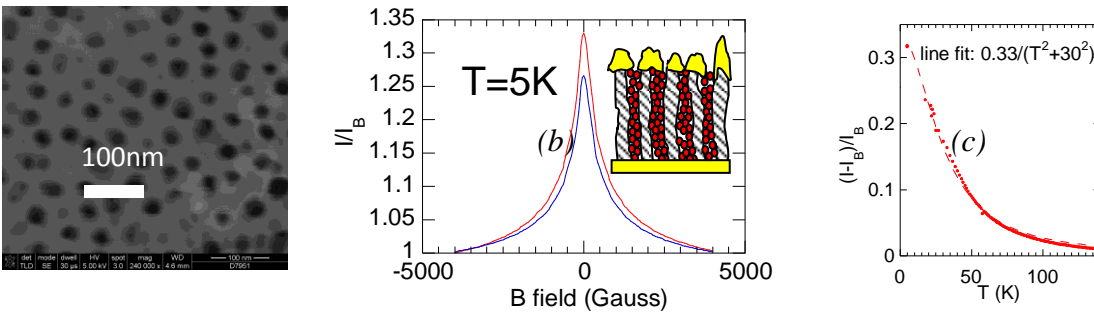


Figure 2: a) SEM image of the pores at the AAO surface. b) MR at 4V (red curve) and 5 V (blue curve) through a film of $\sim 400\text{nm}$ thick AAO filled with CdSe dots and capped with a porous Au layer. c) Temperature dependence of the MR response. A guide to the eye fit uses a Lorentzian with 30K half-width.

Future plans

The investigation of magnetic doped colloidal dots is on-going, and the study of the electrical properties of HgTe quantum dot films is on-going as well. The study of spin-blockade in AAO

channels is nearly finished. Our studies of electrical conductivity in colloidal dot films brought about the issue of conductance noise in these systems. The $1/f$ noise is very large, orders of magnitude larger than in a homogeneous conductor of similar gap and average carrier density. We therefore have started looking into noise in the transport of colloidal dot solids. Figure 3 shows preliminary results for HgTe.

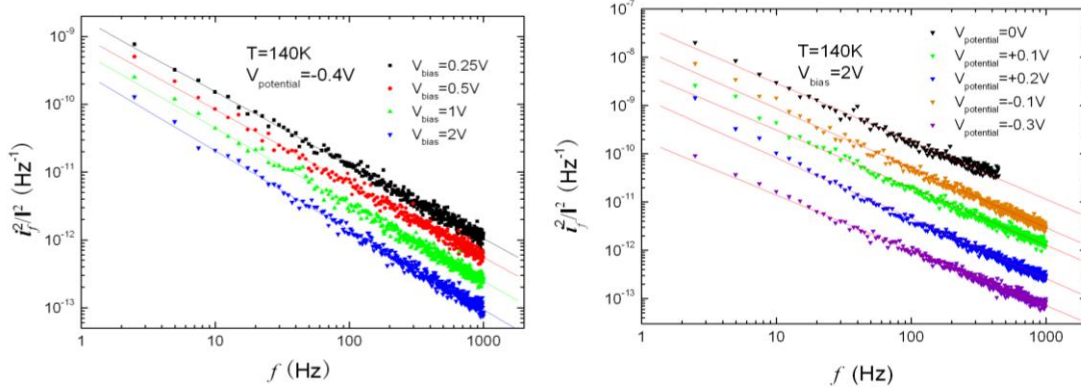


Fig 3: $1/f$ noise power spectrum density normalized by the DC current at different biases (left) and potentials (right) for HgTe colloidal dots. Left: at one fixed potential, -0.4V corresponding to about 2 electrons/dot, the normalized spectral density of the noise decreases under increasing bias. Right: at a fixed bias (2V), the sample is charged to different levels, from the intrinsic regime with $\sim 10^{-3}$ electron/hole per dot to ~ 1 electron/dot and the normalized spectral density of the noise decreases by about 3 orders of magnitude. All lines are linear fits and the slopes vary from 1 to 1.2

Noise has been investigated in granular conductors,^{9 10 11} with predictions¹² of $1/f$ noise in the hopping regime. There is however no quantitative modeling of the magnitude of the noise and its physical origin remains uncertain. In our observations, the noise is reduced with increased bias, lower temperature, and higher charge density. Noise sources may come from single quantum dots as well as the assembly. At the single dot level, PL blinking already exhibits a $1/f$ power law while a film of dots has a granular structure with many possible constricted paths.

We will therefore compare different realization of colloidal dots solids, metals (Au) and semiconductor (CdSe and HgTe). With their tunable properties including their surfaces, size and monodispersivity, packing, and electron occupation, they are promising systems to investigate noise.

List of publications

1. “Thermal Properties of Mid-infrared Colloidal Quantum Dot Detectors” by Emmanuel Lhuillier, Sean Keuleyan, Paul Rekkemeyer and Philippe Guyot-Sionnest, accepted by *J. Appl. Phys.*
2. “Mid-infrared HgTe colloidal quantum dot photodetectors” by Sean Keuleyan, Emmanuel Lhuillier, Vuk Brajuskovic and Philippe Guyot-Sionnest, accepted by *Nature Photonics*.
3. “Mott and Efros-Shklovskii Variable Range Hopping in CdSe Quantum Dots Films” by Liu H (Liu, Heng), Pourret A (Pourret, Alexandre), Guyot-Sionnest P (Guyot-Sionnest, Philippe) *ACS nano* Volume: 4 Pages: 5211-5216 (2010)

4. “Magnetoresistance of CdSe/CdS quantum dot films” by Pourret A (Pourret, Alexandre), Ramirez A (Ramirez, Adan), Guyot-Sionnest P (Guyot-Sionnest, Philippe) *Appl. Phys. Lett.* Volume: 95 Article Number: 142105 (2009)
5. “Atomic Layer Deposition of ZnO in Quantum Dot Thin Films” by Pourret A (Pourret, Alexandre), Guyot-Sionnest P (Guyot-Sionnest, Philippe), Elam JW (Elam, Jeffrey W.) *Adv. Mat.* Volume: 21 Pages: 232-+ (2009)

References:

- ¹ Exciton magnetic polaron in semimagnetic semiconductor nanocrystals, Bhattacharjee AK, laGuillaume CBA, PHYSICAL REVIEW B Volume: 55 Issue: 16 Pages: 10613-10620 Published: APR 15 1997
- ² Ferromagnetism mediated by few electrons in a semimagnetic quantum dot, Fernandez-Rossier J, Brey L PHYSICAL REVIEW LETTERS Volume: 93 Issue: 11 Article Number: 117201 Published: SEP 10 2004
- ³ Optically controlled magnetization of zero-dimensional magnetic polarons in CdMnTe self-assembled quantum, Mackowski S, Gurung T, Nguyen TA, Jackson HE, Smith LM, Kossut J, Karczewski G, PHYSICA STATUS SOLIDI B-BASIC RESEARCH Volume: 241 Issue: 3 Pages: 656-659 Published: MAR 2004
- ⁴ Magnetic polarons in a single diluted magnetic semiconductor quantum dot, Maksimov AA, Bacher G, McDonald A, Kulakovskii VD, Forchel A, Becker CR, Landwehr G, Molenkamp LW, PHYSICAL REVIEW B Volume: 62 Issue: 12 Pages: R7767-R7770 Published: SEP 15 2000
- ⁵ Room-Temperature Electric-Field Controlled Ferromagnetism in Mn_{0.05}Ge_{0.95} Quantum Dots, Xiu FX (Xiu, Faxian)¹, Wang Y (Wang, Yong)², Kim JY (Kim, Jiyoung)¹, Upadhyaya P (Upadhyaya, Pramey)¹, Zhou Y (Zhou, Yi)¹, Kou XF (Kou, Xufeng)¹, Han W (Han, Wei)³, Kawakami RK (Kawakami, R. K.)³, Zou J (Zou, Jin)², Wang KL (Wang, Kang L.)¹ ACS NANO Volume: 4 Issue: 8 Pages: 4948-4954 Published: AUG 2010
- ⁶ Light-Induced Spontaneous Magnetization in Doped Colloidal Quantum Dots, Beaulac R (Beaulac, Remi)¹, Schneider L (Schneider, Lars)^{2,3}, Archer PI (Archer, Paul I.)¹, Bacher G (Bacher, Gerd)^{2,3}, Gamelin DR (Gamelin, Daniel R.)¹ SCIENCE Volume: 325 Issue: 5943 Pages: 973-976 Published: AUG 21 2009 \
- ⁷ Mott and Efros-Shklovskii Variable Range Hopping in CdSe Quantum Dots Films Liu H (Liu, Heng), Pourret A (Pourret, Alexandre), Guyot-Sionnest P (Guyot-Sionnest, Philippe) ACS nano Volume: 4 Pages: 5211-5216 (2010)
- ⁸ Magnetoresistance of CdSe/CdS quantum dot films Pourret A (Pourret, Alexandre), Ramirez A (Ramirez, Adan), Guyot-Sionnest P (Guyot-Sionnest, Philippe) *Appl. Phys. Lett.* Volume: 95 Article Number: 142105 (2009)
- ⁹ 1/f noise of granular metal-insulator composites, Mantese JV, Webb WW, Phys. Rev. Lett. 55, 2212-2215 (1985)
- ¹⁰ Low-frequency noise in monodisperse platinum nanostructures near the percolation threshold Romyantsev SL, Levinshtein ME, Gurevich SA, Kozhevnikov VM, Yavsin DA, Shur MS, Pala N, Khanna A, Physics of the solid state 48, 2194-2198 (2006)
- ¹¹ Current and voltage noise in WO₃ nanoparticle films, Hoel A., Vandamme LKJ, Kish LB, Olsson E, J. Appl. Phys. 91, 5221-5226 (2002)
- ¹² Many electron theory of 1/f noise in hopping conductivity, Burin AL, Shklovskii BI, Kozub VI, Galperin YM, Vinokur V, Phys. Rev. B74, 075205 (2006)

Novel sp²-Bonded Materials and Related Nanostructures

PI: Alex Zettl, University of California, Berkeley / LBNL

Spectroscopy of Degenerate One-Dimensional Electrons in Carbon Nanotubes

Junichiro Kono

*Department of Electrical and Computer Engineering and Department of Physics and Astronomy,
Rice University,
Mail Stop 366, PO Box 1892, 6100 Main St., Houston, Texas 77251-1892, U.S.A.
Telephone: 713-348-2209, E-mail: kono@rice.edu*

1 Project Scope

We are studying the fundamental properties of degenerate one-dimensional (1-D) electrons in single-walled carbon nanotubes (SWNTs) using *dynamical methods* to probe and understand **electronic correlations and many-body phenomena**. SWNTs are an ideal 1-D system for studying novel quantum effects in nanostructures. There have been transport and optical studies on SWNTs by a number of groups during the past decade, revealing some characteristic features of 1-D systems. However, most of the predicted *exotic properties of interacting 1-D electrons* have yet to be observed, and some of the reported experimental evidence remains controversial. Here, using spectroscopic methods from terahertz (THz) to optical ranges, we aim to achieve a **fundamental understanding of correlations and many-body effects** in this prototypical 1-D nanostructure. These studies can provide a wealth of new insight into the nature of strongly correlated carriers in the ultimate 1-D limit and lead to novel nanodevice concepts and implementations.

2 Recent Progress

During the last year, we have made significant progress in three aspects of 1-D dynamic phenomena in SWNTs, which are summarized below:

2.1 Large Magnetic Susceptibility Anisotropy of Metallic SWNTs

Unusual magnetic properties have been predicted for SWNTs due to the combined effects of the Aharonov-Bohm effect and the large diamagnetic susceptibility of the graphene lattice. Their orbital magnetic susceptibility χ is expected to be 2 orders of magnitude larger than their spin magnetic susceptibility, and the value of χ is predicted to be strongly dependent on the strength of the applied magnetic field, B , and the Fermi energy. Furthermore, the sign of χ can be either positive (paramagnetic) or negative (diamagnetic), depending on the nanotube chirality as well as the magnetic field orientation. See Fig. 1(left). Here, through magnetic linear dichroism spectroscopy, we have successfully extracted the anisotropy of χ of metallic SWNTs for the first time and found it to be 2-4 times greater than values for semiconducting nanotubes. This large anisotropy can be understood in terms of large orbital paramagnetism of metallic nanotubes arising from the Aharonov-Bohm-phase-induced gap opening in a parallel magnetic field, and our calculations quantitatively reproduced these results. We also compared our values with previous work for semiconducting nanotubes, which confirm that the anisotropy of χ does not increase linearly with the diameter for small-diameter nanotubes.

Figure 1(Right)(a) shows polarization-dependent optical absorption spectra at 0 and 35 T. None of the spectra are intentionally offset, indicating an increase (decrease) in absorbance for light polarized parallel (perpendicular) to the field. This is a direct result of magnetic alignment, together with the fact that only the light-field component parallel to the tube axis is strongly absorbed in SWNTs. Namely, at 35 T there is a finite degree of alignment in the magnetic field direction within the nanotube ensemble, resulting in stronger (weaker) absorption for light polarized parallel (perpendicular) to the field. From the theory of linear dichroism for an ensemble of anisotropic molecules, the following quantity can be shown to be constant, independent of the degree of alignment:

$$A_0 \equiv \frac{A_{\parallel} + 2A_{\perp}}{3}, \quad (1)$$

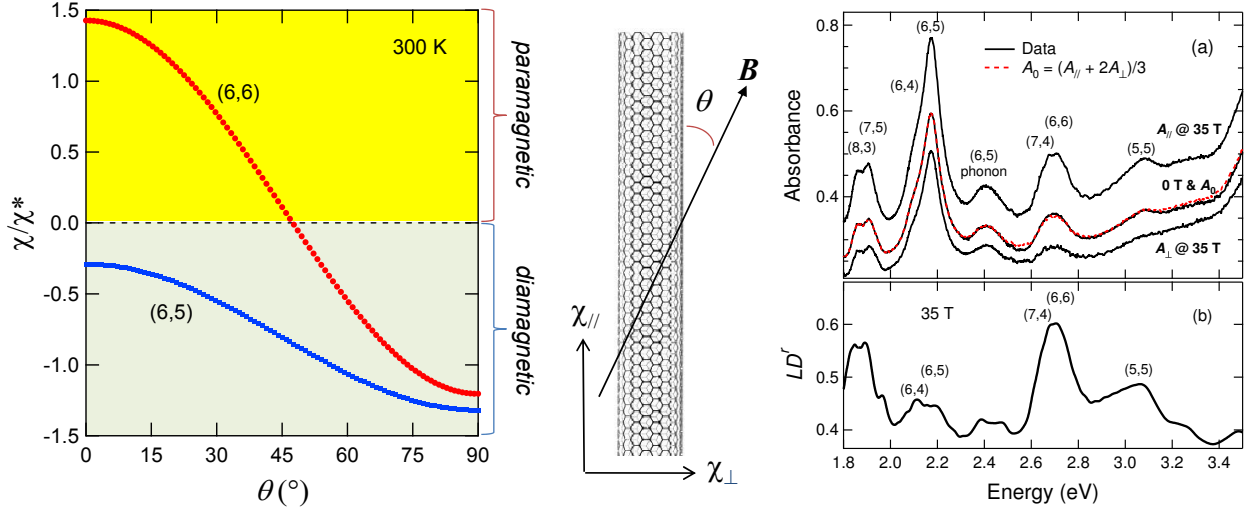


Figure 1: **(Left)** Calculated magnetic susceptibility anisotropy of single-walled carbon nanotubes. The susceptibility χ is expressed in units of $\chi^* = (2\pi\gamma/a)(\pi a^2/\phi_0)^2 a^{-2} = 1.46 \times 10^{-4}$ emu/mol, where $\gamma = 6.46$ eV·Å, $a = 2.5$ Å, and $\phi_0 = ch/e$ is the magnetic flux quantum. The (6,6) nanotube (metallic) is paramagnetic along the tube axis and diamagnetic in the perpendicular direction ($\chi_{\parallel} > 0 > \chi_{\perp}$), whereas the (6,5) nanotube (semiconducting) is diamagnetic in all directions but most strongly diamagnetic in the perpendicular direction ($\chi_{\perp} < \chi_{\parallel} < 0$). In both cases, $\Delta\chi = \chi_{\parallel} - \chi_{\perp} > 0$, leading to alignment in an external magnetic field B . **(Right)** (a) Absorption spectra (solid black) for 0 T and 35 T with all peaks assigned to specific chiralities. No trace is intentionally offset, indicating greater (smaller) absorption for parallel (perpendicular) polarization. The unpolarized isotropic absorbance (dashed red), calculated from the 35 T spectra via Eq. (1), agrees well with the 0 T data. (b) Reduced linear dichroism versus energy from data taken at 35 T. The largest peak is from metallic nanotubes (6,6) and (7,4).

where A_{\parallel} (A_{\perp}) is the absorption for light polarized parallel (perpendicular) to the orientation axis, i.e., the magnetic field direction. We calculated A_0 at 35 T using Eq. (1) and plotted it in Fig. 1(Right)(a) as a red dashed line. The agreement between the calculated A_0 and the zero-field absorption spectrum confirms that A_0 is independent of alignment (or B), because at 0 T $A_{\parallel} = A_{\perp} = A_0$. We further confirmed that at any fields between 0 and 35 T the increase in A_{\parallel} and decrease in A_{\perp} are such that A_0 is preserved through Eq. (1). Since linear dichroism, $LD = A_{\parallel} - A_{\perp}$, directly depends on the absorbance, LD alone cannot be used for comparing different spectral features. To adjust for differences in relative absorbances due to the fact that our sample is enriched for (6,5), the LD was divided by A_0 , yielding the *reduced* linear dichroism, $LD^r = LD/A_0$, which is plotted in Fig. 1(Right)(b) for 35 T. It is immediately evident from this plot that the spectral region where metallic peaks [(6,6) and (7,4)] exist has much larger LD^r than the region where the most prominent semiconducting peaks [(6,5) and (6,4)] exist. This is evidence that the (6,6) and (7,4) tubes are aligning more strongly than the (6,5) and (6,4) tubes.

2.2 Resonant Raman Spectroscopy of Armchair Carbon Nanotubes: Absence of “Metallic” Signature

Recently, much progress has been made in understanding electron-phonon interactions and their consequences in Raman scattering spectra in “metallic” SWNTs, in which the chiral indices (n,m) satisfy $\nu \equiv (n - m) \bmod 3 = 0$, as opposed to semiconducting SWNTs, for which $\nu = \pm 1$. Note that, while armchair ($n = m$) nanotubes are metallic (gapless), non-armchair (or $n \neq m$) $\nu = 0$ tubes have small curvature-induced bandgaps, i.e., they are in fact narrow-gap semiconductors. Of particular interest is the so-called G-band, a Raman-active optical phonon feature originating from the in-plane C-C stretching mode of sp^2 -hybridized carbon. In SWNTs, the G-band is split in two, the G^+ and G^- peaks, due to the curvature-induced inequality of the two bond-displacement directions. For $\nu = 0$ tubes, the higher-frequency mode (G^+)

is a narrow Lorentzian peak, while the lower-frequency mode (G^-) is extremely broad. Earlier theoretical studies described this broad feature as a Breit-Wigner-Fano lineshape due to the coupling of phonons with an electronic continuum or low-frequency plasmons, but there is now accumulating consensus that the broad G^- peak is a softened and broadened longitudinal optical (LO) phonon feature, a hallmark of Kohn anomalies. Through either scenario, this broad G^- feature has conventionally been known to be a “metallic” feature, indicating the presence of metallic tubes.

Here, we have performed detailed wavelength-dependent Raman scattering measurements on a macroscopic ensemble of SWNTs enriched in armchair (or $n = m$) nanotubes produced via density gradient ultracentrifugation. Our G-band spectra clearly show that the broad G^- mode is absent for armchair structures and only occurs for non-armchair (or $n \neq m$) “metallic” nanotubes. Namely, the conventional method for identifying metallic nanotubes by observing a broad G^- peak does not apply to the only truly metallic species, i.e., armchair nanotubes. This supports an earlier conclusion based on a small number of single-tube measurements and negates some claims that armchair nanotubes also show a broad G^- feature. Furthermore, this result firmly establishes a general correlation between G-band lineshape and nanotube structure due to the sampling of a statistically significant number ($\sim 10^{10}$) of nanotubes.

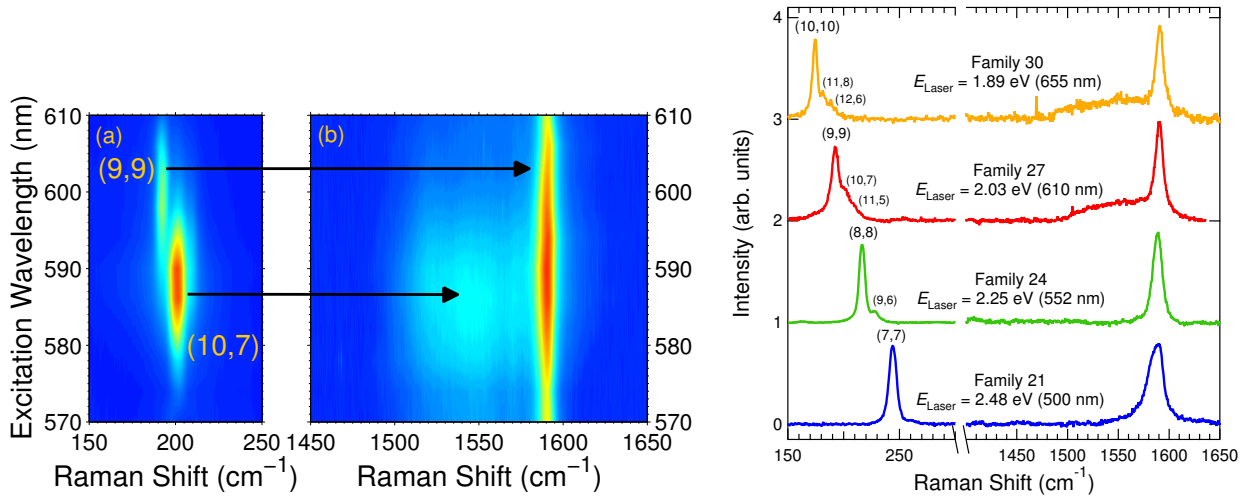


Figure 2: **(Left)** Raman intensity for armchair-enriched SWNTs as a function of Raman shift and excitation wavelength for Family $(2n+m) = 27$. (a) RBM region where RBMs due to the (9,9) and (10,7) are observed. (b) Corresponding G-band region where only the G^+ peak is observed when resonating with the (9,9) and the appearance of the broad G^- coincides with the maximum of the (10,7) RBM. **(Right)** Selected resonant Raman spectra at 655 nm, 610 nm, 552 nm, and 500 nm, where resonance occurs with (10,10), (9,9), (8,8), and (7,7), respectively. In each case, the G-band reflects contribution mainly from the G^+ peak only.

In Fig. 2(Left)(a), we see only two RBMs, from (9,9) and (10,7), reflecting enrichment toward armchair-like species. The corresponding G-band [Fig. 2(Left)(b)] shows only a single G^+ peak centered at $\sim 1590 \text{ cm}^{-1}$ at the longest excitation wavelengths ($\sim 610 \text{ nm}$) coinciding primarily with resonance of the (9,9) RBM. As the wavelength is decreased, a broad G^- peak appears in addition to the G^+ peak. This broad G^- peak, centered at $\sim 1550 \text{ cm}^{-1}$, reaches a maximum in intensity at $\sim 587 \text{ nm}$, which coincides with the RBM resonance maximum of the (10,7). The simultaneous appearance of the G^- peak with the Raman resonance maximum of the (10,7) and its absence with pure resonance with the (9,9) point out a clear correlation between (n,m) chirality and G-band lineshape. Namely, the broad G^- peak appears only in the presence of non-armchair $\nu = 0$ nanotube species, and (n,n) armchair species consist of only one single, narrow peak. Figure 2(Right) shows selected Raman spectra of the (7,7), (8,8), (9,9), and (10,10) armchair families taken at 500, 552, 610, and 655 nm excitations, respectively. These wavelengths are close to the general resonance maxima for each respective family. Data taken across a diameter range of 0.96-1.38 nm shown here clearly demonstrates that the appearance and dominance of a single G^+ feature is a general result and indicator for the predominance of armchair species in a SWNT sample.

3 Future Plans

- To produce water-free and surfactant films of metallic nanotubes for DC transport, THz conductivity, electron spin resonance, and optical pump-probe measurements.
- To conduct THz conductivity measurements on metallic-enriched films to provide insight into the origin of the ~ 4 THz peak observed by many groups on various types of SWNTs.
- To fabricate device structures based on armchair SWNTs for i) investigating the possibility of Peierls instability in small-diameter armchair tubes and ii) resistively detecting electron spin resonance on a single-tube level.

4 List of Publications

- L. Ren, C. L. Pint, L. G. Booshehri, W. D. Rice, X. Wang, D. J. Hilton, K. Takeya, I. Kawayama, M. Tonouchi, R. H. Hauge, and J. Kono, “Carbon Nanotube Terahertz Polarizer,” *Nano Letters* **9** (2009), pp. 2610-2613.
- Y. Murakami and J. Kono, “Existence of an Upper Limit on the Density of Excitons in Carbon Nanotubes by Diffusion-Limited Exciton-Exciton Annihilation: Experiment and Theory,” *Physical Review B* **80** (2009), 035432 [10 pages].
- E. H. Háróz, W. D. Rice, B. Y. Lu, S. Ghosh, R. H. Hauge, R. B. Weisman, S. K. Doorn, and J. Kono, “Enrichment of Armchair Carbon Nanotubes via Density Gradient Ultracentrifugation: Raman Spectroscopy Evidence,” *ACS Nano* **4** (2010), pp. 1955-1962.
- Y.-S. Lim, J.-G. Ahn, J.-H. Kim, K.-J. Yee, T. Joo, S.-H. Baik, E. H. Háróz, L. G. Booshehri, and J. Kono, “Resonant Coherent Phonon Generation in Single-Walled Carbon Nanotubes through Near-Band-Edge Excitation,” *ACS Nano* **4** (2010), pp. 3222-3226.
- T. A. Searles, Y. Imanaka, T. Takamasu, H. Ajiki, J. A. Fagan, E. K. Hobbie, and J. Kono, “Large Magnetic Susceptibility Anisotropy of Metallic Carbon Nanotubes,” *Physical Review Letters* **105** (2010), 017403 [4 pages].
- J. G. Duque, H. Chen, A. B. Swan, E. H. Háróz, J. Kono, X. Tu, M. Zheng, and S. K. Doorn, “Revealing New Electronic Behaviors in the Raman Spectra of Chirality-Enriched Carbon Nanotube Ensembles,” *physica status solidi (b)* **247** (2010), pp. 2768-2773.
- L. G. Booshehri, C. L. Pint, G. D. Sanders, L. Ren, C. Sun, E. H. Háróz, J.-H. Kim, K.-J. Yee, Y.-S. Lim, R. H. Hauge, C. J. Stanton, and J. Kono, “Polarization Dependence of Coherent Phonon Generation and Detection in Highly-Aligned Single-Walled Carbon Nanotubes,” *Physical Review B* **83** (2011), 195411 [9 pages].
- E. H. Háróz, J. G. Duque, W. D. Rice, C. G. Densmore, J. Kono, and S. K. Doorn, “Resonant Raman Spectroscopy of Armchair Carbon Nanotubes: Absence of Metallic Signature,” submitted to *Physical Review B*; see also <http://arxiv.org/abs/1101.1331>.
- W. D. Rice, R. T. Weber, S. Nanot, P. Nikolaev, S. Arepalli, A.-L. Tsai, and J. Kono, “Motional Narrowing of Electron Spin Resonance in Single-Wall Carbon Nanotubes,” submitted to *Physical Review Letters*; see also <http://arxiv.org/abs/1105.5095>.
- J.-H. Kim, K.-J. Yee, Y.-S. Lim, L. G. Booshehri, E. H. Háróz, and J. Kono, “Optical Phonon Dephasing in Single-Walled Carbon Nanotubes Probed via Impulsive Stimulated Raman Scattering,” submitted to *Physical Review Letters*; see also <http://arxiv.org/abs/1106.2858>.

Symmetries, interactions, and correlation effects in carbon nanotubes

DOE award DE-SC0002765

Gleb Finkelstein

Physics Department, Duke University, gleb@phy.duke.edu

Project Scope

Our work focuses on studying electronic interactions in carbon nanotube quantum dots by low temperature magneto-transport methods. Our main result is the observation of the dissipation-induced quantum phase transitions in an artificial quantum impurity (*i.e.* quantum dot). The possibility of a quantum phase transition (QPT) induced by dissipation has attracted significant attention to 2-dimensional systems, such as superconducting films, Josephson junction arrays, and electron gases in the regime of the quantum Hall effect. We observe what we believe is a QPT in a very simple system – a resonant level in a carbon nanotube coupled to two competing dissipative bath, realized in two metallic contacts. We focus on this exciting result in the next two pages. Our other two major directions of studies are briefly listed below:

Kondo box in a carbon nanotube

The concept of the "Kondo box" describes a single spin, antiferromagnetically coupled to a quantum dot that has a finite level spacing. The model has attracted significant theoretical attention, due to an interesting competition between the electronic correlations and confinement. In our recent publication, we have presented the first measurement of the Kondo box, which is formed in a carbon nanotube quantum dot interacting with an electron spin localized nearby. We have studied the excitations of the Kondo box and characterized the spin of the first few eigenstates. In the regime of partially open tunnel barriers between the quantum dot and the electrical leads, the nanotube conductance has exhibited non-monotonic temperature dependence. We have interpreted this behavior as a two-stage Kondo effect, resulting from competition between two correlated states: the Kondo-box state and the more 'conventional' Kondo state coupling the quantum dot and the leads.

Graphene-based Josephson junctions

In this project, we have explored graphene-based Josephson junctions, which are unified with our main subject by the role played by their dissipative environment. We fabricated the junctions with contacts made from lead. The high transition temperature of this superconductor allows us to observe the supercurrent branch at temperatures up to ~2 K, at which point we can detect a small, but non-zero, resistance. We attribute this

resistance to the phase diffusion mechanism, which has not been yet identified in graphene. By measuring the resistance as a function of temperature and gate voltage, we can further characterize the nature of the environment and dissipation in our samples.

Recent Progress:

Dissipation-induced quantum phase transitions in an artificial quantum impurity

We investigate tunneling through a resonant level formed in a carbon nanotube quantum dot, contacted by resistive metal leads. These leads create a “dissipative environment” for the electrons tunneling across the nanotube, suppressing the tunneling rate at a power law of temperature, $\sim T^{2r}$ (with an anomalous exponent $2r=2R/R_Q$, where R is the leads resistance and $R_Q=h/e^2$ is the quantum resistance). We developed side-gated nanotube samples, which allow us to control the tunneling barriers between the nanotube quantum dot and the leads (Figure 1). By using the side gates, we can easily tune the tunneling rates from the dot to the two leads to become identical (symmetric coupling) or strongly asymmetric. We study the shape of the resonant peak in the nanotube conductance, while controlling the ratio of the two tunneling rates.

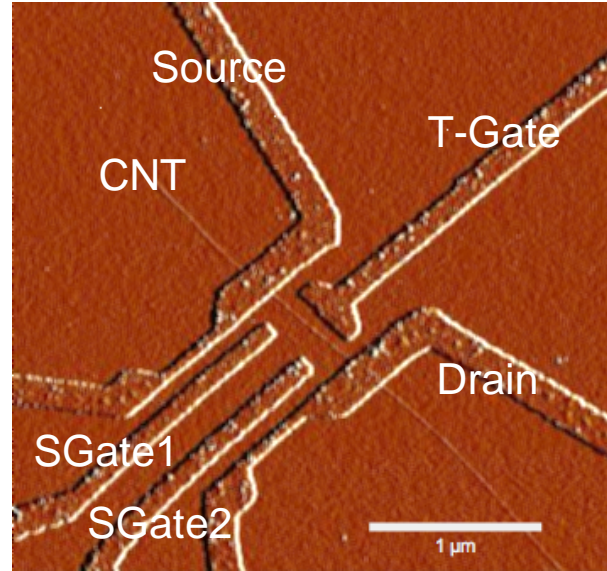


Figure 1. AFM image of the sample. The nanotube is marked CNT. It is contacted by two pairs of metal leads (Source and Drain). Two side-gates (SG1 and SG2) control the barrier asymmetry. The T gate is used to change the number of electrons in the dot.

Intuitively, one might expect that both the width and the height of the resonant peak would be suppressed by the dissipative environment, since they both depend on the tunneling rate. However, we find that the result strongly depends on the ratio of the tunneling rate to the two leads (Figure 2). For asymmetric coupling, the peak conductance drops with decreasing temperature, while the peak width saturates. For symmetric coupling, the situation is reversed: the peak width is suppressed at low temperatures, while the peak height saturates at e^2/h .

The observation of unitary conductance in the symmetric case is highly non-trivial. Indeed, one could have expected that coupling to the dissipative modes would reduce the resonant conductance from its unitary value of e^2/h . Another key observation is that the width of the resonant peak in the symmetric case monotonically decreases with

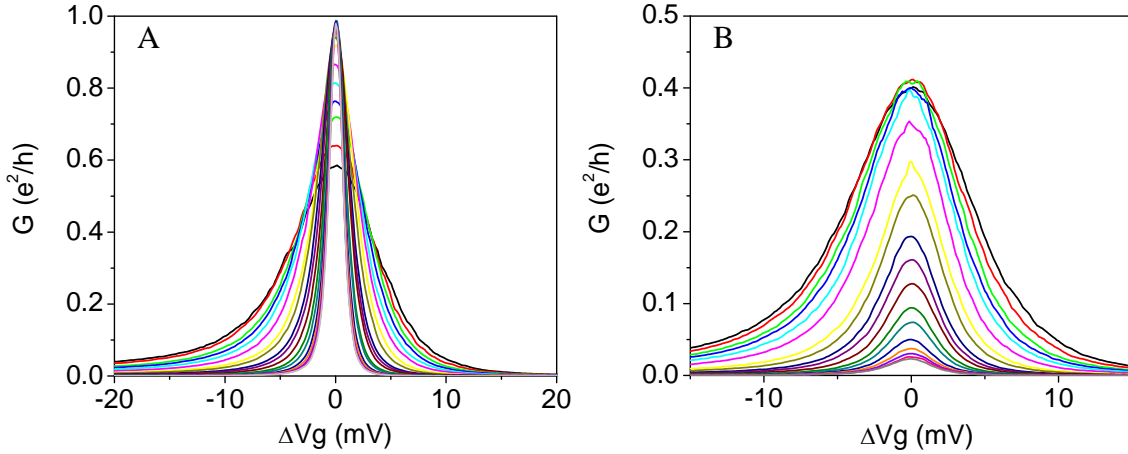


Figure 2: Resonant peak conductance vs. gate voltage at several temperatures from 3.0 K to 50 mK. The two panels compare the (A) symmetric and (B) asymmetric coupling of the resonant level to the two leads. Note that at the highest T , the peaks in (A) and (B) have similar width and height ($\sim 0.5e^2/h$). For symmetric coupling, as the temperature drops, the peak reaches e^2/h , while the peak width monotonically decreases. For asymmetric coupling, the situation is reversed: the peak height drops, while the width saturates. The left panel corresponds to the QPT case (see text).

lowering temperature. We analyze the temperature dependence of the peak height as a function of temperature, and observe that it scales as a power of temperature. A resonant conductance peak separates distinct quantum states of the system, which differ by one electron in the dot. The fact that the transition region between these two states appears to shrink in the limit $T=0$ indicates the presence of a boundary quantum phase transition (QPT; at the boundary QPT, a sub-system of a larger system undergoes a QPT). The dissipation-induced QPTs have been predicted (but never observed!) in more involved quantum impurity models, although surprisingly not for our, more basic, case.

The shape of the resonant peak vs. temperature has not been, to the best of our knowledge, considered theoretically for tunneling into dissipative leads. To understand our observations, we invoke the similarity between tunneling in dissipative environment and tunneling between two Luttinger liquids. In both cases, the tunneling electron excites one-dimensional bosonic modes, resulting in suppression of differential conductance through a single tunneling junction as $G \sim T^\alpha$ at low temperature. It appears that theoretical predictions of the resonant tunneling between the Luttinger liquid correctly describe many of the behaviors of the peak height and width that we observe both in the symmetric and asymmetric cases. However, we stress that our experiment does not study a Luttinger liquid either in the leads or in the nanotube: the electron motion in metallic leads contacting the nanotube is diffusive, while the nanotube segment is short enough so that the electron motion is fully quantized.

Future plans

I plan to continue the work on carbon nanotube quantum dots, which turn out to be very convenient for experimentally ‘modeling’ the behavior of a quantum impurity in dissipative environment. Specifically, after completing the work on the simplest case – the resonant level (see above) – it would be natural to focus on the Kondo effect in dissipative environment. This system is thought to be prototypical for certain types of strongly correlated bulk materials, and one can hope to gain valuable information by studying a well-controlled system that may share similar physics.

Publications

Two-stage Kondo effect and Kondo-box level spectroscopy in a carbon nanotube,
Yu. Bomze, I. Borzenets, H. Mebrahtu, A. Makarovski, H. Baranger, and G. Finkelstein,
Phys. Rev. B 82, 161411R (2010).

Phase diffusion in graphene-based Josephson junctions,
I.V. Borzenets, U.C. Coskun, S.J. Jones, and G. Finkelstein, submitted to PRL.

Dissipation-Induced Quantum Phase Transition in a Resonant Level,
H. Mebrahtu, I. Borzenets, Yu. Bomze, and G. Finkelstein, Preprint.

Session 7

Superconductivity

Quantum Materials

Investigators: R.J. Birgeneau, E. Bourret-Courchesne, A. Lanzara, D. H. Lee, J. Orenstein, R. Ramesh, and A. Vishwanath.

Scope of the program: Quantum physics provides the theoretical basis for our understanding of the electronic properties of all materials. The Quantum Materials program at LBNL focuses on an important sub-class of systems, now widely known as ‘quantum materials,’ in which quantum mechanics plays an especially profound role in determining important properties. In some cases, such as superconductors, the order parameter is explicitly a quantum mechanical object, while in other systems, quantum effects may dominate because of proximity to quantum critical points. Our team focuses primarily on the electronic properties of transition metal oxides, in both thin film and crystalline form, where the interplay between competing order, frustration, strong interactions lead to an especially rich and diverse range of quantum physical phenomena.

Recent progress: Time-resolved ARPES and optical spectroscopy of cuprates

As it is not possible to present an overview of all the research in the Quantum Materials group in this format, we highlight one of the areas in which significant progress has been made. The research described below is the result of a collaboration among the Lanzara, Orenstein, and Lee groups (with BSCCO samples provided by H. Eisaki, AIST, Japan). Lanzara and collaborators have developed instrumentation for performing time-resolved measurements of angle-resolved photoemission (ARPES), while the Orenstein group has developed tools for time-resolved optical measurements. D.H. Lee and his group are providing theoretical support for the team as a whole.

Despite intense research, the most basic question concerning copper oxides – the underlying mechanism for their high- T_c superconductivity – remains unresolved. One of the keys to solving the mystery is deeper understanding of the interactions between quasiparticles (electrons not bound into Cooper pairs) that lead to their net attraction. In principle, a direct path to probing such interactions is to measure the rate of quasiparticle recombination, *i.e.* the rate at

which two quasiparticles of opposite spin interact, emit energy, and re-enter the superfluid condensate.

Although the importance of quasiparticle recombination has been recognized from the earliest days of superconductivity research, historically it has proved difficult to measure rates directly in conventional small-gap superconductors. This is because a phenomenon known as the “phonon bottleneck” intervenes and obscures the rates of the underlying microscopic processes. When a nonequilibrium density of quasiparticles is created in a superconductor, for example by pulsed photoexcitation, their subsequent recombination is accompanied by creation of acoustic phonons of energy 2Δ , that is, twice the BCS energy gap. Once created, such phonons will undergo the reverse process of decay into quasiparticles. In this manner, quasiequilibrium is rapidly established between electrons and phonons. Accordingly, the decay rate of excess

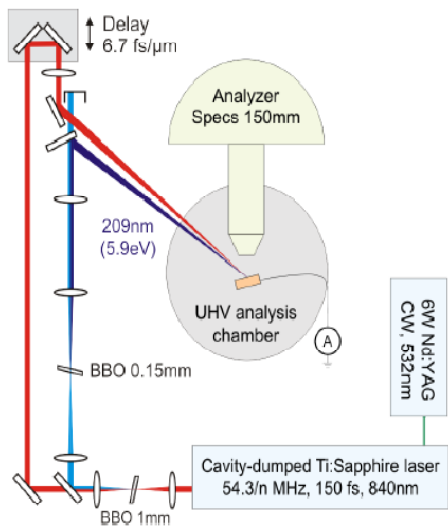


Figure 1: Apparatus for performing time-resolved ARPES measurements. A beam of pulses from a single Ti:Sapphire laser is split into two: one beam at 1.5 eV photogenerates electronic excitations, a second quadrupled and time-delayed beam is used as a photoemission source.

quasiparticles is governed by the rate at which 2Δ phonons either leave the excited region of superconductor or decay into phonons with energy below 2Δ , rather than the underlying recombination rate.

In contrast with the behavior of conventional superconductors, quasiparticle recombination rates in high- T_c materials are not hidden by a phonon bottleneck. The evidence for this statement is that in high- T_c superconductors the rate of decay of the excited quasiparticle

population is proportional to their density, *i.e.* the rate of quasiparticle-quasiparticle scattering, whereas it is independent of density in conventional systems. The contrast with low T_c superconductors is likely to be a straightforward consequence of the much larger gap in high- T_c materials; when 2Δ is as large as 50 to 100 meV, the energy released by recombination is much more likely to decay into lower energy bosonic excitations than to regenerate a broken Cooper pair.

population is proportional to their density, *i.e.* the rate of quasiparticle-quasiparticle scattering, whereas it is independent of density in conventional systems. The contrast with low T_c

The ability to probe the microscopic quasiparticle recombination rate provides a tremendous opportunity for further investigation of quasiparticle interactions by time-resolved ARPES. This experiment can selectively probe the decay rate of quasiparticles as a function of their energy and momentum, thus revealing the details of their interaction. The apparatus developed by the Lanzara group to perform time-resolved ARPES is shown schematically in Fig. 1. A beam of ultrashort pulses from a Ti:Sapphire laser is split in two; one beam of 1.5 eV pulses is used to inject excess quasiparticles, the second beam is quadrupled in frequency and used to induce photoemission from the sample surface. By varying the delay between the 1.5 eV pump pulses and the 6 eV probe, the occupation of quasiparticle states is measured as a function of energy, momentum, and time delay after pulsed photoinjection.

To facilitate comparison of optical and ARPES data, we have set-up a time-resolved optical reflectivity apparatus that uses the same laser as used for photoemission experiments. Fig. 2 shows time-resolved reflectivity data for a slightly underdoped sample of BSCCO ($T_c \cong 90$ K) measured at 20 K. The curves show the decay of the photoinduced change in reflectivity at 1.5 eV as a function of time for different intensities of the pump beam. The curves are

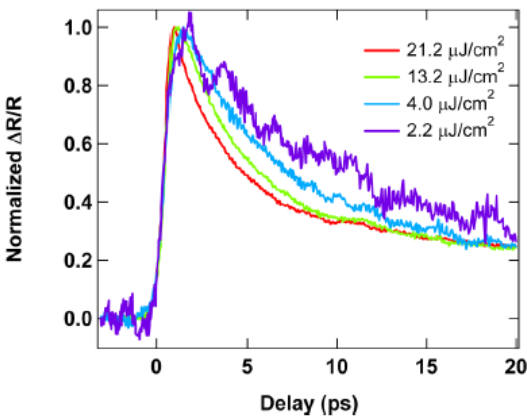


Figure 2: Decay of photoinduced change in optical reflectivity measured at different pump laser intensities and normalized to the same value at zero time delay.

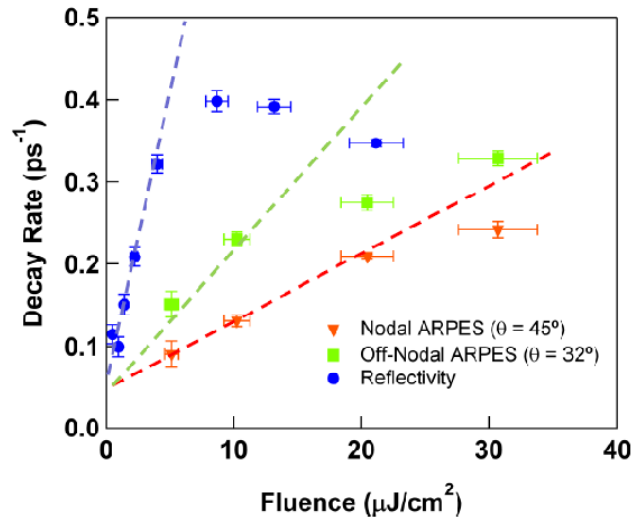


Figure 3: Comparison of the pump intensity dependence of the decay rates of photoinduced optical reflectivity and ARPES signals measured at the gap node and at an angle of 13 degrees away from the gap node.

normalized to illustrate that the decay slows as the initial density of quasiparticles is decreased. Fig. 3 compares the decay rate of the optical reflectivity with that of ARPES signal measured under the same excitation conditions. To

illustrate the trend, we plot the ARPES intensity measured for momentum along the nodal direction and at a direction that is 13° away from the node. The rate of decay of ARPES signal increases with angular distance from the nodal direction while the decay of the optical reflectivity is faster still. This trend is consistent with the assumption that the optical reflectivity probes a momentum and energy average of the quasiparticle distribution function that is weighted in the antinodal direction, where the density of quasiparticle states is much larger.

Future work: The results emerging from time-resolved spectroscopy of cuprates suggest that the microscopic quasiparticle recombination rate is a strong function of quasiparticle momentum. That the rate is fastest for antinodal quasiparticles suggests that recombination may proceed with emission of bosonic excitations with wavevector near π, π , which would conserve momentum for recombination between quasiparticles at adjacent antinodes. We believe that through more detailed measurement and modeling of quasiparticle recombination rates a detailed picture of quasiparticle interactions will emerge. Future work will emphasize:

- use of higher energy photons in the photoemission process, which will enable direct measurement of antinodal quasiparticle recombination rates.
- increased sensitivity which will translate to higher energy resolution, allowing exploration of very slow recombination that may occur at the zero energy nodal states.
- the theoretical problem of recovering the momentum and energy dependence of quasiparticle interactions from the time-resolved ARPES observable, $f(\omega, k; t)A(\omega, k; t)$, the product of the time-dependent occupation and spectral functions.

Recent publications on time-resolved optics and ARPES

Nodal quasiparticle meltdown in ultrahigh-resolution pump-probe angle-resolved photoemission . J. Graf *et al.*, Nature Physics (Published online July 3, 2011).

From a single-band metal to a high-temperature superconductor via two thermal phase transitions. Ruihua He, Science **331**, 1579-1583 (2011).

Vacuum space charge effect in laser-based solid-state photoemission spectroscopy. J. Graf *et al.*, J. Appl. Phys. **107**, 014912 (2010).

Infrared and angle resolved photoemission studies of high-temperature superconductors and related systems

Christopher C. Homes, Tonica Valla, and Peter D. Johnson
homes@bnl.gov, valla@bnl.gov, pdj@bnl.gov
Condensed Matter Physics & Materials Science Department
Brookhaven National Laboratory, Upton, NY 11973-5000

Project Scope

The focus of this program is the detailed investigation of the nature of the interactions in strongly-correlated electron systems as probed by infrared and angle-resolved photoemission spectroscopy (ARPES); the former yields information about the complex optical properties, including the real part of the optical conductivity, while ARPES probes the momentum dependence of the electronic structure and associated dynamics below the Fermi surface. Methods of analysis in the latter include energy distribution curves (EDC's) and momentum distribution curves (MDC's). Both insulating and metallic systems have been studied, with special emphasis on the copper-oxide and the new iron-based superconductors in which there are other phases that compete with superconductivity, such as charge- and spin-stripe order. Understanding the nature of these interactions may provide the key to unlocking the mystery of high-temperature superconductivity in these compounds. Other studies include the topological insulators and graphene.

Recent Progress

Optical properties of an iron-chalcogenide superconductor. The discovery of superconductivity in the iron-pnictide and iron-chalcogenide materials has forced the condensed matter physics community to re-examine the definition of high-temperature superconductivity and the mechanism responsible for it. While FeTe is not superconducting, FeSe is superconducting at ambient pressure with a critical temperature of $T_c \sim 8$ K. The alloyed material $\text{FeTe}_{1-x}\text{Se}_x$ has a superconducting phase with a maximum $T_c \sim 14$ K at $x=0.45$. We have measured the complex optical properties of $\text{FeTe}_{0.55}\text{Se}_{0.45}$ over a wide frequency range for a variety of temperatures above and below T_c [22]; the real part of the optical conductivity is shown in Fig. 1. At room temperature the conductivity appears to be flat and incoherent, but a low temperature (100 K) it can be modeled quite well using a simple Drude-Lorentz model (inset of Fig. 1). Below T_c there is a significant suppression of the low-frequency optical conductivity. This so-called “missing area” may be used to estimate the strength of the superconducting plasma frequency $\omega_{p,S} \cong 3000 \pm 300 \text{ cm}^{-1}$ ($\rho_{s0} = \omega_{p,S}^2$), as well as the effective penetration depth $\lambda_{\text{eff}} \cong 530 \text{ nm}$ (lower than the values observed in the cuprate materials). This material also falls on the universal scaling line $\rho_{s0}/8 \cong 4.4 \sigma_{\text{dc}} T_c$ [1,13], which is consistent with the observation of strong dissipation in the normal state. Finally, we remark that this is a multiband system, with both electron and hole pockets at the Fermi surface. While the conductivity can be fit reasonably well using a single isotropic energy gap and a Mattis-Bardeen dirty limit approach, there is a substantial amount of low-frequency conductivity that is not reproduced unless a second smaller gap is also considered. The values for the two gaps of $\Delta \sim 2.5$ and 5 meV are in good agreement with ARPES measurements, and represent either the

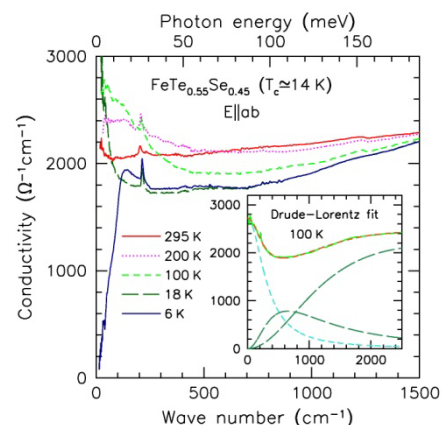


Fig. 1 The real part of the optical conductivity of $\text{FeTe}_{0.55}\text{Se}_{0.45}$ in the infrared region for several temperatures above and below T_c .

gapping of the electron and hole bands, or possibly an anisotropic gap on the electron band – both interpretations are consistent with the s^\pm model.

Photoemission studies of the underdoped cuprates. A new method of analysis to remove the broadening effects associated with the finite experimental resolution, has allowed the identification of a particle-hole asymmetry in the nodal region. Several calculations indicate that such an asymmetry is indicative of the presence of hole pockets on the Fermi surface in the pseudogap region of the phase diagram. By measuring the particle hole asymmetry as a function of doping and associated T_c it is possible to determine the structure of the Fermi surface as indicated in figure 2(a). Note however that in models such as the YRZ phenomenological mode [31], the Green's function $G(\mathbf{k}, \epsilon_F)$ associated with the backside of the pocket obtained in such an analysis is zero. This, of course, results in the absence of intensity in the photoemission spectrum.

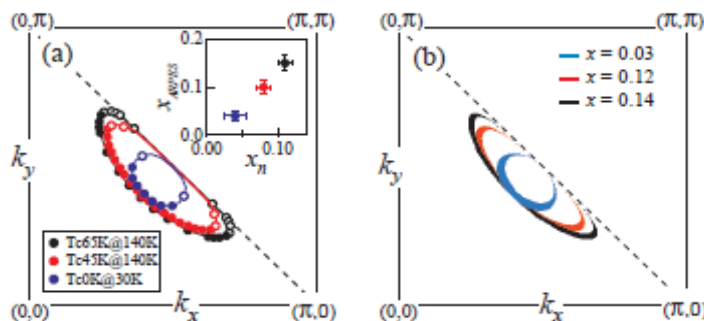


Fig. 2 (a) Experimentally determined hole pockets; (b) Calculated pockets.

For comparison, Fig. 2(b) shows the doping dependent hole pockets calculated within the YRZ ansatz [31]. The area of the pockets scale approximately with the doping level, consistent with Luttinger's theorem which states that the volume of the Fermi surface is equal to the carrier concentration, as shown in the inset of Fig. 2(a). However, we note that at higher doping levels there appears to be an increasing discrepancy between the measured pocket size and the doping level. It is unclear at the present time whether this discrepancy reflects the presence of electron pockets appearing on the Fermi surface at higher coverage's or some other phenomenon.

Future Plans and Beamline Development at NSLS II

We plan to pursue work on the complex optical properties of superconductors, including the iron-chalcogenide materials as well as their non-superconducting parent compounds. The parent compounds are bad metals in which the role of electronic correlations becomes increasingly important at below the magnetic and structural transitions. We will examine the effects of excess iron, as well as other impurities, on the normal-state transport properties and the strength of the electronic correlations in the parent compounds. We will adopt a similar strategy for the superconducting materials to see how iron and other transition metal substitutions alter the normal and superconducting state properties. The role of high-pressure studies of low-dimensional materials will also be expanded.

The Electron Spectroscopy group will participate in the development of two new facilities at NSLS II, including capabilities in both high resolution photoemission and infrared spectroscopy. We have co-authored an approved proposal for a high-resolution Electron Spectro-Microscopy Beamline at NSLS II. A high-resolution, high-flux, wide-range and micro-focused beamline has been designed to provide monochromatic radiation into three separate branches, serving three different electron microscopes. A full-field PEEM microscope, for the *in-situ* growth and characterization of artificial nanomaterials, and two scanning photoemission microscopes, one optimized for ultra-high energy- and angle-resolution

(HR-ARPES) and one optimized for chemical analysis of samples in reactive environments at ambient atmosphere (AP-PES). The two scanning microscopes will be coupled with the PEEM microscope and with a common sample preparation chamber. Further, each chamber will have its own sample storage and load-lock for fast sample insertion.

The proposal for a broadband, high-brightness optical spectroscopy beamline at NSLS II has also been favorably reviewed by the Scientific Advisory Committee. The beamline will sit on one of the dipole bending magnets and will have the potential for magneto-optical spectroscopy, ellipsometry, and time-resolved optical spectroscopy (“METRO”). The principal use of this beamline in our studies will center around “aperture-limited” techniques, specifically the challenges presented by small apertures in measuring the reflectance or transmission in a diamond-anvil or clamped-pressure cell, as well as the use of infrared microscopy to measure small samples.

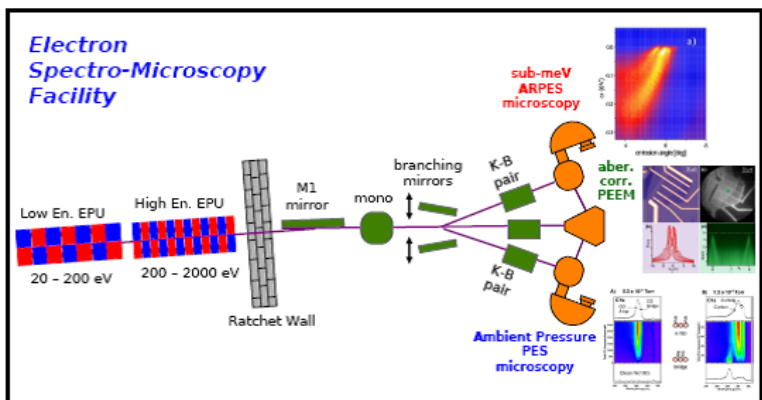


Fig. 3 Electron Spectro-Microscopy Facility at NSLS II. A high-resolution, high-flux, wide-range and micro-focused beamline will provide high-quality monochromatic radiation to three different electron microscopes: 1) PEEM, 2) ultra-high energy- and angle-resolution ARPES (HR-ARPES) and 3) ambient pressure photoemission (AP-PES).

Publications (FY08-FY10)

1. *High- T_c superconductors: Universal scaling relations*, C. Homes, Encyclopedia of Materials: Science and Technology (short monograph), pp. 1-4 (2008).
2. *An inhomogeneous Josephson phase in thin-film and High- T_c superconductors*, Y. Imry, M. Strongin, and C. Homes, Physica C **468**, 288-293 (2008).
3. *Doping of a one-dimensional Mott insulator: Photoemission and optical studies of $Sr_2CuO_{3+\delta}$* , T. E. Kidd, T. Valla, P. D. Johnson, K. W. Kim, G. D. Gu, and C. C. Homes, Phys. Rev. B **77**, 054503 (2008).
4. *Bound excitons on Sr_2CuO_3* , K. W. Kim, C. Bernhard, G. D. Gu, and C. C. Homes, Phys. Rev. Lett. **101**, 177404 (2008).
5. *K-doping dependence of the Fermi surface of the iron-arsenic $Ba_{1-x}K_xFe_2As_2$ superconductor using angle-resolved photoemission spectroscopy*, C. Liu, G. D. Samolyuk, Y. Lee, N. Ni, T. Kondo, A. F. Santander-Syro, S. L. Bud'ko, J. L. McChesney, E. Rotenberg, T. Valla, A. V. Fedorov, P. C. Canfield, B. N. Harmon, and A. Kaminski, Phys. Rev. Lett. **101**, 17705 (2008).
6. *Spin-orbit interaction effect in the electronic structure of Bi_2Te_3 observed by angle-resolved photoemission spectroscopy*, H.-J. Noh, H. Koh, S.-J. Oh, J.-H. Park, H.-D. Kim, J. D. Rameau, T. Valla, T. E. Kidd, P. D. Johnson, Y. Hu, and Q. Li, Europhysics Lett. **81**, 57006 (2008).
7. *Multiple bosonic mode coupling in the charge dynamics of the electron-doped superconductor $(Pr_{2-x}Ce_x)CuO_4$* , E. Schachinger, C. C. Homes, R. P. S. M. Lobo, and J. P. Carbotte, Phys. Rev. B **78**, 134522 (2008).
8. *Infrared optical properties of ferroperricline $(Mg_{1-x}Fe_xO)$: experiment and theory*, T. Sun, P. B. Allen, D. G. Stahnke, S. D. Jacobsen, and C. C. Homes, Phys. Rev. B **77**, 134303 (2008).
9. *Electronic structure of a Co-decorated vicinal Cu(775) surface: High-resolution photoemission spectroscopy*, S. Wang, M. Yilmaz, K. Knox, N. Zaki, J. I. Dadap, T. Valla, P. D. Johnson, and R. M. Osgood, Phys. Rev. B **77**, 115448 (2008).
10. *Emergence of preformed Cooper pairs from the doped Mott insulating state in $Bi_2Sr_2CaCu_2O_{8+\delta}$* , H.-B. Yang, J. D. Rameau, P. D. Johnson, T. Valla, A. Tselik, and G. D. Gu, Nature **456**(6), 77-80 (2008).

11. *Infrared phonon anomaly in BaFe₂As₂*, A. Akrap, J. J. Tu, L. Li, G. Cao, X. Xu, and C. C. Homes, Phys. Rev. B **80**, 180502(R) (2009).
12. *Infrared spectra of the low-dimensional quantum magnet SrCu₂(BO₃)₂: Measurements and ab initio calculations*, C. C. Homes, S. V. Dordevic, A. Gozar, G. Blumberg, T. R  m, D. Hivonen, U. Nagel, A. D. LaForge, D. N. Basov, and H. Kageyama, Phys. Rev. B **79**, 125101 (2009).
13. *Scaling of the superfluid density in strongly underdoped YBa₂Cu₃O_{6+y}: Evidence for a Josephson phase*, C. C. Homes, Phys. Rev. B **80**, 180509(R) (2009).
14. *Electronic properties of iron arsenic high temperature superconductors revealed by angle resolved photoemission spectroscopy (ARPES)*, C. Liu, T. Kondo, A. D. Palczewski, G. D. Samolyuk, Y. Lee, M. E. Tillman, N. Ni, E. D. Mun, R. Gordon, A. F. Santander-Syro, S. L. Bud'ko, J. L. McChesney, E. Rotenberg, A. V. Fedorov, T. Valla, O. Copie, M. A. Tanatar, C. Martin, B. N. Harmon, P. C. Canfield, R. Prozorov, J. Schmalian, and K. A. Kaminski, Physica C **469**, 491-497 (2009).
15. *Coupling of low-energy electrons in the optimally doped Bi₂Sr₂CaCu₂O_{8+δ} superconductor to an optical phonon mode*, J. Rameau, H.-B. Yang, G. Gu, and P. D. Johnson, Phys. Rev. B **80**, 184513 (2009).
16. *Enhanced superconducting transition temperature in FeSe_{0.5}Te_{0.5} thin films*, W. Si, Z.-W. Lin, Q. Jie, W.-G. Yin, J. Zhou, G. Gu, and P. D. Johnson, Appl. Phys. Lett. **95**, 052504 (2009).
17. *Quasiparticles in the pseudogap phase of underdoped cuprate*, K.-Y. Yang, H. Yang, P. D. Johnson, T. M. Rice, and F.-C. Zhang, EPL **80**, 37002 (2009).
18. *Atom-wide Co wires on Cu(775) at room temperature*, N. Zaki, D. Potapenko, P. D. Johnson, and R. M. Osgood, Phys. Rev. B **80**, 155419 (2009).
19. *Anisotropic electron-phonon coupling and dynamical nesting on the graphene sheets in superconducting CaC₆ using angle-resolved photoemission spectroscopy*, T. Valla, J. Camacho, Z.-H. Pan, A. V. Fedorov, A. C. Walters, C. A. Howard and M. Ellerby, Phys. Rev. Lett. **102**, 107007 (2009).
20. *Breakdown of the N=0 quantum hall state in graphene: two insulating regimes*, L. Zhang, J. Camacho, H. Cao, Y. Chen, M. Khodas, D. Kharzeev, A. Tselik, T. Valla, and I. Zaliznyak, Phys. Rev. B **80**, 241412(R) (2009).
21. *Non-equilibrium band mapping of unoccupied bulk states below the vacuum level by two-photon photoemission*, Z. Hao, J. Dadap, K. Knox, M. Yilmaz, N. Zaki, P. D. Johnson, and R. M. Osgood, Phys. Rev. Lett. **105**, 017602 (2010).
22. *Electronic correlations and unusual superconducting response in the optical properties of FeTe_{0.55}Se_{0.45}*, C. C. Homes, A. Akrap, J. S. Wen, Z. J. Xu, W. Lin, Q. Li, and G. D. Gu, Phys. Rev. B **81**, 180508(R) (2010); Ibid: Publisher's Note: Phys. Rev. B **81**, 189901(E) (2010).
23. *Coupling of spin and orbital excitations in the iron-based superconductor FeSe_{0.5}Te_{0.5}*, S.-H. Lee, G. Xu, W. Ku, J. S. Wen, C. C. Lee, N. Katayama, Z. J. Xu, S. Ji, W. Lin, G. Gu, H.-B. Yang, P. D. Johnson, Z.-H. Pan, T. Valla, M. Fujita, T. Sato, S. Chang, K. Yamada, and J. Tranquada, Phys. Rev. B **81**, 220502 (2010).
24. *Application of the Lucy-Richardson deconvolution procedure to high resolution photoemission spectra*, J. Rameau, H.-B. Yang, and P. D. Johnson, J. Electron Spectroscopy and Related Phenomena **181**, 35-43 (2010).
25. *Breakdown of the universal Josephson relation in spin ordered cuprate superconductors*, A. A. Schafgans, C. C. Homes, G. D. Gu, S. Komiyama, Y. Ando, and D. N. Basov, Phys. Rev. B **82**, 100505(R) (2010).
26. *Superconductivity in epitaxial thin films of Fe_{1.08}Te:O_x*, W. Si., Q. Jie, Lijun Wu, Lijun, J. Zhou, G. Gu, P. D. Johnson, and Q. Li, Phys. Rev. B **81**, 092506 (2010).
27. *Optical properties of the iron-arsenic superconductor BaFe_{1.85}Co_{0.15}As₂*, J. J. Tu, J. Li, W. Liu, A. Punnoose, Y. Gong, Y. H. Ren, L.J. Li, G. Cao, Z. A. Xu, and C. C. Homes, Phys. Rev. B **82**, 174509 (2010).
28. *Particle-hole asymmetry and the pseudogap phase of the high-T_c superconductors*, H.-B. Yang, J. D. Rameau, P. D. Johnson, and G. D. Gu, J. Supercond. Nov. Magn. **23**, 803-806 (2010).
29. *Metal to insulator transition on the N=0 Landau level in graphene*, L. Zhang, Y. Zhang, M. Khodas, T. Valla, and I. A. Zaliznyak, Phys. Rev. Lett. **105**, 046804 (2010).
30. *Incoherent c-axis interplane response of the iron chalcogenide FeTe_{0.55}Se_{0.45} superconductor from infrared spectroscopy*, S. J. Moon, C. C. Homes, A. Akrap, Z. J. Xu, J. S. Wen, Z. W. Lin, Q. Li, G. D. Gu, and D. N. Basov, Phys. Rev. Lett. **106**, 217001 (2011).
31. *Reconstructed Fermi surface of underdoped Bi₂Sr₂CaCu₂O_{8+δ} cuprate superconductors*, H.-B. Yang, J. D. Rameau, Z.-H. Pan, G. D. Gu, P. D. Johnson, H. Claus, D. G. Hinks, and T. E. Kidd, Phys. Rev. Lett. **107**, 047003 (2011).

The Nature of Fermi Arcs, Pseudogaps, and Electron Scattering Rates in Cuprate High- T_c Superconductors

Dan Dessau

Department of Physics, University of Colorado, Boulder, CO 80309, USA.

Dessau@Colorado.edu 303-492-1607

The “normal”, i.e. non-superconducting state of underdoped cuprate superconductors is an extremely unusual state of matter, widely argued to be more exotic and interesting than the high temperature superconducting state to which it is linked. This normal state is characterized by three key phenomena – a) a confusing “Fermi arc” typically described as a discontinuous locus of quasiparticle excitations at the Fermi energy, b) a “pseudogap” corresponding to weakly gapped states above the superconducting transition temperature and c) a non-Fermi Liquid behavior usually indicated by unusual electronic scattering rates, and a lack of quasiparticle excitations at the Fermi surface. We show, via the introduction and application of a new type of quantitative

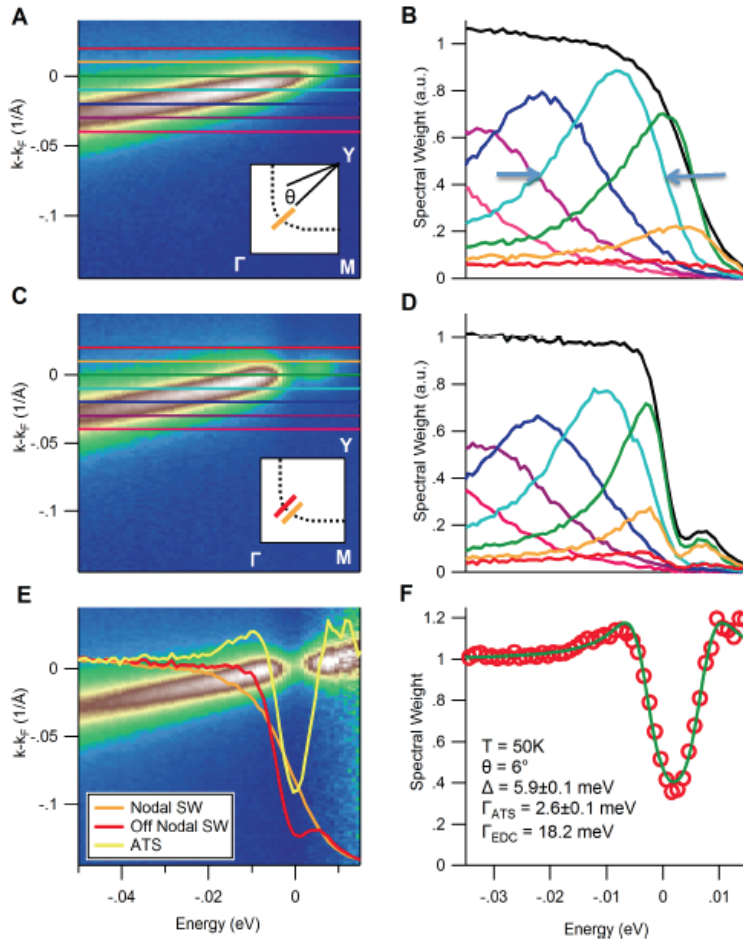


Fig 1: Creation and Fitting of the ARPES Tunneling Spectra (ATS). **a,c)** Nodal and near-nodal ARPES spectra of optimally doped ($T_c = 92\text{K}$) Bi2212 at $T=50\text{K}$. **b,d)** 7 out of a total of 170 individual EDCs from the plots at left. The sum of all 170 individual EDCs gives the spectral weight curves (black. **e)** normalized off-nodal spectra and the spectral weight curves from panels B and D (orange and red curves, respectively). The red curve is normalized to the orange curve to create the ARPES tunneling spectra (Yellow). **f)** Fit of the ATS to the Dynes tunneling formula, with parameters indicated. In particular, the extracted scattering rate $\Gamma_{\text{ATS}} = 2.6 \text{ meV}$ is much smaller than the value $\sim 20 \text{ meV}$ determined by the peak widths (blue arrows in panel b).

ARPES-based spectroscopy (fig 1), that the Fermi arcs as well as much of the pseudogap phenomenology are naturally explained as a consequence of the interplay of the temperature and doping dependence of a d-wave superconducting gap/pseudogap with a dynamical electronic scattering rate which is experimentally determined for the first time. In particular, we show a) the

Fermi arc is not a discontinuous locus of quasiparticle excitations at the Fermi surface but is rather a continuous locus of non-quasiparticle excitations due to the weight scattered into the gap, b) there is a prepairing pseudogap, and c) these non-quasiparticle excitations around the Fermi arc are natural candidates to explain much of the anomalous non-Fermi-liquid like behavior of cuprates (fig 2).

Future studies will extend this new technique to many different doping levels, as well as other classes of superconductors, so as to bring enlightenment to the phase diagram and potentially the mechanism of superconductivity.

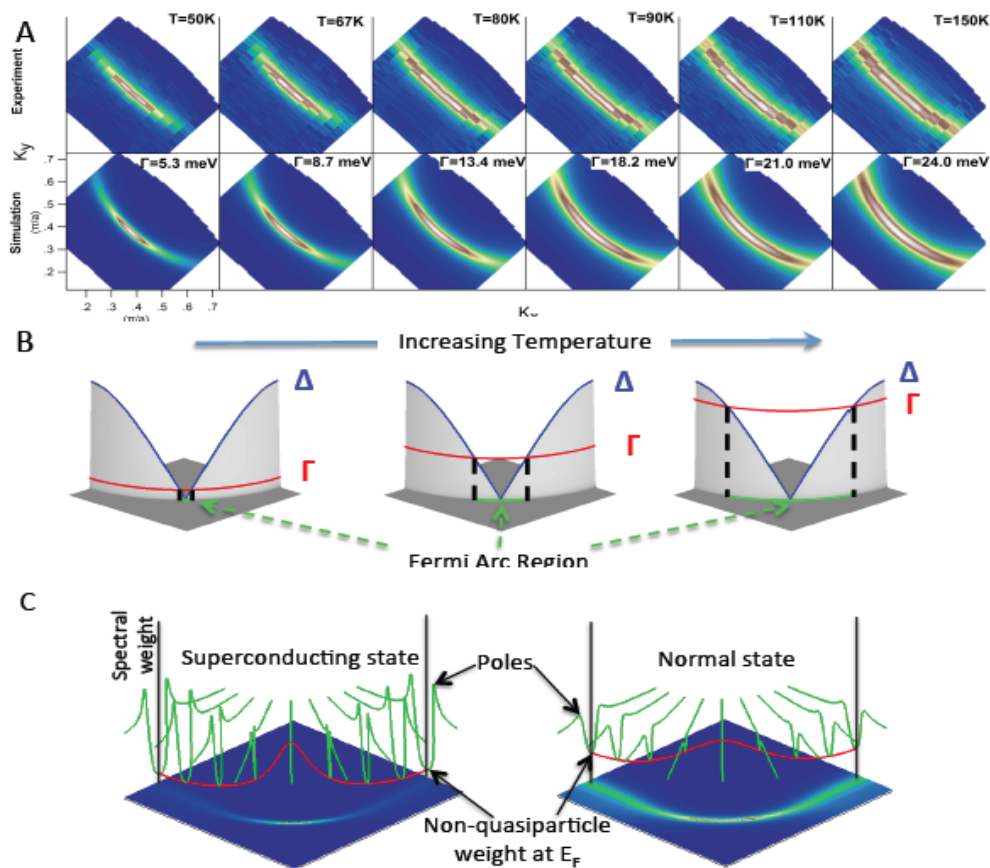


Fig 2: Experimental Fermi “arcs” vs. temperature (top), and simulated arcs (bottom) from a $T_c=67\text{K}$ underdoped $\text{Bi}_2\text{Sr}_2\text{CaCu}_2\text{O}_8$ sample. **A)** The unusual temperature-dependent arc length is seen in both the data and simulations. Inputs to the simulations are directly extracted from the experimental ARPES data, especially from the ATS curves that give the gap and the temperature-dependent scattering rate Γ_{ATS} . **B)** Simple picture for the temperature dependence of the Fermi arc length. The arc is approximately the region where $\Gamma_{\text{ATS}} > \Delta$, with the arc growing rapidly with temperature as Γ_{ATS} grows. **C)** Cartoon showing change in spectral weight (red) along the Fermi surface due to increasing Γ_{ATS} between the superconducting and normal states as determined by the ATS (green).

- T. J. Reber, N. C. Plumb, Z. Sun, Y. Cao, Q. Wang, K. McElroy, H. Iwasawa, M. Arita, J. S. Wen, Z. J. Xu, G. Gu, Y. Yoshida, H. Eisaki, Y. Aiura, and D. S. Dessau “The Non-Quasiparticle Nature of Fermi Arcs in Cuprate High- T_c Superconductors” (under review)
- N. C. Plumb, J. D. Koralek, J. F. Douglas, T. J. Reber, Z. Sun, Y. Aiura, K. Oka, H. Eisaki, and D. S. Dessau “Low-energy (< 10 meV) feature in the nodal electron self-energy and strong temperature dependence of the Fermi velocity in $\text{Bi}_2\text{Sr}_2\text{CaCu}_2\text{O}_{8+d}$ ” *Phys. Rev. Lett.* 105, 046402 (2010)
- H. Iwasawa, J.F. Douglas, K. Sato, T. Masui, Y. Yoshida, Z. Sun, H. Eisaki, H. Bando, A. Ino, M. Arita, K. Shimada, H. Namatame, M. Taniguchi, S. Tajima, S. Uchida, T. Saitoh, D.S. Dessau, Y. Aiura Oxygen isotope effect in optimally doped $\text{Bi}_2\text{Sr}_2\text{CaCu}_2\text{O}_{8+\delta}$ studied by low-energy ARPES *Physica C: Superconductivity*, Volume 470, S134-S136 (2010)
- Q. Wang, Z. Sun, E. Rotenberg, F. Ronning, E. D. Bauer, H. Lin, R. S. Markiewicz, M. Lindroos, B. Barbiellini, A. Bansil, and D. S. Dessau Uniaxial “nematic-like” electronic structure and Fermi surface of untwinned CaFe_2As_2 (arXiv:1009.0271v1)
- K. Sato, H. Iwasawa, N. C. Plumb, T. Masui, Y. Yoshida, H. Eisaki, H. Bando, A. Ino, M. Arita, K. Shimada, H. Namatame, M. Taniguchi, S. Tajima, Y. Nishihara, D. S. Dessau, and Y. Aiura, “Enhancement of oxygen isotope effect due to out-of-plane disorder in $\text{Bi}_2\text{Sr}_2\text{Ln}_{0.4}\text{CuO}_{6+\delta}$ superconductors” *Phys. Rev. B* 80, 212501 (2009)
- Q. Wang, Z Sun, E Rotenberg, H. Berger, D.S. Dessau “Energy-dependent scaling of incoherent spectral weight and the origin of the waterfalls in high- T_c cuprates” arXiv:0910.2787
- S. Danzenbacher, D.V. Vyalikh, Yu. Kucherenko, A. Kade, C. Laubschat, N. Caroca-Canales, C. Krellner, C. Geibel, A.V. Fedorov, D.S. Dessau, R. Follath, W. Eberhardt, and S.L. Molodtsov, “Hybridization Phenomena in Nearly Half-Filled f Shell Electron Systems: Photoemission Study of EuNi_2P_2 ” *Phys. Rev. Lett.* 102, 026403 (2009)
- H. Iwasawa, J. F. Douglas, K. Sato, T. Masui, Y. Yoshida, Z. Sun, H. Eisaki, H. Bando, A. Ino, M. Arita, K. Shimada, H. Namatame, M. Taniguchi, S. Tajima, S. Uchida, T. Saitoh, D.S. Dessau, Y. Aiura “An isotopic fingerprint of electron-phonon coupling in high temperature superconductors” *Phys Rev Lett* 101, 157005 (2008)
- Z. Sun, J.F. Douglas, A.V. Fedorov, D.S. Dessau, H. Lin, Sahrakorpi Seppo, Bernardo Barbiellini, Bob Markiewicz, A. Bansil, H. Zheng, J.F. Mitchell, “Electronic structure of $\text{La}_{2-2x}\text{Sr}_{1+2x}\text{Mn}_2\text{O}_7$ ($x=0.59$) and its comparison with $\text{La}_{2-2x}\text{Sr}_{1+2x}\text{Mn}_2\text{O}_7$ ($x=0.36, 0.38$) revealed by ARPES” *Phys. Rev. B.* 78, 075101 (2008)
- Philip A. Casey, J. D. Koralek, Nick Plumb, D.S. Dessau and Philip W. Anderson “Accurate theoretical fits to laser-excited photoemission spectra in the normal phase of high temperature superconductors” *Nature Physics* 4, 210 (2008)

DOE BES Experimental Condensed Matter Physics PI Meeting 9-12 August 2011.

Project Title: Experimental study of severely underdoped ultrathin cuprate films.

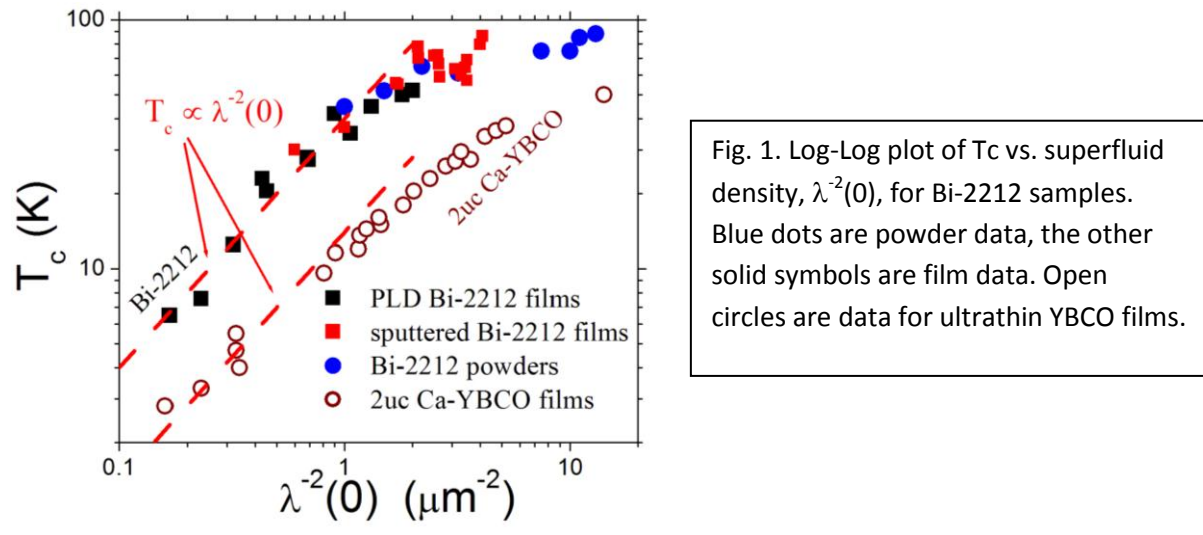
P.I.: Thomas R. Lemberger, Ohio State University. trl@physics.osu.edu.

Project Scope:

The primary physics focus of our DOE research is on quantum critical points and associated quantum and thermal fluctuations in novel superconductors, including cuprates and Fe-based superconductors. Cuprate compounds of primary interest include thick and ultrathin films of YBCO and Bi-2212, grown at OSU and at Technion in Israel. We also study films of LSCO and the novel e-doped compound Pr_2CuO_4 grown by MBE by our longtime collaborator in Japan. In addition, we have extended our work into Fe-based superconducting films grown at U. Wisconsin. Our research involves a range of measurements. Superfluid density measurements on films are essential in order to determine that the films are of sufficient quality to warrant detailed study. Beyond that, we study resistivity and Hall coefficient at OSU, THz transmission measurements with Simon Fraser U., local superfluid density with Stanford, and resistance fluctuations in collaboration with U. Illinois-Urbana. A secondary focus involves working with other film-growing labs to provide feedback on film quality through superfluid density measurements. This has been quite successful for us in the past, in work on electron-doped cuprates and on LSCO. We are working in this fashion with groups in Germany, Wisconsin, and Japan.

Recent Progress:

1. We found that quantum fluctuations in highly-anisotropic, severely-underdoped $\text{Bi}_2\text{Sr}_2\text{CaCu}_2\text{O}_{8+x}$ (B-2212) are strong and are two-dimensional (2D), as opposed to the 3D fluctuations found in the less anisotropic cuprates YBCO and LSCO. These results rest on the measured linear scaling of T_c with “superfluid density”, $\lambda^{-2}(0)$, in Bi-2212 films. The figure shows that Bi-2212 scaling is similar to that of ultrathin YBCO films. And, it shows that data on Bi-2212 powders (blue) agree with sputtered films (red - Technion) agree with PLD films (black - OSU), over doping ranges where the data overlap. To our knowledge, we are the first group to successfully grow severely underdoped Bi-2212 films. (Figure is from our soon-to-be submitted paper listed below.)



1.5. The temperature dependence of superfluid density in Bi-2212 exhibits the same “universal” trend found in underdoped YBCO, namely, that the regime of critical thermal fluctuations near T_c seems to disappear. This observation supports the interpretation of scaling data in terms of critical quantum fluctuations.

2. We found that the magnitude and temperature dependence of the superfluid density of pulsed-laser-deposited (PLD) films of the electron-doped pnictide superconductor, $\text{Ba}(\text{Fe}_{1-x}\text{Co}_x)\text{As}_2$, are comparable to those of single crystals. (Films grown by C.B. Eom at U. Wis.) The T-dependence in particular agrees with crystal data in great detail. This result has two ramifications. First, from a fundamental point of view, the T-dependence of superfluid density in this compound is insensitive to the extra disorder expected in films relative to crystals. Theories predict various degrees of sensitivity, due to scattering between electron-like and hole-like Fermi surfaces with gaps of opposite sign. Second, despite the structural and chemical flaws observed in PLD films by x-rays and TEM, their superconductivity properties are still quite good, and will only get better as film deposition protocols improve. This result was published in: Yong et al., Phys. Rev. B 83, 104510 (2011).

Future Plans:

Right now we are working hard on growing underdoped ultrathin films of Bi-2212 using Bi-2201 for protective buffer layers above and below. Ultrathin cuprate films are of central interest because the fluctuation regime above their T_c 's should be more pronounced than for any bulk cuprate sample. We want to look for Kosterlitz-Thouless-Berezinskii behavior in the superfluid density near T_c in ultrathin Bi-2212, as we observed in ultrathin YBCO. Since "thick" Bi-2212 already exhibits 2D scaling, will we see the same scaling in ultrathin films, just with a different T-dependence near T_c ? Normal-state transport (resistivity, Hall coefficient, and magnetoresistance) should provide great insight into the fluctuation regime above T_c .

We are anxious to get results of resistance-fluctuation measurements on our ultrathin YBCO films from our collaborators at U. Illinois. These fluctuations are presumably due to some mesoscopic ordering, such as charge and spin stripes, that should grow with underdoping and be especially prominent in ultrathin films. We've sent some films already. Similarly, we are hopeful that THz transmission measurements (at Simon Fraser Univ.) on ultrathin films will provide insight into the electrodynamics at frequencies comparable to $2k_B T_c$, where the gap frequency might reside.

We are excited about continuing our collaborations with C.B. Eom on Fe-pnictide films, hoping to follow superfluid density into compounds other than $\text{Ba}(\text{FeCo})_2\text{As}_2$ to study superfluid density near quantum critical points in the phase diagram. There should be features associated with antiferromagnetism turning on as T decreases for films near the QCP where AF appears.

More speculatively, we are working on a novel electron-doped cuprate superconductor $\text{Pr}_2\text{CuO}_{4-x}$, where superconductivity arises due to oxygen reduction, not cation substitution. Our collaborator, Michio Naito in Tokyo, has sent us a film grown by MBE. T_c is as high as 26 K in his annealed films of $\text{Pr}_2\text{CuO}_{4-x}$, which is higher than for the traditional e-doped compound, $\text{Pr}_{2-x}\text{Ce}_x\text{CuO}_4$. It is extremely important to compare properties of e-doped cuprates with the similarly structure LSCO-type hole-doped cuprates. It would be very exciting to get ultrathin films of this compound to compare with YBCO and Bi-2212 ultrathin films.

Publications:

1. "Anomalous Noise in the Pseudogap Regime of $\text{YBa}_2\text{Cu}_3\text{O}_7$ " D. S. Caplan, V. Orlyanchik, M. B. Weissman, D. J. Van Harlingen, E. H. Fradkin, M. J. Hinton, and T. R. Lemberger, Phys. Rev. Lett. 104, 177001 (2010). n.b., We provided some sample films and helped in writing the paper; all measurements were done at Illinois.
2. "Superfluid density measurements of $\text{Ba}(\text{Co}_x\text{Fe}_{1-x})_2\text{As}_2$ films near optimal doping", Jie Yong, S. Lee, J. Jiang, C. W. Bark, J. D. Weiss, E. E. Hellstrom, D. C. Larbalestier, C. B. Eom, and T. R. Lemberger, Phys. Rev. B 83, 104510 (2011).
3. "2-D Quantum Critical Point in Severely Underdoped $\text{Bi}_2\text{Sr}_2\text{CaCu}_2\text{O}_{8+x}$ Films Revealed by Superfluid Density Measurements" Jie Yong, A. McCray, M. Randeria, M. Naamneh, A. Kanigel, and T.R. Lemberger, to be submitted soon.

SPECTROSCOPIC IMAGING STM STUDIES OF COMPLEX ELECTRONIC MATTER

Principal Investigator:

J. C. (Séamus) Davis

Brookhaven National Laboratory

P.O. Box 5000

Upton, NY 11973-5000

Department of Physics, 622 Clark Hall

Cornell University, Ithaca, NY 14850

Phone: 607-220-8685 (mobile)

Email: jcdavis@ccmr.cornell.edu

Project Scope

We focus upon a spectroscopic imaging STM research program covering four major areas of complex electronic matter. The first consists of studies of the electronic structure of **cuprates**, and includes searching for the mechanism of high temperature superconductivity therein. The second is a program focused on the recently discovered high temperature superconducting **pnictides** to study symmetry of the order parameter, effect of the dopant atoms, and the electron pairing mechanism. Our third program focuses on electronic nematic states, especially in the **ruthenates**. Here the key challenge is to image a high magnetic field induced transition to a nematic state at sub kelvin temperatures. The fourth program is the SI-STM study of the mechanism of heavy fermion electronic structure in **intermetallic** metals and of heavy fermion superconductivity.

Recent Progress

Several recent achievements include:

Evolution of the electronic excitation spectrum in superconducting $\text{Bi}_2\text{Sr}_2\text{CaCu}_2\text{O}_{8+\delta}$

We measure the spectrum of electronic excitations $N(E)$ over a wide range of hole density p in superconducting $\text{Bi}_2\text{Sr}_2\text{CaCu}_2\text{O}_{8+d}$ and demonstrated that a form of $N(E)$ enables successful fitting of spectra throughout the $\text{Bi}_2\text{Sr}_2\text{CaCu}_2\text{O}_{8+d}$ phase diagram. We found that $\Delta_i(k)$ values rise with falling p along the familiar trajectory of excitations to the pseudogap energy, whereas the inelastic scattering rate seems to be an intrinsic property of the electronic structure and rises steeply for $p < 16\%$. Such diverging inelastic scattering may play a key role in suppression of superconductivity near the Mott insulator; **Nature Physics** **4**, 319 (2008).

Discovery of Momentum-space Arcs supporting Cooper Pairing in $\text{Bi}_2\text{Sr}_2\text{CaCu}_2\text{O}_{8+d}$

We have imaged the electronic structure of $\text{Bi}_2\text{Sr}_2\text{CaCu}_2\text{O}_{8+d}$ in r -space and k -space simultaneously and discovered that, although the low-energy excitations are Bogoliubov quasi-particles, they occupy only a restricted arc in k -space which is terminated on the line between $(0,\pi)$ and $(\pi,0)$. This arc shrinks rapidly with diminishing p in a fashion that would satisfy Luttinger's Theorem. Concomitantly, spectral weight is transferred to higher energy r -space states that lack the characteristics of excitations from delocalized Cooper pairs and break locally translational & rotational-symmetry; **Nature** **454**, 1072-1078 (2008).

Heavy d-electron Quasiparticle Interference in $\text{Sr}_3\text{Ru}_2\text{O}_7$

Electronic liquid-crystalline phases represent an unexplored frontier of condensed-matter physics and are proposed to be important in the physics of cuprate high- T_c superconductivity. Classical liquid crystal physics was transformed by microscopies that enabled imaging of real-space structures and patterns. To obtain equivalent data in the purely electronic systems we use SI-STM in $\text{Sr}_3\text{Ru}_2\text{O}_7$ because it exhibits a field-induced transition to an electronic liquid crystalline phase; *Nature Physics* **5**, 800 (2009).

Spectroscopic Fingerprint of Phase-Incoherent Superconductivity in Pseudogap Phase

A possible explanation for the existence of the cuprate “pseudogap” state is that it is a d-wave superconductor without quantum phase rigidity. One spectroscopic signature of d-wave superconductivity is the particle-hole symmetric “octet” of dispersive Bogoliubov quasiparticle interference modulations. We explored this octet’s evolution from low temperatures to well into the underdoped pseudogap regime. No pronounced changes occur in the octet phenomenology at the superconductor’s critical temperature T_c , and it survives up to at least temperature $T \sim 1.5 T_c$. In this pseudogap regime, we observed the detailed phenomenology that was theoretically predicted for quasiparticle interference in a phase-incoherent d-wave superconductor. *Science* **325**, 1099 (2009)

Real-space and Momentum-space Imaging of Heavy Fermions

Within a Kondo lattice, the strong hybridization between electrons localized in \mathbf{r} -space and those delocalized such that they are defined in \mathbf{k} -space, generates exotic electronic states called ‘heavy fermions’. We used imaged the evolution of URu_2Si_2 electronic structure simultaneously in \mathbf{r} -space and \mathbf{k} -space. At low temperatures in this material we achieved the first visualization of the quantum mechanical process of heavy fermion formation and thereby opened exciting new avenues for research into heavy fermions and their superconductivity; *Nature* **465**, 570 (2010).

Proposed Research

HEAVY FERMION SUPERCONDUCTORS

Effect of individual ‘Kondo Hole’ on a Heavy Fermion Electronic Structure

Substituting individual Th atoms on the U sites can allow us to image the effect of absence of a single magnetic atom from an otherwise translationally invariant Kondo lattice. This is the well-known ‘Kondo Hole’ idea that has been studied theoretically for decades. However, this state has never actually been imaged by STM because convectional STM studies use magnetic adatoms on metal surfaces, so that creating a ‘Kondo-hole’ is not possible.

We propose exploration of individual ‘Kondo-hole’ phenomenology at individual Th atoms ($S=0$) substituted on the U sites in URu_2Si_2 which is a rather simple heavy fermion system at low temperatures. Our first objective is to determine the changes in density-of-states (within the hybridization energy range occurring at the Th sites. Second we will attempt to use Fourier transform STM to determine the changes in the hybridization process itself (surrounding each Th atom).

Superconducting Quasiparticle Interference in Heavy Fermion Compounds

We also propose to generalize our heavy-fermion QPI techniques from the normal heavy-fermion state into the heavy fermion superconductive state below 1.7K in URu_2Si_2 . This system should have an exotic symmetry order parameter because of the hidden order state

in the background. Superconductive QPI is a very powerful technique to determine the k -space electronic structure and the complex structure of the energy gap

ELECTRONIC NEMATIC MATERIALS

Visualization of the Field-Induced Nematic Transition Imaging in $Sr_3Ru_2O_7$

Grigera *et al* reported that the itinerant metamagnet $Sr_3Ru_2O_7$ undergoes a phase transition to a new state of electronic matter whose transport properties are strongly anisotropic. We propose imaging this field induced phase transition which occurs near 8.2 Tesla and at which the electronic structure spontaneously reduces its symmetry and domains of size approximately 0.5 micron square (from deHaas-VanAlpen measurements) are formed. These domains are believed to separate regions within which the rotational symmetry of the r -space and k -space electronic structure is reduced from that of the crystal but in two possible different ways (at 90° to each other).

COPPER-OXIDE SUPERCONDUCTORS

Imaging Quantum Oscillation Effects in Very High Magnetic Fields

When studied by ARPES, underdoped cuprates appear highly anomalous in that they seem to have no closed Fermi surface, but only disconnected 'Fermi arcs'. However, quantum oscillations in the electrical resistance of $YBa_2Cu_3O_{6.5}$ established the existence of a well-defined Fermi surface in the high-field state of underdoped cuprates. The Fermi surface is made of small pockets, in contrast to the large cylinder characteristic of the overdoped regime. However, after several years of study, it is unknown whether these pockets are electron-like, hole-like, and how many there are, and where they are in k -space. Thus it has proven virtually impossible to make progress on this issue which is profoundly important to our understanding of high- T_c superconductivity. And the standard approach of using ARPES to explore the k -space electronic structure is ruled out because this technique does not work in magnetic fields.

However there is one technique which can determine k -space electronic structure in high magnetic fields – quasiparticle interference imaging. Bogoliubov quasiparticle interference (QPI) occurs when these quasiparticle waves are scattered by impurities and the scattered waves undergo quantum interference. We propose to pursue such QPI studies to the highest magnetic fields at which it is presently possible to achieve a persistent magnetic field – namely 20 Tesla. If the magnetic field were to introduce changes which alter the cuprate k -space electronic structure from its well understood zero-field arrangement, this would become apparent immediately in the QPI patterns. For example, if as proposed an electron pocket were to appear near the Brillouin zone face, an additional new set of QPI vectors would appear.

FERRO-PNICTIDE SUPERCONDUCTORS

Effect of Dopant Atoms on Disorder & Transport Anisotropy in FeAs Compounds

The parent phase of AFe_2As_2 ($A=Ca, Sr$ and Ba) ferropnictide family exhibits very peculiar properties in terms of transport anisotropy. When the crystals are most orthorhombic, the anisotropy is minimal (at most a few %) and it only becomes robust when dopant atoms are added and the system moves toward the orthorhombic \rightarrow tetragonal phase transition point. Beyond this, the anisotropy disappears. The reasons for

these unusual phenomena, and their impact on the mechanism of superconductivity which exhibits its maximum T_c just at the point of disappearance of the anisotropy, are unknown.

We propose to study $\text{Ca}(\text{Fe}_{1-x}\text{Co}_x)_2\text{As}_2$ as a function of Co doping. We will image the locations of the Co dopant atoms in search of a process whereby they could enhance the transport anisotropy. In doing so we will use the knowledge of the band structure in detwinned samples of $\text{Ca}(\text{Fe}_{1-x}\text{Co}_x)_2\text{As}_2$ to analyze the effects of different scattering processes on the transport, and also on the QPI signatures which have remained unexplained.

Publications

1. Interplay of Electron-Lattice Interactions and Superconductivity in $\text{Bi}_2\text{Sr}_2\text{CaCu}_2\text{O}_{8+\delta}$ Jinho Lee, K. Fujita, K. McElroy, J. A. Slezak, M. Wang, Y. Aiura, H. Bando, M. Ishikado, T. Masui, J.-X. Zhu, A. V. Balatsky, H. Eisaki, S. Uchida, and J. C. Davis *Nature* **442**, 546-550 (2006)
2. The Ground State of the Pseudogap in Cuprate Superconductors T. Valla, A. V. Fedorov, Jinho Lee, J. C. Davis, G. D. Gu *Science* **314**, 1914-1916 (2006)
3. An Intrinsic Bond-Centered Electronic Glass with Unidirectional Domains in Underdoped Cuprates, Y. Kohsaka, C. Taylor, K. Fujita, A. Schmidt, C. Lupien, T. Hanaguri, M. Azuma, M. Takano, H. Eisaki, H. Takagi, S. Uchida, J. C. Davis, *Science* **315**, 1380-1385 (2007)
4. Imaging the impact on cuprate superconductivity of varying the inter-atomic distances within individual crystal unit cells, J. A. Slezak, Jinho Lee, M. Wang, K. McElroy, K. Fujita, B. M. Anderson, P. J. Hirschfeld, H. Eisaki, S. Uchida, J. C. Davis, *Proc. Nat. Acad. Sci. USA* **105**, 3203 (2008).
5. How Cooper pairs vanish approaching the Mott insulator in $\text{Bi}_2\text{Sr}_2\text{CaCu}_2\text{O}_{8+\delta}$ Y. Kohsaka, C. Taylor, P. Wahl, A. Schmidt, Jinhwan Lee, K. Fujita, J. W. Allredge, K. McElroy, Jinho Lee, H. Eisaki, S. Uchida, D.-H. Lee & J. C. Davis, *Nature* **454**, 1072 (2008).
6. Spectroscopic Fingerprint of Phase-Incoherent Superconductivity in the Cuprate Pseudogap State Jinhwan Lee, K. Fujita, A. R. Schmidt, Chung Koo Kim, H. Eisaki, S. Uchida, J. C. Davis *Science* **325**, 1099 (2009)
7. Heavy d-electron quasiparticle interference and real-space electronic structure of $\text{Sr}_3\text{Ru}_2\text{O}_7$ Jinho Lee, M. P. Allan, M. A. Wang, J. Farrell, S. A. Grigera, F. Baumberger, J. C. Davis and A. P. Mackenzie *Nature Physics* **5**, 800 (2009)
8. Imaging the Fano lattice to 'hidden order' transition in URu_2Si_2 , A. R. Schmidt, M. H. Hamidian, P. Wahl, A. Balatsky, J. D. Garrett, T. J. Williams, G. M. Luke & J. C. Davis *Nature* **465**, 570 (2010)

Session 8

Topological Insulators

ABSTRACT FOR BES-ECMP MEETING - PABLO JARILLO-HERRERO

Project Title: Quantum Transport in Topological Insulator Nanoelectronic Devices

Principal Investigator: Pablo Jarillo-Herrero

Institution: Massachusetts Institute of Technology

E-mail address: pjarillo@mit.edu

Project Scope

The research objective of this proposal is to study the novel quantum properties of topological insulators (TIs). It is part of the broad context of the PI's research activities, which focus on the conceptually new behavior of electrons in low dimensional nanostructures, and in particular in solids where the effective Hamiltonian is described by the Dirac equation. Our experimental approach includes the fabrication of quantum TI devices and their investigation via electronic transport techniques.

Recent Progress

We developed two alternative fabrication approaches for TI devices. The first approach is based on single crystal Bi_2Se_3 exfoliated onto a substrate, with the resulting flakes subsequently connected by electrodes. Using this first approach we have established¹ that the surface channel supports electronic transport, and that its density is tunable by a gate voltage. A second approach is based on using thin-film of Bi_2Se_3 grown in an ultra-high vacuum chamber. Thin film growth offers fine control over geometry and composition and a straightforward approach for growth of heterostructures. We recently fabricated low carrier density thin-film devices where the surface density is tunable by a top-gate. The devices exhibit remarkable conductance modulation, up to 500% on/off ratio (Fig. 1(a)), and a cross-over of the Hall coefficient to positive values (Fig. 1(b)) which indicates that the dominant Hall current-carrying population changes from electrons to holes.

We use these devices as a platform to study the fundamental transport physics of TIs. The thin film material exhibits a pronounced Weak Antilocalization (WAL) correction to conductance. This correction allows to extract the coherence length and the effective number of coherently independent channels. We find the WAL correction depends on the applied gate voltage such that the effective number of parallel channels is gate-tunable. We interpret this as arising from a competition between two time-scales: A phase coherent transport time scale τ_ϕ and a surface-bulk scattering time τ_{SB} . Our results

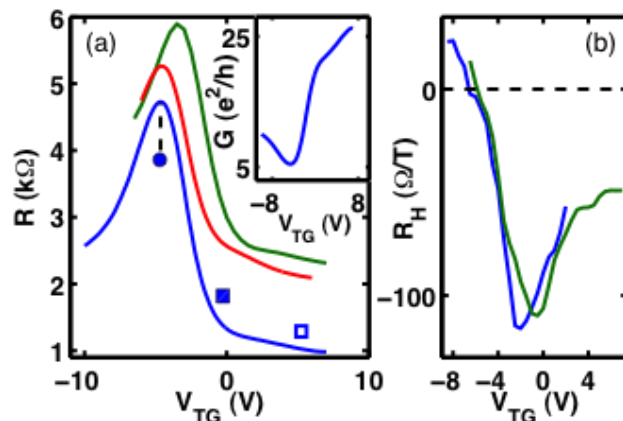


Figure 1. (a) Resistance R vs. Top-gate voltage V_{TG} measured on three different devices. Inset: Conductance of one of the devices. (b) Hall coefficient R_{H} in 2D units. R_{H} crosses over to positive values at $V_{\text{TG}} \sim -7\text{V}$.

suggest that the gate voltage tunes the system between a regime where $\tau_\phi > \tau_{SB}$ where the surface and the bulk merge into a single coherent channel, and an opposite regime where $\tau_\phi < \tau_{SB}$ and the surface and bulk are coherently separate. The gate tunability of τ_{SB} is likely due to the formation of a depletion layer between the surface and the bulk carriers.

Future Plans

High Field Magnetoconductance

We intend to carry out magnetoconductance experiments of our low density devices at high fields. At low field we observe incipient oscillations which are likely to become more pronounced at lower temperatures and higher fields. Our density tunable devices could help resolve some of the outstanding questions relating to the quantum oscillations of the surface states, such as the role of band curvature, the Zeeman effect, and the role of bulk carriers.

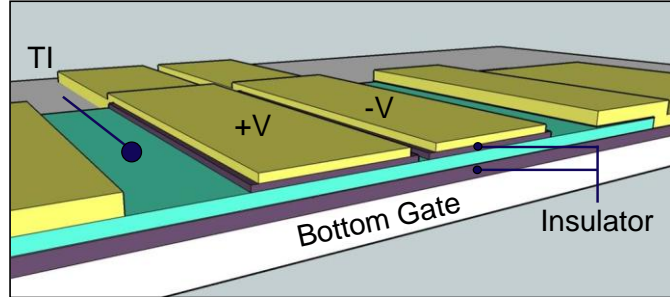


Figure 2: Field-effect TI device. The TI flake (light blue) is gated from the bottom by highly doped Si and from the top by metallic gates. Carrier density on the top and bottom surfaces is tuned by combination of top and bottom gate voltages. A p - n junction is created by tuning adjacent regions to p - and n -type doping.

Magneto-capacitance measurements

Our top-gated devices are suitable for capacitance measurements. In particular, we are interested in characterizing the depletion-layer which is expected to form when gate voltage is applied to the surface. At high magnetic fields, capacitance measurements could elucidate the interplay between the surface and bulk carriers in quantum oscillations.

TI PN Junctions

We are developing a TI PN junction (see geometry in Figure 2). In PN junctions transport is expected to be sensitive to Klein tunneling, detected in graphene but not on the Dirac electrons of the TI surface state. Since the TI top surface cannot be gated using a back-gate (as done in graphene), we are developing an approach for using two local top-gates deposited over different regions of a device.

TI Josephson Junctions

Majorana states are expected to be found in narrow Josephson junctions. We are fabricating Josephson junctions by in-situ growth of heterostructures consisting of a TI and a superconducting (SC) material. This is expected to ensure optimal coupling between the SC and TI. The SC can then be selectively removed by a standard etching process, leaving a narrow junction, and a dielectric and a gate electrode can be subsequently added. We plan to study the effect of TI thickness and junction geometry. In particular we are interested to test how deeply into the TI does the proximity effect

penetrate, and whether the proximity effect induces supercurrent on both the top and bottom surfaces.

List of Publications

This project is starting in July 2011, and no publication resulting from this funding has appeared yet.

References

1. Surface state transport and ambipolar electric field effect in Bi_2Se_3 nanodevices. H. Steinberg, D. Gardner, Y. Lee & P. Jarillo-Herrero. *Nano Letters* **10**, 5032-5036 (2010).

Project Title: Focused Research Center in Correlated Electron Materials

PIs: Ziqiang Wang, Co-PIs: Hong Ding, Vidya Madhavan, and Willie Padilla

Institution: Department of Physics, Boston College, Chestnut Hill, MA 02467

Email addresses: wangzi@bc.edu, madhavan@bc.edu, willie.padilla@bc.edu, dingh@aphy.iphy.ac.cn

Project Scope

This Single-Investigator and Small Group Research Grant commenced on 9/15/09. The grant supports the collaborations among theory and complimentary experimental efforts (STM, ARPES, and Optics) in one of the DOE grand challenge areas of correlated electron and complex materials.

Recent Progress

The research activities have led to 7 published papers from 2010 to 2011, including 2 in Nature Physics, 2 in Physical Review Letters, 1 in Nature Communications. In addition, there are 5 manuscripts that have been submitted or to be submitted for publication. A few selected highlights of the research activities are summarized below.

Iron-based high-T_c superconductors

- 1) In this work, we studied the three-dimensional superconducting gap function in optimally-doped iron-pnictides. We obtained valuable insights by probing the out-of-plane (k_z) dependence of the electronic structure and the superconducting gap using the k_z -capability of angle-resolved photoemission with varying photon energy. We discovered that the superconducting gap on the inner hole-like FS shows large k_z dispersion that can only derive from 3D pairing. The gap on the electron-like FS sheets around $(\pi, 0)$, on the other hand, has a much weaker k_z dependence. We gave a complete description of all the measured gaps by a single 3D gap function that is consistent with the existence of only two dominate pairing energy scales, the in-plane and out-of-plane pairing strengths and suggest a common origin for the pairing strength in all of the observed FS sheets.
- 2) We have studied the correlation effects on the electronic structure and spin density wave order in Fe-pnictides. Starting from the multi-orbital Hubbard model, we developed a finite-U Gutzwiller approximation and showed that non-perturbative correlation effects are essential to stabilize the metallic spin density wave phase for the intermediate correlation strengths appropriate for pnictides. We found that the ordered moments depend sensitively on the Hund's rule coupling J_H but weakly on the Coulomb repulsion U , varying from $0.3\mu_B$ to $1.5\mu_B$ in the range $J_H=0.3\sim 0.8\text{eV}$ and $U=3\sim 4\text{eV}$. We obtained the phase diagram and discuss the effects of orbital order and electron doping, the evolution of the Fermi surface topology with the ordered moment, and compared to recent experiments.

High T_c cuprate superconductors

- 1) We used scanning tunneling microscopy (STM) and neutron scattering to provide the first direct evidence that antiferromagnetism and superconductivity coexist spatially in electron-doped superconducting $\text{Pr}_{0.88}\text{LaCe}_{0.12}\text{CuO}_{4-d}$ (PLCCO) with $T_c = 21\text{ K}$. Combining neutron and STM data on nominally identical samples, we showed that the AF order as well as the superconductivity are inhomogeneous and compete locally on nanometer length scales.

Topological Insulators

- 1) We utilize Fourier transform scanning tunneling spectroscopy (FT-STs) to probe the surface of the magnetically doped TI, $\text{Bi}_{2-x}\text{Fe}_x\text{Te}_3$. Our measurements show the appearance of a hitherto unobserved channel of electronic backscattering along the surface q-vector GK. By comparing the FT-STs with angle-resolved photoemission spectroscopy (ARPES) data, we formulate a simple model showing that these new GK vectors are fully consistent with spin-flip scattering. Our combined data therefore present compelling evidence for the first momentum resolved measurement of enhanced backscattering due to magnetic impurities in a prototypical TI.

Future Plans

In the coming year, we will continue to carry out the proposed and the newly initiated research projects.

The Group will continue the study of high-T_c cuprates and iron-pnictides using complimentary techniques (ARPES, STM, Optics, and theory). In the case of the pnictides, the focus will be on the mechanism of superconductivity and pairing symmetry which have been the most important unresolved issues of intensive debate. The doping dependence of the superconducting gap and the question of coexistence of superconductivity and spin density wave state in Ni-doped Ba122 pnictides will also be studied. For the cuprates, the focus will be to continue the investigation of the origin of the pseudogap in the underdoped regime. STM spectroscopic studies will be conducted to study the evolution pseudogap phase in La-Bi2201 as a function of temperature to test the scenario of competing order that has received increasing experimental support.

We will continue our study on topological insulators, which have drawn tremendous theoretical and experimental interests. We will continue to collaborate with our neutron and sample growth group at BC. STM and spin-polarized STM studies will be carried out to probe the magnetic correlations in doped topological insulator Bi₂Te₃. In addition, we will study the effects of strong correlations in the strontium iridate class of topological insulators.

Our optics group will continue the investigation of the electromagnetic properties of novel metamaterials. These systems show remarkably interesting electromagnetic responses such as negative diffraction index with potential applications. Since the beginning of the project, work completed by the group has primarily been the design, fabrication of experimental equipment for optical characterization. We have successfully constructed a custom vacuum system which will permit accurate characterization of both absolute value transmission and reflection of samples over a broad range of the electromagnetic spectrum from THz to ultraviolet wavelengths. Recently we have redesigned and ordered new toric mirrors which should permit higher quality measurements with greater signal to noise. Additionally we will be able to measure samples from temperatures of liquid helium to 500 degrees Celsius. We are currently writing two manuscripts intended for publication.

Publications

1. J. Zhao, F. C. Niestemski, Shankar Kunwar, Shiliang Li, P. Steffens, A. Hiess, H. J. Kang, S. D. Wilson, Z. Wang, P. Dai, V. Madhavan, "Electron-Spin Excitation Coupling in an Electron Doped Copper Oxide Superconductor", **Nature physics**, advance online publication, 22 May (2011) .
2. Y.-M. Xu, Y.-B. Huang, X.-Y. Cui, R. Elia, R. Milan, M. Shi, G.-F. Chen, P. Zheng, N.-L. Wang, P.-C. Dai, J.-P. Hu, Ziqiang Wang, H. Ding, "Observation of a ubiquitous three-dimensional superconducting gap function in optimally-doped Ba_{0.6}K_{0.4}Fe₂As₂", **Nature Physics**, vol. 7, p. 198-202 (2011).
3. Yoshinori. Okada, C. Dhital, WenWen Zhou, Erik D. Huemiller, Hsin Lin, S. Basak, A. Bansil, Y. -B. Huang, H. Ding, Z. Wang, Stephen D. Wilson , V. Madhavan, "Direct Observation of Broken Time-Reversal Symmetry on the Surface of a Magnetically Doped Topological Insulator", **Phys. Rev. Lett.** vol. 106, 206805 (2011).
4. M. Neupane, P. Richard, Y.-M. Xu, K. Nakayama, T. Sato, T. Takahashi, A. V. Fedorov, G. Xu, X. Dai, Z. Fang, Z. Wang, G.-F. Chen, N.-L. Wang, H.-H. Wen, H. Ding, "Electron-Hole Asymmetry in Superconductivity of Pnictides Originated from the Observed Rigid Chemical Potential Shift", **Physical Review B**, vol. 83 p. 094522, (2011).
5. H. Ding, K. Nakayama, P. Richard, S. Souma, T. Sato, T. Takahashi, M. Neupane, Y.-M. Xu, Z.-H. Pan, A.V. Federov, Z. Wang, X. Dai, Z. Fang, G.F. Chen, J.L. Luo, and N.L. Wang, "Electronic structure of optimally doped pnictide Ba_{0.6}K_{0.4}Fe₂As₂: a comprehensive angle resolved photoemission spectroscopy investigation", **Journal of Physics: Condensed Matter**, p. 135701, vol. 23, (2011).
6. Y.-M. Xu, P. Richard, K. Nakayama, T. Kawahara, Y. Sekiba, T. Qian, M. Neupane, S. Souma, T. Sato, T. Takahashi, H. Luo, H.-H. Wen, G.-F. Chen, N.-L. Wang, Z. Wang, Z. Fang, X. Dai, H. Ding, "Fermi surface dichotomy of superconducting gap and pseudogap in underdoped pnictides", to be published in **Nature Communications** (2011).
7. Sen Zhou and Ziqiang Wang, "Electron correlation and spin density wave order in iron pnictides", **Physical Review Letters**, vol. 105, p. 096401 (2010).

Infrared Hall Effect in correlated electronic materials

Principle investigator: Dr. H. Dennis Drew
CNAM, Physics Department University of Maryland
College Park, MD 20742
hdrew@physics.umd.edu

Project scope

The research in this program is on the magneto-optical response of electronic materials at THz frequencies. The emphasis is on measurements of the Faraday and Kerr rotations and circular dichroism and their interpretation. The program focuses on two classes of materials: the cuprate superconductors and topological insulators. The main goal of the proposed research on the cuprates is to combine measurements of the IR magneto-transport on cuprate superconductors performed in our laboratory at the University of Maryland with the data acquired from Angular Resolved Photoemission Spectroscopy and other experiments such as DC transport, and neutron scattering to critically examine the extent to which Fermi liquid theory provides an adequate description of transport and infrared properties across the phase diagram of the cuprate high temperature superconductors. In topological insulators the goal of the program and its main intellectual merit is the observation and study of the quantization of the Faraday and Kerr rotation in these materials which are key predicted topological effects. This quantization is topologically protected only at zero frequency. The experiments examine the breakdown of these topological invariants with frequency which is important to our understanding of these important fundamental condensed matter constraints. Also, the quantization is in units of the fine structure constant, α , so that the measurement technique may provide precision metrology of this fundamental constant.

Recent progress

Cuprates: IR Hall Effect in BSCCO

Measurements of the Faraday rotation and circular dichroism were performed on optimally doped Bi-2212 at THz frequencies in order to elucidate the nature of the anomalous DC Hall Effect long studied in hole doped cuprates[1]. Recent results are shown in FIG. 1. Above T_c , the spectral weight of the IR Hall response, characterized by the Hall frequency ω_H , is found to be significantly larger than the value calculated within a Boltzmann formalism using ARPES measured parameters. This observation is the THz manifestation of the well-known anomalous dc-Hall effect where dc- R_H enhancements are much larger than the values expected from Luttinger's theorem as well as the ARPES+RTA value. These enhancements as well as the frequency and temperature dependence of the dc- and IR Hall response were found to be well described by a Fermi-liquid theory which incorporates current vertex corrections in the conductivity and electron-electron interactions mediated by antiferromagnetic fluctuations. Therefore this work provides strong evidence for an interpretation of the anomalous Hall Effect in the cuprates in terms spin fluctuations.

Topological Insulators.

A special effort was carried out this past year on topological insulators because of the great interest in the predicted properties of these materials and because of the availability of especially good samples at Maryland. Topological insulators (TIs) are a predicted new quantum state of matter occurring in certain materials with a strong spin orbit coupling (e.g., Bi_2Se_3 and Bi_2Te_3). Topological insulators are predicted to have exotic properties including a topologically protected spin polarized conducting surface state, an intrinsic magneto-electric effect and Majorana fermions induced by the proximity effect with a superconductor. One of the signature exotic properties of a topological insulator is a quantized Faraday rotation and/or Kerr rotation due to the intrinsic magneto-electric effect. In our work we first characterized the Maryland low impurity density samples through measurements of the IR response [2]. The

response is well described in terms of Lorentzian phonons and a Drude response of the bulk electrons. In these measurements the bulk response dominates the signals even for our lowest doped ($n=10^{17} \text{ cm}^{-3}$) samples. The electron-phonon interaction is observed to be weak in Bi_2Se_3 . Magneto-optical measurements yields a cyclotron mass for a low-doped Bi_2Se_3 single crystal which is close to the mass observed in SdH measurements. Free carriers are electrons as determined from the sign of the Faraday angle [2].

In order to investigate the predicted quantization of the Kerr and Faraday angles in topological insulators we extended our THz magneto-optical measurement facility to include the Kerr Effect [3]. This allows measurement of magneto-optical effect on opaque samples which is important at this stage of research on TIs because of their bulk

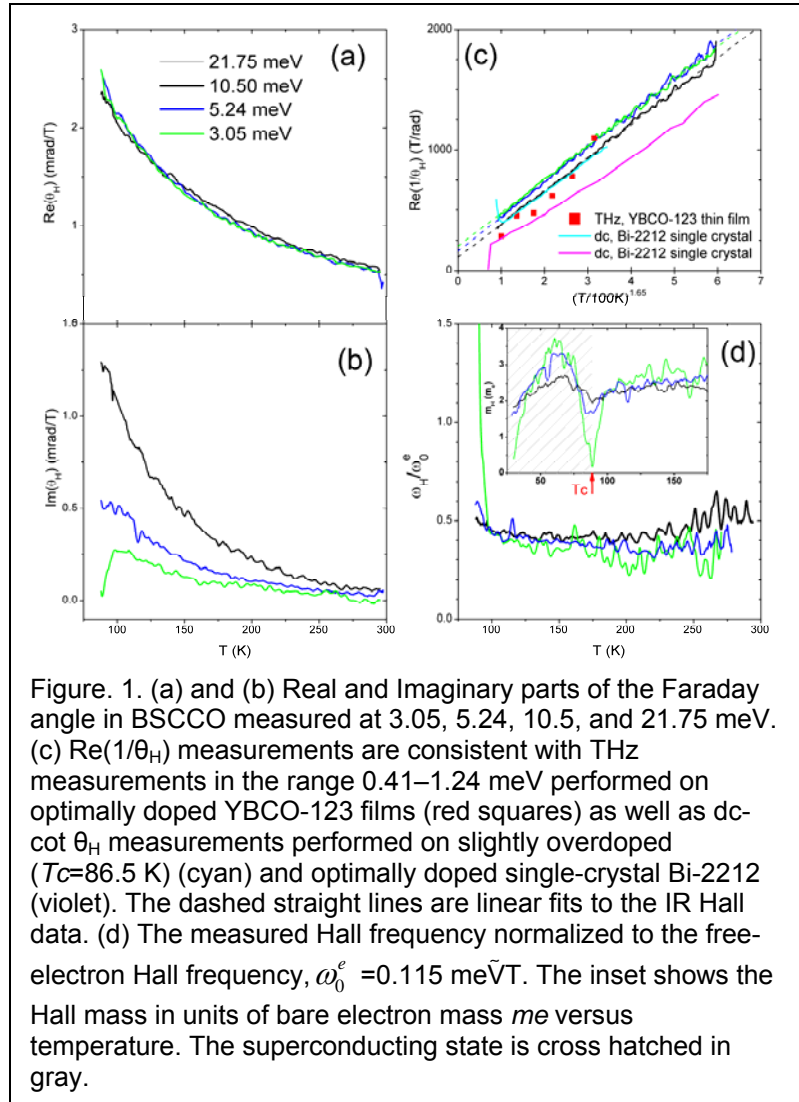


Figure 1. (a) and (b) Real and Imaginary parts of the Faraday angle in BSCCO measured at 3.05, 5.24, 10.5, and 21.75 meV. (c) $\text{Re}(1/\theta_H)$ measurements are consistent with THz measurements in the range 0.41–1.24 meV performed on optimally doped YBCO-123 films (red squares) as well as dc θ_H measurements performed on slightly overdoped ($T_c=86.5 \text{ K}$) (cyan) and optimally doped single-crystal Bi-2212 (violet). The dashed straight lines are linear fits to the IR Hall data. (d) The measured Hall frequency normalized to the free-electron Hall frequency, $\omega_0^e = 0.115 \text{ meV}\cdot\text{T}$. The inset shows the Hall mass in units of bare electron mass m_e versus temperature. The superconducting state is cross hatched in gray.

conduction. We also, examined the predicted magneto-optical effects in more depth by taking into account the multiple reflections in the bulk samples or thin films of TIs on a substrate [4]. The optical configuration is shown in Fig. 2. It was discovered that measurements of the Faraday rotation at an etalon peak of the TI crystal the transmission is 100% which yields a quantized Faraday rotation that is independent of the material properties. Thus $\tan(\theta_F) = \alpha$.

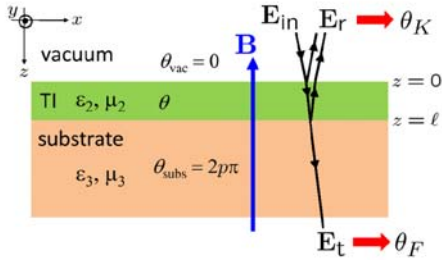


Figure 2. Measurement of Kerr and Faraday angles for a TI thick film of thickness l and optical constants ϵ_2, μ_2 on a topologically trivial insulating substrate with optical constants ϵ_3, μ_3 , in a perpendicular magnetic field B . (We consider normal incidence in the actual proposal but draw light rays with a finite incidence angle in the figure for clarity.) The external magnetic field can be replaced by a thin magnetic coating on both TI surfaces.

Therefore this effect allows the possibility of precision measurements of the fine structure constant. We also developed a method for measuring separately the Faraday rotation of the two surfaces on a transparent topological insulator [4].

THz Faraday and Kerr Effect measurements were made on Bi_2Se_3 single crystals to initiate a study of the intrinsic magneto-electric effect [3]. This work addressed the issue that the optical response of the topological surface state is inextricably mixed with the response of the residual bulk carriers that result from anti-site defect doping. To deal with this problem, that is ubiquitous to currently existing TI samples, we have developed a gate modulated Kerr measurement. When a negative gate voltage, large enough to deplete the bulk, is applied further increases change the response of the surface states but not the bulk. This allows an isolation of the surface response of one surface of the TI. Evidence for the THz magneto-response of the surface carriers was observed as shown in Figure 3. Improved measurements of the gated Kerr response are currently underway.

III. Planned activities: 2011-2012

Our preliminary work on the Kerr measurements on topological insulators has made as much progress as can be expected with the currently existing materials. It is clear that major developments on materials will be required before the fundamental quantized Kerr angle measurements can be realized. We are currently seeking additional support that includes materials development in addition to the magneto-optical measurements on these interesting new materials.

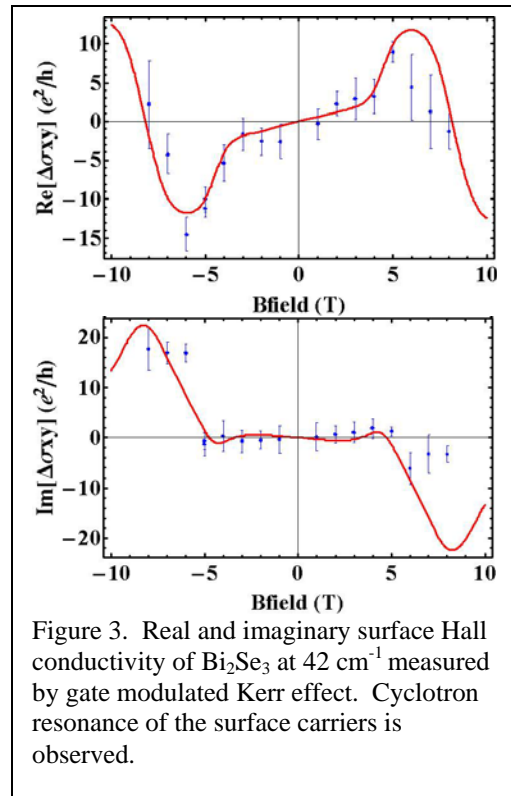


Figure 3. Real and imaginary surface Hall conductivity of Bi_2Se_3 at 42 cm^{-1} measured by gate modulated Kerr effect. Cyclotron resonance of the surface carriers is observed.

For the second year of this project we plan to focus on the IR Hall measurements on underdoped cuprates. The main effort will be made on underdoped BSCCO single crystals which we have available from Brookhaven (Genda Gu). We will also extend our preliminary studies on underdoped $\text{Pr}_{2-x}\text{Ce}_x\text{CuO}_4$. The main goal will be to critically compare the THz IR Hall data with the extensive ARPES data available on BSCCO. We will measure the IR Hall Effect at far IR frequencies which are below any energy gaps, pseudogaps, or interaction energy scales and where we will be probing the states near the Fermi energy. This will allow direct contact with quantum oscillations experiments in cuprates and with DC transport in general. We will examine fundamental issues in cuprate physics using our unique magneto-optical capabilities. These issues include the question of whether Fermi liquid theory adequately describes the transport in cuprates as they are doped closer to the Mott state at zero carrier density. We will also examine the effects of Fermi surface reconstruction and the Fermi arcs observed in ARPES on the THz magneto-transport. The relation between the gaps observed in electron underdoped materials and the pseudogaps observed in hole underdoped materials will be examined by extending our preliminary studies on underdoped $\text{Pr}_{2-x}\text{Ce}_x\text{CuO}_4$ to more extensive doping dependences. The Hall mass m_H as a function temperature and frequency for underdoped these two cuprate systems will be fully characterized. We will also examine $\sigma_{xy}(\omega, T)$ in comparison with $\sigma_{xx}(\omega, T)$ and the frequency dependence of R_H .

Publications

1. “*Terahertz Kerr and reflectivity measurements on the topological insulator Bi_2Se_3* ”, Jenkins, G. S. and Sushkov, A. B. and Schmadel, D. C. and Butch, N. P. and Syers, P. and Paglione, J. and Drew, H. D., Phys. Rev. B **82**, 125120, (2010).
2. “*Terahertz Hall measurements on optimally doped single-crystal $\text{Bi}_2\text{Sr}_2\text{CaCu}_2\text{O}_{8+x}$* ”, Jenkins, G. S., Schmadel, D. C., Sushkov, A. B., Gu, G. D., Kontani, H. and Drew, H. D., Phys. Rev. B **82**, 094518, (2010).
3. “*Topological quantization in units of the fine structure constant*” Joseph Maciejko, Xiao-Liang Qi, H. Dennis Drew, and Shou-Cheng Zhang, Phys. Rev. Letters **105**, 166803 (2010).
4. “*Simultaneous measurement of circular dichroism and Faraday rotation at terahertz frequencies utilizing electric field sensitive detection via polarization modulation*”, G. S. Jenkins, D. C. Schmadel and H. D. Drew, Review of Scientific Instruments **81**, 083903 (2010).
5. “*Terahertz Kerr and Reflectivity Measurements on the Topological Insulator Bi_2Se_3* ”, Gregory S. Jenkins, A.B. Sushkov, D.C. Schmadel, N.P. Butch, P. Syers, J. Paglione, M.-H. Kim, H.D. Drew, J.G. Analytis and I.R. Fisher, Bull. Am. Phys. Soc., **56**, **1** (2011).

Session 9

Superconductivity

Cluster PIs:

Peter Abbamonte (abbamont@illinois.edu)
 Raffi Budakian (budakian@illinois.edu)
 James N. Eckstein (eckstein@illinois.edu)
 Laura H. Greene (lhgreene@illinois.edu)
 Anthony J. Leggett (aleggett@illinois.edu)
 Dale J. Van Harlingen (dvh@illinois.edu)

Alexey Bezryadin (bezryadi@illinois.edu)
 S. Lance Cooper (slcooper@illinois.edu)
 Eduardo H. Fradkin (efradkin@illinois.edu)
 Taylor Hughes (hughest@illinois.edu)
 Nadya Mason (nadya@illinois.edu)
 Smitha Vishveshwara (smivish@illinois.edu)

RESEARCH OVERVIEW

The central aim of the *Quantum Materials at the Nanoscale* (QMN) cluster is to explore—by combining advanced experimental capabilities, sophisticated theoretical analysis, and the outstanding facilities of the FS-MRL—the collective organization and dynamics of charges, spins, orbitals, and ions that arise at the nanoscale in a broad class of important, correlated electronic materials. Our goal is to understand and control how collective phenomena govern the macroscopic and microscopic properties of materials, principally by *exploring the intersection of strong-correlation physics and nanoscience*. Some highlights of our recent work are described below:

Highlight 1: Measuring fractional vortices in Sr₂RuO₄

Recent Progress - Most known superconductors are characterized by the spin-singlet pairing of the electrons that constitute the superconducting flow. An exception is Sr₂RuO₄ (SRO), which—much like superfluid ³He—may be a spin-triplet *p*-wave superfluid. Superconductivity of this type may support remarkable vortex excitations that carry half a unit of magnetic flux (half quantum vortices, or HQVs) and provide topologically-protected states for quantum computation. HQVs have not been observed in large samples of SRO, but may be more stable (and thus observable) in mesoscopic samples.

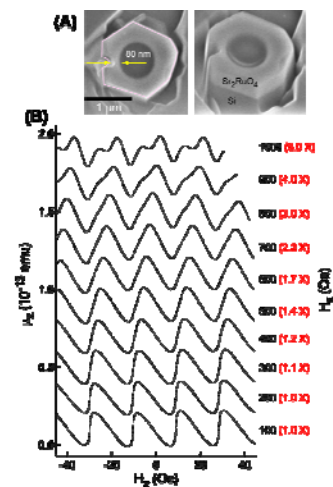


Fig. 2 (A) Image of an SRO nanocrystal ring with an 80-nm wide weak-link constriction. (B) Cantilever magnetometry data showing the evolution of the Josephson currents taken by varying the flux through the ring at a fixed value of the field applied parallel to the ring face.

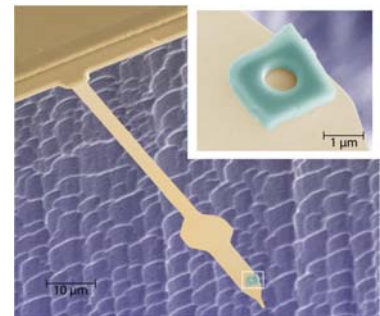


Fig. 1 False color image of an SRO nanocrystal ring attached to the tip of a cantilever.

Following a suggestion by **Leggett, Budakian** fabricated micron-sized, ring-shape structures from high-quality samples of SRO (from Y. Maeno, Kyoto U.) using the focused ion-beam capabilities at the MRL Central Facilities. They made ultra-sensitive cantilever magnetometry measurements on these SRO rings (see Fig. 1) and discovered vortex states exhibiting a magnetic response consistent with the presence of HQVs. **Leggett** and **Goldbart** played an essential role in interpreting these measurements, which were recently published in *Science* and featured in a Search and Discovery article in *Physics Today*. Motivated by **Budakian's** experiments, **Vishveshwara** proposed a two-path vortex interferometry experiment based on the Aharonov-Casher effect for detecting the non-Abelian nature of the fractional vortices observed in SRO. The effect is based on observing vortex interference patterns upon enclosing a finite charge of externally controllable magnitude within the interference path. **Vishveshwara** predicts that when the interfering vortices enclose an odd number of identical vortices in their path, the interference pattern disappears only for non-Abelian vortices.

Future Plans – Vishveshwara’s proposal will be implemented using **Van Harlingen’s** expertise in nanofabrication and measurement of mesoscopic devices, and **Budakian’s** expertise in fabricating nanometer-scale SRO samples. In preliminary measurements, **Budakian** created an SRO rf-SQUID by fabricating a single weak-link junction into a ring-shaped SRO particle (see Fig. 2). To interpret the behavior of Josephson currents in these devices, **Leggett** and **Goldbart** are working with **Budakian** to model the current-phase relationship of spin-triplet Josephson junctions.

As a first step toward establishing the statistics of the fractional vortices, **Budakian** and **Van Harlingen** plan additional measurements of the current-phase relationship of weak-link SRO Josephson junctions. A key distinguishing feature of HQVs that possess non-Abelian statistics is the existence of zero-energy Majorana quasiparticles in the vortex core. In the ring geometry, the Majorana modes would be localized near the boundaries of the ring. Theoretically, such quasiparticles would give rise to an h/e supermodulation which would be in addition to the $h/2e$ period Josephson currents. While these measurements would not directly establish the non-Abelian nature of the quasiparticles, they would establish the existence of edge modes, an important first step. Ongoing theoretical work by **Vishveshwara** is aimed at estimating the magnitude of the Majorana quasiparticle contribution to the Josephson currents and estimating the temperature dependence of this effect.

Highlight 2: Fundamental studies of electronic correlations and phase coherence using graphene

Recent progress - Andreev reflection—where an electron in a normal metal backscatters off a superconductor into a hole—forms the basis of low energy transport through superconducting junctions. Andreev reflection in confined regions gives rise to discrete Andreev bound states (ABS), which can carry a supercurrent and have been proposed as the basis of qubits. Although many measurements have invoked ABS to explain the existence of supercurrents (e.g., in long SNS junctions), it has been difficult to directly probe individual ABS. Recent work of **Hughes**, **Goldbart**, and **Mason** succeeded in

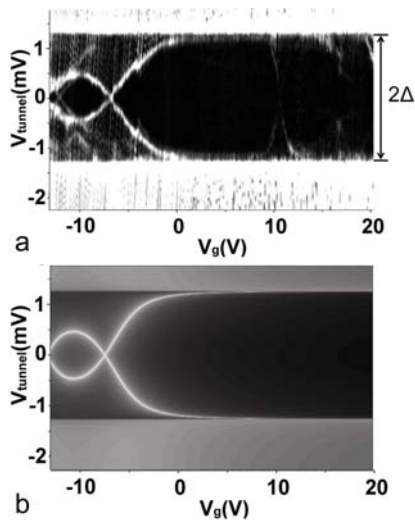


Fig. 4 (a) 2D map of tunneling differential conductance vs. backgate voltage (x-axis) and bias voltage (y-axis) for tunneling into single-layer graphene. Bright white lines inside the superconducting gap (marked as 2Δ) are ABS. (b) Transport calculations for ABS in a quantum dot having two levels, a finite charging energy, and couplings to normal metal and superconducting leads.

determining the spectra of individual ABS that formed in a graphene quantum dot; the results were reported in a recent *Nature Physics* paper. For the experiments, **Mason** fabricated narrow superconducting tunnel probes, as well as normal-metal end contacts, on top of exfoliated graphene flakes (see Fig. 3). Opposite sign work function mismatches at the normal metal and superconducting contacts led to the creation of potential wells, or quantum dots, underneath the superconducting probes. These quantum dots were also proximity-coupled to the superconducting leads. The interplay of the resulting Andreev reflections with Coulomb charging effects gave rise to low-energy ABS, which appeared as subgap conductance peaks in the tunneling measurements. As seen in Figure 4(a), the ABS have a striking gate-voltage dependence. The gate-dependence was explained by **Hughes** and **Goldbart** both phenomenologically and via a microscopic Hamiltonian for ABS in a graphene quantum dot. Figure 4(b) shows transport calculations based on this model, demonstrating a remarkable correspondence with experiment.

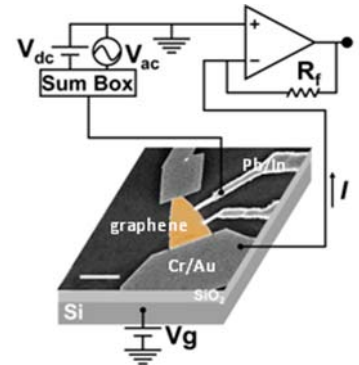


Fig. 3 SEM micrograph of a graphene device (false colored orange) with overlaid measurement circuit, for tunneling from superconductor (Pb/In) into graphene. Scale bar is 5 μm .

Future plans – **Mason** will work with **Hughes** to study manipulation of the ABS via gates and quantum dot configuration; for example, they will test the prediction of **Hughes** and collaborators that the system can be tuned through a quantum phase transition (marked by zero-energy ABS) as the dot size is varied. The technique of superconducting tunneling spectroscopy will also be applied to other systems, such as topological insulators (TIs). In three-dimensional TIs, Majorana modes are predicted to appear when the spin-polarized surface states are coupled to superconductors. **Mason, Van Harlingen** and **Hughes** will collaborate to measure signatures of unusual modes in the tunneling signal between a superconductor and a TI.

Highlight 3: Measurement of the effective fine structure constant of graphene

Recent progress - Electrons in graphene behave like massless Dirac fermions, permitting phenomena with parallels in high-energy physics to be studied in a solid-state setting. Several authors have argued that the electrons in graphene should form a strongly correlated electron system, and might form any of a variety of exotic ground states. Surprisingly, such effects have not been observed in transport experiments; at low temperatures, graphene behaves as a simple semimetal. The reason for this has been a mystery. In most materials, the effect that most directly influences the strength of correlations is screening. To investigate how screening influences the strength of interactions in graphene, **Abbamonte** performed inelastic x-ray scattering experiments on single crystals of graphite at Sector 9 at the Advanced Photon Source (APS). Using new reconstruction algorithms developed in collaboration with **Fradkin** and postdoc Bruno Uchoa, **Abbamonte** was able to image the dynamical screening of charge in a freestanding graphene sheet (Fig. 5). They found that the polarizability of graphene is approximately 3.5 times larger than expected from past estimates based on the random phase approximation. This enhanced screening is a consequence of excitonic effects in transitions between the π and π^* bands, which dominate screening at long distances and low energies. **Abbamonte** and **Fradkin** argued, further, that the strength of Coulomb interactions is characterized by a scale-dependent, effective fine-structure constant, $\alpha_g^*(\mathbf{k}, \omega) = e^2 / \hbar v_F \varepsilon(\mathbf{k}, \omega)$, which approaches the value $0.14 \pm 0.092 \sim 1/7$ at low energies and large distances. This value is substantially smaller than past estimates and suggests that graphene is more weakly interacting than previously believed. This study—which recently appeared in *Science*—demonstrates that a two-dimensional system can exhibit strong dielectric screening over finite distances, provided its excitation spectrum is gapless. These results have implications for all two-dimensional Dirac systems, including transition metal dichalcogenides, copper-oxide superconductors with nodal quasiparticles, and surface states in topological insulators.

Future plans - **Abbamonte** will expand these studies to higher resolution and to study excitations in other Dirac systems. The quantity that is important for interactions is the low-momentum, asymptotic value of α_g^* , but the lowest momentum achieved in the above measurements were $2\pi/k \sim 10$ lattice parameters. To establish the proper asymptotic properties of α_g^* , we are developing, in collaboration with **Diego Casa** at Argonne National Laboratory, a small-angle inelastic x-ray scattering setup in Sector 9 at the APS. This instrument will allow IXS experiments to be carried out at scattering angles down to 3° , allowing the proper, long-wavelength value of α_g^* to be determined. With this setup we should also be able to see the 2d-3d dimensionality crossover in graphite, as well as study other Dirac systems, such as transition metal dichalcogenides, which exhibit nodal quasiparticles and mimic many of the properties of the cuprate superconductors.

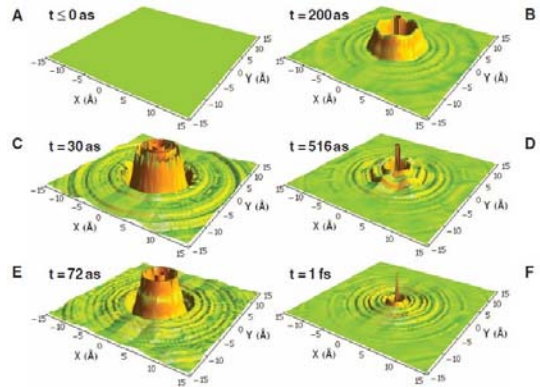


Fig. 5 Snapshots of the dynamical electronic screening in graphene, reconstructed from inelastic x-ray scattering experiments. These images were produced with a spatial resolution of 0.53 \AA and a time resolution of 10.3 attoseconds.

SELECT PUBLICATIONS 2008-2011

1. Barath, H., M. Kim, J.F. Karpus, **S.L. Cooper**, **P. Abbamonte**, **E. Fradkin**, E. Morosan, and R.J. Cava, "Quantum and classical mode softening near the charge-density wave/superconductor transition of Cu_xTiSe_2 ", *Physical Review Letters*, **100**, 106402-1-4 (2008).
2. Frolov, S.M., M.J.A. Stoutimore, T.A. Crane, **D.J. Van Harlingen**, V.A. Oboznov, V.V. Ryazanov, A. Ruosi, C. Granata, and M. Russo, "Imaging spontaneous currents in superconducting arrays of π -junctions", *Nature Physics*, **4**, 32-36 (2008).
3. Sahu, M., M.-H. Bae, A. Rogachev, D. Pekker, T.-C. Wei, N. Shah, **P.M. Goldbart**, and **A. Bezryadin**, "Individual topological tunneling events of a quantum field probed through their macroscopic consequences", *Nature Physics*, **5**, 503-508 (2009).
4. Vakaryuk, V. and **A.J. Leggett**, "Spin polarization of half-quantum vortex in systems with equal spin pairing", *Physical Review Letters*, **103**, 057003 (2009).
5. Chen, Y.-F., T. Dirks, G. Al-Zoubi, N.O. Birge, **N. Mason**, "Nonequilibrium tunneling spectroscopy in carbon nanotubes", *Phys. Rev. Lett.*, **102**, 1-4 (2009).
6. Coridan, R. H., N. W. Schmidt, G. H. Lai, G. R. Rahul, M. Krisch, S. Garde, **P. Abbamonte**, G. C. L. Wong, "Hydration dynamics at femtosecond time scales and Angstrom length scales from inelastic x-ray scattering", *Physical Review Letters*, **103**, 237402 (2009).
7. May, S.J., P.J. Ryan, J.L. Robertson, J.-W. Kim, T.S. Santos, E. Karapetrova, J.L. Zarestky, X. Zhai, S.G.E. te Velthuis, **J.N. Eckstein**, **S.D. Bader**, **A. Bhattacharya**, "Enhanced ordering temperatures in antiferromagnetic manganite superlattices", *Nature Materials*, **8**, 892 (2009).
8. Unaruntai, S., Y. Murata, C.E. Chialvo, H-K. Kim, **S. MacLaren**, **N. Mason**, **I. Petrov**, and **J.A. Rogers**, "Transfer of graphene layers grown on SiC wafers to other substrates and their integration into field effect transistors", *Applied Physics Letters*, **95**, 202101 (2009).
9. D.S. Caplan, V. Orlyanchik, M.B. Weissman, **D.J. Van Harlingen**, **E. Fradkin**, M.J. Hinton, and T.R. Lemberger, "Anomalous Noise in the Pseudogap Regime of $\text{YBa}_2\text{Cu}_3\text{O}_{7-\delta}$ ", *Physical Review Letters*, **104**, 177001 (2010).
10. M. Fogelström, W.K. Park, **L.H. Greene**, G. Goll, and **M.J. Graf**, "Point-contact spectroscopy in heavy-fermion superconductors", *Physical Review B*, **82**, 014527 (2010).
11. A.B. Shah, Q.M. Ramasse, X. Zhai, **J.G. Wen**, S.J. May, **I. Petrov**, **A. Bhattacharya**, **P. Abbamonte**, **J.N. Eckstein**, and J.-M. Zuo, "Probing interfacial electronic structures in atomic layer LaMnO_3 and SrTiO_3 superlattices", *Advanced Materials*, **22**, 1156-1160 (2010).
12. Y.-F. Chen, M.-H. Bae, C. Chialvo, T. Dirks, **A. Bezryadin**, and **N. Mason**, "Magnetoresistance in single layer graphene: weak localization and universal conductance fluctuation studies", *Journal of Physics - Condensed Matter*, **22**, 205301 (2010).
13. M. Kim, X. Chen, Y.I. Joe, **E. Fradkin**, **P. Abbamonte**, and **S.L. Cooper**, "Mapping the magnetostructural quantum phases of Mn_3O_4 ", *Physical Review Letters*, **104**, 136402 (2010).
14. J.P. Reed, B. Uchoa, Y.-I. Joe, Y. Gan, **D. Casa**, **E. Fradkin**, and **P. Abbamonte**, "Effective fine structure constant of freestanding graphene measured in graphite", *Science*, **330**, 805-808 (2010).
15. T. Dirks, **T.L. Hughes**, S. Lal, B. Uchoa, Y-F. Chen, C. Chialvo, **P.M. Goldbart**, and **N. Mason**, "Transport through Andreev Bound States in a Graphene Quantum Dot", *Nature Physics*, **7**, 386-390 (2011).
16. E. Grosfeld, B. Seradjeh, and **S. Vishveshwara**, "Proposed Aharonov-Casher interference measurement of non-Abelian vortices in chiral p-wave", *Physical Review B*, **83**, 104513 (2011).
17. J. Jang, D.G. Ferguson, **V. Vakaryuk**, **R. Budakian**, S.B. Chung, **P.M. Goldbart**, and Y. Maeno, "Observation of Half-Height Magnetization Steps in Sr_2RuO_4 ", *Science*, **331**, 186-188 (2011).
18. S. Scharfenberg, D.Z. Rocklin, C. Chialvo, R.L. Weaver, **P.M. Goldbart**, and **N. Mason**, "Probing the Mechanical Properties of Graphene Using a Corrugated Elastic Substrate", *Applied Physics Letters*, **98**, 091908 (2011).
19. J. Jang, **R. Budakian**, and Y. Maeno, "Phase-Locked Cantilever Magnetometry", *Applied Physics Letters*, (in press, 2011).

Project Title: Engineering of mixed pairing and non-Abelian quasiparticle states of matter in chiral p -wave superconductor Sr_2RuO_4

Principal Investigator: Ying Liu

Institution: Department of Physics, Pennsylvania State University, 104 Davey Laboratory, University Park, PA 16802

Email: liu@phys.psu.edu

1. Project Scope

The goal of this project is to seek out novel phenomena in Sr_2RuO_4 and related Ru- Sr_2RuO_4 eutectic phase, especially mixed pairing and non-Abelian states of matter. There is strong evidence for p -wave superconductivity in Sr_2RuO_4 . Therefore at the interface between Sr_2RuO_4 and s -wave superconductor Ru found in the eutectic phase of Ru- Sr_2RuO_4 , both p - and s -wave pairs are expected, which should then form a novel mixed pairing state. Similar states may also present in ultrasmall samples of Sr_2RuO_4 . Furthermore, half-integer flux quanta were observed in Sr_2RuO_4 recently, suggesting that half-flux-quantum vortices may also exist in this material. If the half-flux-quantum vortex comes from a chiral $p_x \pm ip_y$ pairing, Majorana quasiparticles, which are both particle and holes), are expected, leading to a non-Abelian state. We propose to engineer material and device systems on Sr_2RuO_4 to create experimental conditions that will allow direct observation of mixed pairing and non-Abelian Majorana states of matter. Specifically, we will: 1) prepare thin flakes of Sr_2RuO_4 and characterize them by scanning micro Raman spectroscopy, by scanning transmission (STEM) and by electron energy loss spectroscopy (EELS); 2) perform tunneling as well as electrical transport measurements on Ru- Sr_2RuO_4 eutectic phase and ultrasmall flakes of Sr_2RuO_4 to search for mixed pairing states; 3) explore ways to detect the presence of domains and domain walls, and that of chiral edge currents; 4) use a c -axis magnetic field to induce a d-vector rotation and detect the rotation by measuring the orientation dependence of Josephson coupling; and finally, 5) search for half-flux-quantum vortices and the associated Majorana quasiparticles. It was proposed Majorana quasiparticles may be used as basis for quantum computing. Therefore work proposed here will not only lead to fundamental discoveries in unconventional superconductors, but also contribute to the development of future information technologies.

2. Recent Progress

Even though there is strong evidence for p -wave superconductivity in Sr_2RuO_4 and that for a time-reversal symmetry breaking superconducting state from μSR and polar Kerr rotation measurements, whether it is chiral is less clear as domains and domain walls expected in a chiral p -wave superconductor have not been observed directly in this material. Therefore, further experimental studies that can prepare and detect domains and domain walls are needed. These experiments require structures that are prepared by microfabrication. Recently, we have succeeded in preparing thin flakes of Sr_2RuO_4 . The work was motivated originally by the need of superconducting Sr_2RuO_4 material that can be microfabricated. This was difficult to achieve without superconducting films of Sr_2RuO_4 . The synthesis of superconducting thin films of Sr_2RuO_4 by pulse laser deposition (PLD) has been reported very recently (Y. Krockenberger, M.

Uchida, K. S. Takahashi, M. Nakamura, M. Kawasaki, and Y. Tokura, “Growth of superconducting Sr_2RuO_4 thin films,” *App. Phys. Lett.* 97, 082502 (2010)), however, they are not widely available. The thin flakes prepared by mechanical exfoliation of bulk single crystals should feature better crystallinity than PLD films. Furthermore, these flakes interact very weakly with the substrate, which may be useful for certain experiments.

We prepared thin flakes of Sr_2RuO_4 by mechanical exfoliation. Some results are shown in Figs. 1 and 2. To begin with, slightly Ru deficient single crystals of Sr_2RuO_4 were grown (by our collaborator, Professor Zhiqiang Mao of Tulane), making crystals easier to cleave. The exfoliation procedure is different from the procedure used to prepare graphene flakes as even Ru-deficient crystals of Sr_2RuO_4 are not nearly as cleavable as graphite. In addition, the oxide is more brittle than graphene, and easy to break. The thickness of the flakes can be estimated roughly by its color under an optical microscope, and measured relatively precisely by atomic force microscope. Micro Raman spectroscopy measurements have confirmed that the Raman spectrum of the flakes as thin as 30 nm is the same as that of the bulk. These flakes have been characterized by HRTEM by our collaborator, Dr. Yan Xin of NHMFL in Florida.

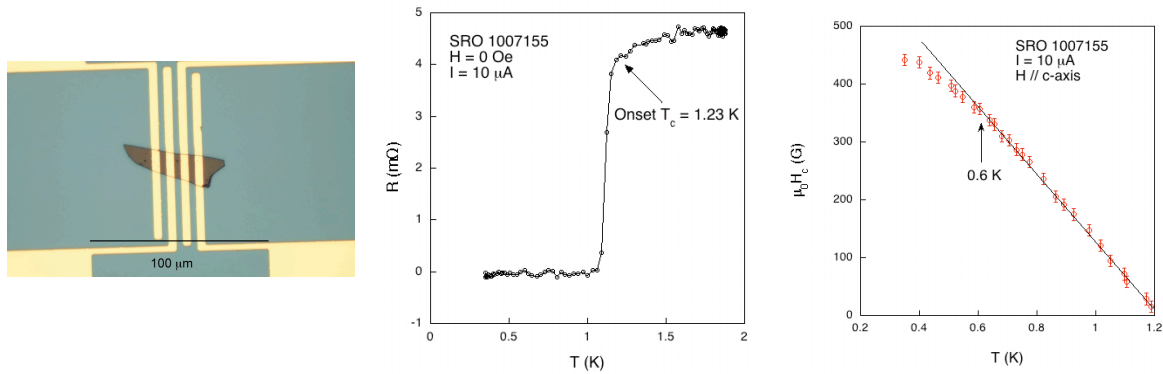


Fig. 1. A sample of a pure flake of Sr_2RuO_4 that features a single transition. The transition temperature and the critical field are similar to those of the bulk.

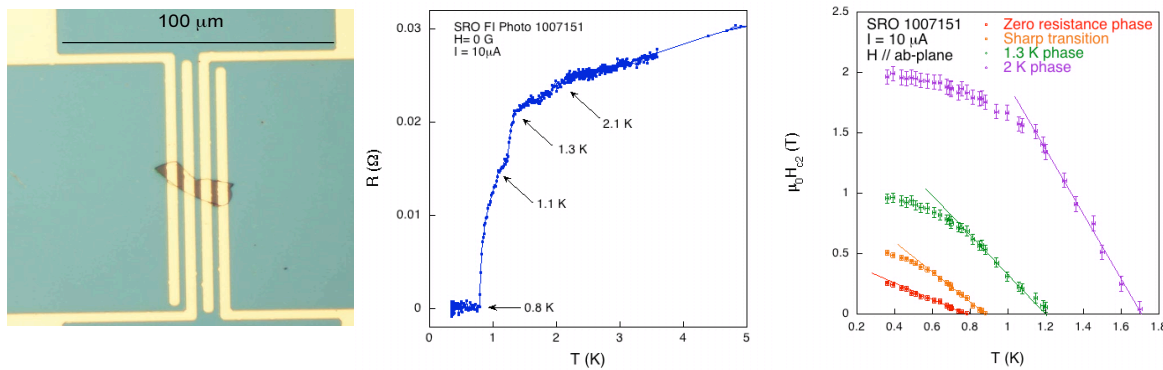


Fig. 2. A sample of a flake of Sr_2RuO_4 that features multiple transitions. The 1.3 K and 2.1 K transitions correspond to the pure and 3K phases of Sr_2RuO_4 .

3. Future Plans

In the next year, we plan to carry out the following two experiments:

Mixed pairing state: Previously we carried out measurements on tunnel junctions prepared on a single Ru island recently. However, Ru islands chosen for this study, found on a polished surface of the Ru-containing Sr_2RuO_4 single crystal, feature a relatively rough surface (Fig. 3), which may prevent the detection of the mixed pairing state. We plan to minimize the amount of the disorder on the surface of Ru island and prepare tunnel junctions on Ru island by wet etching the Ru island (most gentle approach) using sodium hypochlorite (NaOCl) diluted in de-ionized water mixture that seems to be an effective Ru etchant to remove the top layer of damaged Ru.

We will also attempt to prepare tunnel junction on Ru containing flakes of Sr_2RuO_4 . In this case, the Ru island tends to locate at the edge of flake. This will allow a tunnel junction be prepared on the Sr_2RuO_4 side of the interface, which is the bulk of the flake. Mixed pairing state is expected in the flake, which should be detected in both transport and tunneling measurement. We plan to use focus ion beam to prepare the flake samples.

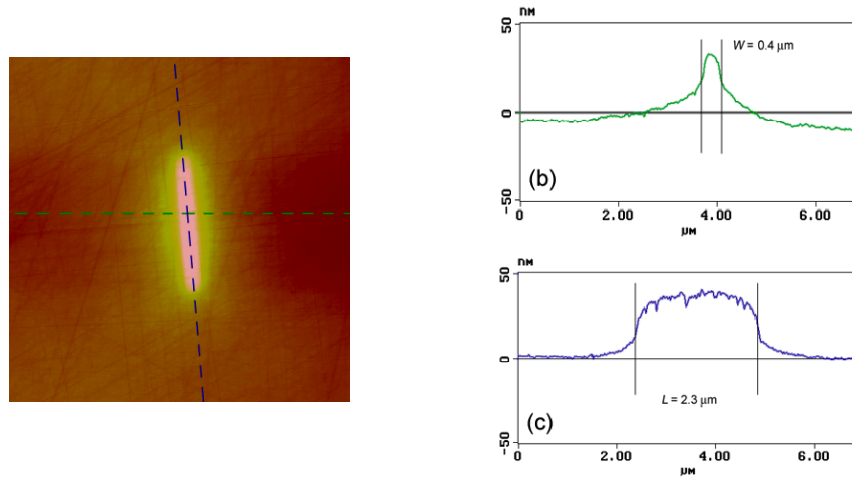


Fig. 3. a) AFM image of a Ru island marked by the red box in (a); b) Line scans along the directions marked in (a) by dashed lines. The height of the Ru island is about 35 nm. The RMS value for the height of the polished Sr_2RuO_4 surface and top surface of the Ru island is $\text{RMS}_{\text{Sr}_2\text{RuO}_4} = 0.49$ nm for Sr_2RuO_4 and $\text{RMS}_{\text{Ru}} = 2.63$ nm for Ru.

2. Domain and domain walls. We plan to detect the presence of domains and domain walls in Sr_2RuO_4 using flake-based phase-sensitive measurements. In the original phase-sensitive measurements (K.D. Nelson, Z.Q. Mao, Y. Maeno, and Y. Liu, “Odd-parity superconductivity in Sr_2RuO_4 ,” *Science* **306**, 1151-1154 (2004)), we used a carefully controlled, slow cooling procedure to prepare a trapped-flux-free, single-domain sample across the crystal (with a width of ~ 0.5 mm). However, no active control of domain formation was attempted.

In thin-flake-based experiment, we plan to prepare $\text{Au}_{0.5}\text{In}_{0.5}/\text{Sr}_2\text{RuO}_4$ SQUIDs for controlling and detecting domains in Sr_2RuO_4 . The device will be prepared by photo lithography and ion milling. Small magnetic field coils prepared by photo lithography can be used to create conditions favoring the formation of two domains opposite chiralities during a slow field cool. Quantum oscillation patterns obtained in zero-field and finite-field cools will be compared to see if there are signs for the present of domains. Essentially, with and without the presence of the

domain correspond to a 180-degree intrinsic phase shift, which will in turn lead to a shift in the minimum position in the quantum oscillation. In addition, we will also explore the physical behavior of the flakes when their sizes become smaller and smaller. In sufficiently small flakes only a single domain exist as the domain wall is expected to be around 1 μm wide, which will show feature not present in flakes that can host multiple domains.

4. Publications resulting from DOE sponsored research (2008-2011)

- 1) Xiangfan Xu, Zhuan Xu, Tijiang Liu, David Fobes, Zhiqiang Mao, and Ying Liu, "Band-dependent normal-state coherence in Sr_2RuO_4 : Evidence from Nernst and thermopower measurements," **Phys. Rev. Lett.** 101, 057002 (2008).
- 2) Neal E. Staley, Linjun Li and Zhuan Xu, and Ying Liu, "Electric field effect on superconductivity in atomically thin flakes of NbSe_2 ," **Phys. Rev. B** 80, 184505 (2009).
- 3) Yiqun A. Ying, Karl Nelson, Iosef G. Deac, Peter Schiffer, Peter Khalifah, Robert J. Cava, and Ying Liu, "Magneto electrical transport properties and possible quantum critical fluctuation in $\text{La}_4\text{Ru}_6\text{O}_{19}$," **Phys. Rev. B** 80, 024303 (2009).
- 4) Y. A. Ying, Y. Xin, B. W. Clouser, E. Hao, N. E. Staley, R. J. Myers, L. F. Allard, D. Fobes, T. Liu, Z. Q. Mao, and Y. Liu, "Suppression of proximity effect and the enhancement of p -wave superconductivity in the Sr_2RuO_4 -Ru system," **Phys. Rev. Lett.** 103, 247004 (2009).
- 5) Tong Zhang, Peng Cheng, Wen-Juan Li, Yu-Jie Sun, Guang Wang, Xie-Gang Zhu, Ke He, Lili Wang, Xucun Ma, Xi Chen, Yayu Wang, Ying Liu, Hai-Qing Lin, Jin-Feng Jia, and Qi-Kun Xue, "Superconductivity in one-atomic-layer metal films grown on $\text{Si}(111)$," **Nature Physics** 6, 104 - 108 (2010).
- 6) T. J. Liu, X. Ke, B. Qian, J. Hu, D. Fobes, E. K. Vehstedt, H. Pham, J.H. Yang, M.H. Fang, L. Spinu, P. Schiffer, Y. Liu, and Z.Q. Mao, "Charge carrier localization induced by excess Fe in the $\text{Fe}_{1+y}(\text{Te},\text{Se})$ superconducting system," **Phys. Rev. B** 80, 174509 (2009).
- 7) Ying Liu, "Phase-sensitive measurement determination of odd-parity, spin-triplet superconductivity in Sr_2RuO_4 ," **New Journal of Physics** 12, 075001 (2010).
- 8) Ying Liu, "Half-flux redux," **Nature Physics** 6, 245 - 246 (2010).

Project Title: Tunneling and Transport in Nanowires

Principal Investigator: Allen M. Goldman

Address: School of Physics and Astronomy
University of Minnesota
116 Church St. SE
Minneapolis, MN 55455

Email Address: goldman@physics.umn.edu

Scope: The goal of this program is to study phenomena that might be relevant to the performance of devices and circuits at the limit of the smallest realizable feature sizes. Structures will be prepared using *physical* rather than chemical or biological techniques. The nanowires will be either quasi-one-dimensional (quasi-1D) or one-dimensional (1D). The appropriate term depends upon the size of the widths and thicknesses, or radii, characterizing the transverse dimensions of a wire relative to some characteristic length associated with a physical property. When these lengths are smaller than the inelastic scattering, phase coherence, or superconducting coherence lengths, the wires are quasi-1D. This distinguishes them from wires for which the transverse dimensions are smaller than the Fermi wavelength for which only the longitudinal electronic degree of freedom is relevant. For such 1D wires, Landau's Fermi liquid theory fails and is replaced by Tomonaga-Luttinger Liquid (TLL) theory. It is important to probe this regime and to understand the entry into the TLL regime produced by either reducing wire size or by changing the wire carrier concentration. We propose two types of experiments on nanowires prepared using electron beam lithography (EBL). The first type involves quasi-1D superconducting nanowires. We will determine the mechanism for the recently discovered restoration of superconductivity of quasi-1D nanowires driven resistive by current that occurs upon the application of magnetic field. We will search for h/e flux quantization in nanometer scale superconducting loops, which may reveal the nature of Cooper pairing in mesoscopic systems. We will study the superconductor-insulator transition in nanowires, by varying their thicknesses, their coupling to dissipation, and their charge densities. The latter will be accomplished using electronic double layer transistor configurations. The second type of experiment will be directed at exploring the TLL regime of 1D wires prepared from a low carrier density material, either electrostatically doped SrTiO₃ or KTaO₃. We will employ electron beam lithography to form a surface mask, and will then use an ionic liquid to induce charge in an exposed line of SrTiO₃ or KTaO₃. If the wires can be made sufficiently narrow, then they should exhibit TLL behavior, which can be ascertained by studying charge transport. We would then study charge and spin transport in detail, and by employing electrostatic gating, tune between the 1D and quasi-1D regimes so as to determine the phase diagram as a function of carrier concentration.

Recent Progress:

We discovered that superconductivity could be restored upon the application of small magnetic fields to nanowires driven out of equilibrium and into a resistive state by an externally supplied current. Standard four-terminal configurations of a single Zn wire connected with 1 μ m wide Zn electrodes. These were prepared using EBL. Standard four-terminal configurations of a single Zn

wire connected with $1\mu\text{m}$ wide Zn electrodes, $1.5\mu\text{m}$ apart, in the case of the sample shown in Fig.1 (a). The current dependence of the resistance for the sample of Fig. 1 (a) is shown in Fig. 1 (b). As shown in Fig. 2(a), the higher resistance part of the transition moved to lower temperatures with increasing magnetic field. The lower resistance part exhibited a different behavior, moving to higher temperatures with increasing field. Also the temperature at which the wire resistance vanished increased. As a result, the transition sharpened with increasing field. However this eventually stopped and the onset temperature as well as the temperature at which the resistance vanished, both moved together towards lower values upon increasing the field. In effect, there is a magnetic field induced restoration of the superconducting state over the range of temperatures corresponding to the lower part of the zero field transition as illustrated in Fig. 2(b).

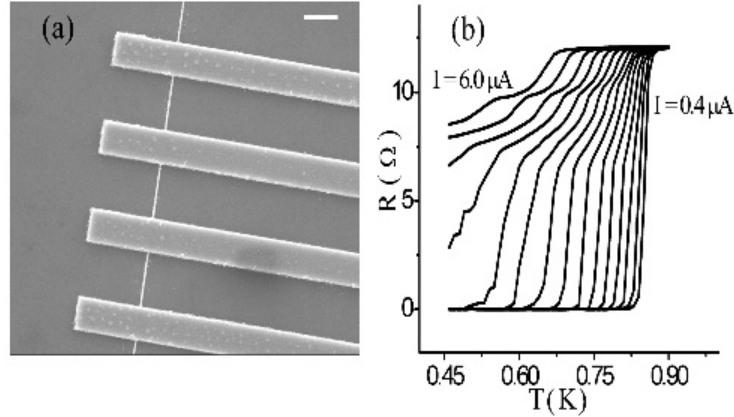


FIG. 1 (a) A Scanning Electron Microscope image of the sample, the white scale bar is $1\mu\text{m}$ long. **(b)** Temperature dependence of the wire resistance, at $H = 0$ Oe, with current ranging from $0.4\mu\text{A}$ to $6\mu\text{A}$, every $0.4\mu\text{A}$.

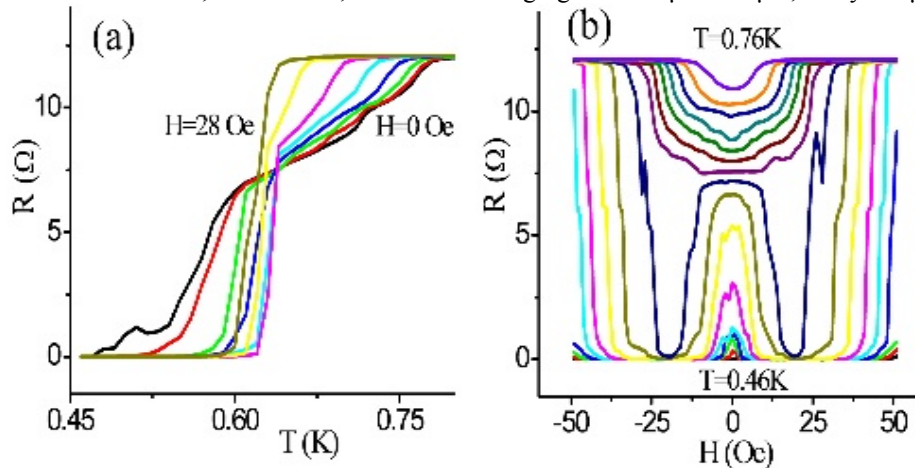


FIG. 2 (a) Temperature dependence of the wire resistance, at $I = 4.4\mu\text{A}$, with varying applied magnetic fields from 0 Oe to 28 Oe, every 4 Oe. **(b)** Magnetic field dependence of the wire resistance, at $I = 4.4\mu\text{A}$, with temperatures ranging from 0.46 K to 0.76 K, every 0.02 K.

Extensive studies of the phenomenon involving changing wire lengths and the orientation of the magnetic field with respect to the sample plane were carried out. The major conclusion was that the action of the magnetic field on the electrodes is to generate quasiparticles, which dampen resistance generating phase fluctuations, leading to the restoration of superconductivity.

There was also progress in the fabrication of superconducting loops for the search for h/e flux quantization, and in the fabrication of low-carrier density conducting SrTiO_3 layers for the study of Tomonaga-Luttinger Liquid phenomena

Future Plans: Superconducting Nanowires and the Tomonaga-Luttinger Liquid

Flux quantization with h/e quanta: We are investigating the possible emergence of h/e period oscillations in the critical temperature of small superconducting rings threaded by magnetic flux. The question arises when the radius of a ring becomes comparable to or smaller than the coherence length. Numerous calculations using various techniques have shown h/e period oscillations in a traditional Little-Parks measurement. Preliminary investigations appear to support the theoretical predictions. However in loops with reduced transition temperatures, $h/4e$ oscillations have also been observed. This work depends upon preparing ultra small superconducting loops using electron beam lithography with ultra-clean, long coherence length Al films.

Magnetic field induced restoration of superconductivity in out-of-equilibrium Zn and Al nanowires:

We have constructed a phenomenological scenario to explain our observations. Increasing the current results in phase slip generation, which results in nonzero resistance. When a magnetic field is applied, quasiparticles are produced in the electrodes. These quasiparticles dampen the phase slip processes that produce resistance by increasing the dissipation, resulting in the wire recovering its zero resistance state. Measurements at temperatures down to 50mK have revealed that the transition as a function of current, widens at lower temperatures. This suggests that the phase slips producing resistance might be driven by quantum fluctuations, even though quantum phase slip models (QPSs) do not describe the data. If the resistance seen in the transition region is indeed driven by QPSs, the field-enhanced superconductivity could be explained by the effect of dissipation associated with quasiparticles generated by the magnetic field. As a possible test of this scenario, we propose to introduce dissipation in a direct manner. The idea would be to fabricate wires on an AlGaAs heterostructure containing a delta-doped layer, located not too far from the surface, whose conductance is electrostatically tunable. Phase fluctuations and phase slips might then be controlled by tuning the conductivity of this delta-doped layer.

Superconductor-Insulator Transitions in Quasi-1D wires: The measurements of Bezryadin and coworkers on carbon nanotube templated nanowires involved comparing the properties of MoGe coated wires of different thicknesses prepared using separate sputtering runs. We propose to produce narrow wires and tune the SI transition using several techniques including: (1) *in situ* cyclic evaporation and measurement of amorphous Bi (*a*-Bi) wires, (2) the use of dissipation as a tuning parameter for InO_x nanowires and (3) the modification of the carrier concentration of InO_x wires using electronic double layer field effect transistor configurations.

Patterning 1D Electron Gas Structures-Tomonaga-Luttinger Liquid Behavior: A simple approach to producing low carrier density nanowires may be realized by inducing conductivity in a narrow patterned line in SrTiO_3 (STO) by gating using an electric double layer transistor (EDLT) employing an ionic liquid (IL) as the gate dielectric. Electron beam lithography can be used to produce a mask that will leave a narrow line on the surface of a material such as SrTiO_3 , exposed to the ionic liquid. If the line can be made the order or narrower than the Fermi wavelength, which depends upon the charge density, then the resultant wires should exhibit TLL behavior and their carrier concentrations should be tunable over a wide range. This configuration could then be used to study spin and charge transport as well as the superconducting character of these systems. (A similar approach can be used to tune the carrier concentration of superconducting nanowires in the quasi-1D limit to explore the quasi-1D superconductor-insulator transition.) The first step in such studies was to demonstrate that we are able to electrostatically dope single crystals of insulating SrTiO_3 into a conductive state. We have characterized the results of such doping over broad ranges of temperature and carrier concentration in work published in *Physical Review Letters*. We propose to combine nanowire fabrication technology with the EDLT

transistor technology used to induce charge in the surface of a single-crystal of an insulator such SrTiO₃ (STO). We would cover the surface of a STO crystal, leaving exposed a line, equipped with various electrodes, which would then be electrostatically gated using an EDLT configuration. With the new EBL system at Minnesota, lines 5 to 8 nm wide may be possible. Charge transport studies will be used to determine whether structures are 1D or quasi-1D. The systematics of conductance variation with voltage and temperature as a function of wire carrier concentration will be determined. Using magnetic and non-magnetic electrodes, we propose to study the transport properties of quantum wires using spin-polarized or partially spin-polarized carriers employing the four-terminal nonlocal spin valve geometry first employed by Johnson and Silsbee, and used by Tombros, van der Molen and van Wees to study carbon nanotubes.

Publications

Phase Diagram of Electrostatically Doped SrTiO₃

[Yeonbae Lee](#); [Clement, C.](#); [Hellerstedt, J.](#); [Kinney, J.](#); [Kinnischtzke, L.](#); [Xiang Leng](#); [Snyder, S.D.](#); [Goldman, A.M.](#) *Physical Review Letters*, v 106, n 13, p 136809 (4 pp.), 1 April 2011.

Stabilization of superconductivity by magnetic field in out-of-equilibrium nanowires

[Yu Chen](#); [Yen-Hsiang Lin](#); [Snyder, S.D.](#); [Goldman, A.M.](#) *Physical Review B (Condensed Matter and Materials Physics)*, v 83, n 5, p 054505 (8 pp.), 1 Feb. 2011.

Indications of superconductivity at somewhat elevated temperatures in strontium titanate subjected to high electric fields

[Yen-Hsiang Lin](#); [Yu Chen](#); [Goldman, A.M.](#) *Physical Review B (Condensed Matter and Materials Physics)*, v 82, n 17, p 172507 (4 pp.), 1 Nov. 2010.

Magnetic-field-induced superconducting state in Zn nanowires driven in the normal state by an electric current

[Yu Chen](#); [Snyder, S.D.](#); [Goldman, A.M.](#), *Physical Review Letters*, v 103, n 12, p 127002 (4 pp.), 18 Sept. 2009.

Transport properties of organic field effect transistors modified by quantum dots

[Nishioka, M.](#); [Yu Chen](#); [Goldman, A.M.](#), *Applied Physics Letters*, v 92, n 15, p 153308-1-3, 14 April 2008.

A simple approach to the formation of ultra-narrow metal wires

[Yu Chen](#) ; [Goldman, A.M.](#) *Journal of Applied Physics*, v 103, n 5, p 054312-1-4, 1 March 2008.

**Single Atom and Molecule Manipulation and Its Application to Nanoscience and
Technology
(DE-FG02-02ER46012)**

Saw-Wai Hla

Ohio University

Clippinger 251B, Physics & Astronomy Department, Ohio University, Athens, OH 45701.

Email: hla@ohio.edu

1. Program Scope

Charge transfer in donor and acceptor molecules alters the electronic states of the molecular complexes, and thus it is useful to tailor novel materials having a wide range of properties. We explore structural and electronic properties of molecular charge transfer complexes and molecular devices utilizing the unique capabilities of scanning tunneling microscopy, atom/molecule manipulations, and tunneling spectroscopy.

2. Progress

We have made several advances in superconducting¹, semiconducting² and magnetic³ properties of charge transfer base molecular materials for nanoelectronics, for charge and energy transfer applications.

2.1. Molecular Superconductor

A class of charge transfer based molecular superconductors known as the *Bechgaard* superconductors are formed by donor and acceptor type molecules. They are non-BCS superconductors and STM studies of Bechgaard superconductors have not been done extensively. One of the reasons is due to the difficulty of getting atomically flat cleavage surfaces. Albeit scanning tunneling spectroscopy (STS) has been used to probe bulk Bechgaard crystals, the lack of direct structural imaging makes the data interpretation incomplete. Atomic and molecular level studies involving structural information are crucial to understand the superconductivity in these materials. To overcome this barrier, we have developed a new technique of preparing the samples; the epitaxial growth of λ -(BETS)₂-GaCl₄ film on metallic substrates such as Ag(111). Our work demonstrated that a well ordered Bechgaard film could be grown on Ag(111) down to just one sheet of molecular packing (Fig. 1). This opens up possibility of exploring Bechgaard superconductors at atomic or molecular level in a clean UHV environment. The epitaxial growth of (BETS)₂-GaCl₄ on Ag(111) can also form 1-D molecular chains. This again opens more exciting opportunities to probe nanoscale superconducting phenomena¹.

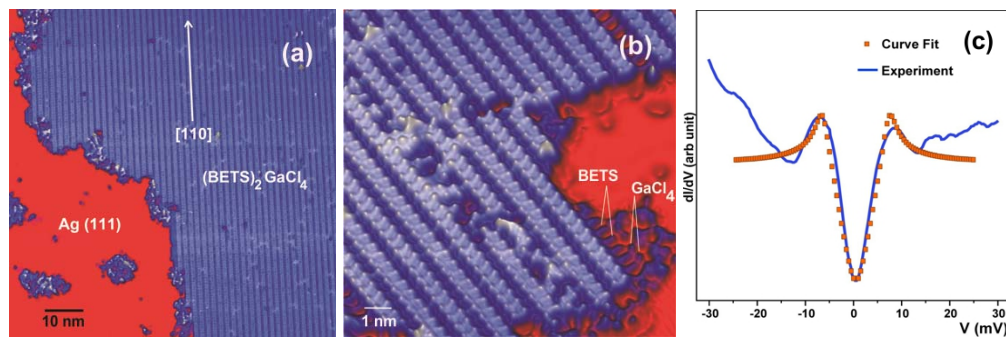
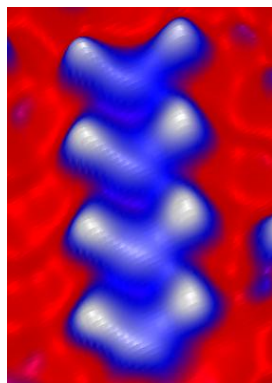
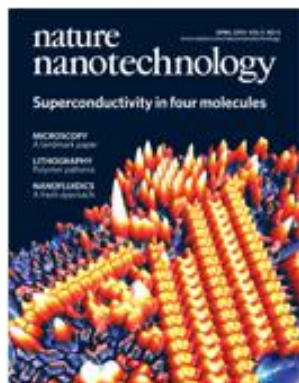


Fig. 1. (a), (b): One layer thick epitaxial film of (BETS)₂-GaCl₄ on Ag(111). (c) dI/dV curve showing superconducting gap and corresponding fit.

Tunneling spectroscopy of $(\text{BETS})_2\text{-GaCl}_4$ molecular layer having just a single constituent thickness ubiquitously show a superconducting gap. $(\text{BETS})_2\text{-GaCl}_4$ is a D_2A type molecular charge transfer system (D = donor, A = acceptor) and each BETS molecule transfers 0.45 electronic charge to GaCl_4 . The charge transfer results in half-filled molecular orbitals in BETS and thus it becomes metallic. Below a critical temperature, the epitaxial film of $(\text{BETS})_2\text{-GaCl}_4$ exhibits superconductivity. Interestingly, the superconducting gap can still be detected down to just four pairs of molecules in these materials.



Abstract: How small can a sample of superconducting material be and still display superconductivity? This question is relevant to our fundamental understanding of superconductivity, and also to applications in nanoscale electronics because Joule heating of interconnecting wires is a major problem in nanoscale devices. It has been shown that ultrathin layers of metal can display superconductivity, but any limits on the size of superconducting systems remain a mystery.

$(\text{BETS})_2\text{-GaCl}_4$, where BETS is bis (ethylenedithio) tetraselenafulvalene, is an organic superconductor, and in the bulk it has a superconducting transition temperature T_c of approximately 8 K and a two-dimensional layered structure that is reminiscent of the high- T_c cuprate superconductors. Here, we use scanning tunneling spectroscopy to show that a single layer of $(\text{BETS})_2\text{-GaCl}_4$ molecules on an Ag (111) surface displays a superconducting gap that increases exponentially with the length of the molecular chain. Moreover, we show that a superconducting gap can still be detected for just four pairs of $(\text{BETS})_2\text{-GaCl}_4$ molecules. Real-space spectroscopic images directly visualize the chains of BETS molecules as the origin of the superconductivity.

2.2. Charge Transfer Induced Molecular Magnetism

Here we show that an interfacial charge transfer can alter properties of molecular spin. After adsorption on a Cu(111), the spin of Co atom in a TBrPP-Co molecule is delocalized and redistribution of spin density from the Co atom to the organic ligands of the molecule occurs due to an interfacial charge transfer process. As a result, the entire molecule becomes magnetic. This effect is reflected in the Kondo resonance, which is observed over the entire molecule.

Abstract: An extensive redistribution of spin density in TBrPP-Co molecules adsorbed on a Cu(111) surface is investigated by monitoring Kondo resonances at different locations on single molecules. Remarkably, Kondo resonance is found to be much larger on the organic ligands than on the central cobalt atom reflecting enhanced spin-electron interactions on molecular orbitals. This unusual effect is explained by means of first principles and numerical renormalization group calculations highlighting the possibility to engineer spin polarization by exploiting interfacial charge transfer.

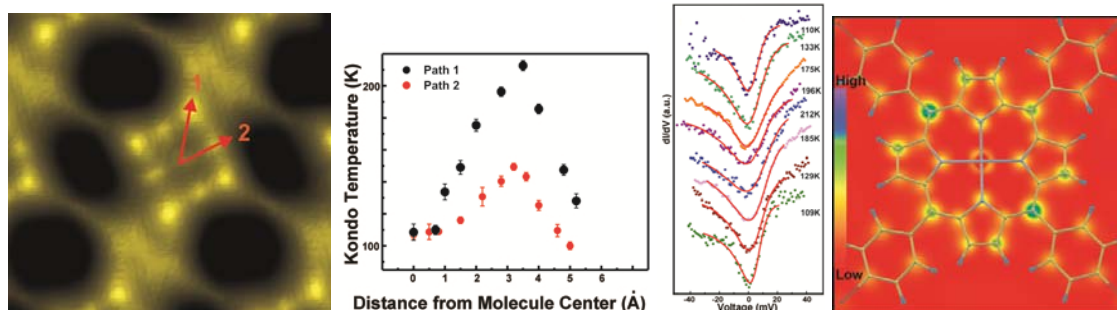


Fig. 2. Kondo resonance of a TBrPP-Co layer on Cu(111) is determined in two paths; 1 and 2 (Left). The Kondo temperature increases over the organic ligands (middle plots). The DFT calculation reveals the distribution of spin density throughout the molecules due to an interfacial charge transfer process (right).

2.3. Modification of Interfacial Charge Transfer by Doping Single Molecules

The ability to modify the electronic properties of materials by the interaction between donor and acceptor molecules plays a significant role in molecular electronics. Formation of molecular charge transfer complexes have been observed for different donor acceptor system in a lateral configuration on surfaces. Here, we studied the changes of interfacial electronic structure in TCNQ (7,7,8,8-tetracyanoquinodimethane) on Au(111) surface caused by adsorption of single decamethyl-manganocene ($\text{Mn}(\text{C}_5\text{Me}_5)_2$) molecules using low temperature STM and STS. The molecular complexes were formed by depositing manganocene onto pre-deposited TCNQ ordered layer on Au(111). Perpendicular interaction between the manganocene and TCNQ were determined by means of conductance tunneling spectroscopy, which reveal formation of new hybrid molecular orbitals upon adsorption of manganocene on TCNQ layer as well as the screening of the surface state electrons of Au(111). This work provides an important step for manipulating and tuning charge state of molecules using donor-acceptor molecular systems.

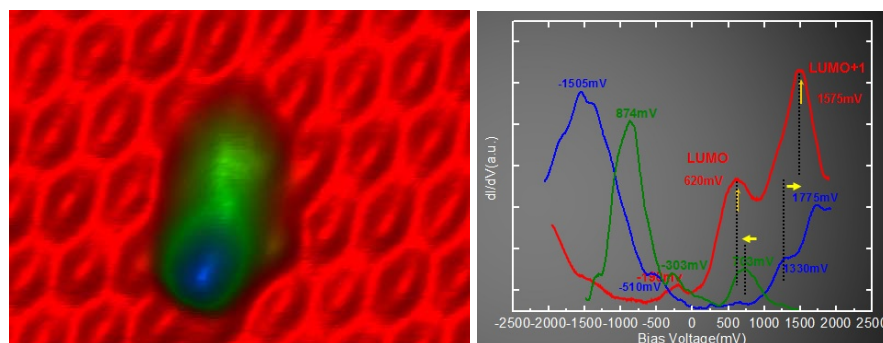


Fig. 3. A manganocene molecule on top of a TCNQ layer (left). Tunneling spectroscopy data reveal the charge transfer process at TCNQ – Au(111) interface.

3. Future Plan

Following the achievement of molecular superconductivity, we are investigating the proximity effect, and the Cooper pair formation mechanism in this unconventional superconductor. We are also investigating charge transfer processes in other molecular complexes involving various metallo organic molecules such as porphyrin, and manganocene.

References

- [1]. K. Clark, A. Hassanien, S. Khan, K.-F. Braun, H. Tanaka, and S.-W. Hla. *Nature Nano* **5**, 261-265 (2010).
- [2]. F. Jäckel, U.G.E. Perera, V. Iancu, K.-F. Braun, N. Koch, J.P. Rabe, & S.-W. Hla, *Phys. Rev. Lett.* **100**,126102 (2008).
- [3]. U.G.E. Perera, H. Kulik, V. Iancu, L.G.G.V. Dias da Silva, S.E. Ulloa, N. Marzari, & S.-W. Hla. *Phys. Rev. Lett.* **105** (2010) 106601.

4. DOE Sponsored Publications in 2008 – 2011

- 1. U.G.E. Perera, H. Kulik, V. Iancu, L.G.G.V. Dias da Silva, S.E. Ulloa, N. Marzari, & S.-W. Hla. *Spatially Extended Kondo State in Magnetic Molecules Induced by Interfacial Charge-Transfer*. *Phys. Rev. Lett.* **105** (2010) 106601. [DOE-ER46012-25]
- 2.* K. Clark, A. Hassanien, S. Khan, K.-F. Braun, H. Tanaka, & S.-W. Hla. *Superconductivity in Just Four Pairs of (BETS)2-GaCl4 Molecules*. *Nature Nanotechnology* **5**, (2010) 261-265. [DOE-ER46012-24]
- 3. K.-F. Braun, & S.-W. Hla, "Charge Transfer in the TCNQ-Sexithiophene Complex", *J. Chem. Phys.* **129** (2008) 064707. [DOE-ER46012-23]
- 4. S.-W. Hla, "Scanning Tunneling Microscope Atom and Molecule Manipulations: Realizing Molecular Switches and Devices", *Jap. J. Appl. Phys.* **47** (2008) 6063-6069. [DOE-ER46012-22]
- 5. F. Jäckel, U.G.E. Perera, V. Iancu, K.-F. Braun, N. Koch, J.P. Rabe, & S.-W. Hla. *Investigating Molecular Charge Transfer Complexes with a Low Temperature Scanning Tunneling Microscope*. *Phys. Rev. Lett.* **100**, (2008) 126102. [DOE-ER46012-21]

*Media news: www.phy.ohiou.edu/~hla/HotResearch.html

Figure 1 shows a schematic diagram of the pump-probe facility.² The sample is first irradiated with a short, relatively high-power, “pump” pulse, creating a nonequilibrium photoexcited state. These excitations, their interactions, and their dynamics modify the frequency-dependent optical properties of the material; these changes are detected using a “probe” pulse, which irradiates the material with a known time delay after the pump pulse. The evolution of these photoinduced changes in optical properties can be followed by varying the time delay. Beamlines U4IR and U12IR have been used for pump-probe spectroscopy. The high brightness of synchrotron and the available magnet makes them outstanding locations for linear spectroscopy as well. The following paragraphs describe first linear and second pump-probe spectroscopy of superconducting thin films in a magnetic field.

2.2. Magnetic field induced pair breaking in superconducting $Nb_{0.5}Ti_{0.5}N$ thin films

We measured the complex optical conductivity of a superconducting thin-film of $Nb_{0.5}Ti_{0.5}N$ in an external magnetic field. The field was applied parallel to the film surface and the conductivity extracted from far-infrared transmission and reflection measurements. The real part shows the superconducting gap, which we observe to be suppressed by the applied magnetic field. We compare our results with the pair-breaking theory of Abrikosov and Gor’kov³ and confirm directly the theory’s validity for the optical conductivity.

The normalized optical conductivities at 0, 5, and 10 T are shown in panels (a)–(c) of Fig. 2. A weak interference fringe in both the transmission and reflection measurements results in the excess σ_2/σ_N over the 40 to 80 cm^{-1} range. The solid lines are fits to the data using the pair-breaking theory as extended by Skalski *et al.*⁴ to calculate σ_1/σ_N at 0 K. Panel (d) shows the fitted σ_1/σ_N at six different fields. Clearly, the absorption edge moves to lower energy as the field increases. The field-induced pair breaking also smears out the gap-edge singularity in the quasiparticle density of states⁴,

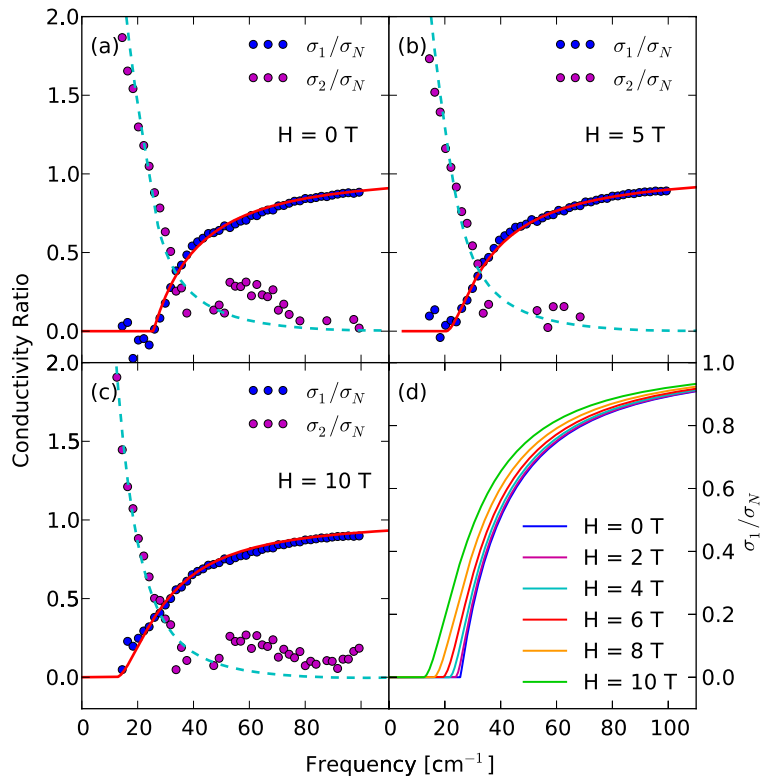


Fig. 2.(a)–(c): The real and imaginary parts of the $T = 3$ K superconducting state optical conductivity (normalized to the normal state conductivity) at three different applied magnetic fields. The solid lines are fits to σ_1/σ_N using the pair-breaking theory. The dashed lines show the fitted σ_2/σ_N as determined by a Kramers-Kronig transform of the real part. (d): The fitted σ_1/σ_N at six fields.

so that the initial rise of σ_1 becomes less abrupt for increasing fields, as can be seen by comparing the 0 T and the 10 T results in Fig. 2. Our analysis⁵ finds that the suppression of both the superconducting order parameter and the spectroscopic gap is in good accord with the pair-breaking theory.³

2.3. Quasiparticle dynamics tuned by external magnetic fields

We used pump-probe spectroscopy to measure quasiparticle recombination dynamics in metallic superconductors ($\text{Nb}_{0.5}\text{Ti}_{0.5}\text{N}$ and NbN thin films) in an external magnetic field. The field was applied parallel to the film surface, and found to break time-reversal symmetry of the electron pairing and suppress the energy gap. This allows us to tune the quasiparticle recombination rate by an external magnetic field. We compared our data with a model of recombination that considers both quasiparticle paramagnetic spin polarization and finite pair-lifetime effects, with the latter appearing to be more important.

Figure 3 shows a summary of our results. The measured quantity is the photoinduced signal, which is proportional to the photoinduced excess quasiparticle density: $S(t) \propto N_{ex}(t)$. We define $-(dS/dt)/S(t)$ as an effective instantaneous relaxation rate, and observe that the effective rate is linear in the photoinduced signal. This behavior is expected for bimolecular recombination. The effect of field is to decrease the rate, an effect we can understand within the same pairbreaking theory³ used to explain the linear spectroscopy.

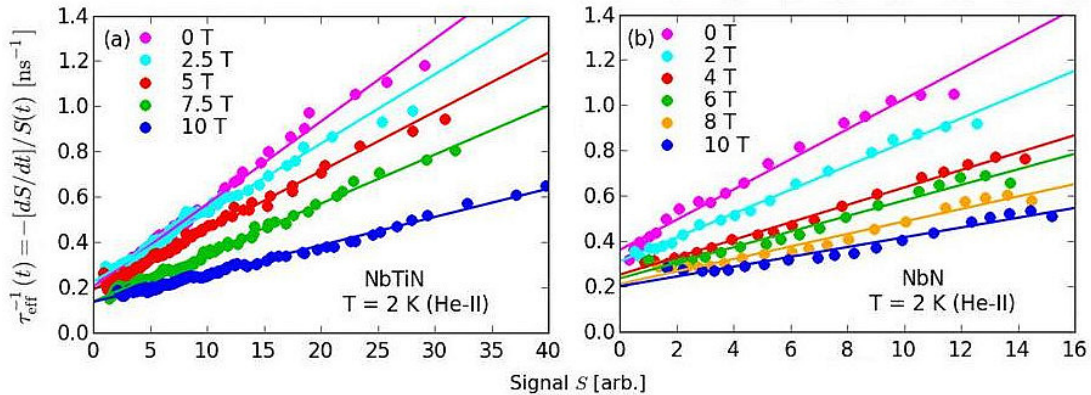


Fig. 3. Effective instantaneous relaxation rate vs the photo-induced transmission at various fields. (a) For NbTiN , data at each field include fluence ranging from 0.37 to 10.70 nJ/cm^2 . (b) For NbN , data at each field are only at the fluence of 18.1 nJ/cm^2 . The straight lines are linear fits to the data.

3. Future Plans

A unifying theme of our research, both over the past few years and in the future, is the relaxation of electronic excitations in systems having an energy gap. A gap in the excitation spectrum for a solid can have many origins, e. g., a periodic lattice (semiconductors and insulators), collective phenomena (superconductivity), or low dimensionality (size effects). Much interesting and novel physics occurs at the boundaries separating these behaviors and provides the motivation for much of our time-resolved research program. Our time-resolved infrared spectroscopy facility provides unique opportunities to explore the electronic spectrum of such systems, especially their dynamical processes. The availability of high magnetic fields gives us sensitivity to the spin of excitations as well as to their charge.

Consequently, we plan to emphasize compound semiconductors, in particular magnetic semiconductors. We will study metallic superconductors in the other field orientation, where the vortex lattice dominates the magnetic response. As part of the work, we will also make detailed theoretical predictions for the time and photon energy dependence of the photoinduced signals.

References

1. D.L. Ederer, J.E. Rubensson, D.R. Mueller, R. Shuker, W.L. O'Brien, J. Jai, Q.Y. Dong, T.A. Calcott, G.L. Carr, G.P. Williams, C.J. Hirschmugl, S. Etemad, A. Inam, and D.B. Tanner, *Nucl. Instrum. Methods* **A319**, 250–256 (1992).
2. R.P.S.M. Lobo, G.L. Carr, J. LaVeigne, D.H. Reitze, and D.B. Tanner, *Rev. Sci. Instrum.* **73**, 1 (2002).
3. A.A. Abrikosov and L.P. Gor'kov, *Soviet Phys. JETP* **12**, 1243 (1961).
4. S. Skalski, O. Betbeder-Matibet, and P.R. Weiss, *Phys. Rev.* **136**, A1500 (1964).
5. Xiaoxiang Xi, J. Hwang, C. Martin, D.B. Tanner, and G.L. Carr, *Phys. Rev. Lett.* **105**, 257006/1–4 (2010).

4. Selected publications since 2008

1. “High-resolution far-infrared spectroscopy at NSLS beamline U12IR,” G.L. Carr, R.J. Smith, L. Mihaly, H. Zhang, D.H. Reitze, and D.B. Tanner, *Infrared Phys. Technol.* **51**, 404–406 (2008).
2. “Unusual thickness dependence of the superconducting transition of α -MoGe thin films,” H. Tashiro, J.M. Graybeal, D.B. Tanner, E.J. Nicol, J.P. Carbotte, and G.L. Carr, *Phys. Rev. B* **78**, 014509/1–7 (2008).
3. “Bosonic spectral density of epitaxial thin-film $\text{La}_{1.83}\text{Sr}_{0.17}\text{CuO}_4$ superconductors from infrared conductivity measurements,” J. Hwang, E. Schachinger, J.P. Carbotte, F. Gao, D.B. Tanner, and T. Timusk, *Phys. Rev. Lett.* **100**, 137005/1–4 (2008).
4. “Wide-range optical spectra of carbon nanotubes: a comparative study,” K. Kamarás Á. Pekker, M. Bruckner, F. Borondics, A.G. Rinzler, D.B. Tanner, M.E. Itkis, R.C. Haddon, Y. Tan, and D.E. Resasco, *Phys. Stat. Sol. (b)* **245**, 2229–2232 (2008).
5. “Superfluorescence from Magnetically Formed Quantum Dots: the Excitation Pulse-Width Dependence,” Young-Dahl Jho, Jinho Lee, Gary D. Sanders, Christopher J. Stanton, David H. Reitze, Junichiro Kono, Alexey A. Belyanin, *J. Opt. Soc. Korea* **12**, 57 (2008).
6. “Aerogel waveplates,” P. Bhupathi, J. Hwang, R.M. Martin, J. Blankstein, L. Jaworski, N. Mulders, D.B. Tanner, and Y. Lee, *Opt. Express* **17**, 10599–10605 (2009).
7. “Supermetallic conductivity in bromine-intercalated graphite,” S. Tongay, J. Hwang, H.K. Pal, D.B. Tanner, D. Maslov, and A.F. Hebard, *Phys. Rev. B* **81**, 115428/1–6 (2010).
8. “Optical birefringence in uniaxially compressed aerogels,” P. Bhupathi, L. Jaworski, J. Hwang, D.B. Tanner, S. Obukov, Y. Lee, and N. Mulders, *New J. Phys.* **12**, 103016/1–21 (2010).
9. “Magnetodielectric coupling of infrared phonons in single crystal Cu_2OSeO_3 ,” K.H. Miller, X.S. Xu, H. Berger, E.S. Knowles, D.J. Arenas, M.W. Meisel, and D.B. Tanner, *Phys. Rev. B* **82**, 144107/1–8 (2010).
10. “Time-resolved magnetospectroscopy of quasiparticle dynamics in superconducting $\text{Nb}_{0.5}\text{Ti}_{0.5}\text{N}$,” X. Xi, J. Hwang, H. Zhang, C.J. Stanton, D.H. Reitze, D.B. Tanner, and G.L. Carr, *Physica C* **470**, S714–S715 (2010).
11. “Far-infrared conductivity measurements of pair breaking in superconducting $\text{Nb}_{0.5}\text{Ti}_{0.5}\text{N}$ thin-films induced by an external magnetic field,” Xiaoxiang Xi, J. Hwang, C. Martin, D.B. Tanner, and G.L. Carr, *Phys. Rev. Lett.* **105**, 257006/1–4 (2010).
12. “Raman study of the phonon modes of bismuth pyrochlores,” D.J. Arenas, L.V. Gasparov, Wei Qiu, J.C. Nino, D.B. Tanner, and C. Patterson, *Phys. Rev. B* **82**, 214302/1–8 (2010).
13. “Terahertz Emission from Nanophononic Heterostructures: the Nexus Between Scale and Origin,” H. Jeong, J. Jeong, Y.D. Jho, E. Oh, D.S. Kim, C. J. Stanton, *J. Korean Phys. Soc.* **56**, 247 (2010).
14. “Ultrafast carrier relaxation and diffusion dynamics in ZnO,” C.J. Cook, S. Khan, G.D. Sanders, X. Wang, D.H. Reitze, Y.D. Jho, Y.-W. Heo, J.-M. Erie, D.P. Norton, and C.J. Stanton, in *Oxide-based Materials and Devices*, edited by F.H. Teherani, D.C. Look, C.W. Litton, and D.J. Rogers, (SPIE, Bellingham, 2010).
15. “Cyclotron Resonance in P-doped InSb Quantum Wells,” M.B. Santos, M. Edirisooriya, T.D. Mishima, C.K. Gaspe, J. Coker, R.E. Doezema, X. Pan, G.D. Sanders, C.J. Stanton, L.C. Tung, and Y.-J. Wang, *Phys. Procedia* **3**, 1201–1205 (2010).
16. “Ultrapure multilayer graphene in Br_2 intercalated graphite,” J. Hwang, J.P. Carbotte, S. Tongay, A.F. Hebard, and D.B. Tanner, *Phys. Rev. B*, in press. (Rapid Communications)

Session 10

Magnetism

Properties of Spintronic Materials and Nanostructures via Novel Characterization Techniques

Charles S. Fadley¹, Peter J. Fischer, Frances Hellman², Jeffrey B. Kortright

Program: Magnetic Materials

Materials Sciences Division, Lawrence Berkeley National Laboratory

¹ Dept. of Physics, UC Davis

² Dept. of Physics, UC Berkeley

➤ **Program Overview:** New techniques based on heat capacity measurements and synchrotron radiation photoemission, x-ray scattering and x-ray microscopy are developed and applied to a variety of magnetic materials and nanostructures, synthesized in-house and by other groups.^{1,2,3,4,5,6,7,8,9,10,11,12,13,14} Heat capacity measurements, using unique nanocalorimeters capable of measuring films of thickness a few nm, with recently added capability for measurements of epitaxial thin films, provide information on the electron density of states, as well as phonons and phase transitions¹³. Soft x-ray resonant scattering provides information concerning depth-dependent properties at surfaces and in nanolayer magnetic structures⁵. We also make use of full-field zone-plate x-ray microscopy to image magnetic domains⁴, with time resolution into the ps range. Newly-developed hard x-ray photoemission (HXPS or HAXPES) measurements using excitation in the 3-6 keV regime permit determination of the bulk electronic properties of novel magnetic and semiconductor materials^{1,2,3}, as well as the study of buried layers and interfaces^{6,7,8}. Beyond this, nm-scale standing-wave excitation in multilayer spintronic structures reveals depth-dependent composition, magnetization, and densities-of-states^{9,10,11,12}, and, in our most recent data, k-resolved electronic structure via angle-resolved photoemission (ARPES)¹⁰. Standing-wave excitation has also been shown to add the third dimension in photoelectron microscopy^{11,12}. Finally, anomalous Hall effect (AHE) and conversion electron Mössbauer spectrometry (CEMS) are used as additional characterization techniques.

➤ **Recent Research Highlights:**

● **Electronic and magnetic structures of epitaxial semiconducting $\text{Cr}_{1-x}\text{Al}_x$, $\text{Fe}_{1-x}\text{Si}_x$ binary Heusler alloys, and FeRh from hard x-ray photoemission, heat capacity, and Mössbauer spectroscopy:** We have studied the properties of several magnetic alloys: antiferromagnetic $\text{Cr}_{1-x}\text{Al}_x$ (together with a pure Cr reference sample), $\text{Fe}_{1-x}\text{Si}_x$ near the Fe_3Si Heusler composition, as well as the metamagnetic transition in FeRh, with bulk-sensitive hard x-ray photoemission at 5956 eV and with nanocalorimetry and CEMS.

▶ **$\text{Cr}_{1-x}\text{Al}_x$ ¹:** Our HXPS data reveal among other things a semiconducting energy band gap of 95 ± 14 meV in a $\text{Cr}_{0.80}\text{Al}_{0.20}$ thin film (see **Fig. 1**). The valence-band measurements are compared to theoretical density-of-states calculations, which agree in predicting the opening of a gap in the alloy. Core-level spectra are also found to exhibit shifts and satellite effects, and these have been analyzed. Nonequilibrium thin film growth and density functional theory have also been used to elucidate the cause of the semiconducting gap in $\text{Cr}_{1-x}\text{Al}_x$ near $x=0.20$: this is found to be a combination of chemical ordering and itinerant antiferromagnetism.

▶ **$\text{Fe}_{1-x}\text{Si}_x$ ^{2,14}:** We have investigated the electronic and magnetic properties of crystalline and amorphous $\text{Fe}_{1-x}\text{Si}_{x1-x}$ with x from 0.45 to 0.75. These alloys are considered to be binary Heusler alloys, with theory predicting significant spin polarization at the Fermi energy, and they thus have possible spintronic applications. The shapes and positions of Si 1s, 2s, & 2p and Fe 2p, 3s, & 3p core levels were investigated for two compositions ($x = 0.72$ and 0.67) and for both crystalline and amorphous samples. In the amorphous alloy, in spite of the disordered structure that could lead to a broad distribution of chemical environments, core spectroscopy shows that the Si environment is relatively unique, consistent with recent DFT calculations. Analysis of the valence spectra, dominated by Fe 4s, Si 3s and Fe 3d character, revealed significant differences between the compounds of the two compositions and degrees of crystallinity. We find excellent agreement with one-step photoemission calculations based on the coherent potential model and including matrix-element effects. Additionally, we observe an anomalous Hall effect (AHE) in all samples in this composition range, providing direct evidence of spin-polarized carriers. The amorphous samples, in particular, exhibit a *very* large AHE. With this material system, it is possible to span multiple orders of magnitude in longitudinal conductivity, thus leading to insight into the fundamental mechanisms of the AHE, which still remain an open question. Remarkably, the amorphous films exhibit a very large magnetization in comparison to crystalline films of the same composition, effects which agreeing extremely well with theoretical DFT calculations (see **Fig. 2**). X-ray absorption fine structure (XAFS) measurements and theoretical calculations show that this enhanced moment is due to a decreased coordination number in the

amorphous alloys. We have also investigated the effect of chemical order on magnetization by conversion electron Mössbauer spectrometry (CEMS), and as disorder increases the magnetic moment also increases¹⁴.

► **FeRh³**: Stoichiometric FeRh undergoes a temperature-induced antiferromagnetic (AFM) to ferromagnetic (FM) transition at ~350 K, making it of interest for thermally assisted magnetic writing. The cause of this transition has been variously attributed to differences in electronic, magnetic, or lattice properties. We have investigated changes in the bulk electronic structure of strained epitaxial FeRh thin films accompanying this transition via core- and valence HXPS with a photon energy of 5.95 keV. Clear differences between the AFM and FM states are observed across the entire valence-band spectrum and these are very well reproduced by density functional theory (**Fig. 3**). Changes in the Fe 2p core-levels of Fe are also observed and interpreted using Anderson impurity model calculations. These results suggest that significant electronic structure changes are involved in this AFM-FM transition. Full-field magnetic microscopy experiments to image the evolution of the morphology and size of the ferromagnetic domains through the AFM-FM phase transition are in progress at the ALS (P. Fischer et al.), using a heater stage developed in the Hellman group.

Complementary more surface sensitive XMCD-XLD experiments in a PEEM are also being performed (Fadley group) to get a better understanding of the influence of surfaces and interfaces in this first-order phase transition. FeRh films grown on MgO and on MgO grown by ion-beam assisted deposition (IBAD) have also been studied by CEMS (with J. Juraszek) to investigate the effect of strain on the Fe magnetic moment in both phases. Also, magnetic thermal fluctuations have been identified as the dominant contribution to the entropy of the metamagnetic transition by specific heat measurements from 2-380K on epitaxial AFM and FM Fe-Rh alloy films grown on IBAD MgO.

• **Development of nanocalorimetry and the ion-beam assisted growth (IBAD) technique for growing epitaxial magnetic films on thin amorphous membrane with heaters and thermometers for temperature-resolved phase transition studies¹³**: A silicon-nitride membrane-based nanocalorimeter has been developed for measuring the heat capacity of 30 nm films from 300 mK to 800 K and in high magnetic fields with absolute accuracy 2%¹³. IBAD growth has been used to provide a biaxially oriented MgO template on the membrane-based calorimeter in order to measure the specific heat of *epitaxial* thin films. Synchrotron x-ray diffraction showed the high epitaxial quality of FeRh and Fe/Cr multilayer films grown onto this MgO template. The contribution of the MgO layer to the total heat capacity was measured to be just 6.5%. Nanocalorimetry of FeRh films and Fe/Cr multilayers showed differences in the electronic density of states for each system that elucidate the AFM/FM phase transition and GMR respectively. Thermal simulations including radiation and convection effects have demonstrated that these devices can be used for temperature and time resolved spectroscopy and microscopy techniques, with such techniques now being used to measure magnetic domains in the ALS full-field microscope at high temperature in FeRh.

• **Development of hard x-ray photoemission: bulk electronic structure from hard x-ray angle-resolved photoemission: W(110) and a (Ga,Mn)As ferromagnetic semiconductor⁸**: We have demonstrated hard angle-resolved x-ray photoemission spectroscopy (HARPES) in the multi-keV regime and used it to investigate the electronic structure of W(110) as a first proof-of-principle test case and of ferromagnetic Ga_{1-x}Mn_xAs (001) (x ≈ 0.05) compared to pure GaAs as a system of interest in spintronics, measuring in detail both core-level spectra and angle-resolved valence-band spectra. Data were obtained with photon energies of 3.2 keV and 6.0 keV. The Ga_{1-x}Mn_xAs samples were synthesized by ion implantation and pulsed-laser melting. Measuring at these energies should yield about 10-20 times more bulk-sensitivity than traditional ARPES in the 20-130 eV regime. Dispersive bands are clearly seen in the data for W, GaAs, and Ga_{1-x}Mn_xAs, particularly after correction for density of states (DOS)-like intensity due to phonon effects and associated x-ray photoelectron diffraction (XPD) effects (**see Fig. 4**). Core-level photoelectron diffraction, multiplet splittings and screening satellites also permit better defining the bulk electronic structure. The valence-level data are compared with one-step photoemission calculations, and found to be in excellent agreement (**again Fig. 4**). This includes differences between GaAs and Ga_{1-x}Mn_xAs.

• **Depth resolved electronic structure of an LSMO/STO superlattice via standing-wave excited angle-resolved photoemission¹⁰**. We have determined the depth-resolved composition profiles and electronic structure of a SrTiO₃/La_{0.67}Sr_{0.33}MnO₃ superlattice via standing-wave (SW) excited angle-resolved soft and hard x-ray photoemission. The epitaxial superlattice samples consisted of 48 and 120 bilayers of STO (15.6 Å-4 unit cells) and LSMO (15.5 Å-4 unit cells). These were studied using excitation energies of 833.2 eV near the La 3d_{5/2} resonance at the ALS, and at 5,946 eV at SPring-8. Analyzing rocking curves at both energies permits determining the precise profiles of the bilayers in the superlattice, which varies slightly in thickness from top to

bottom, as well as depth-resolved composition profiles and optical constants through the STO/LSMO interface. Measurements of core-level binding energies through the soft x-ray rocking curve also reveal a shift of the Mn 3p photoemission peak near the interface which is not found for the peaks in any other element (**see Fig. 4**); this suggests a change in the Mn bonding near the STO/LSMO interface, and is consistent with Anderson-impurity-model (AIM) calculations incorporating a crystal-field distortion effect. The valence-band density of states also reveals signatures of Mn 3d e_g and t_{2g} and Ti-derived states in the rocking curves, together with their localization character. Finally, some first SW-excited soft x-ray ARPES data shows distinctly different k -space maps of the Mn 3d e_g and t_{2g} states, together with changes near the STO/LSMO interface¹⁰. These last data represent a first step towards depth-resolved ARPES.

• **Depth-resolved photoelectron microscopy of nanostructures via soft x-ray standing wave excitation**^{11,12} We have demonstrated the addition of depth resolution to the usual two-dimensional images in photoelectron emission microscopy (PEEM), with application to a wedge-profile sample and a square array of circular magnetic microdots. The method is based on excitation with a soft x-ray standing-wave (SW) generated by Bragg reflection from a multilayer-mirror substrate on which the sample is grown. The standing wave is moved vertically through the sample by imaging the wedge with several SW cycles along it, or by varying the photon energy around the Bragg condition. Depth-resolved PEEM images were obtained for all of the observed elements. Photoemission intensities based on different core peak intensities as functions of photon energy were compared to x-ray optical theoretical calculations in order to quantitatively derive the depth-resolved film structure of the samples. This SW approach thus provides complementary information to the usual lateral information provided by PEEM, and should have wide applicability to studies of magnetic and other nanostructures in the future, particularly with the new reflection geometry beamline and microscope described below.

➤ **Future Plans:** We will continue with the development, refinement, and application of nanocalorimetry, the hard x-ray and nm-scale standing wave photoemission techniques, soft x-ray microscopy and resonant scattering, with specific systems of interest being magnetic oxide multilayer structures, metallic compounds and alloys such as FeRh and NiMnGa and Heusler alloy thin films of interest for spintronic and magnetocaloric applications. We will also establish a facility at the ALS for carrying out HXPS measurements, as well as a next-generation beamline for resonant soft x-ray scattering measurements. We will continue to develop measurement and especially analytical capabilities for resonant x-ray scattering with emphasis on allowing modeling in which resonant optical properties as well as structure are varied in fitting experimental data. We will further develop the capability of growing epitaxial films on thin amorphous membranes with built in heaters and thermometers suitable for nanocalorimetry, spectroscopy and microscopy by developing IBAD techniques for SrTiO₃, SrRuO₃, etc. A next generation full field soft x-ray microscope at an elliptically polarized undulator (EPU) will enable us to provide microspectroscopic information down to <10nm spatial resolution in various sample environments (low temperatures, high magnetic fields). Depth resolution can also be obtained through microscopy in a reflection geometry with standing-wave excitation and full polarization control also opens this technique to AF systems (e.g. FeRh) as well.

Figures:

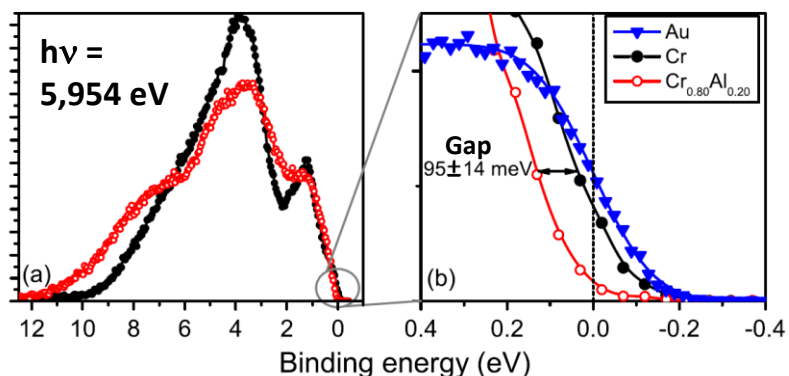


Figure 1: Hard x-ray photoemission valence-band spectra from (a) Cr and Cr_{0.80}Al_{0.20} and (b) blowup near E_F with Au reference shown. [PRL 105, 236404 (2010)]

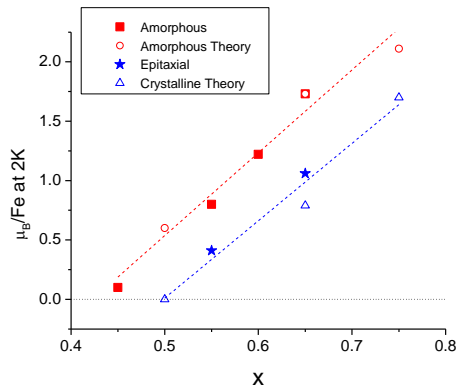


Figure 2: Fe magnetic moment as a function of x in $\text{Fe}_x\text{Si}_{1-x}$ for amorphous (red square) and epitaxial (blue star) thin films, with theory for amorphous (red circle) and crystalline (blue triangle). [Ref. 14]

Figure 4: Hard x-ray angle-resolved photoemission from GaAs (001): (a) Room temp., (b) 20K, (c) 20K, corrected for XPD and DOS, plus free-electron theory, (d) One-step photoemission theory [Ref. 8]

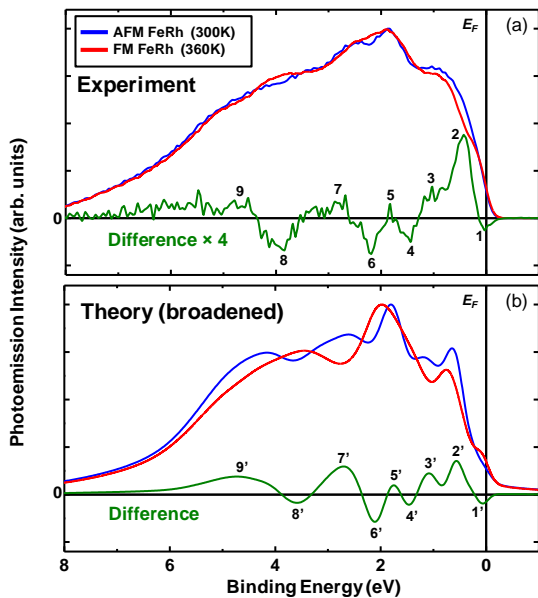
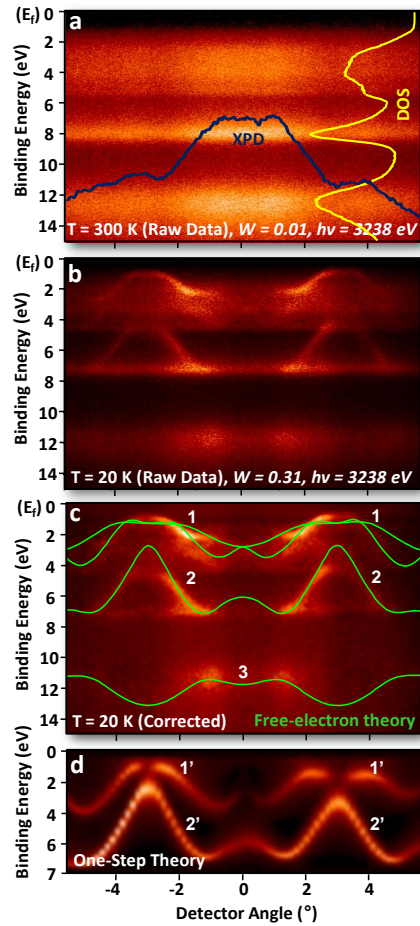


Figure 3: Hard x-ray photoemission valence-band spectra from anti-ferromagnetic and ferromagnetic FeRh: (a) Experiment, (b) Theory. [Ref. 3].

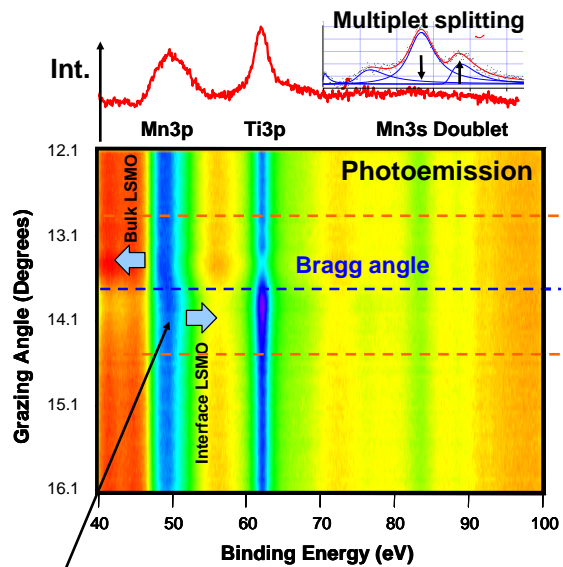


Figure 5: Soft x-ray standing-wave photoemission (833 eV) from a $\text{SrTiO}_3/\text{La}_{0.67}\text{Sr}_{0.33}\text{MnO}_3$ superlattice, with interface Mn 3p shift noted. [Ref. 10]

References: **R** = longer review article, program PIs and other LBNL PIs highlighted

- ¹ “Band Gap and Electronic Structure of an Epitaxial, Semiconducting $\text{Cr}_{0.80}\text{Al}_{0.20}$ Thin Film”, Z. Boekelheide, A. X. Gray, C. Papp, B. Balke, D. A. Stewart, S. Ueda, K. Kobayashi, **F. Hellman**, and **C. S. Fadley**, *Phys. Rev. Letters* **105**, 236404 (2010).
- ² “Hard X-ray Photoemission Study of Near-Heusler $\text{Fe}_x\text{Si}_{1-x}$ Alloys”, A. X. Gray, J. Karel, J. Minár, C. Bordel, H. Ebert, J. Braun, S. Ueda, Y. Yamashita, L. Ouyang, D. J. Smith, K. Kobayashi, **F. Hellman**, and **C. S. Fadley**, *Physical Review B* **83**, 195112 (2011)
- ³ “Electronic Structure Changes across the Metamagnetic Transition in FeRh”, A. X. Gray, D. W. Cooke, P. Krüger, C. Bordel, A. M. Kaiser, S. Ueda, Y. Yamashita, C.M. Schneider, K. Kobayashi, **F. Hellman**, and **C. S. Fadley**, submitted to *Physical Review B*.
- ⁴ **R P. Fischer**, Viewing spin structures with soft X-ray microscopy, *Materials Today* **13**(9) 14 (2010); **P. Fischer**, Exploring nanoscale magnetism in advanced materials with polarized X-rays, *Materials Science & Engineering R72* 81-95 (2011)
- ⁵ M. Valvidares, M. Huijben, P. Yu, R. Ramesh, and **J. B. Kortright**, “Native SrTiO_3 (001) surface layer from resonant Ti $L_{2,3}$ reflectance spectroscopy,” *Physical Review B* **82**, 235410 (2010).
- ⁶ “Band Mapping in Higher-Energy X-Ray Photoemission: Phonon Effects and Comparison to One-Step Theory”, L. Plucinski, J. Minár, B.C. Sell, J. Braun, H. Ebert, C.M. Schneider and **C.S. Fadley**, *Phys. Rev. B* **78**, 035108 (2008).
- ⁷ “Meeting Report: International Workshop for New Opportunities in Hard x-ray Photoelectron Spectroscopy: HAXPES 2009”, J. C. Woicik, D. A. Fischer, E. Vescovo, D. A. Arena, D. E. Starr, B. O. Wells, **C. S. Fadley**, *Synchrotron Radiation News*, **23**, 1 (2010), with program and presentations at: <http://www.nsls.bnl.gov/newsroom/events/workshops/2009/haxpes/>
- ⁸ “Probing Bulk Electronic Structure with Hard-X-Ray Angle-Resolved Photoemission: W and GaAs”, A. X Gray, C. Papp, S. Ueda, B. Balke, Y. Yamashita, L. Plucinski, J. Minár, J. Braun, E. R. Ylvisaker, C. M. Schneider, W. E. Pickett, H. Ebert, K. Kobayashi, and **C. S. Fadley**, *Nature Materials*, to appear, and results for GaAs and (Ga,Mn)As to be published with **O. Dubon**.
- ⁹ “Determination of buried interface composition and magnetism profiles using standing-wave excited soft x-ray emission and inelastic scattering”, B.C. Sell, S.-H. Yang, M. Watanabe, B.S. Mun, L. Plucinski, N. Mannella, S.B. Ritchey, A. Nambu, J. Guo, M.W. West, F. Salmassi, **J.B. Kortright**, S.S.P. Parkin, and **C.S. Fadley**, *J. Appl. Phys.* **103**, 083515 (2008).
- ¹⁰ “Interface properties of magnetic tunnel junction $\text{La}_{0.7}\text{Sr}_{0.3}\text{MnO}_3/\text{SrTiO}_3$ superlattices studied by standing-wave excited photoemission spectroscopy”, A. X. Gray, C. Papp, B. Balke, S.-H. Yang, M. Huijben, E. Rotenberg, A. Bostwick, S. Ueda, Y. Yamashita, K. Kobayashi, E. M. Gullikson, **J. B. Kortright**, F. M. F. de Groot, G. Rijnders, D. H. A. Blank, **R. Ramesh**, and **C. S. Fadley**, *Phys. Rev. B* **82**, 205116 (2010), and to be published.
- ¹¹ “Depth-resolved soft x-ray photoelectron emission microscopy in nanostructures via standing-wave excited photoemission, F. Kronast, R. Ovsyannikov, A. Kaiser, C. Wiemann, S.-H. Yang, D. E. Bürgler, R. Schreiber, F. Salmassi, **P. Fischer**, H. A. Dürr, C. M. Schneider, W. Eberhardt, and **C. S. Fadley**, *Appl. Phys. Lett.* **93**, 243116 (2008).
- ¹² “Standing-wave excited soft x-ray photoemission microscopy: application to nanodot Co magnetic arrays”, C. Papp, F. Kronast, A. Gray, A. Kaiser, C. Wiemann, S.-H. Yang, D. E. Bürgler, R. Schreiber, F. Salmassi, **P. Fischer**, H. A. Dürr, C. M. Schneider, and **C. S. Fadley**, *Appl. Phys. Lett.* **97**, 062503 (2010).
- ¹³ “Thin film nanocalorimeter for heat capacity measurements of 30 nm films”, D. R. Queen and **F. Hellman**, *Rev. Sci. Instrum.* **80**, 063901 (2009).
- ¹⁴ “Enhanced magnetism in amorphous $\text{Fe}_x\text{Si}_{1-x}$ thin films”, J. Karel, C. Bordel, Y.N. Zhang, J. Hu, R. Q. Wu, S.M. Heald and **F. Hellman**, submitted to *Phys. Rev Lett.* (2011).

Digital Synthesis: A Pathway to New Materials at Interfaces of Complex Oxides

Anand Bhattacharya

anand@anl.gov

Materials Science Division & Center for Nanoscale Materials
Argonne National Laboratory, Argonne, IL 60439

(i) Program Scope

The complex oxides host many fascinating and diverse collective states of condensed matter, with spin, charge and lattice degrees of freedom all playing their part. In our program, we seek to create, characterize, understand and manipulate novel states of condensed matter at interfaces of complex oxides using digital synthesis. Digital synthesis is a technique where ordered, undoped layers are stacked in integer sequences, and all charge transfer or doping takes place at atomically sharp interfaces, without the disorder that is associated with the usual chemical doping strategies. The richness of observed phenomena in the complex oxides, which have also presented some of the greatest challenges to our understanding, are due to the strongly interacting degrees of freedom in the materials. Surfaces and interfaces between complex oxides provide a unique environment for these degrees of freedom to ‘reconstruct’ and create new systems with properties that are qualitatively different from their bulk constituents. In this sense, they provide a pathway for discovering new materials. More specifically, we seek to discover and explore novel states of condensed matter with attributes such as tunability of collective states with external electric fields and electric currents. These include multiferroic single-phase materials and heterostructures, superconductivity at interfaces between materials that may not be superconducting themselves, spin-polarized two-dimensional electron gases, and materials where strong spin-orbit coupling is the determinant property of the material. We seek to explore properties of materials that are known to have interesting phases, such as the manganites and cuprates, where the effects of disorder have been engineered away by digital synthesis. We create these materials systems using state-of-the-art, ozone-assisted oxide Molecular Beam Epitaxy (MBE) at the Center for Nanoscale Materials (CNM) at Argonne, and characterize them using the major DOE facilities for neutron and photon scattering, and at the new DOE Nanoscale Science Research Centers.

(ii) Recent Progress (since 2009):

Since 2009, we have published on a number of topics. We list some of these developments below:

- *Enhanced Neel Temperatures in Digital LSMO:* We studied superlattices of $(\text{LaMnO}_3)_m/(\text{SrMnO}_3)_{2m}$ for $m = 1$ and 2 and also random alloys of the same composition. These superlattices are ordered analogues of the composition $\text{La}_{1/3}\text{Sr}_{2/3}\text{MnO}_3$, an antiferromagnetic insulator. We show that chemical ordering creates an enhancement of the Neel temperature by >70 K. Our initial work showed signatures in transport of enhanced ordering temperatures (published in *Applied Physics Letters* in 2007.) Our recent work (published in *Nature Materials* **8**, 892 (2009)) includes measurements of the temperature dependence of the antiferromagnetic order, and corresponding changes in the c -axis lattice parameters, via neutron (HFIR) and x-ray (APS) scattering. The work establishes a definitive

link between these two, and also demonstrates that there is a strong *in-plane* modulation in the lattice for the random alloy that is far less pronounced in the superlattice.

- *Disentangling effects of dimensionality and disorder in manganites*: We studied cation ordered analogs of $\text{La}_{2-x}\text{Sr}_x\text{MnO}_4$. This has a spin glass phase at low T instead of being a usual ferromagnet as in the 3D perovskite analogs, and we wanted to see if ordering the cations would create a 2-D ferromagnet. With postdoc Brittany Nelson-Cheeseman, we have synthesized and characterized ordered analogs of this material. We discovered that cation ordering created a novel magnetic anisotropy and reduced the resistivity by over an order of magnitude at $T < 100\text{K}$. However, we did not observe any long range ferromagnetic order. (*Applied Physics Letters*, 2011)
- *Correlating structure and electronic properties at $(\text{LaMnO}_3)/(\text{SrMnO}_3)$ interfaces*: LaMnO_3 (Mn^{3+}) is a Jahn-Teller/Mott Hubbard insulator with an A-type (layered) antiferromagnetic (AF) ground state, while SrMnO_3 (Mn^{4+}) is a correlated insulator and a G-type (cubic) AF. The interfaces between these materials show properties related to mixed $3^{+}/4^{+}$ valence. Using STEM (scanning transmission electron microscopy) and EELS (electron energy loss spectroscopy) (with Amish Shah and Jim Zuo, UIUC) we studied the correlation between structure and electronic properties with atomic resolution in $(\text{LaMnO}_3)/(\text{SrMnO}_3)$ superlattices. (*Phys. Rev. B* 2010).
- Using high resolution x-ray diffraction at the Advanced Photon Source, we quantified the dependence of octahedral tilts on epitaxial strain in LaNiO_3 thin films grown with oxide MBE at Argonne. We followed this with a study of how these tilts in LaNiO_3 are affected when they are incorporated into superlattices with SrMnO_3 . This work demonstrates a pathway to tune octahedral tilts with a control parameter other than epitaxial strain. (*Phys. Rev. B* 2010; *Phys. Rev. B* 2011).
- There were two papers published on aspects of scanning transmission electron microscopy of different materials by Jian-Min Zuo and Amish Shah (supported by this FWP) with other collaborators, which have appeared in *Advanced Functional Materials* (2010) and in *Surface Science Reports* (2010).

(iii) Future Plans

(a) Using our digital synthesis technique, we can create materials where the cation disorder associated with usual chemical doping strategies is nearly absent. As we have observed in our recent work with the manganites, this may have profound effects on long-range magnetic order. In our proposed research, we plan to extend these ideas to superconducting perovskites to better understand the role of cation disorder in their properties, particularly how this relates to competing order parameters, and how it might impact transition temperatures. (b) Interfaces may also allow the control of collective states. In this regard, we will explore how collective states such as superconductivity and magnetism, and phase transitions such as metal-insulator transitions may be controlled with electric fields and electric currents, an area of research we refer to as ‘Mottronics’. (c) Lastly, we propose to create and study a new class of oxides where spin-orbit interactions coupled with Mott correlations and frustrated spin degrees of freedom may lead to novel states, including superconductivity, and exotic conducting states that may appear at surfaces or in the bulk. In these materials, there may be strong coupling of the momentum and spin of charge carriers leading to new phenomena, which may have relevance for spintronics. An understanding of these materials and their underlying physics may lead to

entirely new concepts where the interface or surface ‘is the material’¹ and provides the desired functionalities.

Synthesis Cluster: Synthesis of novel materials with single atomic layer control forms the basis for our research program. We are planning to create an oxide ‘synthesis cluster’ at the Material Science Division at Argonne for oxide thin films and heterostructures, with capabilities that will be in some ways complementary to those we currently use at the Center for Nanoscale Materials. The complex oxides are diverse in their chemical makeup, and not all can be created with the same techniques. For example, thin dielectrics grown with MBE can sometimes be leaky, and refractory elements such as Ru and Ir cannot be evaporated easily from Knudsen cells in an MBE system. Volatile elements such as Bi and K are probably not very compatible with elements that evaporate at much higher temperature, as they may vaporize from the walls and contaminate films of the more refractory metals. To address these issues, we seek to create a cluster of compact deposition tools that will each have a unique capability (volatiles, reactive sputtering, pulsed laser deposition etc.), where samples can be readily transferred between them under ultra-high vacuum conditions. This will enable us to create a broader range of heterostructures where the constituent materials are grown using techniques optimal to each material, while preventing interfacial contamination. At the first stage of this cluster, we are in the process of acquiring a compact state of the art oxide-MBE system, which we shall interface with a reactive oxide sputtering system. We anticipate that this stage will be operational by end of 2011/ early 2012.

(iv) Publications resulting from work supported by DOE BES from 2008-2011:

1. “Control of octahedral rotations in $\text{LaNiO}_3/\text{SrMnO}_3$ superlattices”, S. J. May, C. R. Smith, J. –W. Kim, E. Karapetrova, A. Bhattacharya, P. J. Ryan, *Phys. Rev. B* **83**, 153411 (2011).
2. “Cation-ordering Effects in the Single layered Manganite $\text{La}_{2/3}\text{Sr}_{4/3}\text{MnO}_4$ ”, B. B. Nelson-Cheeseman, A. B. Shah, T. S. Santos, S. D. Bader., J.-M. Zuo and A. Bhattacharya, *Appl. Phys. Lett.* **98**, 072505 (2011).
3. “Practical Spatial Resolution of Electron Energy Loss Spectroscopy in Aberration Corrected Scanning Transmission Electron Microscopy”, A.B. Shah, Q.M. Ramasse, J.G. Wen, A. Bhattacharya and J.M. Zuo, *Micron*, (2011) (in press) [doi:10.1016/j.micron.2010.12.008](https://doi.org/10.1016/j.micron.2010.12.008)
4. “Presence and spatial distribution of interfacial electronic states in $\text{LaMnO}_3\text{-SrMnO}_3$ superlattices”, A. B. Shah, Q. M. Ramasse, S. J. May, J. Kavich, J. G. Wen, X. Zhai, J. N. Eckstein, J. Freeland, A. Bhattacharya and J. M. Zuo, *Phys. Rev. B* **82**, 115112 (2010).
5. “Quantifying octahedral rotations in strained perovskite oxide films”, S. J. May, J.-W. Kim, J. M. Rondinelli, E. Karapetrova, N. A. Spaldin, A. Bhattacharya and P.J. Ryan, *Phys. Rev. B* **82**, 014110 (2010).
6. "DNA Sensing Using Nanocrystalline Surface-Enhanced Al_2O_3 Nanopore Sensors", B. M. Venkatesan, A. B. Shah, J. M. Zuo, and R. Bashir, *Advanced Functional Materials* **20**, 1266 (2010).
7. “Probing Interfacial Electronic Structures in Atomic Layer LaMnO_3 and SrTiO_3 Superlattices”, Amish B. Shah, Quentin M. Ramasse, Xiaofang Zhai, Jian Guo Wen, Steve J. May, Ivan Petrov, Anand Bhattacharya, Peter Abbamonte, James N. Eckstein, Jian-Min Zuo, *Advanced Materials* **22**, 1156 (2010).

8. "Instability, intermixing and electronic structure at the epitaxial $\text{LaAlO}_3/\text{SrTiO}_3(001)$ heterojunction," S. A. Chambers, M. H. Engelhard, V. Shutthanandan, Z. Zhu, T. C. Droubay, L. Qiao, P. V. Sushko, T. Feng, H. D. Lee, T. Gustafsson, E. Garfunkel, A. B. Shah, J. M. Zuo, and Q. M. Ramasse, *Surface Science Reports* **65**, 317-352 (2010).
 9. "New Optical Absorption bands in Atomic Layer Superlattices" X. Zhai, C. S. Mohapatra, A. B. Shah, J.-M. Zuo and J. N. Eckstein, *Advanced Materials* **22**, 1136 (2010).
 10. "Enhanced ordering temperatures in antiferromagnetic manganite superlattices", S. J. May, P. J. Ryan, J. L. Robertson, J.-W. Kim, T. S. Santos, S. G. E. te Velthuis, E. Karapetrova, J. L. Zarestky, J. N. Eckstein, S. D. Bader, and A. Bhattacharya, *Nature Materials* **8**, 892 (2009).
 11. "Tuning between the metallic antiferromagnetic and ferromagnetic phases of $\text{La}_{1-x}\text{Sr}_x\text{MnO}_3$ near $x=0.5$ by digital synthesis", T. S. Santos, S. J. May, J. L. Robertson and A. Bhattacharya, *Phys. Rev. B* **80**, 155114 (2009).
 12. "Onset of metallic behavior in strained $(\text{LaNiO}_3)_n/(\text{SrMnO}_3)_2$ superlattices", S. J. May, T. S. Santos and A. Bhattacharya, *Phys. Rev. B* **79**, 115127 (2009).
 13. "Substrate orientation dependence of ferromagnetism in $(\text{Ga,Mn})\text{As}$ ", M. J. Wilson, G. Xiang, B. L. Sheu, P. Schiffer, N. Samarth, S. J. May, and A. Bhattacharya *Applied Physics Letters* **93**, 262502 (2008).
 14. "The metal-insulator transition and its relation to magnetic structure in $(\text{LaMnO}_3)_{2n}/(\text{SrMnO}_3)_n$ superlattices". A. Bhattacharya, S. J. May, S. G. E. te Velthuis, M. Warusawithana, X. Zhai, A. B. Shah, J.-M. Zuo, M. R. Fitzsimmons, S. D. Bader, J. N. Eckstein, *Phys. Rev. Lett.* **100**, 257203 (2008).
 15. "Magnetically asymmetric interfaces in a $\text{LaMnO}_3/\text{SrMnO}_3$ superlattice due to structural asymmetries," S. J. May, A. B. Shah, S. G. E. te Velthuis, M. R. Fitzsimmons, J.-M. Zuo, X. Zhai, J. N. Eckstein, S. D. Bader and A. Bhattacharya, *Physical Review B* **77**, 174409 (2008).
 16. "Viscous spin exchange torque on precessional magnetization in $(\text{LaMnO}_3)_{2n}/(\text{SrMnO}_3)_n$ superlattices" H. B. Zhao, K. J. Smith, Y. Fan, G. Lüpke, A. Bhattacharya, S. D. Bader, M. Warusawithana, X. Zhai, J. N. Eckstein, *Phys. Rev. Lett.* **100**, 117208 (2008).
-

**Time-Resolved Spectroscopy of Insulator-Metal Transitions: Exploring
Low-Energy Dynamics in Strongly Correlated Systems
(Grant No. DE-FG02-04ER46127)**

Gunter Luepke
Department of Applied Science, College of William & Mary,
Williamsburg, VA 23187, email: Luepke@wm.edu

1) Project Scope

Our research program focuses on the study of the low-energy dynamics in complex transition metal oxide thin films and heterostructures using time-resolved optical techniques. Our program concentrates on two major themes: (i) to determine the interface magnetism and coherent spin dynamics in various manganite thin-film superlattices using the interface-specific magnetization-induced second-harmonic generation technique, and (ii) to elucidate and reveal the important underlying physics behind the coupled ferromagnetic and ferroelectric order at the heterointerfaces of multiferroic heterostructures, which plays a crucial role in determining their multifunctional behavior. The science addresses issues of energy dissipation and the coupling between electronic and magnetic order in such materials, of fundamental importance to our understanding of solid-state properties and has numerous applications.

2) Recent Progress

Recently, we investigated photoinduced spin precessions for geometry with negligible canting of the magnetization in ferromagnetic perovskite $\text{La}_{0.67}\text{Ca}_{0.33}\text{MnO}_3$ (LCMO) thin films by the time-resolved magneto-optical Kerr effect. We observe weak demagnetization but strong spin precessions over a wide range of fields (0-2.5 T) applied along the in-plane easy axis. The precession amplitude monotonically decreases with increasing field, in contrast to the precession induced by transient anisotropy field in the state of canted magnetization. These observations indicate that the coherent spin rotation may be triggered by a transient exchange field other than by demagnetization and/or anisotropy modulation. We attribute the emergence of the exchange field to antiferromagnetic interaction caused by charge transfer and alteration of kinetic energy of e_g electrons in LCMO under optical excitation.

We have measured the magnetization precession dynamics for LCMO films over a wide range of temperatures. Figure 1 shows that spin precessions are excited at $T < T_c$ (~270K) and only a negligible Kerr signal is observed for $T > T_c$. The precession frequency, shown in the inset, exhibits no significant variance between 20 and 150K. Since the frequency is strongly dependent on the anisotropy fields, we conclude that the thermal modification of the anisotropy is less than 10% at $T=20$ K by considering

that the rise of the temperature is less than 30 K after laser interaction.

In the state of canted magnetization, such anisotropy modulation will indeed lead to a transient field, triggering the spin precession. This transient anisotropy field increases with increasing field and the resulting precession amplitude reaches a maximum at the field approximately equal to the static anisotropy field. Correspondingly, we expect the precession

amplitude to show the same tendency. Figure 2(a) shows the field dependence of the precession amplitude obtained when H is applied at an angle of 45° to the easy axis, a state with canted magnetization. We note that the amplitude is sharply enhanced with increasing field and then slowly decreases at fields larger than ~ 0.3 T, consistent with our expectation. Similar results are obtained from the other LCMO samples, as well as a Fe film with the field applied along the hard axis and at an angle of $\sim 10^\circ$ to the easiest axis (Fig. 2(c)-(d)).

In contrast, the precession for easy axis of LCMO shows the opposite dependence, i.e., the amplitude decreases with increasing field for all three LCMO samples, as shown in Fig 2(b). This result strongly speaks against the canted magnetization, and therefore it confirms our previous conclusion that the transient anisotropy field, either due to demagnetization or modification of anisotropy constant, is not the major contributor to launch the spin precessions when H is applied parallel to the easy axis.

We propose that the transient field results from modification of the exchange coupling between the ferromagnetic metallic (FM) and antiferromagnetic insulating (AFI) states in the film caused by the optical excitation. The coexistence of distinct FM and AFI phases in doped manganites has long been established, and the AFI domain may be melted in the presence of an external field. In the case of LCMO, several reports indicated the presence of the AFI phase down to the lowest temperatures. Very slow photoinduced drops in conductivity and demagnetization have been observed in LCMO and interpreted as a photoinduced shift in the FM/AFI phase balance triggered by the photoexcited carriers that promote the cooperative Jahn-Teller distortions and formation of AFI clusters.

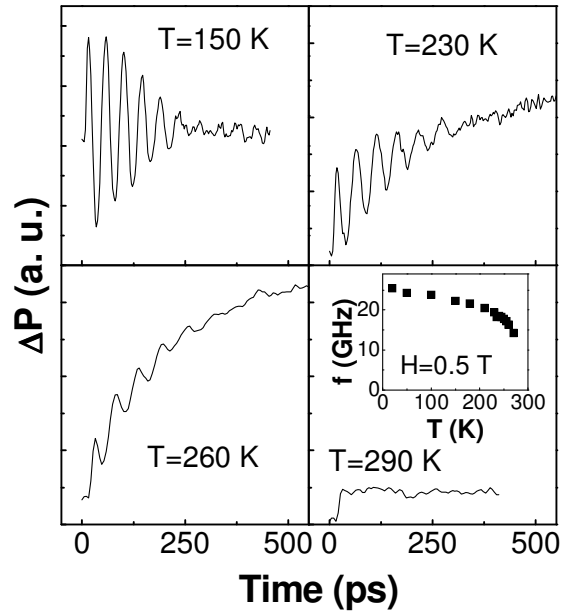


Fig. 1. Transient Kerr rotations of the LCMO film at various temperatures. The inset shows the precession frequency as a function of temperature.

The reorientation of the spins to form AFI clusters may take a long time due to the finite precession frequency and slow spin-lattice thermalization process to dissipate spin angular momentum. However, the exchange interaction may be modified in a much faster time regime, because the local carrier concentration and its kinetic energy play a crucial role in determining the magnetic phases. Both photoinjected carriers to Mn e_g band from O_{2p} orbital and the thermalized electrons may suppress the double exchange interaction and promote the AF coupling to form small Jahn-Teller polarons. Therefore, the exchange field pulse may be generated within the electron phonon relaxation time, much faster than the emergence of the demagnetization caused by real formation of AFI cluster.

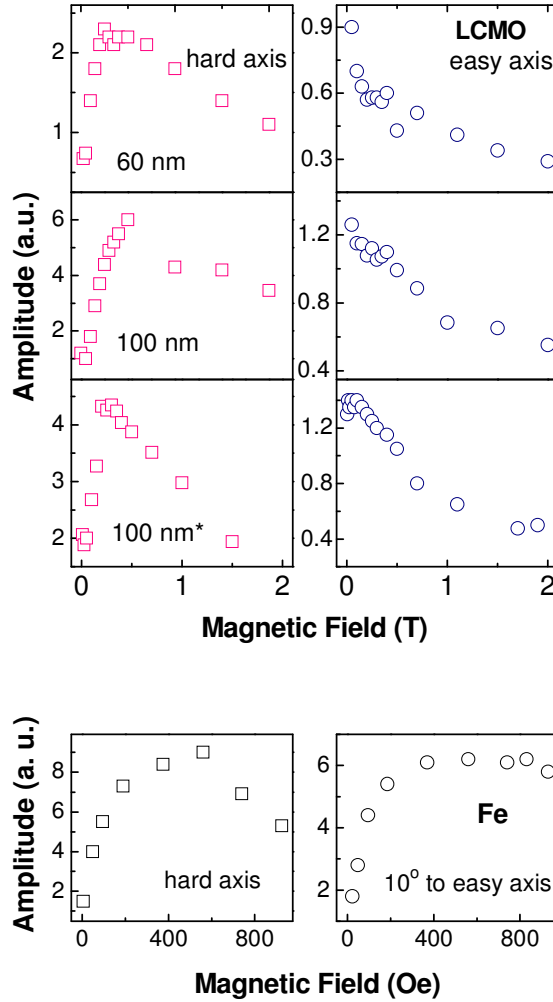


Fig. 2. Amplitude of the precession of (a) 60nm and 100-nm LCMO films with field applied at 45° to easy axis and along easy axis at 20K, and (b) Fe film with field applied at 55° to easy axis and of 10° to easy axis at RT.

This hypothesis is supported by the temperature dependence of the magnetization dynamics shown in Fig. 1. At temperature below 150 K, the magnetization dynamics show negligible demagnetization. With increasing temperature, a slow demagnetization (>500 ps) is clearly identified. Despite the dramatic difference of the demagnetization strength and time, the spin precession is launched nearly at the same time at all temperatures lower than T_c . Here, the reduction of the precession amplitude at higher temperature is mainly caused by the decrease of the saturated magnetization. This result therefore supports our model that the precession is triggered by the transient exchange field in the absence of spin lattice thermalization.

3) Future Plans

Multiferroic, magnetoelectric heterostructure systems have recently attracted great research interest, due to their potential application in multifunctional devices, such as magnetic memories, sensors and spintronics. Indeed, impressive progress has been made, such as the fabrication of room-temperature multiferroic heterostructures, and the observation of a four-state resistance state in a multiferroic tunneling junction. However, most of these studies cannot reveal the important underlying physics behind the coupled ferromagnetic and ferroelectric order at the heterointerfaces, which plays a crucial role in determining multifunctional behavior. Our experimental techniques, Magnetic Second Harmonic Generation (MSHG) and Time Resolved Magneto-Optic Kerr Effect (TRMOKE), can provide a direct probe of the magnetic state and spin dynamics at the heterointerface, and hence turn out to be effective tools to investigate this magnetoelectric coupling. We plan to measure with MSHG the variance of hysteresis loop and magnetic anisotropy at the interface of multiferroic heterostructures under different applied electric fields. Electric field-modulated spin dynamic behavior of such system will be probed by TRMOKE which will provide information on spin pinning centers at the interface. We expect to see variances of the pinning state and the distribution of spin population at the interface by applying different electric fields.

4) Publications

1. H. B. Zhao, K. J. Smith, Y. Fan, G. Lüpke, A. Bhattacharya, S. D. Bader, M. Warusawithana, X. Zhai, J. N. Eckstein, Viscous spin exchange torque on precessional magnetization in $(\text{LaMnO}_3)_{2n}/(\text{SrMnO}_3)_n$ superlattices, *Phys. Rev. Lett.* 100, 2008, pp. 117208-11.
2. Y. H. Ren, M. Ebrahim, H. B. Zhao, G. Lüpke, Z. A. Xu, V. Adyam, Qi Li, Time-resolved optical studies of spin and quasiparticle dynamics in colossal magnetoresistance materials: $\text{La}_{0.67}\text{Ca}_{0.33}\text{MnO}_3$, $\text{La}_{0.67}\text{Sr}_{0.33}\text{MnO}_3$ and $\text{Sr}_2\text{FeMoO}_6$, *Phys. Rev. B* 78, 2008, pp. 014408-13.
3. Lucarelli, A. Frey, R. Yang, G. Lüpke, T. J. Haugan, G. A. Levin, and P. N. Barnes, Dynamic investigation of the transport current in $\text{YBa}_2\text{Cu}_3\text{O}_{7-\delta}$ thin films, *Supercond. Sci. Technol.* 21, 2008, pp. 115003-7.
4. Y. H. Ren, M. Ebrahim, Z. A. Xu and G. Lüpke, Ultrafast quasi-particle dynamics of charge/orbital ordered and ferromagnetic clusters in $\text{La}_{0.7}\text{Ca}_{0.3}\text{MnO}_3$, *New Journal of Physics* 11, (2009) 113013.
5. Andrea Lucarelli, Ran Yang, Francesco Grilli, Timothy Haugan, Paul Barnes, Gunter Lüpke, Dynamic field and current distributions in multi-filamentary $\text{YBa}_2\text{Cu}_3\text{O}_{7-\delta}$ thin films with magnetic coupling, *J. Appl. Phys.* 106, (2009) 063904.
6. Andrea Lucarelli, Francesco Grilli, Gunter Lüpke, Timothy J Haugan and Paul N Barnes, Finite-element simulations of field and current distributions in multifilamentary superconducting films, *Supercond. Sci. Technol.* 22, (2009) 105015.
7. H. B. Zhao, D. Talbayev, Y. H. Ren, A. Venimadhav, Qi Li and G. Lüpke, Optical excitation of coherent spin precession via transient exchange field in $\text{La}_{0.67}\text{Ca}_{0.33}\text{MnO}_3$, submitted to *Phys. Rev. Lett.*

Project Title: “Competing Interactions in Complex Transition Metal Oxides”

L. E. De Long¹, PI (delong@pa.uky.edu); Gang Cao¹ (cao@uky.edu, Todd Hastings² (hastings@enr.uky.edu) and S. S. Seo¹ (a.seo@uky.edu), Co-PI's

¹Department of Physics and Astronomy, University of Kentucky

²Department of Electrical and Computer Engineering, University of Kentucky

Project Scope

One class of next-generation spintronic devices is based upon the injection of spin-polarized electrons into commercial semiconductors such as doped Si or GaAs, which requires a highly transmissive interface with a *room-temperature, ferromagnetic (FM) semiconductor*. However, the rarity of suitable narrow-gap semiconductors that are also FM above room temperature remains an obstacle to the development of semiconductor devices for spintronics. *We are investigating perovskite variants $ABO_{3-\delta}$ ($A=Ca, Sr, Ba$; $B=Mn, Fe, Ru$) and R-type ferrites $(Ba, Sr)M_{2\pm x}Ru_{4\pm x}O_{11}$ ($M=Fe, Co, Mn, Ti$) that exhibit electric and magnetic properties suitable for spin injection. In particular, Fe-bearing R-type ferrites exhibit a rare coexistence of long-range FM order accompanied by narrow-gap semiconducting properties at temperatures above 400 K.*

Our current research addresses the following questions and phenomena:

- 1) We are identifying *fundamental physical and chemical factors* that govern the occurrence of FM order above room temperature in both ferrite and perovskite phases that are narrow-gap semiconductors.
- 2) We are expanding on a preliminary study of certain perovskite materials ABO_3 that appear to exhibit a *rare coexistence of magnetic and electric polarizations on the same B lattice sites*, and various R-type ferrites that show evidence for coexisting magnetic and electric polarizations, whose interplay can be controlled by modest applied fields or electric currents. These materials may have promise for magnetoelectric applications.
- 3) Both ferrites and perovskites exhibit highly anisotropic physical properties that can be sensitively controlled by varying the relative concentration of 3d versus 4d or 5d elements, which we intend to show *adjusts the strengths of the crystal field and spin-orbit interactions* that compete with magnetic frustration and other fundamental interactions to determine the wide-ranging ground states exhibited by these materials.

Recent Progress

We have conducted X-ray and neutron diffraction, magnetotransport, magnetic moment, and soft X-ray scattering measurements on single crystals of hexagonal R-type ferrites $(Ba, Sr)M_{2\pm x}Ru_{4\pm x}O_{11}$. Alterations of the 3d-element ($M = Fe, Co, Mn, Ti$) composition yield a wide range of physical properties desired in practical epitaxial heterostructures. For example, these materials exhibit long-range FM order at temperatures as high as 490 K, accompanied by practical narrow-gap semiconducting properties that include a large anomalous Hall conductance, low resistivity, high carrier concentration and low coercive field. The hexagonal R-type ferrites also exhibit fundamentally interesting phenomena driven by magnetic frustration of antiferromagnetic (AFM) interactions on a disordered Kagomé lattice. Remarkably, simple substitution of $M = Fe$ for Co or Mn results in an evolution from metallic to semiconducting behavior, and a shift from frustrated “all-in/all-out” AFM order that sets in well below 200 K, to collinear FM states ordering well above room temperature. This evolution is accompanied by giant “topological” Hall effect anomalies that are driven by complex changes of spin chirality and Berry phase with only modest applied magnetic fields.

Future Plans

1. We intend to expand our investigation of competing interactions in R-type ferrites by undertaking specific heat experiments covering a wide range of temperatures $4 \text{ K} \leq T \leq 300 \text{ K}$ and magnetic fields up to 14 T. We expect to find multiple phase transitions, some of which have not been obvious in previous magnetic moment or electrical resistivity experiments.

2. We intend to continue XAS and XMCD experiments at Argonne's APS to accurately measure the oxidation state and magnetic moments residing on Ru, Fe, Co and Mn sites in several R-type ferrite compositions. These data should provide information regarding the electronic structure, anisotropy and bonding that underpin the high- T_C ferromagnetism and other unusual properties of these materials.

3. We will attempt to grow thin films of several R-type ferrite compositions via pulsed laser deposition and related techniques. Thin-film samples would make possible improved ferromagnetic resonance, as well as XAS and optical studies of the semiconducting gap and electronic structure. If this effort is successful, we will also explore fabrication of simple heterostructures of R-type ferrites having a range of properties that are required for spin injection studies and magnetotransport experiments.

Our current and future research is motivated by a broad view of the "heavy" 4d and 5d transition elements (HTE). First, the heavy d-elements have more extended d-orbitals compared to lighter 3d electron materials. Stronger p-d hybridization, spin-orbit (SO) and electron-lattice couplings, and reduced intra-atomic Coulomb U and crystalline electric field (CEF) interactions generate competitions between metallic and insulating states or paramagnetic and magnetic order. Small variations of composition, pressure or applied fields can induce drastic changes in the varied ground states exhibited by HTE oxides (ferroelectric, orbital or magnetic order, superconductivity, density waves), as well as control technologically important phenomena such as colossal magnetoresistance (CMR) and giant magnetoelectric effects (GME). We intend to explore materials in which HTE such as Ir, Pt and Rh play key roles in unusual physical properties.

We intend to take an *integrated, interdisciplinary approach* to the discovery and characterization of novel HTE oxides whose physical properties reflect competing interactions: We synthesize and identify novel materials, grow bulk single crystals to comprehensively study physical properties relevant to fundamental theories, as well as fabricate and study thin films and heterostructures relevant to device applications.

Our broad expertise and technical assets permit comprehensive investigations of electrical transport, magnetic, dielectric and thermodynamic properties over a wide range of temperatures $0.05 < T < 1000 \text{ K}$ and magnetic fields $0 < \mu_0 H < 14 \text{ T}$, and high-pressure electrical resistivity and magnetic moment measurements to 10 GPa. We are using National Laboratory facilities and/or external collaborators to conduct EXAFS, and magnetic soft X-ray and neutron scattering experiments to characterize small single crystals and thin films that are not easily studied via conventional electrical transport, magnetic or optical techniques.

Publications (03/15/08-11/15/10)

1. "Structural, magnetic and transport properties of a novel class of ferromagnetic semiconductors: $\text{SrM}_{2\pm x}\text{Ru}_{4\pm x}\text{O}_{11}$ ($M = \text{Fe}, \text{Co}$)", L. Shlyk, L. E. De Long, S. Kryukov, B. Schüpp-Niewa and R. Niewa, *J. Appl. Phys.* **103**, 07D112 (2008).
2. "Observation of Strong Spin Valve Effect in Bulk $\text{Ca}_3(\text{Ru}_{1-x}\text{Cr}_x)_2\text{O}_7$ ", G. Cao, V. Durairaj, S. Chikara, L. E. De Long and P. Schlottmann, *Phys. Rev. Lett.* **100**, 016604, 159902 (Erratum), (2008). (This paper was selected for January 21, 2008 issue of *Virtual Journal of Nanoscale Science & Technology* (American Institute of Physics and the American Physical Society))
3. "High Temperature Ferromagnetism and Tunable Semiconductivity of $(\text{Ba},\text{Sr})\text{M}_{2\pm x}\text{Ru}_{4\pm x}\text{O}_{11}$ ($M = \text{Fe}, \text{Co}$): A New Paradigm for Spintronics", L. Shlyk, S. Kryukov, B. Schüpp-Niewa, R. Niewa and L. E. De Long, *Adv. Mat.* **20**, 1315-1320 (2008).

4. “Horizontally Aligned Single Array of Co Nanowires Fabricated in One-Dimensional Nanopore Array Template”, Rui Zhu, Hongguo Zhang, Zhi Chen, Sergiy Kryukov and Lance De Long, *Electrochem. Solid-State Lett.* **11**, K57 (2008).
5. “A Novel Class of High- T_C Ferromagnetic Semiconductors”, L. V. Shlyk, S. A. Kryukov, L. E. De Long, B. Schupp-Niewa, R. Niewa, J. W. Lynn, Qing Huang, E. Arenholz and C. Piamonteze, in: *Proceedings of the 17th Biennial University Government Industry Micro-Nano Symposium*, Louisville, KY, July 13-16, 2008 (IEEE Conference eXpress Publishing, Piscataway, NJ, 2008), pp. 142-147.
6. “Non-Fermi-Liquid Behavior in Single-Crystal CaRuO_3 : Comparison to Ferromagnetic SrRuO_3 ”, G. Cao, O. Korneta, S. Chikara, L. E. De Long and P. Schlottmann, *Solid State Commun.* **148**, 305-309 (2008).
7. “Giant magnetoelectric effect in the $J_{\text{eff}} = \frac{1}{2}$ Mott insulator Sr_2IrO_4 ”, S. Chikara, O. Korneta, W. P. Crummett, L. E. De Long, P. Schlottmann and G. Cao, *Phys. Rev. B* **80**, 140407(R) (2009).
8. “New Materials for Spintronics”, L. E. De Long, L. Shlyk and Gang Cao, *Proceedings of the International Conference on Electromagnetics in Advanced Applications 2009*, pp. 929-932, *IEEE Xplore*, 978-1-4244-3386-5/09.
9. “Pressure-induced Insulating State in Single-crystal $\text{Ba}_{1-x}\text{Gd}_x\text{IrO}_3$ ”, O. Korneta, S. Chikara, L.E. DeLong, P. Schlottmann and G. Cao, *Phys. Rev. B* **81**, 045101 (2009).
10. “Crystal Structures of Ternary Ruthenium Ferrites $\text{SrM}_{2\pm x}\text{Ru}_{4\pm x}\text{O}_{11}$ with $M = \text{Fe, Co}$ and Magnetic and Transport Properties of Al-doped Single Crystals”, Rainer Niewa, Larysa Shlyk, Barbara Schüpp-Niewa and Lance E. De Long, *Z. Anorg. Allg. Chem.* **636**, 331-336 (2010).
11. “Successive magnetic transitions of the kagome plane and field-driven chirality in single-crystal $\text{BaMn}_{2.49}\text{Ru}_{3.5}\text{O}_{11}$ ”, L. Shlyk, S. Parkin and L. E. De Long, *Phys. Rev. B* **81**, 014413 (2010).
12. “Giant magnetoelectric effect in the $J_{\text{eff}} = \frac{1}{2}$ Mott insulator Sr_2IrO_4 ”, S. Chikara, O. Korneta, W. P. Crummett, L. E. De Long, P. Schlottmann and G. Cao, *J. Appl. Phys.* **107**, 09D910 (2010).
13. “ $\text{Ca}_3(\text{Ru}_{1-x}\text{Cr}_x)_2\text{O}_7$: A new paradigm for spin valves”, G. Cao, O. Korneta, S. Chikara, L. E. De Long and P. Schlottmann, *J. Appl. Phys.* **107**, 09D718 (2010).
14. “Complex magnetic order and spin chirality on the Kagomé lattices of $\text{BaMn}_{2.49}\text{Ru}_{3.51}\text{O}_{11}$ and $\text{BaFe}_{3.26}\text{Ti}_{2.74}\text{O}_{11}$ ”, L. Shlyk, S. Parkin and L. E. De Long, *J. Appl. Phys.* **107**, 09E109 (2010).
15. “Magnetic Structure, Magnetization and Magnetotransport Properties of $(\text{Ba,Sr})\text{M}_{2\pm x}\text{T}_{4\pm x}\text{O}_{11}$ ($M = \text{Fe, Co}$; $T = \text{Ru, Ti}$)”, L. Shlyk, B.G. Ueland, J.W. Lynn, Q. Huang, L.E. De Long and S. Parkin, *Phys. Rev. B* **81**, 184415 (2010).
16. “Staircase magnetization anomalies in superconducting Pb/Au bilayer films patterned with antidot lattices”, L. E. De Long, S. A. Kryukov, V. V. Metlushko, M. J. A. Stoutimore and D. J. Van Harlingen, *Physica C* **470**, 739-743 (2010).
17. “The Promise of Strong Spin-Orbit Coupling: Novel Materials with Novel Properties for Novel Devices” (Invited), L. E. De Long, L. Shlyk, Gang Cao and R. Niewa, *Proceedings of the International Conference on Electromagnetics in Advanced Applications 2010*, pp. 929-932, *IEEE Xplore*, 978-1-4244-3386-5/09.
18. “Electron-Doped $\text{Sr}_2\text{IrO}_{4-\delta}$ ($0 \leq \delta \leq 0.04$): Evolution of a Disordered $J_{\text{eff}} = \frac{1}{2}$ Mott Insulator into an Exotic Metallic State”, O. B. Korneta, Tongfei Qi, S. Chikara, S. Parkin, L. E. De Long, P. Schlottmann and G. Cao, *Phys. Rev. B* **82**, 115117 (2010).
19. “Anomalous Hall Effect in High Temperature Ferrimagnetic Semiconductors $\text{BaFe}_{2\pm x}\text{Ru}_{4\pm x}\text{O}_{11}$ ”, L. Shlyk, R. Niewa and L. E. De Long, *Phys. Rev. B* **82**, 134432 (2010).
20. “Negative Volume Thermal Expansion via Orbital and Magnetic Orders in $\text{Ca}_2\text{Ru}_{1-x}\text{Cr}_x\text{O}_4$ ($0 < x < 0.13$)”, T. F. Qi, O. B. Korneta, S. Parkin, L. E. De Long and G. Cao, *Phys. Rev. Lett.* **105**, 177203 (2010).

KEY WORDS: transition metal oxides, ferromagnetic semiconductors, magnetoelectrics, multiferroics, spin injection, anomalous Hall effect, Berry phase, ferromagnetic resonance, magnetic nanostructures, magnetic multilayers, magnetic frustration, spin chirality

Exploration of Artificial Frustrated Magnets

Principal Investigators: Peter Schiffer (pes12@psu.edu), Vincent Crespi (vhc2@psu.edu), and Nitin Samarth (nxs16@psu.edu)

Institution: Pennsylvania State University, University Park, PA

Project Scope

This program encompasses experimental and theoretical studies of lithographically fabricated arrays of nanometer-scale single-domain ferromagnetic islands in which the array geometry results in frustration of the magnetostatic interactions between the islands. Such geometrical frustration can lead to multiple energetically equivalent configurations for the magnetic moments of the islands and a variety of associated novel collective behavior. These systems are analogs to a class of magnetic materials in which the lattice geometry frustrates interactions between individual atomic moments, and in which a wide range of novel physical phenomena have been recently observed. The advantage to studying lithographically fabricated samples is that they are both designable and resolvable: i.e., we can control all aspects of the array geometry, and we can also observe how individual elements of the arrays behave. In previous work, we have demonstrated that we can fabricate and probe frustrated magnet arrays, including some geometries that are directly analogous to the “spin ice” materials. We have designed frustrated lattices, controlled the strength of interactions by changing the spacing of the islands, and demonstrated that the island magnetic moment orientation is controlled by the inter-island interactions. We are investigating a range of frustrated lattice geometries in both small clusters and extensive arrays of islands, thus accessing a range of different types of frustration. We are also examining how these systems respond to disorder and the effects of both static and dynamic external magnetic fields. In related efforts, we will model the interplay of kinetics and effective thermodynamics in the manifolds of degenerate states of the island moment configurations.

Recent Progress

The first year of this grant has included the continuation and completion of some projects that had been initiated before the DOE support began, as well as the initiation of new projects. Each of these projects is described below.

The role of collective interactions in nanomagnet assemblies: We have studied the moment correlations within triangular lattice arrays of single-domain co-aligned nanoscale ferromagnetic islands. Independent variation of lattice spacing along and perpendicular to the island axis tunes the magnetostatic interactions between islands through a broad range of relative strengths. For certain lattice parameters, the sign of the correlations between near-neighbor island moments is opposite to that favored by

the pair-wise interaction. This finding, supported by analysis of the total correlation in terms of direct and convoluted indirect contributions (a modified Ornstein-Zernike equations), indicates that indirect interactions and/or those mediated by further neighbors can be dominant, with implications for the wide range of systems composed of interacting nanomagnets.

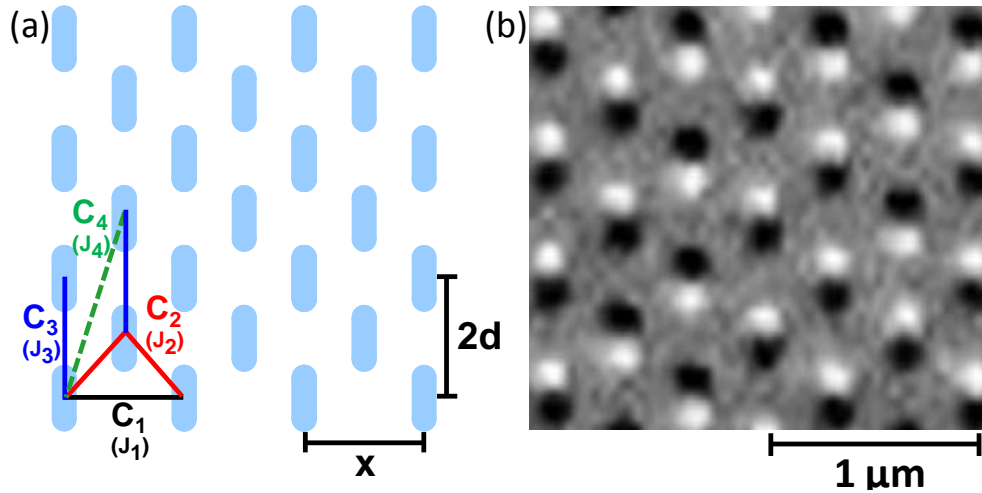


Figure 1 (a) Schematic of triangular lattice arrays of single domain nanomagnets with frustrated magnetostatic interactions. The near-neighbor pair types are labeled C1, C2, C3, and C4, and the convolution of all four pairs can affect moment correlations. (b) MFM image of a section of one triangular lattice array ($x = 680 \text{ nm}$, $d/x = 0.4$). Black and white halves represent the north and south poles of each ferromagnetic island. [S. Zhang et al., preprint]

Magneto-optical Kerr effect studies of square artificial spin ice: We have performed a magneto-optical Kerr effect study of the collective magnetic response of artificial square spin ice. We find that the anisotropic inter-island interactions lead to a non-monotonic angular dependence of the array coercive field, and comparisons with micromagnetic simulations indicate that the two perpendicular sublattices exhibit distinct responses to changing magnetic field that drive the magnetization reversal process. Furthermore, such comparisons demonstrate that island shape disorder plays a hitherto unrecognized but essential role in the collective behavior of these systems. This technique holds promise for a range of extended studies of artificial frustrated magnets, including frequency-dependent ac measurements.

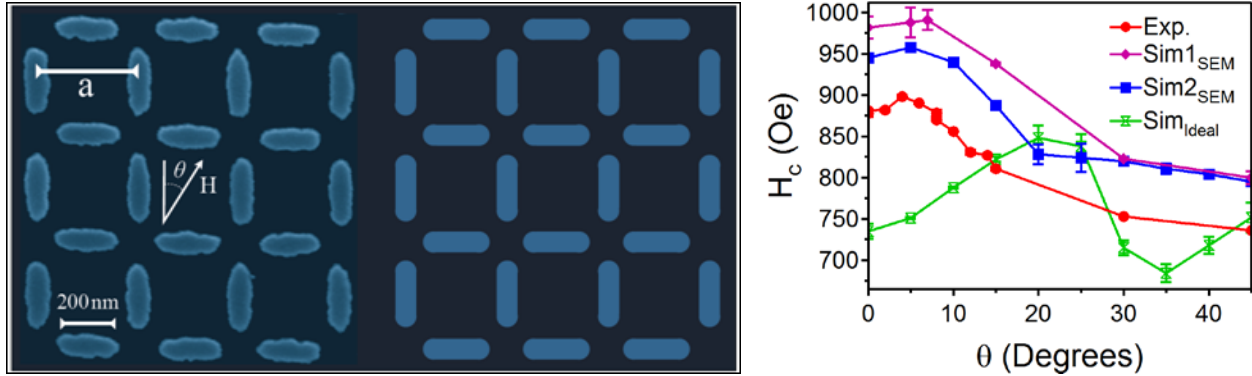


Figure 2 (left frame) An SEM image of a square array with 320 nm lattice spacing and an equivalent array of 24 ideal stadium-shaped islands. (right frame) Coercivity as a function of angle for a square array with 320 nm lattice spacing. Simulations were run on a 24-island cluster similar to that of Fig. 1 for both ideal (green) and SEM-derived (blue, purple) island shapes [K. Kohli et al., preprint].

Magnetization states and switching in gapped ferromagnetic nanorings: We had previously examined small clusters of ferromagnetic islands with arrangements mimicking those of artificial square ice. As an extension of those studies, we also examined permalloy nanorings that are lithographically fabricated with gaps that break the symmetry of the ring while retaining the vortex ground state. We investigated the magnetic properties of these gapped nanorings with both micromagnetic simulations and magnetic force microscopy (MFM), and we find that the ring edge characteristics (i.e., edge profile and gap shape) are critical in determining the magnetization switching field. We demonstrate that the vortex chirality can be set in these structures with an in-plane magnetic field, and easily probed by MFM due to the field within the gap, suggesting such rings for possible applications in storage technologies.

Future Plans:

Future plans for this research program include a number of different thrusts, in particular the development of MOKE microscopy for close imaging of the arrays with better time resolution than MFM allows. We also plan to study a range of artificial frustrated magnets formed from different materials. For example, we will explore perpendicular anisotropy materials: while artificial frustrated magnets have previously been formed from materials with in-plane moments, we plan studies of systems composed of circular islands of perpendicular anisotropy materials. These systems will have the advantage that the inter-island interactions are isotropic, and that they thus are more amenable to simple theoretical models. We also plan studies of arrays that have intentionally introduced disorder, including disorder in the location of the islands and structural disorder in the islands themselves.

Poster Sessions

POSTER SESSION I

Wednesday, August 10, 2011

1. Experimental Study of Correlations and Induced Superconductivity in Graphene
Eva Andrei, Rutgers
2. Probing Nanocrystal Electronic Structure and Dynamics in the Limit of Single Nanocrystals
Moungi Bawendi, MIT
3. Magnetic and Superconducting Properties of Materials Studied by the ^{99}Ru , ^{189}Os , ^{119}Sn , ^{57}Fe and ^{191}Ir Mössbauer Effects in External Magnetic Fields
Michael DeMarco, Buffalo State
4. Advanced Techniques for the Characterization of Novel Magnetic and Strongly Correlated Materials
Peter Fischer and Jeff Kortright, LBNL
5. Linear and Nonlinear Optical Properties of Metal Nanocomposite Materials
Richard Haglund, Vanderbilt
6. High Resolution Photoemission Studies of Strongly Correlated Materials
Chris Homes, BNL
7. Emerging Materials
B.J. Kim, ANL
8. Ballistic Acceleration Phase of a Supercurrent
Milind Kunchur, South Carolina
9. Transport Studies of Quantum Magnetism: Physics and Methods
Minhyea Lee, Colorado
10. Studies of Interband Modes and Fermi Surface Features in Very Clean MgB_2 Films
Qi Li, Penn State
11. Electronic and Optical Processes in Novel Semiconductors for Energy Applications
Angelo Mascarenhas, NREL
12. Correlation Effects in Graphene
Nadya Mason, Illinois
13. Investigating the Material Dependences in the Casimir Force
Umar Mohideen, UC Riverside

14. Nanostructure Studies of Strongly Correlated Materials
Doug Natelson, Rice
15. Domain Wall Functionality in Complex Oxides
Joe Orenstein, LBNL
16. Thermopower Near the 2D Metal-Insulator Transition
Myriam Sarachik, CCNY
17. Photonic Systems
Joe Shinar, Ames Lab
18. Indirect Excitons in Coupled Quantum Wells: New Studies with Dark Excitons
David Snoke, Pittsburgh
19. Anisotropy of the Normal and Superconducting States in Iron Pnictide Superconductors
Makariy Tanatar, Ames Lab
20. Simulating Strongly Correlated Electrons with a Strongly Interacting Fermi Gas
John Thomas, NC State
21. A Synergistic Approach to the Development of New Hydrogen Storage Materials
Part II: Nanostructured Materials
Jeff Urban, LBNL
22. Fabrication of Graphene for Electron Flow Imaging
Robert Westervelt, Harvard

POSTER SESSION II

Thursday, August 11, 2011

1. Quantum Transport in Magnetic and Non-Magnetic 2D Correlated Insulators
Philip Adams, LSU
2. Developing Functionality in Quantum Dots
Jonathan Bird, Univ. of Buffalo
3. ARPES Studies of Transition Metal Substituted BaFe_2As_2
Paul Canfield, Ames Lab
4. Integrated Growth and Ultra-Low Temperature Transport Study of the 2nd Landau Level of the Two-Dimensional Electron Gas
Gabor Csathy, Purdue
5. Experiments on Quantum Hall Topological Phases in Ultra Low Temperatures
Rui-Rui Du, Rice
6. Science at 100 Tesla
Neil Harrison, LANL
7. Optical and Electrical Properties of III-Nitrides and Related Materials
Hongxing Jiang, Texas Tech
8. Interfaces in Epitaxial Complex Oxides
Ho Nyung Lee
Zac Ward, ORNL
9. Spintronic Bandgap Materials
Jeremy Levy, Pittsburgh
10. Emergent Behavior of Magnet-Superconductor Hybrids
Igor Lyuksyutov, Texas A&M
11. Quantum Electronic Phenomena and Structures
Wei Pan, SNL
12. Magnetic Nanostructures and Spintronic Materials
Michael Pechan, Miami-Ohio
13. Insights from Newly Discovered Heavy Fermion Superconductors
Filip Ronning, LANL

14. Exploring Origins of Enhanced Thermoelectric Properties in Complex Materials: Anharmonic Phonons, Strong Electron-Phonon Coupling and High Dielectric Constant
Brian Sales, ORNL
15. Infrared Optical Study of Graphene in High Magnetic Fields
Dmitry Smirnov, NHMFL - FSU
16. Probing the Origins of Conductivity Transitions in Correlated Solids: Experimental Studies of Electronic Structure in Vanadium Oxides
Kevin Smith, Boston Univ.
17. Investigations of Electron Correlation in Complex Systems
Jim Tobin, LLNL
18. Spatial Extent of Near-Band Edge Modification due to Lattice Disorder
Norman Tolk, Vanderbilt
19. Novel Nanoscale Morphologies and Atomistic Processes Control on Surfaces
Michael Tringides, Ames Lab
20. Phase Diagram for Iron-Chalcogenide Superconducting Films
Barry Wells, Connecticut
21. Synchronization and Chaos in Intrinsic Josephson Junctions
Ulrich Welp, ANL

Poster Abstracts

Quantum Transport in Magnetic and Non-Magnetic 2D Correlated Insulators

Philip W. Adams
Louisiana State University
adams@phys.lsu.edu

1. Project Scope

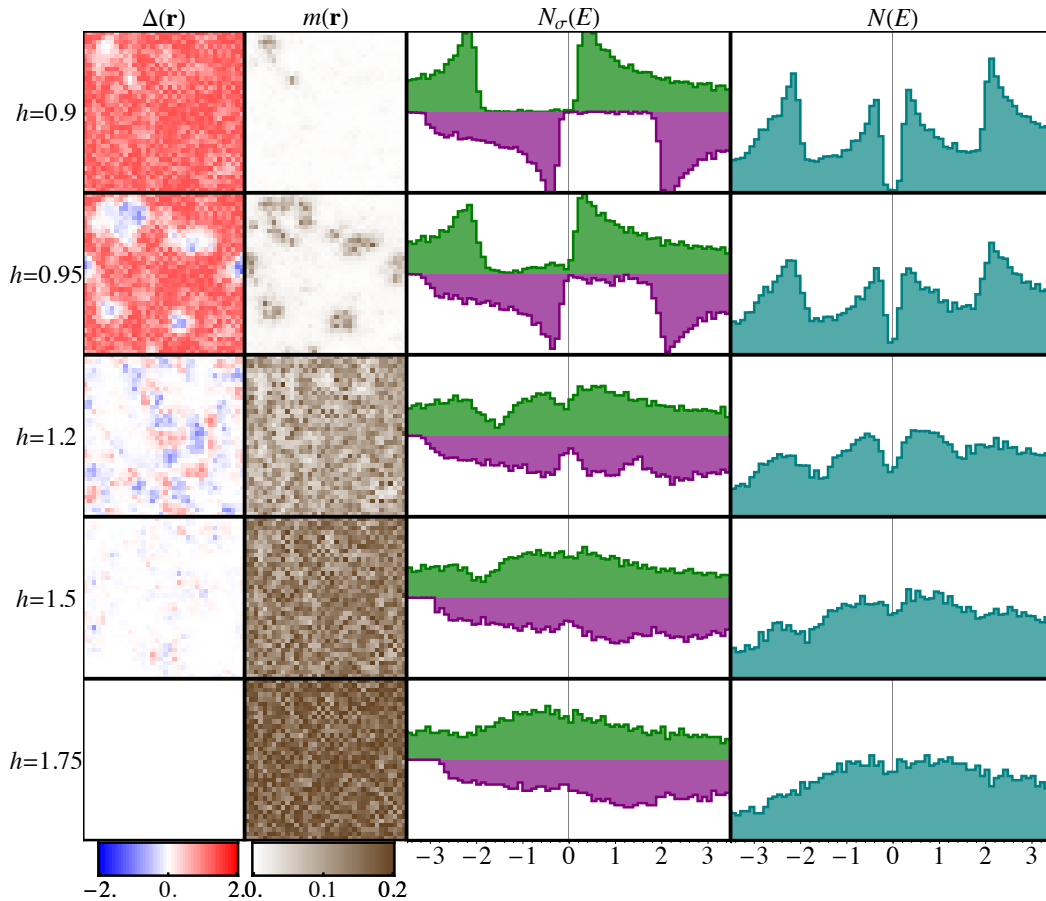
Our experimental research program is focused on the magneto-transport, non-equilibrium relaxation, and spin-resolved density-of-states properties of disordered two dimensional electron gases. In particular, we are studying spin-resolved correlation effects in three different classes of systems. The first is non-magnetic ultra-thin Be films that are produced by e-beam deposition onto liquid nitrogen cooled glass substrates. Beryllium forms non-granular films that are homogeneously disordered on length scales greater than ~ 1 nm. The films exhibit a multifold negative magneto-resistance deep in the correlated insulator phase that is associated with a field suppression of the Coulomb gap. Interestingly, the high-field resistance is asymptotic to the quantum resistance h/e^2 , suggesting the emergence of a novel *quantum metal* ground state. We are particularly interested in the relationship between the Coulomb gap, quantum metallicity, and glassy dynamics in very high resistance films. The second class of systems is ultra-thin CR_3 magnetic films ($R = \text{Ni, Co, Fe}$) formed via e-beam deposition from arc-melted buttons of these metastable, covalently bonded ferromagnetic compounds. We have recently shown that CNi_3 forms dense, amorphous, homogeneously disordered films, with an extremely low thickness threshold of electrical continuity. In this respect they are similar to Be films, but with the added property of being magnetic. Consequently, in addition to following the magneto-transport and tunneling properties deep into the correlated insulator regime, we can also follow the magnetic behavior via the anomalous Hall effect and spin polarized tunneling. Finally we are investigating proximity-induced exchange fields in EuS-Al and EuS-Be bilayers, where EuS is a ferromagnetic semiconductor. The bilayer geometry allows us to produce a tunable exchange field in the Be and Al films. The evolution of such exchange fields and their influence on the spin properties of the films are being studied as a function of disorder.

2. Recent Progress

Over the past 18 months we have been working on two separate but related projects. The first is a systematic study of the exchange field produced in superconducting Al films when the films are deposited onto a thin ferromagnetic insulator. In particular, we are using spin-resolved electron tunneling to study the exchange field in the Al component of EuS/Al bilayers, in both the superconducting and normal-state phases of the Al. Contrary to expectation, we have found that the exchange field, H_{ex} , is a non-linear function of applied field, even in applied fields that are well beyond the EuS coercive field. Ours are the first experiments to directly probe this, and it now seems pretty clear that the interface mechanism that produces the exchange field is not well understood. This work has been recently reported in *Phys. Rev. Lett.* **106**, 247001 (2011).

The second project arose out of ongoing discussions with Nandini Trivedi's theory group at Ohio St. regarding the nature of the Zeeman-mediated critical field transition in a superconductor in which spin is a good quantum number. In particular we have used tunneling density of states measurements of disordered superconducting (SC) Al films in high Zeeman fields to show that a significant population of sub-gap states emerges near the critical field transition which cannot be explained by standard BCS theory. We provide a natural explanation

of these excess states in terms of a novel disordered Larkin-Ovchinnikov (d-LO) phase that is related to the FFLO state that was conjectured more than 40 years ago. It is widely believed that the finite momentum pairing that underlies the FFLO phase is completely destroyed by even small levels of disorder. Our work shows that this is, in fact, not the case. Although the long range order of the FFLO phase is destroyed by disorder, local patches of the phase remain and produce a significant effect on the density of states. The d-LO state is characterized by SC puddles separated from insulating regions. Within a SC puddle, the order parameter modulates between positive and negative values forming domain walls. The excess magnetization carried by the Andreev bound states resides primarily in these domain walls and gives rise to an anomalous low energy quasiparticle population. A summary of Prof. Nandini's calculations is presented in the figure above, where h represents the applied field. The Zeeman critical field is near $h = 1$. A manuscript reporting these results has recently been accepted for publication in *Physical Review Letters*.



The first two columns show spatial maps of the local pairing amplitude Δ and the magnetization m . The last two columns show the densities of states (DoS's) of up and down electrons $N_{\sigma}(E)$ as well as the total density of states $N(E)$. For intermediate fields the system exhibits disordered Larkin-Ovchinnikov states with domain walls at which m is finite and the sign of $\Delta(r)$ varies in space (as indicated by the red and blue patches). The appearance of such states is associated with the filling-in of the gap in the DoS.

3. Future Plans

Dr. Tijiang Liu joined my group as a postdoc on June 1st 2011. Dr. Liu just has recently completed his PhD at Tulane University under Prof. Zhiqiang Mao. We plan to pursue the exchange field studies by trying to modulate the strength of exchange field via a gating strategy. Since the exchange field arises from an interface coupling between the ferromagnet and the superconductor, we hope to be able to modify the strength of the coupling by applying an electric field normal to the interface. If successful, we could then control the exchange field with an applied voltage and hopefully produce a superconducting switch or perhaps a voltage-controlled spin polarized electron source.

In order to get a complete characterization of the d-LO phase in Al films, we will need to make a systematic study of the tunneling conductance as a function of film resistance. We also need a more complete data set on the temperature dependence of zero-bias conductance.

In addition, we will also continue the electron glass studies of high resistance Be films. We plan to measure the temperature dependence of the electron glass dynamics, which has never been done. We will also investigate the evolution of the dynamics as a function of applied field. We are particularly interested in the behavior very high resistance films in pure Zeeman fields.

4. Publications (2008 - 2011)

1. “Self-Assembly of Multiwall Carbon Nanotubes From Quench-Condensed CNi_3 Films”, D.P. Young, A.B. Karki, **P.W. Adams**, J.N. Ngunjiri, J.C. Garno, H. Zhu, B. Wei, D. Moldovan, *J. App. Phys.* **103**, 053503 (2008).
2. “Critical Current Behavior of Superconducting MoN and Mo_3Sb_7 Microfibers”, A.B. Karki, D.P. Young, **P.W. Adams**, E.K. Okudzeto, and J.Y. Chan, *Phys. Rev. B* **77**, 212503 (2008).
3. “Fermi Liquid Effects in the Gapless Phase of Marginally Thin Superconducting Films”, G. Catelani, X.S. Wu, and **P.W. Adams**, *Phys. Rev. B* **78**, 104515 (2008).
4. “Spin-Orbit Scattering and Quantum Metallicity in Ultra-Thin Be Films”, Y.M. Xiong, A.B. Karki, D.P. Young, and **P. W. Adams**, *Phys. Rev. B* **79**, 020510 (2009).(RC)
5. “Superconducting and Magnetotransport Properties of ZnNNi_3 Microfibers and Films”, A.B. Karki, D.P. Young, Y.M. Xiong, and **P.W. Adams**, *Phys. Rev. B* **79**, 212508 (2009).
6. “The Pairing Resonance as a Normal-State Spin Probe in Ultra-Thin Superconducting Al Films”, G. Catelani, Y.M. Xiong, X.S. Wu, and **P.W. Adams**, *Phys. Rev B* **80**, 054512 (2009). (*Editor’s Choice*)
7. “Measurement of Conduction Electron Polarization Via the Pairing Resonance”, Y.M. Xiong, **P.W. Adams**, and G. Catelani, *Phys. Rev. Lett.* **103**, 067009 (2009).
8. “Temperature dependence of resistivity and Hall-coefficient in a strongly disordered metal: NbN”, Madhavi Chand, Archana Mishra, Y. M. Xiong, Anand Kamlapure, S. P. Chockalingam, John Jesudasan, Vivas Bagwe, Mintu Mondal, **P. W. Adams**, Vikram Tripathi, and Pratap Raychaudhuri, *Phys. Rev. B* **80**, 134514 (2009).
9. “Saturation of the Anomalous Hall Effect in Critically Disordered Ultra-thin CNi_3 Films”, Y.M. Xiong, **P.W. Adams**, and G. Catelani, *Phys. Rev. Lett.* **104**, 076806 (2010).
10. “Crystal Growth, Structure, and Physical Properties of $\text{Ln}(\text{Cu},\text{Al})_{12}$ ($\text{Ln} = \text{Y}, \text{Ce}, \text{Pr}, \text{Sm}$, and Yb) and $\text{Ln}(\text{Cu},\text{Ga})_{12}$ ($\text{Ln} = \text{Y}, \text{Gd-Er}$, and Yb), B.L. Drake, J.Y. Cho, C. Capan, K.

- Kuga, Y.M. Xiong, A.B. Karki, Y. Nambu, S. Nakatsuji, **P.W. Adams**, D.P. Young, and J.Y. Chan, *J. Phys.: Cond. Mat.* **22**, 066001 (2010).
11. “Structure and physical properties of the noncentrosymmetric superconductor $\text{Mo}_3\text{Al}_2\text{C}$ ”, A.B. Karki, Y.M. Xiong, I. Vekhter, D. Browne, **P.W. Adams**, D.P. Young, K.R. Thomas, J.Y. Chan, H. Kim, and R. Prozorov, *Phys. Rev. B* **82**, 064512 (2010). (*Editor’s Choice*).
 12. “Crystal growth and properties of $\text{Ln}_2\text{Ag}(1-x)\text{Ga}(10-y)$ ($\text{Ln}=\text{La}, \text{Ce}$), a disordered variant of the $\text{Ce}_2\text{NiGa}_{10}$ -structure type”, M.C. Menard, Y.M. Xiong, A.B. Karki, B.L. Drake, **P.W. Adams**, F.R. Fronczek, D.P. Young, J.Y. Chan, *J. Solid State Chem.* **183**, 1935 (2010).
 13. “Crystal growth, structure, and physical properties of $\text{Ln}(\text{Ag}, \text{Al}, \text{Si})_2$ ($\text{Ln} = \text{Ce}$ and Gd)”, B.L. Drake, M.J. Kangas, C. Capan, N. Haldolaarachchige, Y. Xiong, **P.W. Adams**, D.P. Young, and J.Y. Chan, *J. Phys.: Cond. Mat.* **22**, 426002 (2010).
 14. “Intrinsic Electron Glassiness in Strongly Localized Be Films”, Z. Ovadyahu, Y.M. Xiong, and **P.W. Adams**, *Phys. Rev. B* **82**, 195404 (2010).
 15. “Magnetotransport Properties of Thin CFe_3 Films”, J. C. Prestigiacomo, K. L. Lusker, Y.M. Xiong, S. Stadler, A.B. Karki, D.P. Young, J. C. Garno, and **P. W. Adams**, *Thin Solid Films* **519**, 2362 (2011).
 16. “Physical Properties of the Non-centrosymmetric Superconductor $\text{Nb}_{0.18}\text{Re}_{0.82}$ ”, A.B. Karki, Y.M. Xiong, N. Haldolaarachchige, S. Stadler, I. Vekhter, **P.W. Adams**, D.P. Young, W.A. Phelan, and J.Y. Chan, *Phys. Rev. B* **83**, 144525 (2011).
 17. “Dimensional Crossover in the Electrical and Magnetic Properties of the Layered LaSb_2 Superconductor Under Pressure: The Role of Phase Fluctuations”, S. Guo, D.P. Young, **P.W. Adams**, X.S. Wu, J.Y. Chan, G.T. McCandless, and J.F. DiTusa, *Phys. Rev. B* **83**, 174520 (2011).
 18. “Effect of Partial Substitution of Ni by Co on the Magnetic and Magnetocaloric Properties of $\text{Ni}_{50}\text{Mn}_{35}\text{In}_{15}$ Heusler Alloy”, A.K. Pathak, I. Dubenko, Y.M. Xiong, **P.W. Adams**, S. Stadler, and N. Ali, *J. App. Phys.* **109**, 07A916 (2011).
 19. “Spin-Resolved Tunneling Studies of the Exchange Field in EuS/Al Bilayers”, Y.M. Xiong, S. Stadler, **P.W. Adams**, and G. Catelani, *Phys. Rev. Lett.* **106**, 247001 (2011).
 20. “Origin of Excess Low-Energy States in a Disordered Superconductor in a Zeeman Field”, Y. L. Loh, N. Trivedi, Y. M. Xiong, **P. W. Adams**, and G. Catelani, *Phys. Rev. Lett.*, in press.

Experimental study of correlations and induced superconductivity in graphene
PI: Eva Y. Andrei (eandrei@physics.rutgers.edu)

Rutgers University

Scope

Graphene, a two-dimensional crystal consisting of a single atomic plane of carbon, can give access to extraordinary electronic properties reflecting charge carriers that mimic ultrarelativistic elementary particles. Beyond providing a platform that can extend the range and scope of the core capabilities in the electronic and computer industries, these crystals constitute a vast playing field for unconventional physical phenomena. The research will explore the emergence of new physical phenomena and the feasibility of devices based on the unique charge carriers in graphene. It will address basic questions about the properties of graphene and about the nature of its charge carriers: what is the role of interactions; can one observe new phases in a magnetic field including fractional quantum Hall effect and broken symmetry phases; what is the interplay between massless Dirac fermions and Cooper pairs at the boundary between graphene and a superconductor. Based on these findings, we will investigate the feasibility of devices to generate charge neutral spin currents in superconductor/graphene/superconductor junctions. The experiments will be carried out on graphene samples that are minimally disturbed by substrates. We will study either suspended samples (from leads or as a membrane) or decoupled graphene on conducting substrates and will employ a combination of scanning tunneling microscopy and spectroscopy, atomic force microscopy and magneto-transport.

Recent Progress

We have developed methods to decouple graphene from environmental disturbances and devised non-invasive experimental probes which allowed us to access the intrinsic electronic properties of graphene. We developed a technique to fabricate devices consisting of suspended single layer graphene which allowed access to electronic properties controlled by the Dirac point and opened the door to a new generation of experiments. In these devices we have demonstrated mobilities approaching $10^6 \text{ cm}^2/\text{Vs}$ for densities below $5 \times 10^9 \text{ cm}^{-2}$, a range unattainable in non-suspended-graphene or in 2d electron systems in semiconductors. This allowed us to observe ballistic transport on micron length scales; to measure new quantum Hall plateaus associated with lifting the spin and valley degeneracy; to observe electron-electron correlations through the appearance of a fractional quantum Hall effect. We have found that it is possible to decouple a graphene sample from substrate induced perturbations not only by suspending it from the leads but also by using a non-intrusive substrate such as graphite. By using scanning tunneling spectroscopy this allowed us to directly measure the intrinsic density of states of graphene, the anomalous sequence of Landau levels in the presence of a magnetic field, effects of electron-electron and electron-phonon interactions. In addition we have shown that it is possible to alter and control the properties of graphene by manipulating the orientation between overlapping graphene layers.

- **Observation of the fractional quantum Hall effect and insulating phase in suspended graphene.**

In search of interaction effects and manifestations of correlations between the relativistic charge carriers in graphene we employed suspended samples to decouple the charge carriers from environmental perturbations such as substrate induced potential fluctuations which are typically too strong to allow the observation of the much weaker interaction effects. This led to the discovery of strong magnetically induced correlations manifest as a fractional quantum Hall effect at filling factor of $\nu=1/3$. This result demonstrated that interactions play an important role in the physics of ultrarelativistic charge carriers.

•**Two terminal technique for measuring the quantum Hall effect in mesoscopic samples.** The failure to observe the FQHE in graphene samples long after the first observation of the integer quantum Hall effect in this system, even in suspended samples, where the transport is ballistic on micron size length scales, led to speculation that interactions between the relativistic electrons in graphene are absent or suppressed. Our work has demonstrated that the absence of the FQHE in graphene was not the reflection of an intrinsic property of relativistic charge carriers but rather the result of an invasive measurement technique. While the standard Hall bar measurement geometry is the optimal configuration for extracting information about energy gaps and for eliminating the lead resistance in a Hall measurements of 2-dimensional electron system, it is not suitable for measuring the quantum Hall effect in mesoscopic samples. The reason is the formation of hot-spots at the diagonal corners of the sample where the equipotential lines accumulate and dissipation takes places. If the voltage leads are placed within these hot-spot regions the Hall voltage is partially or fully shorted out. We were able to directly demonstrated this fact by using large graphene samples on a Si/SiO₂ substrate with a multi-lead configuration. When the voltage leads were kept outside the hot spots the full Hall voltage was observed. However when the voltage leads were placed in the hot spot region the Hall voltage was shorted out. Using numerical simulations we have shown that on “good” quantum Hall plateaus where the longitudinal resistance is vanishingly small, a two-terminal resistance measurements gives the correct value of the quantum Hall resistance. This is the key element which made it possible for us to measure the quantum Hall effect in suspended graphene samples and in particular to observe the fractional Quantum Hall effect. Together with our theoretical collaborators we have shown that by using conformal mapping it is possible to extract the longitudinal and transverse voltage components from a two terminal measurement. This enabled us to obtain the activation energies for the $\nu=1/3$ fractional quantum Hall plateau and for the $\nu=1$ plateau.

• **Observation of Van Hove singularities in twisted graphene layers.**

Instabilities in the electronic density at the crossing of the Fermi energy with a Van Hove singularity often lead to novel phases of matter such as superconductivity, magnetism or density waves. However in most materials this condition is difficult to attain. In the case of graphene, although the band structure does have a Van Hove singularity, its energy is too far from the Fermi energy to reach by standard doping techniques. We demonstrated that in twisted graphene layers it is possible to induce in a controlled way Van Hove singularities in the density of states and to tune their position with respect to the Fermi energy by controlling the angle of rotation. Using scanning tunneling spectroscopy we showed that the interlayer rotation in a twisted graphene bilayer produces sharp Van Hove singularity peaks in the density of states whose position is controlled by the angle of rotation. At the same time we observed a strong spatial modulation in the electronic density suggesting an impending Fermi surface instability.

Future Plans

We will use transport and STM to explore the interplay between relativistic electrons in graphene and superconducting correlations. We will focus on electrical and spin transport across a superconducting/graphene (SG) interface, specular Andreev reflections, and explore the feasibility of generating pure spin currents.

Superconductor /Graphene (SG) junctions and spin transport. The search into ways of using the spin degree of freedom in the design of electronic devices, is motivated by the prospect of substantially enhanced performance and efficiency. In this respect, graphene is a promising material due to the low intrinsic spin orbit interaction and the low hyperfine interaction of the electron spins with the carbon nuclei which make it possible to maintain spin coherence over long distances. To explore the potential

of graphene based spintronics we will fabricate and characterize superconductor-graphene-superconductor (SGS) junctions. The transport through superconducting/normal (SN) interfaces is mediated by Andreev reflections. In undoped graphene, when the Fermi energy coincides with the Dirac point, Andreev reflections are expected to be specular at all excitation energies. Specular Andreev reflection (SAR) does not exist in usual metals, where there is an excitation gap between conduction and valence band. Based on the specular nature of the Andreev reflections in graphene it is expected that SGS junctions will efficiently filter the charge out of a current of spin-polarized quasiparticles, leaving behind a pure spin current.

- **SGS junctions.**

To study the interplay between superconductivity and the relativistic electrons in graphene we fabricated SGS junctions on Si/SiO₂ with Al superconducting electrodes. We found that in these junctions it is quite easy to observe proximity induced superconducting state with gate tunable critical currents. Transparent SG interfaces were routinely achieved as seen by the presence of multiple Andreev reflections. However the transport characteristics were clearly not those expected for SAR in a ballistic Josephson junction. Instead, we were able to show that the gate dependence of the critical current, I_c and of the Andreev conductance, are well described by a model of diffusive junctions. The absence of SAR in these SGS junctions is attributed to smearing of the Dirac point due to the substrate induced random potential. If the smearing exceeds the superconducting gap the Andreev reflections are no longer specular and the junction characteristics become indistinguishable from those of standard SNS junctions. Indeed, for SGS junctions on Si/SiO₂ substrates, the typical Dirac point smearing (~ 40 meV) is significantly larger than the gap in any known superconductor. Not surprisingly these junctions do not show signatures of SAR. To overcome the problem of substrate induced random potential we fabricated suspended graphene devices where fluctuations can be reduced to values well below the superconducting gap energy in common superconductors. This makes it possible to achieve the necessary conditions for SAR, in an SGS device with standard superconducting lead materials. We will fabricate suspended SGS devices with Nb or Pb leads to search for signatures of SAR and ballistic transport. The SAR should give rise to new features in the bias dependence of the differential conductance of the SGS junctions as well as strong gate dependence of the critical current. We will use these criteria to confirm the presence of the SAR and their robustness as a function of geometry and various fabrication parameters.

- ***Spin transport in SGS junctions***

A remarkable consequence of SAR is the unusual transport in an SGS channel. Since for electron energies below the superconducting gap, no spin can be injected into the superconductor, the spin of the incident electron is transferred to the reflected hole. In a graphene strip bounded by two superconducting strips the SAR lead to spin propagation along the channel. For a long channel, after averaging over all initial angles of incidence the net charge flow along the channel vanishes leaving a charge neutral spin current to flow along the strip. We will investigate the charge filtering properties and the ability to transport pure spin currents in suspended SGS devices. To access the spin transport we will use a four-terminal non-local spin valve geometry. The device will employ ferromagnetic electrodes making contact with the graphene sheet through a thin tunnel barrier. The tunnel barriers between the ferromagnetic electrodes and the graphene layer underneath, were shown to significantly increase the spin-injection efficiency of the ferroelectric electrodes. The spin polarized current injected from a ferromagnetic electrode induces an imbalance between the two spin populations, that, for diffusive systems, extends over a distance of $\lambda_{sf}=(D\tau_{sf})^{1/2}$ from the interface. τ_{sf} is the spin lifetime and D the electron diffusion constant. For graphene $\lambda_{sf} \sim 1 \mu\text{m}$. If a second ferromagnet is present within λ_{sf} from

the injector, it can be used to detect the spin accumulation. We expect that the presence of the SGS channel will significantly increase the spin propagation distances.

Publications (BES funding)

1. Self-navigation of an STM tip toward a micron sized sample, A. Luican, Guohong Li, and E.Y. Andrei, *Rev. Sci. Instrum.* 82, 073501 (2011)
2. Single Layer Behavior and Its Breakdown in Twisted Graphene Layers, A. Luican, Guohong Li, A. Reina, J. Kong, R. R. Nair, K. S. Novoselov, A. K. Geim and E.Y. Andrei, *Phys. Rev. Lett.* 106, 126802 (2011).
3. Quantized Landau level spectrum and its density dependence in graphene, A. Luican, Guohong Li, and E.Y. Andrei, *Phys. Rev. B* 83 041405(R) (2011)
4. Observation of Van Hove singularities in twisted graphene layers, Guohong Li, A. Luican, J.M. B. Lopes dos Santos, A. H. Castro Neto, A. Reina, J. Kong and E.Y. Andrei, *Nature Physics* 6, 109 (2010).
5. Fractional quantum Hall effect in suspended graphene: Transport coefficients and electron interaction strength, D.A. Abanin, I. Skachko, X. Du, E.Y. Andrei, and L.S. Levitov, *Physical Review B*, 81, 115410 (2010) .
6. Integer and Fractional Quantum Hall Effect in Two-Terminal Measurements on Suspended Graphene, I. Skachko, X. Du, F. Duerr, A. Luican, D. A. Abanin, L. S. Levitov, E.Y. Andrei, *Phil. Trans. R. Soc. A* 368, 5403-5416 (2010)
7. Fractional quantum Hall effect and insulating phase of Dirac electrons in graphene, X. Du, I. Skachko, F. Duerr, A. Luican and E. Y. Andrei, *Nature* 462, 192, (2009)
8. Scanning Tunneling Spectroscopy of Graphene on Graphite, G. Li, A. Luican and E. Y. Andrei, *Phys. Rev. Lett* 102, 176804 (2009)
9. Scanning tunneling microscopy and spectroscopy of graphene layers on graphite, A. Luican, G. Li and E.Y. Andrei, *Solid State Commun.*(2009) doi:10.1016/j.ssc.2009.02.059
10. Electronic states on the surface of graphite, G. Li, A. Luican and E. Y. Andrei, *Physica B*, (2009).
11. Approaching ballistic transport in suspended graphene, X. Du, I. Skachko, A. Barker and E. Y. Andrei, *Nature Nanotechnology* 3, 491 (2008).
12. Towards ballistic transport in graphene, X. Du, I. Skachko, A. Barker and E. Y. Andrei, *International Journal of Modern Physics B: Condensed Matter Physics; Statistical Physics; Applied Physics; Vol. 22 Issue 25/26, p4579-4588, (2008).*
13. Josephson Current and Multiple Andreev Reflections in Graphene SNS Junctions, X. Du, I. Skachko and E.Y. Andrei, *Phys. Rev. B* 77, 184507 (2008).
14. Observation of Landau Levels of Dirac Fermions in Graphite, G. Li and E.Y. Andrei, *Nature Physics*, 3, 623 (2007)

Project Title: Probing nanocrystal electronic structure and dynamics in the limit of single nanocrystals
Principal Investigator: Mounji G. Bawendi
Institution: Massachusetts Institute of Technology
Email: mgb@mit.edu

Project Scope

Nanocrystals (NCs) of semiconductors have been incorporated into hybrid organic/inorganic solar photovoltaic devices for increased light absorption, increased charge separation rate, and enhanced mobilities. NCs of semiconductors of the II-VI family such as CdSe or CdTe and of the IV-VI family such as PbS and PbSe have recently been the subject of increasing study and controversy for their potential in improved 3rd generation solar cells through the generation of more than one electron-hole pair per photon. Morphologies ranging from spherical quantum dots, high aspect ratio quantum nanorods, and branched morphologies such as tetrapods have been studied as potential materials for an optimized hybrid solar cell. Hybrid nanostructures or organic/nanocrystal structures that aim to break up excitons and funnel charge within a device are actively being pursued. The foundation of all this activity is the synthesis and thorough characterization, both structural and optical, of the nanocrystals themselves. Given the potential impact of devices that use NCs as a functional material in the energy field, it is crucial to understand at a very basic level the optical physics, both static and dynamic, of NCs of a variety of materials and morphologies. Without such understanding, designing novel structures, novel device architectures, and understanding the potential and limitations of present materials and devices is haphazard at best. A basic understanding of the optical physics of semiconductor NCs is the core aim of our work. We use, in large part, single NC spectroscopy to directly probe exciton and multiexciton spectroscopy and dynamics in a variety of NCs and NC hybrid structures.

Recent Progress

Quantum dot nanocrystals (NCs) possess spectral properties that are more complex than ensemble-averaged studies could have inferred. Spontaneous spectral shifts, lineshape fluctuations and spectral diffusion result in inhomogeneous spectra undergoing spectral wandering. Single NC spectroscopy has brought to light some of these surprising dynamics but conventional methods require acquisition times longer than milliseconds, leaving faster spectral changes unresolved. Photon correlation Fourier

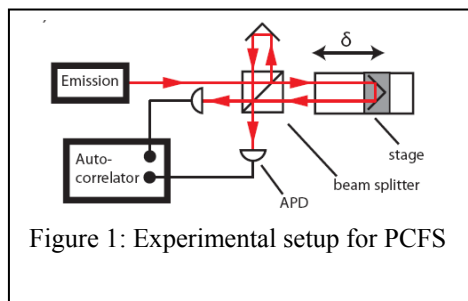


Figure 1: Experimental setup for PCFS

spectroscopy (PCFS) is a fundamentally different approach to obtaining dynamic spectral information with high temporal and frequency resolution. By combining an interferometer with a single photon counting Hanbury-Brown and Twiss correlation setup, PCFS allows us to monitor spectral changes on timescales several orders of magnitude faster than what conventional single-molecule methods can access. Our group has combined PCFS with Fluorescence Correlation Spectroscopy to observe the spectral dynamics of the average single chromophore from an ensemble in solution.

In addition to the analytical theory, we have performed numerical simulations to confirm the ability of PCFS to measure spectral dynamics over timescales ranging from the excited state lifetime (~ 30 ns) up to 100s of ms in the cases of isolated single emitters and emitters diffusing in solution. We have experimentally executed PCFS under a variety of conditions. At liquid helium temperatures, the single NC spectrum narrows and becomes significantly more dynamic. We have successfully used PCFS to measure the evolving linewidth of single NCs at short (μs – ms) timescales. Our unique setup simultaneously allows for conventional spectrometer-based measurements of dynamics on longer (1000 's

of seconds) timescales. This dual pronged approach allows us to observe spectral dynamics over nearly 8 orders of magnitude of time. At room temperature, we have experimentally demonstrated the ability to extract single emitter spectral information from an ensemble in solution and discovered that surprisingly, no significant spectral diffusion occurs from ~ 40 ns to 10 ms. In addition, we have found that the spectral linewidth for the average single emitter in solution varies greatly with material and synthetic scheme but appears uncorrelated with nanocrystal size.

Semiconductor nanocrystals emit light intermittently; i.e., they “blink,” under steady illumination. The dark periods have been widely assumed to be due to photoluminescence (PL) quenching by an Auger-like process involving a single additional charge present in the nanocrystal. This charging model predicts that the dark state exciton has a higher PL quantum yield (QY) than that of the biexciton and also predicts that multiexciton emission should exhibit very weak intermittency. Close examination of exciton PL intensity time traces of single CdSe(CdZnS) core (shell) nanocrystals reveals that the dark state PL QY can be 10 times less than the biexciton PL QY. In addition, from the spectrally resolved multiexciton emission, we find that it also blinks with an on/off ratio greater than 10:1. These results directly contradict the predictions of the charging model.

Multiexciton properties strongly affect the usability of a light emitter in quantum photon sources and lasers. However, it is difficult to measure multiexciton properties for single fluorophores at room temperature due to luminescence intermittency and bleaching at the high excitation fluences usually required. We can observe the biexciton (BX) to exciton (X) to ground state photoluminescence cascade of single nanocrystals (NCs) under weak excitation in a second-order photon cross-correlation measurement. We show that the normalized amplitude of the cascade feature is equal to the ratio of the BX and X fluorescence quantum yields. This imposes a limit on the attainable depth of photon antibunching and provides a robust means to study single emitter biexciton physics. In NC samples, we find that the BX quantum yield is considerably inhomogeneous, consistent with the defect sensitivity expected of the Auger nonradiative recombination mechanism.

For nanocrystals that are optically active in the visible part of the spectrum (e.g. cadmium selenide), a tremendous amount of work detailing the “exciton lifecycle” within these particles has emerged over the past 15 years as a result of our ability to optically interrogate them one at a time using fluorescence methods. Unfortunately, a dearth of photon detectors with high detection efficiencies and low noise in the shortwave infrared (SWIR, 1-2 μm) has prevented the community from extending single NC studies to the lead chalcogenides, indium arsenide and other narrow-band-gap material systems.

We have implemented a new approach that utilizes highly-efficient, multi-element superconducting nanowire single-photon detectors (SNSPDs) for

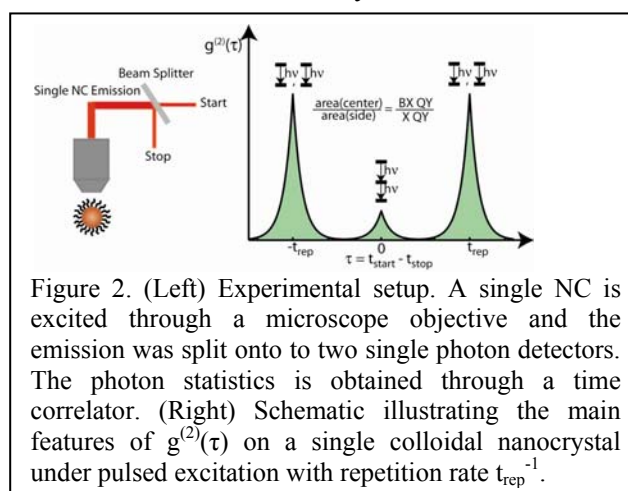


Figure 2. (Left) Experimental setup. A single NC is excited through a microscope objective and the emission was split onto two single photon detectors. The photon statistics is obtained through a time correlator. (Right) Schematic illustrating the main features of $g^{(2)}(\tau)$ on a single colloidal nanocrystal under pulsed excitation with repetition rate t_{rep}^{-1} .

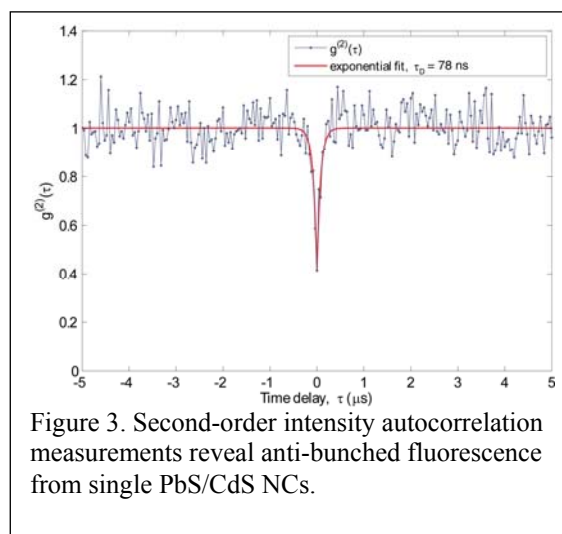


Figure 3. Second-order intensity autocorrelation measurements reveal anti-bunched fluorescence from single PbS/CdS NCs.

imaging single SWIR-emitting NCs. Upon isolating a single NC, we measure the photoluminescence intensity as a function of time and determine the statistics of their intermittency, or “blinking”. In addition, photon events are recorded in time-tagged-time-resolved (TTTR) mode, allowing us to calculate second-order intensity correlation functions in order to determine the extent of antibunching from single SWIR nanocrystals. We have demonstrated that measuring single emitter emission is feasible in the SWIR which is a vital first step towards studying single nanocrystals at these previous inaccessible wavelengths.

Future Plans

The results from the PCFS experiments on nanocrystals at room temperature and solution raise a number of questions. What gives rise to the heterogeneous spectral dynamics observed at low temperature? In solution at room temperature, what is the timescale for spectral diffusion and in turn, what is the mechanism? Overall, what chemical and physical properties of the NCs govern these spectral linewidths and dynamics? We are exploring these questions by applying PCFS on NCs in various controlled experimental conditions (temperature, excitation power, host matrix, chemical synthesis procedure) to disentangle their roles in the spectral linewidths, lineshapes and dynamics of single nanocrystals.

We plan to expand the study of biexciton recombination dynamics in single nanocrystals to low temperatures such as 10K which will reveal more detailed structural and electronic information. In addition, the exciton and biexciton transitions are polarization-dependent. Using the previously discussed method based on photon statistics, it is possible to measure BX quantum yield and correlation of polarizations of the BX and X photons at 10 K. Furthermore, the excitation wavelengths will be varied so that we can study the effect of the initial excitonic state on biexciton dynamics. The measurement can be extended to other materials, such as NCs with different structures or composition, or CdSe nanorods.

Our single-photon measurement capabilities in the SWIR open up an enormous number of possibilities in the study of single nanocrystals. Many of the narrow band-gap nanocrystals possess electronic structures very different from that of CdSe and thus potentially very different photophysical properties. In addition to studying blinking kinetics, we can observe multiexciton properties and spectral diffusion by combining this detector with our newly developed methods for extracting biexciton and spectral dynamics. By cooling these dots to low temperature, we may be able to explore the excitonic transitions and fine structure for these materials that, until now, have been unobservable at the single particle limit.

List of Publications

1. G. Nair, S. M. Geyer, L.-Y. Chang, M. G. Bawendi, “Carrier multiplication yields in PbS and PbSe nanocrystals measured by transient photoluminescence,” *Physical Review B* **78**, 125325 (2008).
2. X. Brokmann, L. F. Marshall, M. G. Bawendi, “Revealing single emitter spectral dynamics from intensity correlations in an ensemble fluorescence spectrum,” *Optics Express* **17**, 4509-4517 (2009).
3. B. J. Walker, G. P. Nair, L. F. Marshall, V. Bulovic, M. G. Bawendi, “Narrow-Band Absorption-Enhanced Quantum Dot/J-Aggregate Conjugates,” *Journal of the American Chemical Society* **131**, 9624-9625 (2009).
4. J. Zhao, G. Nair, B. R. Fisher, M. G. Bawendi, “Challenge to the charging model of semiconductor-nanocrystal fluorescence intermittency from off-state quantum yields and multiexciton blinking,” *Phys. Rev. Lett.* **104**, 157403 (2010).
5. L. Marshall, J. Cui, X. Brokmann, M. G. Bawendi, “Extracting spectral dynamics from single chromophores in solution,” *Phys. Rev. Lett.* **105**, 053005 (2010).
6. B. J. Walker, V. Bulovic, M. G. Bawendi, “Quantum dot/J-aggregate blended films for light harvesting and energy transfer,” *Nano Lett.* **10**, 3995-3999 (2010).

7. G. Nair, J. Zhao, M. G. Bawendi, "Biexciton quantum yield of single semiconductor nanocrystals from photon statistics," *Nano Letters* **11**, 1136-1140 (2011).
8. G. Nair, L.-Y. Chang, S. M. Geyer, M. G. Bawendi, "Perspective on the prospects of a carrier multiplication nanocrystal solar cell," *Nano Letters* **11**, 2145-2151 (2011).

Project Title: Developing Functionality in Quantum Dots

Principal Investigator: Jonathan Bird

Recipient: University at Buffalo

Email Address: jbird@buffalo.edu

Project Scope

There has long been great interest in the modifications to material properties that arise when charge carriers are confined in nanostructures, such as nanotubes, nanowires, and quantum dots. The strong many-body interactions characteristic of these structures, and the interplay of these interactions with quantum size effects, can lead to the formation of novel correlated states of matter, not normally associated with their bulk counterparts. In this research, we provide a specific illustration of these ideas, by focusing on the consequences of many-body interactions for electron transport in the quasi-one-dimensional conductors known as quantum point contacts (QPCs). It has been widely suggested that the interplay of quantum confinement and carrier-carrier interactions can give rise to an unusual spin polarization in these structures. In our currently-funded DoE research, we have provided strong evidence that this behavior is related to the formation of a self-consistent bound state near pinch-off, which essentially allows the QPC to serve as a natural, single-electron trap. While this idea is certainly exciting, there are a number of important questions regarding the microscopic character of the self-consistently formed bound state that remain unresolved. These include the characteristics “storage time” of electrons on the bound state, the manner in which the bound state forms as the QPC is tuned from open conduction to pinch-off, and the spin-dependent structure of the bound state. To address these issues, this work develops new experimental techniques to probe the microscopic properties of the bound states in QPCs, thereby revealing the fundamental processes that give rise to their formation. A major direction for our research involves the development of transient-measurement schemes, as a means to investigate the localization of single electrons on QPC bound states. In parallel with this, we also investigate the application of QPCs as an “on-demand” source of quantum states that can be used to implement sophisticated systems, in which spatially-remote quantum states interact with each other via a common continuum. Resolving these questions addresses key fundamental issues in condensed matter physics, while offering new approaches to quantum control of charge carriers.

Recent Progress

The interaction of discrete quantum objects allows for the emergence of complex phenomena in solid-state physics, with prominent examples provided by the interaction of localized and mobile spins in the Kondo effect, and the phonon-mediated pairing of electrons in superconductivity. When the interaction arises from wavefunction overlap among different atoms, the result is the emergence of covalent bonding that supports the formation of stable molecules and crystals. Yet another important form of interaction is that which arises widely in atomic physics, when the discrete levels of a particular atom are coupled to a continuum of unconstrained states. The characteristic signature of the interference of these channels is the Fano resonance (FR) that is observed in scattering experiments, with a lineshape that intimately reflects the relative transmission amplitudes of the two ionization pathways. An important goal that has emerged in the field of mesoscopic physics is to mimic the interactions that arise in nature, as a means to extend the functionality of semiconductor nanodevices. In addition to the technological importance of this issue, this approach provides an invaluable means to explore quantum-mechanical interactions at the microscopic level, with a control that is simply not possible in conventional atomic systems. Building on these ideas, in the most recent period of our DoE support we have succeeded in demonstrating how a robust interaction can be achieved between mesoscopic devices, by, perhaps counter intuitively, separating them from each other. In this approach, which utilizes the discrete-state/continuum coupling that is the hallmark of the FR, localized states are formed on two separate “quantum dots” and interact indirectly with each other through an inter-connecting continuum. In spite of this non-local coupling, our

In our latest research, we have demonstrated how the technique that we have developed for probing QPC BSs can be extended to realize systems in which two BSs, formed on separate QPCs, are configured to interact through a common 2DEG. The manner in which this is achieved is illustrated in Fig. 1, in which Fig. 1(a) is a schematic that shows the key mechanisms for interaction in the multi-QPC system. In Fig. 1(b), we use micrographs of the actual device to show the two different gate configurations that were used to implement the interacting BSs. In both of these configurations, which are actually geometrically equivalent, the detector gates (biased at V_d) are indicated with red shading, while those of the swept-QPC (biased at V_s) that defines one of the BSs (BS_1) are shown in blue. The other BS (BS_2) is realized within the control-QPC, which is formed by one of the gates of the swept-QPC, and by the additional control gate (biased at V_c) highlighted in yellow. The resulting system is one in which the two BSs, being separated by a distance of as much as four-hundred nanometers, are not coupled directly to each other, but rather interact through a mutual 2DEG that also supports their wavefunction overlap with the detector. The key observation of our experiments performed using the configurations of Fig. 1 is that the detector now exhibits two distinct resonances, one associated with each of the bound states. By varying the voltages applied to the swept- and control-QPCs these two resonances can be brought close to coincidence where an avoided crossing is actually observed, indicative of an interaction between the BSs. Remarkably, this avoided crossing is found to be much stronger than that typically reported for coupled quantum dots. In order to explain this result, we have developed a theoretical model that attributes it to the fact that the coupling of the two BSs is mediated by a highly-degenerate sets of states in the intervening continuum. While one often views the continuum as a source of decoherence, our work therefore suggests the possibility of using this medium to support the interaction of quantum states, a result that has the potential to open up new approaches to coherently couple nanostructures in complex geometries.

Future Plans

A useful means by which to explore the microscopic structure of the multi-state Fano resonance that we have demonstrated should be through the application of a magnetic field, directed either parallel or perpendicular to the plane of the two-dimensional electron gas. In the former case, the coupling is primarily to the spin degree of freedom, allowing for a controlled tuning of the singlet and triplet states of any collective multi-spin system. In the case of a perpendicular magnetic field, in addition to probing the spin states via the Zeeman energy, the magnetic field can also be used to induce wavefunction shrinkage within the “self-assembled” quantum dot that localizes the BS. A comparison of the influence of parallel and perpendicular fields can therefore provide useful spectroscopic information of the system of coupled BSs, and may even open up new means to control the collective state formed between the two BSs. The results of our experiments in this area will be analyzed within the context of the theoretical model that our collaborators have recently developed to describe the multi-state FR.

In parallel with our investigations of the multi-state FR, we have also recently initiated experimental investigations of the transient response of QPCs. The objective of these investigations is to try to use electrical transients to explore the formation of long-lived electron states in QPCs near pinch-off. Experimentally, this is a challenging task, due to the large impedance mismatch between 50-Ohm microwave circuitry and the QPC impedance ($> 25 \text{ k}\Omega$) near pinch-off. Nonetheless, in the past few months we have succeeded in using transient pulsing to investigate the conductance on QPCs on nanosecond time scales, with time resolution in the pico-second range. These experiments are currently ongoing, and our analysis of their results remains at a preliminary stage, but an initial evaluation suggests that we are able to observe – in real time- heating of electrons inside (or, locally, around) the QPC, over a characteristic time scale of order a few nanoseconds. As the 1-D mode structure of the device is modified, by varying the gate-voltage induced confinement of the QPC, this heating behavior shows a dramatic variation, indicating a strong dependence of energy relaxation on the 1-D levels. This phenomenon will also be investigated in our future research.

PUBLICATIONS RELATED TO DoE RESEARCH, 2008 – 2011

1. J. W. Song, G. R. Aizin, J. Mikalopas, Y. Kawano, K. Ishibashi, N. Aoki, J. L. Reno, Y. Ochiai, and J. P. Bird, “*Bolometric terahertz detection in pinched-off quantum point contacts*”, Appl. Phys. Lett. **97**, 083109 (2010).
2. T.-Y. Lin, K.-M. Lim, A. M. Andrews, G. Strasser, and J. P. Bird, “*Nonspin related giant magnetoresistance $\leq 600\%$ in hybrid field-effect transistors with ferromagnetic gates*”, Appl. Phys. Lett. **97**, 063108 (2010).
3. J. W. Song, G. R. Aizin, Y. Kawano, K. Ishibashi, N. Aoki, Y. Ochiai, J. L. Reno, and J. P. Bird, “*Evaluating the performance of quantum point contacts as nanoscale terahertz sensors*”, Optics Express **18**, 4609 – 4614 (2010).
4. J. W. Song, Y. Kawano, K. Ishibashi, J. Mikalopas, G. R. Aizin, N. Aoki, J. L. Reno, Y. Ochiai, and J. P. Bird, “*Current-voltage spectroscopy of the subband structure of strongly pinched-off quantum point contacts*”, Appl. Phys. Lett. **95**, 233115 (2009).
5. T.-Y. Lin, J.-U. Bae, K.-M. Lim, G. Bohra, J. L. Reno, and J. P. Bird, “*Influence of quantum interference on the fringing-field magneto-resistance of hybrid ferromagnetic/semiconductor devices*”, Appl. Phys. Lett. **95**, 143113 (2009).
6. Y. Yoon, M.-G. Kang, P. Ivanushkin, L. Mourokh, T. Morimoto, N. Aoki, J. L. Reno, Y. Ochiai, and J. P. Bird, “*Non-local bias spectroscopy of the self-consistent bound state in quantum point contacts near pinch-off*”, Appl. Phys. Lett. **94**, 213103 (2009).
7. Y. Yoon, M.-G. Kang, T. Morimoto, L. Mourokh, N. Aoki, J. L. Reno, J. P. Bird, and Y. Ochiai, “*Detector backaction on the self-consistent bound state in quantum point contacts*”, Phys. Rev. B **79**, 121304(R) (2009).
8. J.-U. Bae, T.-Y. Lin, Y. Yoon, S. J. Kim, J. P. Bird, A. Imre, W. Porod, and J. L. Reno, “*Characterization of nanomagnet fringing fields in hybrid semiconductor/ferromagnetic devices*”, IEEE Trans. Magn. **44**, 4706 – 4710 (2008).
9. J.-U. Bae, T.-Y. Lin, J. L. Reno, and J. P. Bird, “*Non-linear characteristics of the hysteretic magneto-resistance of a hybrid nanomagnetic field effect transistor*”, Appl. Phys. Lett. **93**, 143109 (2008).
10. A. Ramamoorthy, L. Mourokh, J. L. Reno, and J. P. Bird, “*Tunneling spectroscopy of a ballistic quantum wire*”, Phys. Rev. B **78**, 035335 (2008).
11. J.-U. Bae, T.-Y. Lin, Y. Yoon, S. J. Kim, A. Imre, J. L. Reno, W. Porod, and J. P. Bird, “*Large tunneling magneto-resistance in a field-effect transistor with a nanoscale ferromagnetic gate*”, Appl. Phys. Lett. **92**, 253101 (2008).
12. J. W. Song, N. A. Kabir, Y. Kawano, K. Ishibashi, G. R. Aizin, L. Mourokh, J. L. Reno, A. G. Markelz, and J. P. Bird, “*Terahertz response of quantum point contacts*”, Appl. Phys. Lett. **92**, 223115 (2008).
13. T. Morimoto, N. Yumoto, Y. Ujie, N. Aoki, J. P. Bird, and Y. Ochiai, “*Phenomenological investigation of many-body induced modifications to the one-dimensional density of states of long quantum wires*”, J. Phys.: Condens. Matt. **20**, 164209 (2008).
14. Y. Yoon, T. Morimoto, L. Mourokh, N. Aoki, Y. Ochiai, J. L. Reno, and J. P. Bird, “*Detecting bound spins using coupled quantum point contacts*”, J. Phys.: Condens. Matt. **20**, 164216 (2008).
15. M.-G. Kang, T. Morimoto, N. Aoki, J.-U. Bae, Y. Ochiai, and J. P. Bird, “*Aharonov-Bohm effect in the magneto-resistance of a multi-walled carbon nanotube with tunneling contacts*”, Phys. Rev. B **77**, 113408 (2008).
16. H. Kothari, R. Akis, S. M. Goodnick, D. K. Ferry, J. L. Reno, and J. P. Bird, “*Linear and non-linear conductance of ballistic quantum wires with hybrid confinement*”, J. Appl. Phys. **103**, 013701 (2008).

Title: Integrated growth and ultra-low temperature transport study of the 2nd Landau level of the two-dimensional electron gas

Principal Investigators: Gabor Csathy and Michael Manfra

Institution: Purdue University

Address: 525 Northwestern Ave., West Lafayette, IN 47907

E-mail of PIs: gcsathy@purdue.edu, mmanfra@purdue.edu

Program Scope

Our primary focus is the study of the fractional states of the second Landau level, corresponding to Landau level filling factors $2 \leq \nu \leq 4$. There is mounting theoretical and experimental evidence that several fractional quantum Hall states in this region are not well described by the model of non-interacting composite fermions. For example, the even denominator state at $\nu=5/2$ may result from an unusual pairing mechanism of the composite fermions described by the Pfaffian wavefunction. Because the pairing is believed to be p -wave, the $5/2$ state may resemble other condensed matter systems of current interest such as strontium ruthenate, certain fermionic atomic condensates, and the quantum liquid He-3. Moreover several odd denominator fractional states in the 2nd LL such as the $2+2/5$ and $2+6/13$ are quite distinct from their well understood lowest LL ($\nu < 2$) counterparts.

The study of the $5/2$ state has been reenergized with the prediction that its excitations obey exotic non-Abelian statistics. The $\nu=5/2$ and other novel states in the 2nd LL are not only of fundamental interest as they may manifest behavior not seen in any other physical system, but also may find technological utility in fault-tolerant schemes for quantum computation. These exotic states are, however, fragile and hence they develop only in the highest quality GaAs host crystals and typically only at the lowest electron temperatures.

Building on a recently established combination of expertise and infrastructure at Purdue University, we will carry out an integrated growth and experimental study of the two-dimensional electron gas in GaAs in the 2nd LL. We plan to use incisive techniques that are expected to offer new insight into the nature of the exotic correlated states of the 2nd LL. We will focus on:

- 1) Growth of ultra-high quality GaAs/AlGaAs heterostructures specifically tailored to study the impact of various growth parameters on the stability of the various fractional quantum Hall ground states in the 2nd LL.
- 2) Application of novel techniques together with transport measurements in the most interesting but technologically difficult ultra low temperature regime ($T \sim 5$ mK). As this regime is still largely unexplored, new and unanticipated results can be expected.

Recent Progress

This project builds on the ongoing collaboration at Purdue University established over the last two years. *Our team has recently developed a unique combination next generation growth and measurement capabilities needed to address several of the outstanding problems in the field of 2D electron physics.* Such a work calls for a highly focused and in house collaboration between

sample design and growth specifically tailored to our experimental objectives and state-of-the-art ultra low temperature measurement capabilities.

Manfra has designed and built a highly customized MBE chamber designed for the growth of high mobility GaAs/AlGaAs heterostructures at the Birck Nanotechnology Center at Purdue University (see Figure 1). Highlights of his new machine include: 1) vastly increased pumping capacity as compared to standard commercial MBE systems, 2) modification of standard effusion cell design to increase thermal efficiency and minimize outgassing of undesirable impurities, 4) the addition of increased cyropaneling around the cells to trap impurities, 5) redesign of access ports to allow greater optical access and ease of machine maintenance, 6) built-in expandability – the new machine is designed to allow for the addition of new *in-situ* tools and pumping capabilities as experiments warrant. At present there is a dearth of groups in the United States focused *entirely* on high mobility GaAs growth. Our sample growth effort strives to ensure continuous progress in sample quality which has led to numerous discoveries in the past and will contribute to the vitality of this field in the future.

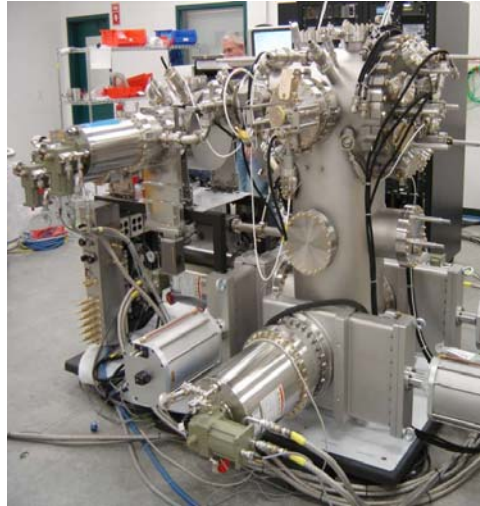


Fig.1. Manfra's custom-designed MBE installed at Purdue. Based on Manfra's 10+ years experience in high mobility semiconductor growth, this new machine will produce samples specifically tailored for our experiments.

Emergent phenomena are often unanticipated but many examples, such as superfluidity, superconductivity, the fractional quantum Hall effect, and Bose-Einstein condensation in atomic gases were enabled by the developments in cryogenic technology. Ultra-low temperature measurement has not yet been used to its full potential in the study of quantum Hall physics. Csathy's background in both Helium and fractional quantum Hall physics research has enabled him to build an ultra-low temperature refrigerator [1] capable of *cooling electrons in GaAs to 5mK* (see in Fig. 2). We emphasize that due to very weak electron-phonon coupling in GaAs in the mK regime, simply cooling the mixing chamber of a dilution refrigerator to $T < 10\text{mK}$ will not result in low electronic temperatures. One needs specialized heat sinking of the sample using sintered Silver heat exchangers which are immersed in a Helium-3 bath. This setup not only cools the electrons but also allows for a reliable magnetic field independent temperature measurement of the local bath via He-3 viscometry [1]. Our close collaboration between growth and ultra-low temperature measurement will facilitate rapid progress.



Fig.2. Csathy's He-3 immersion cell allows reaching temperatures of 5mK (left). A sample mounted on sintered Silver heat sinks (right). Reliable temperature measurement is achieved using a novel quartz He-3 viscometry.

Our collaboration has already produced exciting new physics. We have recently produced state-of-the-art magnetoresistance data in the second Landau level in both single layer two-dimensional electron [2] (see Figure 3) and hole samples [3]. Our progress is evident in the observation of new fractional quantum Hall states [2,3]. The observation of these states is already influencing our understanding of the second Landau level.

We are particularly encouraged by our recent progress in the growth of ultra-high quality GaAs two-dimensional electron systems. In particular our peak mobility has risen to $22 \times 10^6 \text{ cm}^2/\text{Vs}$ and appears far from saturation. More importantly, we have had the opportunity to cool one of our samples grown at Purdue to $T=7\text{mK}$ and found some quite astounding results. The sample under discussion has a density of $2.8 \times 10^{11}/\text{cm}^2$ and a mobility of $15 \times 10^6 \text{ cm}^2/\text{Vs}$ and displays extraordinary fractional quantum Hall features in the 2nd Landau level.

What is most interesting about this sample is that it displays all fractional states ever observed in the highest mobility samples produced despite its significantly lower mobility. In fact the transport in this sample grown at Purdue compares favorably with any yet produced. The fine details of the transport features near $\nu=5/2$ are also shown. In particular, we find a completely well-formed $\nu=2+2/5$ state. This feature has only been reported in 2 samples during the past 6 years, yet it appears quite strong in our sample.

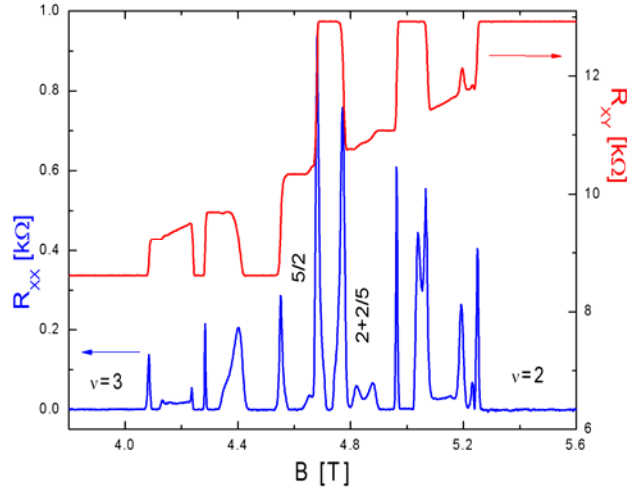
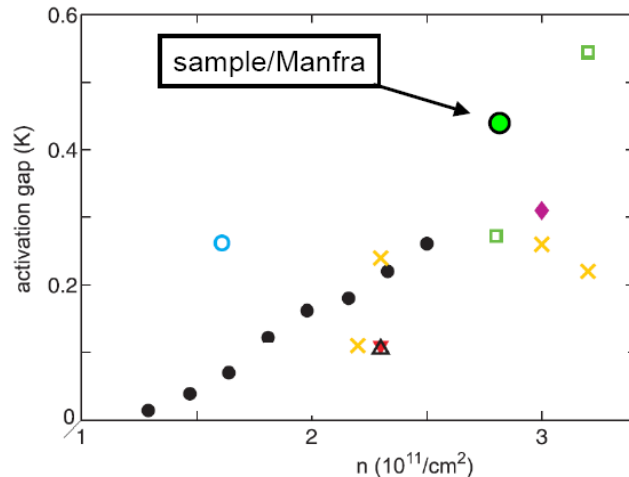


Fig.3. A recently measured magnetoresistance trace of a sample from Manfra's MBE measured at 6mK in Csathy's setup. Some of the important filling factor are marked.

We have also measured the excitation gap of the $\nu=5/2$ state in our sample. A representative temperature scan is shown in the figure. From this data we can extract an excitation gap of 446meV, among the highest ever reported for this density range.

To put this gap energy in prospective, we add our data to the recent publication of Nuebler *et al.* published in PRB in 2010. In this plot they study the excitation gap as a function of density at $\nu=5/2$ in a gate tunable high mobility 2D electron gas. They also compile a fairly complete set of gap measurements published in the literature by other groups. While this plot is somewhat busy, we have inserted our measured gap energy represented by the large green circle with the black outline. The upshot of this plot is that our $\nu=5/2$ gap is



among the highest ever measured at this density, independent of mobility.

We believe our data on samples grown at Purdue to be a significant finding for the field of fractional quantum Hall physics as it emphatically punctuates the notion that zero magnetic-field mobility is neither a primary indicator of the visibility nor the strength of fragile quantum Hall states in the 2nd Landau level. While it has been known in the community that all high mobility samples are not created equal, and that some display better quantum Hall features than others, it has always been assumed that the path new fractional quantum Hall physics is through higher mobility. Our data calls this assumption into question. If a 15 million mobility sample can display all the features of a 30 million mobility sample, then how can we meaningfully state one sample is “better” than another with zero field mobility alone? We of course cannot fully answer this question at present, but we do want to emphasize that this is precisely one of the major focuses of our proposed work. We speculate that sample homogeneity is a particularly important property as any homogeneity will tend to smear out the narrow features in the 2nd Landau level.

Future Plans

The experiments we plan will attempt to answer several of the current outstanding questions in the physics of the 2nd LL. What is the spin polarization of the $\nu=5/2$ state? How do several growth parameters influence the stability of the different fractional quantum Hall and insulating ground states in the 2nd LL? What other competing ground states will emerge as the purity of the GaAs host crystal is improved?

Such investigations call for a coordinated effort between growth and ultra-low temperature measurement and are part of our long term effort aimed at exploring unconventional collective behavior in low-dimensional systems. We think that progress with the experiments will uncover fundamental properties of the states in the 2nd LL and will also lead us in new and unanticipated research directions.

References

1. N. Samkharadze, A. Kumar, M.J. Manfra, L.N Pfeiffer, K.W. West, and G.A. Csathy, “Integrated Electronic Transport and Thermometry at milliKelvin Temperatures and in Strong Magnetic Fields”, *Review of Scientific Instruments* **82**, 053902 (2011)
2. A. Kumar, G.A. Csathy, M.J. Manfra, L.N Pfeiffer, and K.W. West, “Nonconventional Odd Denominator Fractional Quantum Hall states in the Second Landau Level”, *Physical Review Letters* **105**, 246808 (2010)
3. A. Kumar, N. Samkharadze, G.A. Csathy, M.J. Manfra, L.N Pfeiffer, and K.W. West, “Particle-Hole Asymmetry of Fractional Quantum Hall States in the Second Landau Level of a Two-Dimensional Hole System”, *Physical Review B* **83**, 201305 (2011)

Project Title:

Magnetic and Superconducting Properties of Materials Studied by the ^{99}Ru , ^{189}Os , ^{119}Sn , ^{57}Fe and ^{191}Ir Mössbauer Effects in External Magnetic Fields

Principal investigators:

Michael DeMarco, Department of Physics, Buffalo State College, Buffalo NY 14222,

email: demarcmj@buffalostate.edu or mjde@buffalo.edu

Dermot Coffey, Department of Physics, Buffalo State College, Buffalo NY 14222,

email: coffeyd@buffalostate.edu

Project Scope

The project involves the use of the Mössbauer Effect (ME), principally the ^{99}Ru ME, to investigate the ruthenates and other Ru containing compounds. This provides detailed information on the local electronic environment of the Ru sites. High-activity ^{99}Ru sources have been developed by DeMarco over the last few years which made possible the measurement of well-resolved ^{99}Ru Mössbauer spectra (MS) on a wide range of ruthenate and Ru containing rare-earth intermetallic compounds (RRu_2) at previously unattainable temperatures. The analysis of these spectra has provided detailed information on the environment of Ru ions in magnetic, superconducting, and disordered phases, in the form of electric field gradients, isomer shifts and hyperfine magnetic fields. Sources for the ^{189}Os and ^{191}Ir Mössbauer Effects (ME) have been developed and, recently, we have measured the ^{57}Fe ME of one of the new Fe-based superconductors and its antiferromagnetic parent compound. We now use external magnetic fields to further probe questions which our research has raised in ongoing projects and to develop the use of MS to investigate the response of bulk superconductors to external fields. In the near future a source for the ^{119}Sn ME will be developed so that we can concentrate on measuring the ^{57}Fe and ^{119}Sn ME in external fields.

Recent Progress**Rare Earth Intermetallics**

We have solved a fifty year old puzzle concerning GdRu_2 (Phys. Rev. B **81** (2010)). This compound is a ferromagnet due to the ordering of the Gd moments with a Curie temperature of 90K. One would expect to measure a reasonably large transferred hyperfine magnetic field at the Ru site but we measured a nearly a zero hyperfine magnetic field using the ^{99}Ru ME. The discrepancy between the size of the ordered rare earth moments and the measured hyperfine field at the Ru site is also seen in HoRu_2 . The electronic properties were calculated in the LDA approximation using the Wien2k software package and the resulting calculated hyperfine magnetic fields and electric field gradients at the Ru sites were found to provide good fits to the measured GdRu_2 and HoRu_2 MS. The reason for the small magnitude of $B_{\text{hyperfine}}$ at the Ru sites is that the 4d Ru electrons form broad conduction bands rather than localized moments. As a result the electron spin at the Ru sites is effectively unpolarized which leads to a very small $B_{\text{hyperfine}}$. These Ru-4d conduction bands are polarized in the region of the Fermi energy and mediate the interaction between the localized 4-*f* rare-earth moments. The calculated hyperfine magnetic fields at Ru sites in the magnetically ordered members of the RRu_2 series, where R is a lanthanide, are anomalously small.

SmFe_{1-x}Co_xAsO

Recently, we have published a paper studying the coexistence of magnetism and superconductivity in the compounds SmFe_{1-x}Co_xAsO [Phy Rev B, (in press, June 2011)] by the ⁵⁷Fe ME. In the parent compound, x=0, we found a small hyperfine magnetic compound of about 5T. The x = 0.05 compound is a superconductor (T_{SC} ≈ 5.1K) and we found that the linewidth was broadened over the natural width and that the linewidth decreased as the temperature was increased until the enhancement vanished above 25K. We found that the same temperature dependent enhancement of the linewidths up to 25K in external magnetic fields up to 9T. A fluctuating magnetic moment model was developed to understand the broadened line in both the external field and zero field. The enhanced linewidth is due to the slowing down of a fluctuating magnetic field due to the Fe moments, suggesting that 5% Co doping just being sufficient to prevent the ordering of the Fe moments and that at the boundary between magnetic order and superconductivity in the phase diagram magnetic fluctuations coexist with superconductivity. In the x= 0.1 compound (T_{SC} ≈ 17K) the linewidths are independent of temperature from 298K to 4.2K and of applied field up to 9T. We conclude that the spin fluctuations seen in the x=.05 compound are not associated with a magnetic mechanism for superconductivity, but with proximity to the magnetic phase.

Eu₂Ru₂O₇

This investigation of magnetism in this cubic pyrochlore is a collaboration with Sean Cadogan (Univ. of Manitoba). There are magnetic transitions at 23K and 118K. Our measured isomer shift, hyperfine magnetic field and electric quadrupole moment at 4.2K are very similar to those measured previously in Y₂Ru₂O₇ in spite of the difference in the Néel temperature, 76K, for that compound. The value of the isomer shift, ~ -0.26mm/sec is consistent with the Ru⁴⁺(S=1) state. The corresponding moment is smaller than that determined from high temperature susceptibility and the difference remains to be understood.

GdSr₂Ru(Cu_{1-x}Fe_x)₂O₈

GdSr₂RuCu₂O₈ has a Néel temperature at about 134K and superconducting transition at much lower temperatures which depends strongly on sample synthesis. The superconductivity is thought to be in the CuO planes with magnetic order in the RuO planes. We have shown that there is essentially no difference in the ⁹⁹Ru MS above and below the superconducting transition [PRB80,14442 (2008)], see Figure 1. How are magnetic correlations between RuO planes, necessary for three-dimensional order, transmitted through the CuO planes without affecting the superconductivity?. We have been studying the samples of GdSr₂RuCu₂O₈ doped with Fe provided by Torikachvili (San Diego State U.) to answer this question.

Our assumption is that the Fe atoms are distributed between the CuO and RuO planes. This allows us to monitor the effects of the superconducting transition through the ⁵⁷Fe MS in both types of planes. First we consider a sample (x=0.03) which does not have a superconducting transition. We have discovered that there is a phase transition between ~30K and ~40K using the ⁵⁷Fe ME in which roughly half of the Fe sites cease to see an ordered magnetic field. This is well below the Néel temperature. In Fig.2 we show the MS at 30K and 40K for a sample with x=.03. The same transition is seen in a different x=.03 sample and in an x=.01 sample in the same temperature range, showing that the transition does not depend on Fe concentration. The transition takes place over a range of temperatures with the region between the inner lines of the six line magnetic ⁵⁷Fe MS filling in. Beyond ~40K the ⁵⁷Fe MS consists of a central non-magnetic peak and a magnetic spectrum. The temperature dependence of the ⁹⁹Ru MS for the same sample will show whether the Fe's which see this transition are in the RuO planes. The effect of applied field on GdSr₂RuCu₂O₈ is to decrease the size of the hyperfine field in the ⁹⁹Ru MS. This is consistent with the sample becoming more ferromagnetic with the hyperfine magnetic field in the opposite direction to the

Comparison 4.2K and 9.9K (rescaled) data

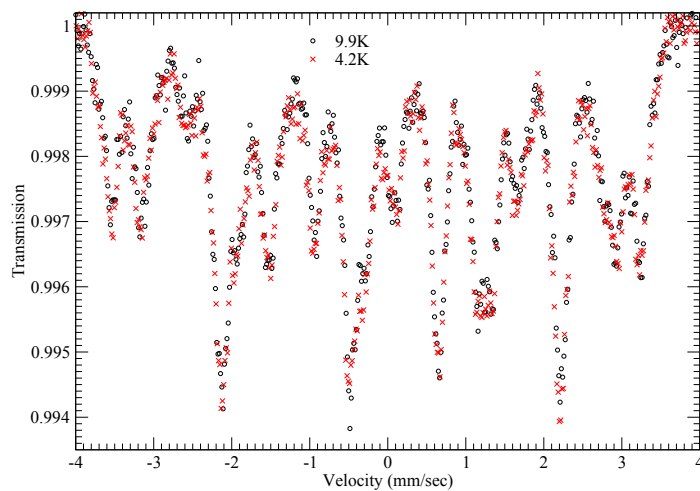


Figure 1: MS spectrum of $GdSr_2RuCu_2O_8$ above and below the superconducting transition

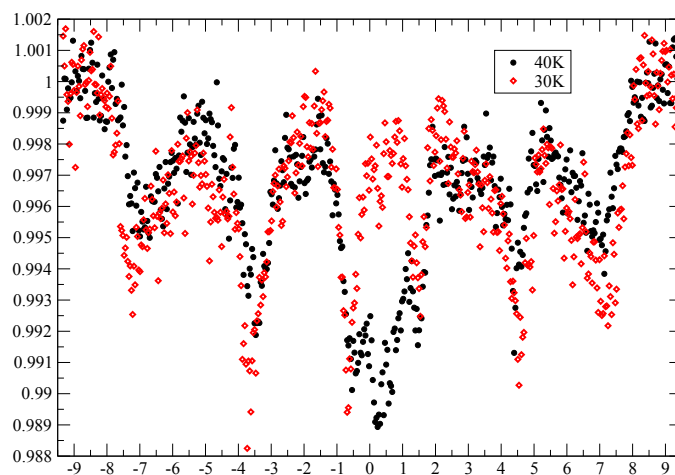


Figure 2: Transition between 30K and 40K seen in ^{57}Fe MS in $GdSr_2Ru(Cu_{0.97}Fe_{0.03})_2O_8$

applied field, as is also the case in other materials. The ability to polarize $\text{GdSr}_2\text{RuCu}_2\text{O}_8$ in a 4T field points to very weak magnetic anisotropy, unlike what we found in either $\text{GdSr}_2\text{Ru}(\text{Cu}_{0.97}\text{Fe}_{0.03})_2\text{O}_8$ or SmFeAsO using the ^{57}Fe ME. The magnetic field dependence of the ^{57}Fe MS in $\text{GdSr}_2\text{Ru}(\text{Cu}_{0.97}\text{Fe}_{0.03})_2\text{O}_8$ remains to be fully analyzed. The MS of SmFeAsO was found to be due to a random distribution of the relative orientations of the internal ordered field of each crystallite with the external field.

Future Plans:

$\text{GdSr}_2\text{Ru}(\text{Cu}_{1-x}\text{Fe}_x)_2\text{O}_8$

We are conducting a comprehensive investigation of the temperature and magnetic field dependences of the ^{99}Ru and ^{57}Fe MS on the same $\text{GdSr}_2\text{Ru}(\text{Cu}_{1-x}\text{Fe}_x)_2\text{O}_8$ samples.

Nb_3Sn

We intend to use the ^{119}Sn ME to detect the superconducting transition in a single-crystal of Nb_3Sn . A ^{119}Sn source for the experiment will be produced at the University at Buffalo cyclotron using a (p,3n) reaction on a ^{121}Sb target. The creation of a vortex lattice will lead to the development of a distribution of hyperfine fields at known lattice positions, from which the vortex lattice could be imaged. Once successful in ordinary superconductors the technique can be applied to other classes of superconductor.

$\text{PrOs}_{4-x}\text{Ru}_x\text{Sb}_{12}$

We intend to study the $\text{PrOs}_{4-x}\text{Ru}_x\text{Sb}_{12}$ system using the ^{189}Os and ^{99}Ru ME. The source for the ^{189}Os ME will be produced at the cyclotron using a cubic Ir metal foil target. ^{189}Pt will be produced by the reaction $^{191}\text{Ir}(p,3n)$. The Mössbauer source, ^{189}Ir (half-life=13 days), is ready after a few days due to the decay of ^{189}Pt (half-life=10 hours).

List of Publications:

G. Long, M. DeMarco, M. Chudyk, J. Steiner, D. Coffey, H. Zeng, Y.K. Li, G. H. Cao, and Z. A. Xu, "Coexistence of magnetic fluctuations and superconductivity in $\text{SmFe}_{0.95}\text{Co}_{0.05}\text{AsO}$ seen in ^{57}Fe Mössbauer spectroscopy", *Phys. Rev. B* (in press June,2011).

S. Smeekens, S. Heylen, K. Villani, K. Houthoofd, E. Godard, M. Tromp, J.-W. Seo, M. DeMarco, C. E. A. Kirschhock and J. A. Martens, "Reversible NO_x storage over Ru/NaY zeolite", *Chem. Sci.*, 2010, 1, 763-771

D. Coffey, M. DeMarco, P.C. Ho, M.B. Maple, T. Sayles, J. W. Lynn, Q. Huang, S. Toorongian and M. Haka, "Absence of the hyperfine magnetic field at the Ru site in ferromagnetic rare earth intermetallics", *Phys. Rev. B* **81**, 184404 (2010).

D. Coffey, M. DeMarco, B. Dabrowski, S. Kolesnik, S. Toorongian and M. Haka "Magnetic properties of $\text{RuSr}_2\text{GdCu}_2\text{O}_8$ using the temperature dependence of the Mössbauer spectrum", *Phys. Rev. B* **77**, 214412 (2008).

C. Westman, S. Jang, C. Kim, S. He, G. Harmon, N. Miller, B. Graves, N. Poudyal, R. Sabirianov, H. Zeng, M. DeMarco, and J.P. Liu, "Surface Induced Suppression of Magnetization in Nanoparticles", *J. Phys. D: Appl. Phys.* **42**, 225003 (2008).

M. A. Goodman, A. Y. Nazarenko, M. DeMarco, M. Scott Goodman and G. Long "Tris(5-methylpyrazolyl)methane: Synthesis and properties of its iron(II) complex", to be submitted.

J. Steiner, A. Anderson and M. DeMarco, "Production of ^{239}Pu from a natural Uranium disk and "hot" rock using a neutron howitzer", arXiv:0805.3665 (2008),

Project Title:**Experiments on Quantum Hall Topological Phases in Ultra Low Temperatures (DE-FG02-06ER46274)****Principal Investigator:** Rui-Rui Du**Institution:** William Marsh Rice University**Email:** rdd@rice.edu**Project Scope**

This project is to cool electrons in semiconductors to extremely low temperatures (1 millikelvin), and to study new states of matter formed by low-dimensional electrons. At such low temperatures (and with an intense magnetic field), electronic behavior differs completely from ordinary ones observed at room temperatures. Studies of electrons at such low temperatures would open the door for fundamental discoveries in condensed matter physics. Understanding low-temperature electron transport in low-dimensional and nanoscale devices is the foundation for developing next generation quantum information and quantum computation technologies.

Our research is based on a demagnetization refrigerator (base $T \sim 0.2$ mK), which was built during previous DOE support. This project consists of the following components: 1) Development of efficient sample cooling techniques and electron thermometry: Our goal is to reach 1 mK electron temperature and reasonable determination of electron temperature; 2) Experiments at ultra-low temperatures: Our goal is to understand the energy scale of competing quantum phases, by measuring the temperature-dependence of transport features. Focus will be placed on such issues as the energy gap of the $5/2$ state, and those of $12/5$ (and possible $13/5$); resistive signature of instability near $1/2$ at ultra-low temperatures; 3) Measurement of the $5/2$ gaps in the limit of small or large Zeeman energies: Our goal is to gain physics insight of $5/2$ state at limiting experimental parameters, especially those properties concerning the spin polarization; 4) Experiments on gate-controlled nuclear spin polarization and detection of spin states at $5/2$: Our goal is to determine the spin-polarization of the $5/2$ ground state utilizing hyperfine interaction effect between the electron spin and the nuclear spin in the GaAs crystal; the experiments will be in the dc transport regime and without the application of microwave excitations.

A specific materials challenge is to fabricate Molecular Beam Epitaxy wafers of mobility $\gg 1 \times 10^7$ cm²/Vs with the designed gating properties. The materials will be prepared by Dr. Loren Pfeiffer of Princeton University. Dr. Pfeiffer is a world leader in MBE growth of ultra pure GaAs/AlGaAs quantum well structures. This material is essential for the success of the proposed project.

Recent Progress**• Studies of Half-Filled $N = 0, 1$ Landau Levels in Extremely Low Temperatures**

As shown in FIG. 1, at ultra low temperatures we have observed the $5/2$ fractional quantum Hall state and the more fragile QH phases at filling factor $12/5$ (and also possible $13/5$), which are considered by theories as "para-fermions", the cluster of quasiparticles. Continue experiment investigation in this parameter regime is planned. The ability to control electron density and potential profile in a very high mobility, modulation-doped GaAs/AlGaAs 2D electron system by voltage gates is a key ingredient in realizing confinement of quasiparticles in the FQHE. We

have succeeded in constructing high quality gate using Si₃N₄ dielectric layer on the very high mobility quantum wells and will apply this technique in studies of resistively-detected NMR in the fractional quantum Hall effect in ultralow temperatures provided by the demagnetization refrigerator. Our ultra low temperature capability also helped to study quantum phases at the half-filling in the lowest Landau level (LL). FIG. 1 (right) shows the magnetotransport data for a low electron density, very-high mobility GaAs/AlGaAs quantum well. Using this high quality 2D electron sample, we are able to measure the electronic state at Landau level filling factor $\nu = 1/2$ at ~ 5 T. To the best of our knowledge, this is the first time that a $\nu = 1/2$ state is measured at $T < 10$ mK. We have observed a sharp minimum in longitudinal resistance at $\nu = 1/2$. Concomitant Hall resistance at $1/2$ shows a change of slope (as indicated by the blue trace, $\propto B \cdot \partial R_{xy} / \partial B$).

• *Studies of 5/2 State in the Limits of Large and Small Zeeman Energy*

The energetics relevant for the QH system are cyclotron energy $E_\omega = \hbar eB / m^* \propto B$, where $m^* \sim 0.067 m_e$ is the electron effective mass; Zeeman energy $E_Z = g\mu_B B \propto B$, where g is the effective g -

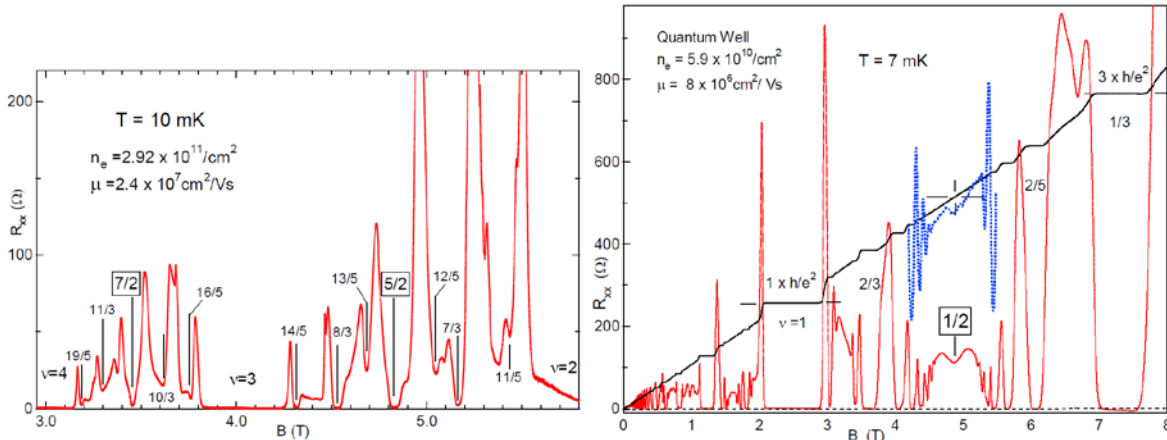


FIG. 1 New results in the fractional quantum Hall regime in the second Landau level (left) and that in the first Landau level (right), measured in our system.

factor in GaAs, μ_B is the Bohr magneton; and electron interaction energy $E_C = e^2 / \epsilon l_B \propto B$, where $\epsilon = 12.9$ is the dielectric constant in GaAs, and l_B is the magnetic length. Although the bare g factor $g \approx -0.44$ in GaAs is small in magnitude, increasing magnetic field favors E_C / E_ω . On the other hand the LL mixing $\kappa \equiv E_C / E_\omega = l_B / a_0$ decreases as $\sim 1 / B$, where $a_0 \sim 10$ nm is the effective Bohr radius in GaAs. Since for $5/2$ the magnetic field $B_{2/5} = \hbar n_e / (5/2)$, using very -high mobility quantum wells having various densities n_e , we have investigated the $5/2$ plateau in the high- and low magnetic field limit and its response to a tilted magnetic field.

a. 5/2 FQHE observed at 10T

Recently we have observed for the first time a $5/2$ quantum Hall plateau at $B \sim 10T$. Together with a vanishing R_{xx} , these data establish unambiguously a true FQHE gap at $5/2$. These results confirm the observation of the FQHE minimum in a magnetic field $B \geq 10T$ and strengthen the case for a high- B version of the $5/2$ quantum liquid. Since here the Zeeman energy $E_z \sim 3K$ exceeds the theoretically calculated energy gap $\Delta_{5/2} \sim 2.5K$, a spin unpolarized ground state is unlikely. We have also systematically studied the Hall plateau and the activation energy in a tilted B , and our data support the notion that the Landau level filling factor $\nu = 5/2$ FQHE is indeed spin-polarized, a significant step towards experimentally proving the $5/2$ state as being non-Abelian. We have also measured the activation energies of the $7/3$, and $8/3$ fractional quantum Hall states as a function of tilted magnetic field. The results indicate a spin-polarized ground state at both the $7/3$ and $8/3$ fractions.

b. Enhancement of $\nu = 5/2$ quantum Hall plateau by an in-plane B

The proposed Pf (or APf) wavefunction for $5/2$ requires the spin being at least partially polarized. Recent numerical results indicate that at $5/2$ in realistic systems is spin-polarized even in the limit of vanishing Zeeman energy. It is anticipated that increasing the Zeeman energy would help to stabilize the spin-polarized ground state in the presence of fluctuations. Therefore, a tilted magnetic field is supposed to enhance the FQHE at $5/2$. However, to date all the experimental results have been contradicted to this simple prediction: $5/2$ FQHE are found to be weakening in a tilted field. Competition with a striped many-electron phase could be responsible for the complex response of the $5/2$ state to a tilted field. Surprisingly, we have observed a $\nu = 5/2$ FQHE at a magnetic field $B = 1.5 \sim 1.7 T$, and found that its energy gap values increase in an in-plane magnetic field. Here the data were taken in a standard dilution refrigerator ($\sim 25 mK$ base T) in the National High Magnetic Field Lab. Completely solving the spin-polarization problem in this context, which is one of the key issues in the $5/2$ non-Abelian physics, would require much lower temperatures ($T < 10 mK$) and *in situ* sample rotation (without warming up sample to room temperature). Our demagnetization system should work well for this task.

Future Plans

The proposed experiments on the $5/2$ quantum Hall effect and other novel many-particle electron phases will be performed in synchronization with the attainment of the lower electron temperatures as this project develops. Our objective during this funding period is to investigate quantum Hall physics in a new temperature window at one millikelvin. Our proposed experiments will be centered on the electrical transport properties of the $5/2$ many-body phases and related high Landau level states. We will develop novel approaches in addition to standard DC magnetotransport for investigation. In particular, we propose to utilize temperature scaling of the quantum Hall plateau-to-plateau transition as an electron thermometer, and develop gate-controlled nuclear spin polarization technique to detect the spin states at $5/2$. These work present formidable challenges concerning both the low-temperature measurements and the 2DES nanofabrication (e.g., gating for ultra high mobility GaAs/AlGaAs quantum well) techniques, but the scientific results they would bring in could be extremely exciting. Based on the submillikelvin instrumentation and expertise developed during the previous and current DOE grant support, we are very well placed for the task. The proposed research is outlined as:

•Development of efficient sample cooling techniques and electron thermometry

Our goal is to reach 1 *mK* electron temperature and reasonable determination of electron temperature.

•Magnetotransport at ultra-low temperatures

Our goal is to understand the energy scale of competing phases, by measuring the temperature dependence of transport features. Focus will be placed on such issues as the energy gap of the 5/2 state, and those of 12/5 (and possible 13/5); resistive signature of instability near 1/2 at ultralow temperatures.

•Measurement of the 5/2 gaps in the limit of small or large Zeeman energies

We propose to continue on experiments of 5/2 state at limiting experimental parameters, such as very low electron density (for example, 5/2 at $\sim 1 T$) and very high density (5/2 at $B \geq 10 T$). In such limits a materials challenge is to fabricate MBE wafers of mobility $> 1 \times 10^7 \text{ cm}^2/\text{Vs}$. We plan also to install a precision, piezoelectric in site sample rotator suitable for tilt magnetic field experiments in the mK environment.

•Experiments on gate-controlled nuclear spin and detection of spin states at 5/2

A technique of gate-controlled nuclear spin polarization and relaxation has been demonstrated to study the electron spin polarization of quantum Hall phases for filling factors 1/2, 3/2, and on both sides of $\nu = 1$. We will adapt this method to the studies of spin polarization at 5/2. The major challenge is the MBE growth of ultra-high-mobility structures that can be reliably gated; Dr. Loren Pfeiffer will develop the special MBE samples for proposed experiments.

Publications

- 1) Enhancement of the $\nu = 5/2$ Fractional Quantum Hall State in a Small In-Plane Magnetic Field, Guangtong Liu, Chi Zhang, Aaron Levine, D. C. Tsui, R. R. Du, L. N. Pfeiffer, and K. W. West, Preprint.
- 2) $\nu = 5/2$ Fractional Quantum Hall Effect at 10 T: Implications for the Pfaffian State, Chi Zhang, T. Knuutila, Yanhua Dai, R. R. Du, L. N. Pfeiffer, and K. W. West, Phys. Rev. Lett. **104**, 166801(2010).
- 3) Resistance Minimum Observed at Landau Level Filling $\nu = 1/2$ in Ultra-High Magnetic Field, Jian Zhang, R. R. Du, J. A. Simmons, and J. L. Reno, Phys. Rev. B **81**, 041308R (2010).
- 4) Magnetotransport in Zener Tunneling Regime in a High-Mobility Two-Dimensional Hole Gas, Yanhua Dai, Z. Q. Yuan, C. L. Yang, R. R. Du, M. J. Manfra, L. N. Pfeiffer, and K. W. West, Phys. Rev. B **80**, 041310R (2009) (Editor's Suggestion).
- 5) Landau Level Spectrum in a Two-Dimensional Hole Gas in C-doped (100) GaAs/Al_{0.4}Ga_{0.6}As Square Quantum Well, Z. Q. Yuan, R. R. Du, M. J. Manfra, L. N. Pfeiffer, and K. W. West, Appl. Phys. Lett. **94**, 052103 (2009).
- 6) 5/2 States in High Electron-Density GaAs/AlGaAs Quantum Wells, R. R. Du, T. Knuutila, Chi Zhang, L. N. Pfeiffer, and K. W. West, 18th International Conference on High Magnetic Field in Semiconductors and Nanotechnologies, 08/03/08-08/08/08, Sao Pedro, Brazil.
- 7) Abstract for APS March10 Meeting: Gated Magnetotransport in a Very-High Mobility GaAs/AlGaAs Quantum Well, Guangtong Liu, D. C. Tsui, L. N. Pfeiffer, K. W. West, Ivan Knez, Chi Zhang, and R. R. Du, Portland, 2010.
- 8) Abstract for APS March10 Meeting: Activation Energies for the $\nu = 5/2$ Fractional Quantum Hall Effect at 10 Tesla, Chi Zhang, R. R. Du, L. N. Pfeiffer, and K. W. West, Portland, 2010.

Fabrication of Graphene Devices for Electron Flow Imaging

Adam Graham³, Wei Li Wang¹, Sagar Bhandari¹, David C. Bell^{1,3}, Robert Westervelt^{1,2}

¹*School of Engineering and Applied Science, Harvard University, Cambridge, MA U.S.A.*

dcb@seas.harvard.edu

²*Physics Department, Harvard University, Cambridge, MA U.S.A.*

³*Center for Nanoscale Systems, Harvard University, Cambridge MA U.S.A.*

A major challenge researchers face is to understand how electrons move through nanoscale graphene structures. The carriers are quite unlike those in conventional semiconductors or metals. The electrons and holes are chiral particles that pass through potential barriers easily (the Klein paradox) and the edges of graphene reconstruct and create new electron states.¹ Graphene is promising for atomic scale devices - to make and understand these structures we need nanoscale probes. We have addressed this challenge directly; by developing a process for fabricating and imaging ballistic electron flow in graphene and controlling graphene quantum dots using cooled SPM instruments and techniques adapted from our earlier work.²

Our current research fabricates graphene structures with nanosculpting and imaging using TEM, STEM and Helium Ion Microscopy. Using the Helium Ion and electron beams it is possible to etch and mill graphene to fabricate such as ribbons and quantum point contact structures.³ The Helium Ion Microscope operates like a scanning electron microscope, except that the image is provided by a scanned He ion beam, providing new contrast mechanisms and a novel way to etch “soft” materials (Fig. 1).⁴ The quantum point contact (QPC) sample size scales (~ 10 -100 nm) are large enough to transfer between the STEM and SPM for electron flow measurements (Fig. 2). Our second phase is toward the atomic scale - done directly inside a Zeiss Libra aberration-corrected STEM by using the electron beam to both cut and image graphene structures. A review of current progress will be presented.

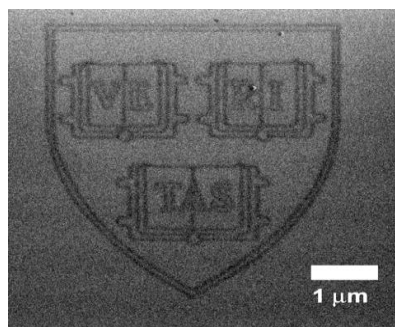


Figure 1. Helium ion beam etching of a graphene sheet (from Ref. 2)

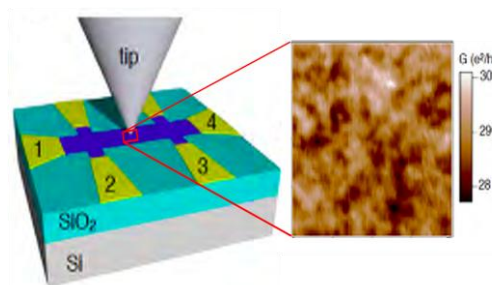


Figure 2. (left) SPM tip above a graphene Hall bar sample; the conducting tip creates a movable scatterer in the 2DEG below.² (right) SPM image of universal conductance fluctuations at 4K.

¹ Kyoko Nakada, Mitsutaka Fujita, Gene Dresselhaus and Mildred S. Dresselhaus, "Edge state in graphene ribbons: Nanometer size effect and edge shape dependence," *Phys Rev B* **54**, 17954 (1996).

² J. Berezovsky, M.F. Borunda, E.J. Heller and R.M. Westervelt, "Imaging Coherent Transport in Graphene (Part I): Mapping Universal Conductance Fluctuations," *Nanotechnology* **21**, 274013 (2010); "Imaging Coherent Transport in Graphene (Part II): Probing Weak Localization," *Nanotechnology* **21**, 274014 (2010).

³ David C. Bell, Max C. Lemme, Lewis A. Stern, Jimmy R. Williams, Charles M. Marcus, "Precision cutting and patterning of graphene with helium ions", *Nanotechnology* **20**, 455301 (2009).

⁴ David C. Bell "Contrast Mechanisms and Image Formation in Helium Ion Microscopy", *Microscopy and Microanalysis*, **15** (2009), pp. 147-153.

LINEAR AND NONLINEAR OPTICAL PROPERTIES OF METAL NANOCOMPOSITE MATERIALS

Principal Investigator: RICHARD F. HAGLUND, JR.

Department of Physics and Astronomy

6301 Stevenson Center Lane

Vanderbilt University

Nashville TN 37235-1807

richard.haglund@vanderbilt.edu

PROJECT SCOPE

The explosive growth of plasmonics has been fueled by a combination of nanofabrication, microscopy and time- and space-resolved spectroscopies, coupled to powerful computational and analytical tools. The scientific themes in our project are (1) nonlinear optical physics in active or nonlinear metamaterials and (2) ultrafast nonlinear optical dynamics in complex plasmonic structures. Aided by finite-difference time-domain and finite-element calculations, we design and fabricate plasmonic structures on which we can excite quasiparticles (e.g., excitons, phonons, plasmons) using optical signals, electrical impulses and laser-induced photomechanical stresses, and map the material response down to femtosecond time and nanometer length scales. The complex phenomenology of these structures is elucidated using coherent and time-resolved second- and third-order nonlinear optical spectroscopies, confocal and near-field optical microscopies, scanning-probe microscopies, and coherent spectroscopy, such as interferometric second-order autocorrelation. The project themes are situated at the intersection of condensed-matter and optical physics, emphasizing (1) optics in active and nonlinear metamaterials in which plasmonic functionality is controlled by solid-solid phase transformations or geometric construction; and (2) ultrafast dynamics in heterostructures designed to highlight novel coupling mechanisms.

RECENT PROGRESS

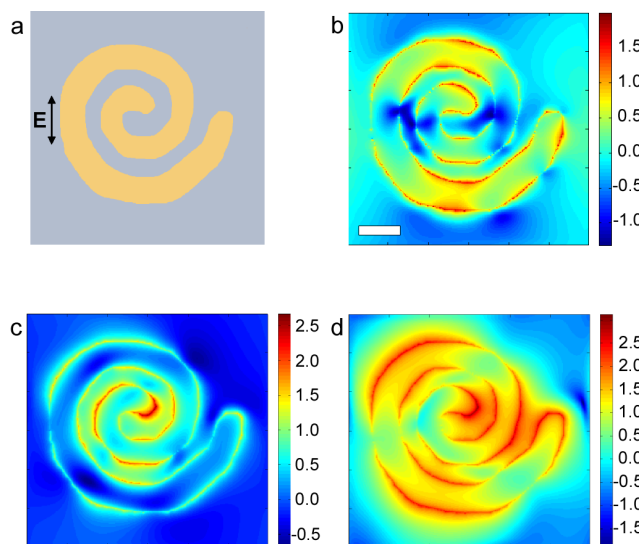


Figure 1. (a) Nanofabricated Archimedean spiral. Near-field distributions from FDTD simulations showing (b) hourglass, (c) focusing and (d) standing-wave modes.

A crucial development in the theory of plasmonics is based on the analogy between bonding and anti-bonding orbitals in molecular physics, and the hybridization of optical modes in complex plasmonic structures. This formalism has been applied to problems ranging from nanoparticle assemblies composed of dissimilar elements to nanoparticle arrays with various kinds of broken symmetries that exhibit hybridized sub-radiant and super-radiant modes. It has also provided a way to understand the plasmonic interactions in complex nanoscale metallic structures and suggested a variety of novel functionalities. However, up to now these studies have focused on coupled dipole and quadrupole oscillations defined by incident polarization in structures with broken symmetry.

We have fabricated nanostructures — Archimedean spirals — with a topologically robust structure, in which polarization response, resonant enhancement and symmetry-breaking are defined by track width, track spacing and winding number. In fact, lack of symmetry produces many modes with spectrally distinct near-field configurations. The spirals (Figure 1a) have sub-wavelength dimensions thereby confining plasmonic activity to the near-field region and winding numbers between 1 and 2 (2π and 4π) in which emergent properties are manifest in complex intra-particle interactions. Using scanning electron micrographs and measured spectra, we simulated the optical response with finite-difference time-domain (FDTD) software (Lumerical) to investigate the observed near-field interactions and mode structures. Figures 1(b)-(d) display three characteristic mode structures: a radially oriented “hourglass” mode (Figure 1b); a *standing-wave* mode (Figure 1d) analogous to longitudinal nanorod modes; and a *focusing* mode (Figure 1c) that centers the confined energy at one or both ends of the spiral. Each characteristic mode is confined to a spectrally distinct region; the correlation between spectral features and winding number allows us to control the number, intensity, and spectral position of the resonant modes. The results obtained so far suggest applications in plasmonic focusing, nanoscale manipulation of dielectric objects, chiral interactions, and enhanced chemical and optical processes such as surface-enhanced Raman scattering (SERS) and second-harmonic generation.

We have also developed a novel heterostructure that makes it possible to study coupling of the ZnO band-edge exciton and localized surface plasmons (LSPs) and propagating surface-plasmon polaritons (SPPs), over a continuous range from the weak- to the strong-coupling regimes. The heterostructures [Figure 2(a)] comprise a ZnO film or quantum well, a MgO or $\text{Zn}_x\text{Mg}_{1-x}\text{O}$ spacer layer of variable thickness, and a plasmonic element that could range from a rough metallic film to a lithographically fabricated array of metallic nanoparticles. Using this heterostructure and photoluminescence (PL) and ultrafast pump-probe spectroscopy, we have been able unambiguously to identify a Zn_i impurity transition previously conjectured theoretically, a state that shows up at the interface of the ZnO and the MgO spacer layer only after an appropriate annealing regime. In this case, the pump-probe measurement is critical to resolving ambiguities from the PL spectra.

The virtue of being able to vary the geometry of the excitonic emitter and plasmonic elements of the heterostructure is exhibited in Figure 2(b), showing optical density as a function of the diameter of lithographically fabricated Al nanodisks spaced on 225 nm centers, for a fixed spacer distance of 20 nm. The growth of the resonance structure in the center of the spectrum corresponds to the passage to the strong-coupling limit when the plasmonic density of states overlaps the band-edge exciton wavelength in the quantum well. Evidence suggests that this is a new kind of hybridized quadrupole-plasmon-exciton feature.

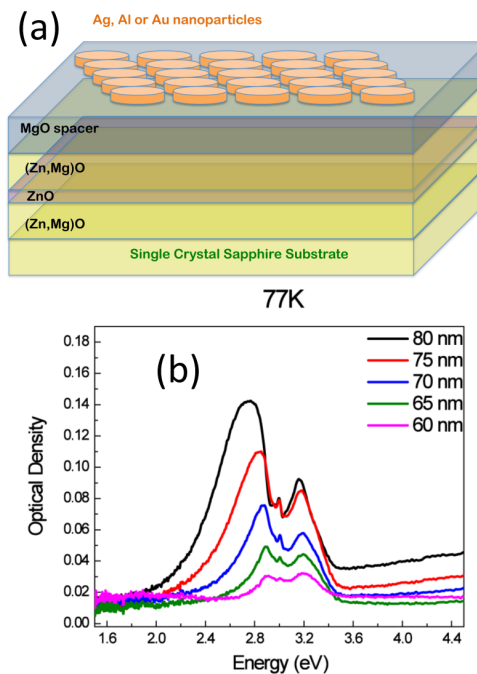


Figure 2. (a) Schematic of a ZnO-plasmonic heterostructure. (b) Transition from weak to strong exciton-plasmon coupling, showing the growth of a Fano-resonance structure.

FUTURE PLANS

Based on our success with initial studies of the correspondence between the spatial distribution of electromagnetic modes and identifiable spectral features in Archimedean spirals, we plan two different classes of ultrafast experiments in these unsymmetric structures. The first class of experiments capitalizes on the fact that the spiral has two different extinction modes that can couple to rod-like plasmons, at 600 and 730 nm. Thus, for example, one can pump at one wavelength and measure the redistribution of plasmon energy at the other wavelength by probing with the second, in-phase beam from a dual optical parametric amplifier (OPA) system. The second class of experiments will focus on second-harmonic generation and second-order interferometric autocorrelation measurements due to the coupling between simple linear structures (*e.g.*, nanorods or rows of disks) and spirals. We expect that the broken symmetries in these structures will have strong effects not only on electron dephasing, but also on polarization and wavelength dependence of the generated harmonic radiation. We will use the femtosecond OPA for frequency-dependent pump-probe and second-harmonic measurements, and a recently built second-order interferometric autocorrelation setup for measuring dephasing times in complex structures.

Relatively little is known about the *dynamics* of exciton-plasmon coupling in low-dimensional structures such as ZnO quantum wells and wires near metal nanodisks and gratings. The lifetime of the ZnO band-edge exciton is of order ps, but it is not known how that time scale is by exciton-plasmon coupling in metamaterials. Nor is it known how doping of the ZnO affects exciton-plasmon interactions — information essential to implementing active plasmonics with ZnO.

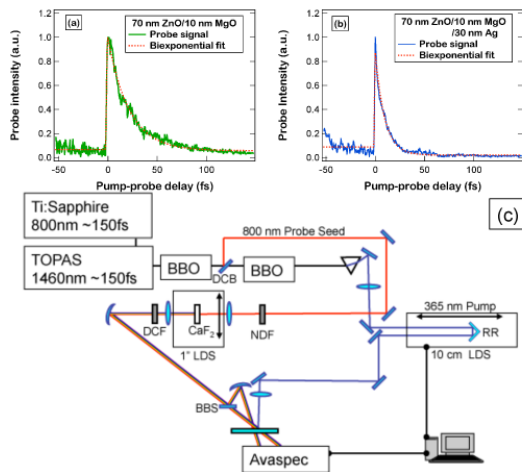


Figure 3. Degenerate pump-probe measurements of the decay of the ZnO band-edge exciton without (a) and in the presence of (b) a gold island nanoparticulate film. (c) Schematic of the setup for pump-probe measurements with a white-light supercontinuum.

We have already fabricated heterostructures with controllable excitonic emission energies and plasmon resonances, growing ZnO/MgO/metal heterostructures on which to carry out degenerate pump-probe studies of the the band-edge exciton decay due to plasmonic interactions. Representative time-resolved data are shown in Figs. 3(a) and (b). Going forward, we plan to implement dynamical studies in ZnO/Zn_{0.85}Mg_{0.15}O quantum wells grown by pulsed laser epitaxy. The QW PL spectra are blue-shifted from the bulk ZnO bandgap — demonstrating that quantum confinement dominates the quantum confined Stark effect (QCSE) in these structures. The RMS surface roughness on these heterostructures is less than 3 nm, smooth enough to allow lithographic fabrication of metal nanoparticle arrays. The localized surface plasmon resonances of these arrays can be tuned from the near-UV to the near-IR by varying the particle diameter, and by changing from Al to

Ag to Au nanoparticles. By varying the barrier width and the MgO spacer thickness in the QWs and bilayer structures respectively, the plasmon exciton coupling dynamics can be mapped as a function of interaction length and coupling strength.

PUBLICATIONS 2008-2011

1. “Pulsed infrared laser annealing of gold nanoparticles embedded in a silica matrix,” A. Halabica, J. C. Idrobo, S. T. Pantelides, R. F. Haglund, Jr., R. H. Magruder III and S. J. Pennycook, *Journal of Applied Physics* **103**, 083545 (2008).
2. “Modulation of the gold particle-plasmon resonance by the metal-semiconductor transition of vanadium dioxide,” J. Y. Suh, E. U. Donev, D. W. Ferrara, K. A. Tetz, L. C. Feldman and R. F. Haglund, Jr., *Journal of Physics A: Pure and Applied Optics* **10**, 055202 (2008). Selected for listing as one of the Highlight Papers of the journal for 2008; see <http://herald.iop.org/jopahighlights2008/m173/kaa/124703/link/2409>.
3. “Using a Semiconductor-to-Metal Transition to Control Optical Transmission through Subwavelength Hole Arrays,” E. U. Donev, J. Y. Suh, R. Lopez, L. C. Feldman, R. F. Haglund, Jr., invited review article for *Advances in OptoElectronics* (an open access journal), volume 2008, doi 739135, (2008).
4. “Confocal Raman microscopy across the metal-insulator transition of single vanadium-dioxide nanoparticles,” E. U. Donev, R. Lopez, L. C. Feldman and R. F. Haglund, Jr., *Nano Letters* **9** (2), 702-706 (2009).
5. “Dichroism in Ag Nanoparticle Composites with Bimodal Size Distribution,” R. H. Magruder III, S. Robinson, C. Smith, A. Meldrum, A. Halabica and R. F. Haglund, Jr., *Journal of Applied Physics* **105**, 024303 (2009).
6. “Optical Properties of Ag Nanocrystals in Sc and O Sequentially Implanted Silica,” R. H. Magruder III and A. Meldrum, *Journal of Non-Crystalline Solids* **355**, 17-22 (2009).
7. “Universal optical response of Si-Si bonds and its evolution from nanoparticles to bulk crystals,” J. C. Idrobo, A. Halabica, R. H. Magruder III, R. F. Haglund, Jr., S. J. Pennycook and S. T. Pantelides, *Physical Review B* **79**, 125322 (2009).
8. “Size effects in the structural phase transition of VO₂ nanoparticles studied by surface-enhanced Raman scattering,” E. U. Donev, J. I. Ziegler, R. F. Haglund, Jr. and L. C. Feldman, *Journal of Optics A: Pure and Applied Optics* **11**, 125002 (2009).
9. “Excitation and detection of surface acoustic phonon modes in Au/Al₂O₃ multilayers,” A. Halabica, S. T. Pantelides, R. F. Haglund, Jr., R. H. Magruder III and A. Meldrum, *Physical Review B* **80**, 165422 (2009). Also selected for inclusion in the American Institute of Physics *Virtual Journal of Ultrafast Science*.
10. “Coupling of photoluminescent centers in ZnO to localized and propagating surface plasmons,” R. F. Haglund, Jr., B. J. Lawrie and R. Mu, *Thin Solid Films* **458**, 4637-4643 (2010). *Invited review paper* from the European Materials Research Society Spring Meeting, June 2009.
11. “Plasmonic response of nanoscale spirals,” J. I. Ziegler and R. F. Haglund, Jr., *Nano Letters* **10**, 3010-3015 (2010).
12. “Substrate dependence of Purcell enhancement in ZnO-Ag multilayers,” B. J. Lawrie, R. Mu and R. F. Haglund, Jr., *Physica Status Solidi C* **8**(1), 159-162 (2011). DOI: 10.1002/pssc.201000773.
13. “Plasmon-Enhanced Low-Power Laser Switching of Gold::Vanadium Dioxide Nanocomposites,” D. W. Ferrara, E. R. MacQuarrie, A. B. Kaye, R. F. Haglund, Jr., *Applied Physics Letters* **98**, 241112 (2011).

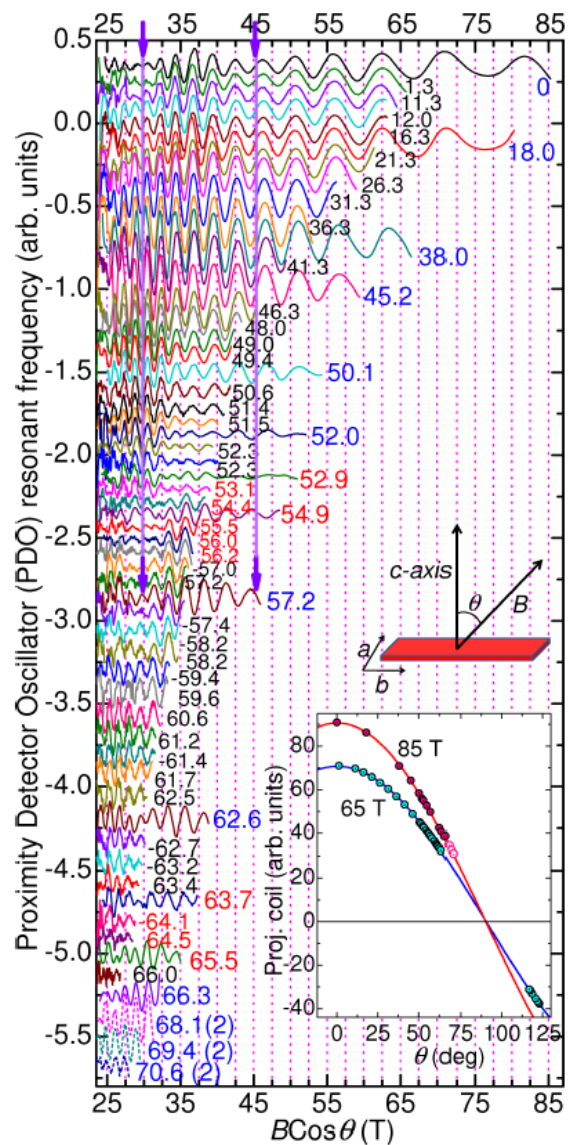
Project Title “Science at 100 Tesla”

Participants: Neil Harrison (PI), Fedor F. Balakirev, Jonathan Betts, Scott Crooker, Marcelo Jaime, Ross McDonald, Albert Migliori, John Singleton

Project Scope: This project utilizes the Multi-Shot Magnet (100TMSM) for fundamental science in condensed-matter physics systems. Designed to achieve 100T nondestructively, it is presently fully operational to 85T for 10ms-duration pulses. The intent is to use the high magnetic fields to examine outstanding questions and emergent themes in condensed matter physics and materials science, and to search for new phenomena. The concept represents a considerable advance over competing technologies, in that the sample, magnet outsert and cryostat are designed to survive thousands of pulses, and each pulse lasts thousands of times longer than in destructive 100 T magnets. The 100 T multi-shot magnet provides a non-invasive, reversible probe that couples directly to the spin and orbital degrees of freedom of electrons in solids, producing very significant energy shifts that disturb the basic energy balance of the system, inducing phase transitions and other effects. The energy shifts in 100 T fields match the scale of many of the robust electronic phenomena characterized by transitions occurring at temperatures ~ 100 K, which are as yet poorly understood. In addition, high magnetic fields provide a tunable magnetic length scale ($l = (25.7/B^{1/2})$ nm) that parameterizes the spatial extent of the wavefunctions of band electrons. For instance, at 100 T, l is comparable to the smallest nanostructures or even moderately-sized organic molecules.

Recent Progress: Technical progress has been made in several key areas. These include significant advances in using magnetic quantum oscillations to probe the electronic structure and origin of superconductivity in high temperature superconducting cuprates, high magnetic field studies of the electronic structure and superconducting properties of Fe-based superconductors/antiferromagnets and extensive studies of quantum magnets.

High Magnetic Field Measurements of the Electronic structure of High Temperature Cuprate Superconductors: Our previously reported doping-dependent effective mass is gaining considerable attention, with features consistent with a concomitant reduction in the Fermi velocity with decreasing doping being seen now in angle-resolved photoemission spectroscopy. Following on



from these measurements, we made use of a newly developed sample rotator for the 100T magnet for making comprehensive measurements of magnetic quantum oscillations in the underdoped high- T_c cuprate $\text{YBa}_2\text{Cu}_3\text{O}_{6.56}$ as a function of the inclination of magnetic field from the crystalline axis (plotted versus $B\cos\theta$ in the attached figure). Such measurements enable the Fermi surface topology to be mapped with higher resolution than has previously been possible, and enable the Zeeman splitting of the spin-up and spin-down Fermi surface components to be determined unambiguously. The field range over which oscillations can be observed (~ 22 -85 T) greatly exceeds that achievable in other laboratories. These quantum oscillation measurements play a crucial role in determining the high magnetic field ground state in underdoped high- T_c superconductors, which is pertinent to understanding the origin of the pseudogap. The contactless conductivity technique unique to Los Alamos continues to be vital for high precision measurements in strong magnetic fields. The most recent measurements point to a form of charge ordering rather than spin-density wave ordering.

High Magnetic Field Studies of the Newly Discovered Fe-pnictide Superconductors: Using pulsed magnetic fields, the LANL team were the first to discover the absence of anisotropy of the upper critical field in FeAs pnictides. Such measurements have since been extended to fields of 85 T, enabling the lack of anisotropy to be followed all the way to optimal doping and beyond in the $(\text{Ba,K})\text{Fe}_2\text{As}_2$ family. The reduced anisotropy compared to the cuprates also implies that the Fe-pnictide superconductors are much more promising candidates for the development of superconducting wires operating in strong magnetic fields and high temperatures.

Quantum Magnets. The crystalline solid $\text{C}_{18}\text{H}_{36}\text{N}_4\text{O}_2\text{Cr}_3\text{C}_{19}$ containing chromium trimers arranged in isosceles triangles, provides an ideal system in which to investigate the role of frustration upon magneto-electric coupling. This is because the material is both strongly in the Mott limit, where the onsite coulomb repulsion preventing double site occupancy is much greater than the wave function overlap, facilitating comparison with theory, and that the magnitude of the resulting exchange interactions are comparable to available magnetic fields. While systems containing dimers can be understood almost entirely in terms of the Heisenberg exchange model, compact trimers give rise to the possibility of loop currents resulting from a residual itinerancy of the charge within the triangle. Loop currents can lift the degeneracy of the groundstate, leading to a coupling between magnetic and dielectric properties. Magnetic torque measurements performed to 85 tesla reveal the magnetic anisotropy to change sign abruptly between different field-induced states. This enables the symmetry-breaking terms responsible for the new purely electronic form of magneto-electric coupling to be identified.

Future Plans. We expect to focus on science with the following themes:

Electronic Structure of high temperature superconductors: The abundance of magnetic quantum oscillation results and the high quality of the experimental data are already having a significant impact on the field. New questions are beginning to emerge from our studies, opening up new directions for research in high magnetic fields: The continued observation of magnetic quantum oscillations as the hole doping is significantly changed suggests the possibility of observing magnetic quantum oscillations in stoichiometric $\text{YBa}_2\text{Cu}_3\text{O}_7$ — close to optimal doping. The key challenges are sample quality and magnetic field of strength sufficient to access the normal carriers. Preliminary unpublished measurements indicate that the latter may be adequate. The bore of the insert magnet has

recently been reduced so as to enable the peak magnetic field to be increased to 95 T, increasing the likelihood of success. Having performed the most comprehensive mapping of the low energy electronic structure of $\text{YBa}_2\text{Cu}_3\text{O}_{6+x}$ to date, we plan to extend similar measurements to $\text{YBa}_2\text{Cu}_4\text{O}_8$, in which only very rudimentary measurements have been made. The high upper critical field of $\text{YBa}_2\text{Cu}_4\text{O}_8$ is likely to require the utilization of magnetic fields extending to 95 T. Such measurements are a crucial step for determining whether there exists a universal electronic ground state at low temperatures and high magnetic fields.

Quantum magnets: We are currently planning experiments on quantum magnets using an optical strain gauge, which has been shown to produce magnetostriction data in pulsed magnetic fields with a much higher signal to noise ratio than produced using conventional techniques. There are two systems of interest for studies to fields of up to 95 T: Preliminary studies of magnetostrictive effects in $\text{SrCu}_2(\text{BO}_3)_2$ made using an optical fiber strain gauge (or fiber Bragg gratings) in regular pulsed magnets show that very high signal-to-noise measurements of the magnetostriction can be obtained in strong magnetic fields. Soon we plan to implement this technique during the testing of the new 95 T insert magnet. One question is whether a clear feature can be detected at fields of 80 T or higher that coincides with our previously reported magnetization plateau (the magnetization within the plateau being half that of full saturation). The second principle area concerns the possibility of a supersolid phase. Geometric frustration has the capacity for yielding complex phase diagrams exhibiting new physics. Recent theoretical models point to the possibility of a spin supersolid phase — in the same way that quantum magnets provide the spin analog of Bose-Einstein Condensation. While the possibility of such a supersolid phase in ^4He continues to be the subject of debate, the metallic frustrated antiferromagnetic AgNiO_3 provides a candidate for its spin analog to be studied by tuning the magnetic field.

New directions: Within the last year, there have been significant discoveries in interacting electron systems whose understanding is likely to require strong magnetic fields. One of these developments concerns topological insulating materials in which gapless states exist at the surface of a sample while its bulk remains insulating. Strong magnetic fields are likely to play a vital role in determining whether the states are fully two-dimensional (as expected for surface states) and whether the dispersion is of the Dirac form. Preliminary measurements made in magnetic fields extending to 85 T indicate that very strong magnetic fields can be utilized to extract the value of the Berry phase — strong magnetic fields are required in order to reach the quantum limit (where only a single Landau level is occupied) at which the Berry phase can be accurately determined.

Unconventional superconductors containing $4f$ or $5f$ electrons are another family of materials in which strong magnetic fields can significantly perturb the electronic structure — usually by polarizing the hybridized bands in strong magnetic field causing them to be decoupled from the conduction electrons. The low resistivity of such materials makes these materials challenging to measure in strong magnetic fields. Recently, focused ion beam (FIB) lithography, in which the sample is cut to dimensions of a few microns, has been found to greatly increase the sensitivity of transport experiments in high magnetic fields — the reduced cross-sectional area causing the resistance to be increased to a more easily measured size.

Selected publications

J.G. Analytis, R.D. McDonald, S.C. Riggs, J.-H. Chu, G.S. Boebinger, I.R. Fisher, “Two-dimensional surface state in the quantum limit of a topological insulator,” *Nature Physics* **6**, 960 (Dec. 2010).

P.J.W. Moll, R. Puzniak, F. Balakirev, K. Rogacki, J. Karpinski, N.D. Zhigadlo, B. Batlogg, “High magnetic-field scales and critical currents in SmFeAs(O, F) crystals,” *Nature Materials* **9**, 628 (Aug. 2010).

J.G. Analytis, J.-H. Chu, R.D. McDonald, S.C. Riggs, I.R. Fisher, “Enhanced Fermi-surface nesting in superconducting $\text{BaFe}_2(\text{As}_{1-x}\text{P}_x)_2$ revealed by the de Haas-van Alphen Effect,” *Physical Review Letters* **105**, 207004 (Nov. 2010).

S.E. Sebastian, N. Harrison, P.A. Goddard, M.M. Altarawneh, C.H. Mielke, R.X. Liang, D.A. Bonn, W.N. Hardy, O.K. Andersen, G.G. Lonzarich, “Compensated Electron and Hole Pockets in an Underdoped High T_c Superconductor,” *Physical Review B* **81**, 214524 (June 2010).

S.E. Sebastian, N. Harrison, M.M. Altarawneh, R.X. Liang, D.A. Bonn, W.N. Hardy, O.K. Andersen, G.G. Lonzarich, “Fermi-liquid behavior in an underdoped high- T_c superconductor,” *Physical Review B* **81**, 140505 (Apr. 2010)

S.E. Sebastian, N. Harrison, M.M. Altarawneh, C.H. Mielke, R.X. Liang, D.A. Bonn, W.N. Hardy, G.G. Lonzarich, “Metal-insulator quantum critical point beneath the high T_c superconducting dome,” *Proceedings of the National Academy of Sciences of the United States of America* **107**, 6175 (Apr. 2010).

J. Singleton, C. de la Cruz, R.D. McDonald, S.L. Li, M. Altarawneh, P. Goddard, I. Franke, D. Rickel, C.H. Mielke, X. Yao, P.C. Dai, “Quantum Oscillations in $\text{YBa}_2\text{Cu}_3\text{O}_{6.61}$ and $\text{YBa}_2\text{Cu}_3\text{O}_{6.69}$ in Fields of Up to 85 T: Patching the Hole in the Roof of the Superconducting Dome,” *Physical Review Letters* **104**, 086401 (Feb. 2010).

H.Q. Yuan, J. Singleton, F.F. Balakirev, S.A. Baily, G.F. Chen, J.L. Luo, N.L. Wang, “Nearly isotropic superconductivity in $(\text{Ba},\text{K})\text{Fe}_2\text{As}_2$,” *Nature* **457**, 565 (Jan. 2009).

E.A. Yelland, J. Singleton, C.H. Mielke, N. Harrison, F.F. Balakirev, B. Dabrowski, and J.R. Cooper Quantum Oscillations in the Underdoped Cuprate $\text{YBa}_2\text{Cu}_4\text{O}_8$, *Phys. Rev. Lett.* **100**, 047003 (2008).

S.E. Sebastian, N. Harrison, P. Sengupta, C.D. Batista, S. Francoual, E. Palm, T. Murphy, N. Marcano, H.A. Dabkowska, B.D. Gaulin Fractalization drives crystalline states in a frustrated spin system, *Proceedings of the National Academy Of Sciences Of The USA.* **105**, 20157 (2008).

Emerging Materials FWP 58916

Principal Investigators:

John F. Mitchell
FWP Leader
Senior Chemist
mitchell@anl.gov

Kenneth E. Gray
Senior Physicist
kengray@anl.gov

B. J. Kim
Assistant Physicist
bjkim@anl.gov

Material Science Division
Argonne National Laboratory
Argonne, IL 60439

Project Scope

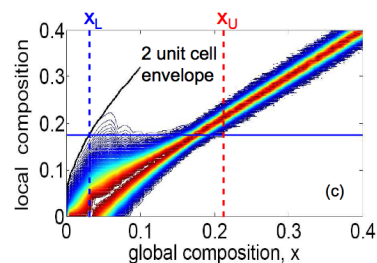
Emerging Materials tightly couples synthesis and crystal growth with insight-driven science as an efficient and reliable pathway to breakthrough results in materials physics. In our program, materials synthesis and crystal growth meet on equal footing to generate fundamental insights, to provide research efficiency through close-connected feedback loops, and to generate pedigreed samples for a worldwide collaborator network. Following this synthesis-science approach, our program plans to expand our established activities beyond *3d* transition metal oxides (TMO)—in which spin, charge, and orbital sectors are distinct, identifiable, and measurable—to address *5d* systems that lie beyond the regime of ‘delicately balanced and tightly coupled’ interactions found among these sectors in the *3d* systems.

Inspired by the novel Mott state recently identified in the nominally $J_{eff} = 1/2$ state of Sr_2IrO_4 , we will use high quality single crystals grown within our program to explore how relativistic spin orbit coupling entangles these notionally separable spin-, charge-, and orbital-order parameters to expose new quantum phases in the presence of electron correlation in *5d* oxides. Specifically, we will explore metal insulator transitions in the presence of this entanglement and search for links to unconventional superconductivity. We will create frustrated lattice structures in both *3d* and *5d* compounds to expose spin-sector and spin-lattice sector interactions for insights into control of magnetic short-range order. We will use reduced dimensionality to test the generality of magnetic and electronic phase segregation. And we will explore nonequilibrium transport effects in both *3d* and *5d* systems, as part of an overarching objective of bridging the gap between the separable and mixed facets of competing interactions. The choice of these materials physics focus areas is based on a program mission to address the Basic Energy Sciences emphasis areas of (1) understanding and controlling correlated-electron phenomena and (2) directing materials discovery and synthesis.

Recent Progress

Our research activities cluster in two general topics in TMO: correlated electron physics and geometric frustration. Below is a brief highlight from each of these areas, which will provide a working framework for exploring the physics of iridates or related $5d$ systems.

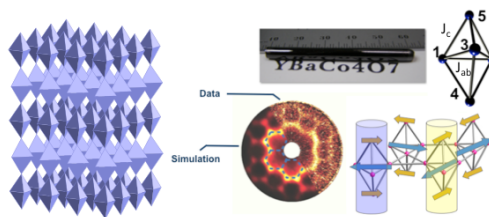
I. *Intrinsic Dopant Fluctuations in $La_{1-x}Sr_xCoO_3$* Our work over the past few years with Chris Leighton (U. Minnesota), Mike Hoch (Florida State and National High Field Magnet Lab) and Frank Bridges (UC Santa Cruz) has deepened the understanding of this system significantly (e.g., EXAFS evidence for missing Jahn-Teller distortions, arguing against significant $S=1$ Co sites in $LaCoO_3$). Perhaps the most important result of this collaboration has come from a comprehensive suite of SANS, magnetization, transport, and heat capacity data on a series of single crystals spanning $0 < x < 0.3$. We showed that the nanoscale ‘phase separation’ in the cobaltites can be quantitatively understood by an inevitable statistical dopant ion inhomogeneity established during growth, thus obviating the need for more exotic explanations for the observed nanoscale phase inhomogeneity in LSCO. This result may in principle extend beyond cobaltites to other randomly doped TMO and represents an *intrinsic* property of the material — statistical fluctuations cannot be avoided during the growth.



Calculated distribution of local Sr doping as a function of the global (i.e., nominal) doping, x , for sampling volumes equal to experimentally determined magnetic correlation volume. Compositions X_U and X_L represent the extreme values of global composition where mixed non-FM and FM regions coexist due to dopant fluctuations. For $x < X_L$ or $x > X_U$, uniform non-FM or long-range FM states are stable, respectively.

II. *Exploring Novel Geometrically Frustrated Lattices* We have

recently been exploring a class of materials with the general formula $RBaM_4O_7$ (R-114; R=Y, Ca, Tb-Lu; M = Co, Fe) that contain the Kagomé lattice motif. Specifically, we have grown tailored single crystals that reveal novel magnetic topologies and have demonstrated control of both structural and magnetic long-range order via oxygen sublattice modification. The structure of R-114, shown at left, is related to that of the pyrochlore lattice when only the magnetic ions are considered. Both pyrochlores and the R-114



Left: Magnetic sublattice of $YBaCo_4O_7$ in trigonal symmetry. Right: single crystal magnetic diffuse scattering comparing data to Monte Carlo simulation, and model of short-range ordered magnetic state just above T_N . All spins lie in the a - b plane.

compounds can be considered as intergrowth structures of Kagomé layers and triangular layers. However, while in a pyrochlore the triangular layers stack (...ABC...), the triangular layers in R-114 stacks (...AAA...). Its absence of chemical disorder (e.g., Zn/Cu mixing in herbertsmithite or Sr/Ga in SCGO) makes this attractive as a model system for magnetic frustration. The availability of two distinct exchange pathways (in-plane and out-of-plane) offers materials design opportunities to tune magnetic frustration in ways not found in pyrochlores for instance. Indeed, we have found from magnetic diffuse scattering studies on long-range ordered antiferromagnetic $YBaCo_4O_{7.0}$ single crystals at a $T > T_N$ that this structure leads to a unique magnetic topology not previously reported, shown schematically in the figure. Chains of

well-ordered Co bipyramids propagating along the c -axis are only weakly correlated with one another in the a - b plane. The most striking feature is that this structure is a composite between order and disorder, with the apical Co atoms (labeled 4 and 5) rigorously coupled ferromagnetically, while the in-plane Co sites (1,2,3) are partially magnetically disordered, albeit with a *net* moment opposing that of the apical sites. Looking ahead, this materials system presents a promising platform for selectively tuning the magnetic coupling between Kagomé sheets.

Future Plans

Research objectives in the upcoming years will emphasize understanding the impact of strong relativistic spin-orbit coupling (SOC) in TMO. Our agenda will be organized along scientific themes that crosscut $3d$ to $5d$ TMO physics and will be guided by an approach that maps specific science issues to the following materials control strategies:

- Dimensionality and Disorder: Impact on TMO Electronic and Magnetic States
- Geometric Frustration: Topological States and Exchange Architecture

We will use both of these materials strategies in the context of this proposal to address the larger question of how SOC impacts the spin-charge-lattice model of TMO. In $5d$ systems we will explore the connection between correlation and SOC. For $3d$ materials, we will advance our understanding of chemical disorder and its impact on electronic states by searching for ‘ordered’ dopant states made possible in some cases by reduced dimensionality. In addition, we will systematically bridge the $3d$ to $5d$ axis by looking at isostructural and isoelectronic low-dimensional systems, thus isolating SOC from extraneous parameters to the largest extent possible. We will explore new topological states in the case of $5d$ iridates by creating magnetic lattices with geometric frustration. This work will join existing efforts focusing on novel $3d$ TMO-based geometrically frustrated magnets that we have pursued in the quest for model systems related structurally to pyrochlores,

Dimensionality and Disorder: Impact on TMO Electronic and Magnetic States

Control of dimensionality is a powerful strategy for isolating competing interactions in TMO, as we have convincingly demonstrated in bilayer manganites. Disorder, typically in the form of random cation and/or anion arrangements arising from chemical doping, has likewise been shown by many groups to be an important ingredient in the physics of $3d$ TMO, leading for instance to ‘phase segregation’ on multiple length scales. In $3d$ TMO mature questions can be readily phrased. For instance, the connection between quenched disorder and phase inhomogeneity in $3d$ systems is well established, yet questions remain open: why is this ‘phase separation’ less prevalent in reduced dimensionality? How do seemingly random dopant landscapes yield extremely narrow phase stability fields? Is there a link between *intrinsic* chemical inhomogeneity and attendant electronic states? We will make headway toward answering these questions by focusing on low-dimensional $3d$ TMO compounds where we propose to grow specimens from heretofore-unexplored regions of phase space. The nascent $5d$ TMO arena brings science issues driven by competing correlation and SOC terms that may provide the basis to test current theories of high temperature superconductivity and topologically controlled states of matter.

Geometric Frustration: Topological Phases and Exchange Architecture

Magnetic ions decorating triangular lattices, Kagomé lattices, pyrochlores, spinels, etc. have long been known to open a window to understanding competing interactions and frustration in the spin sector. Examples include ‘spin ice’ in pyrochlores, and ‘weathervane’ defects in Kagomé lattices. They also provide a structural platform for exposing novel phases of matter, such as quantum spin liquids, Dirac strings (“monopoles”), and potentially topological insulators. We will pursue studies of such novel states of matter and the competing interactions underlying them using $5d$ and $3d$ model systems. In the former our objective is creation of structures that will enable us to test model Hamiltonians not accessible in the absence of SOC. In the latter, we will modify magnetic linkages to build tailored ‘exchange architectures,’ from underlying cobaltites and ferrites. The purpose of building such exchange architectures is to create isolated Kagomé layers, to control short-range order, and to potentially create a new ‘spin ice.’ We will also test fundamental mechanisms of the anomalous Hall effect using frustrated lattices as a materials platform.

Select Recent Publications

1. "Spontaneous formation of an exchange-spring composite via magnetic phase separation in $\text{Pr}_{1-x}\text{Ca}_x\text{CoO}_3$," El-Khatib, S; Bose, S; He, C; Kuplic, J; Laver, M; Borchers, JA; Huang, Q; Lynn, JW; Mitchell, JF; Leighton, C. *Phys. Rev. B* 82, 100411 (SEP 2010).
2. "Spin correlations in the geometrically frustrated RBaCo_4O_7 antiferromagnets: Mean-field approach and Monte Carlo simulations," Khalyavin, DD; Manuel, P; Mitchell, JF; Chapon, *Phys. Rev. B* 82, 094401 (SEP 2010).
3. "Selective Substitution of Cr in CaFe_4As_3 and Its Effect on the Spin Density Wave," Todorov, I; Chung, DY; Claus, H; Gray, KE; Li, QA; Schlueter, J; Bakas, T; Douvalis, AP; Gutmann, M; Kanatzidis, MG. *Chem. Mater.* 22, 4996-5002 (SEP 2010).
4. "d-d excitations in bilayer manganites probed by resonant inelastic x-ray scattering," Weber, F; Rosenkranz, S; Castellán, JP; Osborn, R; Mitchell, JF; Zheng, H; Casa, D; Kim, JH; Gog, T. *Phys. Rev. B* 82, 085105 (AUG 2010).
5. "Muon Spin Rotation Study of the Magnetic Penetration Depth in the Intercalated Graphite Superconductor CaC_6 ," D. Di Castro, A. Kanigel, A. Maisuradze, A. Keren, P. Postorino, D. Rosenmann, U. Welp, G. Karapetrov, H. Claus, D.G. Hinks, A. Amato, and J.C. Campuzano, *Phys. Rev. B* 82, 014530 (JUL 2010).
6. "High-pressure synthesis, crystal and electronic structures of a new scandium tungstate, $\text{Sc}_{0.67}\text{WO}_4$," Varga, Tamas; Mitchell, J. F.; Wang, Jun; Arnold, Lindsay G.; Toby, Brian H.; Malliakas, Christos D. *J. Solid State Chem.* 183, 1567-1573 (JUL 2010).
7. "Observation of a d-Wave Nodal Liquid in Highly Underdoped $\text{Bi}_2\text{Sr}_2\text{CaCu}_2\text{O}_{8-d}$," U. Chatterjee, M. Shi, D. Ai, J. Zhao, A. Kanigel, S. Rosenkranz, H. Raffy, Z.Z. Li, K. Kadowaki, D.G. Hinks, Z.J. Zu, J.S. Wen, G. Gu, C.T. Lin, H. Claus, M.R. Norman, M. Randeria, and J.C. Campuzano, *Nature Physics* 6, 99 (FEB 2010).
8. "Counterintuitive consequence of heating in strongly-driven intrinsic junctions of $\text{Bi}_2\text{Sr}_2\text{CaCu}_2\text{O}_{8+d}$ mesas," Kurter, C.; Ozyuzer, L.; Proslir, T.; Zasadzinski, J. F.; Hinks, D. G.; Gray, K. E. *Phys. Rev. B* 81, 224518 (JUN 2010).
9. "High-pressure crystal growth and magnetic and electrical properties of the quasi-one dimensional osmium oxide Na_2OsO_4 ," Shi, YG; Guo, YF; Yu, S; Arai, M; Belik, AA; Sato, A; Yamaura, K; Takayama-Muromachi, E; Varga, T; Mitchell, JF. *J. Solid State Chem.* 183, 402-407 (FEB 2010).
10. "Heat capacity study of magnetoelectronic phase separation in $\text{La}_{1-x}\text{Sr}_x\text{CoO}_3$ single crystals," He, C; Eisenberg, S; Jan, C; Zheng, H; Mitchell, JF; Leighton, C. *Phys. Rev. B* 80, 214411 (DEC 2009).
11. "Bilayer splitting and c-axis coupling in bilayer manganites showing colossal magnetoresistance," Jozwiak, C; Graf, J; Zhou, SY; Bostwick, A; Rotenberg, E; Zheng, H; Mitchell, JF; Lanzara, A. *Phys. Rev. B* 80, 235111 (DEC 2009).
12. "Transport signatures of percolation and electronic phase homogeneity in $\text{La}_{1-x}\text{Sr}_x\text{CoO}_3$ single crystals," He, C; El-Khatib, S; Eisenberg, S; Manno, M; Lynn, JW; Zheng, H; Mitchell, JF; Leighton, C. *Appl. Phys. Lett.* 95, 222511 (NOV 2009).
13. "Surface-Stabilized Nonferromagnetic Ordering of a Layered Ferromagnetic Manganite," Nascimento, VB; Freeland, JW; Saniz, R; Moore, RG; Mazur, D; Liu, H; Pan, MH; Rundgren, J; Gray, KE; Rosenberg, RA; Zheng, H; Mitchell, JF; Freeman, AJ; Veltruska, K; Plummer, EW. *Phys. Rev. Lett.* 103, 227201 (NOV 2009).
14. "Terahertz wave emission from intrinsic Josephson junctions in high- T_c superconductors," Ozyuzer, L; Simsek, Y; Koseoglu, H; Turkoglu, F; Kurter, C; Welp, U; Koshlev, AE; Gray, KE; Kwok, WK; Yamamoto, T; Kadowaki, K; Koval, Y; Wang, HB; Muller, P. Conference Information: 12th International Superconductive Electronics Conference (ISEC 09), June 16-19, 2009) Fukuoka, JAPAN. *Supercond. Sci. Tech.* 22, 114009 (NOV 2009).
15. "Structural behavior of the kagome antiferromagnet $\text{TmBaCo}_4\text{O}_7$: Neutron diffraction study and group-theoretical consideration," Khalyavin, DD; Chapon, LC; Radaelli, PG; Zheng, H; Mitchell, JF. *Phys. Rev. B* 80, 144107 (OCT 2009).
16. "Study of the local distortions of the perovskite system $\text{La}_{1-x}\text{Sr}_x\text{CoO}_3$ ($0 \leq x \leq 0.35$) using the extended x-ray absorption fine structure technique," Jiang, Y; Bridges, F; Sundaram, N; Belanger, DP; Anderson, IE; Mitchell, JF; Zheng, H. *Phys. Rev. B* 80, 144423 (OCT 2009).
17. "Signature of checkerboard fluctuations in the phonon spectra of a possible polaronic metal $\text{La}_{1.2}\text{Sr}_{1.8}\text{Mn}_2\text{O}_7$," Weber, F; Aliouane, N; Zheng, H; Mitchell, JF; Argyriou, DN; Reznik, D. *Nature Mater.* 8, 798-802 (OCT 2009).

Title: "Ballistic acceleration phase of a supercurrent"
Authors; Milind N. Kunchur and Gabriel Saracila

One of the primitive but elusive current-voltage (I-V) responses of a superconductor is when its supercurrent grows steadily after a voltage is first applied, as per the first London equation. Because this phase lasts for a relatively short duration---until dissipative processes set in---it is difficult to conduct a correlated time-domain I-V measurement of it. The present work employed a measurement system that can simultaneously track and correlate $I(t)$ and $V(t)$ with sub-nanosecond timing accuracy, resulting in a clear time-domain measurement of this transient phase where the quantum system displays a Newtonian like response. The highly controlled technique used here measures the near equilibrium response and should be distinguished from an impulse response measurement, which may probe non-equilibrium processes. The present technique should be of value for the controlled investigation of other types of time-dependent and non-equilibrium phenomena.

Note: This research was supported by the U. S. Department of Energy through grant number DE-FG02-99ER45763.

Interfaces in Epitaxial Complex Oxides (ERKCS80)

Principal Investigators: **Hans M. Christen, Gyula Eres, Ho Nyung Lee, and T.Zac Ward**

Co-Investigators: **Christopher M. Rouleau, Jon Z. Tischler, Ben C. Larson, Anter El-Azab***

Materials Science and Technology Division, Oak Ridge National Laboratory, Oak Ridge, TN 37831

**Department of Scientific Computing, The Florida State University, Tallahassee, FL 32306*

Project Scope

This program seeks a fundamental understanding of the factors that affect novel properties emerging at epitaxial interfaces between dissimilar complex-oxide materials. Specifically, we ask: (1) How can interfacial properties be controlled and tuned by the appropriate choice of materials and synthesis parameters? (2) How are electronic, magnetic, structural and chemical reconstruction interrelated? (3) How do interfaces interact to yield macroscopic properties? (4) How do spatial constraints influence how a system responds to interfacial effects? The synthesis of perovskite heterostructures is controlled at the atomic scale in advanced pulsed-laser deposition (PLD) techniques using electron and x-ray scattering methods for real-time, in-situ diagnostics. A broad range of macroscopic measurements (magnetization, ferroelectricity, transport, optical properties, neutron diffraction, etc.) is combined with spatially-resolved methods (electron microscopy, atom probe tomography, neutron reflectometry, scanning probe microscopy and spectroscopy, etc.) to yield a complete picture of interfacial effects. Specific emphasis is placed on electronic transport both along and across the interfaces or in patterned wires, the emergence of electron gases and magnetization at interfaces between insulating materials, and the coupling between different order parameters. The anticipated impact of this work is an ability to create artificial materials with predetermined macroscopic properties by the deliberate stacking of epitaxial interfaces.

Recent Progress

Recent efforts within this program have focused on structural and electronic effects at interfaces, interfacial-strain stabilization of metastable structural phases, tuning of metal-insulator transitions via interfacial coupling to magnetic nanodots, and a quantitative determination of interlayer transport during PLD growth. The following paragraphs list only specific examples in these areas.

Electronic conduction and structural reconstruction at interfaces.

Two examples illustrate the type of effects that occur when two electronically and/or structurally dissimilar perovskite materials are joined at an atomically-abrupt interface. In the first example, we combined layers of the Mott insulator LaTiO_3 and of the band insulator SrTiO_3 in a delta-doping geometry. At low temperatures, the magnetic field dependence of the Hall resistivity is strongly non-linear. This is attributed to multichannel conduction of interfacial charges generated by an electronic reconstruction (Fig. 1 [Kim 2010]). The second example probes small atomic displacements at interfaces between dissimilar materials with polar discontinuities, relying on aberration-corrected electron microscopy and synchrotron x-ray microdiffraction. The sub-angstrom determination of interfacial polarization reveals how ferroelectric properties can compensate interfacial charges and how a piezoelectric response can be transferred to a non-ferroelectric layer [Chisholm 2010, Jo 2010].

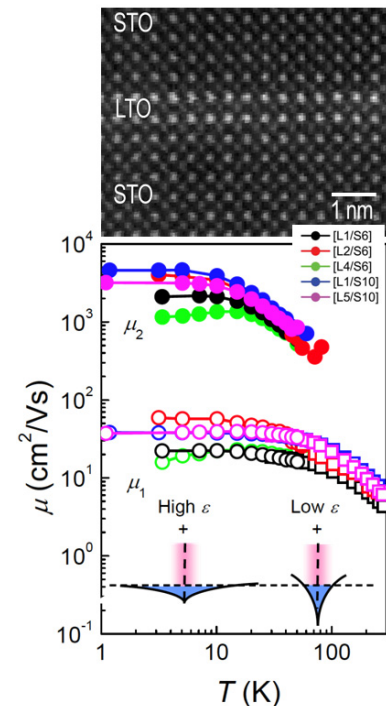


Fig. 1. Z-contrast cross-sectional image of a $\text{LaTiO}_3 / \text{SrTiO}_3$ superlattice, and transport data obtained for various superlattices. Mobilities (extracted from Hall data) for the high-mobility minority carriers are shown as solid circles, those for the lower-mobility minority carriers as open symbols.

Stabilization of metastable phases via interfacial strain.

Related to our work on structural changes at perovskite interfaces we study how such interfaces stabilize materials in crystalline structures that would not exist without the epitaxial constraint. In the specific case of the highly-distorted structure of the multiferroic material BiFeO_3 [e.g. Béa *et al.*, PRL **102**, 217603(2009), Zeches *et al.*, Science **326**, 977 (2009)] we show that the strain-induced phase transition is monoclinic-to-monoclinic and related to those observed in Pb-based solid-solution perovskites [Christen 2011, Bennett 2011], and that additional structural [Siemons 2011] and magnetic [MacDougall 2011] transitions occur near room temperature (work including neutron scattering).

Interfacial coupling of manganite surfaces to magnetic nanodots. We have found that it is possible to exert strong control over the electronic phase competition in the frustrated complex manganite $\text{La}_{1-x}\text{Ca}_x\text{MnO}_3$ (LCMO) [Ward 2011] by coupling the magnetic properties of iron nanodots to the electron spins across the film/nanodot interface. In fact, while the magnetic transition temperatures in ultrathin or highly-strained films are strongly reduced with respect to bulk values, they recover and can be tuned by this coupling.

Kinetics of sharp interface formation. The formation of sharp interfaces is governed by two atomic surface transport processes – intralayer (i.e. redistribution of the growth species within a layer), and interlayer (i.e. redistribution in the vertical direction). As these processes are difficult to study, experimental data yielding an understanding of the formation of oxide surfaces is scarce. We use time-resolved surface x-ray diffraction measurements (SXR) to study the kinetics of oxide film. The specular component of the SXR signal describes the distribution of atoms in the layers perpendicular to the growing surface (related to interlayer process) while the diffuse component contains the intralayer information. Our results include 1) the direct

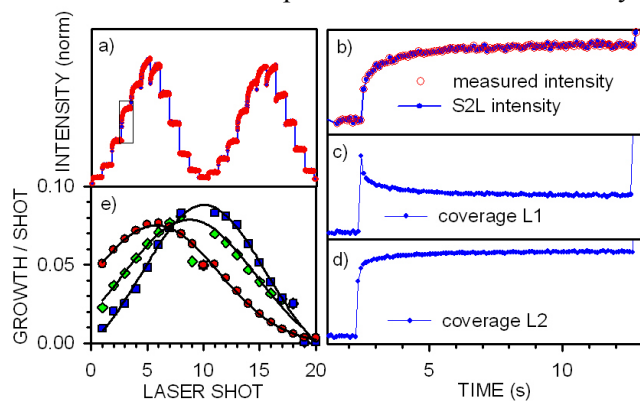


Fig. 3. a) SXR growth intensity oscillation data. b) single shot data corresponding to the window in (a) used to extract the time dependent coverages in (c) and (d) for S2L growth. e) Coverages as a function of laser shot number after plume arrival (red dots), after non-thermal (fast) interlayer transport (green diamonds), and after thermal transport (blue squares). The differences between these curves quantitatively show the relative importance of the different interlayer transport mechanisms [Eres 2011].

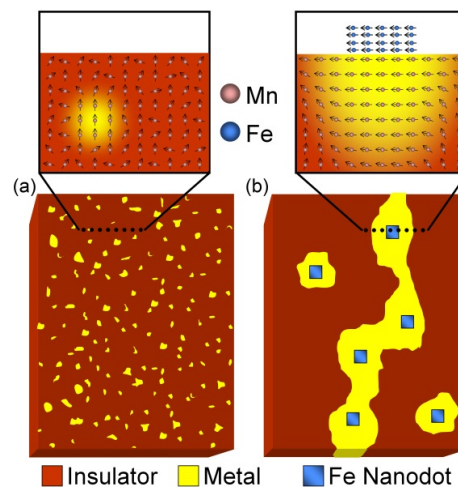


Fig. 2. Schematic diagrams of local spin state cross-sections and top views of LCMO films. a) as-grown LCMO film exhibiting weak spin orientation which leads to only small pockets of the ferromagnetic metallic phase. b, Ferromagnetic Fe nanodots at the surface act to align spins in the LCMO film and allow for the metallic phase to form and open conduction paths at a greatly increased T_C .

measurement of the crystallization time of SrTiO_3 , which occurs on microsecond time scale and separates the non-thermal and thermal components of PLD film growth that occur on vastly different time scales, 2) the demonstration that high-quality (non-step-flow) film growth (by PLD or other methods) proceeds by a variant of layer by layer growth that occurs on two layers simultaneously (simultaneous 2-layer growth, S2L), and 3) the quantitative determination of a strong, energy enhanced (non-thermal) interlayer transport (Fig. 3 [Eres 2011]). It is this fast interlayer transport that is the primary process responsible for the redistribution of the growth species that promotes the formation of smooth layer, while thermal processes occur on a much slower time scale and play a minor role.

Future Plans

The combination of the demonstrated abilities to create electronic carriers at interfaces between insulators, to modify the local crystalline structure across an interface, to stabilize entirely meta-stable phases via interfacial strain, and to influence the spin-behavior near a surface or an interface via magnetic nanodots, and our understanding of how such materials are formed during PLD, opens up a broad range of possibilities for creating materials in which the interfaces themselves lead to novel and enhanced properties that are not found within the constituents. Rather than describing the entire spectrum of anticipated future experiments, we simply illustrate a few specific examples:

Formation of interfacial materials. We will further develop the necessary methods to grow three-dimensional epitaxial structures, including superlattices and fractional superlattices (assemblies incorporating embedded wires or islands), to probe the effects of interfacial magnetism, conductivity, and spatial confinement. For example, we will seek to induce low-dimensional magnetism within epitaxial heterostructures and differentiate it from bulk magnetism in chemically similar but structurally different materials, and develop oxide nano-junctions that hold the potential to generate a large amount of photo-induced carriers. Three-component superlattices will be used to isolate the effects of specific interfaces and asymmetries in magnetic and ferroelectric structures.

Effects of interfacial coupling on laterally-confined structures. Previous work [Ward *et al.*, *Phys. Rev. Lett.* **102**, 087201 (2009)], relying on lithographically-patterned nanowires of manganites, shows that laterally-confined structures enable time-resolved studies of electronic phase transitions. This opens up the possibility to investigate the effects of interfaces and of surface nanodot decorations onto such systems, and to investigate superlattice structures that are spatially-confined in two dimensions and include interface-interface coupling.

Real-time studies of growth kinetics and combination with RHEED. In the next phase of this work, we will investigate the impact of island nucleation and growth kinetics – as observed using time-resolved specular and diffuse synchrotron x-ray scattering – on the electrical, magnetic and optical response of the heteroepitaxial interface region. Most importantly, we will extend the real-time SXRD studies by using simultaneous Reflection High Energy Electron Diffraction (RHEED) observations.

Neutron studies of epitaxial systems. We have shown that neutron diffraction is a powerful tool to probe magnetic properties in epitaxial films, and will continue to perform experiments at both ORNL neutron sources (elastic scattering, reflectometry), for investigations of antiferromagnetism and interfacial magnetization.

Publications

2011 (through June 30):

- C. J. C. Bennett, H. S. Kim, M. Varela, M. D. Biegalski, D. H. Kim, D. P. Norton, H. M. Meyer III, and H. M. Christen, *J. Mater. Res.* **26**, 1326 (2011).
- W. S. Choi, D. W. Jeong, S. Y. Jang, Z. Marton, S. S. A. Seo, H. N. Lee, and Y. S. Lee, *J. Kor. Phys. Soc.* **58**, 569 (2011).
- W. S. Choi, D. W. Jeong, S. S. A. Seo, Y. S. Lee, T. H. Kim, S. Y. Jang, H. N. Lee, and K. Myung-Whun *Phys. Rev. B* **83**, 195113 (2011).
- H. M. Christen, J. H. Nam, H. S. Kim, A. J. Hatt, and N. A. Spaldin, *Phys. Rev. B* **83**, 144107 (2011).
- Gyula Eres, J. Z. Tischler, C. M. Rouleau, P. Zschack, H.M. Christen, and B.C. Larson, submitted to *Phys. Rev. B* (2011).
- H. Ko, K. Ryu, H. Park, C. Park, D. Heon, Y. K. Kim, J. Jung, D.-K. Min, Y. Kim, H. N. Lee, Y. Park, H. Shin, and S. Hong, *Nano Lett.* **11**, 1428 (2011).
- G. J. MacDougall, H. M. Christen, W. Siemons, M. D. Biegalski, J. L. Zarestky, S. Liang, E. Dagotto, and S. E. Nagler, submitted to *Phys. Rev. Lett.* (2011).
- W. Siemons, M. D. Biegalski, J. H. Nam, and H. M. Christen, *Applied Physics Express*, accepted for publication (2011).
- T. Z. Ward, Z. Gai, X. Y. Xu, H. W. Guo, L. F. Yin, and J. Shen, *Phys. Rev. Lett.* **106**, 157207 (2011).

- X. Y. Xu, K. Seal, X. S. Xu, I. Ivanov, C.-H. Hsueh, N. A. Hatab, L. Yin, X. Zhang, Z. Cheng, B. Gu, Z. Zhang, and J. Shen, *Nano Lett.* **11**, 1265 (2011).
- S. M. Yang, S. Y. Jang, T. H. Kim, H. H. Kim, H. N. Lee, J.-G. Yoon, *J. Kor. Phys. Soc.* **58**, 599 (2011).
- 2010:**
- M. F. Chisholm, W. Luo, M. P. Oxley, S. Pantelides, and H. N. Lee, *Phys. Rev. Lett.* **105**, 197602 (2010).
- H. M. Christen, G. J. MacDougall, H.-S. Kim, D. H. Kim, L. A. Boatner, C. J. Callender Bennett, J. L. Zarestky, and S. E. Nagler, *J. Phys. Conf. Series* **251**, 012021 (2010).
- J. W. Freeland, J. Chakhalian, A. V. Boris, J.-M. Tonnerre, J. J. Kavich, P. Yordanov, S. Grenier, P. Popovich, H. N. Lee, and B. Keimer, *Phys. Rev. B* **81**, 094414 (2010).
- B. Gray, H. N. Lee, J. Liu, J. Chakhalian, and J. W. Freeland, *Appl. Phys. Lett.* **97**, 013105 (2010).
- J. Y. Jo, R. J. Sichel, E. M. Dufresne, H. N. Lee, S. M. Nakhmanson, and P. G. Evans, *Phys. Rev. B* **82**, 174116 (2010).
- J. Y. Jo, R. J. Sichel, H. N. Lee, S. M. Nakhmanson, E. M. Dufresne, and P. G. Evans, *Phys. Rev. Lett.* **104**, 207601 (2010).
- J. Y. Jo, R. J. Sichel, H. N. Lee, E. Dufresne, and P. G. Evans, *Mater. Res. Soc. Symp. Proc.* **1199**, 1199-F01-06 (2010).
- H. S. Kim and H. M. Christen, *J. Phys. Condens. Matter.* **22**, 146007 (2010).
- H. S. Kim, H. M. Christen, M. D. Biegalski, and D. J. Singh, *J. Appl. Phys.* **108**, 054105 (2010).
- J. S. Kim, S. S. A. Seo, R. K. Kremer, H.-U. Habermeier, B. Keimer, and H. N. Lee, *Phys. Rev. B* **82**, 201407(R) (2010).
- M.-H. Kim, G. Acbas, M.-H. Yang, M. Eginligil, P. Khalifah, I. Ohkubo, H. M. Christen, D. G. Mandrus, Z. Fang, and J. Cerne, *Phys. Rev. B* **81**, 235218 (2010).
- H. Pan, B. Gu, G. Eres, and Z. Zhang, *J. Chem. Phys.* **132**, 104501 (2010).
- M. Varela, J. Gazquez, A. R. Lupini, J. T. Luck, *et al. Int. J. Mater. Res.* **101**, 21 (2010).
- S. M. Yang, J. Y. Jo, T. H. Kim, J.-G. Yoon, T. K. Song, H. N. Lee, Z. Marton, S. Park, Y. Jo, and T. W. Noh, *Phys. Rev. B* **82**, 174125 (2010).
- 2009:**
- W. S. Choi, Z. Marton, S. Y. Jang, S. J. Moon, B. C. Jeon, J. H. Shin, S. S. A. Seo, T. W. Noh, K. Myung-Whun, H. N. Lee, and Y. S. Lee *J. Phys. D: Appl. Phys.* **42**, 165401 (2009).
- M. Z. Li, Y. G. Yao, B. A. Wu, Z. Y. Zhang, and E. G. Wang, *Europhys. Lett.* **86**, 16001 (2009).
- M. M. Özer, C.-Z. Wang, Z. Y. Zhang, and H. H. Weitering, *Journal of Low Temperature Physics* **157**, 221 (2009).
- S. S. A. Seo and H. N. Lee, *Appl. Phys. Lett.* **94**, 232904 (2009).
- S. S. A. Seo, Z. Marton, W. S. Choi, G. W. J. Hassink, D. H. A. Blank, H. Y. Hwang, T. W. Noh, T. Egami, and H. N. Lee, *Appl. Phys. Lett.* **95**, 082107 (2009).
- D. A. Tenne, H. N. Lee, R. S. Katiyar, and X. X. Xi, *J. Appl. Phys.* **105**, 054106 (2009).
- 2008:**
- J. Cao, J. L. Musfeldt, D. J. Singh, B. Rahaman, T. Saha-Dasgupta, C. C. Torardi, B. C. Sales, H. M. Christen, and O. Swader, *Phys. Rev. B* **77**, 717 (2008).
- H. M. Christen and G. Eres, *J. Phys. Cond. Matter* **20**, 264005 (2008).
- H. M. Christen, D. H. Kim, and C. M. Rouleau, *Appl. Phys. A* **93**, 807 (2008).
- H. M. Christen, M. Varela, and D. H. Kim, *Phase Transitions* **81**, 717 (2008).
- W. Hong, Z. Suo, and Z. Y. Zhang, *J. Mech. Phys. Solids* **56**, 267 (2008).
- D. H. Kim, H. N. Lee, M. D. Biegalski, and H. M. Christen, *Appl. Phys. Lett.* **92**, 12911 (2008).
- D. Lott, F. Klose, H. Ambaye, G. J. Mankey, P. Mani, M. Wolff, A. Schreyer, H. M. Christen, and B. C. Sales, *Phys. Rev. B* **77**, 132404 (2008).
- J. Ma, E. G. Wang, Z. Y. Zhang, and B. A. Wu, *Phys. Rev. B* **78**, 125303 (2008).
- Y. N. Mo, W. G. Zhu, E. Kaxiras, and Z. Y. Zhang, *Phys. Rev. Lett.* **101**, 216101 (2008).
- C. M. Rouleau, H. M. Christen, H. Cui, G. Eres, A. A. Puretzky, and D. B. Geohegan, *Appl. Phys. A* **93**, 1005 (2008).

Project Title: Transport Studies of Quantum Magnetism: Physics and Methods

Principal Investigator: Minhyea Lee

Institution: University of Colorado at Boulder

Email: minhyea.lee@colorado.edu

Project Scope:

The collective behavior arising from many interacting degrees of freedom is a key feature of many physics problems. It not only characterizes a given state of matter but determines the measurable signatures. It is manifested in a set of elementary excitation that can carry charge, energy and other quantum numbers like spin. The type of excitations present and the nature of their propagation and scattering provide a wealth of information about the state of matter from which they arise. Moreover, the same information determines the behavior of fundamentally and technologically important transport properties such as electric and thermal conductivity. In turn, this information can be probed by driving the system slightly off-equilibrium and measuring the resulting linear response in a transport experiment. In many cases, transport results have been essential to uncover the crucial signatures of low-lying excitations. The aim of this project is to investigate the elementary excitations in quantum spin systems via electrical and thermal transport study. There are two main classes of quantum magnetic system of our interest: One is insulating quantum magnets, where geometrical frustration and quantum fluctuation are believed to lead to unusual elementary excitations. The other is metallic magnetic systems in which magnetic structures have an influence on the elementary charge carrying excitations and thus leads to unusual electrical transport properties. As a part of work on insulating quantum magnets, we will develop a new thermometry particularly tailored for the low temperature thermal transport properties measurement. The new technique is based on shot noise from a tunnel junction and is expected to overcome significant limitations of existing methods for thermal conductivity measurement in low temperature. This will serve as particularly useful tool for studying the insulating quantum magnets.

Recent Progress:

Not Applicable: expected project start date is mid August 2011.

Future Plans:

In metallic quantum magnets, we will seek for new types of electronic behavior as a result of unusual spin structures. Anomalous Hall effect (AHE) is known as a sensitive probe to examine such situations. We will particularly focus on AHE generated from non-zero spin chirality both in the presence and in the absence of long-range magnetic order (i.e time reversal symmetry broken). In this way we will be able to make a distinction between the signals coming from underlying spin structure and spin-chirality. We will explore the possibility to probe mobile spin textures with non-zero chirality via Nernst effect measurement in analogy with vortices in type II superconductors.

We will also study insulating *quantum spin liquids* using thermal transport measurements, searching for the itinerant nature of spin excitation and probing the role of dimensionality and/or disorder. The quantities of interest are thermal conductivity (κ_{xx}), and thermal Hall effect, which appears in the transverse thermal conductivity (κ_{xy}) when a magnetic field is applied in the z-direction, and is the thermal analog of Hall effect. In particular, κ_{xx} in the limit $T \rightarrow 0$ directly probes the presence or absence of an energy gap and the itinerant or localized nature of excitations. The magnetic field dependence along different crystal directions is expected to provide further information on the nature of elementary excitation of the system. In quasi-one-dimensional spin chain systems, some work on highly enhanced ballistic thermal conductivity has been reported, but such measurements have been done only sparsely for two-

and three-dimensional systems. The thermal Hall effect is also a very interesting quantity. Most simply, it provides a means of separating spin and lattice contributions to thermal transport, because the lattice hardly responds to an applied field and hardly contributes to thermal Hall effect. Also, there is a recent theoretical prediction of substantial thermal Hall effect in certain quantum magnets, which results from the coupling between applied magnetic field and a hypothesized spinon gauge field. If this effect is observed, it could be the first clear evidence for the presence of a spinon gauge field in some systems.

Since the interesting temperature range for these systems are often very low, existing thermal transport properties measurement methods need to be improved for various reasons. We will develop a new methodology for resilient and micrometer scale thermometry using a shot noise tunnel junction. Shot noise from a normal metal-insulator-normal metal tunnel junction is related to the voltage across the junction via the Fermi-Dirac distribution in such way that it is determined by only the temperature, DC voltage across the junction, junction resistance, and fundamental constants of electron charge, Planck constant and Boltzmann constant. Thus, the junction temperature can be determined from the noise power measurement, which has been already demonstrated down to 10 mK. This new thermometry is extremely attractive for use in thermal transport measurements for several reasons: First, because the temperature is determined by physical laws and fundamental constants, no separate calibration of the thermometer is necessary. Moreover, effects of external conditions such as high magnetic field or pressure are expected to be unimportant, as compared to the large magnetic field dependence and unknown/unexplored pressure dependence of low temperature resistive thermometers. Second, the thermometer is lithographically defined, even directly on the surface of sample, with much smaller size than any conventional resistive sensors; this will improve the accuracy of the measurement greatly. Finally, there is no need to switch to another thermometer as T changes. We believe this technique will greatly advance experimental accuracy and efficiency in thermal transport measurements. It is particularly suited to measurements on magnetic insulators because of the low energy scales and importance of tuning with magnetic field. In addition, it has a great potential to become a standard ultra-low temperature thermometry in research and industrial settings.

List of Publications:

Not Applicable: expected project start date is mid August 2011.

Studies of interband modes and Fermi surface features in very clean MgB₂ films

PI: Qi Li

Department of Physics, Pennsylvania State University, University
Park, PA 16802
e-mail: qill@psu.edu

I. Project scope

The multiband nature of MgB₂ may lead to new physical phenomena that do not exist in single-band superconductors. For example, a proposed collective excitation corresponding to small fluctuations of the relative phase of the two superconducting condensates in two different bands (the "Leggett mode") may be observable. A strong electric field may cause local breakdown of the phase locking between the two superconducting order parameters. On the other hand, many physical properties of MgB₂ are different from conventional single-band superconductors, which are significantly influenced by the intraband scattering in different bands. A direct way to quantify the scattering and Fermi surface features of each band is needed. The objectives of this research project are (a) to investigate the new physical phenomena due to interband phase correlation in MgB₂ which do not exist in single-band superconductors; and (b) to study in depth the scattering and Fermi surface features in the different bands of MgB₂, which is one of the most important factor in determining its physical behaviors. For this project, very clean MgB₂ thin films deposited by HPCVD and high quality MgB₂ Josephson junctions and tunnel junctions with the presence of both gaps will be used. One of the research goals will focus on phenomena associated with the phase difference of the two superconducting condensates in MgB₂. MgB₂ tunnel junctions will be used to detect the resonance coupling between the Josephson current and the Leggett mode in MgB₂. Microbridges will be used to measure the phase textures and voltage oscillations induced by an electric current. The other research goal will focus on the details of the the gaps features in the tunneling spectrum of each band, and magnetoresistance measurements and quantum oscillation of magnetoresistance at the National High Magnetic Field Lab to probe the scattering rates and Fermi surface features in each band.

II. Recent Progress

Multi-band superconductivity has attracted significant renewed interest due to its existence in MgB₂, iron-based superconductors, and other superconducting materials. In MgB₂, besides the widely-observed two superconducting energy gaps

arising from the σ and π bands, theoretical calculations taking into account the fully anisotropic electron-phonon interaction further predict a distribution of gap values for both σ and π bands on the Fermi surface of MgB_2 . However, only two distinct gaps have been observed experimentally before, leading to the suggestion that the two-band model is sufficient for real MgB_2 samples. Our recent results focus on electron tunneling spectroscopy study on planar MgB_2 /native oxide/Pb junctions grown on different substrate orientations. The results clearly show the distribution of energy gaps within one band in very clean samples for junctions with different orientations. By deconvoluting the tunneling spectrum based on the density of state of Pb, we have derived the momentum-dependent energy gaps of MgB_2 , which are in good agreement with the anisotropic Eliashberg calculation. The result affirms the importance of the anisotropic electron-phonon interaction and Coulomb repulsion in MgB_2 and momentum dependence of the energy gaps. On samples with different amount disorders, the gap features become narrower with disorder until it becomes a single gap. This is consistent with the theoretical prediction that scattering will smear out the multigap features. The gap values and their spreads from the tunnel junction measurements provide a valuable experimental test for the development of various theoretical approaches of multi-band superconductivity in MgB_2 .

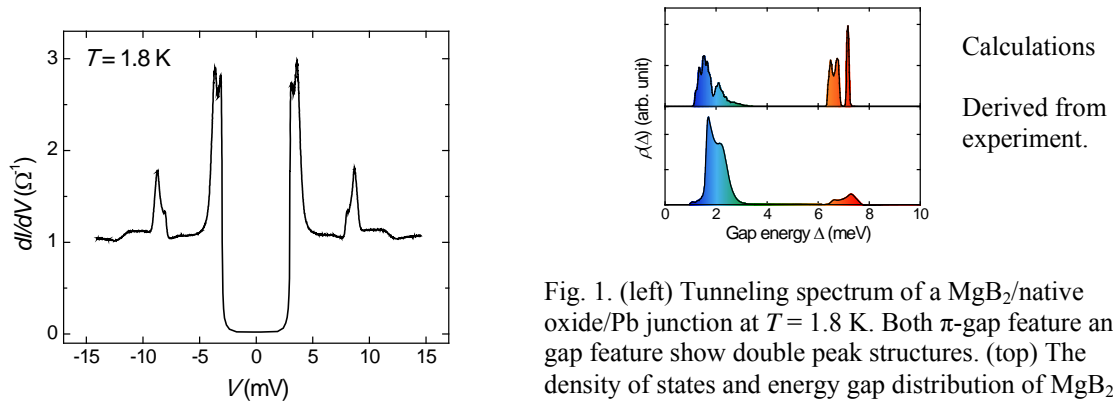


Fig. 1. (left) Tunneling spectrum of a MgB_2 /native oxide/Pb junction at $T = 1.8$ K. Both π -gap feature and σ -gap feature show double peak structures. (top) The density of states and energy gap distribution of MgB_2 .

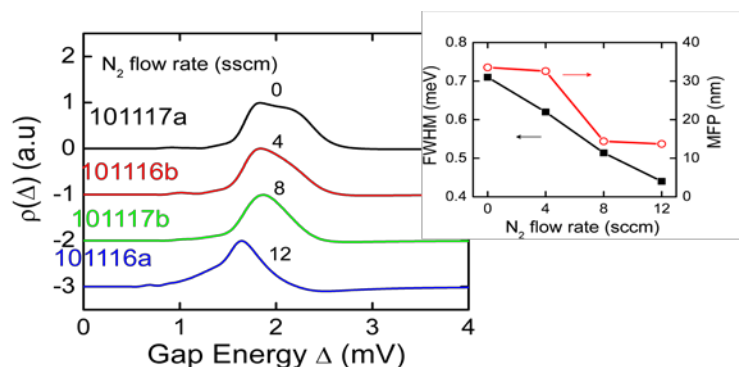


Fig. 2. π gap distribution of four junctions with different level of N_2 during growth. (inset) The FWHM of the gap peaks.

III. Future plans

Multiband superconductivity has gained tremendous attention recently owing to the discovery of superconductivity in MgB₂ and iron pnictides. Many new physical phenomena, such as the "Leggett mode", interband interference, soliton, and Andreev bound state, have been proposed. They are collective modes due to phase relationship or fluctuations between bands. In previous studies, we have observed, for the first time, that MgB₂ does not just have two gaps as previously thought. Each band has a distribution of gap values associated with different parts of the Fermi surface, depending on the momentum. We will continue working in the area to fully investigate the relationship between the gap distributions and other changes in the system, the interband modes, and expand the research into new superconductors. The future research will investigate (a) the effect of intra- and inter-band scattering, carrier doping, and crystal orientation on the momentum distribution of the gap values and evolution of each band in MgB₂; (b) the Josephson-Leggett mode, interband interference, and Andreev bound state in MgB₂ and iron pnictides through resonance tunneling; and (c) the topological superconducting states induced through proximity effect between a topological insulator and MgB₂.

The first activity will provide a deeper understanding of the energy gap features of different parts of Fermi surfaces, and the effect of scattering and doping on their evolution towards two gap. This is not only important to multiband superconductors, but also single gap superconductors with multiple conduction bands, like Nb. The second activity detects new physical phenomena that do not exist in conventional superconductors. Therefore, to experimentally verify these effects will be very significant in advancing our understanding of condensed matter physics. The third activity, the topological superconducting states are a completely new system. By inducing surface topological superconductors, we may explore completely new phenomena in superconductivity.

IV. Publications

1. Y. Huang, Y.L. Wang, L. Shan, Y. Jia, H. Yang, H.H. Wen, G.C. Zhuang, Q. Li, Y. Cui, X.X. Xi, Field Dependence of π -Band Superconducting Gap in MgB₂ Thin Films from Point-Contact Spectroscopy, Chinese Phys. Lett. 25, 2228 (2008)
2. K. Chen, Y. Cui, Qi Li, C. G. Zhuang, Zi-Kui Liu, and X. X. X, Study of MgB₂/I/Pb tunnel junctions on MgO (211) substrates, Appl. Phys. Lett. 93, 012502 (2008)
3. H. Yang, Y. Liu, C.G. Zhuang, J.R. Shi, Y.G. Yao, S. Massidda, M. Monni, Y. Jia, X.X. Xi, Qi Li, Z.K. Liu, Q. R. Feng, and H.H. Wen, Fully band-resolved scattering rate in MgB₂ revealed by the nonlinear Hall effect and magnetoresistance measurements, Phys. Rev. Lett. 101, 067001 (2008).

4. Shufang Wang, A. Venimadhav, Shengming Guo, Ke Chen, Qi Li, A. Soukiassian, Darrell G. Schlom, Michael B. Katz, X. Q. Pan, Winnie Wong-Ng, Mark D. Vaudin, and X. X. Xi, Structural and thermoelectric properties of $\text{Bi}_2\text{Sr}_2\text{Co}_2\text{O}_y$ thin films on LaAlO_3 (100) and fused silica substrates, *Appl. Phys. Lett.* 94, 022110 (2009)
5. Daniel R. Lamborn, Rudiger H.T. Wilke, Qi Li, X.X. Xi, David W. Snyder, and Joan M. Redwing, Modeling studies of an impinging jet reactor design for hybrid physical-chemical vapor deposition of superconducting MgB_2 films, *J. Crystal Growth* 311, 1501 (2009).
6. Sanghan Lee, Ke Chen, Seung Hyup Baek, Wenqing Dai, Brian H. Moeckly, Qi Li, Xiaoxing Xi, Mark S. Rzchowski, and Chang Beom Eom, Growth of MgB_2 Thin Films *In Situ* by RF Magnetron Sputtering With a Pocket Heater, *IEEE Trans. Appl. Superc.* 19, 2811 (2009).
7. T.P. Chen, K. Wu, Q. Li, B. Chen, S. Z. Wang, H. Kandel, Y. Soo, U. Tipparach, J. B. Cui, H. Seo, C.J. Chen, Structure and transport studies on nanometer YBCO/PBCGO multilayers, *Chinese Sci Bull* 54, 2698 (2009).
8. P. Orgiani, Ke Chen, Yi Chui, Qi Li, V. Ferrando, M. Putti, M. Iavarone, R. Di Capua, R. Ciancio, R. Valio, L. Maritato, and X.X. Xi, Anisotropic transport properties in tilted *c*-axis MgB_2 thin films, *Superc. Sci. Technol.* 23, 025012 (2010)
9. Ke Chen, C. G. Zhuang, Qi Li, Y. Zhu, P. M. Voyles, X. Weng, J. M. Redwing, R. K. Singh, A. W. Kleinsasser, and X. X. Xi, High- J_c MgB_2 Josephson junctions with operating temperature up to 40 K, *Appl. Phys. Lett.* 96, 042506 (2010)
10. C.G. Zhuang, Ke Chen, J.M. Redwing, Qi Li, X.X. Xi, Surface morphology and thickness dependence of the properties of MgB_2 thin films by hybrid physical-chemical vapor deposition, *Superc. Sci. Technol.* 23 055004 (2010).
11. Y. W. Yin, M. Raju, W. J. Hu, X. J. Weng, X. G. Li, and Q. Li, Coexistence of tunneling magnetoresistance and electroresistance at room temperature in $\text{La}_{0.7}\text{Sr}_{0.3}\text{MnO}_3/(\text{Ba}, \text{Sr})\text{TiO}_3/\text{La}_{0.7}\text{Sr}_{0.3}\text{MnO}_3$ multiferroic tunnel junctions, *J. App. Phys.* 109, 07D915 (2011).
12. Ke Chen, C.G. Zhuang, Qi Li, X. Weng, J.M. Redwing, Y. Zhu, P.M. Voyles, X.X. Xi, $\text{MgB}_2/\text{MgO}/\text{MgB}_2$ Josephson Junctions for High-Speed Circuits, *IEEE Trans. on Appl. Superconductivity* 21, 115 (2011).

Project Title: Emergent Behavior of Magnet-Superconductor Hybrids

Principal Investigator: Igor F. Lyuksyutov (lyuksyutov@physics.tamu.edu)

Institution: Texas A&M University, Department of Physics and Astronomy

Co-Investigators: W. Wu (wwu@physics.tamu.edu), D. G. Naugle (naugle@physics.tamu.edu)

Project Scope

We study emergent behavior which appears when two mutually exclusive states of matter, magnetism and superconductivity, are combined at the nanoscale in a unified system. Arrays of nanomagnets, either embedded into the superconducting film or placed outside on a thin insulating layer, provide Tesla range magnetic fields penetrating into the superconducting film and changing sign at distances as small as 60 nm. Magnetoresistance of such hybrid systems differs dramatically from the magnetoresistance of a conventional superconducting film. Two main mechanisms are responsible for the novel behavior:

- nanometer scale inhomogeneity of the magnetic field and superconducting regions;
- strong magnetic interaction of the superconducting vortices with magnetic nanostructures.

The first factor dramatically changes the phase diagram, and the second one creates a strong magnetic pinning potential for vortices and in this way strongly increases the critical current or its anisotropy. We have experimentally shown by using embedded Ni or Co nanomagnets that the critical current can be increased up to several orders of magnitude in finite (several hundreds of Gauss) magnetic field in comparison with the conventional film. This result can be useful in design of YBCO thin film based power cables. We have generated Tesla range magnetic fields that periodically change sign on the scale of the Cooper pair size. This allows us to extend these studies to a new level: from vortex control/pinning to Cooper pair control/localization by magnetic nanostructures.

Results of this project have been published in Ref. [1-13], accepted for publication in Ref. [14-17] or are in preparation for publication.

Recent Progress

Magnetic Nanorods Arrays. We have previously proposed the use of arrays of magnetic nanorods embedded in a superconductor instead of pancake-like dots for more effective vortex pinning [18]. In contrast to a non-magnetic pinning center, the magnetic nanorod can use the whole vortex energy, which

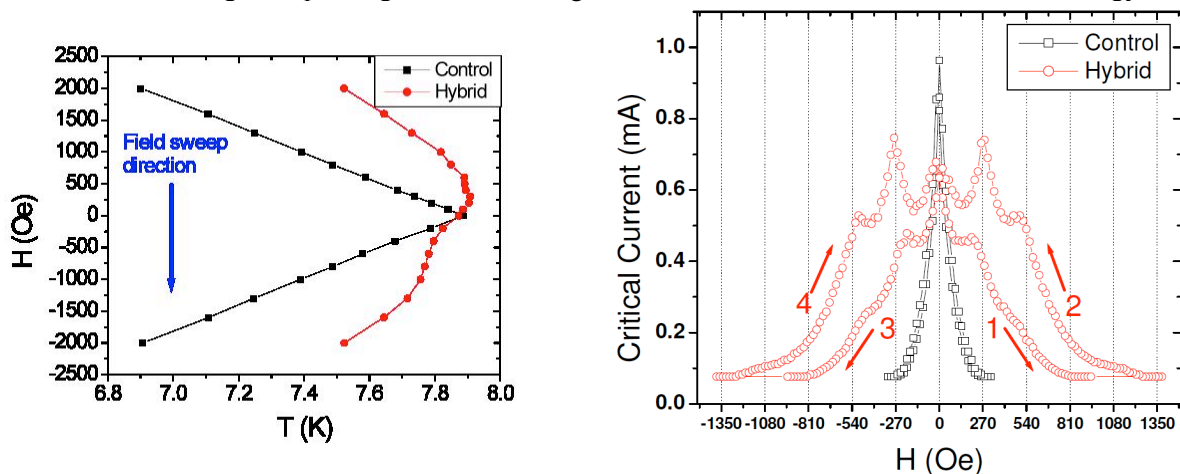


Figure 1. *Left:* Phase diagram for the control (black squares) sample and for the hybrid (red circles) PbBi film with square array of Ni nanorods [13]. *Right:* Critical current as a function of field for the PbBi film with a triangular array of Co nanorods (red circles) and the control film (black squares). Arrows indicate direction of the magnetic field change. Dotted lines show first matching field multiplied by integers [17].

is mainly magnetic, to better pin vortices [18]. In contrast to previous studies [19-22], we have fabricated magnetic columnar nanostructures with high aspect ratio (3-4) magnetic Ni nanorods which have a diameter (100nm) small enough to preserve the magnetization direction (parallel to the rod) even at room temperature. We have studied magnetoresistance of Ni and Co nanorod arrays embedded into a 100nm thick $\text{Pb}_{82}\text{Bi}_{18}$ superconducting film. Fig. 1 left shows the phase diagram of a film with a square Ni nanorod array with 270nm period and of a control film without nanorods. The phase diagram of the hybrid film demonstrates asymmetry due to hysteresis of the Ni nanorod array and a shift of the T_C maximum to the magnetized state. This shift is due to the magnetic field generated by the magnetized array and directed opposite to the applied field [19,20,22]. Fig. 1 right shows the critical current for a 100nm thick $\text{Pb}_{82}\text{Bi}_{18}$ superconducting film with an embedded Co nanorod triangular array with period 270 nm and for the control film. At the first matching field (270 Oe) the film with the magnetized array has orders of magnitude larger critical current than the control film. This proves the suggestion [18] that magnetic pinning can be more effective than traditional pinning.

Magnetic Nanorails for Vortices. Recently we have observed strong anisotropy in the vortex pinning in a superconducting film exposed to a stripe-like magnetic field pattern created by magnetic structures with a period from ten to hundreds of microns [4, 9]. We have observed that the critical current in the direction parallel to the stripes was up to an order of magnitude higher than in the perpendicular direction [4, 9]. In these systems an insulating layer separated the superconductor from the ferromagnet. Therefore, the superconductor and ferromagnet only interact via the magnetic field. The anisotropy in the critical current in this extremely wide range of periods for the magnetic stripe structure is due purely to the magnetic interaction of vortices with the stripe magnetic structure.

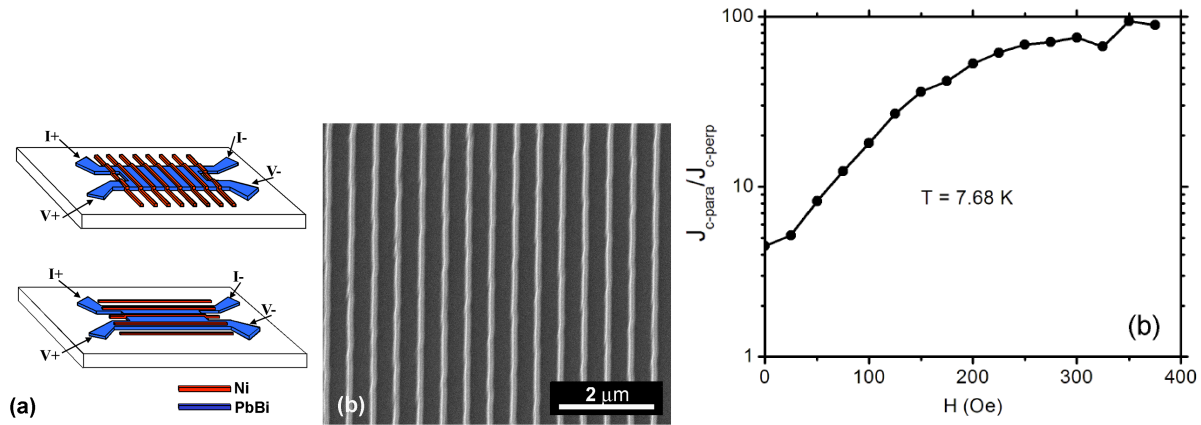


Figure 2. *Left:* (a) Hybrid sample structures. (b) SEM image of the Ni stripes; *Right:* Ratio of the critical current densities as a function of magnetic field for superconducting films with stripes parallel and perpendicular to the applied current at $T = 7.68$ K [11].

When the current is parallel to the magnetic stripes, the Lorentz force acts on vortices in the direction perpendicular to the stripes and vice versa. The magnetic interaction of vortices with the magnetic stripes provides a periodic potential barrier for vortex motion in the direction perpendicular to the stripes. This explains the higher value of critical current in the direction parallel to the stripes in comparison to that perpendicular to the stripes. Fig. 2 right shows critical current measurements for a stripe magnetic nanostructure with width as narrow as 80nm and with a period as small as 300nm, almost 1000 times smaller than in [4].

Fig. 2 (left) illustrates the structure for the hybrid samples with current perpendicular and parallel to the magnetic stripes. Rectangular superconductor film patterns with four contact leads were defined by electron-beam lithography. Superconducting $\text{Pb}_{82}\text{Bi}_{18}$ thin films of thickness ~ 100 nm were thermally evaporated onto the silicon wafer substrates. Stripe patterns were defined by e-beam lithography. The stripes are either perpendicular or parallel to the current. After evaporating a 20 nm thick Ge insulating layer, 120 nm thick Ni

films were thermally evaporated onto the stripe patterns. Fig. 2 (left, b) shows a typical SEM image of the Ni stripes on the $\text{Pb}_{82}\text{Bi}_{18}$ superconducting film. Fig.2 right shows the ratio of the critical current densities, which ranges from 5 to 100, as a function of magnetic field for films with stripes parallel and perpendicular to the applied current. Thus the magnetic nanostructure plays the role of magnetic nanorails for vortices.

Future Plans. We plan to fabricate and study the following systems:

- i. Superconducting films with arrays of magnetic nanorods embedded into the film as discussed above. This type of system will be studied with 2-5 times smaller rod diameters and with higher aspect ratios than with current nanostructures. We plan to study superconducting films with a wide range of coherence lengths and arrays with different symmetries and periods in a wide range of temperatures. We expect to determine system parameters, which result in the highest values of critical current. We will also study such systems in the limit when the coherence length becomes larger than the elementary cell of the magnetic nanorod array.
- ii. We will continue to study magnetic pinning in superconducting films with a periodic array of magnetic stripes as discussed above. We will refine our fabrication technique to get a higher aspect ratio (height/width) for the magnetic stripes. We will explore a wide range of periods, temperatures and coherence lengths (through alloying the film to reduce the coherence length). Special efforts will be taken to improve the quality of our films.
- iii. In the system of the type described in (ii) we will study the situation when the Cooper pair size becomes comparable or exceeds the period of the magnetic field variation. The Cooper pairs can be localized in the direction perpendicular to the stripes, but delocalized along the stripes. At low temperature this may result in a system, which demonstrates high resistance for current in the direction perpendicular to the stripes and superconductivity in the direction parallel to the magnetic stripes. Of course, the real system can demonstrate only a large difference in magnetoresistance due to the inevitable misalignments, local shorts, etc. We will explore a wide range of periods, temperatures and coherence length. Note that this is a different effect from the critical current anisotropy that we have already demonstrated.
- iv. We will fabricate superconducting films with a single magnetic stripe as a weak link and study Cooper pair tunneling through the region of high magnetic field. Such measurements will give important information to understand the system behavior in (iii).
- v. We will try to fabricate superconducting films with arrays of magnetic nanorods atop the film. We plan to study predominantly the magnetic interaction of both vortices and Cooper pairs with the magnetic nanostructure. We will measure transport properties and critical current of these superconducting films with a wide range of coherence lengths, symmetries and periods and in a wide range of temperatures. We expect to observe a set of resistive and superconducting states. In particular we will search for the appearance of a highly resistive (insulating) state with decreasing temperature.
- vi. We will continue to explore superconducting films atop an alumina membrane template with magnetic nanowires. These studies will include magnetic pinning with thinner superconducting films and better ordered membrane nanowires. Another direction will be studies of the magnetic interaction of Cooper pairs with an array of magnetic nanowires. We will also use tunneling spectroscopy with STM to prove if a gap really exists in a region with finite resistivity.
- vii. We will continue work on fabrication methods of magnetic nanorods embedded into a YBCO film with Naugle's Pulsed Laser Deposition System. We will work to extend the critical current enhancement, that we have achieved with magnetic nanorods in films of conventional superconductors, to YBCO films. In this work we will take advantage of the expertise of Haiyan Wang, Associate Professor in the Department of Electrical and Computer Engineering at TAMU, with whom we have collaborated on the YBCO fabrication.

List of publications resulting from DOE sponsored research that have been published in 2008-2011 or that have been accepted for publication:

1. Z. Ye, H. Zhang, H. Liu, W. Wu and Z. Luo, "Observation of Superconductivity in Single Crystalline Bi Nanowires," *Nanotechnology* **19**, 085709 (2008).
2. Z. Ye, H. Liu, Z. Luo, H. Lee, W. Wu, D. G. Naugle and I. Lyuksyutov, *Thickness dependence of the microstructure and magnetic properties of electroplated Co nanowires*, *Nanotechnology* **20**, 045704 (2009).
3. Z. Ye, H. Liu, Z. Luo, H. Lee, W. Wu, D. G. Naugle, and I. Lyuksyutov, *Changes in the crystalline structure of electroplated Co nanowires induced by small template pore size*, *J. Appl. Phys.* **105**, 07E126 (2009).
4. A. E. Ozmetin, K. D. D. Rathnayaka, D. G. Naugle, and I. F. Lyuksyutov, *Strong increase in critical field and current in magnet-superconductor hybrids*, *J. Appl. Phys.* **105**, 07E324 (2009).
5. A. E. Ozmetin, M. K. Yapici, J. Zou, I. F. Lyuksyutov and D. G. Naugle, *Micro Magnet-Superconducting Hybrid Structures with Directional Current flow Dependence for Persistent Current Switching*, *App. Phys. Lett.* **95**, 022506, (2009).
6. K. Kim, D. G. Naugle, W. Wu and I. F. Lyuksyutov, *Large Increase of the Critical Field in a Magnet-Superconductor Nanowire Hybrid*, *Journal of Superconductivity and Novel Magnetism*, **23**, 1075 (2010).
7. I. Lyuksyutov, *Magnetic Nanorod - Superconductor Hybrids*, *Journal of Superconductivity and Novel Magnetism*, **23**, 1047 (2010).
8. Z. Ye, D. G. Naugle, W. Wu and I. Lyuksyutov, *Superconducting Properties of Pb/Bi Films Quenched-condensed on a Porous Alumina Substrate Filled with Co Nanowires*, *Journal of Superconductivity and Novel Magnetism*, **23**, 1083 (2010).
9. I. Lyuksyutov, D. G. Naugle, A. E. Ozmetin, M. K. Yapici, J. Zou, *Vortex Pinning by an Inhomogeneous Magnetic Field*, *Journal of Superconductivity and Novel Magnetism*, **23**, 1079 (2010).
10. K. Kim, A. E. Ozmetin, D. G. Naugle and I. F. Lyuksyutov, *Flux Pinning with a Magnetic Nanorod Array*, *App. Phys. Lett.* **97**, 042501 (2010).
11. Z. Ye, I. F. Lyuksyutov, W. Wu and D. G. Naugle, *Strongly anisotropic flux pinning in superconducting $Pb_{82}Bi_{18}$ thin films covered by periodic ferromagnet stripes*, *Supercond. Sci. Technol.* **24**, 024011 (2011).
12. Z. Ye, I. F. Lyuksyutov, W. Wu and D. G. Naugle, *Superconducting properties of $Pb_{82}Bi_{18}$ films controlled by ferromagnetic nanowire arrays*, *Supercond. Sci. Technol.* **24**, 024019 (2011).
13. K. Kim, I. F. Lyuksyutov and D. G. Naugle, *Magnetic nanorod-superconductor hybrid near the superconducting transition temperature*, *Supercond. Sci. Technol.* **24**, 024013 (2011).
14. K. Kim, K. D. D. Rathnayaka, I. F. Lyuksyutov and D. G. Naugle, *Superconducting film with an array of magnetic nanostripes*. *Journal of Superconductivity and Novel Magnetism*, accepted.
15. K. Kim, K. D. D. Rathnayaka, I. F. Lyuksyutov and D. G. Naugle, *Transport properties of a superconducting film with magnetic nanostripes*, *Journal of Superconductivity and Novel Magnetism*, accepted.
16. I. F. Lyuksyutov, *Controlling superconductivity with magnetic nanostructures*, *Journal of Superconductivity and Novel Magnetism*, accepted.
17. H. Lee, K. Kim, K. D. D. Rathnayaka, I. F. Lyuksyutov and D. G. Naugle, *Superconducting film with embedded cobalt nanorods*. *Journal of Superconductivity and Novel Magnetism*, accepted.

References

18. I. F. Lyuksyutov and D. G. Naugle, *Mod. Phys. Lett. B* **13** 491-7 (1999)
19. M. Lange, M. J. Van Bael, Y. Bruynserade and V. M. Moshchalkov, *Phys. Rev. Lett.*, **90**, 197006 (2003).
20. I. F. Lyuksyutov and V. L. Pokrovsky, *Advances in Phys.* **54**, 67-136, (2005).
21. M. Velez, J.I. Martin, J.E. Villegas, A. Hoffmann, E.M. Gonzalez, J.L. Vicent, and I. K. Schuller, *J. Mag. Mat.* **320**, 2547 (2008).
22. A. Yu Aladyshkin, A. V. Silhanek, W. Gillijins and V. V. Moshchalkov, *Supercond. Sci. Technol.* **22**, 053001 (2009)

Program Title: *Electronic and Optical Processes in Novel Semiconductors for Energy Applications*

Principle Investigators: A. Mascarenhas, Brian Fluegel, Kirstin Alberi, Aleksej Mialitsin

Institution: NREL

Mailing address: 1617 Cole Blvd., Golden, CO 80401

e-mail: angelo.mascarenhas@nrel.gov

Program Scope:

Advanced energy technologies require high-performance materials, which in photovoltaics translates to new semiconductor alloys to efficiently absorb sunlight, and in solid-state lighting (SSL), to new semiconductors for direct conversion of electricity to white light. A goal of this project is fundamental materials research for the realization of semiconductors that transcend the existing limitations that constrain present photovoltaic and solid-state lighting technologies. It specifically addresses the current unavailability of efficient high bandgap (2.1 eV) and low bandgap (1 eV) absorbers for photovoltaics, and efficient green emitters for SSL, via technologies based on GaAs substrates. The key to transcending the present limitations, is the understanding and control of fundamental electronic and optical processes in semiconductors, which is another goal of this project. Towards this, the project focuses on understanding the phenomena of spontaneous ordering in high bandgap lattice-mismatched $\text{Ga}_x\text{In}_{1-x}\text{P}$, and the abnormal electronic structure and properties of isoelectronic dopants N and Bi in GaAs. Additionally, it addresses recent observations of new excitations in bipolar plasmon gasses photogenerated in semiconductors, so as to achieve an understanding of collective phenomena that could enable semiconductors with novel, useful properties. Through collaborative efforts, this project utilizes state-of-the-art resources in growth, spectroscopy, and theory, from three national laboratories, to address the above mentioned issues. By exploiting the use of BES Nanoscience Centers (CINT), and Supercomputer Facilities (LBNL), it brings to bear new tools for the growth and characterization of semiconductors, and connects BES theory and computation programs with the experimental work in this BES supported project at NREL.

Recent Progress: Major Achievements

Our work on exciton photoluminescence (PL) ring patterns has revealed surprising behavior in which upconversion ring patterns can be moved and focused at special sample defects called localized bright spots (LBS)ⁱ. Here photogenerated charge carriers attain lifetimes and diffusion lengths that are orders of magnitude greater than what is typically found in direct gap semiconductors. If fully understood, this might allow photogenerated charge to be swept across a detector array, similar to charge-coupled devices that are presently limited to silicon. Ordinary PL rings result from isotropic 2D diffusion, but our results show that those diffusing carriers can be concentrated and reradiate from the LBS, which are points of enhanced tunneling in the multiple quantum well structure. The LBS collect charge carriers and vertically funnel them into the adjacent layer.

A key point in Fig 1(a) is that the PL occurs through field-assisted upconversion, i.e., it has a photon energy greater than the laser. This process is driven by field-assisted tunneling, and at high field its efficiency can actually be comparable to direct laser excitation. Upconversion favorably modifies the electron and hole QW capture rates, giving a high contrast between the

ring and the laser spot. As Fig. 1(a) shows, upconversion PL (UPL) is relatively weak at the point of laser excitation. Much more intense UPL is emitted in a ring centered at the LBS. Time-resolved UPL in Fig. 1(b) reveals how this occurs. Excitation of the sample with a ns square-wave laser pulse, and use of a streak camera to sweep a horizontal slice of the map image shows how the ring's radius expands in time.

The LBS ring is modeled as a point of weakness in the tunnel barriers that allows greatly increased tunneling of electrons into adjacent wells, where they expand outward before undergoing radiative recombination. By numerically solving rate equations for the electron and hole densities in these layers, we have reproduced the image of Fig. 1(a) and its behavior as a function of laser-LBS separation. By functioning as a collector for electrons, the LBS has greatly modified the carrier transport compared to simple diffusion. Previous works in directing this type of long-range transport have been limited to the indirect excitons of coupled quantum wells^{ii,iii}. By using transport through multiple vertical structures coupled by the LBS, we have now accomplished this with free electrons.

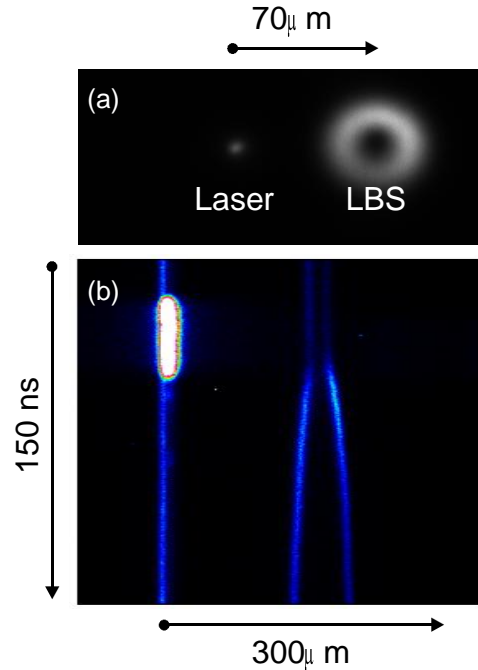


Figure 1. Exciton ring generation centered at a localized bright spot. (a) Spatial PL map showing the point of focused laser excitation at left and the LBS-centered ring at right. The LBS itself is dark. (b) A streak camera sweep of a similar image in which the horizontal vertical axes are space and time.

Work in progress and future plans

We are currently investigating the behavior of collective excitations of photogenerated 2D electron gasses (2DEGs) in multiple quantum well layers. When two distinct charge-carrier gases are present in the same material layer, or in layers that are close enough to be coulomb-coupled, their density oscillations will be coupled to each other; these are generally understood and known as a bilayer plasma. A much more exotic phenomenon occurs when the two layers are within a de Broglie wavelength and tunneling can occur. In this case plasmons modes exist which can be classically envisioned as an electron density that bounces between the two spatially separated layers. The charge density waves have been studied in doped coupled-quantum wells^{iv} (CQWs), but very little is known about the corresponding *spin*-density waves in which electrons oscillate between layers accompanied by a change of spin. Our preliminary results show that these modes can be generated all-optically in a CQW under an applied electric field by working in resonance with the spin-orbit band. Figure A shows light-scattering results in which the moving spectral peak labeled ISP apparently follows a shifting intersubband energy. The origin of the higher energy replicas is entirely unknown and will likely require careful study of the effects of charge separation, band bending and screening of the field.

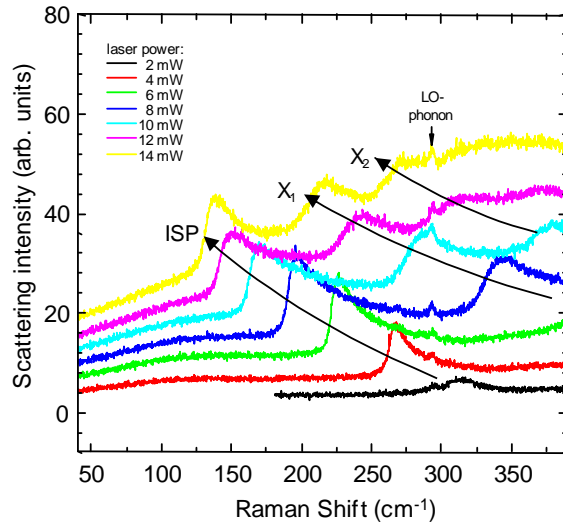


Figure A. Depolarized light scattering intensity from a CQW in an electric field. ISP is likely the spin-density wave associated with the intersubband transition between the CQW's tunneling-split ground state.

ⁱ B. Fluegel, K. Alberi, L. Bhusal, A. Mascarenhas, D. W. Snoke, G. Karunasiri, L. N. Pfeiffer, and K. West, *Phys. Rev. B* **83**, 195320 (2011).

ⁱⁱ L. V. Butov, C. W. Lai, A. L. Ivanov, A. C. Gossard, and D. S. Chemla, *Nature* **417**, 47 (2002).

ⁱⁱⁱ Z. Vörös, D. W. Snoke, L. Pfeiffer, and K. West, *Phys. Rev. Lett.* **97**, 016803 (2006).

^{iv} M.-T. Bootmann, C.-M. Hu, Ch. Heyn, D. Heitmann, and C. Schüller, *Phys. Rev. B* **67**, 121309(R) (2003).

PUBLICATIONS (emanating from this project during the period (2008-2010))

1. "Exciton pattern generation in GaAs/AlGaAs multiple quantum wells", B. Fluegel, K. Alberi, L. Bhusal, A. Mascarenhas, D. W. Snoke, G. Karunasiri, L. N. Pfeiffer and K. West, *Phys. Rev. B.* **83**, 195320 (2011).
2. "Solid-State Lighting", L. Bhusal and A. Mascarenhas, *Handbook of Luminescent Semiconductor Materials*, Book Chapter, Taylor and Francis, (2011).
3. "Effect of Bi alloying on the hole transport in the dilute bismide alloy, GaAs_{1-x}Bi_x", R. N. Kini, A. J. Ptak, R. France, R. C. Reedy and A. Mascarenhas, *Phys. Rev. B.* **83**, 75307 (2011).
4. "III-V semiconductor alloys covering 600~6000 nm", L. Bhusal, and A. Mascarenhas, *Materials Science and Engineering B*, (2010).
5. "Synthesis and photovoltaic effect of vertically aligned ZnO/ZnS core/shell nanowire arrays", Wang K, Chen, J. J., Zeng, Z. M., Tarr, J., Zhou, W. L. Zhang, Y., Yan, Y. F. Jiang, C. S., Pern, J., Mascarenhas A., *Appl. Phys. Lett.* **96**, 123105 (2010).
6. "Direct-Indirect Crossover in GaInP Alloys", K. Alberi, B. Fluegel, M. Steiner, R. France, W. Ollavaria and A. Mascarenhas. *J. Appl. Phys.* (submitted).
7. "Shubnikov-de Haas measurement of electron effective mass in GaAs_{1-x}Bi_x", B. Fluegel, R. N. Kini, A. J. Ptak, D. Beaton, K. Alberi, and A. Mascarenhas, *Appl. Phys. Lett.* (submitted)
8. "Kinetically-limited growth of GaAsBi by molecular-beam epitaxy", A.J. Ptak, R. France, D.A. Beaton, K. Alberi, J.D. Simon, C.-S. Jiang and A. Mascarenhas. (submitted).
9. "Ordering induced direct-indirect transformation in unstrained GaIn_{1-x}P for 0.76 < x < 0.78". Bhusal, L; Fluegel, B; Steiner, MA; et al. *J. Appl. Phys.* **106**, 114909 (2009).
10. "Polarized photoluminescence from point emitters in ordered GaIn_{1-x}P". Fluegel, B; Mascarenhas, A; Geisz, JF. *Phys. Rev. B*, **80**, 125333 (2009).
11. "CuPt ordering in high bandgap GaIn_{1-x}P alloys on relaxed GaAsP step grades". Steiner, MA; Bhusal, L; Geisz, JF; et al. *J. Appl. Phys.* **106**, 063525 (2009).
12. "Electron Hall mobility in GaAsBi". Kini, RN; Bhusal, L; Ptak, AJ; et al. *J. Appl. Phys.* **106**, 043705 (2009).
13. "Comparison of atomistic simulations and statistical theories for variable degree of long-range order in semiconductor alloys". Zhang, Y; Mascarenhas, A; Wei, SH; et al. *Phys. Rev. B*, **80**, 045206 (2009).
14. "Tailoring the electronic properties of GaIn_{1-x}P beyond simply varying alloy composition". Zhang, Y; Jiang, CS; Friedman, DJ; et al. *Appl. Phys. Lett.* **94**, 091113 (2009).
15. "Comparison of the dilute bismide and nitride alloys GaAsBi and GaAsN". Mascarenhas, A; Kini, R; Zhang, Y; et al. *Physica Status Solidi B* **246**, 504 (2009).
16. "Contactless electroreflectance studies of ultra-dilute GaAs_{1-x}Bi_x alloys". Bhusal, L; Ptak, AJ; France, R; et al. *Semicond. Science and Technology* **24**, 035018 (2009).
17. "Interplay of alloying and ordering on the electronic structure of GaIn_{1-x}P alloys". Zhang, Y; Mascarenhas, A; Wang, LW. *Phys. Rev. B* **78**, 235202 (2008).
18. "Low temperature photoluminescence from dilute bismides". Kini, RN; Mascarenhas, A; France, R; et al. *J. Appl. Phys.* **104**, 113534 (2008).
19. "An UV photochromic memory effect in proton-based WO₃ electrochromic devices". Zhang, Y; Lee, SH; Mascarenhas, A; et al. *Appl. Phys. Lett.* **93**, 203508 (2008).
20. "Aberration-free imaging for light and electrons". Fluegel, B; Mascarenhas, A. *Appl. Phys. Lett.* **93**, 161105 (2008).
21. "Growth and properties of the dilute bismide semiconductor GaAs_{1-x}Bi_x a complementary alloy to the dilute nitrides". Tiedje, T; Young, EC; Mascarenhas, A. *Int. Journal of Nanotechnology* **5** (9-12): 963 (2008).
22. "Direct growth of highly mismatched type II ZnO/ZnSe core/shell nanowire arrays on transparent conducting oxide substrates for solar cell applications". Wang, K; Chen, JJ; et al. *Advanced Materials* **20** (17): 3248 (2008).
23. "Non-bloch nature of alloy states in a conventional semiconductor alloy: GaIn_{1-x}P as an example". Zhang, Y; Mascarenhas, A; Wang, LW. *Phys. Rev. Lett.* **101**, 036403 (2008).
24. "Bi isoelectronic impurities in GaAs". Francoeur, S; Tixier, S; Young, E; et al. *Phys. Rev. B*, **77**, 085209 (2008).

Title: Investigations of the Material Dependence of the Casimir Force

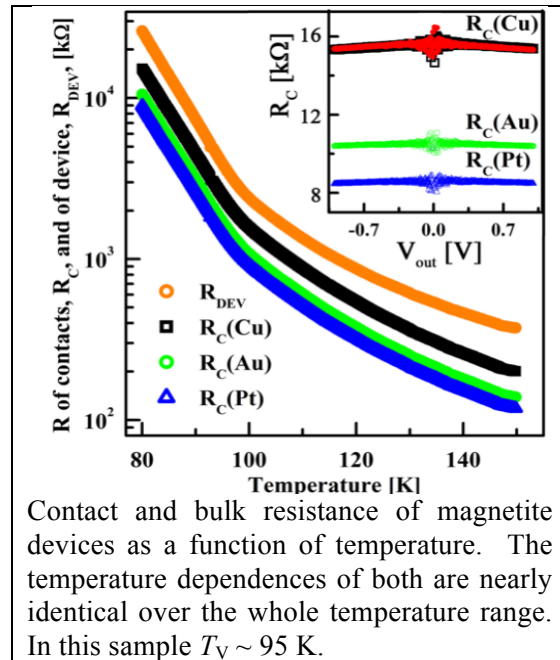
The Casimir force, which for some simple geometries can be crudely approximated by the many body retarded van der Waals force, is critical to the function, design and yield of micro mechanical systems, where moving segments are placed at submicron separations. The material dependence of the Casimir force are very interesting and we will present recent experiments of reducing the Casimir force with transparent materials and by UV treatment. In addition, we will also review ongoing investigations of the role of magnetic materials in the Casimir force.

Project Scope

This project applies nanostructure techniques to strongly correlated electronic materials (SCEMs). Strong electronic correlations often lead to competing electronic ground states, and as a result, SCEMs often exhibit rich phenomenology, including metal-insulator transitions, magnetic ordering, colossal magnetoresistance, and high temperature superconductivity. Nanostructure methods have become highly developed over the last two decades, and have chiefly been applied to semiconductor materials. Nanoscale devices enable probes of SCEMs that can shed light on the underlying physics in ways not possible in macroscale devices. Closely spaced electrodes allow the application of extremely large perturbing dc electric fields with comparatively modest voltages, delineating field-driven effects from those triggered by available energy per electron. Complementary to scanned probe techniques, nanoscale electrodes and nanoscale SCEMs can examine the physics of strong correlations in the presence of geometric confinement, and probe systems on length scales comparable to intrinsic and extrinsic inhomogeneities. Nonequilibrium studies of SCEMs also benefit from nanoscale device engineering. Field effect structures allow the tuning of carrier density at fixed disorder, a modification of material properties not possible in macroscale systems. Thus far, we have concentrated on applying these techniques to two SCEMs, magnetite (Fe_3O_4) and vanadium dioxide (VO_2). Both materials exhibit first order transitions between high temperature conducting states and low temperature insulating states, accompanied by structural transitions to low temperature phases of reduced symmetry. Magnetite experiments revealed a nonequilibrium transition, with the application of large dc electric fields destabilizing the correlated insulating state. These studies have examined the mechanism of this transition, as well as the nature of the charge injection and transport process, and the relative importance of electronic correlations. Vanadium dioxide experiments have concentrated on attempts at electrolytic gating, and have led to the development of hydrogen doping as a means of drastically altering the electronic properties of the material.

Recent Progress

Magnetite. Our recent progress concerning magnetite has focused on using nanoscale multiterminal devices fabricated on 50 nm thick films grown by oxide-assisted molecular beam epitaxy. Magnetite has a moderately conducting “bad metal” phase at room temperature, separated by a first-order “Verwey” transition from a correlated insulating state below $T_V \sim 120$ K in the bulk. The nature of the correlations in the ground state and the physics of the Verwey transition remain controversial. Specifically debated are the relative importance of electron-electron and electron-phonon interactions (in essence, is the transition more Mott-like vs. more Peierls-like). Below T_V , the nonequilibrium transition driven by the application of a large in-plane electric field kicks the material out of the insulating state, providing a new handle for accessing the physics of the correlated state.



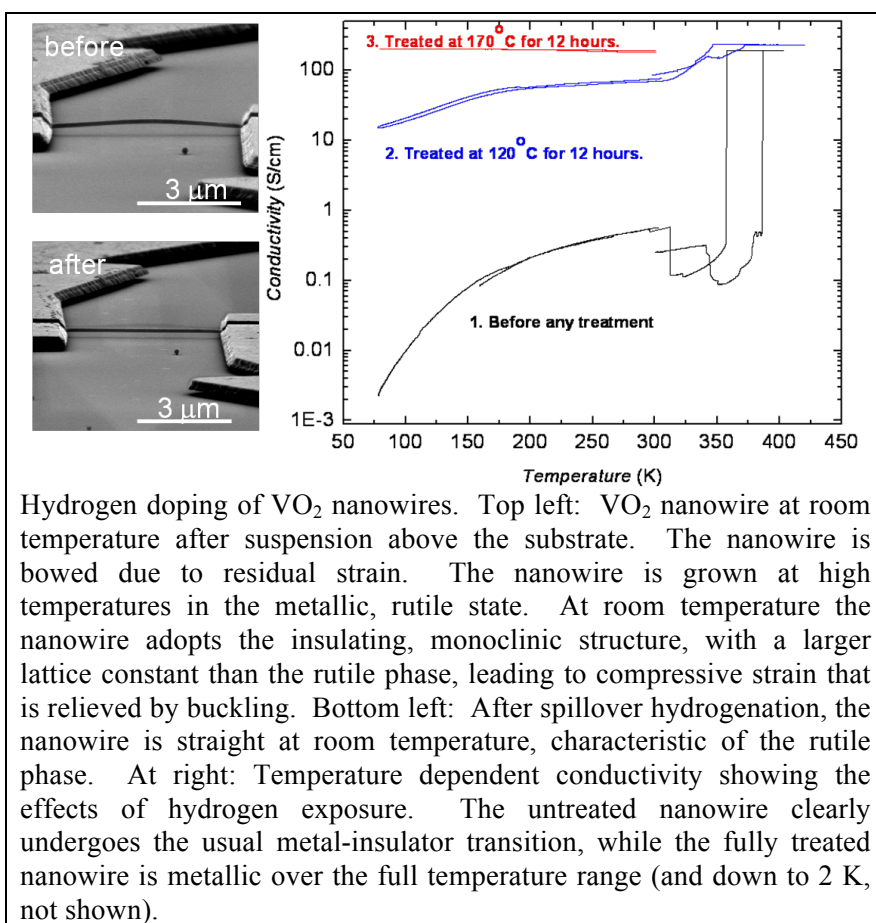
Pulsed measurements demonstrated that the electric field-driven transition is intrinsic and not due to self-heating.

Recent results using the multiterminal measurements have demonstrated that, as the critical electric field is exceeded, the contact resistance at the metal/oxide interfaces drops, along with the bulk resistance. This is consistent with the idea that the destabilization of the gapped insulating state comes as a result of physics analogous to Landau-Zener breakdown. Comparisons of contact resistance and bulk resistance as a function of temperature for three different contact metals (Cu, Au, Pt) have been revealing; contact resistance is found to be directly proportional to bulk resistivity over the whole temperature range including across T_V . This is consistent with models of injection into a system where bulk conduction takes place through hopping between localized states. Most recently, we have examined the statistical variation in the switching voltage, and how that distribution evolves with temperature and magnetic field. Observations suggest a connection between magnetization orientation and the stability of the insulating state, providing a hint for a theoretical approach to the breakdown mechanism.

Vanadium dioxide. At 68 °C, VO₂ undergoes a first-order phase transition between a low temperature, insulating, monoclinic state (gap = 0.6 eV) and a high temperature, metallic, rutile state. As in magnetite, the relative importance of electronic correlations and electron-phonon coupling are much debated in VO₂. We have conducted a series of experiments using single-crystal VO₂ nanowires and nanoplates grown by physical vapor transport.

We first attempted to use an ionic liquid (DEME-TFSI) as an electrolytic gate to modulate the conductance in these nanowires. Electrolytic gating permits the accumulation of surface charge densities exceeding 10^{14} carriers/cm², approaching the level of one carrier per unit cell. In a Mott insulator such gating experiments may enable a “Mott transistor”. Remarkably, we found *no sign* of direct field-effect modulation of the metal-insulator transition. The lack of conventional gate response, even in the semiconducting regime, is surprising. We did discover surface electrochemistry can modulate nanowire conductivity by orders of magnitude. When the ionic liquid contained dissolved water, and the electrochemical biasing was in the range needed to split that water, enormous (slow, hysteretic) changes in nanowire conductance were observed.

These observations led to our major VO₂ achievement: *spillover hydrogenation of VO₂ nanowires at very moderate temperatures leads to stabilization of the metallic phase.* The effects of hydrogen exposure



are remarkable, changing the low temperature conductivity of VO₂ by more than 10⁴. Electron diffraction shows that the rutile structure is stabilized after hydrogenation. The metallic state may be stabilized down to cryogenic temperatures. Elastic strain in VO₂ drastically affects the hydrogenation process. In nanowires freed from the substrate, hydrogenation and attendant conductance changes proceed readily. However, in nanowires stuck to the growth substrate, or in thin, plate-like VO₂ that is under high lateral strain, hydrogenation is greatly inhibited. These strain issues also make full temperature-dependent studies of the newly resulting, correlated metal H_xVO₂ nanowires challenging. Conversely, inhomogeneous hydrogen concentration leads to dramatic temperature-dependent conformational changes in unanchored or cantilevered beams, due to local variation in the modified transition temperature and the differing lattice constants of the metallic and insulating phases. These results are in the process of being written for publication.

Future Plans

Magnetite. One important next step is to confirm and better characterize the coupling between magnetization orientation and the stability of the correlated state. This requires measurements of the statistics of the electric field-driven breakdown process as function of external magnetic field in at least two field orientations, over a broad temperature range. If preliminary data is borne out, this may bear directly on the role of electronic correlations and spin-orbit coupling in the low temperature Verwey state. So far, breakdown voltages are altered at the few percent level as the magnetization is reoriented, while the actual low-bias resistivity (set by direct hopping of carriers) is comparatively unaffected. This suggests that spin-orbit coupling, known to be important in the reported multiferroic ordering of magnetite below 40 K, plays an important role in the stability of the insulating state.

Additionally, we shall conduct high speed (nanosecond) pulsed measurements of the breakdown process. Preliminary data suggests that the breakdown field is actually reduced in high speed pulses, and that the typical timescale between bias application and breakdown is tens of nanoseconds. Understanding the kinetics of the destruction of the ordered state will shed light on the role of disorder and the free energy landscape associated with this finite-temperature nonequilibrium transition. We shall also examine the effect of ionic gating on the stability of the insulating state. Ionic liquids provide a means of applying enormous electrostatic fields normal to the surface of the SCEM, in the absence of net current flow. It remains to be seen whether the gapped Verwey state is stable in the presence of such a field.

Vanadium dioxide. Central to our investigations are the opportunities opened by our discovery of hydrogen's ability to tune the MIT in VO₂ and stabilize the metallic state down to low temperatures. First, it is essential to ***understand the mechanism whereby hydrogen stabilizes the metallic structure***. Is this a case of doping altering the band filling to suppress Mott physics, or does the presence of hydrogen in the lattice affect the softening of the phonon modes associated with the rutile to monoclinic transition? This question is likely to require a strong collaborative effort with theorists, and we have begun appropriate discussions. Closely related, what is the ***critical hydrogen concentration*** required for the stabilization? This is very challenging, given that the hydrogenation process is most controllably performed in individual nanocrystals, and extremely light elements like hydrogen can be very difficult to detect directly. Collaboration again may be needed, with users of advanced TEM and other local probes. Solving this challenge will be of more general use to the nanomaterials community, with respect to the related problems of hydrogen storage and lithiation. We hope to assess the spatial location of the phase boundary between metallic and insulating states as a function of temperature through study of the temperature-dependent deformation of inhomogeneously doped nanocrystals. The kinetics of hydrogenation are also important – the related (not correlated) rutile TiO₂ structure has extremely anisotropic diffusion of hydrogen that can be enhanced by orders of magnitude under infrared illumination. Systematic studies of hydrogenation and resulting properties under different, controlled strain conditions are also of much interest.

We need to ascertain the *properties of the stabilized metallic state*, including a measure of the importance of correlations, down to low temperatures. Some methods (magnetotransport) are readily accomplished at the single nanocrystal level. However, other techniques that would be extremely useful (magnetization measurements to search for magnetic order; low temperature heat capacity measurements to assess the “heaviness” of the charge carriers) are more readily accomplished if large quantities of hydrogenated material can be prepared. Accordingly, while embarking on magnetotransport measurements, we are working to use Pd nanoparticles and related materials to attempt hydrogenation of bulk amounts of VO₂ powder. Combining optical illumination and electronic transport measurements is another avenue to pursue. We have the capability to examine local photoconduction in undoped nanocrystals at MIT phase boundaries, as well as in inhomogeneously doped material.

We will also examine potential *energy-related applications* of this new material. Rutile TiO₂ is an important photocatalyst, and has been considered for energy-related hydrogen production. Many researchers have labored to dope that material to achieve catalytic activity at small overpotentials when illuminating in the visible and infrared. Stabilized rutile VO₂ is metallic by nature, and we have begun collaborative investigations of its photocatalytic properties. Likewise, vanadium oxides have been considered as high capacity cathode materials for lithium ion battery applications. The channels in the rutile lattice that allow hydrogenation are also well suited to lithiation, and we have begun investigations to see whether this VO₂ nanomaterial has worthwhile properties under battery conditions.

Other strongly correlated nanostructures. Finally, we want to apply nanostructure techniques to other strongly correlated materials, to address outstanding questions regarding their underlying basic science as well as possible technical applications. To our existing array of tools (nanospaced electrodes down to the single nanometer scale; ionic liquids as gates; combined electronic and optical measurements), we can now add spill-over hydrogenation. Materials of interest are the manganites and correlated layered materials such as the dichalcogenides. The general idea is to consider the effect of tuning carrier density (via ionic gate or hydrogen doping) and apply perturbations (e.g., dc electric field) and see how that affects the competing electronic ground states.

Publications

S. Lee, A. A. Fursina, J. T. Mayo, C. T. Yavuz, V. L. Colvin, R. G. S. Sofin, I. V. Shvets, and D. Natelson, “[Electrically-driven phase transition in magnetite nanostructures](#)”, *Nature Materials*, **7**, 130-133 (2008).

A. A. Fursina, S. Lee, R. G. S. Sofin, I. V. Shvets, and D. Natelson, “[Nanogaps with very large aspect ratios for electrical measurements](#)”, *Appl. Phys. Lett.* **92**, 113102 (2008).

A. A. Fursina, R. G. S. Sofin, I. V. Shvets, and D. Natelson “[The origin of hysteresis in resistive switching in magnetite is Joule heating](#)”, *Phys. Rev. B* **79**, 245131 (2009)

A. A. Fursina, R. G. S. Sofin, I. V. Shvets, and D. Natelson, “[Interplay of bulk and interface effects in the electric field driven transition in magnetite](#)”, *Phys. Rev. B* **81**, 045123 (2010).

A. A. Fursina, R. G. S. Sofin, I. V. Shvets, and D. Natelson, “[Interfacial transport properties between a strongly correlated transition metal oxide and a metal: Contact resistance in Fe₃O₄/M \(M=Cu, Au, Pt\) nanostructures](#)”, *Phys. Rev. B* **82**, 245112 (2010).

A. A. Fursina, R. G. S. Sofin, I. V. Shvets, and D. Natelson, “Magnetic field dependence of the electric field driven switching of the Verwey state in Fe₃O₄”, in revision.

J. Wei and D. Natelson, “Nanostructure studies of strongly correlated materials”, *Nanoscale* (in press).

MAGNETIC NANOSTRUCTURES AND SPINTRONIC MATERIALS

Principal Investigator

Michael Pechan
620 E. Spring Street
17 Culler Hall
Oxford, OH 45056-3653
Ph: (513)529-4518
pechanmj@muohio.edu

Institution

Miami University
500 E. High Street
102 Roudebush Hall
Oxford, OH 45056-3653

SCOPE

Nanoscale systems are the basis for a wealth of novel phenomena in condensed matter magnetism. Of particular significance are effects arising from epitaxial and otherwise laterally constrained systems, which include spintronic systems, exchange biased structures and patterned nano-structures. In all such systems ferromagnetic resonance is becoming an increasingly significant probe of anisotropy and magnetic relaxation. For example, both anisotropy and relaxation of the magnetization to equilibrium are key parameters in recording technology and knowledge of anisotropy, precession frequency and damping are crucial in the development of devices based upon spin torque phenomena. Pechan's group explores magnetodynamics and magnetostatics in spintronic related materials, coupled nanostructures, bio-related nanoparticles and single crystal transition metals. A more powerful and sensitive microwave source has been installed for the technique of ferromagnetic resonance. Pechan works in collaboration with scientists from other universities and industrial and national laboratories.

Pechan Recent Results

Coupled Nano-dots Recently, in collaboration with Hitachi Storage Technologies, we reported novel magnetostatic and magnetodynamic effects in coupled nano-dot chain arrays. Permalloy (PY) dots 300 nm in diameter and 40 nm thick were formed, via e-beam lithography, into a square lattice with 350 nm lattice constant. Samples were prepared with five dot chains coupled by PY bridge widths of 0, 20, 40 and 60 nm. Fig. 1 shows the 20 nm bridge width sample. Bridge exchange coupling significantly suppresses vortex formation and the ensuing

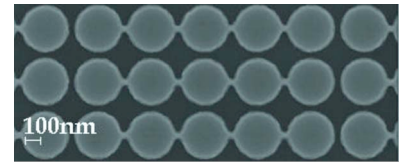


Fig. 1. SEM image of a nanodot chain array with 20 nm bridge width.

buildup of exchange energy is release by simultaneous reversal of the magnetization and vortex nucleation. The magnetodynamics were investigated with the magnetization saturated normal to the film plane, a summary of which is shown in Fig. 2. The no-bridge spectrum is consistent with ‘drum-head’ type Bessel function modes. Coupled dots produce increasingly complex mode structures with increasing coupling strength. Simulations demonstrated that the additional satellite structure on the higher order (lower field) modes arise from a single dot-bridge component within the chain – the structure increasing in complexity as the bridge becomes a larger part of this component. Simulations also demonstrated that normal mode excitations arising from interdot coupling appear as satellites on the immediate low field side of the lowest order (highest field) resonance, which increase in intensity and separation with increasing coupling strength.

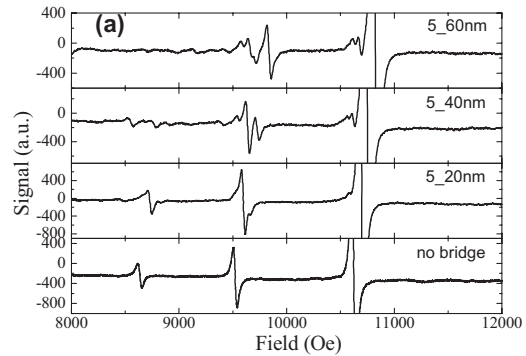


Fig. 2. Perpendicularly magnetized FMR spectra.

Spintronic Materials In collaboration with Chris Leighton at the University of Minnesota, we are investigating CoS_2 a promising model system for fundamental studies of spintronic processes. This system has - 55% spin polarization (P) at the Fermi level, a value that is tunable with Fe doping in $\text{Co}_{1-x}\text{Fe}_x\text{S}_2$, reaching + 85%. Of interest is whether the ferromagnetic damping is influenced by P . Single crystals of $\text{Co}_{1-x}\text{Fe}_x\text{S}_2$ with close to ideal sulfur stoichiometry are ground into powder for the FMR studies. The linewidth exhibits a minimum at T_C (Fig. 3), which provides a measure of both T_C and the breadth of the FM transition. In contrast to expectations based on NMR, the linewidth is observed to increase rather than decrease with increasing P (Fig. 3 inset). This suggests that other mechanisms, such as two-magnon scattering or Fe positional inhomogeneity, dominate the damping. Note also the absence of a paramagnetic resonance well above T_C , indicating the absence of a localized moment above the ordering temperature.

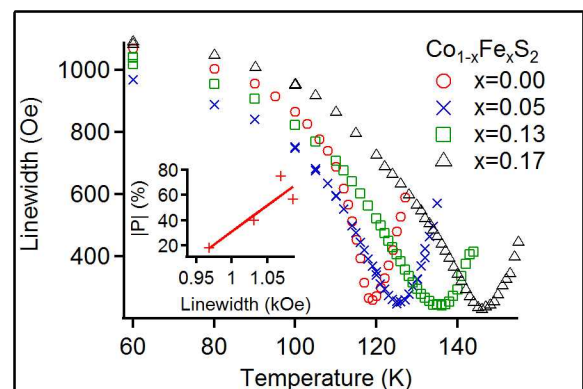


Fig. 3. FMR linewidth vs. temperature. Inset linewidth dependence upon polarization.

Pechan Future Plans

Coupled Nano-wires As an extension of the coupled nano-dot work, we are collaborating with Liesl Folks, Mathew Carey and Jordan Katine at Hitachi Storage Technologies, to investigate coupling between nano-wire samples. Magnetic nanowires are of fundamental interest for studying domain wall propagation and in device applications for sensors, information storage and read/write capabilities. Preliminary simulations indicate intriguing effects associated with coupling between two nano-wires, 40 nm thick, 100 nm wide and 1000 nm long, separated by 50 nm with two 40 nm wide bridges coupling the two. A field sufficient to saturate the magnetization is applied along the long axis (x) of the wire, then the magnetization is pulled slightly away from the x-axis and released. The resulting transverse oscillations (M_y) are recorded as a function of time. This procedure was applied for several symmetric placement of bridges with separation spanning the length of the wires. As seen in Fig. 4, certain positions of the bridges produce dramatic modulations in the time domain, reminiscent of coupled pendula. This apparent transfer of energy from one wire to another has potential application in, for example, microwave assisted recording. We will do a thorough ‘screening’, via simulation, prior to proposing structures for Hitachi to produce. Full frequency/field dispersion characterization will be done on microstrips and co-planar waveguides. Enhanced power and low noise output from our new 67 GHz signal generator will ensure acceptable signals from the small samples utilized in this study.

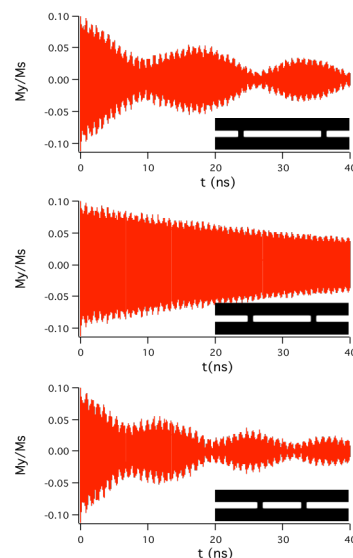


Fig. 4. Transverse oscillations in the time domain for various separation of two bridges between the nano-wires.

Spintronic Materials In collaboration with Casey Miller at the University of South Florida, we are investigating spin polarized Fe_3O_4 epitaxially grown on (100) MgO substrates. Ferromagnetic resonance (FMR) measurements at 35 GHz in the plane of the film revealed four-fold anisotropy confirming high quality (100) epitaxy, with an additional uniaxial contribution present in the samples grown in a magnetic field. Temperature dependent FMR clearly reflects the Verwey transition in the linewidth and in-plane and out-of-plane anisotropies confirming optimal oxygen stoichiometry (Fig. 5). Preliminary evidence suggests the influence of growth field on the anisotropy is thickness dependent. As a result, samples of varying thickness are under investigation.

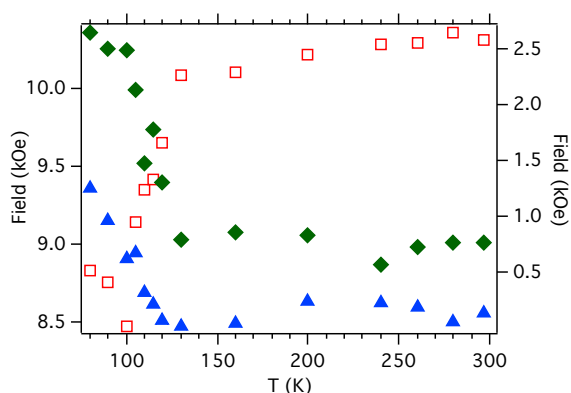


Fig. 5 In-plane anisotropy (blue triangles), out-of-plane anisotropy (red open squares) and FMR linewidth (green diamonds) vs. temperature. Solid markers are associated with the right axis and open markers with the left.

Pechan Publications

“Exchange-coupling modified spin wave spectra in the perpendicularly magnetized permalloy nanodot chain arrays”. Jian Dou, Sarah C.Hernandez *, Chengtao Yu, Michael J. Pechan, Liesl Folks, Jordan A Katine, Matthew J.Carey. *J. Appl. Phys.* **107**, 09B514 (2010).

“Enhancing remote controlled heating characteristics in hydrophilic magnetite nanoparticles via facile co-precipitation”. Reynolds A. Frimpong, Jian Dou, Michael Pechan and J.Z. Hilt. *J. Magn. Magn. Mat.* **322** 326–331 (2010).

“Mechanisms of exchange bias in DyFe₂/YFe₂ exchange-coupled superlattices”. M. R. Fitzsimmons, C. Dufour, K. Dumesnil, Jian Dou and Michael Pechan. *Phys. Rev. B* **79**, 144425 (2009).

“Exchange-coupled suppression of vortex formation in permalloy nanodot chain arrays”. Sarah Hernandez, Jian Dou, Chengtao Yu, Michael Pechan, Liesl Folks, Jordan Katine and Matthew Carey. *J. Appl. Phys.* **105**, 07C125 (2009).

“Ferromagnetic resonance in ferromagnetic/ferroelectric Fe/BaTiO₃/SrTiO₃ (001). Chengtao Yu, Michael J. Pechan, Swadesh Srivastava, Chris J. Palmstrom, Michael Begaslski, Charles Brooks and Darrell Schlom. *J. Appl. Phys.* **103**, 07B108 (2008).

“Driving Mechanism for a Foucault Pendulum (revisited)”, Joseph Priest and Michael J. Pechan, *American Journal of Physics*, **76**, 188(2008).

“Magnetic coupling of CoPt/Ru/CoFe trilayers investigated with magnetometry and ferromagnetic resonance”. Chengtao Yu, Bryan Javorek**, Michael J. Pechan, and Stefan Maat. *J. Appl. Phys.* **103**, 063914 (2008).

Experimental Condensed Matter Physics
Principal Investigators Meeting

TITLE: Thermopower near the 2D Metal-Insulator Transition

PRINCIPAL INVESTIGATORS:

Myriam P. Sarachik, City College of New York, CUNY, New York, NY 10031,

sarachik@sci.ccnycuny.edu

Alex Punnoose, City College of New York, CUNY, New York, NY 10031,

punnoose@sci.ccnycuny.edu

Sergey V. Kravchenko, Northeastern University, Boston MA ,

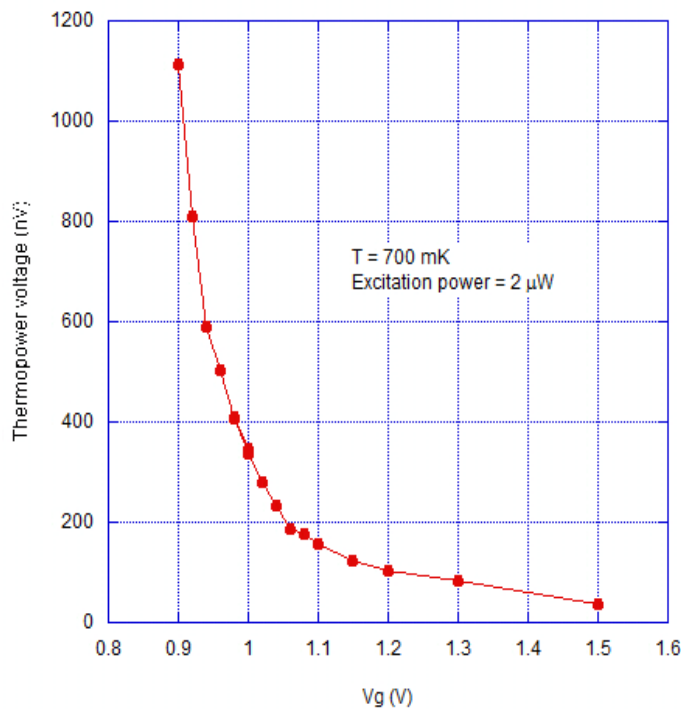
s.kravchenko@neu.edu

PROJECT DESCRIPTION: The availability of two-dimensional electron systems in samples of very high mobility has enabled the study of new and very interesting physics in strongly interacting electron systems, a region that had previously been inaccessible. Measurements of the resistivity, magnetoresistance and Hall effect have provided evidence for a totally unexpected transition to metallic behavior, a transition that is forbidden in weakly interacting systems. In contrast with the extensive transport measurements that have been carried out in a variety of 2D electron systems, there have been very few studies of the thermal properties. The aim of this project is to study the thermoelectric power and the thermal conductivity of dilute two-dimensional electrons systems of high-mobility samples near the 2D metal-insulator transition.

RECENT PROGRESS: The goal of the work supported by this grant is to measure the thermal properties of high-mobility 2D semiconductors at low carrier densities where the electron-electron interactions are very strong, and in which a metal-insulator transition was discovered where none was expected. The system we are measuring is the 2D electron gas in silicon MOSFETs. We are focusing our attention on the interesting region in the vicinity of the transition.

These measurements have turned out to be quite challenging. They must be performed at very low temperatures, where the effect of the phonons is not too large. The thermal gradient necessary for thermopower measurements cannot be established in the superfluid mixture, because the fluid provides a parallel low-impedance heat path and it is therefore difficult to establish and maintain a thermal gradient. The signal is small, and great care must be taken to suppress the noise by frequency filtering and appropriate electrical grounding. By using a unique, ultra low-noise amplifier LI-75A, we succeeded in achieving a resolution of 10^{-10} V. At high densities, where the thermopower is quite small, there is an out-of-phase signal that we believe is due to the contacts. This problem is currently being addressed.

Thermoelectric power measurements currently underway are yielding interesting results that have yet to be fully analyzed and understood. As shown below, the



thermoelectric voltage increases with decreasing electron density and diverges approaching a critical density, $n_c \sim 10^{11} \text{ cm}^{-2}$ for the metal-insulator transition.

Since the thermopower in the diffusive regime is proportional to T/E_F (where T is temperature and E_F is the Fermi energy), the thermopower reflects the behavior of the effective electron mass (through the Fermi energy E_F). The divergence of the thermopower and the electron mass signals that we are approaching a new phase. Our results provide thermodynamic evidence for the occurrence of a much-debated transition that has heretofore been inferred largely on the basis of transport measurements. We note that for a system with no disorder, this would signal the formation of the long-sought-for Wigner solid at low electron densities.

FUTURE PLANS: We are continuing careful study of the density-dependence and the power-dependence of the signal, and working toward eliminating possible contributions from contacts by replacing the leads with superconducting wire.

We plan to extend our investigations to measurements of the thermopower as a function of a magnetic field applied parallel to the 2D plane. Such an in-plane magnetic field affects only electron spins, aligning them and lifting the spin degree of freedom; the Fermi energy is therefore expected to increase by a factor of 2 and the thermopower should reflect this change.

PUBLICATIONS:

1. "Test of scaling theory in two dimensions in the presence of valley splitting and intervalley scattering in Si-MOSFETs", A. Punnoose, A. M. Finkel'stein, A. Mokashi, and S. V. Kravchenko, Phys. Rev. B **82**, 201308 (2010).
2. "Effects of Electron-Electron Interactions in Two Dimensions", S. V. Kravchenko, Int. Jour. Mod. Phys. B **23**, 4186 (2009).
3. "Colloquium: Transport in strongly correlated two-dimensional electron fluids", B. Spivak, S. V. Kravchenko, S. A. Kivelson, and X. P. A. Gao, Rev. Mod. Phys. **82**, 1743 (2010).
4. "A metal-insulator transition in 2D: Established facts and open questions", S. V. Kravchenko and M. P. Sarachik, Int. Jour. Mod. Phys. B **24**, 1640 (2010).
5. "Quantum phase transitions in two-dimensional electron systems", A. A. Shashkin and S. V. Kravchenko, in "Understanding Quantum Phase Transitions" ed. by Lincoln D. Carr (Taylor & Francis, Boca Raton, 2010).
6. "Renormalization group study of intervalley scattering and valley splitting in a two-valley system," A. Punnoose, Phys. Rev. B **81**, 035306 (2010).
7. "Renormalization group study of a two-valley system with spin-splitting," A. Punnoose, Phys. Rev. B **82**, 115310 (2010).

Ames Laboratory Photonic Systems FWP

Joseph Shinar (shinar@ameslab.gov), Rana Biswas (biswasr@ameslab.gov),
Kai-Ming Ho (kmh@ameslab.gov), and Costas Soukoulis (soukoulis@ameslab.gov)

Project Scope (one paragraph)

This FWP was created to address outstanding DOE challenges in efficient energy conversion and utilization through fundamental studies of photonic materials, structures, and devices. These include photonic crystals (PCs), organic semiconductors (OSs), organic light emitting diodes (organic LEDs (OLEDs)), and, in particular, novel systems combining PCs, OSs, and OLEDs. The PIs pioneered the development of 3-dimensional PCs, developed forefront OLEDs and procedures for characterizing them, and conducted pioneering optically detected magnetic resonance (ODMR) studies on organic semiconductors and OLEDs since ~1990. Besides continuing the studies in each of these areas, we are using our extensive expertise in them to enhance light emission from OLEDs. We are also building on our strengths to achieve new functionalities of OSs and PCs, including organic spintronics, lasing and nonlinear effects, and we are utilizing low-cost methods to design and fabricate large-area PC structures relevant to energy-related applications. The work involves a close synergy between theory, simulation, fabrication and experimental studies in these tasks.

Recent Progress (approximately one page)

- Development of wide area submicron laser interference + soft lithography procedures that have yielded extremely high-quality microlens arrays (μ LAs) and nanowire patterns (Fig. 1).
- The μ LAs enhance extraction of light from OLEDs otherwise waveguided through the glass substrate by 100%, a record enhancement (Fig.2).
- Development of the fundamental physics of transmission, absorption and emission of photonic structures relevant to energy-related applications. These have enabled fabrication of nanowire patterns that are transparent and conducting, with the consequent potential to replace indium tin oxide (ITO), a need that is steadily progressing towards a critical stage.
- Ab-initio studies of light emission from OLEDs and enhanced light absorption in organic solar cells that include photonic and/or plasmonic structures.
- Development of novel physics of photonic structures, including surface beaming (Fig. 3), beam steering, and efficient coupling between waveguides and radiation in free space, and supertransmission, and photonic crystal lasing.
- Fabrication and fundamental studies of solution-processable small molecule OLEDs (SMOLEDs) with near-record efficiency (Fig. 4). Such SMOLEDs are strongly preferred over similar OLED fabricated by thermal vacuum evaporation due to the drastically lower cost of solution processing.
- Fabrication and fundamental studies of OLEDs with transparent conducting polymer anode and efficiency strongly exceeding that of similar OLEDs fabricated on ITO.
- Fabrication and fundamental studies of blue-to-red microcavity OLED arrays with MoO_3 hole-injection and spacer layers.

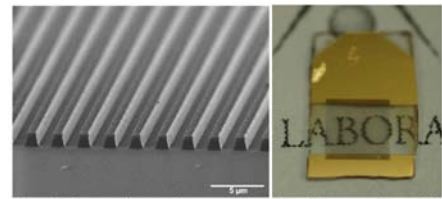


Fig. 1. PC-based transparent conducting nanowire patterns.

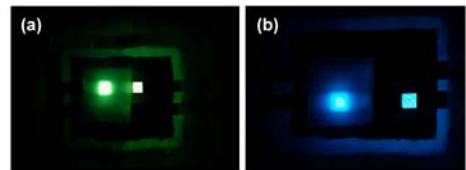


Fig. 2. OLED pixels with & w/o a μ LA.

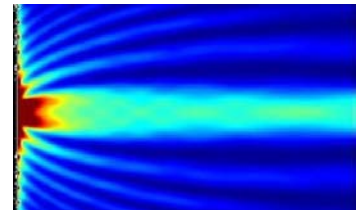


Fig. 3. Surface beaming from a PC.

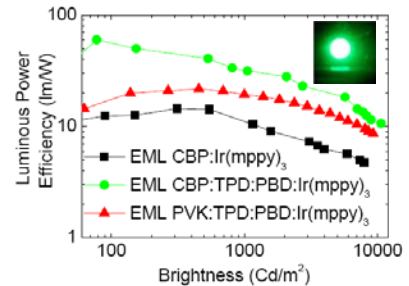


Fig. 4. Solution-processed SMOLEDs with near record efficiency.

Future Plans (approximately one page)

We will address our mission through the following efforts:

- We will expand and deepen the fundamental ODMR and electrically-detected magnetic resonance (EDMR) studies of organic semiconductors and OLEDs, to elucidate various processes such as bipolaron and trion formation, and their effect on carrier transport, light emission (in OLEDs), and carrier collection (in organic solar cells (OSCs)).
- We will also explore the relevance of ODMR and EDMR to organic spintronics. While the latter has exclusively focused on organic magnetoresistance, we will explore the combined effects of a dc magnetic field and a microwave field on the transport properties of organic electronic devices.
- We will expand and deepen the fabrication and fundamental studies of highly efficient solution-processable SMOLEDs. We recently described such SMOLEDs with near-record efficiency (Cai et al., *Adv. Mat.* (2011)), and we will study their stability and explore pathways to improve it.
- We recently exploited a new method to fabricate highly conducting, smooth, and transparent films of poly(3,4-ethylenedioxythiophene):poly(4-styrenesulfonate) (PEDOT:PSS) and fabricated fluorescent tris(8-hydroxyquinoline) Al OLEDs on such anodes. These devices were exhibited a power efficiency up to 80% more than that of those fabricated on indium tin oxide (ITO) (Cai et al., submitted). We will expand this effort to demonstrate phosphorescent spin-coated SMOLEDs with world-record efficiency.
- We will continue to explore novel structures to enhance outcoupling of light from OLEDs. While we recently demonstrated 100% outcoupling enhancement using μ LAs fabricated by UV interference lithography, that enhancement only extracted the light that is otherwise waveguided through the glass substrate. The \sim 50% of the generated photons that are reflected at the ITO/glass interface and consequently waveguided and lost in the organic+ITO layers still beg for a geometry that will extract them, and we will explore various novel geometries and methods to do that.
- We will rigorously design and simulate other novel OLED architectures that show promise for (i) tunable emission over a wide band of wavelengths, and (ii) white light emission. We recently demonstrated combinatorial sky blue-to-red microcavity OLEDs and their promise as integrated microspectrometers (Liu et al., submitted).
- We will invest efforts towards understanding the mechanisms of emission observed in ongoing experiments utilizing rigorous photonic emission calculations.
- We will design and develop novel periodic photonic and plasmonic nanostructures showing enhanced absorption and emission effects.
- We will develop dynamically controllable beam-steering based on surface waves on tunable photonic crystal surfaces and switchable surface beaming facilitated by resonant surface structures.
- We will apply the gain/lasing code we developed for use in loss-compensated metamaterials to lasing in photonic crystals and resonant scattering dominated corrugated surfaces.

Selected 2008 – 2011 Publications

1. Joseph Shinar and Ruth Shinar, "Organic Light-Emitting Devices (OLEDs) and OLED-Based Chemical and Biological Sensors: An Overview," *J. Phys. D: Appl. Phys.* **41**, 133001 (2008). (invited review article).
2. J. Wang, J. Xu, M. Goodman, Y. Chen, M. Cai, J. Shinar, and Z. Lin, "A Simple Biphasic Route to Water Soluble Dithiocarbamate Functionalized Quantum Dots," *J. Mat. Chem.* **18**, 3270 (2008).
3. Yuankun Cai, Ruth Shinar, Zhaoqun Zhou, Chengliang Qian, and Joseph Shinar, "Multianalyte sensor array based on an organic light emitting device platform," *Sensors & Actuators B* **134**, 727 (2008).
4. C. Tapalian, J. Langseth, Y. Chen, J. W. Andereg, and J. Shinar, "Ultrafast Laser Direct-Write Actuable Microstructures," *Appl. Phys. Lett.* **93**, 243304 (2008).
5. R. Biswas, C. Christensen, J. Muehlmeier, G. Tuttle, K-M. Ho, "Waveguide bends and circuits in three-dimensional photonic crystals," *Photonics and Nanostructures* **6**, 208 (2008).

6. R. Biswas, D. Zhou, I. Puscasu, E. Johnson, A. Taylor and W. Zhao, "Sharp thermal emission and absorption from conformally coated metallic photonic crystal with triangular lattice," *Appl. Phys. Lett.* **93**, 063307 (2008). *Virtual J. of Nanoscale Sc. & Tech.* **18** (Sept 2008).
7. D. Zhou and R. Biswas, "Photonic crystal enhanced light-trapping in thin film solar cells," *J. Appl. Phys.* **103**, 093102 (2008).
8. M. Sigalas and R. Biswas, "Slot defect in three-dimensional photonic crystals," *Phys. Rev. B* **78**, 033101 (2008).
9. P. Kohli, J. Chatterton, D. Stieler, G. Tuttle, M. Li, X. H. Hu, Z. Ye, and K. M. Ho, "Fine tuning resonant frequencies for a single cavity defect in three-dimensional layer-by-layer photonic crystal," *Opt. Exp.* **16**, 19844 (2008).
10. J. H. Lee, J. C. W. Lee, W. Leung, M. Li, K. Constant, C. T. Chan, and K. M. Ho, "Polarization engineering of thermal radiation using metallic photonic crystals," *Adv. Mat.* **20**, 3244 (2008).
11. X. H. Hu, M. Li, Z. Ye, W. Y. Leung, K. M. Ho, and S. Y. Lin, "Design of midinfrared photodetectors enhanced by resonant cavities with subwavelength metallic gratings," *Appl. Phys. Lett.* **93**, 241108 (2008).
12. W. Dai, B. Wang, Th. Koschny and C. M. Soukoulis, "Experimental verification of quantized conductance for microwave frequencies in photonic crystal waveguides," *Phys. Rev. B* **78**, 073109 (2008).
13. W. Dai and C. M. Soukoulis, "Converging and waveguiding of a Gaussian beam by two-layer dielectric rods," *Appl. Phys. Lett.* **93**, 201101 (2008).
14. R. Shinar and J. Shinar, Editors, *Organic Electronics in Sensors and Biotechnology*, McGraw Hill (2009).
15. Ruth Shinar, Yuankun Cai, and Joseph Shinar, "Progress and Challenges in Organic Light-Emitting Diode-Based Chemical and Biological Sensors, in *Organic Electronics in Sensors and Biotechnology*, edited by Ruth Shinar and Joseph Shinar, Chap. 5 (McGraw Hill, 2009).
16. Z. Gan, Y. Tian, Z. Zhou, J.-h Kang, Q-H. Park, D. W. Lynch, and J. Shinar, "Spectrally narrowed edge emission from leaky waveguide modes in organic light-emitting diodes," *J. Appl. Phys.* **106**, 094502 (2009).
17. B. Curtin, R. Biswas, V. Dalal, "Photonic crystal based back reflectors for light management and enhanced absorption in amorphous silicon solar cells," *Appl. Phys. Lett.* **95**, 231102 (2009).
18. R. Biswas, W. Zhao, I. Puscasu, E. Johnson, "Angular variation of absorption and thermal emission from photonic crystals," *J. Opt. Soc. of America B* **26**, 1808–1817 (2009).
19. D. Stiehler, A. Barsic, R. Biswas. G. Tuttle. K.-M. Ho, "A planar four-port channel drop filter in the 3-d woodpile photonic crystal", *Optics Express* **17**, 6128-6133 (2009).
20. *High Temperature Photonic Structures*, 2009 Spring Materials Research Symposium J Proceedings, Vol. 1162E (2009). Editors: R. Biswas, V. Shklover, S. Lin, E. Johnson
21. D. Stieler, A. Barsic, R. Biswas, G. Tuttle, and K. M. Ho, "A planar four-port channel drop filter in the three-dimensional woodpile photonic crystal," *Opt. Exp.* **17**, 6128 (2009).
22. D. Stieler, A. Barsic, G. Tuttle, M. Li, and K. M. Ho, "Effects of defect permittivity on resonant frequency and mode shape in the three-dimensional woodpile photonic crystal," *J. Appl. Phys.* **105**, 103109 (2009).
23. J. B. Kim, Y. H. Lu, M. H. Ho, Y. P. Lee, J. Y. Rhee, J.-H. Lee, and K.-M. Ho, "Diffracted Magneto-optical Kerr Effect of a Ni Magnetic Grating," *J. Appl. Phys.* **106**, 093103 (2009)
24. M. Diem, Th. Koschny and C. M. Soukoulis, "Wide-angle perfect absorber/thermal emitter in the THz regime," *Phys. Rev. B* **79**, 033101 (2009).
25. W. Dai and C. M. Soukoulis, "Theoretical analysis of the surface wave along a metal-dielectric interface," *Phys. Rev. B* **80**, 155407 (2009).
26. Srikanth Vengasandra, Yuankun Cai, David Grewell, Joseph Shinar, and Ruth Shinar, "Polypropylene CD-Organic Light Emitting Diode Biosensing Platform," *Lab on a Chip* **10**, 1051 (2010).
27. Yuankun Cai, Alex Smith, Joseph Shinar, and Ruth Shinar, "Data Analysis and Aging in Phosphorescent Oxygen-Based Sensors," *Sensors & Actuators: B. Chemical* **146**, 14 (2010).
28. K. S. Nalwa, Y. Cai, A. L. Thoeming, J. Shinar, R. Shinar, and S. Chaudhary, "Polythiophene-fullerene based photodetectors: tuning of spectral response and application in photoluminescence based (bio)chemical sensors," *Adv. Mat.* **22**, 4157 (2010).
29. Zhengqing Gan, Rui Liu, Ruth Shinar, and Joseph Shinar, "Transient Electroluminescence Dynamics in Small Molecular Organic Light-Emitting Diodes," *Appl. Phys. Lett.* **97**, 113301 (2010).
30. R. Biswas, J. Bhattacharya, B. Lewis, N. Chakravarty, V. Dalal, "Enhanced Nano-crystalline Silicon Solar cell with a Photonic Crystal Back Reflector" *Solar Energy Materials and Solar Cells* **94**, 2337-2442 (2010).
31. J. M. Park, K. S. Nalwa, W. Leung, K. Constant, S. Chaudhary, and K. M. Ho, "Fabrication of Metallic Nanowires and Nanoribbons using Laser Interference Lithography and Shadow Lithography," *Nanotech.* **21**, 215301 (2010).

32. Y. C. Shin, D. H. Kim, D. J. Chae, J. W. Yang, J. I. Shim, J. M. Park, K.-M. Ho, K. Constant, H. Y. Ryu, and T. G. Kim "Effects of Nanometer-Scale Photonic Crystal Structures on the Light Extraction From GaN Light-Emitting Diodes," *IEEE J. Quantum Electr.* **46**, 1375 (2010).
33. Y. C. Shin, D. H. Kim, E. H. Kim, J. M. Park, K. M. Ho, K. Constant, J. H. Choe, Q. H. Park, H. Y. Ryu, J. H. Baek, T. Jung, and T. G. Kim "High Efficiency GaN Light-Emitting Diodes With Two Dimensional Photonic Crystal Structures of Deep-Hole Square Lattices," *IEEE J. Quantum Electr.* **46**, 116 (2010).
34. J. H. Lee, P. Kuang, W. Leung, Y. S. Kim, J. M. Park, H. Kang, K. Constant, and K. M. Ho, "Semicrystalline Woodpile Photonic Crystals without Complicated Alignment via Soft Lithography," *Appl. Phys. Lett.* **96**, 193303 (2010).
35. P. Kuang, J. H. Lee, C. H. Kim, K. M. Ho, and K. Constant "Improved Surface Wettability of Polyurethane Films by Ultraviolet Ozone Treatment," *J. Appl. Polymer Sci.* **118**, 3024 (2010)
36. D. Ates, A. O. Cakmak, E. Colak, R. Zhao, C. M. Soukoulis, and E. Ozbay, "Transmission enhancement through deep subwavelength apertures using connected SRRs," *Opt. Exp.* **18**, 3952 (2010).
37. M. Diem, Th. Koschny, and C.M. Soukoulis, "Transmission in the vicinity of the Dirac point in hexagonal photonic crystals," *Physica. B* **405**, 2990 (2010).
38. W. Dai and C. M. Soukoulis, "Control of beaming angles via a subwavelength metallic slit surrounded by grooves," *Phys. Rev. B* **82**, 045427 (2010).
39. R. Biswas, C. Xu, W. Zhao, R. Liu, R. Shinar, and J. Shinar, "Simulations of emission from microcavity tandem organic light emitting diodes," *J. Phot. Ener.* **1**, 011016 (2011).
40. Teng Xiao, Weipan Cui, James Anderegg, Joseph Shinar, and Ruth Shinar, "Simple routes for improving solution-based organic solar cells" *Org. Electr.* **12**, 257 (2011).
41. J. J. Intemann, J. F. Mike, M. Cai, S. Bose, T. Xiao, T. C. Mauldin, J. Shinar, R. Shinar, and M. Jeffries-El, "Synthesis and Characterization of Poly (9,9-dialkylfluorenevinylene benzobisoxazoles): New Solution Processable Electron-Accepting Conjugated Polymers," *Macromol.* **44**, 248 (2011).
42. J. Shinar and R. Shinar, "An Overview of Organic Light-Emitting Diodes and their Applications," in D. L. Andrews, G. D. Scholes, and G. P. Wiederrecht, Editors, *Comprehensive Nanoscience and Technology, Vol. 1*, 73–107 (Oxford: Academic Press 2011).
43. Y. Chen, M. Cai, E. Hellerich, R. Liu, Z. Gan, R. Shinar, and J. Shinar, "Evidence for holes beyond the recombination zone & trions near the organic/cathode interface in OLEDs," *J. Phot. Ener.* **1**, 011017 (2011).
44. R. Liu, Z. Gan, R. Shinar, and J. Shinar, "Comprehensive Investigation of Transient Electroluminescence Spikes in Small Molecular Organic Light-Emitting Diodes," *Phys. Rev. B* **83**, 245302 (2011).
45. J.-M. Park, Z. Gan, W. Y. Leung, Z. Ye, K. Constant, J. Shinar, R. Shinar, and K.-M. Ho, "Soft lithography microlens fabrication for enhanced OLED light extraction," *Opt. Exp.* **19**, A786 (2011).
46. Min Cai, Teng Xiao, Emily Hellerich, Ying Chen, Ruth Shinar, and Joseph Shinar, "High efficiency solution-processed small molecule electrophosphorescent organic light-emitting diodes," *Adv. Mat.* **xx**, 1 – 7 (2011).
47. R. Biswas, C. Xu, "Nano-crystalline silicon solar cell architecture with absorption at the classical $4n^2$ limit", *Optics Express*, **19**, A664-A672 (2011).
48. J. F. Mike, J. J. Intemann, M. Cai, T. Xiao, R. Shinar, J. Shinar, and M. Jeffries-El, "Efficient Synthesis of Benzobisazole Terpolymers Containing Thiophene and Fluorene," *Polymer Chem.* (accepted).
49. R. Liu, C. Xu, R. Biswas, J. Shinar, and R. Shinar, "MoO₃ as Combined Hole Injection Layer and Tapered Spacer in Combinatorial Multicolor Microcavity Organic Light Emitting Diodes," *Appl. Phys. Lett.* (accepted).
50. K. S. Nalwa, J. M. Park, K. M. Ho, and S. Chaudhary, "On Realizing Higher Efficiency Polymer Solar Cells Using a Textured Substrate Platform," *Adv. Mater.* **23**, 112 (2011).
51. J. Lee, Z. Ye, K. M. Ho, and J. Kim "Two-dimensional optofluidic liquid-core waveguiding based on optimized integration of single- and multiple-layer antiresonance reflection optical waveguides," *J. Opt. Soc. Am. B* **28**, 489 (2011).
52. D. P. Mao, M. Li, W. Leung, K. M. Ho and L. Dong "Photonic-plasmonic integration through the fusion of photonic crystal cavity and metallic structure," *J. Nanophot.* **5**, xx (2011).
53. P. Kuang, J. M. Park, W. Leung, R. C. Mahadevapuram, K. S. Nalwa, T. G. Kim, S. Chaudhary, K. M. Ho, and K. Constant, "A New Architecture for Transparent Electrodes: Relieving the Trade-Off Between Electrical Conductivity and Optical Transmittance," *Adv. Mater.* **23**, 2469 (2011).

Project Title: Infrared Optical Study of Graphene in High Magnetic Fields

Principal Investigator:

Dmitry Smirnov
National High Magnetic Field Laboratory, Florida State University
Phone: 850-644-5399; Email: smirnov@magnet.fsu.edu

Co-PI:

Zhigang Jiang
School of Physics, Georgia Institute of Technology
Phone: 404-385-3906; Email: zhigang.jiang@physics.gatech.edu

Project Scope:

Graphene, a single atomic layer of graphite, has emerged as one of the most intriguing materials for fundamental physics. It also holds great promise for post Si-CMOS nanoelectronics. In particular, high-mobility and ballistic graphene-based electronic/photonic devices are expected to possess intrinsically low power consumption, and the exceptional gate tunability of graphene suggests new functionalities that were hard or impossible to achieve in previous materials. The intriguing properties of graphene result from its unusual low-energy band structure, rendering the charge carriers in it formally identical to massless relativistic particles. In this project, we carry out a systematic infrared optical study of graphene in high magnetic fields. Compared with electronic transport methods, which are dominated by the sample edge in high magnetic fields, infrared spectroscopy directly accesses the intrinsic materials properties, yielding important complementary and/or supportive information about the material. The proposed research is focused on the effects of many-body interactions at the root of the symmetry breaking of the zero energy Landau level and the fractional quantum Hall (QH) effect in graphene. In addition we propose to extend the scope of the project to novel topological insulators, known as “one-quarter of graphene.” The proposed experiments rely on recent successful experimental developments by our group, which allow us to perform infrared magneto-spectroscopy measurements on mesoscopic-size samples in magnetic fields up to 31 T. Moreover, we plan to extend experimental capabilities towards higher magnetic fields, ultimately up to 45 T, and towards the very low, sub-THz frequency range.

Recent Progress:

Many-body effect in graphite: Magnetic-field tunable electron-phonon coupling

We report on the experimental study of magneto-phonon resonance in thin graphite layers, via infrared spectroscopy measurements. We observe two distinct resonant behaviors due to the coupling of charge carriers to the Γ -point phonons or the large momentum K -point phonons, while the interested cyclotron resonance (CR) energy crosses the phonon energies. In particular, we find that the observed resonance is tunable by varying the magnetic field, which might have profound implications in future carbon-based optoelectronic devices.

The first observation of this work is the unusual avoided-level-crossing splitting of the CR at a magnetic field close to 19 T. As shown in Fig. 1(a), the CR consists of two Lorentzian absorption dips, and their magnetic-field dependence follows the typical avoided-level-crossing

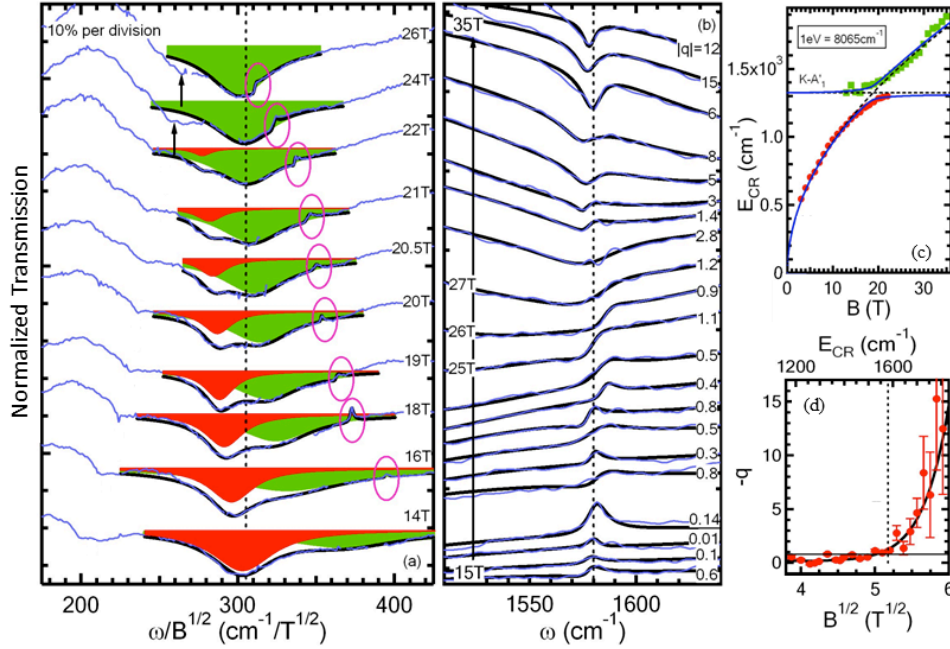


Figure 1: (a) Magneto-infrared spectra of thin graphite layers with respect to scaled frequency, $\omega/B^{1/2}$, at selected magnetic fields near the avoided-level-crossing. Vertical dashed line labels the expected position for the CR without EPC. The thicker lines are best fits to the data (thin lines) using two Lorentzian functions. (b) Magneto-infrared spectra as a function of magnetic field near the Γ -point phonon energy (vertical dashed line). (c) Avoided-level-crossing splitting of the CR near the K -point phonon energy (horizontal dashed line). (d) Fano resonance fitting parameter, q , as the CR energy crosses the Γ -point phonon energy (vertical dashed line).

characteristics (Fig. 1(c)). The crossing energy is found to be ~ 1325 cm⁻¹, corresponding to the zone boundary phonon at the K -point. Based on conventional coupled mode theory, we obtain a dimensionless electron-phonon coupling (EPC) strength parameter, $\lambda = 5.4 \times 10^{-3}$.

Moreover, as highlighted by ovals in Fig. 1(a) and further illustrated in Fig. 1(b), a Fano resonance-like feature is evident in the magneto-infrared spectra and centered ~ 1580 cm⁻¹. We attribute this resonance to EPC between the Γ -point phonon mode and the broad CR of charge carriers. As the CR energy is increased with magnetic field, the lineshape of the resonance evolves systematically from a peak to a dip. The lineshape of Fano resonance is usually characterized by a fitting parameter, q , and as shown in Fig. 1(d), the $|q|$ value is drastically changed after the CR energy exceeds the Γ -point phonon energy in the field range of 25-27 T.

Future Plans:

Photoconductivity of graphene on h-BN in high magnetic fields

Studying the many-body effects in graphene via infrared magnetospectroscopy is a longstanding goal of this program. Recent advances in fabrication of high mobility graphene devices on hexagonal boron nitride (h-BN) surfaces have provided a new playground for this study. With much improved sample quality, electronic transport was able to demonstrate the Landau level symmetry breaking and fractional QH effect in a relatively low magnetic field, preferable for infrared experiments. Owing to the small size of such devices, photoconductivity measurement is employed using a CO₂ laser, with a temperature tunable wavelength in the mid-infrared regime ($\lambda = 10.6 \pm 0.1$ μm).

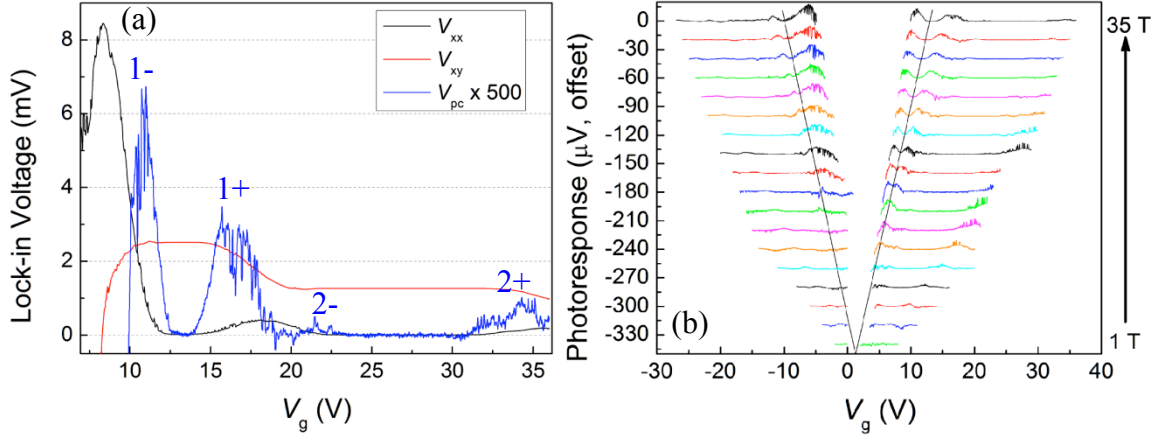


Figure 2: (a) The longitudinal (V_{xx}) and Hall (V_{xy}) voltages, as well as the photoresponse (V_{pc}), of graphene/h-BN as a function of gate voltage (V_g), measured at 4.2 K and 35 T. The photoresponse signals appear near the edge of the QH states, as labeled. (b) Photoresponse of graphene/h-BN at odd integer values of magnetic field between 1 T and 35 T. The curves are offset vertically based on their magnetic field values. The solid lines are visual guides tracking the $\nu = \pm 1$ QH states.

Figure 2 summarizes our preliminary photoconductivity measurement data. The two transport curves (V_{xx} and V_{xy}) in Fig. 2(a) clearly show the presence of the $\nu = +1, +2$ QH states, evidenced by a constant plateau in V_{xy} and vanishing V_{xx} in the same gate voltage ranges. The photoresponse signals appear as peaks near the edge of the QH states. Specifically, there are two large peaks in the photoresponse near the edges of the $\nu = +1$ state (labeled by 1+ and 1-), and two other smaller peaks near the edges of the $\nu = +2$ state (labeled by 2+ and 2-). To track the field dependence, photoconductivity measurements were taken at every odd integer value for magnetic field from 1 T to 35 T. The main features tracked here are the two peaks around both the $\nu = \pm 1$ states, as guided by the solid lines in Fig. 2(b). These states are due to the symmetry breaking of zero energy Landau level, and many-body effect plays an important role in this splitting.

Our photoconductivity measurements show great ability for identifying QH states in graphene that are not necessarily clear in the Hall conductivity data (transport). Future works include employing circularly polarized light to extract the contributions from CR transitions, and to examine the corresponding transition selection rule. Circularly polarized light can filter the energy-degenerated CR transitions by the corresponding angular momentum change, while same amount of heating is caused by the light of different polarization. In addition, we plan to improve the photoresponse detecting sensitivity in our measurements. The signal fluctuations seen in Fig. 2 are more likely due to some light-induced physical process rather than electrical noise. Photoconductivity measurements will also be performed to other types of graphene (particularly bilayer graphene on h-BN) and topological insulators.

List of Publications (2008-2011):

- [1] E.A. Henriksen, Z. Jiang, L.-C. Tung, M.E. Schwartz, M. Takita, Y.-J. Wang, P. Kim, and H.L. Stormer, "Cyclotron resonance in bilayer graphene," Phys. Rev. Lett. **100**, 087403 (2008).
- [2] E.A. Henriksen, P. Cadden-Zimansky, Z. Jiang, Z.Q. Li, L.-C. Tung, M.E. Schwartz, M. Takita, Y.-J. Wang, P. Kim, and H.L. Stormer, "Interaction-induced shift of the cyclotron resonance in monolayer graphene," Phys. Rev. Lett. **104**, 067404 (2010).

- [3] J. Qi, X. Chen, W. Yu, P. Cadden-Zimansky, D. Smirnov, N.H. Tolk, I. Miotkowski, H. Cao, Y.P. Chen, Y. Wu, S. Qiao, and Z. Jiang, “*Ultrafast carrier and phonon dynamics in Bi₂Se₃ crystals*,” *Appl. Phys. Lett.* **97**, 182102 (2010).
- [4] Z. Jiang, E.A. Henriksen, P. Cadden-Zimansky, L.-C. Tung, Y.-J. Wang, P. Kim, and H.L. Stormer, “*Cyclotron Resonance near the Charge Neutrality Point of Graphene*,” Proceedings of the 30th International Conference on the Physics of Semiconductors (2010).

Manuscripts under review:

- [5] L.-C. Tung, P. Cadden-Zimansky, J. Qi, Z. Jiang, and D. Smirnov, “*Measurement of graphite tight-binding parameters using high field magneto-reflectance*,” arXiv:1106.5948.
- [6] Y. Kim, X. Chen, Z. Wang, I. Miotkowski, Y.P. Chen, W. Pan, J. Shi, Z. Jiang, and D. Smirnov, “*Temperature dependence of Raman-active optical phonons in Bi₂Se₃ and Sb₂Te₃*,” submitted (2011).

**Probing the Origins of Conductivity Transitions in Correlated Solids:
Experimental Studies of Electronic Structure in Vanadium Oxides.
*Award DE-FG02-98ER45680***

Institution:

Trustees of Boston University
881 Commonwealth Ave.
Boston MA 02215

Principal Investigator:

Kevin E. Smith
Department of Physics, Boston University,
590 Commonwealth Ave., Boston MA 02215.
e-mail: ksmith@bu.edu; phone: 617-353-6117

Project Scope:

Vanadium oxides are a class of solid that display particularly complex and fascinating properties. Whether as simple binary oxides or as ternary compounds with another metal cation, these oxides are replete with complex conductivity transitions, as well as charge ordering transitions, structural phase transitions, frustrated spin structures, superconductivity, and unusual magnetic properties. As such, vanadates are prototypical correlated materials, and allow important physical themes to be explored both experimentally and theoretically. Key to understanding the origin of all these phenomena in the vanadates is accurate experimental determination of the underlying electronic structure. This program involves the spectroscopic measurement of the electronic properties of a selection of vanadium oxides. The primary goal of this program is to use the knowledge to be gained on the electronic structure of the vanadates to facilitate a deeper understanding of the origins of conductivity transitions in correlated materials. The experimental tools used are soft x-ray emission spectroscopy (XES), soft x-ray absorption spectroscopy (XAS), resonant inelastic soft x-ray scattering (RIXS), x-ray photoemission spectroscopy (XPS), and angle resolved photoemission spectroscopy (ARPES). The use of this suite of techniques enables a wide range of oxides to be studied, since are able to measure electronic structure in electrical conductors and insulators, and samples in crystal, thin film, or powdered form. We measure, and test against theory, vanadate band structures and Fermi surfaces, the coupling between collective excitations and quasi-particles, cation charge states, low energy valence excitations, and most importantly, the changes in electronic structure during metal to non-metal transitions.

Recent Progress:

Our studies in the last year have focused on three vanadates: the quasi-one dimensional conductor β - $\text{Sr}_{0.17}\text{V}_2\text{O}_5$,¹ the room temperature antiferromagnetic insulator $\text{V}_{0.82}\text{Cr}_{0.12}\text{O}_2$,² and the photoactive vanadate BiVO_4 .³

i) The electronic structure of the quasi-one dimensional vanadium beta-bronze β - $\text{Sr}_{0.17}\text{V}_2\text{O}_5$ was measured using XAS, XES, and RIXS.¹ These measurements were used to derive the experimental site-resolved (k -integrated) band structure of a material whose electronic structure is difficult to obtain from first principles. The occupied states, probed by XES, demonstrate the O $2p$ - V $3d$ bonding hybridization at the bottom of the O $2p$ band, with the V $3d_{xy}$ „magnetic orbitals“ well-separated in energy. These results are consistent with the carriers being small polarons. A strong anisotropy in the absorption spectrum was observed, and used to identify the energy and character of the unoccupied states. Additionally, absorption measurements at the V L -edge were compared with atomic multiplet calculations, clarifying the interpretation of the experimental multiplet structure and are consistent with

the presence of both V^{5+} and V^{4+} species. Site specific electronic excitations, probed by RIXS at the V L -edge, were observed at an energy of 1.1 eV, and correspond to transitions from the partially-filled d_{xy} magnetic orbital into the unoccupied $d_{xy,vz}$ orbitals.

ii) The chromium-vanadium oxide system $V_{1-x}Cr_xO_2$ ($0.1 < x < 0.2$) displays *both* insulating character in the rutile phase and room temperature ferromagnetism. A combination of XPS, and XES/RIXS at the V $L_{3,2}$ -, O K - and Cr $L_{3,2}$ -edges was used to study the electronic structure near the Fermi level (E_F) of $V_{0.82}Cr_{0.12}O_2$.² Our results show that the chromium enters as Cr^{3+} with the d^3 configuration, resulting in the formation of Cr^{3+} - V^{5+} ion pairs, in contrast to the simple Cr^{4+} substitution expected from the end members VO_2 and CrO_2 . The occupied Cr $3d$ orbital is located ~ 2 eV below E_F . Comparison with the parent material VO_2 revealed significant changes in the O $2p$ band-width and increased O $2p$ -V $3d$ hybridization in $V_{0.82}Cr_{0.12}O_2$, which are attributed to the reduced atomic spacing upon doping. Two energy loss features due to d - d^* transitions were observed at 0.95 eV and 1.75 eV in the V L_3 -edge x-ray scattering spectra and were explained in terms of the splitting of the t_{2g} -derived π band.

iii) The electronic structure of $BiVO_4$ has been studied using XPS, XAS, and XES, and the results compared with density functional theory calculations.³ This is a vanadate that has attracted attention as having possible applications in photoelectrochemical splitting of water. Our results confirm both the direct band gap of 2.48 eV and that the Bi $6s$ electrons hybridize with O $2p$ to form antibonding “lone pair” states at the top of the valence band. The results highlight the suitability of combining s^2 and d^0 cations to produce photoactive ternary oxides.

Immediate Future Plans:

A very interesting development in the study of metal to non-metal transitions in vanadium oxides is the discovery of a large anisotropy in the dc conductivity of epitaxial tetragonal VO_2 thin films grown on $TiO_2(011)$ substrates.⁴ Figure 1 presents the dc conductivity of the VO_2 film measured along different in-plane directions at room temperature.⁴ The maximum conductivity occurs parallel to the c -axis of the rutile VO_2 , while the minimum occurred perpendicular to the c -axis. The anisotropy ratio, $\sigma_{max}/\sigma_{min}$, was ~ 4.5 in the (011) plane of this VO_2 thin film.⁴ Most significantly, there is a shift in the metal to non-metal transition temperature as a function of orientation. Figure 2 shows the resistivity of the VO_2 film as a function of temperature along two different directions. Remarkably, the transition temperature of ~ 310 K is well below that of bulk VO_2 . We intend to use ARPES to measure the band structure, Fermi surface, and many-body coupling in pure and doped films of stressed VO_2 as a function of sample temperature with the goal of understanding the modified electronic structure of these materials. High quality films will be provided by Professor Stuart Wolf from the University of Virginia.

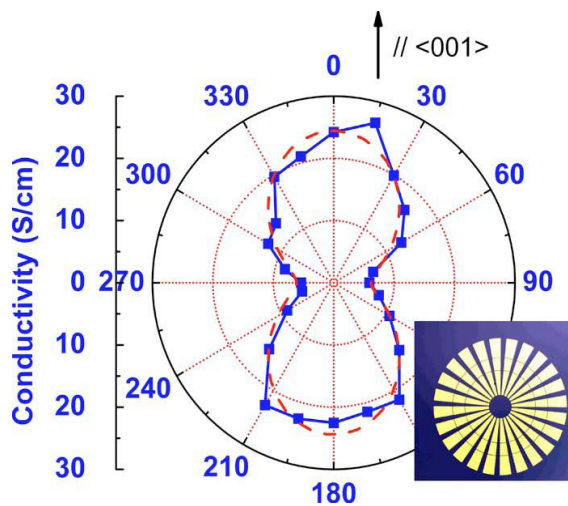


Fig. 1: Angular dependence of the conductivity of VO_2 film grown on a $TiO_2(001)$ substrate. The dashed line is a fit. The inset is a photograph of Au top contacts. From Ref. 4

Samples will be cleaned *in-situ* by UHV annealing, and via low energy inert gas ion bombardment and annealing in low partial pressure of O₂. Stoichiometry changes in the films could have a detrimental effect on the phenomenon we wish to study, so great care will be taken to ensure that the films are not modified by the surface cleaning method. Initial experiments have been undertaken on BL 12.0.1 at the ALS, and we have successfully cleaned the samples by a simple vacuum anneal.

Publications (2008-2011) acknowledging Award DE-FG02-98ER45680:

A total of 19 peer-reviewed papers have been published in the period 2008-2011.^{2,3,5-21}

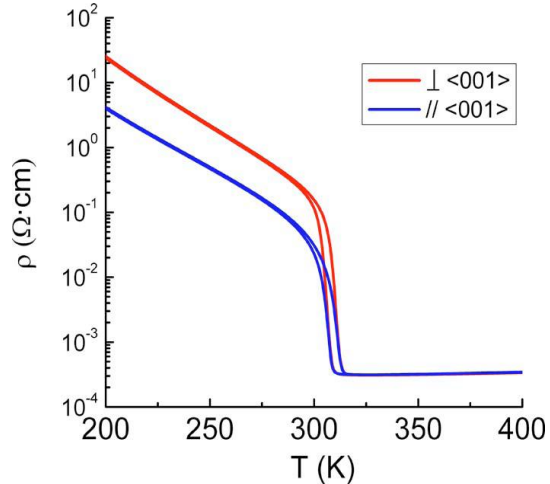


Fig 2: dc resistivity as function of temperature of a VO₂ film grown on a TiO₂(011) substrate measured parallel and perpendicular to the c-axis of rutile VO₂, respectively. From Ref. 4

1. J. Laverock, A.R.H. Preston, L.F.J. Piper, B. Chen, J. McNulty, K.E. Smith, P.A. Glans, J.H. Guo, C. Marin, E. Janod, and V. Ta Phuoc, "Orbital anisotropy and low-energy excitations of the quasi-one dimensional conductor β -Sr_{0.17}V₂O₅", Phys. Rev. B (*submitted*) (2011).
2. L.F.J. Piper, A. DeMasi, S. Cho, A.R.H. Preston, J. Laverock, K.E. Smith, K.G. West, J.W. Lu, and S.A. Wolf, "Soft X-ray Spectroscopic Study of the Ferromagnetic Insulator: V_{0.82}Cr_{0.18}O₂", Phys. Rev. B **82**, 235103 (2010).
3. D.J. Payne, M.D.M. Robinson, R.G. Egdell, A. Walsh, J. McNulty, K.E. Smith, and L.F.J. Piper, "The nature of electron lone pairs in BiVO₄", Appl. Phys. Lett. **98**, 212110 (2011).
4. J. Lu, K.G. West, and S.A. Wolf, "Very large anisotropy in the dc conductivity of epitaxial VO₂ thin films grown on (011) rutile TiO₂ substrates", Appl. Phys. Lett. **93**, 262107 (2008).
5. T. Learmonth, P.A. Glans, J.H. Guo, M. Greenblatt, and K.E. Smith, "Temperature Dependent Resonant Inelastic Soft X-ray Scattering Study of the Correlated Metal BaV_{0.98}Ti_{0.02}S₃", J. Phys. - Cond. Matter **22**, 025504 (2010).
6. L.F.J. Piper, A.R.H. Preston, A.V. Fedorov, S.W. Cho, A. DeMasi, and K.E. Smith, "Direct evidence of metallicity at ZnO (0001)-(1×1) surfaces from angle-resolved photoemission spectroscopy", Phys. Rev. B **81**, 233305 (2010).
7. B. Freelon, A. Augustsson, J.H. Guo, P.G. Medaglia, A. Tebano, G. Balestrino, C.L. Dong, C.L. Chang, P.A. Glans, T. Learmonth, K.E. Smith, J. Nordgren, and Z. Hussain, "Low energy electronic spectroscopy of an infinite-layer cuprate: A resonant inelastic X-ray scattering study of CaCuO₂", Physica C **470**, 187 (2010).
8. D. Shin, J.S. Foord, D.J. Payne, T. Arnold, D.J. Aston, R.G. Egdell, K.G. Godinho, D.O. Scanlon, B.J. Morgan, G.W. Watson, C. Yaicle, E. Mugnier, A. Rougier, L. Colakerol, L.F.J. Piper, and K.E. Smith, "A Comparative Study of Bandwidths in Copper Delafossites", Phys. Rev. B **80**, 233105 (2009).
9. L.F.J. Piper, A. DeMasi, S.W. Cho, K.E. Smith, F. Fuchs, F. Bechstedt, C. Körber, A. Klein, D.J. Payne, and R.G. Egdell, "Electronic Structure of In₂O₃ from Resonant X-ray Emission Spectroscopy", Appl. Phys. Lett. **94**, 022105 (2009).

10. T. Learmonth, C. McGuinness, P.A. Glans, B. Kennedy, J. St.John, J.H. Guo, M. Greenblatt, and K.E. Smith, "Resonant Soft X-Ray Inelastic Scattering and Soft X-Ray Emission Study of the Electronic Structure of α - MoO_3 ", *Phys. Rev. B* **79**, 035110 (2009).
11. H.-K. Jeong, H.-J. Noh, J.-Y. Kim, L. Colakerol, P.-A. Glans, M.H. Jin, K.E. Smith, and Y.H. Lee, "Comment on ``Near-Edge X-Ray Absorption Fine-Structure Investigation of Graphene''", *Phys. Rev. Lett.* **102**, 099701 (2009).
12. T. Arnold, D.J. Payne, A. Bourlange, J.P. Hu, R.G. Egdell, L.F.J. Piper, L. Colakerol, A. DeMasi, P.A. Glans, T. Learmonth, K.E. Smith, D.O. Scanlon, A. Walsh, B.J. Morgan, and G.W. Watson, "X-ray Spectroscopic Study of the Electronic Structure of CuCrO_2 ", *Phys. Rev. B* **79**, 075102 (2009).
13. A. Walsh, J.L.F. Da Silva, S.-H. Wei, C. Korber, A. Klein, L.F.J. Piper, A. DeMasi, K.E. Smith, G. Panaccione, P. Torelli, D.J. Payne, A. Bourlange, and R.G. Egdell, "Nature of the Band Gap of In_2O_3 Revealed by First-Principles Calculations and X-Ray Spectroscopy", *Phys. Rev. Lett.* **100**, 167402 (2008).
14. T. Schneller, H. Kohlstedt, A. Petraru, R. Waser, J.H. Guo, J. Denlinger, T. Learmonth, P.-A. Glans, and K.E. Smith, "Amorphous to Crystalline Phase Transition of Chemical Solution Deposited $\text{Pb}(\text{Zr}_{0.3}\text{Ti}_{0.7})\text{O}_3$ Thin Films Studied by Soft X-ray Absorption and Soft X-ray Emission Spectroscopy", *J. Sol-Gel. Sci. Technol.* **48**, 239 (2008).
15. A. Schleife, C. Rödl, F. Fuchs, J. Furthmüller, F. Bechstedt, P.H. Jefferson, T.D. Veal, C.F. McConville, L.F.J. Piper, A. DeMasi, K.E. Smith, H. Lössch, R. Goldhahn, C. Cobet, J. Zúñiga-Pérez, and V. Muñoz-Sanjosé, "Ab-Initio Studies of Electronic and Spectroscopic Properties of MgO , ZnO and CdO ", *J. Korean Phys. Soc.* **53**, 2811 (2008).
16. A.R.H. Preston, B.J. Ruck, L.F.J. Piper, A. DeMasi, K.E. Smith, A. Schleife, F. Fuchs, F. Bechstedt, J. Chai, and S.M. Durbin, "Experimental Band Structure of ZnO from Resonant X-ray Emission Spectroscopy", *Phys. Rev. B* **78**, 155114 (2008).
17. L.F.J. Piper, A. DeMasi, K.E. Smith, A. Schleife, F. Fuchs, F. Bechstedt, J. Zuniga-Perez, and V. Munoz-Sanjose, "Electronic structure of single-crystal rocksalt CdO studied by soft x-ray spectroscopies and ab initio calculations", *Phys. Rev. B* **77**, 125204 (2008).
18. L.F.J. Piper, L. Colakerol, P.D.C. King, A. Schleife, J. Zúñiga-Pérez, P.-A. Glans, T. Learmonth, A. Federov, T.D. Veal, F. Fuchs, V. Muñoz-Sanjosé, F. Bechstedt, C.F. McConville, and K.E. Smith, "Observation of Quantized Subband States and Evidence for Surface Electron Accumulation in CdO from Angle-Resolved Photoemission Spectroscopy", *Phys. Rev. B* **78**, 165127 (2008).
19. T. Learmonth, P.A. Glans, C. McGuinness, L. Plucinski, Y. Zhang, J.H. Guo, M. Greenblatt, and K.E. Smith, "Electronic Structure of the 1D Conductor $\text{K}_{0.3}\text{MoO}_3$ studied using Resonant Inelastic X-ray Scattering and Soft X-ray Emission Spectroscopy", *J. Phys.: Condens. Matter* **20**, 415219 (2008).
20. J.P. Hu, D.J. Payne, R.G. Egdell, P.-A. Glans, T. Learmonth, K.E. Smith, J. Guo, and N.M. Harrison, "On-site interband excitations in resonant inelastic x-ray scattering from Cu_2O ", *Phys. Rev. B* **77**, 155115 (2008).
21. X. Chen, P.-A. Glans, X. Qiu, S. Dayal, W.D. Jennings, K.E. Smith, C. Burda, and J. Guo, "X-ray spectroscopic study of the electronic structure of visible-light responsive N-, C- and S-doped TiO_2 ", *J. Elec. Spec. Related Phenom.* **162**, 67 (2008).

Project Title: Indirect Excitons in Coupled Quantum Wells: New Studies with Dark Excitons

PI: Dr David Snoke

Institution: University of Pittsburgh

Email: snoke@pitt.edu

Project Scope

This project employs stress-induced trapping of interwell excitons (IXs) in GaAs/GaAlAs coupled quantum wells as a mechanism to produce high-density, equilibrated IX populations. This effort is aimed at investigating the single- and many-body physics of these dipolar excitations and, specifically, the unique characteristics of a Bose-Einstein Condensate (BEC) of these strongly repulsive particles. Through optical excitation, we create populations of IXs, which exist much longer than the time required to thermalize to the lattice temperature and to spatially equilibrate in the harmonic trapping potential created by a localized stress. From time-resolved photoluminescence measurements of these excitons' radiative decay, we directly gain information about the characteristics of this population, and through this analysis, we probe the occupation statistics and dynamics of these excitons.

Recent Progress

In GaAs/AlGaAs coupled quantum wells, localized strain can provide in-plane harmonic traps for interwell excitons, lowering the energy by local hydrostatic expansion, without significantly altering the population lifetime. In the past, we have demonstrated thermal and spatial equilibration within the long lifetimes of these spatially-indirect particles. In order to observe Bose-Einstein Condensation (BEC) in this system of strongly-repulsive aligned dipoles, we must increase the trap depth to be at least commensurate with the density-driven blue shift of the excitons within the trap. When increasing the stress past the point of previous investigations, we have observed a remarkable transition in the spatial profile of the photo-luminescence.

Specifically, we have measured a dimming of the luminescence from the highest density region at the center of the trap (see Fig. 1), and we have shown this effect to vanish at increased temperatures and at lower density. Furthermore, we have demonstrated that the dimmed central spot remains the highest density region in the trap, suggesting some fundamental change in the recombination behavior of the excitons. While consistent with the onset criteria for BEC, our simulations of the effect of strain on the band structure suggest that the effect occurs when, the higher-energy light-hole indirect exciton state starts to cross the heavy-hole state at high stress. In addition, the shear strain resulting from our trapping, which reaches a maximum away from the center of the trap, causes mixing of these different valence band states. Using an exact numerical solution to the problem of an electron and hole in this structure, with Coulomb attraction and applied electric field, we find that the light-hole indirect exciton oscillator strength is much larger than that of the heavy-hole, in contrast to the case of excitons in a single well. Simulations taking into account these effects are able to produce a darkening of the luminescence from centrally-peaked density profiles similar to the data, and they can be used to argue why this effect disappears with decreased stress and decreased density. The simulations are also confirmed by correction prediction of the polarization pattern of the luminescence (see Fig. 2). However, the simulations do not reproduce the following experimental effects: 1) The simulation predicts no temperature dependence, while the experimental effect occurs only at low temperature, 2) the simulation suggests a drastic

decrease in the population lifetime when this pattern emerges, while this is not evident in experiments, and 3) the contrast between center and periphery is much greater in the experiments. This leads us to believe that many-body effects, possible phase separation due to Bose-Einstein condensation, plays a role in this unique pattern formation effect. We have been collaborating with various theorists to understand what role many-body effects may be playing in the hydrodynamics of the excitons.

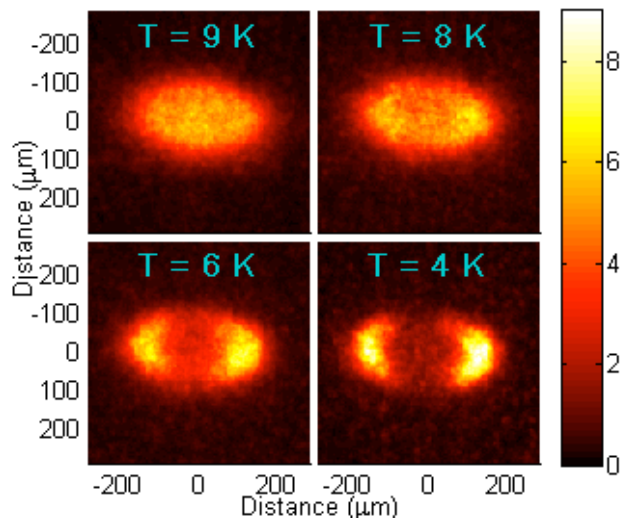


Fig. 1. Spatial image of the luminescence emitted from the interwell excitons in the stress-induced harmonic potential in a GaAs/AlGaAs coupled quantum well structure. The luminescence intensity decreases in the center even as other measurements indicate the density of the excitons is maximum in the center.

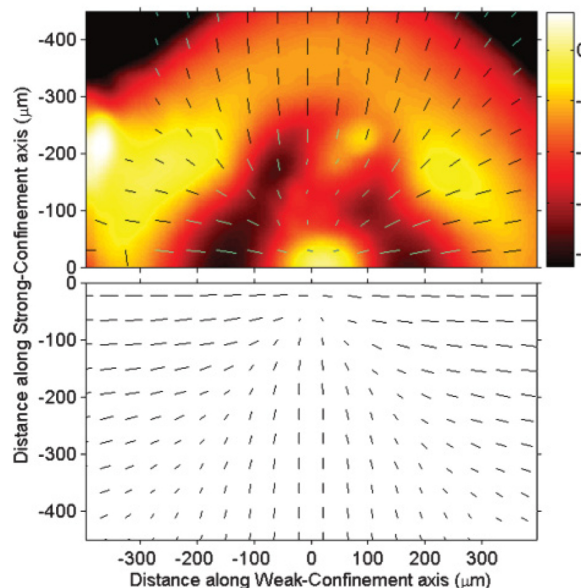


Fig. 2. Upper half: intensity (false color) and polarization degree and direction, for interwell excitons in a deep trap. There is a dark region around the center, and in the very center, the luminescence turns bright again at high stress. Lower half: theoretical prediction of the polarization pattern.

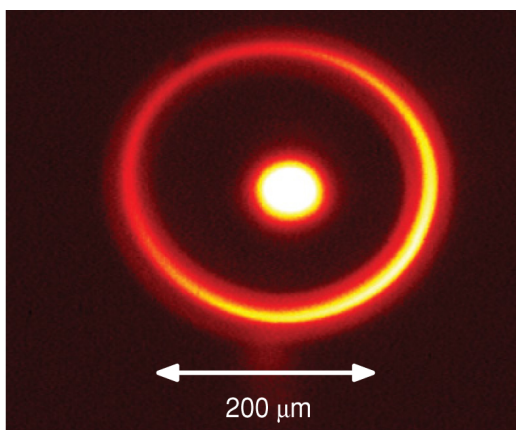


Fig. 3. Spatial image of the luminescence emitted from a GaAs/AlGaAs superlattice structure. The pattern is caused by separation of free electrons and holes in different layers.

In addition, we have collaborated with B. Fluegel and A. Mascarenhas on a very different pattern formation effect which occurs in semiconductor superlattices. In this effect, which produces rings of luminescence (see Fig. 3), optically generated carriers created by a pump laser near the band gap tunnel into superlattice states, which then emit luminescence at photon energy *higher* than the pump laser photon energy. A ring of luminescence is seen at the interface of two regions: one consisting of free holes and the other consisting of free electrons. The two types of carriers have different tunneling rates into the superlattice and therefore have different total populations, creating a charge separation. This effect has been studied before in doped structures, but this is the first time it has been demonstrated in superlattices due to up-conversion and tunneling.

Future Plans

The future work in this system will branch out in three main directions: 1) to observe signals of BEC in the highly-confined light-hole IX state at very high stress and density, 2) further investigation of the spin-structure and dynamics of the stressed system, and 3) incorporation of further post-growth processing, allowing direct contacts to the quantum well for transport measurements and creation of electrostatic traps.

Continuing with the primary thrust of this project, experiments are in progress which push beyond the stress regime of darkened luminescence and examine the luminescence from the very sharply confined light-hole IX state which becomes the lowest energy state at high stress. We specifically hope to identify deviations from the typical uncondensed optical signals, signifying, e.g., classic BEC predictions of optical coherence, superradiance, and spatial/spectral narrowing. In addition, we are interested in deviations from the nearly-ideal BEC predictions arising from the very strong repulsive character of the particles. In fact, if we continue to push to higher and higher density and fail to see any of the traditional characteristics of condensation, this may be the most surprising and interesting result of all.

In support of our previous analysis of the luminescence darkening, we are arranging studies to nail down some of the predictions related to the spin structure and spin-dynamics in that system. First, we would like to establish that the dark ($J=2$) exciton states are not playing a significant role in this darkening process. One possible explanation of the darkening employs a BEC of these dark excitons, and, so far, we have been unable to rule out this possibility, except to say that light/heavy-hole mixing explains most of what we see without employing dark excitons in the process. In order to elucidate the role of dark excitons, we will place the sample in an in-plane magnetic field, which will mix the bright and dark states, allowing us to “turn on” the luminescence of the dark excitons. Our second study in this vein will explore the spin relaxation in the strained and unstrained case. In our analysis of the luminescence darkening, one possible explanation of the discrepancy between our lifetime predictions and measurements is that some long-lifetime state is acting as a reservoir, buffering the lifetime. Again, the dark IX states could play this role, but this would require extremely long spin-relaxation times. However, recently there have been reports of spin-relaxation times exceeding the radiative lifetime of IXs in similar systems, and, hence, we must consider this possibility. We plan to employ time-resolved luminescence measurements to measure the cross-polarization rise-time from a polarized, resonant pump.

In a complementary effort, we will employ further lithographic processing to our samples to allow more flexibility in electrical potential application/measurement and to directly measure the exciton current through electrical contacts.

List of Publications, 2008-2011

D.W. Snoke, "Predicting the Ionization Threshold for Carriers in Excited Semiconductors," *Solid State Communications* **146**, 73 (2008).

Z. Vörös and D.W. Snoke, "Quantum Well Excitons at Low Density," *Modern Physics Letters B* **22**, 701 (2008).

Z. Vörös, D.W. Snoke, L. Pfeiffer, and K. West, "Direct measurement of exciton-exciton interaction energy," *Physical Review Letters* **103**, 016403 (2009) (cover article).

B. Fluegel, K. Alberi, L. Bhusal, A. Mascarenhas, D. W. Snoke, G. Karunasiri, L. N. Pfeiffer, and K. West, "Exciton pattern generation in GaAs/AlGaAs multiple quantum wells," *Physical Review B* **83**, 195320 (2011).

D.W. Snoke, "Coherence and Optical Emission from Bilayer Exciton Condensates," *Advances in Condensed Matter Physics* **2011**, 938609 (2011).

N.W. Sinclair, J.K. Wuenschell, Z. Vörös, B. Nelsen, D. W. Snoke, M. H. Szymanska, A. Chin, J. Keeling, L.N. Pfeiffer and K.W. West, "Strain-induced Darkening of Trapped Excitons in Coupled Quantum Wells at Low Temperature," *Physical Review B* **83**, 245304 (2011).

D.W. Snoke, "Dipole excitons in coupled quantum wells: toward an equilibrium exciton condensate," in *Non-Equilibrium and Finite Temperature Quantum Gases*, (World Scientific, in press).

Simulating strongly correlated electrons with a strongly interacting Fermi gas

Grant #DE-SC-0002712

Report for the Period: 8/14/10-8/15/11

John E. Thomas

Physics Department, North Carolina State University

Raleigh, NC 27695

e-mail: jet@phy.duke.edu

April 23, 2010

1. Scope

The quantum many-body physics of strongly correlated fermions is studied in a degenerate, strongly interacting atomic Fermi gas, first realized by our group with DOE support in 2002. This system, which exhibits strong spin pairing, is now widely studied and provides an important paradigm for testing predictions based on state-of-the-art many-body theory in fields ranging from nuclear matter to high temperature superfluidity and superconductivity.

Strongly interacting mixtures of spin-up and spin-down ${}^6\text{Li}$ fermions are produced by using a bias magnetic field to tune near a collisional (Feshbach) resonance. The resonance permits wide tunability of the s-wave scattering length that determines the interaction strength. In addition, the density, temperature, and spin composition are experimentally controllable. Thermodynamic measurements in this system offer unprecedented new opportunities to provide feedback between theory, computation and experiment, which is essential for testing and comparing the best current nonperturbative quantum many-body calculations.

The purpose of the proposed program is the precision measurement of the thermodynamic properties of this unique quantum system, in both the superfluid and normal fluid regime and in three dimensional and two dimensional trapped gases. As the system is strongly interacting, the normal fluid is nontrivial and of great interest, especially in view of a recent conjecture from the string theory community on the concept of nearly perfect normal fluids, which exhibit a minimum ratio of shear viscosity to entropy density [1].

2. Recent Progress

During this period, we made a major breakthrough in our studies of a strongly correlated, resonantly interacting Fermi gas, as described in our recent *Science* paper on the first measurement of a transport coefficient, the shear viscosity [2]. At resonance, where the gas exhibits universal behavior, we made the first complete measurement of the universal quantum viscosity. This research combines measurements of the thermodynamic properties (energy, entropy, and temperature) with measurements of the hydrodynamic properties (viscosity). As pointed out to us by condensed matter theorists, ^4He and ^3He have similar behavior in the heat capacities, but very different behavior in the viscosities. Indeed, ^4He shows an increase in viscosity below a certain temperature, while ^3He agrees with Fermi liquid theory down to a certain temperature and then drops precipitously, in disagreement with Fermi liquid behavior. Our work was the culmination of a nearly two year effort. In addition, we observed shockwaves by colliding two strongly interacting clouds, which opens up a new paradigm for studying nonlinear hydrodynamics in quantum matter.

Universal Quantum Viscosity in a Strongly-Interacting Fermi Gas [2]

Measurement of the ratio of the shear viscosity η to the entropy density s is at present of great interest in the context of a recent conjecture from the string theory community, that η/s has a universal minimum $\hbar/(4\pi k_B)$ for a broad class of strongly interacting quantum fields. As both the thermodynamic and hydrodynamic properties can be measured, a strongly interacting Fermi gas offers a nonrelativistic, scale-invariant analog for study. Remarkably, a quark-gluon plasma and our ultracold strongly interacting Fermi gas have nearly the same ratio, about 5 times the lower bound, despite the fact that the temperatures and densities differ by 19 and 25 orders of magnitude respectively!

Our measurements were made possible by several breakthroughs, both in the analysis of the hydrodynamic properties and in the measurement of the thermodynamic properties. For the viscosity measurements, we realized that observing anisotropic expansion would permit measurement of the viscosity at high temperature, permitting the first demonstration of the predicted universal high temperature scaling $\eta \propto T^{3/2}$. For the low temperature measurements, we observed the damping rate of the radial breathing mode. A critical step in our analysis of the data was to develop universal hydrodynamic equations that included not only the friction force arising from the viscosity, but the effect of the heating rate on the pressure. We found that the two measurement methods agree nicely in the region of temperature where they overlap, only if the heating rate is properly included. Leaving out the heating rate leads to a factor of 2 discrepancy.

A critical breakthrough was our development a new method of measuring temperature for the viscosity measurements at high temperature. In this high temperature regime, we exploited a universal expression for the local energy density in terms of

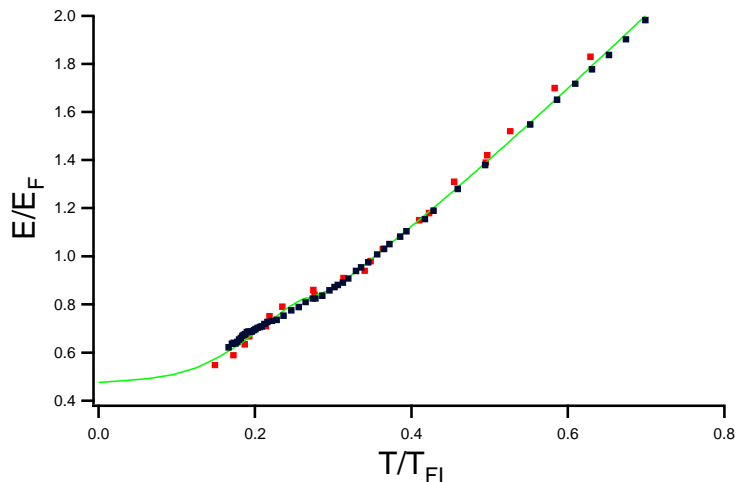


Figure 1: Measured global energy per particle versus the temperature obtained from the calibration (red dots); For comparison, we show the data obtained by the ENS group by integrating the measured local energy density (black dots) and the NSR theory of Hu, Liu and Drummond [*New J. of Phys.*, 12:063038, 2011] (green curve).

the temperature and density (due to Ho and Mueller), based on the universal second virial coefficient. As the pressure is $2/3$ of the local energy density for a universal gas, we were able to use force balance in the trap to relate the measured mean square size of the trapped cloud directly to the temperature. Further, we used the second virial expansion to calculate the global entropy S and energy E at higher temperatures. Combining this high temperature calculation with our previous model-independent measurements of S and E at low temperature, we were able to obtain a smooth curve for E versus S over the entire range of temperatures used in the viscosity experiments [4]. From this curve, we obtained a new temperature calibration, $T = \partial E / \partial S$, which permitted a measurement of viscosity versus reduced temperature at the trap center. To test the new calibration, we plotted the measured global energy in the low temperature region as a function of the temperature obtained from the calibration. The results are shown in Fig. 1. Our calibration of temperature versus energy will find applications in other precision measurements, as the energy of a universal Fermi gas can be measured directly from the mean square cloud profile by exploiting the virial theorem, which holds for a universal strongly interacting gas.

Shock Waves in a Strongly-Interacting Fermi Gas [5]

In addition to measuring the universal viscosity, we made the first observation of shock waves in a strongly interacting Fermi gas, by colliding two strongly interacting clouds in a long, cigar-shaped optical trap. This system will provide a new paradigm for the study of nonlinear hydrodynamics in quantum matter. Of interest

is the interplay between the formation of large density gradients, dispersion arising from quantum pressure, and dissipation arising from the kinetic viscosity, which has a natural unit \hbar/m , where m is the atom mass. In this system, we can study shock wave formation and propagation as a function of the speed of the colliding clouds, interaction strength (by tuning away from the collisional resonance), and as a function of temperature. We are working to understand the thermodynamic features, in particular, the effect of heating, when the clouds collide, on the local pressure and shock wave formation.

3. Future Plans

Our immediate plans involve two experiments. First, we plan to measure the bulk viscosity in a strongly interacting gas, which is predicted to vanish at the Feshbach resonance, where the gas is a scale invariant, but which is nonzero away from resonance. We are also working to understand the role of many-body correlations on the pairing energy of trap-induced pairs in a two-dimensional gas. These experiments use radio frequency spectroscopy to probe the pairing energy near the Feshbach resonance for atoms in a standing-wave optical trap. We will study the how pairing arises from trap induced localization and from many-body physics.

4. References to Publications of DOE Sponsored Research (Past Year)

- 1) J. E. Thomas, “The nearly perfect Fermi gas,” *Physics Today*, pp. 34-37 (May, 2010).
- 2) C. Cao, E. Elliott, J. Joseph, H. Wu, J. Petricka, T. Schäfer, and J. E. Thomas, “Universal Quantum Viscosity in a Unitary Fermi gas,” *Science* **331**, 58 (2011).
- 3) J. E. Thomas, submitted chapter on “Unitary Fermi gases,” in “Ultracold Fermi and Bose Gases,” “Contemporary Concepts of Condensed Matter Science” (A. Fetter, K. Levin and D. Stamper-Kurn, Editors), (Elsevier, 2011; to be published).
- 4) C. Cao, E. Elliott, H. Wu, J. E. Thomas “Searching for perfect fluids: Quantum viscosity in a universal Fermi gas,” *New J. Phys.*, special issue on strongly correlated matter (accepted, 2011).
- 5) J. A. Joseph and J. E. Thomas (with M. Kulkarni and A. G. Abanov), “Observation of shock waves in a strongly interacting Fermi gas,” *Phys. Rev. Lett.* **106**, 150401 (2011).
- 6) J. E. Thomas, “Spin drag in a perfect fluid,” *Nature, News and Views*, **472**, 172 (2011).

**BES Experimental CMP PI Meeting
Rockville, Maryland
August 9 -12, 2011**

Investigations of Electron Correlation in Complex Systems

JG Tobin¹, SW Yu¹, BW Chung¹ and GD Waddill²

1 Lawrence Livermore National Laboratory, Livermore, CA

2 Missouri University of Science and Technology, Rolla, MO

Email Contact: Tobin1@LLNL.Gov

Project Scope:

Electron correlation, the electron-electron interactions outside of simple one-electron models, is the key to resolving outstanding issues concerning the electronic structure of complex materials. These complex materials have intricate physical structures and/or multiple phases with unique electronic-structure properties. We will use cutting-edge techniques such as Resonant Inverse Photoelectron Spectroscopy (RIPES) and Fano Spectroscopy, a sophisticated variant of Photoelectron Spectroscopy (PES), and related techniques to determine the valence electronic structure of complex materials. These complex materials include potential spin-sources for spintronic-devices such as transition-metal, magnetic, ultra-thin films; materials exhibiting correlation effects such as Kondo Shielding and Hidden Order, e.g. the Rare Earth materials; and the crucially important yet poorly understood actinide systems, such as those containing U and Pu. These are each distinctive and separate areas of world-class science, an issue at the core of the DOE Office of Science and Office of Basic Energy Research. Measurements will be performed at the Advanced Light Source (Lawrence Berkeley National Laboratory, Berkeley, CA), the Advanced Photon Source (Argonne National Laboratory, Chicago, IL) and Lawrence Livermore National Laboratory (Livermore, CA). We will solve the Pu electronic structure problem, a goal of tremendous scientific and technological importance to DOE and the USA. We will provide experimental benchmarking for the new theories of Pu and actinide 5f electronic structure, leading to the resolution of a problem that has remained unsolved for the last 60 years, the nature of the 5f electron. A proper modeling of Pu electronic structure will, in turn, lead to an enhanced capability to predict the behavior of Pu over long periods of time, an issue of tremendous importance to environmental cleanup, radioactive waste storage and science based stockpile stewardship.

Recent Progress: Differentiation of 5f and 6d Components in the Unoccupied Electronic Structure of UO₂

One of the crucial questions of all actinide electronic structure determinations is the issue of 5f versus 6d character and the distribution of these components across the density of states. Here, two break-through experiments will be discussed, which have allowed the direct determination of the U5f and U6d contributions to the unoccupied density of states (UDOS) in Uranium Dioxide (UO₂). [1] First, a combined soft X-ray Absorption and Bremsstrahlung Isochromat Spectroscopy (XAS and BIS, respectively) study of UO₂ will be discussed. [2] Second, a novel Resonant Inverse Photoelectron and X-ray Emission Spectroscopy (RIPES and XES, respectively) [3] investigation of UO₂ will be presented, along with an analysis predicated upon the picture of the UDOS generated in the XAS/BIS study. It will be seen that the U5f and U6d components are isolated and identified unambiguously.

the incoming electrons. The horizontal scale on the bottom is the energy of the outgoing photons. The resolution bandpass was 2 eV or better throughout.

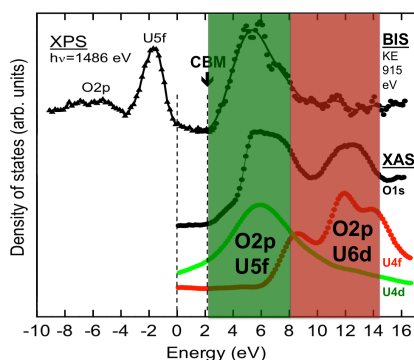


Figure 1: (above) A summary of our earlier results for XPS, BIS and XAS of UO₂ is shown here. The green region represents the part of the UDOS dominated by U5f and O2p states and the red area is that dominated by the U6d and O2p states. CBM is conduction band minimum.

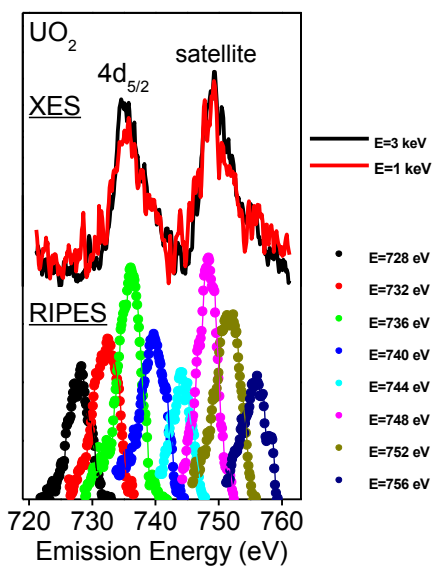


Figure2: (right) The RIPES and XES of UO₂ is presented here. The XES is shown in the upper part of the figure and the RIPES in the lower part of the figure. The legend in the corner denotes the energy of the excitation,

References

1. S.-W. Yu and J.G. Tobin, J. Vac. Sci. Tech. A **29**, 021008 (2011).
2. S.-W. Yu, J.G. Tobin, J. C. Crowhurst, S. Sharma, J. K. Dewhurst, P. Olalde-Velasco, W. L. Yang, W. J. Siekhaus, Phys. Rev. B **83**, 165102 (2011).
3. J.G. Tobin, S.W. Yu, B.W. Chung, G.D. Waddill, L. Duda and J. Nordgren, Phys. Rev B **83**, 085104 (2011).

Acknowledgements

Lawrence Livermore National Laboratory is operated by Lawrence Livermore National Security, LLC, for the U.S. Department of Energy, National Nuclear Security Administration under Contract DE-AC52-07NA27344. This work was supported by the DOE Office of Science, Office of Basic Energy Science, Division of Materials Science and Engineering. The Advanced Light Source (ALS) is supported by the Director, Office of Science, Office of Basic Energy Sciences, of the U.S. Department of Energy under Contract No. DE-AC02-05CH11231.

**BES Experimental CMP PI Meeting
Rockville, Maryland
August 9 -12, 2011**

Proposed Work

Three directions of research into complex systems will be proposed here: highly polarized ultra-thin films; 4f electron correlated systems; and 5f electron correlated systems, especially Pu.

P1 Magnetic systems: highly polarized ultrathin films

Based upon our success with Fe/GaAs system, we will continue to pursue the investigation of highly spin-polarized, ultra thin films at the Advanced Photon Source. Particular emphasis will be placed upon the 3d systems: Fe, Co and Ni and their alloys.

P2 Electron Correlation in 4f systems: Spin Shielding

We would like to return to the issue of 4f electron correlation in Ce. It is well known that the electron correlation effects in Ce are phase dependent, with the principal phases being α , β and δ . It is also well known that the pressure and temperature effects of the pure Ce phases can be mimicked and manipulated by chemical doping. e.g Th. We propose to grow various doped samples of Ce alloys and study the spin composition of the Lower Hubbard band (LHB) and quasiparticle peaks as a function of dopant, dopant concentration, phase and temperature. We will also grow evaporated films in vacuo. We will investigate these Rare Earth samples with our in-house Fano capability, with its chirally mounted dual He I photon sources. This will provide us with a tremendous experimental database to which we will compare theoretical predictions for various models of electron correlation in the literature.

P3 Electron Correlation in 5f systems

Because of their chemical toxicity, radioactivity and political sensitivity, handling 5f materials such as Pu is a nightmare. We propose two parallel approaches to address this problem.

P3i Fano Experiments at LLNL

We propose to grow various doped samples of U, Np, Pu and Am alloys and study the spin composition of the valence peaks as a function of dopant, dopant concentration, phase and temperature. We will investigate these actinide samples with our in-house Fano capability, with its chirally mounted dual He I photon sources. This will provide us with a tremendous experimental database to which we will compare theoretical predictions for various models of electron correlation in the literature.

P3ii Isolation of 5f and 6d components in the UDOS with RIPES and XAS

The nature of this problem, its importance and the solution to it are discussed above under recent results. The limitation for XAS is that only low activity samples can be taken to the soft X-ray synchrotron sources. For low activity samples, we will continue the work at facilities such as the ALS and APS. For higher activity samples, such as those containing Np, Pu, and Am, we will perform the experiments at LLNL.

In our initial studies, both XAS and RIPES, will be directed at UF_4 . This is a compound that is closely related to Uranium Dioxide, but with perhaps greater localization. The increased localization may give a response in RIPES that is between the two limits of complete localization (CeOxide, Ref 14, page 4) and the delocalization and covalency of UO_2 (Ref 15, page 4). It may also provide a sufficiently localized form of U that a Fano effect may be seen, but this may be too optimistic of a hope.

BES Experimental CMP PI Meeting
Rockville, Maryland
August 9 -12, 2011

Peer Reviewed Publications 2008-2011

1. J.G. Tobin, P. Söderlind, A. Landa, K.T. Moore, A.J. Schwartz, B.W. Chung, M.A. Wall, J.M. Wills, R.G. Haire, and A.L. Kutepov, "On the electronic configuration in Pu: Spectroscopy and Theory," *J. Phys. Cond. Matter* **20**, 125204 (2008).
2. S.W. Yu and J. G. Tobin, "Breakdown of spatial inversion symmetry in core level photoemission, *Phys. Rev. B* **77**, 193409 (2008).
3. J.D.W. Thompson, J.R. Neal, T.H. Shen, S.A. Morton, J.G. Tobin, G.D. Waddill, J.A.D. Matthew, D. Greig, and M. Hopkinson, "The Evolution of Ga and As core levels in the formation of Fe/GaAs(001): A high-resolution soft x-ray photoelectron spectroscopic study," *J. Appl. Phys.* **104**, 024516 (2008).
4. S.W. Yu, J.G. Tobin, and P. Söderlind, "An Alternative Model for Electron Correlation in Pu," *J. Phys. Cond. Matter* **20**, 422202 (2008), Fast Track Communication.
5. J.G. Tobin, S.W. Yu, B.W. Chung and G.D. Waddill, "Resolving the Pu Electronic Structure Enigma: Past Lessons and Future Directions," *J. Nucl. Matl.* **385**, 31 (2009).
6. J.G. Tobin, S.-W. Yu, M.T. Butterfield, T. Komesu, and G.D. Waddill, "Investigations of Magnetic Overlayers at the Advanced Photon Source, *J. Vac. Sci. Tech.A* **28**, 697 (2010).
7. S.W. Yu, B.W. Chung, J.G. Tobin T. Komesu, and G.D. Waddill, "A Possible Way for Removing Instrumental Asymmetries in Spin Resolved Photoemission with Unpolarized Light," *Nuclear Instr. Meth. Phys. Res.* **A 614**,145 (2010)
8. J.G. Tobin, S.-W. Yu, S.A. Morton, G.D. Waddill, J.D.W. Thompson, J.R. Neal, M. Spangenberg, and T.H. Shen, "Highly polarized emission in spin resolved photoelectron spectroscopy of alpha-Fe(001)/GaAs(001)," *Surface Science* **604**, 1342 (2010). Perspective Article in *Surface Science*, June 2010. Introduction at *Surf. Sci.* **604**, 1333 (2010).
9. T. Komesu, G.D. Waddill, S.W. Yu, M.T. Butterfield and J.G. Tobin, "Isolation of Exchange- and Spin-orbit- Driven Effects via Manipulation of the Axis of Quantization," *J. Vac. Sci. Tech.A* **28**, 1371 (2010).
10. J.G. Tobin, S.-W. Yu, B.W. Chung, G.D. Waddill and AL Kutepov, "Narrowing the Range of Possible Solutions to the Pu Electronic Structure Problem: Developing a new Bremsstrahlung Isochromat Spectroscopy Capability," *IOP Conf. Series: Materials Science and Engineering* **9**, 012054 (2010).
11. J.G. Tobin, S.W. Yu, B.W. Chung, G.D. Waddill, E. Damian, L. Duda and J. Nordgren, "Observation of Strong Resonant Behavior in the Inverse Photoelectron Spectroscopy of Ce Oxide," *Phys. Rev B* **83**, 085104 (2011).
12. S.-W. Yu and J.G. Tobin, "Confirmation of Sample Quality: XPS and UPS of UO₂", *J. Vac Sci. Tech.* **A 29**, 021008 (2011).
13. J.G. Tobin, S.-W. Yu, B.W. Chung, G.D. Waddill and J.D. Denlinger, "Direct comparison of the X-ray emission and absorption of cerium oxide", *J. Vac. Sci. Tech.* **A 29**, 031504 (2011).
14. S.-W. Yu, J. G. Tobin, J. C. Crowhurst, S. Sharma, J. K. Dewhurst, P. Olalde-Velasco, W. L. Yang, and W. J. Siekhaus, "f-f origin of the insulating state in uranium dioxide: X-ray absorption experiments and first-principles calculations," *Phys. Rev. B* **83**, 165102 (2011).
15. J.G. Tobin and S.-W. Yu, "Orbital Specificity in the Unoccupied States of UO₂ from Resonant Inverse Photoelectron Spectroscopy, sub to *Phys. Rev. Lett*, May 2011.
16. S.-W. Yu, J. G. Tobin, and B. W. Chung, "An instrument for the investigation of actinides with spin resolved photoelectron spectroscopy and bremsstrahlung isochromat spectroscopy," to be sub to *Rev. Sci. Instrum.* 2011.

Spatial extent of near-band edge modification due to lattice disorder

A. Steigerwald¹ (d.steig@vanderbilt.edu), A.B Hmelo¹ (a.hmelo@vanderbilt.edu), K. Varga¹ (kalmna.varga@vanderbilt.edu), L.C. Feldman^{1,2} (l.c.feldman@rutgers.edu),
N. Tolk¹ (norman.tolk@vanderbilt.edu)

¹*Dept. of Physics and Astronomy, Vanderbilt University, Nashville TN 37205*

²*Institute of Advanced Materials, Devices, and Nanotechnology, Rutgers University,
New Brunswick NJ 08901*

Project Scope

We develop and apply an optical probe technique known as coherent acoustic phonon (CAP) spectroscopy to the study of radiation-damaged materials. Our overall effort is two-fold: (a) understanding the behavior and interpretation of the optical response in disordered crystals, and (b) using the CAP technique as a tool to study the effects of disorder on crystal properties. Conceptually, the CAP technique offers the ability to probe local optoelectronic properties as a function of depth with spatial resolution as low as tens of nanometers. As it is an all-optical technique, CAP is extremely sensitive to any aspect (defect, strain, external fields, etc.) that modifies the optoelectronic properties, one of the hallmarks of disorder in semiconductors. Therefore, CAP has great potential as a method to understand the influence of disorder on semiconductor properties.

Recent Progress

Recently we applied the CAP technique to observe near-band edge optoelectronic modification in ion-irradiated GaAs. Disorder (e.g., structural defects) in a crystal lattice induces localized strain, and in turn modifies the optoelectronic structure in some volume surrounding the structural defects. By correlating the change in the optical response with estimated structural disorder (as determined via channeling analysis and simulation), we were able to estimate the number of lattice points that experience optical modification surrounding structural damage. This volume of 'optical damage' is found to be strikingly large, nearly 700 lattice points per unit disorder. Numerous techniques, macroscopic to nano-scopic, have been developed to identify and characterize defects in semiconductors. With regards to defect-induced changes to the electronic structure, most work focuses on the specific defect levels within the original band structure. Little headway has been made in studying delocalized optoelectronic modification surrounding localized structural disorder, particularly how the band edge is modified in a local area by defect-induced strain effects. Understanding such behavior on a microscopic level is particularly important as it creates "pockets" where optoelectronic properties differ significantly from bulk values.

The CAP technique is part of the generalized experimental approach known as ultrafast time-resolved pump-probe spectroscopy. Our measurements monitor ultrafast pump-induced (transient) changes to the reflectivity. Initially, an intense

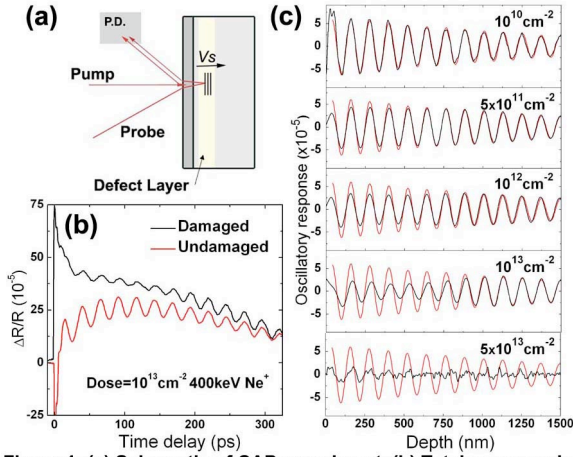


Figure 1: (a) Schematic of CAP experiment, (b) Total pump-probe response for damaged and undamaged sample, and (c) isolated oscillatory responses for a variety of radiation doses.

optical pulse is absorbed by a thin ($\sim 10\text{nm}$) metallic layer deposited on the sample surface, causing rapid thermal expansion and launching an acoustic strain wave into the bulk material (Figure 1a). The acoustic pulse travels at the speed of sound and is roughly $\sim 20\text{nm}$ wide (the phonon distribution is centered around $\sim 100\text{GHz}$). A second, time-delayed probe pulse then reflects off both the sample surface and the optical discontinuity created by the strain pulse. The two components meet at the photodiode, however, a continuously changing phase difference due to the travelling strain wave contributes a persisting oscillatory component in the time-resolved response. These oscillations are analyzed to determine subsurface optoelectronic features as a function of depth. Because the fraction of light reflected from the acoustic pulse, and hence the oscillation amplitude, is dependent on the local optical properties, the technique is very sensitive to any optical modification present.

In the case of irradiated GaAs, when the acoustic wave passes through highly disordered areas of the crystal lattice we observed a significant reduction in CAP amplitude (Figure 1b). As the speed of sound in GaAs is well known ($\sim 4.7\text{nm/ps}$) we were able to plot this change in amplitude as a function of depth, which represented an optical ‘damage’ profile. Additionally, we performed ion channeling analysis and Monte Carlo simulations to determine an estimate of the structural disorder. By comparing the reduction in amplitude with the estimated ion damage (i.e. the degree of optical damage versus defect concentration), we were able to determine how quickly optical properties of the near band edge electronic structure changed as disorder increased. We found that changes in the optical response followed a dependence on point defect concentration of the following form:

$$\frac{\Delta A}{A}(n_d) = K[1 - \exp(-\beta n_d)]$$

Here $\Delta A/A$ is the change in CAP amplitude, n_d is defect concentration, K defines a saturation level, and β defines a characteristic volume within which optical modification occurs. In other words, β provides an estimate of the number of lattice points experiencing optical modification surrounding ion-induced structural disorder. We found this ‘optical footprint’ to be on the order 700 atoms, corresponding to a volume of roughly 16nm^3 . This result is particularly important in nanoscale devices whose size scale is comparable to the optically modified volume (though β most likely differs significantly for various materials).

Future Work

We continue to develop the CAP technique as a robust tool for characterizing various types of materials systems. This entails studying systems of increasing complexity, understanding the interaction between acoustic phonons and artifacts (interfaces, disorder, grain boundaries, impurities, dopants, etc.), and further developing analysis of the observed optical response. Fundamentally, our studies use CAP to measure optical modification caused by some subsurface crystal feature. Yet it is not straightforward to know precisely how any particular feature will modify the optoelectronic structure, or conversely, if we observe a certain amount of optical modification, determining what type of crystal defect is present. Such understanding can come about only through testing CAP in wide variety of material systems and applications. Currently we have collaborations to probe a wide range of systems, including (among others):

- Radiation-damaged oxides (TiO₂/STO)
- CeO₂ nanocrystalline thin films
- Thin *p*- and *n*-doped diamond heterostructures
- Various materials pressurized (~10-100GPa) in a diamond anvil cell

Recent publications

1. Steigerwald, A. *et al.* Spatial extent of near-band edge optical modification due to lattice disorder. *Submitted July 2011, Physical Review B*
2. Park, H., *et al.* Polarization-dependent temporal behaviour of second harmonic generation in Si/SiO₂ systems. *Journal of Optics* **13**, 055202 (2011).
3. Nageswara Rao, S.V.S. *et al.* Reconfiguration and dissociation of bonded hydrogen in silicon by energetic ions. *Physical Review B* **83**, 045204 (2011).
4. Qi, J. *et al.* Mechanical and electronic properties of ferromagnetic Ga_{1-x}Mn_xAs using ultrafast coherent acoustic phonons. *Physical Review B* **81**, 115208 (2010).
5. Spahr, E.J. *et al.* Giant Enhancement of Hydrogen Transport in Rutile TiO₂ at Low Temperatures. *Physical Review Letters* **104**, 205901 (2010) .
6. Park, H. *et al.* Boron induced charge traps near the interface of Si/SiO₂ probed by second harmonic generation. *Physica Status Solidi B* **247**, 1997 (2010).
7. Park, H. *et al.* Photon energy threshold for filling boron induced charge traps in SiO₂ near the Si/SiO₂ interface using second harmonic generation. *Applied Physics Letters* **97**, 062102 (2009).
8. Ciesielski, P.N. *et al.* Enhanced Photocurrent Production by Photosystem I Multilayer Assemblies. *Advanced Functional Materials* **20**, 4048 (2010).
9. Steigerwald, A. *et al.* Semiconductor point defect concentration profiles measured using coherent acoustic phonon waves. *Applied Physics Letters* **94**, 111910 (2009).

10. Qi, J. *et al.* Ultrafast laser-induced coherent spin dynamics in ferromagnetic Ga_{1-x}Mn_xAs/GaAs structures. *Physical Review B* **79**, 085304 (2009).
11. Park, H. *et al.* Characterization of boron charge traps at the interface of Si/SiO₂ using second harmonic generation. *Applied Physics Letters* **95**, 062102 (2009).
12. Spahr, E.J. *et al.* Proton Tunneling: A Decay Channel of the O-H Stretch Mode in KTaO₃. *Physical Review Letters* **102**, 075506 (2009).
13. Lu, X. *et al.* Temperature-dependent second- and third-order optical nonlinear susceptibilities at the Si/ SiO₂ interface. *Physical Review B* **78**, 155311 (2008).

Novel nanoscale morphologies and atomistic processes control on surfaces

K.M. Ho^{1,2}, M.Hupalo¹, P. A. Thiel^{1,3}, M.C.Tringides^{1,2} and C. Z. Wang¹

¹Ames Laboratory, ²Department of Physics-ISU, ³Department of Chemistry-ISU
Ames IA 50011

Emails: kmh@ameslab.gov, hupalo@ameslab.gov, thiel@ameslab.gov, tringides@ameslab.gov,
wangcz@ameslab.gov

Scope

The ability to control the growth of nanostructures could impact many current and future technologies such as microelectronics, catalysis, computer memories, ultrafast switches, lasing materials etc. Different factors are responsible for the emergence of novel properties on nanostructures: electron confinement, lower atom coordination of boundary atoms, etc. Since these properties depend on nanostructure dimensions they can become tunable with size. The goals of the FWP have been two-fold:(i) to discover ways to grow uniform nanostructures epitaxially on a variety of substrates. Since growth is far from equilibrium and a wealth of metastable structures is possible, it requires better understanding of the atomistic processes (diffusion, nucleation, coarsening etc) involved. (ii) Utilizing its previous expertise, the FWP plans to use controllable metal morphologies in three new areas: (a) to investigate enhanced reactivity of adsorbed gases on metal islands (hydrogen adsorption on Mg islands relevant to hydrogen storage and oxygen, ethylene adsorption on Ag islands relevant to ethylene epoxidation); (b) to grow metal defect-free nanowires on carbon coated Si(111) and on epitaxial graphene on SiC for magnetic applications and to elucidate the underlying growth mechanisms. (c) to study metal growth on graphene for improved metal contacts and determine to what extent the metal graphene interaction can modify the ideal graphene electronic structure. In all three problems the synergistic interaction between theory and experiment is essential to attain understanding and predictability.

Recent Progress

The FWP has done pioneering work in the discovery of uniform height metal islands which form spontaneously because of electron confinement[1,2], when the electron wavefunction fits optimally within the confining well. (Pb/Si(111), In/Si(111), Ag/NiAl(110), Ag/Quasicrystals(QC), Bi/QC[11]). Since the formation of the islands requires uphill diffusion of up to ~million of atoms to build an island, this discovery has stimulated sophisticated modeling[3,4] to generate the complex potential energy surface that dictates how the deposited atoms irreversibly move to higher layers. Monte Carlo simulations and analytic work was used to model the formation of 3-layer Ag islands on Ag/QC, 2-layer Ag islands on NiAl(110) and 7-layer Pb islands on Si(111).

A bigger surprise than height selection was the extent QSE can affect atomistic processes. A dramatic dependence of nucleation on height was found after a small amount of Pb was deposited on Pb islands: a low density of fractal islands nucleated on stable (5-layer) vs a high density of small islands on unstable(4-layer) islands[5]. These intriguing results show indeed that island geometry controls nucleation, which is very promising for the future reactivity studies planned by the FWP on Mg and Ag islands. Monte Carlo simulations (in collaboration with the Czech group of Chvoj and Kuntova) have reproduced the experiment using a higher critical size cluster $i_c=5$ on stable vs $i_c=1$ on unstable islands.

Although the growth studies of the uniform height islands are carried out below room temperature, their completion time is only 2-3 minutes. Classical diffusion is not the most efficient mode for mass transport, since distance depends sub-linearly \sqrt{t} on time. From the STM experiments we concluded that the dense wetting layer between the islands is the key player as it moves mass superdiffusively, i.e., linearly in time. This unusual motion was directly confirmed in real time in collaboration with M. S. Altman (Hong Kong Univ. of Science and Technology) using low energy electron microscopy (LEEM)[6] seen in fig.3(a). The superdiffusive motion of the Pb wetting layer was also seen in coarsening experiments. Growth does not follow classical Gibbs Thompson decay and a non-classical behavior “sudden death” type of decay of the unstable islands was observed. Since Ag on Si(111) is one of the systems to be used to study height dependent reactivity, work was performed to understand the Ag growth on the 7×7 and on the Si(111)-Ag($\sqrt{3} \times \sqrt{3}$) phase. Diffusion of Ag on $\sqrt{3} \times \sqrt{3}$ was studied by measuring the nucleated island densities over a wide temperature range. Fig. 3(c) shows unusual large

diffusion length $\sim 1\mu\text{m}$ at 300K, analogous to Pb/Si(111); and fig.3(d) shows the sudden change in island density at $\sim 170\text{K}$ [7].

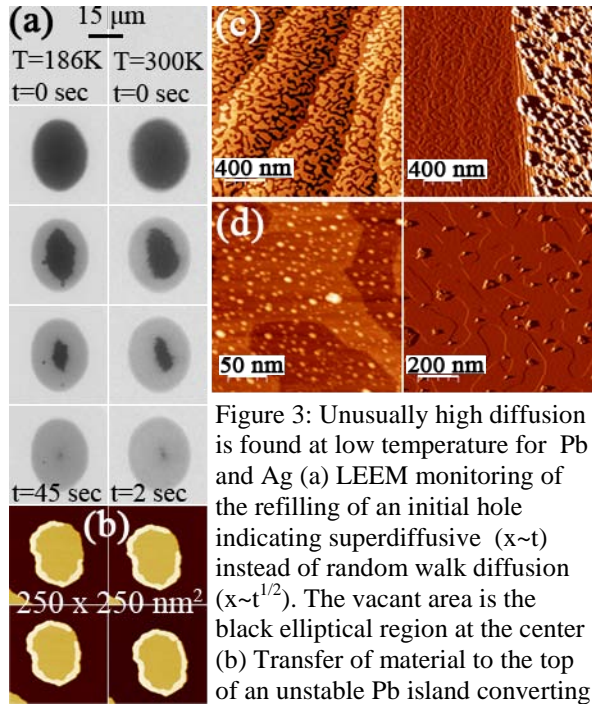


Figure 3: Unusually high diffusion is found at low temperature for Pb and Ag (a) LEEM monitoring of the refilling of an initial hole indicating superdiffusive ($x\sim t$) instead of random walk diffusion ($x\sim t^{1/2}$). The vacant area is the black elliptical region at the center (b) Transfer of material to the top of an unstable Pb island converting it to a stable island at constant speed. (c) Unusually fast diffusion of Ag on Si(111)-Ag $\sqrt{3}\times\sqrt{3}$ at 300K that shows a diffusion length of $1\mu\text{m}$. (d) Diffusion of Ag on Si(111)-Ag $\sqrt{3}\times\sqrt{3}$ switches abruptly from slow (left 115K) to fast (right 180K).

Although graphene has been extensively studied because of its unusual electronic structure and high electron mobility, the adsorption of metals on graphene is limited. With combined STM and DFT calculations we have shown that the metal-C interaction can vary dramatically with adsorbed metal[8]. By measuring the nucleated island densities (which relate to diffusion and adsorption energies) the behavior of metals is classified into two groups: Gd, Dy, Fe show high island densities and strong interaction, while Eu and Pb show low densities and weak interaction.

Future Work

Concerning the use of nanostructures as “tunable” substrates, the promising work carried out by the FWP to control metal nucleation as function of island height will be the basis to study gas reactivity as a function of island height. Additional evidence exists in recent literature that gas adsorption can be controlled by QSE. Ag and Mg films will be grown as flat islands of controllable height to study reactions that have very low yield on bulk surfaces: ethylene epoxidation on Ag and molecular hydrogen adsorption on Mg or Mg-rich compounds. Besides QSE different controllable open morphologies will be generated with different type of low coordination sites with reduced barriers, so adsorption is expected

to be enhanced. Already initial experiments show that oxygen adsorbed on Ag islands can accelerate the kinetics of height conversion from 2- stable islands to 3-layer islands. The Mg films will be used to study the adsorption of molecular hydrogen that is known to have zero sticking coefficient on Mg bulk crystals. This will be accomplished with open morphologies (wedding cakes or films on Si(111)with dislocations due to strain), with the adsorption of small amounts of other metals (Ti, Pd) that are expected to promote H₂ dissociation, or with QSE.

A second area where controllable metal nanostructures will be grown are nanowhiskers and nanowires (NWs). Although the problem has long history[9], still there is no understanding of the fundamental mass transport processes involved. Based on recent experiments [10] that show that high quality metal NWs can be grown on C coated Si(111) we plan to grow NWs using non-magnetic and magnetic metals. Our initial work will focus on Ag because it presents a simple model system and because the work relates to the Ag growth on Si(111) described earlier. Energetics of diffusion and nucleation of Ag on Ag are well established and scientists in this FWP are experts in Ag homoepitaxy. We will also investigate Fe and Co as prototype magnetic transition metals. Dy (hcp) and Eu (bcc) will serve as prototypical rare earth metals because they represent extremes in cohesive energies, and because they exhibit different growth behavior on graphene. The substrates used will be Si (with various forms of C) as in [10] and graphene on SiC.

Control of the microstructures of ferromagnetic materials could lead to high-performance (high coercivity/high Curie temperature) permanent magnets (e.g., spring magnets) using little or even zero rare earth metals. Moreover, ultra-high-density magnetic storage media would also require the ability to grow dense arrays of vertical NWs with diameters of a few tens of nanometers and lengths of several tens of micrometers. About the still unknown growth mechanism there are only indications that the growth is

controlled by the weak bonding of metal atoms to C, so that 3-d metal growth is promoted. This is a result consistent with the preliminary studies of the FWP of metal growth on graphene that show the metal adsorption energy is low[8]. Also, rapid diffusion of metal atoms along the faceted sides of the NW is necessary according to [10], but no quantitative analysis was done. C is important but the nature of the C nucleation sites is unknown. We will also study growth of Ag on the $\sqrt{3}\times\sqrt{3}$ [7] since the high diffusion of Ag on this phase should be conducive to NW growth. The extensive expertise of this FWP on Ag homoepitaxy will be used to learn how mass is transferred to build NWs, to identify the growth mechanism and the controlling barriers. We expect to determine the fundamental energetics relevant to growth and develop a model that predicts the formation of NWs with flux and temperature. We plan also to achieve positional control of the location where NW are grown by nanopatterning the initial substrate. A final goal is to be able to work on multi-component systems (when Ag and Au are codeposited) to form shell structures, if one of the metals diffuses out and away with controlled heating as in [10].

The third future project relates to metal growth on graphene. Graphene has been a key material of the last decade with tremendous interest by many communities, because of its unusual electronic structure and high electron mobility. Despite the numerous studies on clean graphene, the controlled study of metals deposited on graphene is limited. The key question is to determine conditions when the grown morphology is layer by layer growth (so metal contacts are optimal), but without the metal graphene interaction becoming so strong that its desirable properties degrade. Preliminary work[8] has been performed to determine the conditions to grow crystalline islands (Gd, Dy, Fe, Pb, Eu) and to extract the diffusion and adsorption barriers by comparing DFT calculations with STM results. This work will continue over a wider range of growth conditions (T, F, θ) to map out the various metal morphologies grown and whether standard nucleation analysis is applicable [11]. Metal deposition and annealing will be carried out in a controlled way from low to high temperature T, correlating film morphology changes and atom distribution at the graphene/SiC interface to possible changes of the graphene electronic structure measured with ARPES [12]. These experiments are important, first, to clarify the complex processes involved at higher T; and second, many device applications require operations at high temperatures, so the stability range will depend whether graphene electronic structure is affected or not. Additional information about the metal graphene interaction can be obtained at low coverage by direct comparison of STS spectra with the DFT calculated projected density of states (PDOS), to see deviations from the ideal PDOS of clean graphene (which will be another measure of the strength of the interaction).

- [1] K. Budde, E. Abram, V. Yeh, and M.C. Tringides, *Phys. Rev. Rap. Com. B* **61**, 10602 (2000).
- [2] V. Fournée, H. R. Sharma, M. Shimoda, A. P. Tsai, B. Unal, A. R. Ross, T. A. Lograsso, and P. A. Thiel, *Phys. Rev. Lett.* **95**, 155504 (2005).
- [3] B. Unal, V. Fournée, P.A. Thiel, and J.W. Evans, *Physical Review Letters* **102**, 196103 (2009).
- [4] Y. Han, B. Unal, D.P. Jing, F.L. Qin, C.J. Jenks, D.J. Liu, P.A. Thiel, and J.W. Evans, *Physical Review B*, **81**, 115462 (2010).
- [5] S.M. Binz, M. Hupalo, and M.C. Tringides, *Physical Review B* **78**, 193407 (2008).
- [6] K.L. Man, M.C. Tringides, M.M.T. Loy, and M.S. Altman, *Physical Review Letters* **101**, 226102 (2008).
- [7] A. Belianinov, Barış Ünal, K.-M. Ho, C.-Z. Wang, J. W. Evans, M. C. Tringides, and P. A. Thiel, *Jour. of Phys. Cond. Matt* **23**, 265002 (2011).
- [8] M. Hupalo, X. Liu, C. Z. Wang, W.-C. Lu, Y. X. Yao, K. M. Ho, and M. C. Tringides, *Advanced Materials* **23**, Issue 18, 2082–2087 (2011).
- [9] G.T. Galyon, *IEEE Trans. Electronics Packaging Manufacturing* **28**, 94 (2005).
- [10] G. Richter, K. Hillerich, D.S. Gianola, R. Mönig, O. Kraft, and C.A. Volkert, *Nano Lett.* **9**, 3048 (2009).
- [11] J.W. Evans, P.A. Thiel, and M.C. Bartelt, *Surf. Sci. Reports* **61**, 1 (2006).
- [12] C. Virojanadara, S. Watcharinyanon, A. A. Zakharov, and L. I. Johansson *Phys. Rev. B* **82**, 205402 (2010)

Publication list of the FWP in the period (2008-11)

- [1]. S.M. Binz, M. Hupalo, and M.C. Tringides, *Physical Review B*, **78**, 193407 (2008).
- [2]. F.-C. Chuang, C.-H. Hsu, C.Z. Wang, and K.M. Ho, *Physical Review B*, **78**, 245418 (2008).
- [3]. L. Huang, N. Lu, J.-A. Yan, M.-Y. Chou, C.Z. Wang, and K. M. Ho, “*Journal of Physical Chemistry C*, **112**, 15680 (2008).
- [4]. Z. Kuntova, M.C. Tringides, and Z. Chvoj, *Physical Review B*, **78**, 155431 (2008).
- [5]. K.L. Man, M.C. Tringides, M.M.T. Loy, and M.S. Altman *Physical Review Letters*, **101**, 226102 (2008).
- [6]. S.M. Binz, M. Hupalo, and M.C. Tringides *Journal of Applied Physics*, **105**, 094307 (2009).
- [7]. T.-L. Chan, C.Z. Wang, K.M. Ho, and J. Chelikowsky *Physical Review Letters*, **102**, 176101 (2009).
- [8]. M. Hupalo, E.H. Conrad, and M.C. Tringides, *Physical Review RC B*, **80**, 041401 (2009).
- [9]. M. Li, C.Z. Wang, J.W. Evans, M. Hupalo, M.C. Tringides, and K.M. Ho, *Physical Review B*, **79**, 113404 (2009).
- [10]. M.M. Ozer, C.Z. Wang, Z.Y. Zhang, and H.H. Weitering, “*Journal of Low Temperature Physics*, **157**, 221 (2009).
- [11]. M. Svec, V. Chab, and M.C. Tringides *Journal of Applied Physics*, **106**, 053501 (2009).
- [12]. B. Unal, V. Fournee, P.A. Thiel, and J.W. Evans, *Physical Review Letters*, **102**, 196103 (2009).
- [13]. A. Belianinov, B. Ünal, N. Liu, M. Jin, K.M. Ho, C.Z. Wang, M.C. Tringides, and P.A. Thiel, *Physical Review B*, **82**, 245413 (2010).
- [14]. Y. Han, B. Unal, D.P. Jing, F.L. Qin, C.J. Jenks, D.J. Liu, P.A. Thiel, and J.W. Evans,” *Physical Review B*, **81**, 115462 (2010).
- [15]. Z. Kuntova, M.C. Tringides, S.M. Binz, M. Hupalo, and Z. Chvoj *Surface Science*, **604**, 519 (2010).
- [16]. G.D. Lee, C.Z. Wang, E. Yoon, N.M. Hwang, and K.M. Ho *Physical Review B*, **81**, 195419 (2010).
- [17]. N. Liu, Y.-R. Li, N. Lu, Y.-X. Yao, X.-W. Fang, C.-Z. Wang, and K.-M. Ho *Journal of Physics D*, **43**, 275404 (2010).
- [18]. X.J. Liu, C.Z. Wang, M. Hupalo, Y.X. Yao, M.C. Tringides, W.C. Lu, and K.M. Ho *Physical Review B*, **82**, 245408 (2010).
- [19]. M.C. Tringides and M. Hupalo, *Journal of Physics: Condensed Matter*, **22**, 264002 (2010).
- [20]. B. Unal, A. Belianinov, P.A. Thiel, and M.C. Tringides *Physical Review B*, **81**, 085411 (2010).
- [21]. G.P. Zhang, M. Hupalo, M. Li, C.Z. Wang, J.W. Evans, M.C. Tringides, and K.M. Ho *Physical Review B*, **82**, 165414 (2010).
- [22]. A. Belianinov, B. Ünal, K.-M. Ho, C.-Z. Wang, J.W. Evans, M.C. Tringides, and P.A. Thiel *Journal of Physics: Condensed Matter*, **23**, 265002 (2011).
- [23]. Z. Chvoj, M. C. Tringides, and Z. Cromcova *Journal of Physics: Condensed Matter*, **23**, 215307 (2011).
- [24]. M. Hupalo, S. Binz, and M.C. Tringides *Journal of Physics-Condensed Matter*, **23**, 045005 (2011).
- [25]. M. Hupalo, X. Liu, C.Z. Wang, W.-C. Lu, Y.X. Yao, K.M. Ho, and M.C. Tringides *Advanced Materials*, **23**, 2082 (2011).
- [26]. X. Liu, C.Z. Wang, Y.X. Yao, W.C. Lu, M. Hupalo, M.C. Tringides, and K. M. Ho *Physical Review B*, **83**, 235411 (2011).
- [27]. M.C. Tringides, M. Hupalo, K.L. Man, M.M.T. Loy, and M.S. Altman *Nanophenomena at Surfaces: Fundamentals of Exotic Condensed Matter Properties*, Springer ed. M. Michailov (2011).
- [28]. M. Yakes and M. C. Tringides *Journal of Physical Chemistry B* 115 7096 (2011) invited paper for special issue dedicated to Prof. J.P. Toennies
- [29]. M.W. Gramlich, S.T. Hayden, Yiyao Chen, C. Kim, E.H. Conrad, M.C. Tringides, and P.F. Miceli *Physical Review B* (accepted).

A Synergistic Approach to the Development of New Hydrogen Storage Materials Part II: Nanostructured Materials

A. Paul Alivisatos, Jeffrey R. Long, Jeffrey J. Urban, and Alex Zettl
Materials Sciences Division, Lawrence Berkeley National Laboratory

The Berkeley Hydrogen Storage Program consists of a broad-based, multi-investigator effort for developing new types of hydrogen storage materials. In particular, fundamentally new materials with the potential for meeting the 2015 DOE target of a reversible uptake of 5.5% H₂ by mass are sought. Our approach has been to explore numerous possibilities for new materials, and narrow our focus as the research progresses. The synergy of many scientists in one location working toward a common goal is expected to accelerate our progress and lead to new ideas via cross-fertilization. One half of the program (new EERE proposal currently under review) involves development of light-weight microporous metal-organic frameworks with open metal coordination sites. The present proposal represents a renewal of the funding for the other half of the program, which focuses on the development of new nanostructured materials. Specific areas proposed for investigation include: the detailed spectroscopic investigation of the hydrogenation and dehydrogenation processes of individual nanocrystals, the synthesis and characterization of new nanostructured forms of boron nitride, synthesis and evaluation of hydrogen uptake in polymer-embedded magnesium nanocrystals, and the development of robust metal-organic frameworks suitable for templating the formation of metal nanocrystals. A hydrogen storage characterization facility containing one gravimetric and two volumetric high-pressure adsorption analyzers will be maintained in order to provide accurate and immediate feedback on the properties of the many new materials generated. Ultimately, this research is expected to yield fundamentally new materials that could lead to advances in enhancing the range of hydrogen fuel cell-powered vehicles.

Progress Report of the Previous Period

Single-Nanoparticle Studies. Chen and Kasemo's work on employing single particle optical methods for catalytic events has been extended. Using Au as a plasmonic probe, we have tracked hydrogen storage in Pd directly and indirectly at the single particle level. In the case of the indirect sensing experiment, a Pd dot is patterned in the near-field of an Au antenna with great precision. The more hydrogen is stored in the octahedral interstitial sites of Pd, the further Pd acquires the characteristics of a semi-metal. This change in the dielectric function of Pd is reflected in the change of the refractive index in the environment of the Au antenna, and gives rise to a red shift in its localized surface plasmon resonance (LSPR), as shown schematically in Figure 1. The LSPR of Pd is not a good reporter of the reaction, as it is weak and broad compared to Au, especially in the visible wavelengths where we did all our experiments.

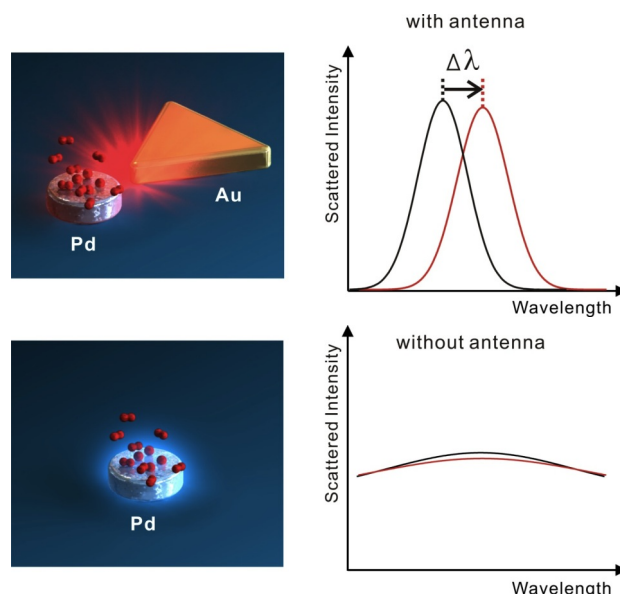


Figure 1. Schematic representation of antenna-enhanced single-particle hydrogen sensing. Hydrogen sensing using a resonant antenna-enhanced scheme (top): The palladium nanoparticle is placed at the nanofocus of a gold antenna, which scatters much more strongly than palladium itself. Hydrogen absorption on the palladium particle changes its complex dielectric function, which causes a resonance shift of the gold antenna that can be optically detected. Hydrogen sensing with a single palladium nanoparticle (bottom) alone causes a negligible change on hydrogen exposure. The palladium nanoparticle scatters weakly, showing an extremely damped and broad spectrum.

We have also made Au/Pd core/shell nanoparticles for the direct sensing experiment. While the mechanism for single particle sensing is the same as before, this time the LSPR shifts are larger as both materials are in contact. Interestingly, we are able to observe shape dependent hydrogen uptake trajectories. Most particles showed red and blue LSPR shifts with increasing and decreasing partial pressures of hydrogen respectively, as expected with PdH formation. However, 20% of the particles, mainly those with thicker Pd shells, show LSPR shifts that can only be explained by Au/Pd interdiffusion or metal silicide formation. This work shows that single particle techniques are vital in retaining information that would be lost in ensemble averaging.

Nanostructured Boron Nitride. We have found a method to prepare monolayer and multilayer suspended sheets of hexagonal boron nitride h-BN, using a combination of mechanical exfoliation and reactive ion etching. Ultrahigh-resolution transmission electron microscope imaging is employed to resolve the atoms, and intensity profiles for reconstructed phase images are used to identify the chemical nature boron or nitrogen of every atom throughout the sample. Reconstructed phase images are distinctly different for h-BN multilayers of even or odd number. Unusual triangular defects and zigzag and armchair edge reconstructions are uniquely identified and characterized. The general atomic structure and in particular the defect structure of BN is relevant to hydrogen adsorption.

We have performed a near-edge x-ray absorption fine-structure (NEXAFS) investigation of multi-walled boron nitride nanotubes (BNNTs). We show that the one-dimensionality of BNNTs is clearly evident in the B K edge spectrum, while the N K edge spectrum is similar to that of layered hexagonal BN (h-BN). We observe a sharp feature at the σ^* onset of the B K edge, which we ascribe to a core exciton state. We also report a comparison with spectra taken after an ammonia plasma treatment, showing that the B K edge becomes indistinguishable from that of h-BN, due to the breaking of the tubular order and the formation of small h-BN clusters.

Magnesium Nanocrystals. We have recently developed a synthetic route to producing a composite material which both enhances the hydridation kinetics via nanostructuring while also rendering the magnesium nanocrystal-containing composite air-stable (see Figure 3).⁶ This was achieved through encapsulation of 5 nm Mg nanocrystals in a polymer, poly (methyl methacrylate) (PMMA). PMMA acts as a gas-selective barrier, allowing H_2 gas in, while preventing water and oxygen access to the Mg nanocrystals. The gas barrier is critical, as magnesium metal quickly and exothermically forms oxides upon exposure to even minute quantities of air or water. The Mg nanocomposites we synthesized are highly air-stable, showing no trace oxide peaks in atomic resolution transmission electron microscope

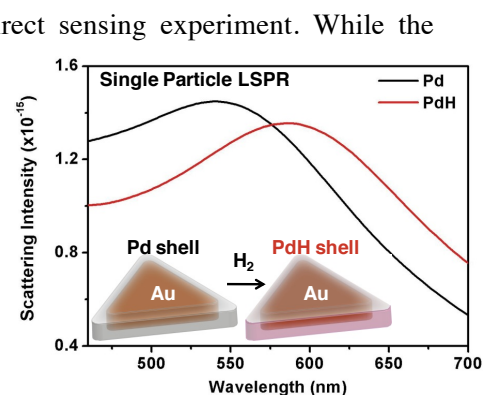


Figure 2. The change in the LSPR allows hydrogen absorption and desorption in Au/Pd core/shell nanocrystals to be monitored at the single particle level. Using colloiddally synthesized nanocrystals, we can investigate the effects of size, shape and facets exposed on the amount of hydrogen stored, and the kinetics involved.

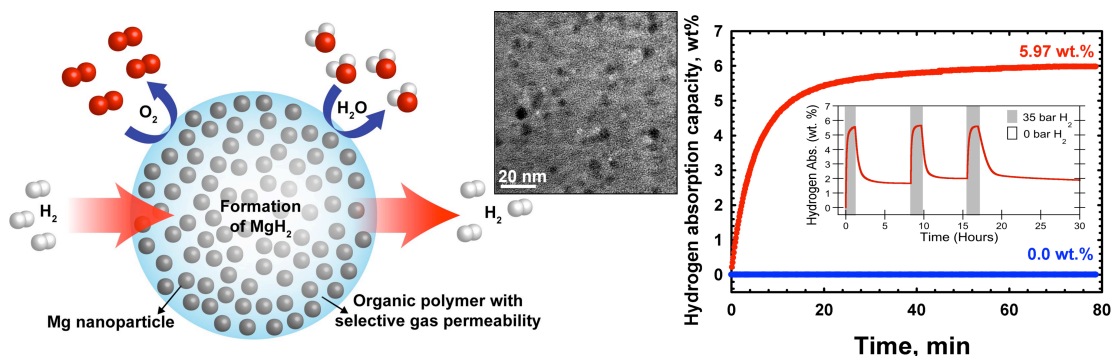


Figure 3. Left: Schematic describing our nanocomposites consisting of metallic Mg nanocrystals embedded in PMMA. Middle: TEM image of the Mg nanocomposites. Right: H_2 absorption capacity of Mg nanocomposites (red) and bulk Mg (blue) at 200 °C and 35 bar H_2 . Inset: Reversible H_2 absorption/desorption.

diffraction patterns after 2 weeks of air exposure. The composites have high H₂ storage capacity (5.97 wt. % Mg, ~4 wt. % in overall composite mass) at temperatures where bulk Mg does not absorb H₂ (200 °C), and demonstrate excellent reversibility of hydrogen sorption without substantial degradation. Moreover, these nanocomposites display enhanced kinetics over bulk magnesium, recording hydriding/dehydriding

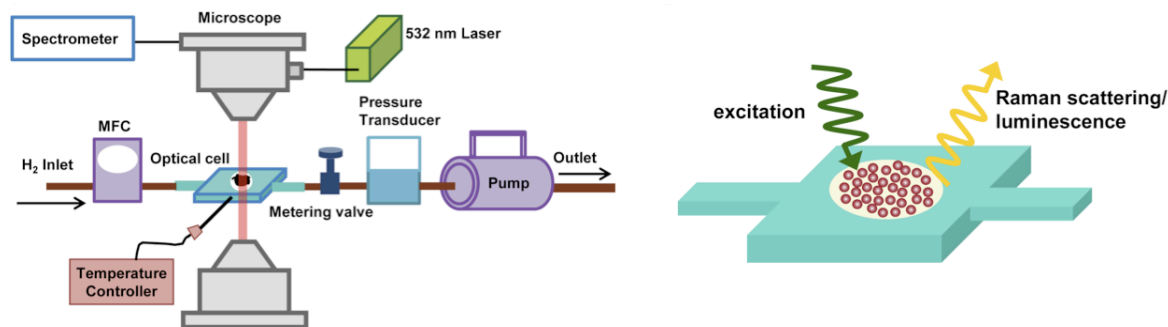


Figure 4. Left: Schematic representation of the *in situ* optical setup for hydriding and dehydriding. Right: A detailed view of the optical cell with metal nanoparticles loaded on the transparent quartz windows for optical excitation and subsequent Raman scattering or emission collection.

activation energies of 25/79 kJ/mol, significantly below the bulk magnesium value of 120-142 kJ/mol.

On the measurement side, we have recently engineered a unique gas-flow setup (see Figure 4) on a Raman microscope currently located in our laboratory. Samples are placed in a uniquely designed gas-tight optical cell with transparent sapphire windows to enable sample illumination. H₂ flow through the cell is controlled with a mass flow controller (MFC); pressure in the cell is manipulated with a metering valve and monitored with a pressure transducer. The optical cell is probed with a Raman microscope, excited with a pump laser, and coupled to a spectrometer for spectral information. Cartridge heaters are also built into the optical cell to controllably heat the samples, whose temperature is measured at the sample for accurate readout. This system will enable us to directly monitor, modulate and measure the dynamics of hydriding and dehydriding *in situ* by directly measuring the changes in electronic (luminescence) and vibrational (Raman) excitations when hydrogen interacts with metal nanoparticles.

Nanocrystals in Metal-Organic Frameworks. A variety of new composite materials in which narrow-dispersity Pd nanocrystals were integrated with high-surface area metal-organic frameworks were prepared and characterized. Unfortunately, all attempts to observe enhanced hydrogen storage via spill-over in the resulting composites failed. Attempts to reproduce spill-over results previously reported by other researchers also met with failure. It should be noted, however, that there are many unknown variables in the manner by which the prior composite materials reported to display this effect were prepared. Thus, it is unclear if we were ever actually able to recreate precisely the materials that were measured previously.

We have also sought to create highly robust metal-organic frameworks capable of serving as templates for the preparation of nanocrystalline phases of hydrogen storage materials such as magnesium or aluminum. Here, it is necessary that the framework host be able to survive repeated cycling at high temperatures, while also being stable upon exposure to strong reductants like magnesium. Along these lines, we have sought to create new metal-organic frameworks built up of strong metal-ligand bonds, which should impart exceptional thermal and chemical stability.

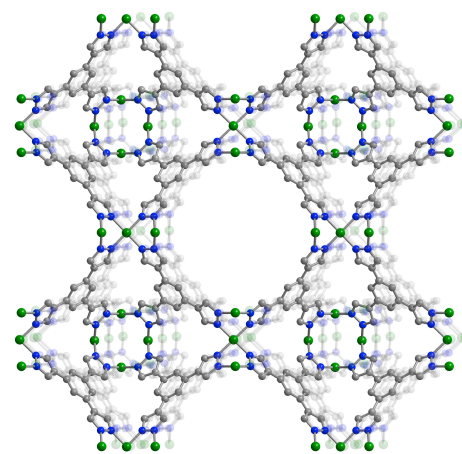


Figure 5. Structure of the new microporous pyrazolate-bridged metal-organic framework Ni₂(BTP)₂ (**1**). Green, blue and gray spheres represent Ni, N, and C atoms respectively; H atoms are not depicted for clarity. Strong Ni^{II}-pyrazolate bonds impart the framework with exceptional thermal and chemical stability. The pores within the material are approximately 1 nm in diameter.

Reactions between the tritopic pyrazole-based ligand 1,3,5-tris(1*H*-pyrazol-4-yl)benzene (H₃BTP) and transition metal acetate salts in DMF were found to afford microporous pyrazolate-bridged metal-organic frameworks of the type M₃(BTP)₂·*x*solvent (M = Ni (**1**), Cu, (**2**), Zn (**3**), Co (**4**)).⁷ *Ab-initio* X-ray powder diffraction methods were employed in determining the crystal structures of these compounds, revealing **1** and **2** to exhibit an expanded sodalite-like framework with accessible metal cation sites (see Figure 5), while **3** and **4** possess tetragonal frameworks with hydrophobic surfaces and narrower channel diameters. Compounds **1-4** can be desolvated without loss of crystallinity by heating under dynamic vacuum, giving rise to microporous solids with BET surface areas of 1650, 1860, 930 and 1027 m²/g, respectively. Thermogravimetric analyses and powder X-ray diffraction measurements demonstrated the exceptional thermal and chemical stability of these frameworks. In particular, **3** is stable to heating in air up to at least 510 °C, while **1** is stable to heating in air to 430 °C, as well as to treatment with boiling aqueous solutions of pH 2 to 14 for two weeks. Unexpectedly, **2** and **3** are converted into new crystalline metal-organic frameworks upon heating in boiling water. With the combination of stability under extreme conditions and 1-nm pore sizes, it is anticipated that **1** may open the way to testing metal-organic frameworks as templates for the formation of nanocrystalline magnesium.

(Selected) List of Publications from the Previous Period

- (1) “Optimization of Metal Dispersion and Hydrogen Adsorption Strength in Doped Graphitic Materials for Hydrogen Storage” Kim, G.; Jhi, S.-H.; Park, N.; Louie, S. G.; Cohen, M. L. *Phys. Rev. B* **2008**, *78*, 085408. [DoE Hydrogen support: All of the work.]
- (2) “Hydrogen Storage in Metal-Organic Frameworks” Murray, L. J.; Dinca, M.; Long, J. R. *Chem. Soc. Rev.* **2009**, *38*, 1294-1314. [Support for writing this review article was split evenly between DoE, the US Defense Logistics Agency, and General Motors Corporation.]
- (3) “Size-Controlled Synthesis and Optical Properties of Monodisperse Colloidal Magnesium Oxide Nanocrystals” Moon, H. R.; Urban, J. J.; Milliron, D. J. *Angew. Chem., Int. Ed.* **2009**, *48*, 6278-6281.
- (4) “One-Step, Gram-Scale Synthesis of Highly Fluorescent, Spectrally Responsive, Porous Carbogenic Nanoparticles” Moon, H. R.; Jeon, K.-J.; Urban, J. J., submitted. [DoE Hydrogen support: All of the work.]
- (5) “The Physics of Boron Nitride Nanotubes” Cohen, M. L.; Zettl, A. *Physics Today* **2010**, *63* 34-38. [DOE Hydrogen support: Hydrogen adsorption studies of defected BN. DOE sp2: synthesis and general characterization of BNNTs]
- (6) “Hydrogen Storage Properties and Neutron Scattering Studies of Mg₂(dobdc)—A Metal-Organic Framework with Open Mg²⁺ Adsorption Sites” Sumida, K.; Brown, C. M.; Herm, Z. R.; Chavan, S.; Bordiga, S.; Long, J. R. *Chem. Commun.* **2011**, *47*, 1157-1159. [DoE Hydrogen support: All of the work performed in Berkeley.]
- (7) “Air-Stable Magnesium Nanocomposites Provide Rapid and High-Capacity Hydrogen Storage without Using Heavy-Metal Catalysts” Jeon, K.-J.; Moon, H. R.; Ruminski, A. M.; Jiang, B.; Kisielowski, C.; Urban, J. J. *Nature Mater.* **2011**, *10*, 286-290. [DoE Hydrogen support: All of the work.]
- (8) “Neutron Scattering and Spectroscopic Studies of Hydrogen Adsorption in Cr₃(BTC)₂—A Metal-Organic Framework with Exposed Cr²⁺ Sites” Sumida, K.; Her, J.-H.; Dincă, M.; Murray, L. J.; Schloss, J.; Pierce, C.; Thompson, B.; FitzGerald, S. A.; Brown, C. M.; Long, J. R. *J. Phys. Chem. C* **2011**, *115*, 8414-8421. [DoE Hydrogen support: All of the work performed in Berkeley.]
- (9) “High Thermal and Chemical Stability in Pyrazolate-Bridged Metal-Organic Frameworks with Exposed Metal Sites” Colombo, V.; Galli, S.; Choi, H. J.; Han, G. D.; Maspero, A.; Palmisano, G.; Masciocchi, N.; Long, J. R. *Chem. Sci.* **2011**, *2*, 1311-1319. [DoE Hydrogen support: All of the work performed in Berkeley.]
- (10) “Nanoantenna-Enhanced Gas Sensing in a Single Tailored Nanofocus” Liu, N.; Tang, M. L.; Hentschel, M.; Giessen, H.; Alivisatos, A. P. *Nature Mater.* **2011**, in press.

Phase Diagram for Iron-Chalcogenide Superconducting Films

PI - Barrett O. Wells
Department of Physics
University of Connecticut
Storrs, CT 06269-3046

Co-PI – Joseph I. Budnick
Department of Physics
University of Connecticut
Storrs, CT 06269-3046

email: wells@phys.uconn.edu

budnick@phys.uconn.edu

Research Scope

Our DOE funded program currently has two main projects: a study of large scale phase separation in super-oxygenated $\text{La}_{2-x}\text{Sr}_x\text{CuO}_{4+y}$ and an investigation of films of Fe-chalcogenide superconductors with an emphasis on properties uniquely associated with film structures. Our group synthesizes interesting materials and we have substantial experience exploring issues connected to intercalation of oxygen into samples. We explore our materials using a variety of techniques as appropriate to the physics problem at hand, mostly pursued at DOE laboratories. Techniques that have been very important for our work include ARPES, neutron scattering, X-ray absorption, and muon Spin Rotation. We are currently moving to emphasize a program to exploit our discoveries in films of Fe-based superconductors, and thus this presentation will thus focus on the discovery of a new superconductor, FeTeO_x films.

Recent Progress – Superconductivity in FeTeO_x Films.

Bulk FeTe is antiferromagnetic and non-superconducting and considered a parent compound for the Fe-chalcogenide family of superconductors. Chemical pressure via isoelectronic substitution of Se or S onto Te sites produces a superconductor [1-3]. However, no form of charge doping or physical pressure on bulk FeTe has been shown to produce a superconductor.

We have grown magnetic, nonsuperconducting FeTe films epitaxially on MgO and STO substrates using pulsed laser deposition (PLD). Further, we recently found [4] that superconductivity can be induced post growth by either a short, low temperature (100°C) annealing in oxygen or a longer term exposure to oxygen in the ambient atmosphere at room temperature. A superconducting transition with a onset temperature of 13 K has been observed. In addition, all of the resistivity vs temperature curves show a broad peak around 65 K for both superconducting and non-superconducting samples. In the bulk, this peak in the resistivity is associated with a concurrent antiferromagnetic (AFM) and structural transition [5-7]. As shown below, our films also appear to have this structural transition, but so far the magnetic state is unknown.

A series of annealing experiments show that the oxygen incorporation process is reversible: the superconducting state can be removed by driving oxygen out through a vacuum anneal and then restored again through another oxygen anneal. The resistivity profiles of these films and the reversible nature of the oxygen absorption is shown in Fig 1a. Fig 1b shows both the shielding (zero field cooled) and Meissner (field cooled) magnetic transition for a superconducting FeTeO_x film. These are large signals with particular notice that the Meissner signal is almost as large as the shielding, rarely the case in cuprate superconductors such as $\text{La}_{2-x}\text{Sr}_x\text{CuO}_4$. The ease of cycling the oxygen content suggests one might be able to perform well controlled experiments on the changes that lead to superconductivity without changing the sample studied.

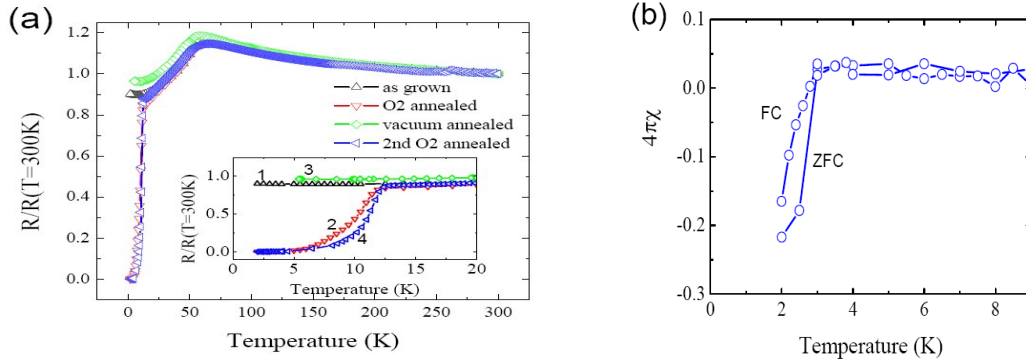


Fig 1. a) Resistivity of an FeTe film after different annealing steps demonstrating the reversibility of the superconducting state with oxygen uptake/expulsion. b) the shielding and Meissner signal from a superconducting film of FeTeO_x .

The process of incorporating oxygen appears to induce only a small change in the structure. Fig. 2 shows a broad, XRD scan of one film in its as-grown non-superconducting state and then in the O_2 annealed superconducting state. There is little change. Higher resolution studies at beamline X22C at the NLS at Brookhaven revealed that there was a small contraction in-plane and a small expansion along the c-axis. Our own DFT calculations indicate that a likely low energy site for excess oxygen is just below the Fe plane, at a symmetry equivalent site to that occupied by the Te atoms. With O in this site, the DFT confirms that FeTeO_x will remain in the tetragonal phase with only a small change in lattice constant.

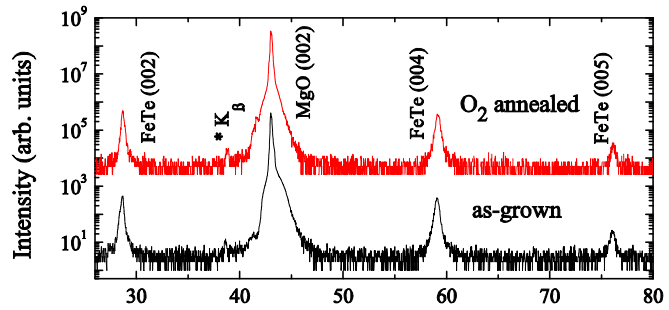


FIG. 2. X-ray diffraction profiles in the (00L) direction of the as-grown and oxygen annealed FeTe films taken at room temperature.

Both neutron and x-ray diffraction studies have revealed a sudden change in the c-axis associated with a structural transition at both 65 K and 12 K. The transition at 65 K is associated with the maximum in the resistivity and presumably the same structural phase transition seen in the bulk. The lower temperature transition is not seen in bulk FeTe but occurs at the superconducting T_C . A complete study of this lowest temperature phase has been hampered by the fact that exposure to a synchrotron x-ray beam alters the sample to eliminate the transition, perhaps due to an x-ray assisted loss of oxygen, but it may point to an alternative cause for superconductivity.

We performed X-ray absorption spectroscopy and X-ray photoemission measurements to understand the changing valence states induced by oxygen incorporation. We found a surprisingly large change in the Fe valence state, from metallic like Fe^0 in the as-grown film to predominantly Fe^{3+} in the superconducting films. Fig. 3 shows a series of XAS measurements taken at different stages of oxidation showing a progression from $\text{Fe}^0/\text{Fe}^{2+}$ in the fresher films to a spectrum reminiscent of Fe^{3+} in the superconductor. Our results on the Fe valence states for the as grown FeTe films are a close match to other XAS results on Fe arsenide and Fe chalcogenide materials, both parent compounds and superconductors, where the Fe L edge was reported to be metallic-like [8,9,10]. However, the spectra we measure for the superconducting films are substantially different from any reports in related compounds. The result indicates that FeTeO_x likely falls into

the category of a heavily hole-doped superconductor, in analogy to the heavily electron doped nature of superconductors of the type $A\text{Fe}_{1.7}\text{Se}_2$ that has recently been reported [11-12].

In summary, by introducing excess oxygen at low temperature, superconductivity was induced in the FeTe films. When the films are superconducting, XRD indicates only a small structural change and XAS indicates that the majority of the Fe has a nominal valence of 3+. A structural transition associated with the superconducting transition has been observed. This method for creating a superconductor is quite different from the better known procedure of substituting isovalent Se or S for Te. However, the two doping procedures can be combined, with the correct combination of both necessary to produce a superconductor. This ability to co-dope with both charge and isovalent dopants makes the Fe chalcogenide system a good candidate for understanding in detail what parameters control whether magnetism or superconductivity becomes the ground state, and thus learn more about the interplay of these phenomena.

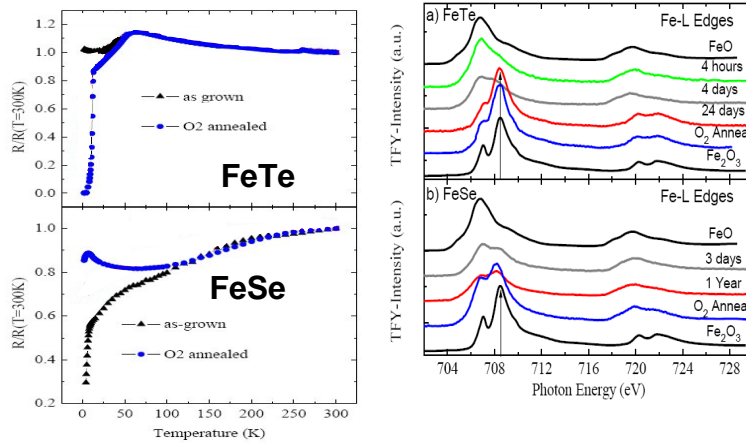


Figure 3. Left Panel: Resistance vs. temperature for FeTe and FeTeO_x (top) and FeSe and FeSeO_x (bottom). Right Panel: XAS-TFY spectra for FeTeO_x (top) and FeSeO_x (bottom) at successive stages of exposure and O₂ annealing. The top spectrum in both panels is an FeO reference and the bottom spectrum is an Fe₂O₃ reference.

Future Plans

We are moving in two main directions to explore the discovery of superconductivity in FeTeO_x films. One is to determine the full phase diagram of the FeTe_{1-y}Se_yO_x system and more thoroughly characterize the materials we have made. Se substitution for Te is an isovalent substitution that primarily modifies the lattice whereas oxygen intercalation is a charge doping process that makes little change to the lattice, and we have shown that the two can be combined. Codoping with various amounts of both dopants should allow us to develop insights into the underlying control parameters for turning an antiferromagnetic parent compound into a superconductor. Further, we are developing better measurements of oxygen content and position. Measuring the oxygen content is made easier by using a non-oxide substrate and we are now growing on CaF₂. We are developing EXAFS experiments to locate the location of the doped oxygen.

A second challenge is to proceed with more sophisticated, microscopic experimental probes. We have some evidence that superconducting FeTeO_x may show coexistence of magnetism and superconductivity, most notably the surprising lack of change in the normal state resistivity versus temperature curves between the parent and superconducting samples. Measuring antiferromagnetism in films can be very difficult. We have begun a collaboration with Ercan Alp of Argonne National Laboratory to use Mossbauer spectroscopy to explore magnetism in our films. Mossbauer gives a dramatic change in signal between magnetic and nonmagnetic samples of FeTe_{1-y}Se_y, [13] and has also been shown to give good signals from film samples. Related, more modern synchrotron techniques such as time-resolved, inelastic nuclear resonant x-ray scattering can give phonon density of states of the films distinct from substrate interference [14].

Ultimately, superconductivity is an electronic phenomenon and understanding the electronic structure is critical. Preliminary experiments have shown that cleaved films of FeTeO_x are suitable samples for ARPES investigations, giving data with distinct peaks in energy

dispersion curves and a well defined hole Fermi surface near the zone center. We expect that FeTeO_x may be a heavily hole doped superconductor in analogy with the heavily electron doped AFe_{1.7}Se₂-type compounds that have shown to be doped such that the central hole pockets have been emptied and only the zone edge electron pockets survive [11-12].

In general we are interested in exploring collaborations conducting experiments that give basic microscopic information for film samples.

Publications since 2008

- D. Telesca, Y. Nie, J. I. Budnick, B. O. Wells, and B. Sinkovic, "Impact of Valence States on Superconductivity of Oxygen Incorporated Iron Telluride and Iron Selenide Films" submitted to *Phys. Rev. B* and *arXiv:1102.2155*
- Y. F. Nie, D. Telesca, J. I. Budnick, B. Sinkovic, R. Ramprasad and B. O. Wells, "Superconductivity and Properties of FeTeO_x Films", *J Phys Chem Solids* **72**, 426 (2011)
- L. Udby, P.K. Willendrup, E. Knudsen, Ch. Niedermayer, U. Filges, N.B. Christensen, E. Farhi, B.O. Wells, K. Lefmann, "Analysing neutron scattering data using McStas virtual experiments" *Nuclear Instruments and Methods in Physics Research Section A: Accelerators, Spectrometers, Detectors and Associated Equipment*, **634**, S138-S143 (2011).
- Y.F. Nie, D. Telesca, J. I. Budnick, B. Sinkovic and B.O. Wells, "Superconductivity induced in iron telluride films by low temperature oxygen incorporation" *Phys. Rev. B* **82**, 020508(R) (2010)
- Y. F. Nie, E. Brahim, J. I. Budnick, W. A. Hines, M. Jain, and B. O. Wells, "Suppression of superconductivity in FeSe films under tensile strain" *Appl. Phys. Lett.* **94**, 242505 (2009)
- L. Udby, N.H. Andersen, F.C. Chou, N.B. Christensen, S.B. Emery, K. Lefmann, J.W. Lynn, H.E. Mohottala, Ch. Niedermayer, B.O. Wells, "Magnetic ordering in electronically phase separated Sr/O co-doped La_{2-x}Sr_xCuO_{4+y}" *Phys. Rev. B* **80**, 014505 (2009)
- S.B. Emery and B.O. Wells, "Properties of Phase-Separated, Super-Oxygenated La_{2-x}Sr_xCuO_{4+y}" *J Supercond Nov Magn*, **22**, 33 (2009)
- Hashini E. Mohottala, B. O. Wells, J. I. Budnick, W. A. Hines, Ch. Niedermayer, and F. C. Chou, "Flux pinning and phase separation in oxygen rich La_{2-x}Sr_xCuO_{4+y} system" *Phys. Rev. B* **78**, 064504 (2008).
- C. K. Xie, J. I. Budnick, W. A. Hines, B. O. Wells, Feizhou He, and A. R. Moodenbaugh, "Direct evidence for the suppression of charge stripes in epitaxial La_{1.67}Sr_{0.33}NiO₄ films" *Phys. Rev. B* **77**, 201403(R) (2008).

References:

- [1] Y. Mizuguchi, *et al.*, *Appl. Phys. Lett.* **94**, 012503 (2009)
- [2] F.-C. Hsu, *et al.*, *Proc. Natl. Acad. Sci. U.S.A.* **105**, 14262 (2008).
- [3] M. H. Fang, *et al.*, *Phys. Rev. B* **78**, 224503 (2008)
- [4] Y. Nie, D. Telesca, J.I. Budnick, B. Sinkovic, B.O. Wells, *Phys. Rev. B* **82**, 020508(R) (2010)
- [5] M. J. Wang, *et al.*, *Phys. Rev. Lett.* **103**, 117002 (2009)
- [6] R. Hu, *et al.*, *Phys. Rev. B* **80**, 214514 (2009)
- [7] G. F. Chen, *et al.*, *Phys. Rev. B* **79**, 140509(R) (2009)
- [8] W. L. Yang, *et al.*, *Phys. Rev. B* **80**, 014508 (2009)
- [9] C. Parks Cheney *et al.*, *Phys Rev B* **81**, 104518 (2010)
- [10] Saini *et al.*, *Phys Rev B* **83**, 052502 (2010)
- [11] Qian *et al.*, *Phys Rev. Lett.* **106**, 187001 (2011)
- [12] D. Mou, *et al.*, *Phys. Rev. Lett.* **106**, 107001 (2011)
- [13] Y. Mizuguchi *et al.*, *Physica C* **470**, 5338 (2010)
- [14] E. E. Alp *et al.*, *Nuclear Instruments and Methods in Physics Research B* **97**, 526 (1995)

Author Index

Author Index

Abbamonte, Peter	139	El-Azab, Anter	225
Adams, Philip W.	183	Engel, Lloyd W.	77
Alberi, Kirstin	239	Ereno, John L.	85
Alivisatos, A. Paul	287	Eres, Gyula	225
Andrei, Eva Y.	187	Fadley, Charles S.	159
Ashoori, Raymond	73	Feldman, L. C.	279
Bader, Sam	21	Finkelstein, Gleb	105
Balakirev, Fedor F.	216	Fischer, Peter J.	159
Balicas, Luis	69	Fluegel, Brian	239
Bawendi, Mounji G.	191	Fradkin, Eduardo H.	139
Bell, C.	13	Goldman, Allen M.	147
Bell, David C.	211	Graham, Adam	211
Betts, Jonathan	216	Gray, Kenneth E.	220
Bezryadin, Alexey	139	Greene, Laura H.	139
Bhandari, Sagar	211	Guyot-Sionnest, Philippe	96
Bhattacharya, Anand	164	Hadjipanayis, George	37
Bird, Jonathan	195	Haglund, Jr., Richard F.	212
Birgeneau, R. J.	109	Harrison, Neil	216
Biswas, Rana	255	Hastings, Todd	172
Boatner, Lynn A.	9	Hellman, Frances	159
Bourret-Courchesne, E.	109	Hikita, Y.	13
Budakian, Raffi	139	Hla, Saw-Wai	151
Bud'ko, S.	1	Hmelo, A. B.	279
Budnick, Joseph I.	291	Ho, K. M.	283
Butov, Leonid	89	Ho, Kai-Ming	255
Canfield, P.	1	Homes, Christopher C.	113
Cao, Gang	172	Hughes, Taylor	139
Carr, G. L.	155	Hupalo, M.	283
Christen, Hans M.	225	Hwang, H. Y.	13
Christen, David K.	9	Jaime, Marcelo	216
Chung, B. W.	275	Jarillo-Herrero, Pablo	127
Civale, Leonardo	65	Jiang, Zhigang	259
Clem, J.	1	Johnson, Peter D.	49, 113
Coffey, Dermot	203	Johnston, D.	1
Cooper, S. Lance	139	Johnston-Halperin, Ezekiel	25
Crabtree, George W.	57	Kaminski, A.	1
Crespi, Vincent	175	Kastner, Marc A.	93
Crooker, Scott	216	Kim, B. J.	220
Csathy, Gabor	199	Kim, Philip	41
Davidović, Dragomir	29	Kogan, V.	1
Davis, J. C. (Séamus)	123	Kono, Junichiro	101
De Long, L. E.	172	Kortright, Jeffrey B.	159
DeMarco, Michael	203	Koshelev, Alexei E.	57
Dessau, Dan	117	Kravchenko, Sergey V.	252
Ding, Hong	130	Kunchur, Milind N.	224
Drew, H. Dennis	134	Kwok, Wai-Kwong	57
Du, Rui-Rui	207	Lanzara, A.	109
Eckstein, James N.	139	Larson, Ben C.	225

Author Index

Lee, D. H.	109	Schuller, Ivan K.	17
Lee, Ho Nyung	225	Sefat, Athena S.	61
Lee, Minhyea	229	Sellmyer, David J.	37
Leggett, Anthony J.	139	Seo, S. S.	172
Lemberger, Thomas R.	120	Shinar, Joseph	255
Li, Qi	231	Singleton, John	216
Lilly, Michael P.	85	Skomski, Ralph	37
Liu, Ying	143	Smirnov, Dmitry	259
Long, Jeffrey R.	287	Smith, Arthur R.	33
Luepke, Gunter	168	Smith, Kevin E.	264
Lyo, Ken S. K.	85	Snoke, David	267
Lyuksyutov, Igor F.	235	Soukoulis, Costas	255
Madhavan, Vidya	130	Stanton, C. J.	155
Mandrus, David G.	9	Steigerwald, A.	279
Manfra, Michael	199	Stohr, J.	13
Mani, Ramesh G.	45	Tanatar, M.	1
Maple, M. Brian	5	Tanner, D. B.	155
Mascarenhas, A.	239	Thiel, P. A.	283
Mason, Nadya	139	Thomas, John E.	271
McDonald, Ross	216	Tischler, Jon Z.	225
Mialitsin, Aleksej	239	Tobin, J. G.	275
Migliori, Albert	216	Tolk, N.	279
Millis, Andy.	49	Tracy, Lisa A.	85
Mitchell, John F.	220	Tringides, M. C.	283
Mohideen, Umar	243	Urban, Jeffrey J.	287
Natelson, Douglas	244	Valla, Tonica	113
Naugle, D. G.	235	Van Harlingen, Dale J.	139
Novotny, Lukas	53	Varga, K.	279
Orenstein, J.	109	Vishveshwara, S.	139
Osgood, Richard	49	Vishwanath, A.	109
Padilla, Willie	130	Vlasko-Vlasov, Vitalii	57
Pan, Wei	85	Waddill, G. D.	275
Pechan, Michael	248	Wang, C. Z.	283
Prasankumar, Rohit P.	85	Wang, George T.	85
Prozorov, R.	1	Wang, Wei Li	211
Punnoose, Alex	252	Wang, Ziqiang	130
Ramesh, R.	109	Ward, T. Zac	225
Reitze, D. H.	155	Wells, Barrett O.	291
Rouleau, Christopher M.	225	Welp, Ulrich	57
Sales, Brian C.	9	Westervelt, Robert	211
Samarth, Nitin	175	Wu, W.	235
Sarachik, Myriam P.	252	Yang, Fengyuan	25
Saracila, Gabriel	224	Yu, S. W.	275
Schiffer, Peter	175	Zettl, Alex	100, 287
Schmalian, J.	1	Zudov, Michael	81

Participant List

Last Name	First Name	Organization	E-mail Address
Abbamonte	Peter	University of Illinois, Urbana-Champaign	abbamonte@mrl.uiuc.edu
Adams	Phil	Louisiana State University	adams@phys.lsu.edu
Andrei	Eva	Rutgers University	eandrei@physics.rutgers.edu
Ashoori	Ray	Massachusetts Institute of Technology	ashoori@mit.edu
Bader	Sam	Argonne National Laboratory	bader@anl.gov
Balicas	Luis	National High Magnetic Field Laboratory	balicas@magnet.fsu.edu
Bhattacharya	Anand	Argonne National Laboratory	anand@anl.gov
Bird	Jon	University at Buffalo	jbird@buffalo.edu
Butov	Leonid	University of California, San Diego	lvbutov@physics.ucsd.edu
Canfield	Paul	Ames Laboratory / Iowa State University	canfield@ameslab.gov
Civale	Leonardo	Los Alamos National Laboratory	lcivale@lanl.gov
Coffey	Dermot	Buffalo State College	coffeyd@buffalostate.edu
Cooper	Lance	University of Illinois	slcooper@illinois.edu
Crockett	Teresa	DOE, Basic Energy Sciences	gcsathy@purdue.edu
Csathy	Gabor	Purdue University	teresa.crockett@science.doe.gov
Cui	Jian	Massachusetts Institute of Technology	gunqwee@mit.edu
Davenport	James	DOE, Basic Energy Sciences	james.davenport@science.doe.gov
Davidovic	Drago	Georgia Institute of Technology	dragomir.davidovic@physics.gatech.edu
Davis	Séamus	Cornell University / BNL	jcdavis@ccmr.cornell.edu
De Long	Lance	University of Kentucky	delong@pa.uky.edu
DeMarco	Mike	Buffalo State College	demarcmj@buffalostate.edu
Dessau	Dan	University of Colorado	Dessau@Colorado.edu
Drew	Dennis	CNAM, University of Maryland	hdrew@physics.umd.edu
Du	Rui-Rui	Rice University	rrd@rice.edu
Engel	Lloyd	NHMFL / Florida State University	engel@magnet.fsu.edu
Fadley	Chuck	University of California, Davis / LBNL	fadley@lbl.gov
Feldman	Leonardo	Rutgers University	l.c.feldman@rutgers.edu
Fiechtner	Gregory	DOE, Basic Energy Sciences	gregory.fiechtner@science.doe.gov
Finkelstein	Gleb	Duke University	gleb@phy.duke.edu
Fischer	Peter	Lawrence Berkeley National Laboratory	PJFischer@lbl.gov
Floro	Jerry	University of Virginia	Floro@Virginia.edu
Gersten	Bonnie	DOE, Basic Energy Sciences	Bonnie.gersten@science.doe.gov
Goldman	Allen	University of Minnesota	goldman@physics.umn.edu
Graham	Adam	Harvard University	agraham@cns.fas.harvard.edu
Guyot-Sionnest	Philippe	University of Chicago	pgs@uchicago.edu
Hadjipanayis	George	University of Delaware	hadji@udel.edu
Haglund	Richard	Vanderbilt University	richard.haglund@vanderbilt.edu
Harrison	Neil	Los Alamos National Laboratory	nharrison@lanl.gov
Hellman	Frances	University of California, Berkeley / LBNL	fhellman@berkeley.edu
Hla	Saw	Ohio University	hla@ohio.edu
Homes	Christopher	Brookhaven National Laboratory	homes@bnl.gov
Horwitz	Jim	DOE, Basic Energy Sciences	james.horwitz@science.doe.gov
Hwang	Harold	Stanford University / SLAC	hyhwang@stanford.edu
Jarillo-Herrero	Pablo	Massachusetts Institute of Technology	pjarillo@mit.edu
Jiang	Hongxing	Texas Tech University	hx.jiang@ttu.edu
Jiang	Zhigang	Georgia Institute of Technology	zhigang.jiang@physics.gatech.edu
Johnston-Halperin	Zeke	The Ohio State University	ejh@mps.ohio-state.edu

Last Name	First Name	Organization	E-mail Address
Kastner	Marc	Massachusetts Institute of Technology	mkastner@mit.edu
Kerch	Helen	DOE, Basic Energy Sciences	helen.kerch@science.doe.gov
Kim	B. J.	Argonne National Laboratory	bjkim@anl.gov
Kim	Philip	Columbia University	pk2015@columbia.edu
Kono	Jun	Rice University	kono@rice.edu
Kortright	Jeff	Lawrence Berkeley National Laboratory	jbkortright@lbl.gov
Koshelev	Alexei	Argonne National Laboratory	koshelev@anl.gov
Kravchenko	Sergey	Northeastern University	s.kravchenko@neu.edu
Kunchar	Milind	University of South Carolina	kunchur@sc.edu
Kwok	Wai-K.	Argonne National Laboratory	wkwok@anl.gov
Lee	Ho-Nyung	Oak Ridge National Laboratory	hnlee@ornl.gov
Lee	Minhyea	University of Colorado, Boulder	minhyea.lee@colorado.edu
Lemberger	Tom	The Ohio State University	trl@physics.osu.edu
Levy	Jeremy	University of Pittsburgh	jlevy@pitt.edu
Li	Qi	Pennsylvania State University	qil1@psu.edu
Lin	Jingyu	Texas Tech University	jingyu.lin@ttu.edu
Liu	Ying	Pennsylvania State University	liu@phys.psu.edu
Luepke	Gunter	College of William and Mary	Luepke@wm.edu
Lyuksyutov	Igor	Texas A&M University	lyuksyutov@physics.tamu.edu
Madhavan	Vidya	Boston College	madhavan@bc.edu
Mailhiot	Christian	Lawrence Livermore National Laboratory	mailhiot1@llnl.gov
Manfra	Mike	Purdue University	mmanfra@purdue.edu
Mani	Ramesh	Georgia State University	rmani@gsu.edu
Maple	Brian	University of California, San Diego	mbmaple@ucsd.edu
Mascarenhas	Angelo	National Renewable Energy Laboratory	angelo.mascarenhas@nrel.gov
Mason	Nadya	University of Illinois at Urbana-Champaign	nadya@illinois.edu
Mebrahtu	Henok	Duke University	htm@duke.edu
Mentzel	Tamar	Massachusetts Institute of Technology	tamarm@mit.edu
Mohideen	Umar	University of California, Riverside	umar.mohideen@ucr.edu
Natelson	Doug	Rice University	natelson@rice.edu
Novotny	Lukas	University of Rochester	lukas.novotny@rochester.edu
Orenstein	Joe	University of California, Berkeley / LBNL	jworenstein@lbl.gov
Osgood	Rick	Columbia University	osgood@columbia.edu
Pan	Wei	Sandia National Laboratories, New Mexico	wpan@sandia.gov
Pechan	Mick	Miami University of Ohio	pechanmj@muohio.edu
Ramesh	Ramamoorthy	DOE, Energy Efficiency and Renewable Energy	ramamoorthy.ramesh@ee.doe.gov
Ronning	Filip	Los Alamos National Laboratory	fronning@lanl.gov
Sales	Brian	Oak Ridge National Laboratory	salesbc@ornl.gov
Sarachik	Myriam	City College of New York, CUNY	sarachik@sci.ccny.cuny.edu
Schiffer	Peter	Pennsylvania State University	pes12@psu.edu
Schuller	Ivan	University of California, San Diego	ischuller@ucsd.edu
Schwartz	Andy	DOE, Basic Energy Sciences	andrew.schwartz@science.doe.gov
Sefat	Athena	Oak Ridge National Laboratory	sefata@ornl.gov
Sellmyer	Dave	University of Nebraska	dsellmyer@unl.edu
Shinar	Joseph	Ames Laboratory / Iowa State University	shinar@ameslab.gov
Simmons	Jerry	Sandia National Laboratories, New Mexico	jsimmon@sandia.gov
Sinclair	Nick	University of Pittsburgh	nws5@pitt.edu

Last Name	First Name	Organization	E-mail Address
Smirnov	Dmitry	Florida State University	smirnov@magnet.fsu.edu
Smith	Art	Ohio University	ohiousmith@gmail.com
Smith	Kevin	Boston University	ksmith@bu.edu
Snoke	David	University of Pittsburgh	snoke@pitt.edu
Stanton	Christian	University of Florida	stanton@phys.ufl.edu
Talley	Lee-Ann	Oak Ridge Institute for Science and Education	lee-ann.talley@orise.orau.gov
Tanatar	Makariy	Ames Laboratory	tanatar@ameslab.gov
Tanner	David	University of Florida	tanner@phys.ufl.edu
Thiyagarajan	Thiyaga	DOE, Basic Energy Sciences	p.thiyagarajan@science.doe.gov
Thomas	John	North Carolina State University	jet@phy.duke.edu
Tobin	Jim	Lawrence Livermore National Laboratory	Tobin1@LLNL.Gov
Tolk	Norman	Vanderbilt University	norman.tolk@vanderbilt.edu
Tringides	Michael	Ames Laboratory / Iowa State University	tringides@ameslab.gov
Urban	Jeff	Lawrence Berkeley National Laboratory	jjurban@lbl.gov
Van Harlingen	Dale	University of Illinois at Urbana-Champaign	dvh@illinois.edu
Ward	Zac	Oak Ridge National Laboratory	5zw@ornl.gov
Wells	Barry	University of Connecticut	wells@phys.uconn.edu
Welp	Ulrich	Argonne National Laboratory	welp@anl.gov
White	Benjamin	University of California, San Diego	whitebd@physics.ucsd.edu
Yang	Fengyuan	The Ohio State University	yang.1006@osu.edu
Zaki	Nader	Columbia University	nz2137@columbia.edu
Zettl	Alex	University of California, Berkeley / LBNL	azettl@physics.berkeley.edu
Zudov	Mike	University of Minnesota	zudov@physics.umn.edu

